Building Simulation Applications BSA 2022 - Proceedings of 5th IBPSA-Italy conference

Konferenzbeiträge / Atti / Proceedings

Building Simulation Applications BSA 2022

5th IBPSA-Italy Conference
Bozen-Bolzano, 29th June –1st July 2022

Edited by
Giovanni Pernigotto, Francesco Patuzzi,
Alessandro Prada, Vincenzo Corrado, Andrea Gasparella

bu,press
bozen
bolzano
university
press

Freie Universität Bozen
Libera Università di Bolzano
Università Liedia de Bulsan

Konferenzbeiträge / Atti / Proceedings

Building Simulation Applications BSA 2022

5th IBPSA-Italy Conference
Bozen-Bolzano, 29th June –1st July 2022

Edited by
Giovanni Pernigotto, Francesco Patuzzi,
Alessandro Prada, Vincenzo Corrado, Andrea Gasparella

bu,press
bozen
bolzano
university
press

bu,press

Bozen-Bolzano University Press, 2022

Free University of Bozen-Bolzano

www.unibz.it/universitypress

Cover design: DOC.bz / bu,press

ISSN 2531-6702

ISBN 978-88-6046-191-9

DOI 10.13124/9788860461919

Table of Contents

Preface

The participation of about 100 attendees at the fifth Building Simulation Applications BSA2022 Conference, one of the first IBPSA conferences held entirely in presence after the pandemic outbreak, can certainly be claimed as a step forward in the process of overcoming the constraints and limitations imposed by the years of the Covid-19 pandemic.

11 conference sessions in two parallel tracks, 66 presentations reporting the contributions by more than 180 authors are some of the most significant figures of this event. In addition, confirming an international profile and its inclusivity call, the Conference saw a small but significant presence of delegates from abroad, especially from Austria and India.

As the previous editions, BSA 2022 focused on providing an overview of the latest applications of building simulation in the following three main fields: the use of simulation for building physics applications, such as building envelope and HVAC system modelling and their design and operation optimization; global performance and multi-domain simulations; the development through simulation of new methodologies, regulations, as well as new calculation and simulation tools.

Nonetheless, the times urged to address indoor air quality, the main topic of this edition, emphasizing the role of simulation to assess strategies able to ensure healthy and safe indoor conditions for occupants.

The engaging opening speech about "The Role of IBPSA and Post-Covid Simulation" by Prof. Lori McElroy, President of IBPSA, was followed by two innovative and capturing keynotes, "Simulation and Optimization: Supporting Building Decarbonization" by Prof. Paolo Baggio, University of Trento, Italy, and "Going Digital – Infrastructure Modeling for Resilience and Decarbonization", by Dr. Drury B. Crawley, vice-President of IBPSA.

The conference also devoted some time to the analysis and discussion of the use of building simulation among building professionals and specialists in terms of education: The "3rd Student School on Building Performance Simulation Applications" addressed the use of building performance simulation in the context of building rating systems and in relation with BIM. We also had an interesting conversation with Lori McElroy on the topic of "Building Simulation in the Profession: Work in Progress", discussing the current most critical aspects and challenges. Finally, after the conference closing ceremony on the third day, the "Round Table for Designers and Practitioners" featured four professional experiences about the use of building simulation, with a discussion about errors, challenges, and opportunities.

The fifth edition of the BSA conference represented an opportunity to restart and revitalize the process of reducing the gaps between academia and the professional world, of rethinking the role of building simulation in the design practice for future buildings, and of opening in the face of unprecedented challenges and opportunities of a new post-pandemic society.

Andrea Gasparella, Free University of Bozen-Bolzano

Optimization of Daylighting and Energy Performance in Bangladesh Ready-Made Garment Factories: Use of Parametric Design, Simulation Modeling, and Genetic Algorithms

Md Ashikur Rahman Joarder – Bangladesh University of Engineering and Technology, Bangladesh – ashikj2000@gmail.com; ashikjoarder@arch.buet.ac.bd
Md Monir Hossain – Bangladesh University of Engineering and Technology, Bangladesh – hossainmonir.2008@gmail.com
Aaron J.E. Bach – Griffith University, Australia – a.bach@griffith.edu.au
Jean P. Palutikof – Griffith University, Australia – j.palutikof@griffith.edu.au
Fahim Tonmoy – BMT Commercial pty, Brisbane, Australia – Fahim.Tonmoy@bmtglobal.com

Abstract

The ready-made garment (RMG) sector is an essential contributor to the economy of Bangladesh. Most RMG buildings in the country are often found to be inefficient in terms of natural light, energy consumption and the thermal comfort of the workers. Computational modeling, simulation and optimization analysis could be used during the building planning and design phases to effectively integrate these three issues and improve the working environment. This research first evaluates both daylighting and energy performance of a real-world existing air-conditioned RMG factory building in Dhaka. Next, an optimized design solution is proposed for the factory. Finally, we correlate the relationship between design variables and performance metrics. Nine independent variables (north, south, east and west window-to-wall ratios and shading; and skylights) are identified to evaluate performance. The variables are connected with parametric sliders (value expressed by a range of numbers despite a constant value), so that performance can be checked for different possible configurations. Rhinoceros, Grasshopper, ClimateStudio, Octopus, TT toolbox, and Energy plus™ software with plugins are used to conduct the optimization process. Genetic Algorithms are used to narrow down the optimization results and identify the best options that comply with the multi-objective goal. Predicted Percentage of Dissatisfaction (PPD) is also analyzed for the best options identified from the optimization process. The result shows the balanced option (best for both daylighting and energy) with changed materials satisfies the thermal comfort of users.

1. Introduction

Ready-made garment (RMG) factories in Bangladesh have been heavily criticized for their working conditions. More than 80 % of the export earnings of Bangladesh come from the RMG sector (Islam, 2021) and about four million people are involved in this industry. In the factories, workers are engaged in sewing, ironing, packing, tailoring, operating machines and other labor-intensive works. Due to the nature of their work and the heat generated from machinery, the indoor environment of the factories is often uncomfortable and workers suffer a range of health problems that affect the individual as well as the overall productivity of the factory. In RMG factories, along with other physical conditions, the quality of the luminous environment is affected by poor natural lighting systems and high internal heat gain from artificial lighting (Hossain & Ahmed, 2013). This creates an intolerably hot and uncomfortable working environment for the workers that is non-compliant with national and international standards. Since lighting directly affects visibility, light is critical to the productivity, safety and healthy working conditions of workers (Zohir & Majumder, 2008). Industrial workers spend more than 90 % of their lives in artificial luminous environments and in such conditions, natural light could work as medicine (Gligor, 2004). Different studies have shown that lighting is one of the biggest consumers of power in the RMG sector, accounting for around 21-35 % of the total

energy consumption (EAC, 2009). Much work has been done to reduce the power consumption of machinery in RMG factories; however, developments in the areas of lighting, heating and ventilation are limited (Godiawala et al., 2014).

Appropriate use of daylight and removing generated heat by effective natural and/or artificial ventilation systems can be an effective means to reduce energy consumption and excessive cooling load. With the appropriate use of technology, it is anticipated that the energy consumption in the building sector can be reduced to about 30 % to 80 % (Gupta, 2017). Due to current environmental concerns, energy saving has become the leading driving force in modern research (Bojic et al., 2013). Appropriate architectural design can reduce the energy consumption of heating or air conditioning systems significantly (Kalmár & Csiha, 2006). The EU energy policy in the buildings sector, including technical solutions and legal procedures, aims to improve the energy performance of buildings and guarantee human comfort (Tronchin & Tarabusi, 2013).

In recent times, to ensure workers' comfort and productivity, the construction of fully air-conditioned factory buildings with excessive artificial lighting has been gaining in popularity among owners and management of RMG factories in Bangladesh. Electricity-based carbon-intensive air conditioning and lighting systems can result in a significant amount of energy consumption. On the other hand, the use of daylight with passive or hybrid ventilation systems requires less energy to operate, while at the same time having less impact on the environment, carbon emissions and climate change. Using a case study approach based on a real RMG factory in Dhaka, this research presents a system for improving indoor lighting conditions and comfort by integrating passive strategies for the existing garment factories of Bangladesh. The research addresses the growing threat to worker health and productivity from the visual and heat stress that may be caused by climate change and seeks to identify sustainable passive strategies that will not add to the burden of greenhouse gas emissions.

2. Case Study

The case building is an 864-square-meter factory building with a pitched roof (Fig. 1). The building is north facing (Fig. 2: top) towards the access road. The roof is made of a metal sheet adjacent to a truss frame structure (Fig. 2: bottom). The north façade of the factory has two large gates (6 meters x 2.5 meters) made of steel. During working hours, these two gates remain closed for security purposes. So, for simulation modeling, the north façade of the base case was provided with no opening.

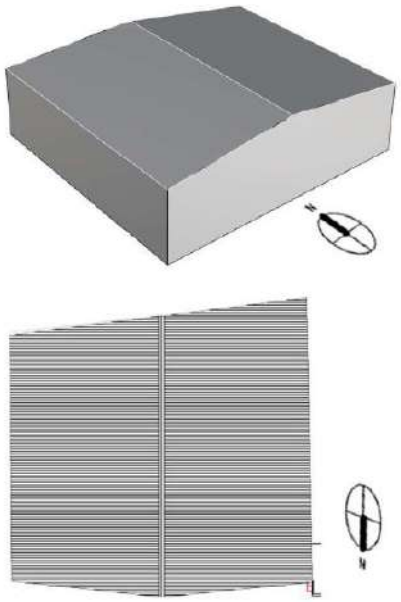

Fig. 1 – Rhinoceros model for case RMG factory (top) and top view of the roof (bottom)

A Kestrel 5400 pro instrument was installed inside the factory to measure air temperature, relative humidity (RH), wind speed, and black and wet bulb globe temperatures (Table 1). Three wireless tag loggers made by OnSolution were also placed at different locations inside the factory to measure temperature and RH. The collected data were cross-checked with the base case simulation modeling for validation.

3. Method

This study seeks to test and verify the effectiveness of optimization processes in the tropical climatic context, in this case, Bangladesh. Based on the

RMG factory described in Section 2, the internal conditions were optimized for the target parameters of daylighting and energy consumption. There are six main steps for the research, as explained below.

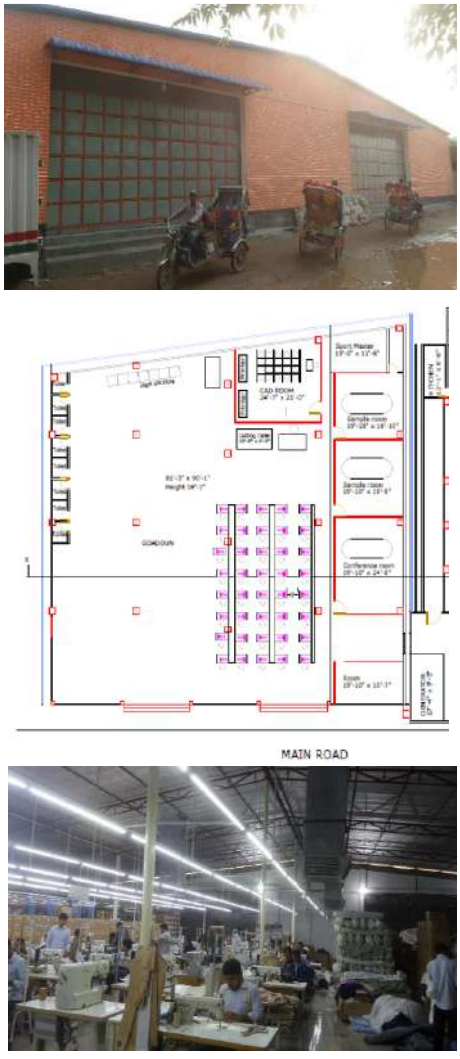

Fig. 2 – North side view of the case factory building (top), floor plan (middle), and inside view of the RMG factory (bottom) (pictures by Photographer Md M A R Joarder, 2020)

The first step is to select an RMG building for a case study. This research selected a single-storey RMG building constructed with steel and brick, located in northwest Dhaka (Fig. 2). The factory undertakes garment manufacture, from cutting through sewing and ironing to packing. A physical survey was conducted in the first step to measure the existing configuration and collect the climate data (Table 1) that is required for simulation analysis.

Table 1 – Indoor and outdoor mean maximum temperature (T_{max}) and mean minimum relative humidity (RH_{min}) between 08:00 and 18:00 on the days the factory was operating in 2021

	Indoor	Outdoor
January (n=308 hours over 28 days)		
T_{max} (°C)	28.6	24.5
RH_{min} (%)	44.2	50.3
March (n=264 hours over 24 days)		
T_{max} (°C)	29.6	33.3
RH_{min} (%)	59.9	38.8
September (n=286 hours over 26 days)		
T_{max} (°C)	30.1*	32.6
RH_{min} (%)	62.4*	64.3
All of 2021 (n=3234 hours over 294 days)		
T_{max} (°C)	30.9^	30.6
RH_{min} (%)	58.7^	55.9

*30 hours of missing data not included
^ 39 hours of missing data not included

The second step was to prepare the 3D model using the data collected during the physical survey. The simulation of the base case factory building was carried out at this step. Materials and other information for zones were transferred into simulation settings and Grasshopper scripts accordingly. In this script, the workflow could be divided into six parts. Part A was the components for developing the building geometry (floor, wall, roof, window, shading and skylight). The geometry was connected to components in Part B for energy and daylighting modeling. In this part, material selection for individual elements of the building, sensor grid settings for daylighting, zone settings, adiabatic and boundary condition settings were operated. The daylight model was connected to components in Part C for daylighting simulation. In this part, various simulation-related settings were identified (e.g., the number and name of the objectives and ClimateStudio Result [CSR] settings). Part D connected both the energy model from Part B and the daylighting simulation output from Part C for energy simulation. Part E was the components for optimization. Part F was the components for data output (Fang, 2017).

The third step was to run the optimization process for Option 1 (the best option for daylighting). Grasshopper script was prepared for modeling the case space with parametric design variables. Phe-

notype toggle in Octopus is connected with daylight performance batteries (LEED: Leadership in Energy and Environmental Design credit; sDA: Spatial Daylight Autonomy; ASE: Annual Sunlight Exposure; and Mean Illuminance) and energy performance batteries were skipped, as the best daylighting option was the target. As windows have a large-scale impact on daylighting and thermal comfort considering their size, orientation and shading configurations, as well as on the energy consumption of the building, it was thus necessary to optimize window design for maximum benefit (Aman, 2017).

The fourth step was to run the optimization process for Option 2 (the best option for energy). The overall procedure was similar to daylighting optimization. The difference was only in the optimization objective, which is Energy Use Intensity (EUI), and CO_2 emissions. Daylighting performance batteries were skipped here, as the best energy option is the target. Therefore, the Phenotype toggle in Octopus was connected with EUI and CO_2 only.

The fifth step was to run the optimization process for option 3 (the balanced option for daylight and energy both). In this step, three performance objectives (e.g., sDA, ASE and EUI) were identified to run the simulation. Octopus by default found the minimum value of each objective, so the objective to be maximized (sDA) should be multiplied by -1. Pareto Frontiers with the trade-off between each performance metric were found after the optimization process.

In the final (6^{th}) step, Percentage of Mean Vote (PMV) and Predicted Percentage of Dissatisfaction (PPD), analyses were carried out to check thermal comfort inside the factory space. ClimateStudio and Grasshopper were used to run this analysis as well. Five simulations were run in this step (for Base case, Op1- Daylighting, Op2- Energy, Op3- Balanced, and Op4- Balanced and changed materials). Comparing the results of these five simulations, the best one complying with both the American Society of Heating, Refrigerating and Air-Conditioning Engineers (ASHRAE) standard and the Bangladeshi standard (BNBC, 2020) and which could provide thermal comfort inside the factory, was identified.

4. Simulation and Results

In this research, the percentage of windows and skylights, and depth of shading was explored for optimal daylighting and energy performance. There were no windows and shading on any of the façades of the factory building, and no skylight on the roof. For the modeling of the optimization process focusing on daylighting and energy, the placement of the doors and the interior partitions was not considered. The model was developed with Rhinoceros 7.1 (Fig. 1) and Grasshopper scripting. ClimateStudio 1.1 plugins were used for simulation. Existing data collected through factory visits were used for zone settings while simulations were conducted. There were 26 daylighting sensors evenly spaced at a height of 0.75 meters above the floor. Some building parameters were fixed throughout the optimization process: the height of the building from the ground to the edge of the pitched roof was 5 meters; windows were considered from 0 to 100% of the façade; areas of skylight were considered from 0 to 20% of the roof surface.

Building material details found during the physical survey were used in the model. To avoid excessive heat gain or heat loss from the skylight, an insulated translucent material was used as its glazing material. The material had a U-value of 0.45 W/(m^2 K). The reflectance of the ceiling, floor, interior, exterior walls, and shading were 0.8, 0.2, 0.5, 0.5, and 0.8 respectively. The windows had a transparent material with visible transmittance of 0.65. Skylights had a translucent material with a transmittance of 0.24. Nine independent design variables for the building geometry were analyzed: north, south, east and west windows to wall ratios [WWR] and shade; and Skylights. Table 2 shows the minimum (0 % for WWR, 0.0m for shade and 2 % for skylight) and maximum (100 % for WWR, 2.0 m for shade and 20 % for skylight) values of the variables and the ranges used during simulation analysis. The daylighting simulation output included sDA and ASE.

The energy simulation output Included annual heating, cooling, equipment and lighting energy loads. Since the equipment load stays the same for studied design options, it was not considered. The

energy optimization objective was to ensure the minimum total energy load. The total energy load was the sum of heating, cooling, and lighting loads. EUI was also calculated by dividing the total energy load by the occupied floor area of the factory building.

Table 2 – Design variables and ranges for simulation analysis

	Variable	Minimum	Maximum
1	WWR-North	 No windows	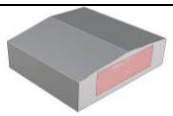 Full-wall windows
2	WWR-East	 No windows	 Full-wall windows
3	WWR-South	 No windows	 Full-wall windows
4	WWR-West	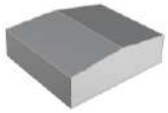 No windows	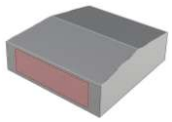 Full-wall windows
5	Shade Depth-North	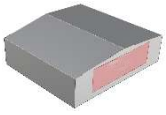 No shade	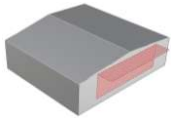 2.0m shade
6	Shade Depth-East	 No shade	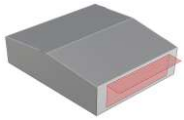 2.0m shade
7	Shade Depth-South	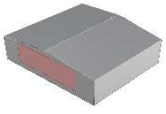 No shade	 2.0m shade
8	Shade Depth-West	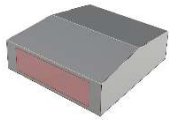 No shade	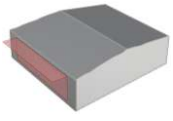 2.0m shade
9	Skylight	 2 %	 20 %

4.1 Base Case Modeling and Analysis

The first simulation was conducted for the base case, to understand the existing status of the building in terms of daylighting and energy performance. The model was prepared considering the exact dimensions of the building collected during the physical survey. The weather data file for Dhaka was used during the simulation process. The building was counted as air-conditioned and values of independent variables (windows, shading and skylight) were set to 0 (zero) representing the existing building. Simulation results for LEED credit, sDA, ASE, mean illuminance values, EUI and CO_2 emissions were 0, 0 %, 0 %, 0 lx, 223 kWh/(m^2 yr) and 198 kg$_{CO2e}$/(m^2 yr), respectively.

4.2 Optimization of Daylighting

The second simulation was conducted for the best daylighting results (Option 1). In this simulation, the population size was set to 20 and maximum generations were set to 10. In total, 200 iteration process were carried out to identify the best daylighting results. Pareto Front algorithm identified the best configurations among these combinations. Four daylighting performance objectives (LEED credits, sDA, ASE and mean illuminance) were set to run this optimization process. Table 3 shows the results of the simulation. LEED credit, sDA, ASE and mean illuminance values for the best daylighting case results are 3, 1 (100 %), 0.134 (13 %) and 1003 lx, respectively. In Fig. 3 (top), Pareto Front 3-dimensional graph shows the optimized results along with the Pareto Frontier (marked with a red circle).

4.3 Optimization of Energy

The third simulation was conducted to find the best energy consumption (Option 2). The process is similar to the prior simulation. The only difference is that two energy performance objectives (EUI and CO_2 emissions) were set to run this optimization. In Table 3, the third column presents the values of the independent variables that resulted from the optimization process and which were identified through the Pareto Front algorithm. The EUI and CO_2 emissions for the best energy case are

56 kWh/(m² yr) and 46 kg_{CO2e}/(m² yr), respectively. In Fig. 3 (middle), the Pareto Front 3-dimensional graph shows the studied iterations with the optimized one highlighted.

Table 3 – Optimization results for three different options

Design Variables	Op 1 (Daylighting)	Op 2 (Energy)	Op 3 (Balanced)
WWR- North (%)	82.5	40	100
WWR-East (%)	43	4	10
WWR-South (%)	7.5	24	22.5
WWR-West (%)	80	34	10
Shading-North (m)	1.17	1.86	1.58
Shading-East (m)	1.72	0.95	1.04
Shading-South (m)	1.52	0.09	1.84
Shading-West (m)	0.32	0.39	1.01
Skylight (%)	23	10	7

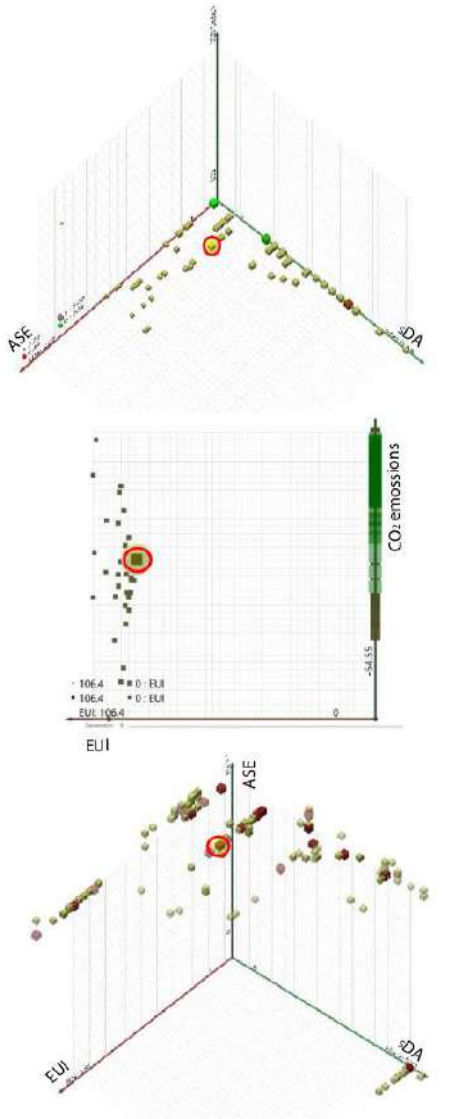

Fig. 3 – Pareto Front analysis for daylighting optimization (top), energy optimization (middle) and multi-objective optimization (bottom)

4.4 Optimization of Balanced Option

A Pareto optimization aims to find the trade-off front (ParetoFront) between multiple outcome objectives. The Octopus plugin handled the multi-objective optimization process using Pareto-Front algorithms (Aman et al., 2021). The fourth simulation was conducted for Option 3 (the balanced option for daylighting and energy combined). The simulation process was similar to the prior two simulations. Fig. 4 (top) shows the factory model while the optimization process of Op3 is running. Fig. 4 (bottom right) shows the ranges slider of nine variables in the Grasshopper script for this optimization. A large number of combinations are possible among these nine variables and within their ranges. Fig. 4 (bottom left) shows the values of six performance metrics (LEED credit, sDA, ASE, mean illuminance, EUI and CO_2 emissions) generated in this process. Later, three performance metrics (sDA, ASE and EUI) were considered for Pareto Front analysis to make the process simplified. The outcomes of the simulation studies are presented in Table 3 (fourth column, Op 3 Balanced; the values of design variables).

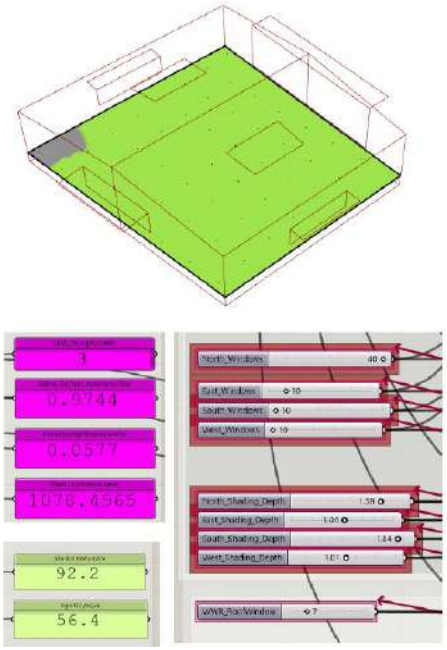

Fig. 4 – Rhinoceros model showing simulation process (top); results for six performance objectives appeared in Grasshopper script (bottom left); and Grasshopper slider for parametric design (bottom right)

In Fig. 3 (bottom), Pareto Front 3-dimensional graphs show different optimized results and locations (marked with a red circle) of the Pareto Frontier (the best one). sDA, ASE and EUI values for balanced option case are 0.90 (90 %), 0.09 (9 %) and 89 kWh/(m² yr), respectively.

Comparing the results of performance metrics for the base case (explained in Section 4.1) and the balanced option case reveals that the latter is performing effectively.

4.5 Thermal Comfort Analysis

By understanding the thermal behavior of the existing situation of factory buildings, owners can improve the indoor environment quality to increase their production (Sayem et al., 2011). The fifth simulation was conducted for analyzing the PPD. In this process, thermal comfort performance was checked for Base case, Op1 (daylighting), Op2 (energy), Op3 (balanced) and Op4 (balanced and changed materials). Design variables found in previous simulation results (presented in Table 3) were used in this study. In the base case, variables remain 0 (zero), as there were no windows, sunshades and skylights in reality. In Op4, variables were kept similar to Op3 (balanced), except for the changes of material for the roof and wall. 300 mm concrete, 80 mm insulation and 80 mm cement screed were used for the roof and walls. ClimateStudio's default script for spatial comfort analysis in the Grasshopper interface was used to run the PPD simulation. The building was considered non-AC during this simulation. Keeping the model static, the PPD analysis was performed by changing the values of design variables presented in Table 3.

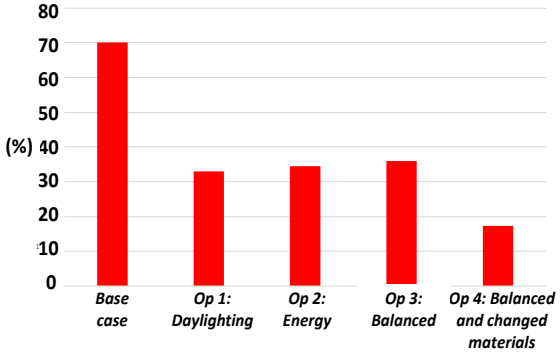

Fig. 5 – PPD results for the base case, daylighting, energy, balanced, and balanced and changed materials

In the case of Op4, in the Grasshopper script, roof and wall materials were changed from zone settings. Fig. 5 shows that the PPD value for the base case is 70 %, for Op1 32.9 %, for Op2 34.4 %, for Op3 35.9 % and for Op4 17.3 %. Although in ASHRAE standard below 10 % is recommended for thermal comfort, the value of 17.3 (below 20 %) for Op4 is also acceptable in the context of Bangladesh climate. The other 4 options do not comply with the ASHRAE standard and Bangladesh Standard (BNBC, 2020).

5. Conclusion

The global increase in demand for energy has generated pressure to save energy. Consequently, energy-efficient buildings are an important factor related to the energy issue (Jahangir et al., 2014). High-energy performance buildings can save primary energy and reduce CO_2 emissions. Optimization processes successfully present the ability to adapt to various design environments and provide design options with significant performance improvement. As a result, this method can be considered a valid approach (Fang, 2017). This research conducts three optimization processes and the results show that the configuration of the variables is changed in terms of Op1 (daylighting), Op2 (energy), and Op3 (balanced) (Table 3). The research recommends variables of Op3 (balanced) for RMG buildings in the context of Bangladesh, as it complies with both daylight and energy optimization. On the other hand, in the case of thermal comfort analysis, Op4 (balanced and changed materials) shows the best results among the options studied. In a nutshell, the features for RMG buildings in the climatic context of Bangladesh are: WWR-north 100 %, WWR-east 10 %, WWR-south 22.5 %, WWR-west 10 %, shade depth north- 1.35 m, shade dept east- 1.58 m, shade depth south- 1.63 m, shade depth west- 1.55 m, skylight- 10 %, roof and wall materials: 300 mm concrete, 80 mm insulation, and 80 mm cement screed performed the best among the options studied in terms of daylight penetration, energy consumption and providing thermal comfort. The features can be incorporated as strategies for sustainable RMG building design in Bangladesh.

Acknowledgement

This work is part of the "Managing heat stress among Bangladesh ready-made clothing industry workers" project funded by Wellcome under the Our Planet Our Health Programme. This work was carried out in the Department of Architecture, Bangladesh University of Engineering and Technology (BUET). The authors gratefully acknowledge the support and facilities provided by BUET.

Nomenclature

AC	Air Conditioning
ASE	Annual Sunlight Exposure
ASHRAE	American Society of Heating, Refrigerating and Air-Conditioning Engineers
CSR	ClimateStudio Results
EUI	Energy Use Intensity
LEED	Leadership in Energy and Environmental Design
PMV	Percentage of Mean Vote
PPD	Predicted Percentage of Dissatisfaction
RH	Relative Humidity
RMG	Ready-Made Garment
sDA	Spatial Daylight Autonomy

References

Aman, J., N. Tabassum, J. Hopfenblatt, J. B. Kim, and M. O. Haque. 2021. "Optimizing Container Housing Units for Informal Settlements - A Parametric Simulation & Visualization Workflow for Architectural Resilience." 26th CAADRIA Conference, Hong Kong. 29 Mar - 1 Apr.

Aman, J. 2017. "Impact of Windows for Daylighting on Thermal Comfort in Architecture Design Studios in Dhaka." 'Masters of Architecture' dissertation submitted to the Dept. of Architecture, BUET, Dhaka.

Bojic, M., A. Patou-Parvedyb, and H. Boyer. 2013. "Optimization of thermal comfort in buildings through envelope design." 25th ECOS Conference, Perugia, Italy. 26-29th June.

EAC. 2009. Energy Management Study on Abony Textile Limited and Abony Knitwear Limited, Hamayatpur, Savar, Dhaka. Energy Audit Cell, Ministry of Energy and Mineral Resources, BD.

Fang, Y. 2017. "Optimization of Daylighting and Energy Performance Using Parametric Design, Simulation Modeling, and Genetic Algorithms." Ph.D. in Design, Graduate Faculty of North Carolina State University.

Gligor, V. 2004. Luminous Environment and Productivity at Workplaces. Thesis (Licentiate). Espoo: Helsinki University of Technology, Finland.

Godiawala, P., N. Anand, and J. M. Patel. 2014. "Sky lighting - A solution to reducing energy consumption in Apparel Sector." *International Journal of Scientific and Research Publications* 4(4).

Gupta, M. 2017. "A path towards net-zero energy buildings." *International Journal of Research in Engineering & Technology (IJRET)* 5(2).

Hossain, M. and K. S. Ahmed. 2013. "Illumination Conditions and Visual Comfort in Production Spaces of Ready-Made Garments Factories in Dhaka." *IACSIT International Journal of Engineering and Technology* 5(5).

Islam, M. 2021. "Ready-made garments exports earning and its contribution to economic growth in Bangladesh." *GeoJournal*. 86 (2021).

Jahangir, A, M. A. Islam, and B. K. Biswas. 2014. "Energy simulation to estimate building energy consumption using EnergyPlus." 3rd ICMIEE Conference. Khulna, Bangladesh. 26-27 Dec.

Kalmár, F. and A. Csiha. 2006. "Interrelation between glazed surfaces, building structure and thermal comfort." 23rd PLEA conference, Geneva, Switzerland, 6-8 Sept.

Sayem, A., H. Ahmad, and T Hayat. 2011. "Indoor thermal condition of factory building in Bangladesh." *Journal of Architecture and Built Environment* 38(2).

Tronchin, L., and V. Tarabusi. 2013. "Energy Performance of Building and Thermal Comfort: a comparison. Recent Researches in Environmental and Geological Sciences." DIENCA–CIARM, University of Bologna, Italy.

Zohir, S. C. and P. Majumder. 2008. "Garment Workers in Bangladesh: Economic, Social and Health Condition." Dhaka: Bangladesh Institute of Development Studies.

Transient Three-Dimensional CFD Modelling of Ceiling Fans: A Comparison Between Detailed and Simplified Models

Francesco Babich – Eurac Research, Italy – francesco.babich@eurac.edu
Akshit Gupta – Eurac Research, Italy – akshit.gupta@eurac.edu
Wilmer Pasut – Ca' Foscari University of Venice, Italy / Korea University – wilmer.pasut@unive.it

Abstract

Ceiling fans have been widely used for decades for providing thermal comfort in warm environments. They are an effective means of completely avoiding the use of energy-intensive air conditioning systems in milder environmental conditions and of reducing the use of such systems in more severe and hotter thermal environments. Ceiling fans can generate an immediate cooling effect on people, as they act on both sensible and latent heat exchange between the human body and the moved air. However, one of the major potential limitations of ceiling fans is that they generate non-uniform velocity profiles, and their effect is highly dependent on the mutual position between body and fan. Thus, it is essential to carefully evaluate the position in which they are installed to maximize their cooling effect where needed by people. CFD is a powerful technique for investigating the air velocity field generated by different ceiling fan configurations. Due to its high demand for computational power and the need for having stable models, previous studies proposed different approaches to model ceiling fans in CFD with some simplifications. As the available computational power increases, so does the possibility of creating more realistic models, but too little is known about when the benefits produced by more complex models are overtaken by their computational costs. The aim of this study was to compare the results obtained by using two approaches to include the ceiling fan into a CFD model, namely a detailed model of the geometry of the fan and a simplified implicit approach that emulates the effect of the fan only. The results illustrate that (a) both models capture the main regions of the air flow, (b) the implicit model provided considerably more accurate air speed values, (c) the computational time of the model with blades is one order of magnitude higher, and (d) fan geometry and meshing are the most critical issues in the model with blades.

1. Introduction

Ceiling fans have been widely used for decades for providing thermal comfort in warm environments. They are an effective means of completely avoiding the use of energy-intensive air conditioning systems in milder environmental conditions, and of reducing their usage in more severe and hotter thermal environments (Babich et al., 2017a; Pasut et al., 2014; Schiavon & Melikov, 2008). Ceiling fans can generate an immediate cooling effect on people, as they act on both sensible and latent heat exchanging between the human body and the moved air.

However, one of the major potential limitations of ceiling fans is that they generate non-uniform velocity profiles, and their effect is highly dependent on the mutual position between body and fan (Babich et al., 2021). Thus, it is essential to carefully evaluate the position in which they are installed to maximize their cooling effect where needed by people.

Computational fluid dynamics (CFD) is a powerful technique for investigating the air velocity field generated by different ceiling fan configurations. Due to its high demand for computational power and the need for having stable models, previous studies proposed different approaches to model ceiling fans in CFD with some simplifications (Babich et al., 2017b). As the available computational power increases, so does the possibility of creating more realistic models, but too little is known about when the benefits produced by more complex models are overtaken by their computational costs.

The aim of this study was to compare the results obtained by using two approaches to include the ceiling fan into a CFD model, namely a detailed model of the geometry of the fan and a simplified implicit approach that emulates the effect of the fan only.

2. Methodology

In this study, two identical set-ups were created in CFD apart from the ceiling fan. In the former, the fan was modeled as a ring to which a body force was applied, while in the latter the actual geometry of the blades was included. As a result, a moving mesh was used in the latter, while this was not needed in the former. Both models were validated with measured air velocity values.

2.1 Features Common to Both Models

In this study, the key features that are common to both models were taken from a CFD model originally developed for thermal comfort studies (Babich et al., 2017b).

The geometry comprises an environmental chamber in which only a 120-cm-diameter ceiling fan was installed (Fig. 1). 36 monitoring points were placed in the model (3 heights; 12 points per height distributed on each level as shown in Fig. 2) in the very same locations of the original measurements.

An unstructured mesh with ten prism layers (added adjacent to the walls to accurately model the boundary layer near surfaces) was adopted.

Transient simulations were performed to better model the real behavior of the ceiling fan. In the original model, 3-minute simulations were performed. In this study, the simulation time was reduced to 1-minute to decrease the computational effort. To ensure that this was not altering the model results, a preliminary test was performed. Using the original air speed values (available for each time step of the 3-minute simulation for all 36 point), the average air speed in each monitoring point was calculated for a set of 60 s intervals (from 0 s – 60 s to 110 s – 170 s). The results showed negligible variations for a study that aimed at comparing two types of ceiling fan CFD modelling. For most points, the ratio between standard deviation and mean (i.e., the mean of the means of each interval) values was equal to 4 % or less (for instance, in point "centre 1300", the std is 0.06 m/s, the mean 2.05 m/s, and their ratio 2.9 %). Only at a very few points was this ratio higher than 10 %. However, all these points were at a higher level (70 cm or 130 cm above the floor) and far from the fan axis, and therefore in regions in which air speed values are considerably lower and less relevant.

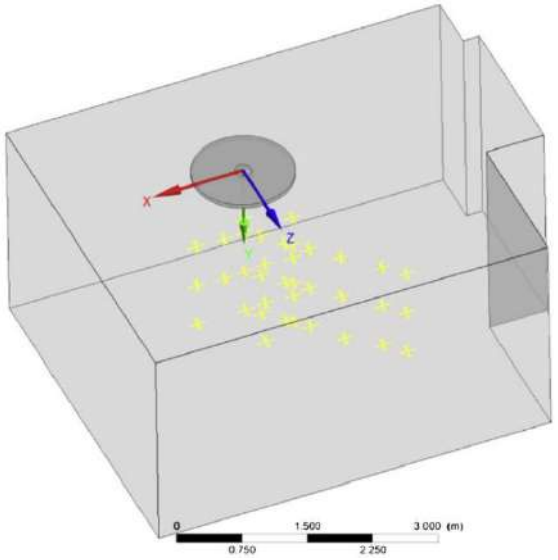

Fig. 1 – CFD model of the environmental chamber. In yellow, 36 monitoring points (Babich et al., 2017b)

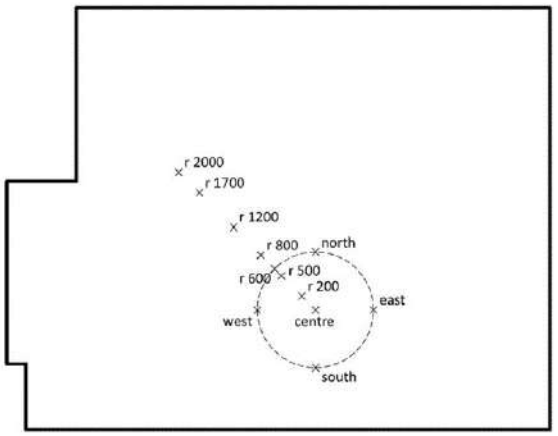

Fig. 2 – Plan view of the environmental chamber with the measurement locations (Babich et al., 2017b)

Convergence criteria were set equal to 1e-05 for the RMS residuals, and an adaptive time step as a function of RMS Courant number was chosen, with the limit for the RMS Courant number set equal to 5. The SST (Shear Stress Transport) k-ω turbulence model was selected as it gave the most accurate results in the original study (best match with measurements).

All CFD simulations were performed with ANSYS CFX version 2021. For the mesh, ICEM CFD was used for its advanced capabilities. All simulations were performed using a workstation equipped with 16 GB RAM and a 6-core Intel Xeon Gold 6154 CPU.

2.2 Fan Implicit Model (Without Blades)

In this former model (Fig. 1), the ceiling fan was modeled as in the original study (Babich et al., 2017b). A ring with the same diameter and distance from the ceiling (30 cm) as the actual fan was created. At the centre of the ring, a cylindrical solid element was added to emulate the fact that, in a real ceiling fan, no air emanates from the centre. A momentum source defined by means of cylindrical components was applied to this ring: axial component 55 kg m^{-2} s^{-2} (push air downwards), theta component 8 kg m^{-2} s^{-2} (rotational movement), and radial component 0 kg m^{-2} s^{-2}. This model led to a 1,933,004-element mesh.

2.3 Fan Explicit Model (With Blades)

In this second model (Fig. 3), the ceiling fan was modeled in more detail by implementing its three blades and central part. To enable the rotation of the fan, two domains were defined in the CFD model, namely a rotating domain (i.e., the cylindrical element shown in Fig. 3), which contained the fan, and a static domain (i.e., the remaining part of the room). One interface was used to link the two domains (lower and upper circles, and vertical side as shown in Fig. 3). In CFX, a "general connection" interface model and "transient rotor stator" were chosen. For mass and momentum, a "conservative interface flux" was used. The selected mesh connection method was "general grid interface" (GGI).

In this case, the model required a rotational velocity as an input, and this was set equal to 290 rpm, which was the corresponding rotational velocity for which the original model (Babich et al., 2017b) was developed. In this model, the total number of mesh elements is 2,088,669 (rotating domain = 217,150; remaining part of the room = 1,871,519).

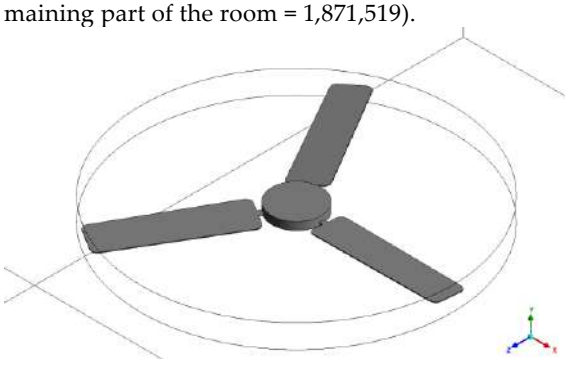

Fig. 3 – Ceiling fan with blades

3. Results

For both models, this section presents their capability of capturing the main regions of the air flow generated by the ceiling fan, the predicted air speed values, and the computational power required.

3.1 Regions of the Air Flow

Both modeling approaches capture the key qualitative features of the air flow generated by a ceiling fan (Fig. 4 and 5). In both cases, the main typical regions of the air flow can be identified (Jain et al., 2004; Wang et al., 2019), namely the region below the fan in which the highest speeds occur (excluding the small area immediately below the motor – also captured by both models), the regions near the floor and then the walls in which air (after having hit the floor) moves horizontally and then vertically to finally return to the blade areas, and lastly the remaining part of the room in which the lowest air speed values are usually recorded. In the region below the fan, like in previous studies (Babich et al., 2017b), the downward flow diverges with a variable half-cone angle depending on which time-step is analyzed.

However, by using the same scale (0.0 m/s to 2.0 m/s) to show the results of both models, it clearly appears that the absolute air speed values generated by the two modeling approaches are considerably different, the values obtained with the detailed model being significantly lower in almost all regions of the flow. This difference is particularly evident in the region below the fan in which the highest values are expected. On the other hand, there are no regions or other qualitative aspects of the flow that seem to be better captured by the detailed model.

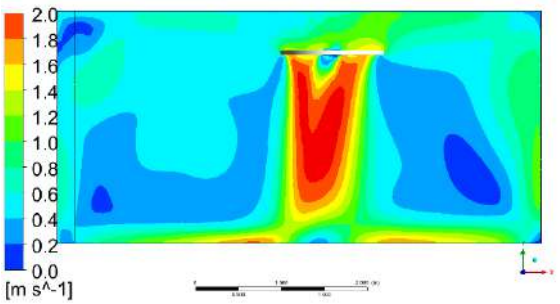

Fig. 4 – Air speed distribution - model without blades (scale from 0.0 m/s to 2.0 m/s)

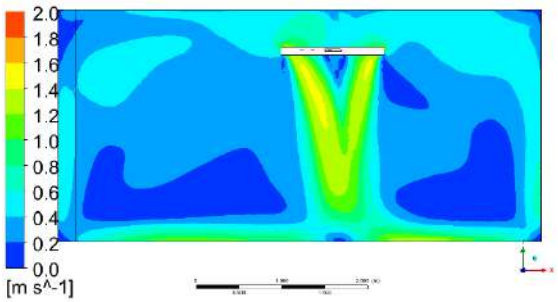

Fig. 5 – Air speed distribution - model with blades (scale from 0.0 m/s to 2.0 m/s)

3.2 Air Speed Values

Comparing the air speed values calculated by the two models and the measured values taken from previous studies (Babich et al., 2017b), in all 36 points the figures of the detailed model are considerably below the predictions of the implicit model (Fig. 6). Moreover, in most points, the output of the model without blades is much closer to the measured values that the predictions of the model with blades.

At the two higher levels (130 cm and 70 cm above the floor), the trend is very similar. Below the center of the fan and in the other points located in the region below the blades (r200 and r500), the air velocity obtained with the detailed model is approximately half the values generated by the implicit model, and the latter are usually in good agreement with measured values. Only in one (point r200 at 130 cm height) does the model without blades also underestimate the air speed, but it is still considerably closer to the measured value.

Focusing on the points that are more distant from the fan (r800 to r2000, i.e., 80 cm to 200 cm away from the fan rotational axis), air speed values are typically below 0.5 m/s, but even in this region the model with blades outperformed the one with blades by providing results that are closer the measurements.

Only in the points placed under the perimeter of the ceiling fan (which are r600, north, west, south and east) the trend is less clear. Both models show limited capability of capturing this region, which is characterized by rapid air speed variations. For the model without blades, this was already noted when it was originally developed (Babich et al., 2017b). On the other hand, modeling the blades did not lead to any noticeable improvement in this region of the flow.

At the lowest level (10 cm above the floor), the model without blades consistently underestimated the air speed values at all 12 points, and in none of them it proved to be superior to the model without blades.

Thus, overall, the model with blades did not lead to better results in any of the regions of the air flow, being considerably less accurate (i.e., less close to measured values) than the implicit model.

3.3 Computational Effort

The computational effort required to complete the simulations is considerably different (Table 1). Using exactly the same workstation and hardware-related settings, the total clock time of the model with blades is one order of magnitude higher than the total clock time of the model without blades. While the former simulation was completed in less than 4 hours, the latter required nearly 9 days.

Table 1 – Computational time

Model	Total clock time	Total clock time
Without blades	1.354e+04 s	3h 45m 40s
With blades	7.643e+05 s	8d 20h 18m 20s

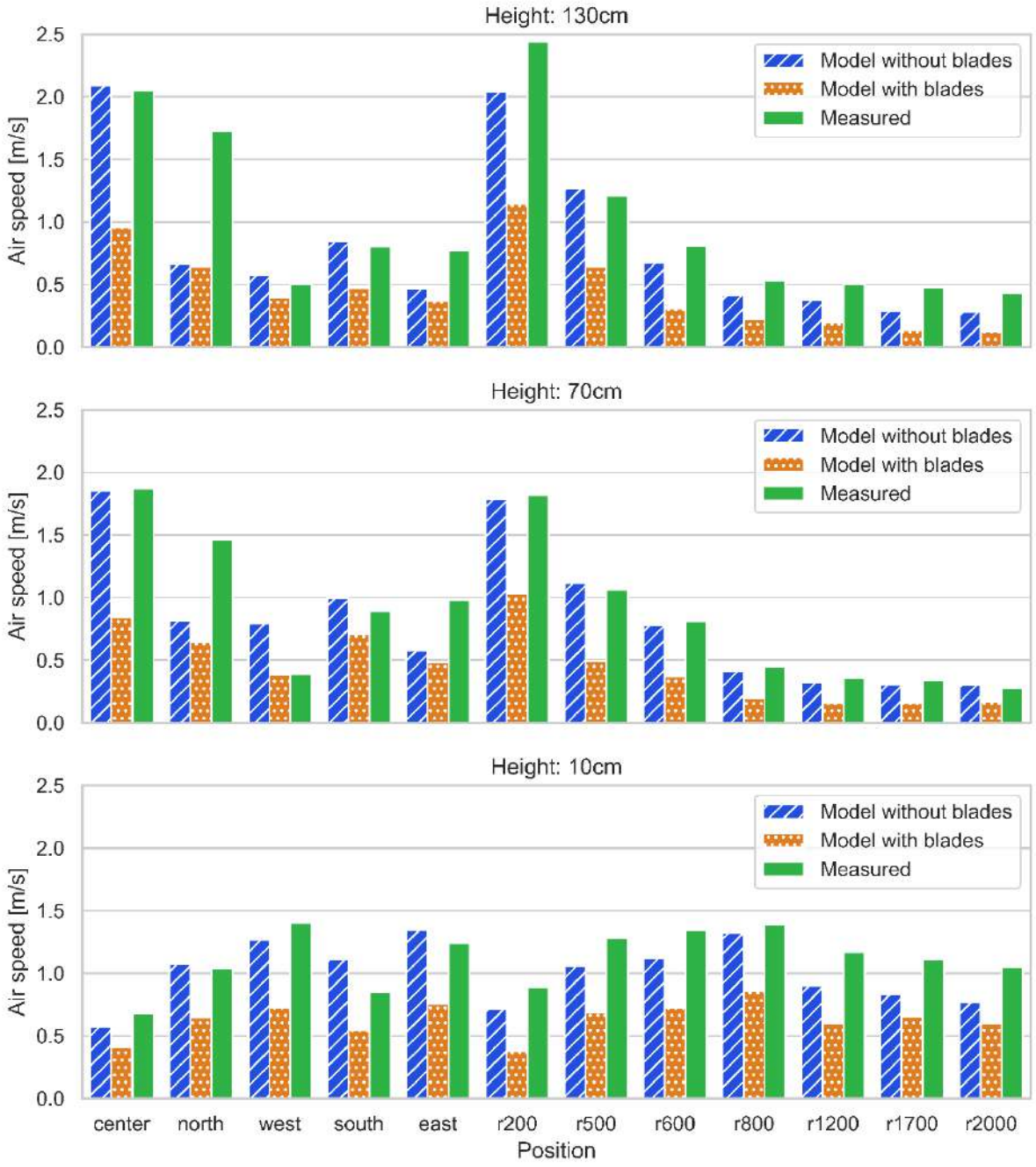

Fig. 6 – Simulated (60 s average) and measured (Babich et al., 2017b) air speed values

4. Discussion

The results of this study showed how the model without blades in which the ceiling fan is implicitly modeled by applying a body force to a cylinder provided more accurate air speed values in less than a tenth of the time, while qualitatively capturing all the main regions of the air flow. Thus, in this study, this modeling approach proved to be superior to a more detailed approach by all aspects. Since the implicit model had previously been fully validated based on experimental data (Babich et al., 2017b), it was expected to be accurate. However, the considerably lower accuracy of the model with blades was less predictable. Therefore, questions arise as to why this happened, and if and when using a model with blades might be the best solution.

In this study, several key parameters were identical in both models. Both used the SST k-ω turbulence mode. For the implicit model, previous studies (Babich et al., 2017b) showed that this turbulence model led to the best agreement with measured values by testing several Reynolds Averaged Navier-Stokes (RANS) turbulence models. For the model with blades, although some tests could be performed, there are no evident reasons to think that the use of a different RANS model, such as the widely used Re-Normalisation Group (RNG) k-ε, might significantly change the results. It might be also possible to explore the usability of other approaches to simulate the turbulence, such as large eddy simulation (LES). While the benefit (intended as better results) should be assessed, an increase in the computational time and in the set-up time would be certain.

Moreover, in both modeling approaches, an adaptive time step was set by using the same target, which is RMS Courant number equal to 5. For the turbulence model, also in this case there is no reason to assume that using a stricter target would considerably affect the results of the model with blades. However, the likelihood of a considerable increase in the computational time would be very high.

Focusing on the model with blades, the elements that are therefore more likely to explain the poor performances are the geometry of the fan, its meshing, and the interface between the two domains (rotating and stationary).

While in the implicit model the geometry is largely simplified (only dimensions of the total and central motor diameters are required), a considerably larger number of geometrical parameters are needed when the blades are modeled. If a computer-aided drafting (CAD) file is made available by the fan manufacturer, then the main effort is usually the cleaning of the geometry to remove all those small details that are required for production, but not CFD simulations, since they would be likely to increase the number of mesh elements and therefore also the computational time. However, an oversimplification might lead to inaccurate results.

On the other hand, if a CAD file is not made available, the geometry must be created by the modeler starting from the measurement taken on the actual fan. In this case, the accurate representation of the blades is usually the most difficult and time-consuming part (especially when there are multiple curvatures and variations of the profile). This is the approach used in this study. Further details could be added to try to improve the model predictions, but this is likely to increase the computational time, too.

Likewise, the use of a finer mesh in the rotating part might enhance the results. In this study, the minimum size of the surface mesh (on the fan surface) was 8 mm. This can be further reduced, and the overall meshing approach investigated in more detail. However, also in this case the computational time is likely to grow.

Focusing on the interface between the two domains, different settings might be evaluated, such as using three separate interfaces for the cylinder that encapsulates the fan to enable its rotation (upper circle, lower circle, and vertical side – Fig. 3). However, there are no evident reasons to expect considerably better results due to a change in the modeling of the domain interface only (ANSYS 2015).

Thus, fan geometry and meshing are likely to be the two most critical issues to be addressed to improve the capabilities of the model with blades. Although this study showed the higher accuracy and lower computational cost of an implicit ceiling fan model, its main limitation is the fact that each rotational speed requires different values for the momentum source, and the definition of the most appropriate values needs experimental data. The outcome might be a discrete set of momentum values (particularly useful for fans with a finite number of rotational speed levels) or a function that calculates the momentum values for any given rotational speed (more appropriate when direct current – DC – motors are used). On the other hand, an explicit CFD model of a ceiling fan uses the rotational speed as an input and therefore would not need experimental validation for multiple rotational speeds.

Thus, the main open question is whether it was better to develop an implicit model (the main effort is the creation of the experimental data) or to opt for an explicit model with blades (the main effort is on geometry and mesh implementation, and then on computational power). Assuming that measurements for different rotational speeds could be taken in one or two days, then the implicit model appears to be the best choice in most cases. However, especially if energy consumption for computing is not

considered, this might not be always the case (e.g., if a considerably high computational power such as a high-performance computing -HPC- cluster with hundreds of cores is available).

5. Conclusion

Ceiling fans are an effective means of completely avoiding the use of energy-intensive air conditioning systems in milder environmental conditions, and for reducing their usage in more severe and hotter thermal environments. CFD can be used to predict the air flow generated by ceiling fans, and therefore to better evaluate their capability of delivering comfort cooling.

The aim of this study was to compare the results obtained by using two approaches to include the ceiling fan into a CFD model, namely a detailed model of the geometry of the fan and a simplified implicit approach that emulates the effect of the fan only. The main findings of this study are as follows.

- both modeling approaches capture the key qualitative features of the air flow generated by a ceiling fan, and no relevant difference was noted.
- comparing the air speed values calculated by the two models and the measured values, the implicit model proved to be considerably more accurate. Especially in the regions of the flow in which the most elevated air speeds occur (such as below the fan), the measured figures and the values predicted by the implicit model were close, while the values obtained by the detailed model were much lower (half on the others in several points).
- using exactly the same workstation and hardware-related settings, the total clock time of the model with blades is one order of magnitude higher than the total clock time of the model without blades (less than 4 hours as opposed to nearly 9 days).
- fan geometry and meshing are likely to be the two most critical issues to be addressed to improve the capabilities of the model with blades. However, the use of a more detailed geometry and finer mesh would increase the computational time (and related energy consumption).
- the implicit model appears to be the best choice in most cases.

Considering that the main limitation of the implicit model is the fact that each rotational speed requires different values for the momentum source, and the definition of the most appropriate values needs experimental data, further work will focus on the geometry and meshing of the fan in the explicit model (in which the rotational speed is directly set).

Acknowledgement

The research presented in this paper was performed within H2020 Cultural-E project, which received funding from the European Union's Horizon 2020 research and innovation programme under grant agreement N. 870072.

References

ANSYS. 2015. "CFX Solver Theory Guide." Canonsburg, PA, USA.

Babich, F., M. Cook, D. Loveday, R. Rawal, and Y. Shukla. 2017a. "A New Methodological Approach for Estimating Energy Savings Due to Air Movement in Mixed Mode Buildings." In IBPSA.

Babich, F., M. Cook, D. Loveday, R. Rawal, and Y. Shukla. 2017b. "Transient Three-Dimensional CFD Modelling of Ceiling Fans." *Building and Environment* 123: 37–49. doi: https://doi.org/10.1016/j.buildenv.2017.06.039

Babich, F., W. Pasut, and A. Belleri. 2021. "The Use of Ceiling Fans in Reverse- Flow Mode for Comfort Cooling : Physiological Aspects and Relationship with International Standards." *ASHRAE Transactions* 127(2).

Jain, A., R. R. Upadhyay, S. Chandra, M. Saini, and S. Kale. 2004. "Experimental Investigation of the Flow Field of a Ceiling Fan." In *Proceedings of the ASME Heat Transfer/Fluids Engineering Summer Conference* 2004, HT/FED 2004, 3:93–99. American Society of Mechanical Engineers. doi: https://doi.org/10.1115/ht-fed2004-56226

Pasut, W., E. Arens, H. Zhang, and Y. Zhai. 2014. "Enabling Energy-Efficient Approaches to

Thermal Comfort Using Room Air Motion." *Building and Environment* 79: 13–19. doi: https://doi.org/10.1016/j.buildenv.2014.04.024

Schiavon, S., and A. K. Melikov. 2008. "Energy Saving and Improved Comfort by Increased Air Movement." *Energy and Buildings* 40(10): 1954–60. doi: https://doi.org/10.1016/j.enbuild.2008.05.001

Wang, H., H. Zhang, X. Hu, M. Luo, G. Wang, X. Li, and Y. Zhu. 2019. "Measurement of Airflow Pattern Induced by Ceiling Fan with Quad-View Colour Sequence Particle Streak Velocimetry." *Building and Environment* 152: 122–34. doi: https://doi.org/10.1016/j.buildenv.2019.02.015

Intelligibility Prediction in Scholar Classrooms

Samantha Di Loreto – Università Politecnica delle Marche, Italy – s.diloreto@pm.univpm.it
Fabio Serpilli – Università Politecnica delle Marche, Italy – f.serpilli@univpm.it
Valter Lori – Università Politecnica delle Marche, Italy – v.lori@univpm.it
Costanzo Di Perna – Università Politecnica delle Marche, Italy – c.diperna@univpm.it

Abstract

In recent Italian Law, the DM 11/01/2017 about Environmental criteria, reference values for the acoustic indoor quality descriptors of public buildings are imposed. These refence values are in compliance with the national standards UNI 11532-1 and UNI 11532-2. Part two of the series standard, in particular, describes the procedures and gives limit values for the acoustic comfort descriptors for schools. Regarding schools, adequate acoustic comfort targets are required in terms of indoor noise level and acoustic quality. Indoor acoustic quality targets refer to reverberation time (RT), Clarity (C50) and/or speech intelligibility (STI). The limit values for these indoor acoustic quality parameters, established by the national standards, are related to the measurement methods results; however, it is necessary to use prediction methods to estimate these parameters during the design phase. The aim of this study is to verify the prediction method accuracy used to determine intelligibility score. The study was developed to model the existing calculation method of speech transmission index (STI) in Matlab software to determine the acoustic speech intelligibility in school classrooms. A school building located in central Italy, in the Marche Region, was taken as a case study. This research aims to determine a correlation factor between the results of predictions and measurement speech intelligibility methods.

1. Introduction

The theme of the acoustic comfort (ambient noise, sound insulation, reverberation time, speech intelligibility) in primary school classrooms, in secondary school classrooms, as well as in university classrooms, has been the focus of several studies all around the world (Sala & Viljanen, 1995; Zannin et al., 2009). High noise levels in classrooms cause students to tire early, their cognitive abilities to decline, and they do not understand the content of the lessons. Excessive noise, too high reverberation, or the combined presence of both these effects in a classroom could reduce speech intelligibility, which is defined as the percentage of a message understood correctly.

The standard UNI EN ISO 9921 (UNI, 2004) specifies the requirements for the performance of speech communication and recommends the level of speech communication quality required for conveying comprehensive messages in several case studies. In (Pickett, 2005) many measurements of the intelligibility of speech were made to calculate the disturbance produced by different amounts of vocal force. The results of this case study show less than 5 % deterioration in intelligibility over the range, from a moderately low voice to a very loud voice (55 to 78 dB in a free field at one m from the lips). Other studies (Bradley et al., 1999; Yang & Bradley, 2009; Yang & Mak, 2018) have shown that speech intelligibility is influenced by reverberation time (RT), as well as by signal-to-noise ratios (SNR).

In (Choi, 2020), speech intelligibility tests were carried out in 12 university classrooms in Korea; the test results indicate that young adult listeners at university have a mean score of 95 % correct at a signal-to-noise ratio (SNR) value of +3 dB(A), which is a considerably lower SNR value than for the younger students in elementary schools. As a result, much attention to the development of effective objective indicators of quality and/or intelligibility are of particular interest, the measured parameters include reverberation time, early decay times, energy ratios, and STI values. The STI is a physical metric related to the intelligibility of speech degraded by additive noise and reverberation (Goldsworthy et al., 2004). Scientists nowadays consider the STI to be the parameter that best reflects the

intelligibility of speech (in a sound transmission system) (Steeneken & Houtgast, 1980). Consequently, the STI measure correlates well with subjective intelligibility scores for stimuli distorted by linear filtering, reverberation, and additive noise. Experiments in literature evaluate the effectiveness of the prevision method at predicting speech intelligibility.

In (Peters, 2020) the potential binaural effect of reducing reflection and reverberation was studied. These conditions create a reduction in intelligibility because echoes and strong discrete reflections, arriving late, lead directly to a wrong assessment when using the STI. Similarly, in (Schwerin & Paliwal, 2014) the STI approach was revisited and a variation was proposed which processes the modulation envelope in short-time segments, requiring only an assumption of quasi-stationarity (rather than the stationarity assumption of STI) of the modulation signal. Based on the tests in (Hongshan et al., 2020), the corresponding relation between STI and speech intelligibility in large spaces was modified, and a new rating threshold of STI was also proposed.

This paper aims to determine a correlation factor between the results of prediction and measurement speech intelligibility methods. The study was developed to model the existing calculation method of speech transmission index (STI) to determine the acoustic speech intelligibility in some classrooms at the Faculty of Engineering of the Università Politecnica delle Marche, Italy.

In this work, two sections are included. In the first, STI values are evaluated and calculated with the calculation method described in the annex L of BS EN 60268–16 (BSI, 2020). In the second, the result of the simulations is compared to the objective intelligibility measures in the same classes.

2. Material And Methods

2.1 Reference Values For Speech Transmission Index (STI)

The STI aims to objectively quantify speech intelligibility at a specific location in one environment when speech is produced through a normalized signal at another specific location in the same environment.

The STI index is based on the measurement of the Modulation Transfer Function (MTF). MTF quantifies the reduction in the modulation index of a test signal, depending on the modulation frequency. For each modulation frequency, the MTF is determined by the ratio between the modulation index of the signal at the listener, m_0, and the modulation index of the test signal, m_i. A family of MTF curves is determined, in which each curve is relative to each octave band of speech emission and is defined by the values that the modulation index reduction factor m assumes for each modulation frequency present in the envelope of a natural speech signal. For the STI index measurement, 7 octave bands, from 125 Hz to 8 kHz, and 14 modulation frequencies, between 0.63 Hz and 12.5 Hz at one-third octave intervals, are considered. The 98 (7x14) *m-values* are finally summarized in a single index, the STI, varying between 0 and 1, which represents the effect of the transmission system on intelligibility.

The STI quantifies the combined effect of background noise interference and reverberation on speech intelligibility reduction, with or without sound amplification systems.

The UNI EN ISO 9921 standard (UNI, 2004) establishes a relationship between STI value and their subjective assessment in terms of intelligibility for a normally hearing user. The values are shown in Table 1:

Table 1 – Relation between STI and Speech Intelligibility according to UNI EN ISO 9921:2004, Table F.1

Intelligibility rating	**Sentence score %**	**STI**
Excellent	100	> 0.75
Good	100	0.60 to 0.75
Fair	100	0.45 to 0.60
Poor	70 to 100	0.30 to 0.45
Bad	< 70	< 0.30

Another classification of speech intelligibility is provided in of BS EN 60268–16 (BSI, 2020); the standard defines qualification intervals for the levels of STI obtained, as shown in the following Fig. 1. The typical STI requirements for dedicated applications are also provided in Fig. 2.

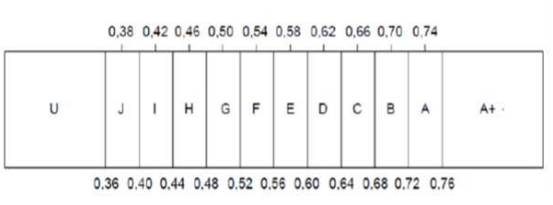

Fig. 1 – Qualification intervals for STI levels

Category	Nominal STI value	Type of message information	Examples of typical uses (for natural or reproduced voice)	Comment
A+	>0,76		Recording studios	Excellent intelligibility but rarely achievable in most environments
A	0,74	Complex messages, unfamiliar words	Theatres, speech auditoria, parliaments, courts, Assistive Hearing Systems (AHS)	High speech intelligibility
B	0,7	Complex messages, unfamiliar words		
C	0,66	Complex messages, unfamiliar words	Theatres, speech auditoria, teleconferencing, parliaments, courts	High speech intelligibility
D	0,62	Complex messages, familiar words	Lecture theatres, classrooms, concert halls	Good speech intelligibility
E	0,58	Complex messages, familiar context	Concert halls, modern churches	High quality PA systems
F	0,54	Complex messages, familiar context	PA systems in shopping malls, public buildings' offices, VA systems, cathedrals	Good quality PA systems
G	0,5	Complex messages, familiar context	Shopping malls, public buildings' offices, VA systems	Target value for VA systems
H	0,46	Simple messages, familiar words	VA and PA systems in difficult acoustic environments	Normal lower limit for VA systems
I	0,42	Simple messages, familiar context	VA and PA systems in very difficult spaces	
J	0,38		Not suitable for PA systems	
U	<0,36		Not suitable for PA systems	

Fig. 2 – Value for STI qualification bands and typical applications

There are two measurement methods for STI: the direct and indirect method. The direct method uses modulated (speech-like) test signals to directly measure the modulation transfer function. Typically modified Pink Noise with modulation frequencies was used. In this case, the measurement signal is either applied as an electric input to the system or through a "human speaker" loudspeaker to a microphone. The indirect method uses impulse response and forward energy integration (Schroeder integral) to derive the modulation transfer function. STI can be measured at the same time as other room acoustic parameters. This means that speech intelligibility will normally be measured using an omnidirectional speaker.

2.2 Room Descriptions and Measurements

The university building is in a suburban area of Ancona city, away from road traffic and other environmental noise sources. In addition, the classrooms are located at the rear of the building in relation to the access road. The external SPL during the daytime period is between 45 and 55 dB(A).

For the assessment of speech intelligibility, the AT2 classroom, belonging to the Engineering Faculty of the Marche Polytechnic University, was chosen as a case study. Classroom AT2 has a volume of 378 m^3, an average height of 3 m and a base area of 126 m^2.

The classroom has a sound-absorbing acoustic ceiling, wooden chairs, and tables. The windowed surface occupies 1/3 of the total surface of the concrete perimeter walls. Fig. 3 shows AT2 classroom, and the measurement positions, as required by UNI 11532-2 (UNI, 2020).

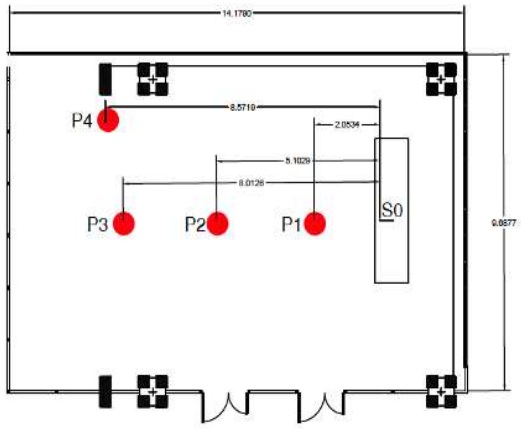

Fig. 3 – Plan of classroom AT2

The measurements in the classroom were done at four measurement points, chosen in compliance with UNI 11532 standard. Three positions were selected along the imaginary line traced on the longitudinal axis of the classroom, between the sound source and the back of the classroom, and a position was selected as representative of the most unfavorable listening condition (due to background noise, distance from the speaker, etc.). The STI measurements were derived from the impulse response measures and background noise measures with the indirect methodology proposed by BS EN 60268–16 (BSI, 2020).

Table 3 shows the results of STI for each measurement point and the STI mean value, without and with measurement uncertainty.

Table 3 – Value of STI for single point of measure, STI mean and STI mean with measurement uncertainty

STI (P1)	**STI (P2)**	**STI (P3)**	**STI (P4)**	**STI mean**
0.61	0.60	0.58	0.56	0.56
STI mean with measurement uncertainty		**Speech quality in accordance with CEI EN 60268-16**		
0.53		FAIR		

3. STI Prediction Using Indirect Method

Prediction of the STI of a sound system may be based on the MTF matrix that is calculated from the predicted room acoustic and electro-acoustic parameters and from the measured or estimated background noise levels, for each octave band contributing to the STI version chosen. The STI measure uses artificial signals (e.g., sinewave-modulated signals) as probe signals to assess the reduction in signal modulation in several frequency bands and for a range of modulation frequencies (0.6–12.5 Hz).

As requested in the reference standard, the speech spectrum at 1 meter in front of the mouth of a male speaker with the ambient noise spectrum reported in the Table H.1 of UNI EN ISO 9921:2004, see Table 4 and Table 5 was concatenated.

Table 4 – Speech spectrum at 1m in front of the mouth of a male speaker to UNI EN ISO 9921:2004, Table H.2

Octave band (Hz)	**125**	**250**	**500**	**1000**	**2000**	**4000**	**8000**
SPL@1m (dB)	62.9	62.9	59.2	53.2	47.2	41.2	35.2

Table 5 – Ambient noise spectrum according to UNI EN ISO 9921:2004, Table H.1

Octave band (Hz)	**125**	**250**	**500**	**1000**	**2000**	**4000**	**8000**
SPL@1m (dB)	41	43	50	53,2	47	42	39

The STI was calculated based on modulation transfer function (MTF) and the calculations used the method of Houtgast and Steeneken (1973).

In (UNI, 2020) for the calculation of the STI in classrooms without amplification system and with volumes > 250 m^3, an emission signal at 1m in axis to the source equal to 70 dB is required. So, for the calculation of the predictive STI, the reference signal of the speech was increased by 10 dB.

The modulation transfer function of the transmission path may be quantified by comparing the ratio of the modulation depth at the output and input of the test signal, and it was be written as Eq. (1):

$$m(fm) = \frac{|\int_0^\infty h(t)^2 e^{-j2\pi f m^t} dt|}{\int_0^\infty h(t)^2 dt} \cdot [1 + 10^{-\frac{SNR}{10}}]^{-1} \qquad (1)$$

where:

- $m(fm)$ is the modulation transfer function of the transmission channel
- $h(t)$ is the impulse response of the transmission channel
- SNR is the signal-to-noise ratio in dB

Considering a diffuse reverberant field, the impulse response was written as Eq. (2):

$$h(t) = \frac{Q}{r^2} \cdot \delta(t) + \frac{13{,}8\ Q}{r_c^2 T} e^{\frac{-13{,}8\ t}{T}} \qquad (2)$$

where:

- Q is the directivity factor for the sound source (talker)
- r is the talker-to-listener distance
- T is the reverberation time of the room space

The reverberation time was calculated with the method described in UNI EN 12354-6 (UNI, 2006), starting from the acoustic absorption of the room. The impulse response of the classroom was calculated in the four different positions of the room.

The standard UNI 11532-2:2020 in Paragraph 4.5 defines an optimal reverberation time, T_{ott} , corresponding with a conventional occupation of the environment equal to 80 % for categories A1, A2, A3, A4. The categories of the environment, in relation to the destined use, are reported in Table 6.

Table 6 – Categories of the environment in relation to the destined use according to UNI 11532-2:2020

CATEGORY	**Activities in the environment**	**Methods of intervention**
A1	Music	Objective achieved with integrated design of geometry, furniture, residual noise control
A2	Spoken / conference	
A3	Lesson / communication as speech and lecture	
A4	Special classroom lecture / communication	
A5	Sport	
A6	Areas and spaces not intended for learning and libraries	Objective achieved with sound absorption and residual noise control

The reference values for optimal reverberation time for A1-A4 categories are reported in Table 7.

Table 7 – Categories of the occupied environment in relation to the destined use according to UNI 11532-2:2020

CATEGORY	Occupied environment 80 %
A1	T_{ott} = (0.45Log(V) + 0.07) (30 m³ < V < 1000 m³)
A2	T_{ott} = (0.37Log(V) - 0.14) (50 m³ < V < 5000 m³)
A3	T_{ott} = (0.32Log(V) – 0.17) (30 m³ < V < 5000 m³)
A4	T_{ott} = (0.26Log(V) - 0.14) (30 m³ < V < 500 m³)

In Fig. 4, the graph of the simulated reverberation time vs measured reverberation time, for a conventional occupation of the environment equal to 80 %, is reported.

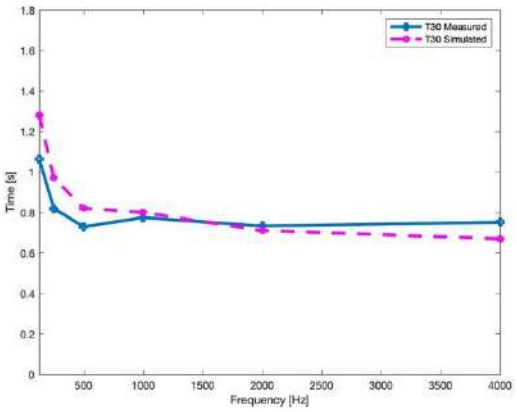

Fig. 4 – Reverberation time value in the octave bands between 125 Hz and 4000 Hz simulated (empty room) and measured

A constant MTF over the modulation frequencies indicates that speech intelligibility is mainly determined by background noise. A continuously decreasing MTF indicates an important influence of the reverberation and an MTF that decreases first and then increases again indicates the presence of an echo. Fig. 5 shows the result of the simulation of the modulation transfer function in the 7 octave bands calculated for P1.

The STI index can be finally obtained by using the weighted average method for the modulation transmission index on the considered octave bands Eq. (3):

$$STI = \sum_{k=1}^{7}(a_k \, x \, MTI_k) - \sum_{k=1}^{6}\beta_k \, x \, (MTI_k \, x \, MTI_{k+1})^{1/2} \quad (3)$$

Where:

- α_k is the weight coefficient of octave band f_m
- β_k is the redundancy factor between octave band k and octave band $k + 1$.

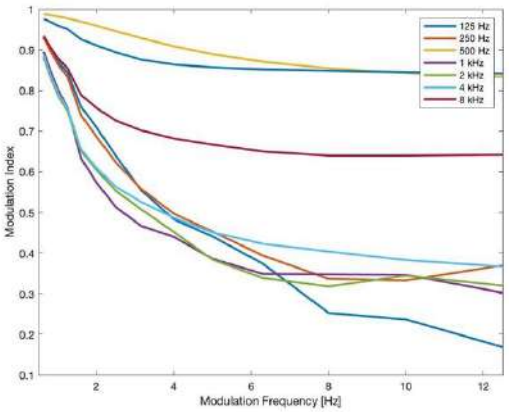

Fig. 5 – Modulation transmission ratio in the 7 octave bands

Table 8 shows the relationship between α_k, β_k and MTI_k to determine the STI for P1.

Table 8 – Result of the calculation for the P1

Frequency [Hz]	125	250	500	1000	2000	4000	8000
a_k male	0.085	0.127	0.230	0.233	0.309	0.224	0.173
Combined MTI_k x a_k weighting	0.054	0.090	0.163	0.157	0.207	0.118	0.071
β_k male	0.085	0.078	0.065	0.011	0.047	0.095	0.000
Combined MTI_k x β_k weighting	0.054	0.055	0.046	0.007	0.032	0.005	0.000
sum a_k * MTI_k	0.860						
sum β_k * MTI_k	0.244						
STI (P1)	0.62						

The same calculation was carried out for all the positions and the STI simulation results are shown in Table 9.

Table 9 – Results of the calculation of STI for P1, P2, P3 P4 and STI mean

STI (P1)	STI (P2)	STI (P3)	STI (P4)	STI mean
0.62	0.55	0.53	0.53	0.55

STI mean with measurement uncertainty	Speech quality in accordance with CEI EN 60268-16
0.53	FAIR

4. Results

From the comparison between the results of STI obtained between measured and simulated values, it can be seen that the difference is very low. This attests that the predictive model turns out to be very effective to ensure a good internal quality of the classrooms during the design phase.

In particular, the STI mean, simulated and measured, is equal and, in both cases, speech intelligibility is FAIR in accordance with the reference standard.

Considering the results of simulations and according to the background literature, a statistical analysis for the case study was carried out.

The proposed correlation model between the measurements of STI versus the simulations of STI is based on a polynomial function, according to the following Eq. 4.

$$y=ax^3+bx^2+cx+d \quad (4)$$

where y is the response variable and a, b, c, d represents partial correlation coefficients (coefficients with 95 % confidence bound).

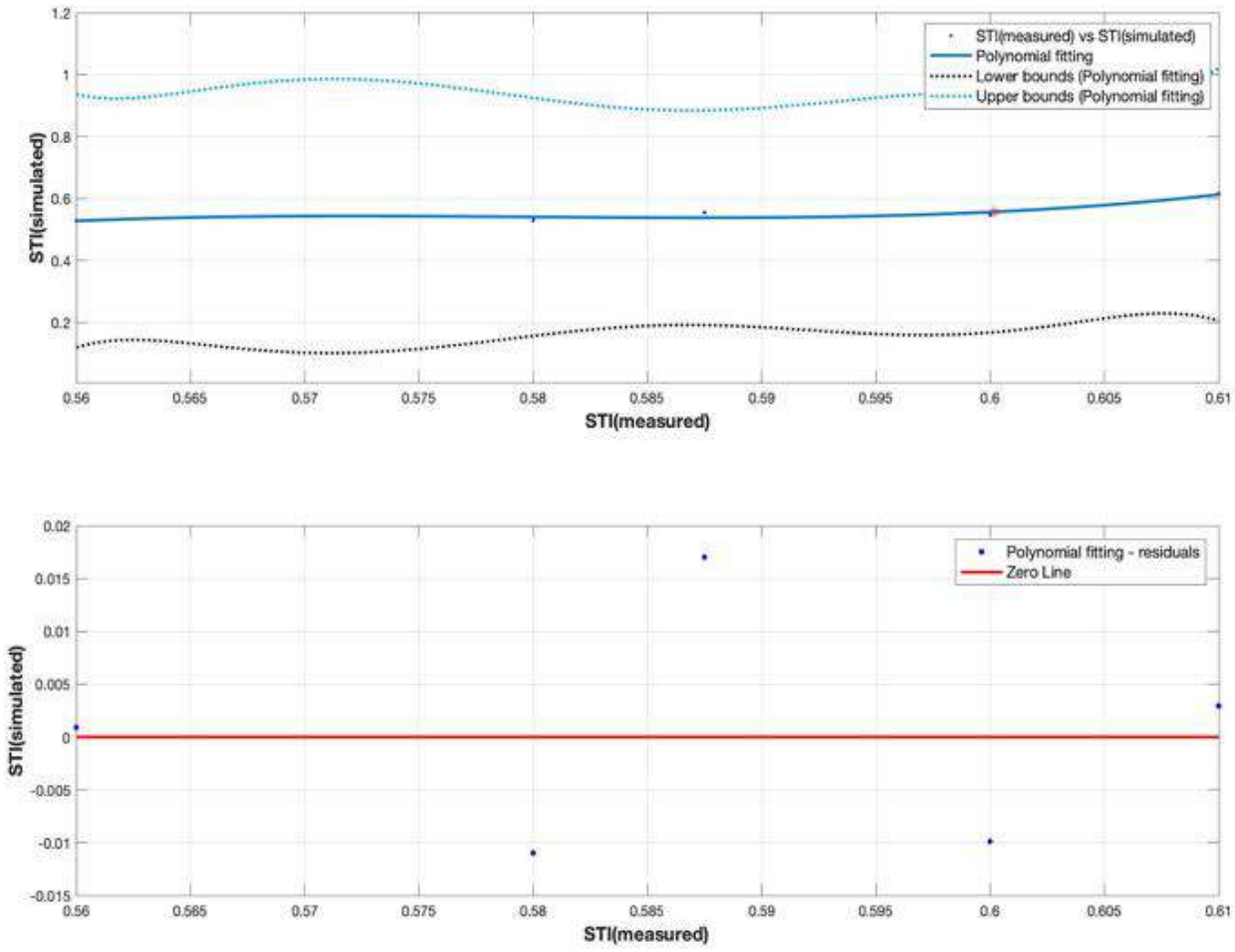

Fig. 6 – Best fit polynomial curve and residuals of the STI_m vs STI_p considered for each point of measure

Table 10 – Results of the polynomial regression

DFE	SSE	R^2	R	RMSE
1	5.18	0.89	0.60	0.02

The result of the correlation shows the statistical significance is indicated by the $R^2 = 0.89$ and this represents a good correlation between the variables (Fig. 6; Table 10).

5. Conclusions

This paper systematically provides the flow of STI indirect test method specified in BS EN 60268-16 and introduces in detail the calculation formula involved in the indirect method, with reference to Schroeder's Frequency analysis and therefore to the limits of validity of the sound equations of classical theory, associated with the simulation of the room.

The study highlighted that the one of the major problems when developing this type of prediction is represented by the error generated by a low signal-to-noise ratio. Therefore, the choice of the speech spectrum, as well as the residual noise setting, represents an important choice in order for overestimation errors of the STI not to be incurred.

Although the standard is clear in recommending standard spectra, a possible solution could be to simulate the environment impulse response using a commercial room acoustic software and enter, in the input phase, an environmental noise that could be representative of the acoustic scene of the room.

Nomenclature

Symbols

STI	Speech transmission index
IS	Intelligibility score
MTF	Modulation transfer function
SPL	Sound pressure level
STI_m	Speech transmission index (measured)
STI_p	Speech transmission index (predicted)

References

Bradley, J. S., R. Reich, and S. G. Norcross. 1999. "On the combined effects of signal-to-noise ratio and room acoustics on speech intelligibility." *The Journal of the Acoustical Society of America* 106: 1820.

BSI. 2020. BS EN 60268–16:2020. Sound system equipment - Objective rating of speech intelligibility by speech transmission index.

Choi, Y.-J. 2020. "The intelligibility of speech in university classrooms during lectures." *Applied Acoustics* 162: 107211. doi: https://doi.org/10.1016/j.apacoust.2020.107211

Goldsworthy, R. L., and J. E. Greenberg. 2004. "Analysis of speech-based speech transmission index methods with implications for nonlinear operations." *The Journal of the Acoustical Society of America* 116: 3679.

Hongshan, L., H. Ma, J. Kang, C. Wanga. 2020. "The speech intelligibility and applicability of the speech transmission index in large spaces." *Applied Acoustics* 167: 107400. doi: https://doi.org/10.1016/j.apacoust.2020.107400

Houtgast, T., and H. J. M. Steeneken. 1973. "The Modula-tion Transfer Function in Room Acoustics as a Predictor of Speech Intelligibility." *Acta Acustica* united with *Acustica*: 66-73.

Peters, R. 2020. Uncertainty in Acoustics. Boca Raton: CRC Press.

Pickett, J. M. 2005. "Effects of Vocal Force on the Intelligibility of Speech Sounds." *The Journal of the Acoustical Society of America* 28(902): 1956.

Sala, E., and V. Viljanen. 1995. "Improvement of acoustic conditions for speech communication in classrooms." *Applied Acoustic* 45: 81-91. doi: https://doi.org/10.1016/0003-682X(94)00035-T

Schwerin, B., and K. Paliwal. 2014. "An improved speech transmission index for intelligibility prediction." *Speech Communication* 65: 9-19. doi: https://doi.org/10.1016/j.specom.2014.05.003

Steeneken, H., and T. Houtgast. 1980. "A review of the MTF concept in room acoustics and its use for estimating speech intelligibility in auditoria." *The Journal of the Acoustical Society of America* 318-326.

UNI. 2004. EN ISO 9921:2004. Assessments of speech communication.

UNI. 2006. EN ISO 12354-6:2006. Building Acoustics - Estimation of acoustic performance of buildings from the performance of elements - Part 6: Sound absorption in enclosed spaces.

UNI. 2020. UNI 11532-2:2020. Internal acoustical characteristics of confined spaces - Design methods and evaluation techniques - Part 2: Educational sector.

Yang, D., and C. M. Mak. 2018. "An investigation of speech intelligibility for second language students in classrooms." *Applied Acoustic* 134: 54-149. doi: https://doi.org/10.1016/j.apacoust.2018.01.003

Yang, W. Y., and J. S. Bradley. 2009. "Effects of room acous-tics on the intelligibility of speech in class-rooms for young children." *The Journal of the Acoustical Society of America* 125: 922-933.

Zannin, P. H. T., D. Petri, and Z. Zwirtes. 2009. "Evaluation of the acoustic performance of classrooms in public schools." *Applied Acoustics* 70: 626-635. doi: https://doi.org/10.1016/j.apacoust.2008.06.007

Hybrid Heat Pump Systems: Is Predictive Control Worth Using?

Patricia Ercoli – Università Politecnica delle Marche, Italy – p.ercoli@pm.univpm.it
Alice Mugnini – Università Politecnica delle Marche, Italy – a.mugnini@univpm.it
Fabio Polonara – Università Politecnica delle Marche, Italy – f.polonara@univpm.it
Alessia Arteconi – Università Politecnica delle Marche, Italy; & KU Leuven, Belgium – a.arteconi@univpm.it

Abstract

One of the possible solutions for renovating building heating systems is the use of hybrid systems, which consists of coupling heat pumps with traditional natural gas boilers. Hybrid Heat Pump systems are typically controlled to run the heat pump when the outside temperature is not too low, maintaining acceptable costs and good energy efficiency levels. However, when buildings also have a certain level of thermal inertia, proper management of the hybrid system can allow some flexibility. Especially in presence of non-programmable renewable sources, the control strategy can play an important role to maximize self-consumption.

The aim of this work is to assess the role of the control strategy in achieving this objective in relation to the cost reduction potential for energy bills. In particular, we investigate how much it is worth using an advanced control technique (e.g., a Model Predictive Control) compared to a Ruled Based Control to regulate the hybrid heating system of a residential building. The paper analyses a case study in which a building, equipped with Hybrid Heat Pump system assisted by photovoltaic panels serving a radiant floor, is controlled both through a Model Predictive and a designed Ruled Based Control. The objective of the controls is to minimize the energy bill for heating. The results are intended to assess whether the added complexity of the best performing model predictive control is justified by the magnitude of the performance increase that is obtained.

1. Introduction

In recent years, Heat Pumps (HPs) have seen an increase in their use in residential buildings. According to the International Energy Agency (IEA, 2021), as of 2015, there has been an upward trend in HP sales within the European market, with an average annual growth rate of 12 %.

In the context of energy transition, HPs can offer a good solution for reducing energy consumption, as they give the possibility of using renewable energy sources such as aerothermal, geothermal and hydrothermal (Madonna et al., 2013), in addition to producing thermal energy through electricity (coming from the grid or produced on site).

The capability to correlate the thermal demand to electricity consumption is one of the most interesting aspects of HPs for unlocking the energy flexibility in buildings: the different levels of thermal inertia, which are already contained in buildings (thermal mass of the envelope or thermal storage devices), can be exploited to provide flexibility to the electricity grid.

One of the most frequently adopted solutions for exploiting the advantages of HPs, while maintaining acceptable costs and good levels of energy efficiency, are hybrid systems. In a Hybrid Heat Pump (HHP) system, the heat demand of the building is met by a HP coupled with a traditional boiler (EHI, 2020). This system is particularly useful in the presence of air-source HPs, since their performance depends heavily on the external climatic conditions. Although most HPs are installed in new constructions (IEA, 2021), hybrid systems present a good solution for home renovations (Dongellini et al., 2021). Indeed, in Italy, where the building stock is rather dated, the market of HHPs is one of the largest in the European Union, with about 7000 units sold in 2018 (EHI, 2020).

As for HP systems, a fundamental role is played by the control technique adopted also in HHP systems. To activate energy flexibility and optimize the ma-

nagement of sources, Model Predictive Controls (MPCs) are widespread. MPCs refer to an optimization problem to select the optimal set of control actions to minimize a given objective function at each time step.

There are many works available in the literature on the evaluation of the effectiveness of a MPC compared to a simpler Rule Based Control (RBC) for HPs. Fischer et al. (Fischer et al., 2017) have compared five different control methods, aimed at considering cases where the cost of electricity is constant, variable or cost-free in order to exploit self-consumption in a multi-family house equipped with an air-source HP supported by Photovoltaic (PV) panels and coupled to storage for domestic hot water. According to the authors, MPCs are more efficient than RBCs, with cost reductions of 6–16 % and 2–4 %, respectively. Zanetti et al. (2020) modeled an HHP, consisting of an air-to-water unit and a gas-fire boiler, assisted by PV panels and coupled to a water tank, serving a school supplied with floor heating. Comparing an RBC with an optimal control, from a thermal comfort point of view, the two controls provide similar results; regarding energy costs, the optimal control performs better as it allows savings of up to 20 % with an increase in self-consumption from 67 % (RBC) to almost 100 %. Ahmad et al. (Ahmad et al., 2013) have modeled a small house with an integrated HP via solar collector through a water tank for heating and hot water production. When compared to a simple RBC, the MPC was able to deliver savings of up to 9 %. From the comparison, the better performance of an optimized control is evident; however, as mentioned in (Fischer et al., 2017), its computational modeling and control fitting effort should be considered.

In this respect, this paper wants to analyze whether such advanced control techniques are worth using to control the heating system of a residential building according to a certain objective. In this regard, the paper proposes an analysis, in a simulation environment, of a case study in which a typical residential building subject to renovation, equipped with a HHP system assisted by PV panels and supplying a radiant floor, is controlled both through an MPC and a properly designed RBC. The main objective of the controls is to minimize the costs in the electricity bill for heating.

2. Methodology

In order to assess the need for predictive control in an HHP system, the use of MPC and RBCs are compared in a residential building. In both cases, the controls aim to select the technology to be used (i.e., boiler or HP) to achieve economic savings, maximize the self-consumption of renewable sources and maintain thermal comfort. The comparison between MPC and RBC is carried out in a simulation environment. TRNSYS (TRNSYS 17, 2014) is selected to model the energy dynamics of the building. RBC is also modeled in TRNSYS, while MATLAB (MATLAB, 2014) is used for the MPC. The performance of RBC and MPC are evaluated by comparing the cost for satisfying the thermal demand of the building, the ability to maintain thermal comfort and the degree of exploitation of electricity produced by a PV plant installed on site. More details regarding the formulation of MPC and RBC are reported in the following subsections: subsection 2.1 describes the RBC, while in subsection 2.2 the formulation of MPC is explained.

2.1 Rule Based Control

RBC control is based on the determination of the external temperature (cut-off temperature) above which it is convenient to use the HP instead of the boiler. The cut-off temperature ($T_{cut\text{-}off}$) is determined through a comparison of the cost required to produce 1 kWh_{th}. For the HP, the cost is obtained considering the price of electricity withdrawal from the grid (c_E). To obtain the electrical energy absorbed by the HP, it was necessary to model the dependence of the COP on the temperatures of the air sources and the capacity ratio (CR). The model is based on the indications contained in EN 14825:2018 (CEN, 2018), starting from the performance map provided by the manufacturers. Since TRNSYS does not currently have a Type that allows modeling of a variable capacity HP, a new Type was developed by the authors, called Type 2701 (Ercoli et al., 2022). For the boiler, the cost of satisfying the heat demand is calculated by

multiplying the price of Natural Gas (c_{NG}) by its volume used. The latter is obtained by dividing the heat by the efficiency of the boiler (η_{BO}) and by the Higher Heating Value, HHV (condensing gas-fired boiler). Since also the availability of electricity from renewable sources is considered, two types of RBC were formulated: (i) base RBC (bRBC) and (ii) advanced RBC (aRBC). The bRBC is the simplest control where the switch between boiler and HP is determined only by $T_{cut\text{-}off}$. In addition, in the bRBC there is a thermostat that maintains the indoor air temperature (T_{air}) within a comfort range (2021 °C). On the other hand, the aRBC is set to force the HP to turn on regardless of $T_{cut\text{-}off}$ when a certain threshold of availability of PV is exceeded. It has been assumed as the minimum electrical power required for the minimum modulation of the HP (minimum CR of 0.3). To take advantage of the storage capacity of the heating system, the aRBC can exploit a wider comfort range (20 - 22 °C). However, in the absence of sufficient availability from PV, the HP and the boiler alternate their operation according to the set $T_{cut\text{-}off}$ and the thermostat is maintained within the 20 – 21 °C range.

2.2 Model Predictive Control

An MPC based on the system model was developed as an advanced control technique. The MPC can be divided into two parts: (i) the model of the system to be controlled and (ii) the optimizer. The system model (i) is responsible for forecasting the building's thermal demand. A lumped-parameter model based on the thermal-electricity analogy is used. Fig. 1 shows the structure of the resistances and capacitances (RC) network. It is composed of three thermal nodes. Each of them is represented by a capacitance (C) and a temperature (T). In particular, the thermal nodes represent the mass of the building envelope (C_e, T_e), the internal air (C_{air}, T_{air}) and the floor (C_f, T_f). The three thermal conductances K_{ea}, K_{fa} and K_{fg} model the heat flow between the three nodes, while the conductances K_w and K_{eo} model the heat flow between the external air (outdoor temperature, T_o) and T_{air} and T_e, respectively. The thermal flows entering the model are the solar gains (G_s) and the heating power provided by the heating system (Q_h). Since, as reported in Section 3, the building is equipped with a radiant floor heating system, Q_H is directly applied to the thermal node of the floor (Fig. 1).

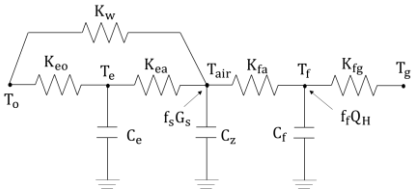

Fig. 1 – Third-order RC network building model

To obtain the numerical values of the parameters (C_e, C_{air}, C_f, K_{ea}, K_{fa}, K_{fg}, K_w, K_{eo}, f_f and f_s), the model was trained starting from the data obtained from the building simulation in TRNSYS (Root Mean Square Error of 0.16 °C in the training period involving the whole month of January).

With this structure, the model can be represented with a discrete state space formulation (Eq. 1 and 2):

$$\mathbf{X}(k+\Delta k) = \mathbf{A}\cdot\mathbf{X}(k)+\mathbf{B}\cdot\mathbf{U}(k) \quad (1)$$

$$\mathbf{Y}(k+\Delta k) = \mathbf{C}\cdot\mathbf{X}(k)+\mathbf{D}\cdot\mathbf{U}(k) \quad (2)$$

with the vector $X = [T_{air}\ T_e\ T_f]^T$, which represents the state of the system at each timestep k (Δk is the time interval between two timesteps), $\mathbf{U} = [T_o\ Q_H\ G_s]^T$ the input vector and Y the vector contains the output (T_{air}). **A**, **B**, **C** and **D** are time-invariant real matrices depending on the parameters of the system.

The model, therefore, can simulate the thermal dynamics of the building. At this point, the optimizer (ii) must select the best control actions of the HHP system to maintain the T_{air} within an accepted comfort range. As in the case of aRBC (subsection 2.1), also in this case a greater tolerance is granted to the thermostat (20 - 22 °C) to increase the exploitation of the thermal inertia of the building.

The control actions to be set are the control signals for the HP and the boiler (1/0 control signals: $ctrl_{HP}$ and $ctrl_{BO}$). The objective of the optimization is to minimize the energy bill over a forecast period (FP). To do this, a Linear Programming optimization problem was formulated (Eq. 3, 4, 5, 6 and 7).

$$minimize \sum_{k}^{FP} \left(\frac{Q_{HP}(k)}{COP(k)} \cdot c_E(k) + \frac{Q_{BO}(k)}{\eta_{BO} \cdot HHV} \cdot c_{NG} \right) \quad (3)$$

$$subject$$

$$\forall k = 1, \dots, FP\ T_{min} \le T_{air}(k) \le T_{max} \quad (4)$$

$$\forall k = 1, \dots, FP\ 0 \le Q_{HP}(k) \le Q_{maxHP}(k) \quad (5)$$

$$\forall k = 1, \dots, FP0 \leq Q_{BO}(k) \leq Q_{maxBP} \quad (6)$$

$$\forall k = 1, \dots, FPQ_{BO}(k) + Q_{HP}(k) = Q_H(k) \quad (7)$$

Referring to Eq. 3, Q_{HP} and Q_{BO} are the thermal powers supplied by the HP and the boiler, respectively. These are the decision variables of the optimization problem. They can assume values between 0 and the maximum capacity of the HP (Q_{maxHP}) and the boiler (Q_{maxBO}), respectively. Eq. 4 contains the predictive model of the building. Eq. 5 and 6 set the boundary conditions for Q_{HP} and Q_{BO}. Finally, the constraint expressed by Eq. 7 is also inserted in order not to operate the HP and the boiler simultaneously (Q_H expresses the building load curve, Section 3). To incentivize the consumption of electricity produced by PV, a cost equal to 0 Eur kWh_e^{-1} is assigned to the electricity produced by PV. In general, Fig. 2 describes the dynamic behavior of the MPC. The MPC solves the optimization problem at each timestep k.

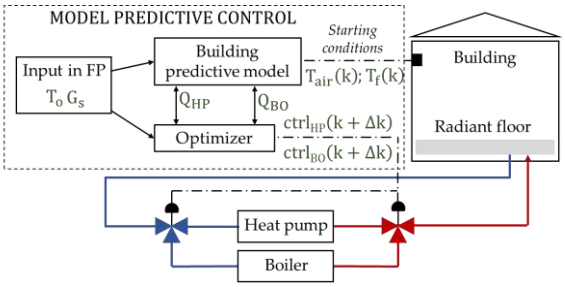

Fig. 2 – Schematic of the MPC

The actual temperatures (T_{air} and T_f) are passed as starting conditions to the MPC. Based on the receding horizon principle (Rawlings & Mayne, 2012), the MPC establishes the values of the control actions $ctrl_{HP}(k+\Delta k)$ and $ctrl_{BO}(k+\Delta k)$. These are derived from decision variables. Especially if $Q_{HP}(k+\Delta k)$ is greater than 0, $ctrl_{HP}(k+\Delta k)$ is 1, otherwise it is 0 (the same for $ctrl_{BO}$).

3. Case Study

A refurbishment for a residential building was considered as a case study. A single-family house whose construction characteristics refer to a period between 1991 and 2005 (Tabula Project (Corrado et al., 2014)) was chosen as an original building. The building has a heated surface of 96 m^2 with a net heated volume of 299 m^3. Table 1 contains the comparison between the thermal transmittances (U-values) of the original and the renovated building. Only the structures of the external walls and the windows were modified in the refurbishment (Table 1). In particular, the updated values were extrapolated from the most recent Italian regulation (DM, 2020).

Table 1 – U-values for renovated and original building

Building Status	Walls ($Wm^{-2}K^{-1}$)	Roof ($Wm^{-2}K^{-1}$)	Floor ($Wm^{-2}K^{-1}$)	Windows ($Wm^{-2}K^{-1}$)
Renovated	0.25	0.69	0.77	1.40
Original	0.59	0.69	0.77	1.70

For the simulations in TRNSYS, the climate file for a typical year of Ancona (43°37'N-13°31'E, Italy) was considered. Given an outdoor design temperature of -2 °C (UNI, 1976) and a T_{air} of 20 °C, the renovated building has a design peak load of 4.25 kW_{th}.

As mentioned, the heating system adopted in the renovated building is an HHP. It is composed of a modulating Air to Water Heat Pump (AWHP) and a condensing gas-fired boiler. To perform the study, commercial sizes of AWHP and boiler were taken as a baseline. For the HP, the operating characteristics were extrapolated from the data provided by a manufacturer. It presents a commercial size with 4.50 kW_{th} and 4.64 as COP, referred to an ambient temperature of 7 °C and a supply temperature of 35 °C. The boiler, on the other hand, has a capacity of 19 kW_{th} and an efficiency of 98 %, referred to the HHV (10.70 kWh Sm^{-3}).

As emission system, radiant floor heating was considered. The regulation of the heating system takes place with a compensation curve for the supply temperature (Fig. 3). The latter was calculated from the building load curve (Q_H) according to the T_o variation (Fig. 3).

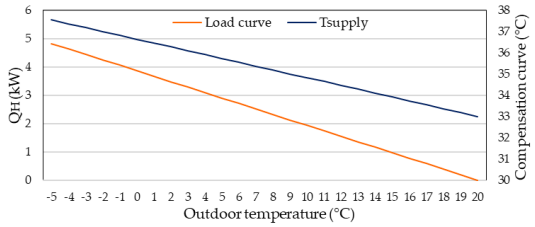

Fig. 3 – Building load curve (Q_H) and compensation curve

By applying the methodology described in Section 2.1 to the case study, the $T_{cut\text{-}off}$ obtained is 4 ° C. This was achieved by considering a natural gas cost of 1.225 Eur Sm^{-3} and an electricity cost of 0.388 Eur kWh_e^{-1} (ENEL, 2022). The renovated building was also equipped with a PV system installed on site. The PV plant consists of 12 monocrystalline silicon panels for a nominal peak power of 3.80 kW_e.

4. Results

A reference period was selected to compare the performance of MPC and RBC, i.e., the first two weeks of January. The analysis of the results will first be presented for the two RBC controls (4.1), to then be extended to the case of MPC (4.2). Finally, in section 4.3, we will try to answer the original question: "Is it worth using predictive control?".

4.1 Results for RBCs

The comparison between the internal air temperature trend in the case of bRBC and aRBC is shown in Figs. 4 and 5. In both bRBC and aRBC, there is a certain period in which the air temperature does not respect the thresholds set on the thermostat (Section 2.1). In the case of bRBC (Fig. 4), the air temperature drops below the minimum threshold (i.e., 20 °C) for the 2 % of the time (7 hours), reaching a minimum of 19.43 °C. From this point of view, better behavior is obtained with the aRBC. In fact, looking at Fig. 5, the air temperature assumes values lower than 20 °C for 1 hr and 30 mins (0.45 % of the time), reaching a minimum of 19.93 °C.

As for the upper temperature threshold, this is different between the two controls when PV is available. In fact, the aRBC can exploit the flexibility of the thermostat to increase PV self-consumption and reach 22 °C. Comparing Fig. 4 and 5, it can be noted that there is a greater exploitation of the upper band granted to the thermostat in case of aRBC. Indeed, the average air temperature in case of bRBC is 20.47 °C, while it becomes 20.62 °C with the aRBC. Furthermore, with the aRBC, the air temperature exceeded the upper limit of 22 °C for a time of 2 hrs and 45 mins (about 0.82 % of the time) with a peak of 22.48 °C.

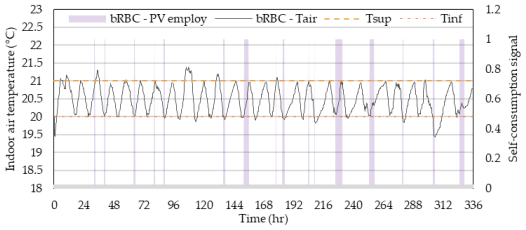

Fig. 4 – Internal air temperature (T_{air}) and self-consumption signals during basic RBC (bRBC) use

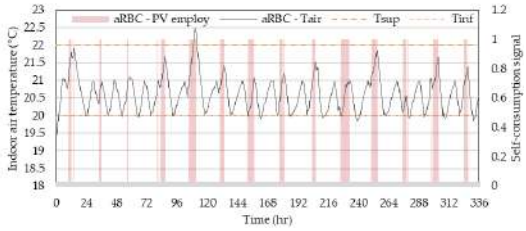

Fig. 5 – Internal air temperature (T_{air}) and self-consumption signals during advanced RBC (aRBC) use

Figs. 6 and 7 show the involvement of the single technologies (AWHP and boiler) in the case of the RBCs. From the comparison of Figs. 6 and 7, with bRBC, there is a higher utilization of the boiler and higher thermal demand peaks than in the case where the aRBC is used. In addition, from Fig. 7, there is an increase in AWHP utilization through use of the aRBC, since, as described in Section 2.1, the control is set to force the AWHP to turn on regardless of $T_{cut\text{-}off}$. In particular, the AWHP is found to be operating for 141 hrs and 45 mins through aRBC, 6.98 % more than bRBC. The boiler, on the other hand, works 7.17 % less during use of the aRBC than the basic one, for a total time of 61 hrs and 30 mins. Also, comparing Figs. 6 and 7, in addition to an increase of AWHP application, it is also possible to see a slight increase in the PV self-consumption by aRBC.

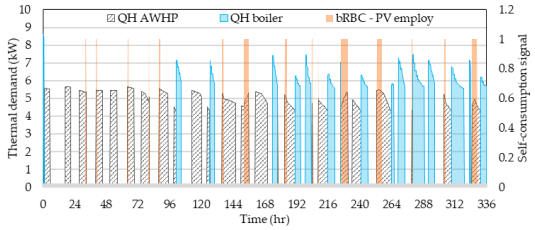

Fig. 6 – Thermal demand (Q_H) trends and self-consumption signals during bRBC use

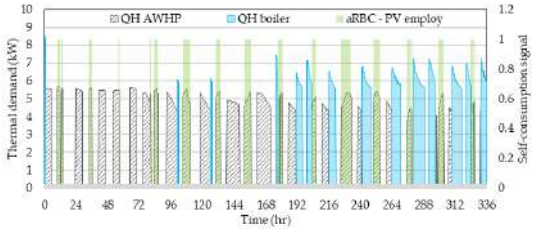

Fig. 7 – Thermal demand (Q_H) trends and self-consumption signals during aRBC use

The difference in utilization between the two RBCs can also be seen through the thermal demand via Fig. 8; from the comparison with the bRBC, the use of the aRBC involves an increase of the thermal demand of 6.46 % covered by the AWHP and a decrease of 7.18 % for the contribution of the boiler.

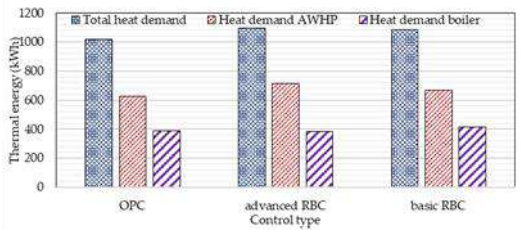

Fig. 8 – Thermal demand of the hybrid system, AWHP and boiler during the application of the three controls

The differences in terms of PV exploitation are also highlighted in Fig. 9, where the self-consumption of electric energy during advanced control is 6.43% higher than that through bRBC.

In terms of performance, the use of aRBC results in a slight reduction of 0.26 % in average COP, with a value of 4.21 compared with that of the bRBC of 4.22. Despite the slight decrease in average COP, the lower boiler utilization by the aRBC resulted in lower energy bill costs. From Fig. 10, a net saving is achieved through aRBC. In particular, the costs due to the boiler, which, compared with the case of the bRBC, decreased by 76.8 %.

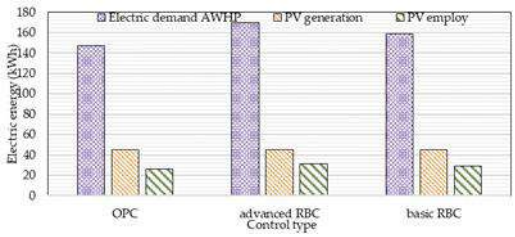

Fig. 9 – Electric consumption required by the AWHP, generated by the PV panels and self-consumed during the application of the three controls

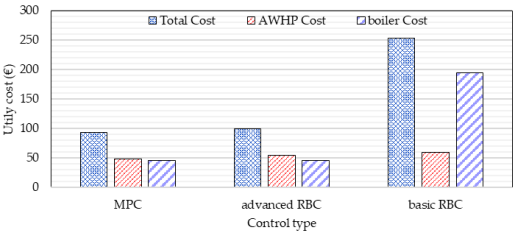

Fig. 10 – Cost due to use of hybrid system, AWHP and boiler during the application of the three types of control

4.2 Results for MPC

As with the two RBCs, Fig.11 shows the trend of the internal air temperature in the reference period for the MPC. It can be noted that the temperature fluctuates frequently around 20 °C with an average value of 20.11 °C. The MPC is able to maintain the air temperature within a narrower range of variation. Both violations towards the lower limit of the thermostat and towards the upper one are reduced in comparison with the RBCs. In fact, as can be seen in Fig. 11, the upper limit of 22 °C is not exceeded, and the air temperature reaches a peak of 21.4 °C.

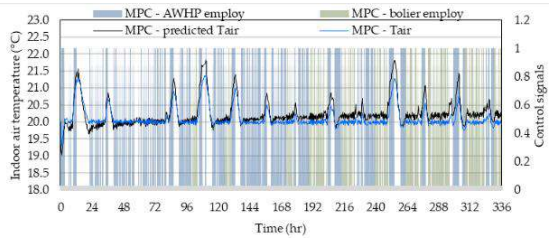

Fig. 11 – Calculated and predicted indoor temperature trends and AWHP and boiler usage signals during MPC application

In terms of running time, the use of the MPC leads to an overall reduction; both the AWHP and the boiler are used for less time, meaning 123 hr and 45 min and 58 hrs and 15 mins, respectively. Overall, there is a reduction in system utilization of less than 10.46 % compared with the aRBC and less than 8.43 % compared with the bRBC. Through Fig. 8, it

can be seen that the use of the MPC also leads to 7.19 % in thermal demand reduction due to the entire hybrid system compared with the aRBC. Even the AWHP provides a lower thermal demand of 11.82 %, probably due to its decreased use. In addition, this could lead to a reduction of the self-consumption, as shown in Fig. 10; in fact, compared with the aRBC there is a reduction of 17.33 % in self-consumption. Moreover, the AWHP, through the MPC, is able to provide better performance, with 4.26 as average COP, 0.94 % higher than the bRBC.
Considering the energy costs, the MPC performs better than the RBCs, given the bill savings objective (Fig. 11). In fact, within a two-week reference period, the use of MPC, in the case study considered, resulted in savings of 63.27 % compared with bRBC and 5.93 % compared with aRBC.

4.3 Is It Worth Using Predictive Control?

The results shown in the previous sections showed that MPC achieved better performance in terms of cost savings and concerning the thermostat. On the other hand, the best performance regarding self-consumption of PV was obtained from the advanced RBC.
What is important to note is that, although the MPC is better at achieving the objective (e.g., cost reduction), modeling difficulties not present in RBC cases should be taken into account. In fact, the MPC being a model-based control, in the case of incorrect or missing data, there could be a wrong estimation of the thermal demand of the building and, consequently, incorrect decision making. Furthermore, the modeling and implementation difficulty that MPC requires compared with RBCs cannot be overlooked.
In the case studied, the advanced RBC turned out to be a good compromise; in fact, it was possible to achieve good savings over the basic RBC with less effort than the MPC. In particular, this was possible through: (i) a good estimation of the $T_{cut\text{-}off}$ (e.g. using the method described in section 2.1), (ii) forcing the AWHP to turn on during PV generation and (iii) the activation of the flexibility of thermostat. Indeed, it is possible to see in Fig. 12 how the $T_{cut\text{-}off}$ varies while using the MPC in comparison with the fixed 4 °C of RBCs. From the comparison, it can be seen that this transition temperature between the two generators was properly estimated through a comparison of the cost required to produce 1 kWh_{th} (section 2.1).

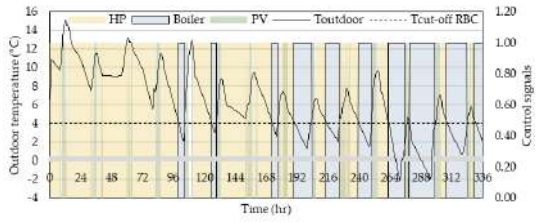

Fig. 12 – Variation of the outdoor temperature and AWHP and boiler use convenience signals based on cost

5. Conclusion

In this paper, we asked whether it is worth using a MPC to control a residential hybrid heating system with PV panels. To do this, a MPC was compared with two RBCs, one basic and one advanced.
From the results, the main conclusions can be summarized in the following points:

- The MPC is more effective in reducing the energy cost: a saving of 63.27 % was estimated in relation to the basic RBC and 5.93 % compared to advanced RBC.
- The advanced RBC allows a higher self-consumption of PV compared with MPC to be obtained (with the MPC a reduction in self-consumption of 17.33 % was achieved in comparison with advanced RBC).
- With the MPC there is no violation of the upper band of the thermostat – a phenomenon that occurs with the advanced RBC (0.82 % of the time, 2 hrs and 45 mins).

Although MPC has shown better performance than RBCs in terms of comfort and savings, its application for a system such as the one analysed should also consider the level of difficulty that its implementation requires. Through advanced RBC, it was possible to achieve good savings over the basic RBC but with less effort than the MPC, thus offering a good compromise between the two controls.
Despite good results from both MPC and advanced RBC, there were still unused amounts of self-

generated electrical power. One way to mitigate wasted electrical power could be to introduce additional integration devices to increase system flexibility and further exploit the building's storage capabilities. In this context, it might be interesting to further explore the comparison between different types of control.

References

Ahmad, M. W., M. Eftekhari, T. Steffen and A.M. Danjuma. 2013. "Investigating the performance of a combined solar system with heat pump for houses" *Energy and Buildings* 63: 138-146. doi: https://doi.org/10.1016/j.enbuild.2013.03.055

CEN (European Committee for Standardization). 2018. *EN 14825:2018. Air Conditioners, Liquid Chilling Packages and Heat Pumps, with Electrically Driven Compressors, for Space Heating and Cooling – Testing and Rating at Part Load Conditions and Calculation of Seasonal Performance*

Corrado, V., I. Ballarini, and S. P. Corgnati. 2014. "Building Typology Brochure – Italy" EPISCOPE. Accessed January 10. https://episcope.eu/communication/download/

Dongellini, M., C. Naldi, and G. L. Morini. 2021. "Influence of sizing strategy and control rules on the energy saving potential of heat pump hybrid systems in a residential building" *Energy Conversion and Management* 235. doi: https://doi.org/10.1016/j.enconman.2021.114022.

EHI (European Heating Industry). 2020. "Heating Market Report 2020" EHI. Accessed March 30. https://ehi.eu/heating-market-report/heating-market-report-2020/

ENEL, 2022. www.enel.it/?ecid=paidsearch-google-alwayson_top_keyword-brand-enel_exact&gclid=EAIaIQobChMI5sa8hvaf9wIVBLLVCh0o4wDQEAAYASAAEgJAH_D_BwE&gclsrc=aw.ds

Ercoli, P., A. Mugnini and A. Arteconi. 2022. github.com/diismunivpm/Type2701-for-TRNSYS.git

Fischer, D., J. Bernhardt, H. Madani, and C. Wittwer. 2017. "Comparison of control approaches for variable speed air source heat pumps considering time variable electricity prices and PV." *Applied Energy* 204: 93-105. doi: https://doi.org/10.1016/j.apenergy.2017.06.110

IEA - International Energy Agency. 2021. "Heat Pumps" IEA. Accessed March 21. https://www.iea.org/reports/heat-pumps

Madonna, F., and F. Bazzocchi. 2013. "Annual performances of reversible air-to-water heat pumps in small residential buildings" *Energy and Buildings* 65: 299-309. doi: https://doi.org/10.1016/j.enbuild.2013.06.016.

MATLAB - Matrix Laboratory. 2014. Version R2014a, MathWorks, Natick, Massachusetts, USA.

Ministero dello sviluppo economico. 2020. "DECRETO 6 agosto 2020 - cd ECOBONUS (In Italian)" Ministero dello sviluppo economico. Accessed January 10. https://www.gazzettaufficiale.it/eli/id/2020/10/05/20A05394/sg

Rawlings, J. B., and D. Q. Mayne. 2012. *Model Predictive Control: Theory and Design*. ISBN 9780975937709.

TRNSYS 17 - Transient System Simulation Tool. 2014. Version 17.2, Solar Energy Laboratory, University of Wisconsin, Madison, USA.

UNI (Italian National Agency for Unification). 1976. *UNI 5364:1976. Hot water heating systems. Rules for presentation of offer and for testing.*

Zanetti, E., M. Aprile, D. Kum, R. Scoccia, and M. Motta. 2020. "Energy saving potentials of a photovoltaic assisted heat pump for hybrid building heating system via optimal control." *Journal of Building Engineering* 27. doi: https://doi.org/10.1016/j.jobe.2019.100854

The Acoustic Adaptation of the Aula Magna at the University of Bologna: Auditorium and Conference Hall Scenarios Simulated in the Main Nave of Santa Lucia's Church

Antonella Bevilacqua – University of Parma, Italy – antonella.bevilacqua@unipr.it
Ruoran Yan – University of Bologna, Italy – ruoran.yan2@unibo.it
Maria Cristina Tommasino – ENEA, Italy – cristina.tommasino@enea.it

Abstract

The main Auditorium of Bologna was created inside the original monastery built during the 16th century by the Jesuits. In the following century, the building was modified to become a Catholic church by the architect G. Rainaldi. After the French invasion led by Napoleon during the 18th century, the church was adapted to fulfil different uses. Nowadays, the main hall, composed of three naves but having audience seats in the central one only, is used for celebrations and civil events organized by the University of Bologna. Numerical simulations have been undertaken considering two different scenarios: acoustic adaptation to become an auditorium and to become a conference hall. The model representing the existing conditions has been calibrated on the measurements undertaken across the seating areas. The two scenarios simulated have been compared with the existing conditions of the Aula Magna: the outcomes highlight an improvement in speech comprehension across all the seating areas by achieving the optimal range of each acoustic parameter analyzed. A historical background has also been introduced to understand the adaptation of the original construction to the different room functions assigned throughout the centuries.

1. Introduction

Increased demand for the utilization of cultural heritage buildings has caused experts and scholars to study the existing historical patrimony (Vecco, 2010). On this basis, this paper deals with the acoustic simulations of two conditions that the old church of Santa Lucia could have: the adaptation to become an auditorium for classical music and to become a conference hall, both room functions in line with academic activities run at the University (Dordevic, 2016). A digital model was utilised for the simulations after being calibrated with the measured values (Vorländer, 2007). The design project of the acoustic measures was digitally tested with the application of absorbing plaster on walls, installation of acoustic panels and addition of heavy curtains to close the main nave from the laterals. The results highlight a significant improvement in the outranges values related to the main acoustic parameters.

2. Historical Background

The main auditorium of the University of Bologna, the Aula Magna, was located inside Santa Lucia's church, and is now no longer in use. It was built during the 11th century, while the surrounding college buildings were erected in the 17th century.
During the 16th century, the original monastery became property of the Jesuits, and, on this occasion, the building was modified into a Catholic church by the architect G. Rainaldi (Wittkower et al., 1992). When the Jesuit order was suppressed by Pope Clement XIV, the church complex was transferred to the Barnabites at the end of the 16th century, and then turned into a military camp at the end of the 17th century. During the 18th century, under the French invasion led by Napoleon, the church was converted to fulfil different uses.
In the 1960s, the buildings were involved in a serious fire. From the 1970s to the 1980s, the restoration and modernization (Bettarello et al., 2010) project began to adapt the buildings to the needs of the

University of Bologna and finally opened to the public in 1988. At the end of the 20th century, Santa Lucia's church was also transformed into a university facility.

Fig. 1 – Internal view of the Aula Magna of Bologna

Nowadays, the Aula Magna is composed of three naves, having walls and ceilings decorated with transparent and hard plaster. The auditorium, with lightly upholstered seats in the central nave, is surrounded by wooden balconies, in place for the occasion of degree celebrations and civil events, as shown in Fig. 1.

3. Architectural Organization

The Aula Magna at the University of Bologna, whose current form can be traced back to 1843, has a total capacity of about 1000 seats. It consists of the main hallway and two high, wide, and solemn side passageways, with a total area of about 30000 m^3, as shown in Fig. 2 and Fig. 3.

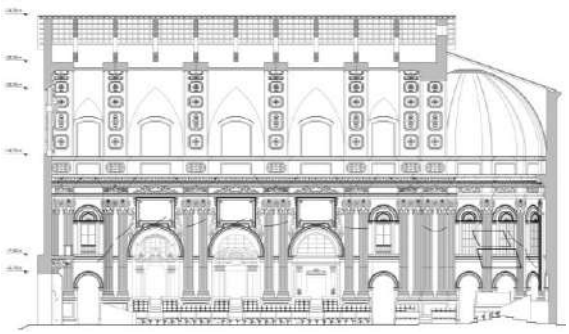

Fig. 2 – Longitudinal section of the Aula Magna of Bologna

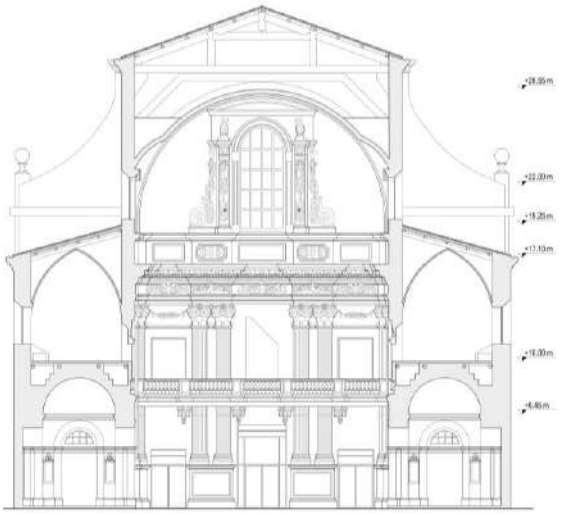

Fig. 3 – Transversal section of the Aula Magna of Bologna

The walls of the main hall are completely plastered, and the central area is decorated with stucco and is 10 to 15 m high. Wooden galleries and low padded seating platforms have been built on the sides of the nave, leaving full view of the auditorium.

3.1 Digital Model

From the architectural drawings, as well as for energy building and musical instruments simulation, (Fabbri et al., 2014; Farina et al., 1998; Manfren et al., 2019, 2021a, 2021b, and 2022; Tronchin, 2005) a digital model was realised to be composed of 3700 surface entities. The vault was realised with polyhedric geometry composed of 16 sides (Antlej, 2022). In a similar way, the apse was modeled by adopting the same methodology, as well as the capitals and the bases of the columns (Bettarello et al., 2021). As such, the model was exported in DXF format (Caniato et al., 2020a and 2020b), ready to be used within Ramsete software.

Attribution of the absorbing and scattering coefficients was carried out based on the acoustic measurements (Caniato et al., 2019), as indicated in Fig. 4.

In particular, the sound source and the receivers were placed in the same positions used during the survey (Caniato et al., 2021).

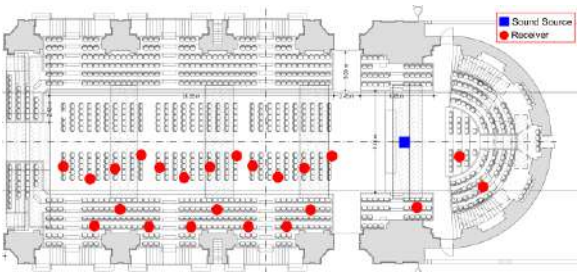

Fig. 4 – Equipment positions during the acoustic survey

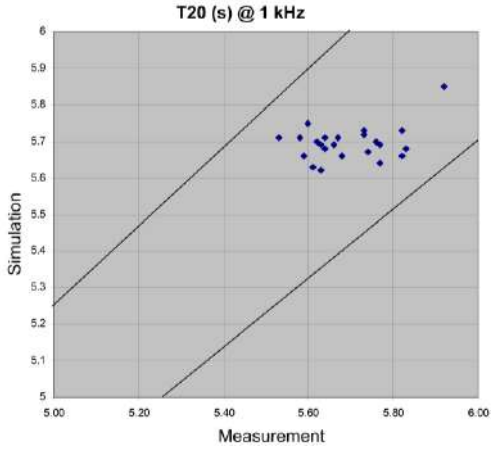

Fig. 5 – Reverberation Time (T_{20}) calibration between simulated and measured results of the existing conditions

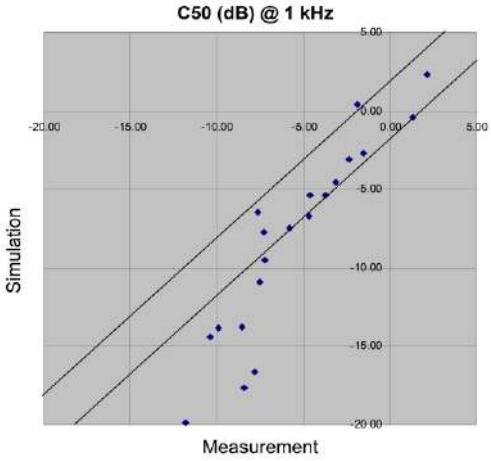

Fig. 6 – Clarity Index (C_{50}) calibration between simulated and measured results of the existing conditions

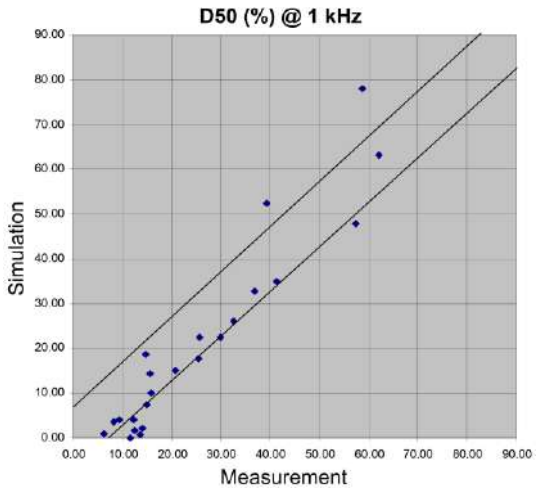

Fig. 7 – Definition (D_{50}) calibration between simulated and measured results of the existing conditions

The tuning process (Tronchin & Knight, 2016; Wang et al., 2004) was carried out upon the reverberation time (T_{20}), clarity index (C_{50}), and definition (D_{50}), as reported in Figs. 5, 6 and 7. The results simulated to be closer to the measured values should stand along the median line between the defined boundaries.

4. Acoustic Simulation

Two sets of simulations were carried out for the Aula Magna of Bologna, based on the functions that were attributed. The first set of simulations adapts the acoustics to auditorium functions, to be used for classical music, while the second set is more centred on speech intelligibility, since the purpose is to adapt the acoustics to suit a conference hall.

During the simulations of the auditorium, an omnidirectional sound source was placed in the location where the orchestra was intended to be located. Based on the room volume of the central nave of Santa Lucia's church being equal to 24000 m^3, the optimal T_{20} value at 500 Hz should be around 2.8 s, as shown in Fig. 8.

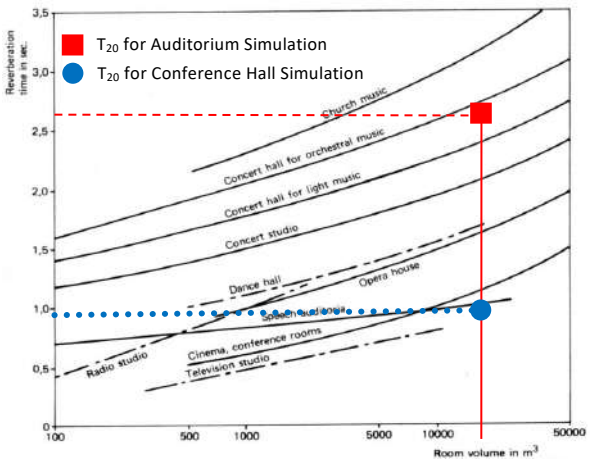

Fig. 8 – Optimal T20 values at 500 Hz, based on room volume

When the simulations have the purpose of adapting the acoustics to suit a conference hall, the sound source was introduced in Ramsete by reproducing the characteristics of the human voice, in terms of spectrum, power, and directivity (Tronchin, 2005). In addition, the existing amplified system was also reproduced with further sound sources having the features of the loudspeakers in place. On this basis, the optimal T_{20} value at 500 Hz for a room of such a volume size used as a conference hall should be around 1.1 s, as indicated in Fig. 8.

In both scenarios, the adopted acoustic measures involve the reduction of reverberation and an improvement in terms of speech intelligibility (Tronchin & Bevilacqua, 2022). Specifically, the measures consist of the following solutions:

- substitution of the standard plaster with an absorbing plaster, to be applied mainly to the surface area of the vault of the central nave;
- introduction of carpet along the corridors serving the seats;
- installation of heavy drapery to close off the lateral naves during conferences.

The application of the absorbing plaster was carried out on a surface area of 853 m², while the introduction of the reflecting panels covers a surface area of 331 m². Table 1 indicates the absorption coefficients of the materials listed above.

Table 1 – Absorption coefficients of the materials used for the project design

Material	Abs. Coeff. α - Octave Bands (Hz)					
	125	250	500	1k	2k	4k
Abs. plaster	0.23	0.30	0.59	0.64	0.67	0.082
Carpet	0.08	0.10	0.20	0.25	0.30	0.35
Drapery	0.08	0.29	0.44	0.50	0.40	0.35

4.1 Auditorium For Classical Music

Based on the acoustic measures being a common factor for the two scenarios, the simulation of the auditorium is focused on the insertion of reflecting panels to be installed above the area of the orchestra and above the stalls. The panels were designed to be in polycarbonate, with a transparency of 90 %, and suspended with steel wires hung to the existing beams. Fig. 9 and 10 show the configuration of the model for an auditorium.

Fig. 9 – Acoustic project design for the adaptation of Santa Lucia's church to an auditorium. Apse side

Fig. 10 – Acoustic project design for the adaptation of Santa Lucia's church to an auditorium. Entrance side

The reflecting panels were installed in such a way as to distribute the sound across the audience uniformly. The results of the conditions simulated for the auditorium scenario are shown in the acoustic maps highlighting the spatial distribution of the main parameters. Fig. 11 shows the $T_{20,}$ while Fig. 12 reflects the results of C_{80}, simulated with and without the audience.

4.2 Conference Hall

The second set of simulations adapts the acoustics of the Aula Magna to a conference hall. The main difference compared with the other configuration consists of the use of heavy curtains and coconut fibres (Fabbri et al., 2021) to be kept closed during conferences to avoid disturbance from people walking in the lateral naves as well as to increase the absorbing surfaces that are useful for lowering the reverberation time (Tronchin et al., 2021a and 2021b). With the acoustic measures, the speech transmission index (STI) values are found to be more than 0.6, falling into a "good" category, as defined by the intelligibility rating according to ISO 9921 (Farina et al., 1998; Tronchin & Bevilacqua, 2021).

5. Results

The results are presented graphically with the plan distribution of the main acoustic parameters, by highlighting the difference between the existing conditions and the simulated environments, as indicated in Figs. 11 to 13. The simulated results shall be considered in unoccupied conditions.

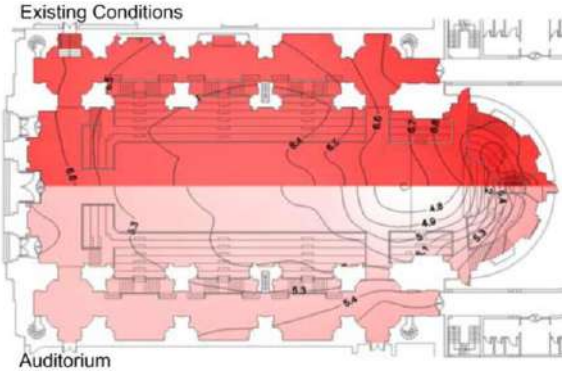

Fig. 11 – Spatial distribution of Reverberation Time (T_{20})

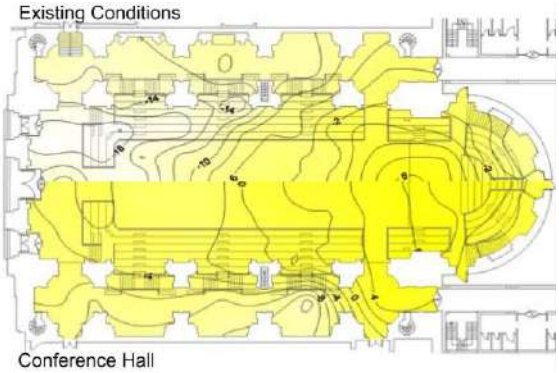

Fig. 12 – Spatial distribution of speech clarity index (C_{50})

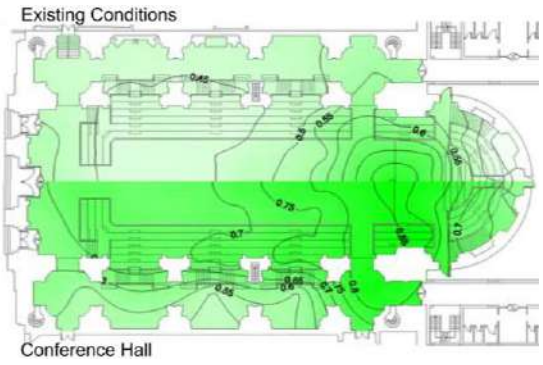

Fig. 13 – Spatial distribution of speech transmission index (STI)

Fig. 11 indicates that the T_{20} values decrease significantly with the introduction of the acoustic measures, passing from 8-9 s to 4.5 s. Such values result in greater uniformity across the plan layout (Mickaitis et al., 2021; Puglisi et al., 2021).

Fig. 12 shows the spatial distribution of the C_{50} values, improved to be within the optimal range as defined by the literature. The C_{50} values equal to -14 dB, especially at the back of the hall, were increased to up to 0 dB in the centre of the hall, and were more uniformly distributed (ISO, 2003; Jeon et al., 2009; Ortega & Rivera, 2012; Steeneken & Houtgast, 1980).

Fig. 13 shows the STI values to be around 0.7, which indicates a good rating. It should be noted that the results with full occupancy of the hall improve the simulated conditions even more, bringing the values closer and within the optimal range limits.

6. Conclusion

The application of the acoustic measures for the Aula Magna at the University of Bologna outlined by the design project has revealed an important benchmark achieved with the accuracy of the digital simulations. The installation of acoustic panels floating at different heights across the plan, along with the absorbing plaster to the vault and the curtains at the openings to the lateral naves, was considered the best option for a cultural heritage site of such historical value. In addition, the criteria of transparency for the suspended panels were assessed to leave the wide view of the indoor space intact as well as to filter the natural lights from the large windows. In summary, the outcomes of the simulated values compared with the existing conditions of the room outline a considerable improvement in speech comprehension, resulting in more appropriate functions assigned to the Aula Magna.

References

Antlej, K. 2022. "Digital Heritage Interpretation of Modernist Modular Architecture: The K67 Kiosk." In: Bartolomei, C., A. Ippolito, S. H. T., Vizioli (eds) *Digital Modernism Heritage Lexicon*. https://doi.org/10.1007/978-3-030-76239-1_23

Bettarello, F., P. Fausti, V. Baccan, and M. Caniato. 2010. "Impact Sound Pressure Level Performances of Basic Beam Floor Structures." *Building Acoustics* 17(3): 305-316. https://doi.org/10.1260/1351-010X.17.4.305

Bettarello, F., M. Caniato, G. Scavuzzo, and A. Gasparella. 2021. "Indoor Acoustic Requirements for Autism-Friendly Spaces." *Applied Science* 11: 3942. https://doi.org/10.3390/app11093942

Caniato, M., F. Bettarello, C. Schmid, P. Fausti. 2019. "The use of numerical models on service equipment noise prediction in heavyweight and lightweight timber buildings." *Building Acoustics* 26(1): 35-55. Doi: https://doi.org/10.1177/1351010X18794523

Caniato, M., C. Schmid, and A. Gasparella. 2020a. "A comprehensive analysis of time influence on floating floors: Effects on acoustic performance and occupants' comfort." *Applied Acoustics* 166: 107339. doi: https://doi.org/10.1016/j.apacoust.2020.107339

Caniato, M., F. Bettarello, P. Bonfiglio, and A. Gasparella. 2020b. "Extensive Investigation of Multiphysics Approaches in Simulation of Complex Periodic Structures." *Applied Acoustics* 166:107356. doi: https://doi.org/10.1016/j.apacoust.2020.107356

Caniato, M., F. Bettarello, and A. Gasparella. 2021. "Indoor and outdoor noise changes due to the COVID-19 lockdown and their effects on individuals' expectations and preferences." *Scientific Reports* 11:16533. https://doi.org/10.1038/s41598-021-96098-w

Dordevic, Z. 2016. "Intangible tangibility: Acoustical heritage in architecture". *Structural Integrity and Life* 16(1): 59–66.

Fabbri, K, L. Tronchin, and V. Tarabusi. 2014. "Energy Retrofit and Economic Evaluation Priorities Applied at an Italian Case Study." *Energy Procedia* 45: 379-384. https://doi.org/10.1016/j.egypro.2014.01.041

Fabbri, K., L. Tronchin, and F. Barbieri. 2021. "Coconut fibre insulators: The hygrothermal behaviour in the case of green roofs." *Construction and Building Materials* 266:1-9. https://doi.org/10.1016/j.conbuildmat.2020.12102

Farina, A., A. Langhoff, and L. Tronchin. 1998. "Acoustic characterisation of "virtual" musical instruments: using MLS technique on ancient violins." *Journal Of New Music Research* 27(4): 359-379. doi: https://doi.org/10.1080/09298219808570753

ISO. 2003. ISO 9921:2003. *Ergonomics - Assessment of speech communication*.

Jeon, J. Y., J. K. Ryu, Y. H. Kim, and S. Sato. 2009. "Influence of absorption properties of materials on the accuracy of simulated acoustical measures in 1:10 scale model test." *Applied Acoustics* 70(4): 615–25. https://doi.org/10.1016/j.apacoust.2008.06.009

Manfren, M., B. Nastasi, E. A. Piana, and L. Tronchin. 2019. "On the link between energy performance of building and thermal comfort: An example." *AIP Conference Proceedings* 2123:1-9. doi: https://doi.org/10.1063/1.5116993

Manfren, M., B. Nastasi, L. Tronchin, D. Groppi, D. A. Garcia. 2021a. "Techno-economic analysis and energy modelling as a key enablers for smart energy services and technologies in buildings." *Renewable and Sustainable Energy Reviews* 150:1-14. https://doi.org/10.1016/j.rser.2021.111490

Manfren, M., M. Sibilla, and L. Tronchin. 2021b. "Energy Modelling and Analytics in the Built Environment—A Review of Their Role for Energy Transitions in the Construction Sector." *Energies* 14:1-29. https://doi.org/10.3390/en14030679

Manfren, M., P. A. B. James, and L. Tronchin. 2022. "Data-driven building energy modelling – An analysis of the potential for generalisation through interpretable machine learning." *Renewable and Sustainable Energy Reviews* 167:1-13. https://doi.org/10.1016/j.rser.2022.112686

Mickaitis, M., A. Jagniatinskis, and B. Fiks. 2021. "Case study of acoustic comfort in conference room". *Proc. 27th International Congress of Sound & Vibration*.

Ortega, G. V., and J. I. S. Rivera. 2012. "Acoustic study of Madrid auditorio nacional de musica: comparison between simulation and measurements." *41st International Congress and Exposition on Noise Control Engineering* (INTER-NOISE 2012).

Puglisi, G. E., A. Warzybok, A. Astolfi, and B. Kollmeier. 2021. "Effect of competitive acoustic environments on speech intelligibility". *Journal of Physics* 2069(1): 175180. https://doi.org/10.1088/1742-6596/2069/1/012162

Steeneken, H. J. M., and T. Houtgast. 1980. "A physical method for measuring speech-transmission quality." *Journal of Acoustic Society of America*, 67(1): 318-326.

Tronchin, L. 2005. "Modal analysis and intensity of acoustic radiation of the kettledrum." *The Journal Of The Acoustical Society Of America* 117(2): 926-933. https://doi.org/10.1121/1.1828552

Tronchin, L, and D. J. Knight. 2016. "Revisiting Historic Buildings through the Senses. Visualising Aural and Obscured Aspects of San Vitale, Ravenna." *International Journal of Historical Archaeology* 20: 127-145. https://doi.org/10.1007/s10761-015-0325-2

Tronchin, L., and A. Bevilacqua. 2021. "Acoustic study of different sceneries at the São Carlos national theatre of Lisbon." *Applied Acoustics* 180:1-11. https://doi.org/10.1016/j.apacoust.2021.108102

Tronchin, L., F. Merli, and M. Manfren. 2021a. "On the acoustics of the Teatro 1763 in Bologna." *Applied Acoustics* 172: 1-9. https://doi.org/10.1016/j.apacoust.2020.107598

Tronchin, L., F. Merli, and M. Dolci. 2021b. "Virtual acoustic reconstruction of the Miners' Theatre in Idrija (Slovenia)." *Applied Acoustics* 172: 1-9. https://doi.org/10.1016/j.apacoust.2020.107595

Tronchin, L., and A. Bevilacqua. 2022. "Historically informed digital reconstruction of the Roman theatre of Verona. Unveiling the acoustics of the original shape." *Applied Acoustics* 185: 1-18. https://doi.org/10.1016/j.apacoust.2021.108409

Vecco, M. 2010. "A definition of Cultural Heritage: From the tangible to the intangible". *Journal of Cultural Heritage* 11: 321–324. https://doi.org/10.1016/j.culher.2010.01.006

Vorländer, M. 2007. "Fundamentals of Acoustics, Modelling, Simulation. Algorithms and Acoustic Virtual Reality".

Wang, L. M., J. Rathsam, and S. R. Ryherd. 2004. "Interactions of model detail level and scattering coefficients in room acoustic computer simulation". *Proceeding International Symposium on Room Acoustics*.

Wittkower, R., I. B. Jaffe, and M. Parizzi. 1992. "Architettura e arte dei Gesuiti". Electa.

Implementation and Calibration of a Model to Treat Naturally Ventilated Complex Fenestration Systems in TRNSYS

Ingrid Demanega – EURAC Research, Italy – ingrid.demanega@eurac.edu
Giovanni Gennaro – EURAC Research, Politecnico di Torino, Italy – giovanni.gennaro@eurac.edu
Giuseppe De Michele – EURAC Research, Italy – giuseppe.demichele@eurac.edu
Francesco Isaia – EURAC Research, Italy – francesco.isaia@eurac.edu
Fabio Favoino – Politecnico di Torino, Italy – fabio.favoino@polito.it
Stefano Avesani – EURAC Research, Italy – stefano.avesani@eurac.edu

Abstract

Adaptive façade systems offer the opportunity to improve building performance and user experience with their ability to adapt the façade configuration to the dynamic variability of the external environment. Nevertheless, the correct deployment of adaptive systems in real buildings is highly dependent on the ability to predict their performance. This is especially relevant in the case of Complex Fenestration Systems (CFS), which are characterized by a complex behavior both from a thermal and daylighting perspective. Often, such CFS are combined with airflow movement when the façade cavity is either mechanically or naturally ventilated, making the performance even more difficult to be characterized. The possibility to use building performance simulation tools to simulate the behavior of these systems integrated in a whole building is central for the proper use and the penetration on the market of these systems.

In this framework, a naturally ventilated window with integrated venetian blinds was modeled in TRNSYS and compared with a FEM-based 2D detailed model, developed in COMSOL Multiphysics. Type56_CFS solves thermal calculation and uses the Bidirectional Scattering Distribution Function for describing optical properties of the façade. This model requires the inlet mass flow rate, which was assessed thanks to an ad-hoc implementation of ISO 15099. The numerical modeling of the coupled heat transfer and fluid flow with COMSOL allowed the TRNSYS model to be calibrated.

The calibration was carried out by increasing the model complexity, focusing on the inlet ventilation flow rate parameter: (a) firstly, it was provided as an input to the Type56_CFS from the FEM-based simulation and then (b) it was calculated by the ISO 15099 internal model and provided to the Type56_CFS. Using this methodology, it was possible to compare the ability of TRNSYS to simulate the thermal behavior of the naturally ventilated cavity against a FEM-based benchmark. Results show a difference of 5 % after the fine tuning of all TRNSYS-related parameters (40 % as un-calibrated starting value).

1. Introduction

Complex Fenestration Systems (CFS) can provide a valuable solution to lower the building energy needs by optimizing solar gains during winter, limiting them during the cooling season and reducing artificial lighting (Huckemann et al., 2010; Pomponi et al., 2016). In order to correctly implement these solutions, it is of crucial importance to predict their thermal and day-light behavior.

To this purpose, two main approaches can be used: on the one hand, FEM methods can be adopted to determine in a detailed way its thermal behavior, since all the system components and the relative thermo-physical properties are taken into account, along with the underlying thermo-physical phenomena (Dama et al., 2017; Li et al., 2017; Wang et al., 2016). As Jankovic and Goia (2021) stated, computational fluid dynamics methods are the most suitable tools for solving problems related to these systems. On the other hand, Building Energy Simulation (BES) tools implement simplified methodologies for taking into account the effect of such complex systems on the building scale and, in the case of open cavity fenestration systems, they are typically designed for modeling mechanically ventilated ones. The unavoidable approximations related

to the impossibility of fully considering the geometries and the detailed physical phenomena, however, strongly limit the modeling possibilities, especially when unconventional complex systems are considered. Catto Lucchino et al. (2021) used different BES tools to predict the behavior of a mechanically ventilated Double Skin Façade, and compared the results with measured data; the conclusions state that these tools can be acceptable for predicting an overall performance over a long period, but for short-term performance assessment the error is too large.

In this study, a CFS characterized by a naturally ventilated cavity with an integrated venetian blind was considered. Through a coupled heat transfer and fluid flow simulation with FEM-based calculation software, it is possible to fully capture the fenestration behavior at system scale, but great limitations are found if its impact on the building scale needs to be assessed. These limitations are particularly related to natural ventilation, which is always harder to predict compared with the mechanical ventilation (Wang et al., 2019). This paper hence aims at identifying the natural ventilation modeling limitations for CFS by comparing two calculation approaches (namely, concentrated-parameters and FEM-based models). To answer this research question, a custom simulation setup was built in TRNSYS 18 with the aim of modeling the naturally ventilated window with integrated venetian blinds and assessing its impact on the building scale. To allow this, a FEM-based 2D detailed model was developed in COMSOL Multiphysics with the purpose of obtaining the necessary data to support and calibrate the implementation of the proposed TRNSYS simulation setup.

2. Methodology

2.1 Case Study

In this study, a CFS consisting of a naturally ventilated window with integrated venetian blinds was studied. Fig. 1 shows how the window cavity is in direct connection with the external environment at the bottom and at the top part. A peculiarity is present in the shape of the external openings, which are not continuous along the fenestration width, but interrupted by solid (closed) parts, as shown in Fig. 1. Additionally, the external openings are covered by a grille characterized by the ratio of blocked area to total area of 1/5. Furthermore, there is a second (internal) vent that is continuous along the fenestration width and characterized by a depth of 5 mm.

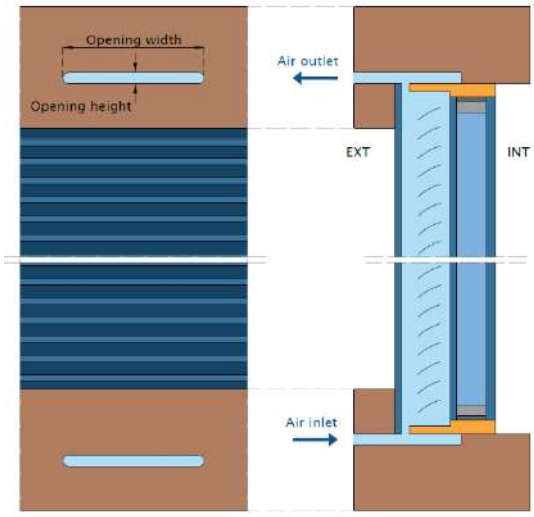

Fig. 1 – Scheme of the considered CFS: front view of a portion of the CFS (left) and vertical cross section (right)

The integrated venetian blind has a direct impact on the airflow and, therefore, on the cavity air temperature in terms of blind type and angles of the slats. In this study, the venetian blind was deployed with slat angles of 0°, 30° and 75° with respect to the horizontal plane. The external cavity (cavity 1) is composed of air, as it is in direct contact with the external environment, while the internal cavity (cavity 2) is filled with a gas mixture of 90 % argon and 10 % air. The external (1) and central (2) glasses are made of single float glass panes of 4mm, while the internal glass (3) is laminated and composed of two float glass panes of 3mm each and one PVB layer. On face 5 (exterior side of the interior glass pane) a low-emissivity coating is placed with an emissivity of 0.013. The geometrical properties of the CFS are listed in Table 1, while the thermal characteristics are reported in Table 2.

Table 1 – *CFS* geometric parameters

Symbol	Parameter	Value
dglass1-2	Glass 1-2 thickness	4 mm
dgap1	Cavity 1 width	30 mm
dgap2	Cavity 2 width	18 mm
dglass3	Glass 3 thickness	6 mm
w	Blind width	16 mm
α	Blind tilt	0°/30°/75°
H	Cavity height	1.33 m
open_w	Opening width	80mm
open_h	Opening height	7mm

Table 2 – *CFS* thermal parameters

Symbol	Unit	Blind	Glass1-2	Glass3	Frame
λ	W/m/K	100	1.0	0.65	0.12
c_p	J/kg/K	900	820	820	2700
ϱ	kg/m³	2700	2500	2500	532
ε_f	-	0.212	0.84	0.013	0.84
ε_b	-	0.489	0.84	0.84	0.84

2.2 Simulation workflow

The workflows adopted in the different modeling and simulation approaches of the CFS (FEM-based at system scale and using TRNSYS at building scale) are described in this chapter. The system scale simulation allowed an assessment of the system's performance in detail and temperature and airflow data to be gathered, later used to support the calibration of the TRNSYS model.

2.2.1 System scale simulation approach

The FEM-based software COMSOL Multiphysics (COMSOL n.d.) was used to compute the coupled heat transfer and fluid flow of the analysed CFS. To simplify the model and reduce computation time, the geometry of the CFS was reduced to a vertical cross section and modeled as a bi-dimensional domain. This assumption was supported by the statement of Pasut and De Carli (2012) describing that the 3D modeling of a fenestration system does not provide a substantial improvement in the results, considering the additional complexity and computation time. The discretization of the domain occurred through the creation of a calculation grid (mesh). This latter was done dividing the geometry into various domains so that, according to the geometric and material characteristics, different types and sizes of the mesh could be adopted. To ensure that the solution is independent from the calculation grid, a mesh refinement study was carried out , and the thermal transmittance was used as control parameter. The final mesh is reported in Fig. 2.

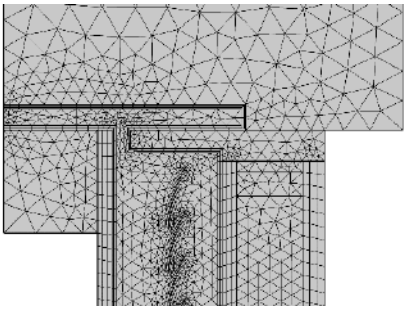

Fig. 2 – Final mesh of the Complex Fenestration System

The modeling of the short-wave radiation exchange due to solar irradiance was done outside the FEM model through a detailed optical calculation using Radiance (Ward, 1994). For each shading configuration, the Bidirectional Scattering Distribution Function (BSDF) was calculated and the solar absorption data for each glass pane and the shading system were derived. The share of incident solar radiation absorbed by each layer of the fenestration system was finally assigned as heat source to single domains within the FEM-based dynamic simulation (Demanega et al., 2020).

To model the natural ventilation through the open window cavity and the top and bottom vents, two additional domains representing the external ambient were added to the model. A relative pressure of 0 Pa was assigned to the top domain's boundaries and of $\frac{1}{2}\rho u^2$ to the bottom ones.

The presence of the grille on the vents was modeled as a pressure drop for a squared mesh described by the equation 1 (COMSOL n.d.), with a solidity σ_s (ratio of blocked area to total area of the screen) equal to 1/5.

$$K = 0.98\ ((1-\sigma_s)^{-2} - 1)^{1.09} \quad (1)$$

To account for the discontinuity of the external vertical opening, which is interrupted by solid (closed) parts along the fenestration width, this non-homogeneity was described analytically in the bi-dimensional FEM model through a localized pressure drop equation of the type Δp = f(u), which was determined by means of a separate FEM CFD 3D model focussed only on the ventilation openings.
The thermal boundary conditions were assigned in terms of convective and radiative heat flux on the internal and external glazing surfaces, while adiabatic conditions were assumed for the top and bottom boundaries. The simulation was run in a stationary regime and considered converged when the relative residuals of the continuity, momentum and energy equations were less than 10e-4.

2.2.2 Building scale simulation approach

TRNSYS 18 was used as building dynamic energy simulation software to assess the impact of the CFS on the building scale. A single thermal zone with one window was modeled using the new version of the multi-zone building model Type 56 CFS. This in-built model enables a detailed CFS thermal simulation according to ISO 15099:2003 and uses the BSDF for describing the façade optical properties in the solar and visual band. This Type has been mainly meant to model mechanically ventilated gaps; indeed, it requires as input the inlet mass flow rate (together with its temperature), which is easily available from fan datasheets; however, in the case of naturally ventilated windows, this data is not known a priori because it is highly dependent on the cavity geometry and boundary conditions. For this reason, a Python-based script was implemented through TRNSYS Type 169, which calculated the inlet mass flow rate according to the ISO 15099. The air moves inside the cavity due to the stack effect, thus the velocity of the air gap depends on the driving pressure difference and the resistance of the openings. The airflow in the cavity is modeled as a pipe flow and the driving force of the flow is set equal to the total pressure loss, which takes into account Bernoulli's pressure loss, steady laminar flow and pressure loss due to the inlet and outlet openings. The resulting model exhibits an inter-dependence between the air gap temperature and velocity and consequently an iterative calculation is performed until the relative convergence limit is less than 1 %.

2.2.3 Model calibration

Given the absence of measured data, the TRNSYS model was calibrated against the FEM one. To support this calibration, parametric simulations were performed with the FEM model considering all combinations of external air temperature ($T_{air,ext}$), internal air temperature ($T_{air,int}$) and solar irradiance (I_{sol}) listed in Table 3.

Table 3 – Boundary conditions for parametric simulations

$T_{air,ext}$ (°C)	0, 5, 10, 15, 25, 30, 35
$T_{air,int}$ (°C)	20, 24, 28
I_{sol} (W/m²)	0, 250, 500, 750, 1000

COMSOL Multiphysics and TRNSYS 18 have two different approaches to simulate the thermal behavior of CFS. Therefore, to minimize these differences and to set the same boundary conditions, the following assumptions were used in the TRNSYS model: a single-zone "shoe-box" model was used as thermal zone, the surface temperatures of the walls were set equal to the indoor temperature and the view factor to the sky of the façade was set to 0.5 (as in the FEM-model).
To achieve steady-state conditions for every combination of the boundary conditions (as listed in Table 3), simulations were run for 100 hours while keeping fixed the values of $T_{air,ext}$, $T_{air,int}$ and I_{sol}. Results correspondent to the last timestep of each simulation were considered as the steady-state ones.
The ad-hoc TRNSYS Type was carried out by increasing the model complexity step by step, focusing on the inlet ventilation flow rate and the total heat flux.
In a first step, the mass flow rate resulting from the thermo-fluid dynamic simulation was provided as input to the TRNSYS type in order to tune the Type 56 CFS parameters and, in a second step, it was calculated by the Python-based Type 169 and provided as input to the TRNSYS building model. Comparing the outcomes of the two models at component level, it was possible to calibrate the natural flow rate Type, particularly focusing on the tuning

of the pressure loss factor along the window cavity, which takes into account the pressure losses caused by the ventilation openings (inlet and outlet), the squared mesh grille and the integrated venetian blinds. The ISO 15099 describes the pressure loss in the inlet and outlet openings through equation 2 and 3, and, in case of zero lateral opening area and equal top and bottom opening area, equation 4.

$$\Delta P_Z = \frac{1}{2}\rho v^2 (Z_{inl} + Z_{out}) \quad (2)$$

$$Z_{inl/out} = \left(\frac{A_s}{0.6 \cdot A_{eq,inl/out}} - 1\right)^2 \quad (3)$$

$$A_{eq,inl/out} = A_{top/bot} + \frac{1}{4}A_h \quad (4)$$

Starting from these expressions, two calibration parameters were introduced in the formulation: the first parameter "x" *5* is used to calibrate the area of the openings in order to consider the effect of the discontinuity along the fenestration width of the ventilation openings, and the second parameter "k" *6* to tune the area of the holes of the venetian blinds.

$$A^*_{top/bot} = x \cdot A_{top/bot} \quad (5)$$

$$A^*_{eq,inl/out} = k \cdot \left(A^*_{top/bot} + \frac{1}{4}A_h\right) \quad (6)$$

Additionally, the pressure drop factor K was included in the total pressure loss equation 2, which becomes equation 7.

$$\Delta P_Z = \rho v^2 \left(Z_{inl/out} + K\right) \quad (7)$$

The parameters were varied parametrically one at a time: x between 0.1 and 10 and k between 0.1 and 1. The calibration procedure was divided into 2 steps: first, the opening parameter x was calibrated considering only the blind-up configuration, then the shading parameter k was calibrated keeping the x parameter fixed. In this way, the equation 4 becomes 8, forcing identical parameter values for all configurations.

$$A^*_{eq,inl/out} = k \cdot \left(x \cdot A^*_{top/bot} + \frac{1}{4}A_h\right) \quad (8)$$

The optimal values were chosen by minimizing two statistical indicators: the Root Mean Squared Error (RMSE) (9) and the Mean Absolute Percentage Error (MAPE) (10), computed for the inlet mass flow rate and the total heat flux for all the cases considered.

$$RMSE = \frac{1}{N}\sqrt{\sum_{i=1}^{N}\left(x_{T,i} - x_{C,i}\right)^2} \quad (9)$$

$$MAPE = \frac{1}{N}\sum_{i=1}^{N}\left|\frac{x_{T,i} - x_{C,i}}{x_{C,i}}\right| \cdot 100\% \quad (10)$$

In this way, the calibration was carried out both at component level (inlet flow rate) and at building level (contribute of the component on the thermal balance of the zone).

3. Results and Discussion

3.1 System Scale Results From COMSOL

The FEM-based simulation performed with COMSOL Multiphysics allowed the temperature, pressure, and velocity field over the fenestration system to be computed and the airflow rate and the total heat flux to be quantified in detail.

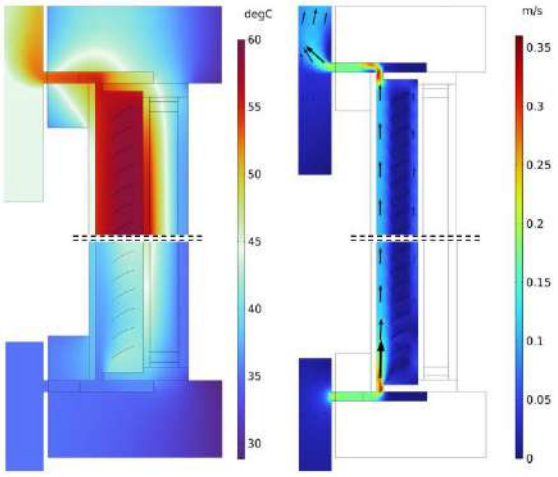

Fig. 3 – Temperature (left) and air velocity (right) distribution over the CFS, $T_{air,ext}$=35°C, $T_{air,int}$ = 28°C, I_{sol} = 500 W/m², blind tilt 30°

To showcase a possible temperature and air velocity distribution over the CFS with a blind tilt angle of 30° and warm summer conditions ($T_{air,ext}$ = 35 °C, $T_{air,int}$ = 28 °C, I_{sol} = 500 W/m²) an illustration of the spatial distribution of the two variables is shown in Fig. 3. It is possible to notice how buoyancy forces the warmer air to rise, resulting in a vertical

temperature gradient and leading to high temperatures in the upper part of the CFS, where 60 °C are reached.

3.2 Building Scale Results From TRNSYS and Calibration Parameters

The FEM model outcomes were used to tune the two calibration parameters 5 and 6 of the Python-based Type 169. As mentioned before, only the blind-up dataset was used for the calibration of the x-parameter and focusing on the statistical indicators of the total heat flux, x=0.5 was found to be the optimal solution. Regarding the configuration with the shading system deployed, the x parameter was kept fixed to 0.5 and the parameter k was varied parametrically in order to identify the optimal value which minimizes the statistical indicators for the three blind tilt angles configuration. Fig. 5 shows the outcomes of the calibration procedure with blinds at 30° angle; models with k = 0.3, 0.7 and 1 were compared to the uncalibrated one (x=1, k =1). For each model, the COMSOL (x-axis) versus TRNSYS (y-axis) results are reported for inlet mass flow rate (a) and total heat flux (b). The scatter plots were clustered by the value of the incident solar irradiance, since it affects both the parameters analyzed. It should be noted that parameter k has a greater impact on the mass flow rate than on the total heat flux, because it directly determines the mass flow rate, which in turn influences the total heat flux. Since the flow rate and the total heat flux have different behaviors to the variation of parameter k, the value that minimizes the statistical indicators of the total heat flux was chosen as the optimal one. This assumption is related to the building scale model approach: the total heat flux of the CFS accounts directly for the contribution of the component on the thermal balance of the zone, therefore a greater weight to this parameter is given in the choice of the optimal value.

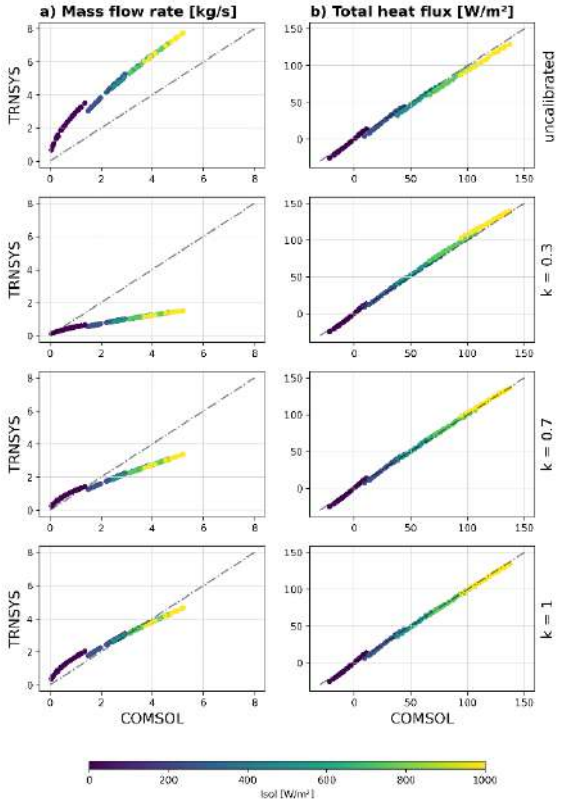

Fig. 4 – Inlet mass flow rate (a) and total heat flux (b) calibration outcomes for blind tilt 30°

The statistical indicator for total heat flux suggests that k=0.7 is the optimal solution, with a reduction of the statical errors of 67 % compared to the uncalibrated model (x=1, k=1). The same calibration procedure was repeated for the other 2 configurations. To avoid redundancy and for sake of brevity, Table 4 summarizes the results of the calibrated model compared to the uncalibrated one in terms of RMSE and MAPE indicators of inlet mass flow rate and total heat flux. A unique value of k parameter was chosen as optimal for all the configurations of the shading system, in order to avoid the need for changing the calibration values x and k for each blind tilt angle.

This, however, leads to a reduction of the model performance, especially with fully closed blinds. Nonetheless, by calibrating x and k parameters for the two extreme conditions (horizontal and fully closed) and one intermediate condition (30°), it can be assumed that the use of these values could be extended for the remaining configurations.

Table 4 – Comparison of RMSE (top) and MAPE (bottom)

Blind mode	Ventilation Type	Mass flow rate	Total heat flux
Blind up	final model	0.19 kg/s 13.2 %	3.12 W/m² 5.6 %
	uncalibrated model	1.59 kg/s 100.8 %	3.74 W/m² 6.7 %
Blind 0°	final model	0.39 kg/s 34.8 %	1.49 W/m² 2.4 %
	uncalibrated model	2.41 kg/s 186.9 %	3.81 W/m² 6.4 %
Blind 30°	final model	0.97 kg/s 37.9 %	1.58 W/m² 1.3 %
	uncalibrated model	2.13 kg/s 125.5 %	4.74 W/m² 5.8 %
Blind 75°	final model	0.98 kg/s 30.9 %	3.42 W/m² 11.0 %
	uncalibrated model	1.67 kg/s 82.7 %	1.88 W/m² 2.0 %

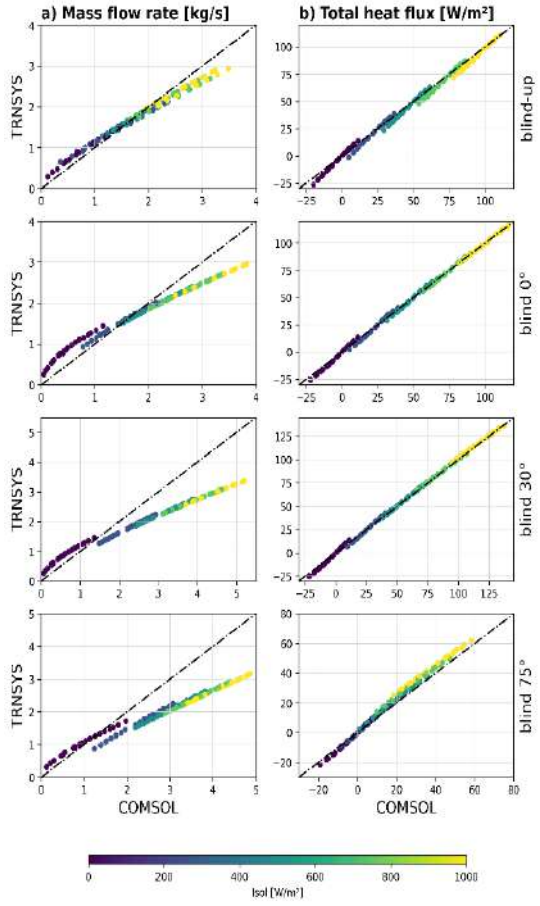

Fig. 5 – Inlet mass flow rate (a) and total heat flux (b) comparison for all blind configurations with the calibrated model

The calibration procedure resulted in a significant reduction of the RMSE in a range of 60 % (blind tilt 0°) to 66 % (blind tilt 30°) and in minimizing the MAPE (especially for blind tilt 0° and 30°). Finally, the comparisons with FEM results for the inlet mass flow rate and total heat flux are shown in Fig. 5 for all configurations. The TRNSYS model overestimates the inlet mass flow rate in the presence of low radiation (< 500 W/m²) and underestimates it in presence of high radiation.

4. Conclusions

To promote the implementation of CFS, it is crucial to enable a relatively simple yet reliable way of assessing their impact at building scale. In this paper, a novel workflow was implemented in one of the most widespread BES tools to assess the performance of a CFS in terms of heat fluxes and airflow rate. The results obtained through FEM simulations were used to calibrate the BES workflow and to assess the error of the calibrated BES tool. Results show a difference of 5 % of the total heat flux through the CFS after the fine-tuning of the ad-hoc Type parameter. The calibration was carried out focusing on the CFS contribution to the thermal balance zone to improve the BES tool's performance in predicting the thermal behavior of such complex components. Moreover, the ad-hoc type can be generalizable for modeling naturally ventilated windows with geometric features similar to the presented CFS (narrow cavity with small vents), since the calibration procedure was carried out by only varying the opening areas.

With this picture, it is possible to state that such workflows allow a consideration of the thermal behavior of CFS at building scale with an acceptable degree of uncertainty. This results in the great advantage of providing the possibility of assessing the impact of a CFS when there is still room for improvement and change in the design.

Acknowledgement

The research presented in this paper has been supported by the Cultural-E project. This project has received funding from the European Union's Horizon 2020 research and innovation program under grant agreement No 870072.

Nomenclature

Symbols

q	Specific heat flux (W/m²)
h_c	Convective heat transfer coefficient (W/(m²K))
T_{air}	Air temperature (°C)
T_{sf}	Surface temperature (°C)
σ	Stefan-Boltzmann constant (5.669×10^{-8} W/m²/K⁴)
ε	Thermal emissivity (-)
ε_f	Thermal emissivity front (-)
ε_b	Thermal emissivity back (-)
ρ	Mass density (kg/m³)
u	Air velocity (m/s)
σ_s	Solidity (ratio of blocked area to total area of the screen)
K	Resistance coefficient (-)
λ	Thermal conductivity (W/m/K)
c_p	Specific heat capacity at constant pressure (J/kg/K)

References

Catto Lucchino, E., A. Gelesz, K. Skeie, G. Gennaro, A. Reith, V. Serra, and F. Goia. 2021. "Modelling Double Skin Façades (DSFs) in Whole-Building Energy Simulation Tools: Validation and Inter-Software Comparison of a Mechanically Ventilated Single-Story DSF." *Building and Environment* 199. doi: https://doi.org/10.1016/j.buildenv.2021.107906

COMSOL. n.d. "COMSOL Multiphysics® v. 5.6."

COMSOL. n.d. "Screen Boundary Condition."

Dama, A., D. Angeli, and O. Kalyanova Larsen. 2017. "Naturally Ventilated Double-Skin Façade in Modeling and Experiments." *Energy and Buildings* 144: 17–29. doi: https://doi.org/10.1016/j.enbuild.2017.03.038

Demanega, I., G. de Michele, M. Hauer, S. Avesani, G. Pernigotto, and A. Gasparella. 2020. "Numerical and Experimental Characterization of the Thermal Behavior of Complex Fenestrations Systems under Dynamic Conditions." In Proceedings of Building Simulation Applications 2019, Bolzano, Italy.

Huckemann, V., E. Kuchen, M. Leão, and É. F. T. B. Leão. 2010. "Empirical Thermal Comfort Evaluation of Single and Double Skin Façades." *Building and Environment* 45(4): 976–82. doi: https://doi.org/10.1016/j.buildenv.2009.10.006

ISO. 2003. *ISO 15099 International Standard ISO 15099:2003. Thermal Performance of Windows, Doors and Shading Devices — Detailed Calculations.*

Jankovic, A., and F. Goia. 2021. "Impact of Double Skin Facade Constructional Features on Heat Transfer and Fluid Dynamic Behaviour." *Building and Environment* 196: 107796. doi: https://doi.org/10.1016/j.buildenv.2021.107796

Li, Y., J. Darkwa, and G. Kokogiannakis. 2017. "Heat Transfer Analysis of an Integrated Double Skin Façade and Phase Change Material Blind System." *Building and Environment* 125: 111–21. doi:https://doi.org/10.1016/j.buildenv.2017.08.034

Pasut, W., and M. De Carli. 2012. "Evaluation of Various CFD Modelling Strategies in Predicting Airflow and Temperature in a Naturally Ventilated Double Skin Façade." *Applied Thermal Engineering* 37:267–74. doi: https://doi.org/10.1016/j.applthermaleng.2011.11.028

Pomponi, F., P. A. E. Piroozfar, R. Southall, P. Ashton, and E. R. P. Farr. 2016. "Energy Performance of Double-Skin Façades in Temperate Climates: A Systematic Review and Meta-Analysis." *Renewable and Sustainable Energy Reviews* 54: 1525–36. doi: https://doi.org/10.1016/j.rser.2015.10.075

Wang, Y., Y. Chen, and C. Li. 2019. "Airflow Modeling Based on Zonal Method for Natural Ventilated Double Skin Façade with Venetian Blinds." *Energy and Buildings* 191: 211–23. doi: https://doi.org/10.1016/j.enbuild.2019.03.025

Wang, Y., Y. Chen, and J. Zhou. 2016. "Dynamic Modeling of the Ventilated Double Skin Façade in Hot Summer and Cold Winter Zone in China." *Building and Environment* 106:365–77. doi: https://doi.org/10.1016/j.buildenv.2016.07.012

Ward, G. J. 1994. "The RADIANCE Lighting Simulation and Rendering System." Proceedings of the 21st Annual Conference on Computer Graphics and Interactive Techniques, SIGGRAPH 1994 459–72. https://doi.org/10.1145/192161.192286

Heat and Mass Transfer Modelling for Moisture-Related Risks in Walls Retrofitted by Timber Materials

Gianpiero Evola – University of Catania, Italy – gevola@unict.it
Alessandra Urso – University of Catania, Italy – alessandra.urso@phd.unict.it
Vincenzo Costanzo – University of Catania, Italy – vincenzo.costanzo@unict.it
Francesco Nocera – University of Catania, Italy – fnocera@unict.it
Luigi Marletta – University of Catania, Italy – luigi.marletta@unict.it

Abstract

The e-SAFE innovation project financed by the Horizon 2020 Programme and led by the University of Catania, is developing, testing and demonstrating an innovative combined energy-and-seismic renovation solution for Reinforced Concrete (RC) framed buildings based on the addition of Cross Laminated Timber (CLT) boards to the outer walls, in combination with wood-based insulation. In this paper, the proposed renovation solution (called e-CLT) is investigated in terms of moisture-related risks, i.e., the mold growth and the increase in heat losses due to Liquid Water Content (LWC) within building materials. To this aim, dynamic simulations are performed by means of Delphin 6.1, thus including combined heat and mass transfer (HAMT) due to water vapor migration and accumulation. The results show that, although there is no significant risk of mold growth in the e-CLT for climate conditions prevalent in Northern Italy, the moisture content within the materials implies an increase by about 10 % in the heat losses if compared with a dry wall. Furthermore, inaccurate material properties and boundary outdoor climate conditions can affect the reliability of the results: for this reason, a more appropriate hygrothermal characterization of materials is recommended, as well as the identification of suitable climate datasets, which, however, are not always available.

1. Introduction

Since around 80 % of the building stock in the European Union was built before 1990, i.e., before the enforcement of most EU regulations regarding the energy performance of buildings, it is apparent that deep renovation is a key challenge towards the decarbonization of the existing building stock.

In this framework, the e-SAFE innovation project financed by the Horizon 2020 Programme and led by the University of Catania, is developing, testing and demonstrating an innovative combined energy-and-seismic renovation solution for Reinforced Concrete (RC) framed buildings based on the addition of Cross Laminated Timber (CLT) boards to the outer walls, in combination with wood-based insulation. In this study, the proposed renovation solution (called e-CLT) is applied to a building with infill walls made of two leaves of lightweight concrete blocks with an intermediate air gap, a very common envelope solution in Italy for the residential buildings from the 1960s to the 1980s.

While the seismic performance ensured by the e-CLT solution is addressed in other studies, this paper aims to investigate moisture-related risks by means of Delphin 6.1 software, which allows transient simulations considering combined heat and moisture transport (HAMT). In fact, wood-based components are particularly prone to moisture storage due to their cellular structure, and – being wood an organic material – they are more sensitive to decay caused, e.g., by mold.

Preliminary investigations by means of Glaser's method revealed that, although the application of the e-CLT solution improves both thermal and hygrothermal behavior of the walls (Evola et al., 2021), interstitial condensation may occur in cold climates in case of high indoor humidity values (Costanzo et al., 2021a). A following study (Costanzo et al., 2021b) tested the e-CLT solution in three different climates in Italy, performing transient hygrothermal simulations and reaching similar conclusions: wood-based materials are likely exposed to mold

growth – although moderate – especially in colder climates.

Building on these previous research experiences, this paper focuses on the reliability of the results, which may be affected by inaccuracy of hygrothermal materials properties and climatic boundary conditions. To this aim, a literature review highlights the dispersion of the hygrothermal property values for wood, and the consequent effects on the simulation results. Moreover, the paper underlines the effects of using different weather datasets, such as a typical meteorological year (TMY) and a weather file available in the Delphin database for the same location. In particular, the simulations refer to Milan, a cold and humid climate in Northern Italy. Finally, moisture-related risks are investigated by looking not only at mold growth, but also at the increase in the heat transfer through the wall due to the liquid water content within building materials.

2. Methodology

The hygrothermal performance and the moisture-related risk of the e-CLT solution are investigated by means of dynamic finite element analyses performed in Delphin 6.1, a commercial program developed at University of Dresden.

The software allows the combined heat and moisture transport (HAMT) within porous building materials to be considered. To this aim, it requires hygrothermal material properties and functions (e.g., porosity, density, specific heat capacity, thermal conductivity, water vapor resistance factor, liquid conductivity, moisture storage curve), and indoor and outdoor climatic boundary conditions (e.g., temperature, relative humidity, driving rain, wind speed, wind direction, short and long wave radiation). The selection of appropriate material properties and climate data is a paramount issue due to their effect on the reliability of the results; for this reason, this paper pays particular attention to these issues, as highlighted in this Section.

2.1 Materials

The e-CLT solution is here applied to a typical Italian wall structure composed of (from internal to external side): cement plaster (20 mm), hollow concrete blocks with volcanic aggregates (80 mm), non-ventilated air cavity (100 mm), hollow concrete blocks with volcanic aggregates (120 mm) and cement plaster (30 mm).

As regards the e-CLT solution, this is composed of (from internal to external side): CLT (100 mm), low density wood fiber (60 mm), scarcely-ventilated air gap (20 mm) and a fiber cement cladding (12 mm).

The proposed solution also includes a vapor-open foil (s_d = 0.04 m) to protect the insulation layer from the effect of wind-driven rain, applied to the external side of wood fiber. Materials are selected from the Delphin database; some properties have been modified according to technical sheets and standards in case of missing materials. Table 1 and Table 2 show the hygrothermal properties of the selected materials. In case of air gaps, the thermal conductivity is defined as an equivalent value calculated from the air gap thermal resistance.

Table 1 – Thermal properties of selected materials: "id" is the identification code on material database, (*) indicates modified properties

id	Material	ρ	c_p	λ_{dry}
		kg·m^{-3}	J·kg^{-1}·K^{-1}	W·m^{-1}·K^{-1}
242	Plaster	1390	850	0.75
508	Hollow blocks (80 mm)	845	1000	0.29*
15	Non-ventilated air gap	1.3	1050	0.56*
508	Hollow blocks (120 mm)	667*	1000	0.39*
712	CLT	450*	1843	0.12*
1762	Wood fiber	50*	1000	0.04
15	Scarcely-ventilated air gap	1.3	1050	0.22*
654	Fiber cement cladding	1160	1188	0.60*

Table 2 – Hygric properties of selected materials: "id" is the identification code on material database, (*) indicates modified properties

id	Material	μ	A	θ80	θeff
		-	g·m^{-2}·s$^{-0.5}$	kg·m^{-3}	kg·m^{-3}
242	Plaster	33	30	40.7	430.0
508	Hollow blocks (80 mm)	15	177	11.4	319.4
15	Non-ventilated air gap	1	-	-	-
508	Hollow blocks (120 mm)	15	177	11.4	319.4
712	CLT	186	2- 5 - 12*	59.8	728.1
1762	Wood fiber	1.1	5	12.7	590.3
15	Scarcely-ventil. air gap	1	-	-	-
654	Fiber cement cladding	26	14	70.9	283.6

The hygrothermal characterization of the CLT requires a more detailed literature review, both because it is a missing material from the Delphin database, and because there are some discrepancies amongst the various sources surveyed. In particular, those parameters related to moisture transport, namely the water vapor resistance factor (μ-value) and the water uptake coefficient (A-value), show a high dispersion of their values. Thus, CLT is represented through the database material Spruce radial (id.: 712), experimentally tested by the Technical University of Dresden. However, since the manufacturing process can make CLT denser than the original wood (Lapage, 2012), density is replaced by the value supplied by manufacturers ($\rho = 450$ kg·m^{-3}), whereas dry thermal conductivity refers to EN ISO 10456 Standard (CEN, 2007a) ($\lambda = 0.12$ W·m^{-1}·K^{-1}).

As regards moisture transport parameters, the glue between lumber boards in a CLT panel can affect the μ-value and A-value because it acts as a seal. Nevertheless, some studies show good agreement between CLT and transverse wood's hygric properties (AlSayegh, 2012; Lapage, 2012): Table 3 sums up experimental μ-value and A-value for softwoods and CLT, based on different species as reported in the literature. As shown in Table 3, moisture transport parameters depend firstly on species and fiber direction. The EN ISO 10456 Standard (CEN, 2007a) reports $\mu = 50$ for timber, i.e., the proposed resistance to vapour diffusion is about four times lower than spruce radial and ten times lower than spruce tangential as gathered from the Delphin database. However, if compared with literature values (AlSayegh, 2012; Kordiziel et al., 2020), the μ-value varies from 146 to 456 for softwoods and CLT boards made of softwood with transverse fiber direction. This means that μ-value of spruce radial ($\mu = 186$) can be assumed as a reliable value for simulations.

Coming to the A-value, this varies between 1.6 g·m^{-2}·s$^{-0.5}$ and 14 g·m^{-2}·s$^{-0.5}$ for transverse fiber direction. The wide range of values covered in the literature mainly depends on the preparation of test specimens. For instance, the presence of wood imperfections (e.g., checks, cracks, holes) could make wood more permeable to moisture, as confirmed by (Raina, 2021) by means of the visual evaluation of absorbed water from a surface with a small hole during the water uptake test. For this reason, (AlSayegh, 2012) selected test specimens that are more representative of the material without checks, thus obtaining A-value = 1.9 – 2.0 g·m^{-2}·s$^{-0.5}$. In contrast, (Lapage, 2012) tested samples including "checks, cracks, pitch pockets and other deviations from ideal conditions", and determined higher A-values (4 – 14 g·m^{-2}·s$^{-0.5}$). The size of the sample can also affect the experimental results: indeed, small samples are likely to minimize the effects of checks and gaps in the boards (McClung et al., 2014). This could explain A-values (2.1–2.8 g·m^{-2}·s$^{-0.5}$) found out by (Kordiziel et. al., 2020), who used samples with smaller surface area than the minimum set in the Standard.

Table 3 – Softwoods and CLT features from literature (SPF: Spruce-Pine-Fir)

Source	Type	ρ	μ*	A
		kg·m^{-3}	-	g·m^{-2}·s$^{-0.5}$
Delphin database	Spruce (radial)	395	186	12
	Spruce (tangential)	395	488	5
	Spruce (longitudinal)	395	5	12
EN ISO 10456 (CEN, 2007a)	Timber	450	50	-
(Lapage, 2012)	CLT, Eastern SPF	486	-	4 - 7
	CLT, Western SPF	500	-	12
	CLT, European softwood	340	-	10 - 11
	CLT, Him-Fir	522	-	14
(Alseyeg, 2012)	CLT, Eastern SPF	370	328	2.0
	CLT, Western SPF	440	456	1.9
	CLT, European softwood	340	311	1.6
	CLT, Him-Fir	380	277	2.5
(Cho et al., 2019)	CLT	602	630	-
(Kordiziel et al., 2020)	CLT, SPF + Douglas Fir	423	-	2.5 -2.8
	SPF without adhesive	426	146	2.8
	SPF with adhesive	426	168	2.4
(Raina, 2021)	CLT, European spruce	-	-	1.9 – 3.6
	CLT, European spruce – without covered edges	-	-	7 - 12
(Chang et al., 2020)	Larch (radial)	570	75	-
	Larch (tangential)	570	109	-
	Larch (longitudinal)	570	5	-
	CLT, larch and plywood	600	79	-

*dry cup, RH chamber = 50 %

Lastly, the sealing of edges could also influence test results. To this purpose, (Raina, 2021) tested various samples with and without sealed edges, demonstrating that the A-value can reach 12 g·m^{-2}·s$^{-0.5}$ due

to water absorbed from longitudinal fiber of the cut uncovered edges. Not surprisingly, the results are close to those reported by (Glass & Zelinka, 2010) for softwood in longitudinal direction (10 – 16 $g \cdot m^{-2} \cdot s^{-0.5}$). In view of this, and considering A-values of 2 and 12 $g \cdot m^{-2} \cdot s^{-0.5}$ as reasonable extreme conditions, this paper assumes 5 $g \cdot m^{-2} \cdot s^{-0.5}$ as an intermediate value for spruce. However, simulations are repeated for other A-values to perform a sensitivity analysis.

2.2 Climate Boundary Conditions

The simulations are carried out for Milan (lat: 45°, long: 9°, altitude: 103 m) a cold and humid climate in Northern Italy. In order to assess the most appropriate available dataset for this location, the paper considers: i) the weather file from the Delphin database and ii) the TMY weather file from Linate (2004 – 2018) downloaded from the website (Climate.OneBuilding.org, 2022) (Fig. 1). In both cases, the investigated wall is oriented facing north, thus excluding the effect of direct solar radiation. For this reason, the plots in Fig. 1 only report the mean diffuse solar radiation.

Considering yearly mean values, the Delphin dataset shows 13 % higher diffuse solar radiation, but it appears colder (by 3 °C on average), more humid (by 6 % on average) and rainier (by 20 % on average) than the Linate dataset. This suggests that it will more likely induce moisture-related risks. Nevertheless, the long wave sky radiation (LWR) data is missing in all Italian weather files within the Delphin database, which implies excluding long wave radiation exchange from the simulation, thus affecting the reliability of results. On the other hand, Linate TMY is not built *ad hoc* for hygrothermal simulations, i.e., it is not representative of the worst climate conditions from the point of view of moisture-related risks. The selection of the most appropriate dataset thus requires preliminary simulations, as discussed in Section 3.1.

The outside heat transfer coefficient and surface vapor diffusion coefficient are 25 $W \cdot m^{-2} \cdot K^{-1}$ and $7.5 \cdot 10^{-8}$ $m \cdot s^{-1}$, respectively, while their indoor values are 8 $W \cdot m^{-2} \cdot K^{-1}$ and $2.5 \cdot 10^{-8}$ $m \cdot s^{-1}$, respectively. The solar absorption coefficient is set to 0.6. The incident wind-driven rain (WDR) is calculated by Delphin according to EN ISO 15927-3 Standard (CEN, 2009), using a splash coefficient of 0.7. In addition, a water source is assigned to the side of the insulation protected by the water-proof membrane, set equal to 1 % of the rain flux incident on external surface. This setting simulates rain leakage through the cladding.

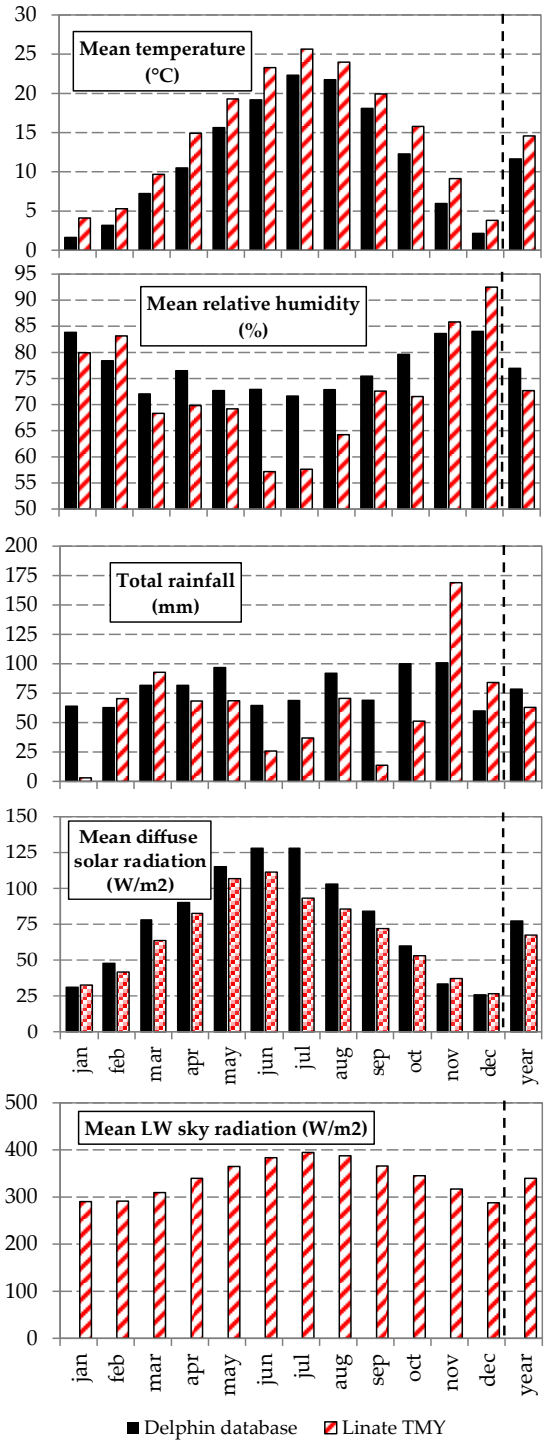

Fig. 1 – Comparison between weather data from Delphin Database and from a web service (Climate.OneBuilding.org, 2022)

On the other hand, the indoor conditions are set according to EN ISO 15026 Standard (CEN, 2007b). The standard offers a simplified approach to take the change in indoor temperature and relative humidity as a function of external conditions into account (Fig. 2). It is here relevant to highlight that moisture-related risks may also depend on the indoor conditions (Brambilla & Gasparri, 2020). This issue will be investigated in future studies.

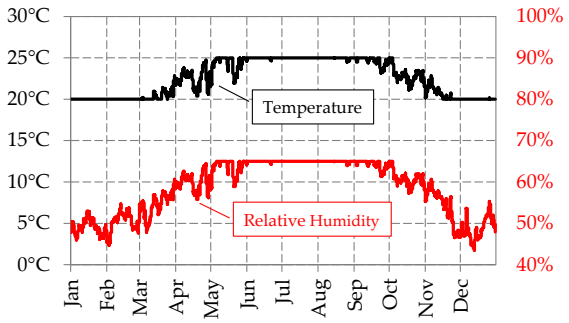

Fig. 2 – Indoor climate conditions as a function of outdoor temperature from Linate TMY, according to EN ISO 15026 (CEN, 2007b)

2.3 Initial Conditions

The simulations are performed over a 10-year-long period, in order to obtain stabilized behavior; the initial conditions correspond to 20 °C temperature and 80 % relative humidity for all materials.

2.4 Outputs

Moisture related-risks are evaluated for the e-CLT solution applied to the investigated existing wall by requesting as outputs from Delphin the time-dependent liquid water content (LWC) in both the CLT and the insulating material, as well as the temperature and relative humidity from which calculating the mold index (MI) by means of the tool PostProc 2.2.3.

In particular, the LWC ($m^3 \cdot m^{-3}$) represents the volume fraction of liquid phase accumulated in the pores of the materials (Bauklimatik Dresden, 2022). Instead, according to the VTT model (Ojanen et al., 2010), MI measures the mold growth rate in a scale from 0 (no mold growth) to 6 (very heavy and tight mold growth); the authors also suggest that MI values above 3 are not acceptable. The model also considers the sensitivity of materials to mold growth: in this specific case, the CLT and the wood fiber are set as "sensitive".

Further outputs are the mean conductive heat flux throughout the wall and the moisture-dependent thermal conductivity for each layer of the wall. They are required to assess the increase of thermal losses and U-value due to humidity within building materials.

More specifically, the moisture-dependent U-value ($W \cdot m^{-2} \cdot K^{-1}$) is calculated as follows:

$$U(LWC) = \left[\frac{1}{h_{0,e}} + \sum_{i=1}^{n} \frac{s_i}{\lambda_i (LWC)} + \frac{1}{h_{0,i}} \right]^{-1} \quad (1)$$

where $h_{0,e}$ and $h_{0,i}$ are respectively the outside and inside heat transfer coefficient, previously defined, n is the number of layers and λ_i ($W \cdot m^{-1} \cdot K^{-1}$) is the moisture-dependent thermal conductivity of each layer, computed by Delphin as a function of LWC, given the dry thermal conductivity λ_{dry} (Vogelsang et al., 2013):

$$\lambda = \lambda(LWC) = \lambda_{dry} + 0.56 \cdot LWC \quad (2)$$

This study does not consider the influence of temperature on thermal conductivity, since Delphin does not include any built-in functions for the selected materials to this scope. However, by taking into account the conversion coefficients reported in Annex A of EN ISO 10456 Standard (CEN, 2007a), the maximum variation of λ within the range of temperatures occurring in this study would be around 3 % for the insulating material, and even less for the other materials.

3. Results And Discussion

3.1 The Role of the Weather Data

As mentioned above, the influence of weather data is preliminarily investigated. The main target is to understand which dataset is more appropriate, or implies more conservative results, in terms of moisture-related risk.

The simulations are repeated with i) weather data from the Delphin database, which does not include the LWR exchanges, ii) weather data from Linate TMY, with and without LWR exchanges. The results are reported in Fig. 3 and Fig. 4.

If looking at the results obtained using the weather file from the Delphin database (grey solid line in Figs. 3-4), the yearly mean LWC is 0.054 $m^3 \cdot m^{-3}$ in

the external side of CLT and 0.012 $m^3 \cdot m^{-3}$ in the external side of wood fiber. There is no risk of mold in both materials. Instead, the results from the simulations run with the TMY from Linate reveal that including LWR exchanges worsens the hygrothermal behavior of the e-CLT. In fact, using Linate TMY with LWR implies temperatures and relative humidity profiles respectively lower and higher than the case without LWR, which also means higher LWC and MI.

In particular, the yearly mean LWC in the external side of both CLT and wood fiber increases by around 4 %. The risk of mold growth is higher in the wood fiber, for which the maximum MI is 2.17 – 0.27 respectively taking and not taking into account LWR exchanges. Although the MI is still below the critical threshold, in the first case its values tend to increase over the years. This means that excluding the LWR exchanges, for instance by using the Italian weather files available in Delphin, can underestimate moisture-related risks.

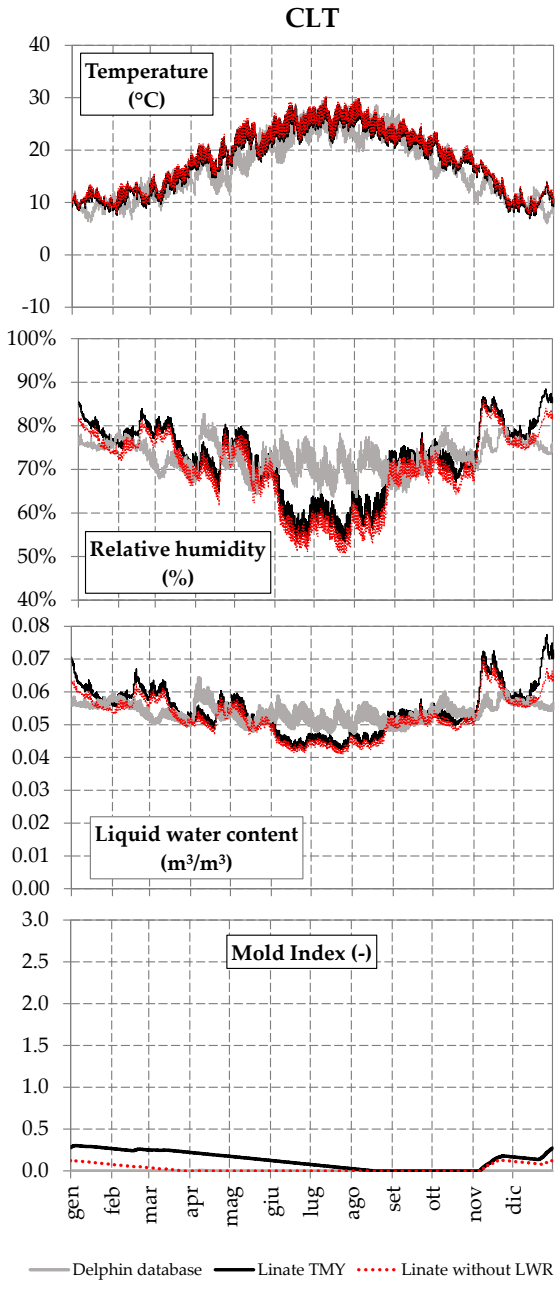

Fig. 3 – Comparison between simulations with weather data from Delphin database and from Linate TMY with/without LWR

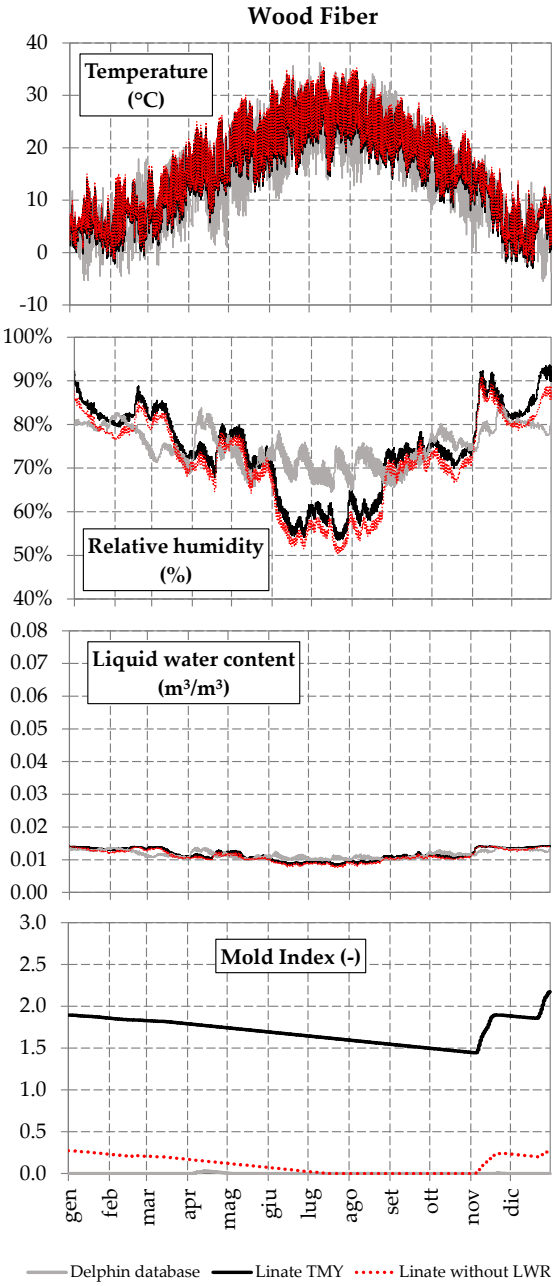

Fig. 4 – Comparison between simulations with weather data from Delphin database and Linate TMY with/without LWR

For this reason, the results discussed in the following sections refer to simulations performed with Linate TMY, even if this weather file is not built *ad hoc* for hygrothermal simulations. Future studies will rely on suitable extreme weather data for Milan, for instance created according to EN ISO 15026 (CEN, 2007b).

3.2 Humidity and Increased Heat Flux

In order to assess the increase in the heat losses due to LWC within building materials, the mean heat flux transferred through the wall is calculated considering thermal conductivity respectively dependent, or independent, on moisture content. Thus, simulations are repeated assuming for each material respectively Eq. 2 and Eq. 3.

$$\lambda = \lambda_{dry} \quad (3)$$

The results are reported in Fig. 5: not taking into account the variation in thermal conductivity due to moisture content within materials would underestimate heat losses by about 9.7 % on average. Similarly, the moisture-dependent yearly mean U-value (U = 0.326 W·m^{-2}·K^{-1}) increases by 11.0 % with respect to the U-value in dry conditions (U = 0.290 W·m^{-2}·K^{-1}).

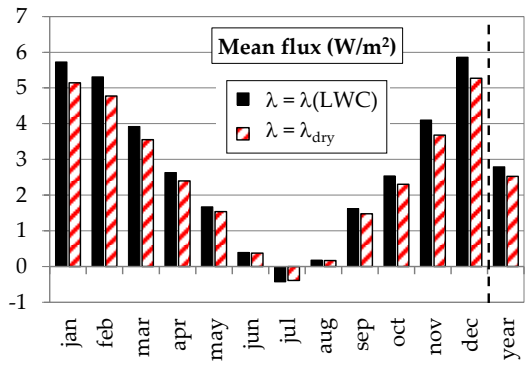

Fig. 5 – Monthly mean conductive heat flux: comparison between simulations taking and not taking into account moisture-dependent thermal conductivity

In a similar study, (Danovska et al., 2019) studied the impact of humidity and temperature on the thermal behavior of insulated timber walls for a series of Italian cities, and found out that the mean increase in heat losses – considering the actual thermal conductivity of materials – is below 6 % on average in Northern Italy locations and below 10 % in Southern Italy, the highest values pertaining to the most insulated wall structures. Finally, Fig. 6 suggests that the monthly mean U-value of the wall retrofitted through the e-CLT solution can be linearly correlated with mean LWC of wood fiber with $R^2 = 0.99$. This means that the thermal performance of the e-CLT solution applied to the investigated wall decreases linearly with the amount of the LWC in the insulation layer.

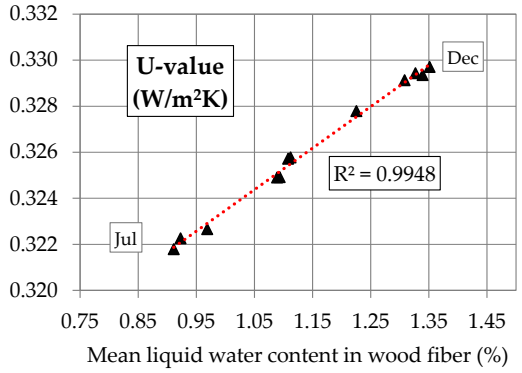

Fig. 6 – Moisture-dependent monthly mean U-value

3.3 The Water Uptake Coefficient

A sensitivity analysis is finally carried out to observe the CLT performance as a function of its A-value. The top plot in Fig. 7 shows the hourly profiles of mean LWC throughout the CLT, respectively with A-value = 2, 5 and 12 g·m^{-2}·s$^{-0.5}$ according to literature. In principle, higher A-values imply higher LWC during winter.

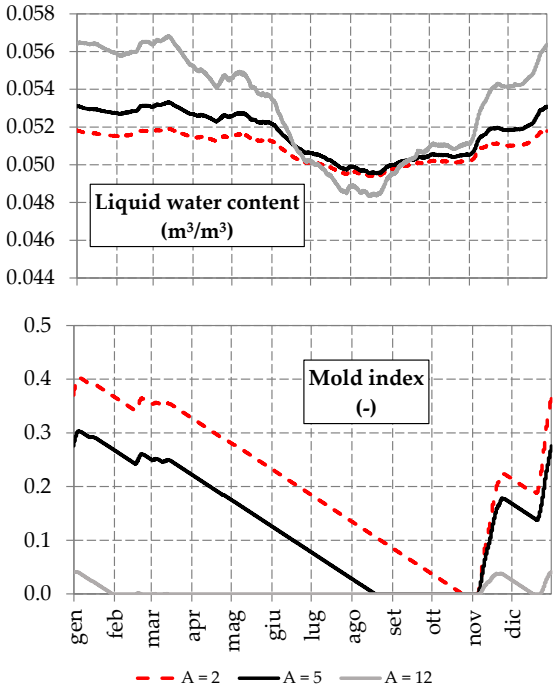

Fig. 7 – Influence of A-value on mean liquid water content and external face mold index. All values in legend are in g/m^{2}s$^{1/2}$

Overall, A-value does not significantly affect the e-CLT thermal performance: indeed, the yearly mean LWC ranges between 0.051 – 0.053 $m^3 \cdot m^{-3}$, which does not imply variations in the heat losses. Finally, looking at the MI in the CLT (bottom plot of Fig. 7), the increase in A-value determines slightly higher mold growth risk. Indeed, in this case the moisture content between CLT and wood fiber is absorbed more rapidly towards the inner side. However, the risk is negligible (MI < 0.4).

4. Conclusion

In this study, the e-CLT building retrofit solution, applied to a typical existing Italian wall, is investigated in terms of moisture related risks, i.e., the mold growth and the increase in heat losses due to liquid water content within building materials. Moreover, this paper focuses on the role of weather data and of the water uptake coefficient of the CLT material on simulations. Since e-CLT is an innovative retrofit solution, this topic is not addressed in the literature except for some preliminary analyses carried out by the same authors (Costanzo et al., 2021b). With respect to the above-referenced study, the current research confirms that a moderate mold growth risk (MI > 1) can occur in a cold and humid Italian climate, while also discussing the role of CLT hygrothermal properties in greater detail. Furthermore, the reliability of the Italian weather files within the Delphin database is assessed in a systematic way.

The conclusions can be summed up as follows:

- excluding the long wave heat transfer from the simulation, for instance, when using Delphin database Italian weather files, leads to underestimate moisture-related risks;
- the inaccuracy on the A-value of CLT does not significantly impact on the LWC and MI;
- the increased heat losses due to LWC within building materials amount to around 10 %
- the monthly mean U-value is linearly dependent on LWC in the insulation layer, and on average can vary by around 11 % if compared to an equivalent dry wall.

The next steps of this research activity will investigate the hygrothermal behavior during extreme meteorological years, selected from long-term weather acquisitions in different climate zones. In addition, further analyses are planned to better characterize hygrothermal properties of materials by means of experimental analyses.

Nomenclature

Symbols

A	water uptake coefficient ($g \cdot m^{-2} \cdot s^{-0.5}$)
CLT	cross laminated timber
c_p	specific heat capacity ($J \cdot kg^{-1} \cdot K^{-1}$)
HAMT	heat and moisture transport
λ	thermal conductivity ($W \cdot m^{-1} \cdot K^{-1}$)
λ_{dry}	dry thermal conductivity ($W \cdot m^{-1} \cdot K^{-1}$)
LWC	liquid water content ($m^3 \cdot m^{-3}$)
LWR	long wave radiation
MI	mold index (-)
μ	water vapor resistance factor (-)
ρ	density ($kg \cdot m^{-3}$)
s_d	equivalent air layer thickness (m)
θ_{80}	moisture content at 80 % RH ($kg \cdot m^{-3}$)
θ_{eff}	effective saturation ($kg \cdot m^{-3}$)
U	thermal transmittance ($W \cdot m^{-2} \cdot K^{-1}$)
WDR	wind-driven rain

Acknowledgement

This paper was carried out within the framework of the "Energy and seismic affordable renovation solutions" (e-SAFE) project, which has received funding from the European Union's Horizon 2020 research and innovation programme under grant agreement No. 893135. Neither the Executive Agency for Small-and-Medium-sized Enterprises (EASME) nor the European Commission is in any way responsible for any use that may be made of the information it contains. The activities are also partially funded by the University of Catania in the framework of the SIS-RENEW research project (Piano di incentivi per la Ricerca 2020–2022).

References

AlSayegh, G. 2012. *Hygrothermal Properties of Cross Laminated Timber and Moisture Response of Wood at High Relative Humidity.* Ottawa, Ontario: Carleton University.

Brambilla, A, and E. Gasparri. 2020. "Hygrothermal behaviour of emerging timber-based envelope technologies in Australia: A preliminary investigation on condensation and mould growth risk." *Journal of Cleaner Production* 276. doi: https://doi.org/10.1016/j.jclepro.2020.124129

Bauklimatik Dresden. 2022. "*Material Editor – Manual*". Material Editor - Manual (bauklimatik-dresden.de). Accessed on March 15.

CEN. 2007a. *EN ISO 10456:2007. Building materials and products, Hygrothermal properties, Tabulated design values and procedures for determining declared and design thermal values.* Brussels, Belgium.

CEN. 2007b. *EN ISO 15026:2007. Hygrothermal performance of building components and building elements - Assessment of moisture transfer by numerical simulation*. Brussels, Belgium.

CEN. 2009. *EN ISO 15127-3:2009. Hygrothermal performance of buildings - Calculation and presentation of climatic data - Part 3: Calculation of a driving rain index for vertical surfaces from hourly wind and rain data*. Brussels, Belgium.

Chang, S. J., S. Wi, S. G. Kang, and S. Kim. 2020. "Moisture risk assessment of cross-laminated timber walls: Perspectives on climate conditions and water vapor resistance performance of building materials." *Building and Environment* 168. doi: https://doi.org/10.1016/j.buildenv.2019.106502

Cho, H. M., S. Wi, S. J. Chang, and S. Kim. 2019. "Hygrothermal properties analysis of cross-laminated timber wall with internal and external insulation systems." *Journal of Cleaner Production* 231: 1353 - 1363. doi: 10.1016/j.jclepro.2019.05.197.

Climate.OneBuilding.org.2022. https://www.climate.onebuilding.org//WMO_Region_6_Europe/ITA_Italy/index.htm. Accessed on March 17.

Costanzo, V., G. Evola, A. Gagliano, L. Marletta, and F. Nocera. 2021a. "Hygrothermal Analysis of CLT-Based Retrofit Strategy of Existing Wall Assemblies According to EN 13788 Standard." *TECNICA ITALIANA - Italian Journal of Engineering Science* 65: 324 – 329. doi: https://dx.doi.org/10.18280/ti-ijes.652-428

Costanzo, V., G. Evola, L. Marletta, and G. Roccella. 2021b. "Preliminary investigation on the transient hygrothermal analysis of a CLT-based retrofit solution for exterior walls." *Journal of Physics: Conference Series* 2042(1). doi: https://doi.org/10.1088/1742-6596/2042/1/012142

Danovska, M., M. Libralato, G. Pernigotto, A. De Angelis, O. Saro, P. Baggio, and A. Gasparella. 2019. "Numerical and Experimental Study on the Impact of Humidity on the Thermal Behavior of Insulated Timber Walls." In *Proceedings of Building Simulation Applications BSA 2019*, 91 – 99. Bolzano.

Evola, G., V. Costanzo, and L. Marletta. 2021. "Hygrothermal and Acoustic Performance of Two Innovative Envelope Renovation Solutions Developed in the e-SAFE Project." *Energies* 14(13). doi: https://dx.doi.org/10.3390/en14134006

Glass, S. V., and S. L. Zelinka. 2010. "Chapter 4 - Moisture Relations and Physical Properties of Wood." In *General Technical Report FPL–GTR–190*. Madison, WI: U.S. Department of Agriculture, Forest Service, Forest Products Laboratory.

Kordiziel, S., S. V. Glass, C. R. Boardman, R. A. Munson, S. L. Zelinka, S. Pei, and P. C. Tabares-Velasco. 2020. "Hygrothermal characterization and modeling of cross-laminated timber in the building envelope." *Building and Environment* 177. doi: https://doi.org/10.1016/j.buildenv.2020.106866

Lapage, R. T. M. 2012. *Moisture Response of Wall Assemblies of Cross-Laminated Timber Construction in Cold Canadian Climates*. Waterloo, Ontario: University of Waterloo.

McClung, R., H. Ge, J. Straube, and J. Wang. 2014. "Hygrothermal performance of cross-laminated timber wall assemblies with built-in moisture: field measurements and simulations." *Building and Environment* 71: 95-110. doi: https://dx.doi.org/10.1016/j.buildenv.2013.09.008

Ojanen, T., H. Viitanen, R. Peuhkuri, K. Lähdesmäki, J. Vinha, and K. Salminen. 2010. "Mold growth modeling of building structures using sensitivity classes of materials." In *Proc. ASHRAE Conf. Buildings XI,* ASHRAE.

Raina, L. 2021. *Capillary movement of water in a radial direction and moisture distribution in a cross-section of CLT panel*. Tallinn: Tallinn University of Technology.

Vogelsang, S., H. Fechner, and A. Nicolai. 2013. "Delphin 6 Material File Specification, Version 6.0." *Technical Report*, Dresden, Germany: Institut für Bauklimatik Technische Universität Dresden.

Multi-Objective Optimization Of Thermo-Acoustic Comfort Of School Buildings

Daniele Colarossi – Università Politecnica Delle Marche, Italy – d.colarossi@pm.univpm.it
Samantha Di Loreto – Università Politecnica Delle Marche, Italy – s.diloreto@pm.univpm.it
Eleonora Tagliolini – Università Politecnica Delle Marche, Italy – e.tagliolini@pm.univpm.it
Paolo Principi – Università Politecnica Delle Marche, Italy – p.principi@univpm.it
Fabio Serpilli – Università Politecnica Delle Marche, Italy – f.serpilli@univpm.it

Abstract

The reduction of the environmental impact of the building sector is one of the top priorities in the "climate change challenge". As the primary energy consumption of the building decreases, a high level of indoor comfort must be maintained. Both thermal parameters, lighting, acoustic level, and indoor air quality affect indoor comfort. These aspects are fundamental, especially in school buildings, where a good level of indoor comfort can help student to stay focused. This paper proposes a methodology for a combined optimization of the energetic and the acoustic performance of a school building. A case study, located in the center of Italy, was analyzed. Firstly, the thermal and acoustic performance was determined. Then a list of interventions was hypothesized and simulated, involving both the building envelope, the lighting and thermal plants. Normalized acoustic insulation of partitions between adjacent rooms, acoustic insulation of the façade and reverberation time were evaluated. The outdoor and ambient noise levels were based on the main characteristics of the façade (type and stratifications of opaque and transparent components, ventilation system, etc.). Results show that the optimal combination of interventions reduces the CO_2 emissions of 88.55 % and the global energy performance index of 85.2 %. The indoor sound pressure level due to traffic noise is reduced by 19 dB after acoustic insulation of the façade, while further treatments to indoor surfaces should be implemented to reduce internal reverberation time and to improve speech intelligibility. The combined optimization shows that the highest reduction of the global impact (89.2 %) is obtained by weighting 80 %/20 % the acoustic/thermal performance.

1. Introduction

Nowadays, the building sector accounts for around 40 % of total global energy consumption and more than 30 % of CO_2 emissions. To achieve net-zero carbon emissions by 2050, the International Energy Agency (IEA) estimates that the sector has to halve its emissions by 2030. In the EU, the situation is similar, with 36 % of CO_2 emissions from the building stock, of which the final energy consumption for heating and cooling is 50 %. Accordingly, improving the energy efficiency and fostering total decarbonization is an essential step towards renewal of the building stock. The current rate of renovation of public buildings ranges from 0.4 % and 1.2 % per year, while it should be around 3 %, as reported by the 2018/844/EU Directive.

In addition, a high level of indoor comfort is required. Indoor comfort is affected by several factors, such as thermal level (air temperature and humidity, air velocity and quality), lighting and acoustic quality. In school buildings, students spend many hours a day in the classroom. The correct environment can help students to be focused and energetic. Different strategies have been proposed to evaluate and optimize the performance of school buildings (MacNaughton et al., 2018), or energy audits (Wang et al., 2015). Díaz-López et al. (2022) identified the 24 best passive intervention strategies, analyzing research trends in 42 countries. Li et al. (2021) proposed a multi-objective optimization method based on the response surface method, where optimal design trade-offs between thermal comfort and energy demand are obtained. Omar et al. (2022) based their optimization on lighting and cooling plant

retrofitting, and on the integration of a photovoltaic plant to increase the share of renewable energy exploited. Results show a gain of renewable fraction of around 82 %. Gamarra et al. (2018) considered water consumption and carbon footprint, resulting in a life-cycle assessment.

Noise in schools derives from its original surrounding environment, which has turned from silent into very noisy over the years (Secchi et al., 2017). The specification regarding sound insulation properties and noise from equipment properties in Italy were defined in the D.P.C.M. 5/12/97. The recent Italian law D.M. 11/01/2017, recalls the Italian standard UNI 11367. According to these standards, new school buildings must guarantee a façade sound insulation of $D_{2m,nT,w} \geq 48$ dB, which is very restrictive. In UNI 11367, the limit value for the normalized acoustic insulation of partitions between adjacent rooms of the same unit was presented: basic performance, with $D_{nT,w} \geq 45$, and high performance, with $D_{nT,w} \geq 50$ dB. UNI 11367 also requires a Speech Transmission Index in classrooms higher than 0.60 and sets the optimum value of reverberation time (Tott) as average value between 500 and 1000 Hz for unoccupied classrooms (s). The limit values for the acoustic indoor room quality are also defined in the UNI 11532-1. In part 2 of the standard, the limit value for reverberation time, STI e/o C50, and sound pressure level for technologic systems installed inside the classroom are defined.

This paper presents a methodology for the thermo-acoustic optimization of an existing school building, based on combinations of interventions (Moazzen et al., 2020). A primary school building located in central Italy was taken as a case study. Firstly, the current state of the building was analyzed using software to estimate the heating energy demand and acoustic performance. The analysis concerns both the design conditions and the dynamic consumption over a period of one year. Then, a list of interventions was hypothesized, involving both building envelope, the lighting system, the thermal plants and the acoustic parameters, to find out the optimal configuration. The novelty proposed is combined analysis, setting and optimizing weighting coefficients between thermal and acoustic performances.

2. Materials and Method

The methodology proposed consists of different steps:

- Identification of the case study building and determination of its properties and climatic conditions.
- Evaluation of energy and acoustic performance by software simulations.
- Proposal of interventions and combination of them.
- Simulation and index calculation.

The building chosen as reference case should be representative of the category of buildings under study, as regards the building geometry, energy performance for both envelope and plants, and climatic conditions. This way, the proposed model, once validated, can be easily applied to other buildings. In this paper, a primary school building has been chosen as reference case. Fig. 1 shows a real image of the building, while Fig. 2 shows the plan view.

Fig. 1 – Real image of the school building under study

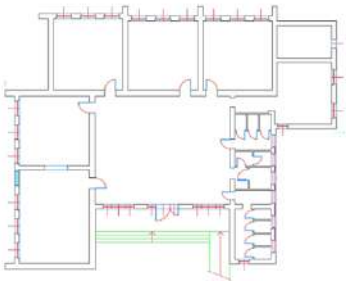

Fig. 2 – Plan view of the school building under study

The reference building presents a floor area of 350 m² and consists of 6 classrooms, with a net height of 3.25 m. The entrance hall has a sloped ceiling, average height 4.8 m. The occupancy has been hypothesized as typical of school buildings, namely on weekdays between 08.00 and 1700. According to the national standards, Italy is divided into six climatic zones, depending on the heating degree days. For each zone, there is a corresponding different annual heating period and number of hours of daily operation. In addition, a series of minimum U-values are provided for each zone. Central Italy, where the reference building is located, is involved in the "E" zone, which corresponds with a heating period from 15 October to 15 April. The specific location of the building presents a minimum temperature of -4 °C, as stated in the UNI 10349 standard. This data is required to calculate the energy performance of the building under the worst-case conditions. Then a dynamic hourly-based method is applied to provide the energy consumptions over a year. The first step for the energy performance calculation is the energy determination of the U-values of all vertical and horizontal, opaque and transparent structures. The U-value is a function of the thickness and type of each material of the stratification. The thermal conductivity is taken from the UNI 10351 standard for homogeneous materials and the UNI 10355 for heterogeneous ones. In the absence of reliable data, the U-value of opaque and transparent structures can be estimated as a function of the year of construction of the building. When data are collected, U-values can be determined. In Tables 1, 2, 3, 4 the stratifications and the thermal and acoustic performance of the opaque structures are presented.

Table 1 – Stratification of the front vertical facade

Total thickness [cm]			50
Surface mass [kg/m²]			1296
U-Value [W/(m² °C)]			2,02
Rw [dB]			54
Layer	**Thickness [cm]**	**Thermal conductivity [W/(m °C)]**	**Density [kg/m³]**
Gypsum plaster	2	0.35	1200
Dolomite stone	48	1.8	2700

Table 2 – Stratification of the external vertical wall

Total thickness [cm]			44
Surface mass [kg/m²]			560
U-Value [W/(m² °C)]			1.1
Rw [dB]			51
Layer	**Thickness [cm]**	**Thermal conductivity [W/(m °C)]**	**Density [kg/m³]**
Gypsum plaster	2	0.35	1200
Perforated brick	40	1.8	2700
Cement mortar	2	1.4	2000

Table 3 – Stratification of the floor

Total thickness [cm]			32
Surface mass [kg/m²]			354
U-Value [W/(m² °C)]			1.64
Rw [dB]			52
Layer	**Thickness [cm]**	**Thermal conductivity [W/(m °C)]**	**Density [kg/m³]**
Ceramic tiles	2	1	2300
Cement mortar	4	1.4	2000
Floor brick	26	0.74	1185

Table 4 – Stratification of the ceiling

Total thickness [cm]			24
Surface mass [kg/m²]			55
U-Value [W/(m² °C)]			0.20
Rw [dB]			48
Layer	**Thickness [cm]**	**Thermal conductivity [W/(m °C)]**	**Density [kg/m³]**
Wood panel	1.3	0.12	450
BARRIER 100	0.1	0.35	950
Rock wool	1.6	0.035	40
Waterproofing	0.1	0.17	1200
Air	5	0.32	1
Roof tiles	1.5	1	2000

The U-values of the transparent components range from 2.8 W/(m² °C), consisting of aluminum frame without thermal break and double glazing, to 5 W/(m² °C) for the oldest ones, consisting of metallic frame and single glazing.

Then the performance of the building was evaluated. Energetically, the building was modeled on MC4software, whose representation is shown in Fig. 3.

For the acoustic characterization of the unoccupied classrooms, forecast calculations were carried out according to the current technical regulations. These can be determined with the aid of performance and functional criteria. The forecast calculations and assessment methods are described in UNI 11532-2.

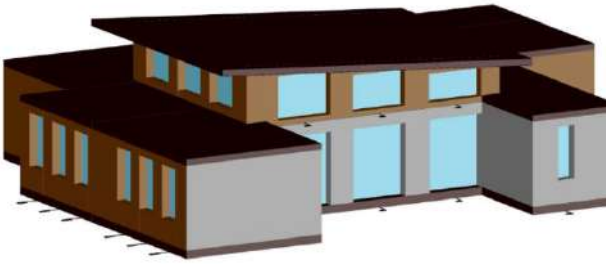

Fig. 3 - 3D model reconstruction for building simulation

The sound insulation performances of typical Italian classrooms were investigated in terms of indoor sound pressure level transmitted through the school façade, reverberation time and sound emitted by technological systems. The estimation of the indoor sound pressure level, L_2, due to the sound from outdoor is obtained with Eq. (1), based on the ISO 12354-3.

$$L2 = L1{,}2m - D2m{,}nT + 10Log(\frac{T}{T0}) \text{ [dB]} \quad (1)$$

where $L_{1,2m}$ is the outdoor sound pressure level 2 m in front of the façade (dB), $D_{2m,nT}$ is the standardized level difference of façade insulation, T is the reverberation time (s) and T_0 is the reference reverberation time (0.5 s).

The prediction method for calculating the Reverberation Time is described in EN 12354-6, while for the $L_{pu,c}$ index the reference standard is the EN 12354-5. Based on the energy efficiency interventions, the acoustic performance of the school has been calculated in parallel as the interventions varied.

A list of intervention has been hypothesized, involving both the building envelope and the thermal plant. Each specific building can require certain interventions. In this work general interventions are proposed, to remain valid in most of the cases. In Table 5 the interventions are listed.

Table 5 – List of interventions

Code	Intervention
GL1	Substitution of glazing
IN1	Insulation of vertical walls
IN2	Insulation of floor and addition of radiant heat floor
L1	Substitution of traditional lighting system with LED-based one
TP1	Substitution of traditional heat generator with heat pump
TP2	Introduction of a photovoltaic plant
TP3	Introduction of mechanic ventilation system

The substitution of glazing (GL1) allows a reduction of the U-value of the transparent components. Triple glass of thickness 5 mm with 12 mm of air gap has been chosen, with an aluminum frame and thermal break. The respective U-value turns out to be in the range 2.8 W/(m² K) and 5 W/(m² K), depending on the size of the window. The insulation of vertical walls (IN1) consists in the addition of a layer of thermal insulation, to increase the thermal resistance. An expanded polystyrene (EPS100) has been chosen, with a thermal conductivity of 0.035 W/m K and a density of 20 kg/m³. A layer of 12 cm, placed externally to the wall stratification, has been provided for the brick-based wall. The front façade instead, has been insulated with 6 cm of the same polystyrene but placed internally, to maintain the aesthetics of the faced stone. The U-value of the two walls becomes 0.2 and 0.5 W/(m² K), respectively.

The intervention on the lighting system (L1) consists in the replacement of traditional lamps with LED ones. The latter reduce the expense of electricity for lighting, considering that a traditional lamp produces 62 lm/W compared to 95 lm/W of a LED one. The number of LED lamps to be installed in each room (n) has been evaluated with the Eq. (2):

$$n = \frac{\Phi_t}{m\, h\, \Phi_l} \quad (2)$$

where Φ_t is the luminous flux of the lamp, m is a coefficient of utilization in function of the shape of the lamp, h is the net height of the room and Φ_l is the luminous flux on the target area.

The substitution of traditional heat generator for heat pump (TP1) increases the heat generation and

distribution efficiency by decreasing the working temperature of the water. In addition, this is a switch from natural gas to electricity. Consequently, the installation of a photovoltaic plant (TP2) is a fundamental step towards exploiting a local renewable energy source to cover the lighting and heat pump energy demand. The last intervention is the mechanical ventilation system (TP3), which improves the indoor air quality of the classrooms. The system is composed of a single machine, to be installed in each room, which provides an air ventilation rate proportional to the CO_2 percentage in the room.
Then the single interventions were combined each other to maximize the energy performance of the building and the energy saving. Different scenarios, later called "packages", have been simulated (Table 6).

Table 6 – Combination of interventions

Package	Building envelope		Lighting		Thermal plant		
P0	-	-	-	-	-	-	-
P1	GL1	-	-	-	-	-	-
P2	-	IN1	-	-	-	-	-
P3	GL1	IN1	-	-	-	-	-
P4	GL1	IN1	IN2	-	TP1	-	-
P5	GL1	IN1	IN2	L1	TP1	TP2	-
P6	GL1	IN1	IN2	L1	TP1	TP2	TP3

3. Results and Discussions

The parameters for the indoor conditions of the rooms were calculated separately for the thermal, acoustic and visual conditions. Energetically, the parameters are the global perfomance index and the CO_2 emitted. The first one, indicated with "$EP_{gl,nren}$" and expressed in kWh/m² yr, considers the amount of energy for the air conditioning over one year, normalized per meter square. This is a useful parameter for comparing different buildings. In addition, the index differentiates the fuel used, applyng a higher coefficient for non-renewable ones and neglecting the share of local energy productions from renewable sources. The CO_2 emitted considers the typology of fuel and its relative emissive factor, while for the electricy from the grid the factors are estimated based on the national energy mix. Results are shown in Fig. 4 and Fig. 5, for the global performance index and the CO_2 emitted, respectively. The reference case is characterized by a global performance index of 407.6 kWh/m2 yr and 38037 kg of CO_2 emissions. Both parameters decrease, while the number of interventions increase. The best scenario allows a reduction of the CO_2 emissions of 88.5 %, 4354 kg, and the global performance index of 85.2 %, 60.3 kWh/m² yr.

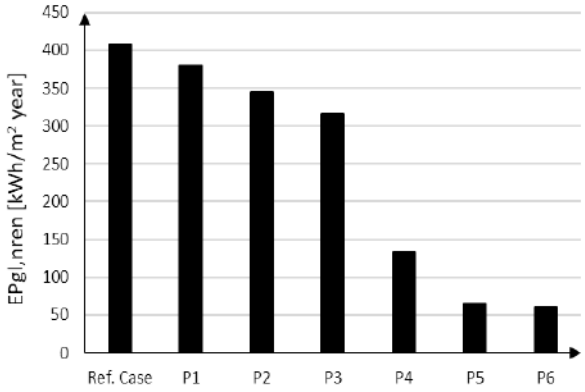

Fig. 4 – Global energy performance index for each scenario

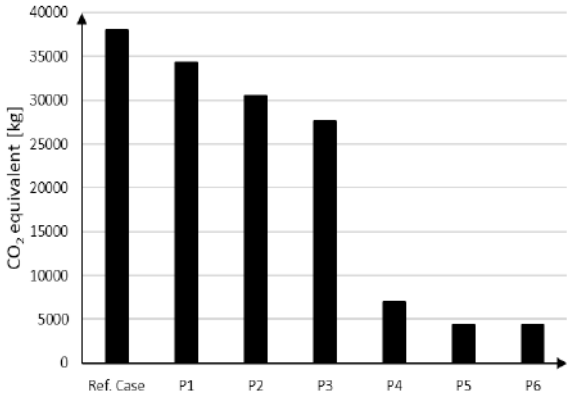

Fig. 5 – CO2 emissions for each scenario

The payback period (PB) was chosen as economic index. It provides information about the time necessary to recover the initial costs, by means of the annual energy saving of the improved scenario. The lower the PB is, the more the scenario becomes a priority. Table 7 summarizes the initial cost and the PB for each scenario analyzed. The best scenario turns out to be the combination of all interventions

except for the mechanical ventilation system, with a payback period of 13 years and 10 months.

Table 7 – Initial cost and payback period of the simulated scenarios

Intervention	Cost [€]	PB [years]
P1	27605	24 years 6 months
P2	37161	14 years 4 months
P3	64766	15 years 6 months
P4	217234	17 years 6 months
P5	283336	13 years 10 months
P6	303336	14 years 9 months

For the acoustic scenarios, results refer to the prediction values of façade sound insulation, to the reverberation time and to the calculated values of unoccupied indoor sound pressure level. Table 8 shows the average values of results of D2m,nT,w and DnT,w calculationsfor all classrooms, respectively. Results concerning corridors, gyms and closets were excluded from this analysis.

Table 8 – Acoustic performance ante and post operam

	Result	Limit value
Ante Operam Average	**D2m,nT,w [dB]**	**D2m,nT,w [dB] D.P.C.M 5/12/97**
	33	48
	DnT,w [dB] Between two classrooms	**DnT,w [dB] high performance UNI 11367**
	45	50
Post Operam Average	**D2m,nT,w [dB]**	**D2m,nT,w D.P.C.M 5/12/97**
	52	48
	DnT,w [dB] Between two classrooms	**DnT,w high performance UNI 11367**
	54	50

Schools with single-glazed windows have typically lower insulation performances. The improvement of acoustic performances is evident because of the better air thickness of the new windows and the insulation of vertical walls.

Fig. 6 shows the average reverberation time calculated in octave bands in all the classrooms.

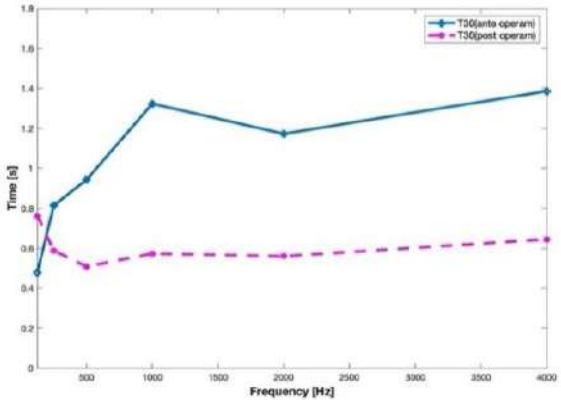

Fig. 6 – Reverberation time in pre (blue) and post operam (pink)

Reverberation time values averaged between the 500 Hz and 1 kHz octave bands, resulting in 1,02 s (ante operam) and 0,59 s (post operam).

The optimal value set by Italian law [16] is a function of the classroom volume. Averaging the volume of the examined classrooms (100 m^3), the optimal average value is 0,47s.

For each façade, the outdoor noise levels ($L_{1,2m}$) were calculated. A weighted outdoor level equal to 60 dB (that is the maximum noise emissions level permitted by the law DCPM 14/11/97) was assumed. Results were compared to the limit values set by Italian legislation or by other relevant national or international references. The analysis of indoor SPL shows that, after the treatments of the façades, the main acoustic problem of the selected classrooms is the indoor reverberation time and it is not the noise from outdoor sources.

A subsequent statistical analysis was performed for the case study. The first correlation model is based on a multivariate regression between the representative thermal parameters and weighted on the non-renewable global energy performance index of the school (Fig. 7). The regression was calculated considering the results obtained by the seven scenarios.

The model is based on the following Eq. 4:

$$Model\ (x,y) = a + bx + cy + dx^2\ exy \qquad (4)$$

where a, b, c, d, e represent the partial regression coefficients (with 95 % confidence bound).

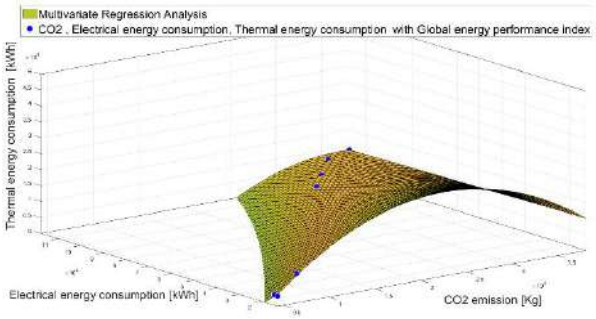

Fig. 7 – Multivariate regression (CO2 emission [kg], electrical energy consumption [kWh], thermal energy consumption [kWh] weighted on the global energy performance index). Several noteworthy results were: R2=0.99, R=0.97, Dfe 2

The second correlation model aims to determine the impact of the acoustic and energetic interventions on processing costs. The model was defined as the weighted sum of the acoustic and thermal resulting parameter. The weights were assigned arbitrarily considering increasing weights to the acoustic performance and subsequently decreasing to the thermal one. The optimization model is represented by the following equation (Eq. 5):

$$opt = b \cdot \%EP_{gl,nren} + a \cdot \%RT + a \cdot \%SA \qquad (5)$$

where a= [0 0.2 0.4 0.6 0.8], b = [1-a], and the $EP_{gl,nren}$, RT(reverberation time (T30)) and SA (sound absorption) are expressed as percentages of saving compared to the reference case.

Results of the polynomial regression are shown in Fig. 8, while Table 9 summarizes the percentage of reduction of the global impact at the various weights.

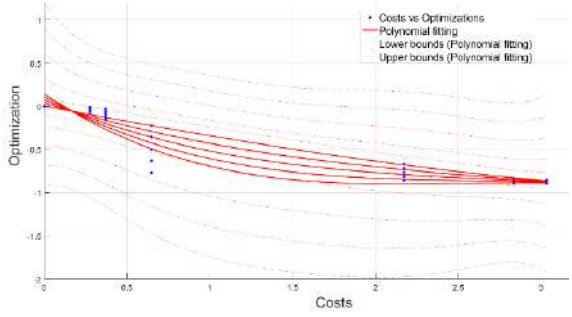

Fig. 8 – Results of linear regression between Thermal-Acoustic optimization and Costs (Euro). Several noteworthy results were: R2=0.85, R=0.70, Dfe 3

Table 9 - Thermal-acoustic optimization vs costs of intervention at the different weights *(w0, w1, w2, w3, w4)*

Intervention	w0	w1	w2	w3	w4
P1	6.9%	5.6%	4.2%	2.8%	1.4%
P2	15.5%	12.3%	9.2%	6.1%	3.0%
P3	22.3%	35.9%	49.5%	63.2%	76.8%
P4	67.1%	71.8%	76.5%	81.1%	85.8%
P5	84.2%	85.4%	86.7%	87.9%	89.2%
P6	85.2%	86.2%	87.3%	88.3%	89.4%

4. Conclusions

This paper proposes a methodology for a combined optimization of the thermal and acoustic performance of a school building. A primary school building located in the center of Italy was chosen as case study. Firstly, the thermal and acoustic performance of the reference building were simulated. Then the proposed methodology was applied. A list of interventions was hypothesized, involving both the building envelope and the thermal and lighting plants. Different interventions were combined in packages, to optimize the overall performance of the building and to find the best scenario. Results show that the optimal scenario, combining all the interventions, reduces the CO_2 emission of 88.5 % (4354 kg, while it is 38037 kg for the reference case) and the global performance index of 85.2 % (60.3 kWh/m² yr, while it is 407.6 kWh/m² yr for the reference case). The acoustic treatment of façades, consisting of the replacement of windows and the insulation of vertical walls, produces good results in the abatement of indoor noise level (19 dB). The average reverberation time is reduced by about 0.40 s, which turns out to be a good result but still not compliant with the optimal time defined by the standards. However, the mechanical ventilation system negatively affects the intelligibility and, in general, the acoustic comfort in a classroom (Serpilli et al., 2022). Consequently, a combined plan between the façade refurbishment and the interior acoustic treatment of the classrooms is recommended. As regard the economic analysis, the best scenario turns out to be the combination of all interventions except for the mechanical ventilation system. This scenario returns the shortest payback period (13 years and 10

months). The combined optimization shows that the best scenario is obtained by weighting the acoustic performance 80 % and the thermal one 20 %, and ensures a global impact reduction of 89.2 %, compared with the reference case. Further research, under analysis, will be proposed extending the presented methodology to other school buildings, to validate the statistical approach and compare the results obtained.

References

Díaz-López, C., A. Serrano-Jiménez, J. Lizana, E. López-García, M. Molina-Huelva, & Á. Barrios-Padura. 2022. "Passive action strategies in schools: A scientific mapping towards eco-efficiency in educational buildings". *Journal of Building Engineering* 45: 103598. doi: https://doi.org/10.1016/j.jobe.2021.103598

D.P.C.M 5/12/97. Determinazione dei requisiti acustici passivi degli edifici.

D.M. 11/01/2017. Criteri Ambientali minimi per l'affidamento di servizi di progettazione e lavori per la nuova costruzione, ristrutturazione e manutenzione di edifici pubblici.

Gamarra, A. R., I. R. Istrate, I. Herrera, C. Lago, J. Lizana, & Y. Lechón. 2018. "Energy and water consumption and carbon footprint of school buildings in hot climate conditions. Results from life cycle assessment". *Journal of Cleaner Production* 195: 1326-1337. doi: https://doi.org/10.1016/j.jclepro.2018.05.153

Li, Q., L. Zhang, L. Zhang, & X. Wu. 2021. „Optimizing energy efficiency and thermal comfort in building green retrofit". *Energy* 237: 121509.
doi: https://doi.org/10.1016/j.energy.2021.121509

MacNaughton, P., X. Cao, J. Buonocore, J. Cedeno-Laurent, J. Spengler, A. Bernstein, & J. Allen. 2018. "Energy savings, emission reductions, and healt co-benefits of the green building movement". *J Expo Sci Environ Epidemiol* 28(307): 12. doi: https://doi.org/10.1038/s41370-017-0014-9

Moazzen, N., T. Ashrafian, Z. Yilmaz, & M. E. Karagüler. 2020. « A multi-criteria approach to affordable energy-efficient retrofit of primary school buildings". *Applied Energy* 268: 115046. https://doi.org/10.1016/j.apenergy.2020.115046

Omar, A. I., N. M. Khattab, &, S. H. A. Aleem. 2022. "Optimal strategy for transition into net-zero energy in educational buildings: A case study in El-Shorouk City, Egypt." *Sustainable Energy Technologies and Assessments* 49: 101701. doi: https://doi.org/10.1016/j.seta.2021.101701

Secchi, S., A. Astolfi, G. Calosso, D. Casini, G. Cellai, F. Scamoni,C. Scrosati & L. Shtrepi. 2017. "Effect of outdoor noise and façade sound insulation on indoor acoustic environment of Italian schools". *Applied Acoustics* 126: 120-130. doi: https://doi.org/10.1016/j.apacoust.2017.05.023

Serpilli, F., S. Di Loreto, V. Lori, & C. Di Perna. 2022. "The impact of mechanical ventilation systems on acoustic quality in school environments. EPD sciences", 52nd A iCARR International Conference. doi: https://doi.org/10.1051/e3sconf/202234305002

UNI 10349, 2016 "Riscaldamento e raffrescamento degli edifici-Dati climatici. Ente Nazionale Italiano Di Normazione

UNI 10351, 2021—Building materials. Thermal conductivities and vapor permeabilities (in Italian: Materiali da costruzione. Conduttività termica e permeabilità al vapore)

UNI 10355, 1994. Walls and floors–Thermal resistance values and calculation method

UNI 11367, 2010. Acustica in edilizia – Classificazione acustica delle unità immobiliari – Procedura di valutazione e verifica in opera.

UNI 11532-1, 2018. Caratterizzazione acustiche interne di ambienti confinati - Metodi di progettazione e tecniche di valutazione – Parte 1: requisiti generali.

UNI 11532-2, 2020. Caratterizzazione acustiche interne di ambienti confinati - Metodi di progettazione e tecniche di valutazione – Parte 2: Settore scolastico.

UNI EN ISO 12354-3, 2017. Building acoustics – Estimation of acoustic performance of buildings from the performance of elements - Part 3: Airborne sound insulation against outdoor sound.

UNI EN ISO 12354-5, 2009. Building acoustics - Estimation of acoustic performance of building from the performance of elements - Part 5: Sounds levels due to the service equipment.

UNI EN ISO 12354-6, 2006. Building acoustics - Estimation of acoustic performance of buildings from the performance of elements - Part 6: Sound absorption in enclosed spaces.

Wang, Y., J. Kuckelkorn, F. Y. Zhao, D. Liu, A. Kirschbaum, & J. L. Zhan. 2015. „Evaluation on classroom thermal comfort and energy performance of passive school building by optimizing HVAC control systems". *Building and Environment* 89: 86-106. doi: https://doi.org/10.1016/j.buildenv.2015.02.023

A Review on the FIVA-Project: Simulation-Assisted Development of Highly-Insulating Vacuum Glass Windows

Ulrich Pont – TU Wien, Austria – ulrich.pont@tuwien.ac.at
Peter Schober – Austrian Forest Products Research Society, Austria – p.schober@holzforschung.at
Magdalena Wölzl – TU Wien, Austria – Magdalena.woelzl@tuwien.ac.at
Matthias Schuss – TU Wien, Austria – Matthias.schuss@tuwien.ac.at
Jakob Haberl – Austrian Forest Products Research Society, Austria – j.haberl@holzforschung.at

Abstract

This contribution provides a review on research and development activities that have been conducted in the field of highly-insulating windows with vacuum glass. In a joint effort with the window-producing industry, different novel solutions for vacuumglass-equipped windows have been studied. Thereby, different methodological approaches have been deployed, including the construction of technology demonstrators, performance measurements on laboratory test sites, and numeric thermal bridge simulation. As a result, the project consortium succeeded in the development, construction, and exhibition to relevant stakeholders in the industry of four, innovative window prototypes. These windows not only employ vacuum glass products, but also in part provide new operation kinematics, motorization, and the implementation of automated ventilation positions. Moreover, the U-values of the windows could be approximated to be around or below 0.70 $W.m^{-2}.K^{-1}$ (i.e., U_{Win}-value) at pane thicknesses of less than a centimeter. The windows include turn windows to inside and outside, as well as a swing-operation window, and a window utilizing an offset- and slide-operation mechanism without visible railings. The contribution not only displays the final prototypes, but also highlights the methods and provides an outlook for future development in this area.

1. Introduction

1.1 Scope of the FIVA Project, Observations and Prerequisites

The present contribution highlights the methodology and results of a joint research effort conducted together with stakeholders of the window producing industry. The ultimate goal of this project, which was named FIVA (*Fensterprototypen mit integriertem Vakuumglas* – in English: Window prototypes that employ vacuum glass) was the development of vacuum-glazing-equipped windows that provide both a very good (thermal) insulating performance and a high degree of innovation in architectural appearance and operation. Moreover, that the resulting prototypes should fully prove their functionality, or in other words, a high TRL (technology readiness level) of the envisioned prototypes was an additional planned goal of the project.

The project's outline was built on and started based on a set of observations (O) and prerequisites (P):

O(bservation)1: Although vacuum glass products finally arrived on the market after intensive research and development efforts by both industry and academia lasting close to a century (Zoller, 1913), there was little to no public and relevant research available about the utilization of such products in contemporary and past window constructions. **O2:** Companies in the window-producing sector agreed about the high potential of vacuum glass for window constructions, however, most companies were reluctant to pioneer vacuum-glazed window constructions. Moreover, there was little knowledge about the required changes to existing window/frame constructions amongst the relevant stakeholders. Furthermore, resentment against vacuum glass pertaining to the durability of the vacuum (and thus its thermal performance) in the products was reckoned. Given that, until 2020, vacuum glass products were not produced in

Europe, but majorly in South-East Asia, another threat was seen in the long delivery times in the case of the need for glass replacement. Moreover, while there have been multiple producers of multi-pane insulation glass, the number of vacuum glass producers was (and still is) limited. **O3:** Stakeholders in the glass-producing industry showed a certain ambivalence toward vacuum glass products. This was majorly because vacuum glass products show similar thermal performances to high-end triple glazing, but do feature one glass pane less (which would potentially have negative effects on feasibility and profit for glass producers). **O4:** Despite major efforts toward improvement of the performance of transparent envelope components, windows are still considered the weak spot in thermal envelopes, and are even considered to be responsible for a major share of building-related energy loss through the envelope. However, current highly-insulating windows are majorly triple-glazing windows coming with large system thickness and correspondingly heavy weight of the overall construction. Vacuum glass is considered to disrupt this situation.

Amongst the prerequisites for the FIVA project were the following: **P(requisite)1:** basic knowledge about the durability and thermal performance of different vacuum glass products was required. This was fulfilled due to the authors' previous research efforts into vacuum glass within the VIG-SYS-RENO project (Pont et al., 2018a). In this exploratory product, not only a wide range of tests pertaining to mechanics, thermal performance and acoustical performance of different glass products was conducted, but also basic challenges pertaining to the integration of vacuum glass into existing and new window frames were addressed. **P2:** A clear objective is required in the development process. While the integration of vacuum glass in existing (historically relevant) windows often needs to consider the upkeep of the appearance of the window (e.g., Kastenfenster / casement windows, compare (Pont et al., 2018b), new windows can be designed toward performance and operation optimization. Moreover, the specifics of vacuum glass (e.g., problematic thermal bridge along the edge seal) determine construction principles. As such, it was decided to design the windows from scratch based on the specific requirements of the vacuum glass, rather than to adapt existing window constructions. **P3:** Subsequently, a set of innovative early-stage window designs (that consider the specifics of vacuum glass) was required. Such innovative and, in part, disruptive approaches to new windows were the result of another preliminary and exploratory research effort by the authors named MOTIVE (Pont et al., 2018c). **P4:** To start and successfully conduct the project, a strong consortium of academic partners and stakeholders from the relevant branches of industry was required who were open to new ideas and agreed upon close collaboration. This consortium consisted in the end of two academic and eight industrial partners (5 window-producing companies, 3 producers of different window constituents, namely fittings, seals, and vacuum glass). **P5:** To be able to explore the space of potential, innovative, high-performing vacuum glass windows, all partners were required to bring in their specific expertise and instruments. Simulation as a method specifically was deployed in the fields of operation kinematics of the innovative windows, and thermal performance assessment. For the latter, numeric thermal bridge simulation was deployed as instrument of choice.

1.2 Vacuum-Glazing Products

To understand the challenges connected with the integration of vacuum glass in windows, one needs to understand the technical specifications of vacuum glass. Vacuum glass products are regularly constituted of two planar, parallel glass panes. Between the glass panes, an interstitial space of rather small dimension (less than a millimeter) houses a grid of distance pillars. The axis-distance between the pillars is regularly between 20 and 40 mm. To close the interstitial space against the surroundings, a vacuum-tight edge seal is set up along the perimeter of both glass panes. Via an opening in one of glass panes, the interstitial space is then evacuated (leading to a high vacuum). The distance pillars mentioned maintain the parallel position of the glass panes, as otherwise the panes would be pushed together by the surrounding air pressure. Another important element is the so-

called getter. This is a highly reactive surface that filters/binds the remaining particles in the interstitial space. Due to the vacuum, heat transfer processes that require media are widely eliminated in the interstitial space (i.e., conduction and convection). Thereby, already rather slim systems (vacuum glass between 6 and 8 millimeters) provide excellent thermal insulation. However, the glass-edge seal, as well as the distance pillars, literally remain as connecting thermal bridges between the two glass panes and need to be considered in designing windows with vacuum glass. In a previous research effort (Pont & Mahdavi, 2017), the heat loss via conduction through the pillars was identified as noticeable but very small (majorly due to their limited physical dimensions). In contrast, the tight edge seal was identified as a major thermal bridge and needs to be covered / insulated as well as possible in window constructions. A sufficient glass edge-cover length can ensure this. Fig. 1 illustrates a schematic section through a (generic) vacuum glass product.

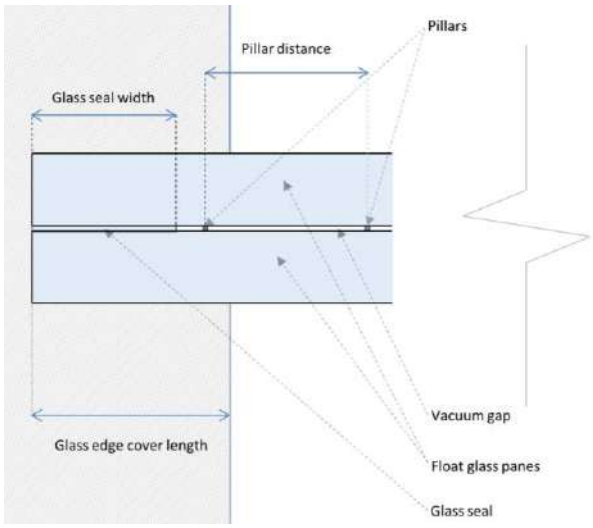

Fig. 1 – Schematic section through a generic vacuum glass product, including the relevant terminology (illustration by the authors)

2. Methodology

2.1 General R&D Efforts Within the Project

The development of new windows requires considerations from different backgrounds. Aspects such as the statics, weight, operation, acoustics, thermal performance, material, form and construction of frames, fittings, glass, seals, and many more need to be considered. To comply with these in part harsh requirements, the following strategy was deployed: in a first attempt, the major aspects to be worked upon were identified, including shifting certain aspects to post-project phases (as final product development done by the industry). Such aspects included production aspects, or the selection of the final components. Rather, the project team decided to work upon three major aspects: (a) The conception of specific window prototypes as such, which includes the operation/movement patterns and the principle architectural appearance. (b) The integration of motorized fittings for the specific window, preferably to be integrated in the fixed window frame (not into the moving part of the window. (c) The integration of the vacuum glass in the moveable wing of each of the windows under consideration of specific requirements of the vacuum glass, such as a well-dimensioned glass-edge seal cover. After setting up a decision fine-tuning of these aspects, an iterative development process started. Thereby, for each of the window prototypes, one of the industrial partners assumed responsibility for development, thus constructing the early prototypes and movement mock-ups, and conducting communicating/coordinating of geometry and semantic data means of their prototype with the consortium. The scientific partners, together with the industrial partners, were continuously developing and designing the corresponding windows. Thereby, one of their major responsibilities was to deliver proof of concept and proof of functionality results. A lot of iterative optimization characterized this later stage of the development. This workflow worked well and offered a lot of productive exploration of the space of possible solutions, mostly due to the many brainstorming and sketching meetings that were set up regularly.

2.2 Simulation and Thermal Performance Assessment

As already mentioned, one of the key tasks of the scientific partners in the project (namely the authors of this contribution) was to continuously assess the impact of design modifications on the thermal performance. To this end, we deployed

numeric thermal bridge simulation as matter of choice in assessing the critical thermal bridge situations along the window frames and highly conductive fitting parts. The tool we used was Antherm v. 10 (Antherm n.d.).

Moreover, the overall performance of the window in view of thermal transmittance was evaluated. Due to the non-off-the-shelf character of the windows, the equations from corresponding standards (i.e., EN ISO 10077 Parts 1 and 2 (EN10077 2017)) were found to be inappropriate for the purposes of vacuum glass windows, and thus slightly adapted. This majorly affected the U_{Win}- equation, in which parts of the frame geometry that were supported with the highly-insulating vacuum glass were considered specific parts of reduced heat transfer in contrast to the otherwise rather weak performance of the frame.

Tables 1 and 2 illustrate both assumed conductivities and boundary conditions that were used for thermal performance assessment. Note that for encapsulated air and the vacuum gap replacement, Lambda-Values were considered, and that the colors in the table correspond with the materials in the illustrations in the Results section.

2.3 Subjective Assessment of Window Prototypes

To ensure that all relevant stakeholders accept new window constructions, it is not sufficient to just promise and provide excellent performance values. Rather, relevant stakeholders need to be convinced about aspects such as aesthetics, contemporaneity, innovation, feasibility of the construction, aspects of mounting, aspects of operation, and general acceptance amongst customers. To collect the opinion of domain experts and non-experts, we developed a short and easy-to-use questionnaire that encompassed these categories and allowed them to be graded (by the Austrian school grading system, starting from excellent to insufficient). Additionally, windows could be ranked by preference in the questionnaire, and additional comments could be written in the questionnaire.

Table 1 – Assumed thermal conductivities of materials and replace materials (vacuum gap, encapsulated air)

Color	Material	Conductivity [$W.m^{-1}.K^{-1}$]
	Timber / Wood	0.11
	Steel	50
	Aluminium	200
	Compac Foam	0.031
	Insulation	0.041
	Seal(ing)	0.3
	Seal encapsuled	0.04
	Glass	1
	Plastic	0.2
	Masonry	0.45
	Purenite	0.096
	Plaster	0.7
	Silicone	0.35
	Vacuum	0.00000975
	Encapsulated Air	0.07

Table 2 – Boundary condition settings.

Colour	Boundary Condition	Rs (H,T) Value [$m^2.K.W^{-1}$]
	Inside	0.13
	Outside	0.04

3. Results

3.1 Developed Window Prototypes

In the project, four different window prototypes were worked upon in depth and finally realized as full-scale functional mock-ups. These were:

- Turn window opening to inside (A): while adopting the traditional, established operation scheme of central Europe, the window provides a glass-inline-with-outer-perimeter appearance. Integration of external shading is easy, and the window operation is widely familiar to users.

- Turn window opening to outside (B): while not common in Central Europe anymore, windows that turn to the outside are familiar in Scandinavia. B comes with a rather reduced and thus aesthetically pleasing appearance.
- Swing window (C): adopting the principles of garage doors, this window provides a rather convenient way of storing the open wing above occupants' heads and thus allows spatial flexibility. The window was engineered to possess maximum flexibility and as few moving parts as possible.
- (Offset and) Sliding window (D): this window allows an offset movement to the outside for the purpose of ventilation. From this position, the window can be slid to one side on telescope railings, which remain totally invisible when the window is in its closed state.

All of the windows were equipped with electrical actuators, so that motorized operation could be realized. Thereby, automated operation in most cases covered the shift from fully closed to a ventilation position, while the classical full opening was still to be carried out manually (however, this has to be understood as a suggestion, both fully manual and fully motorized operation is possible in all four of the prototypes).

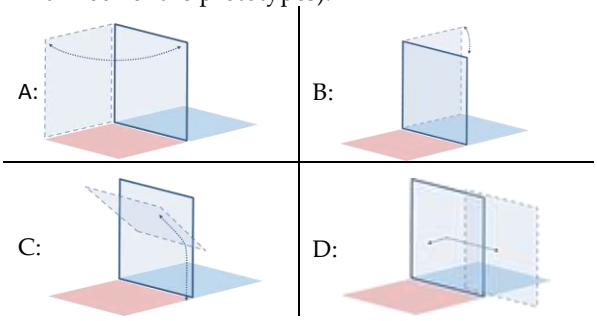

Fig. 2 – Opening/operation schemes of prototype A – D.

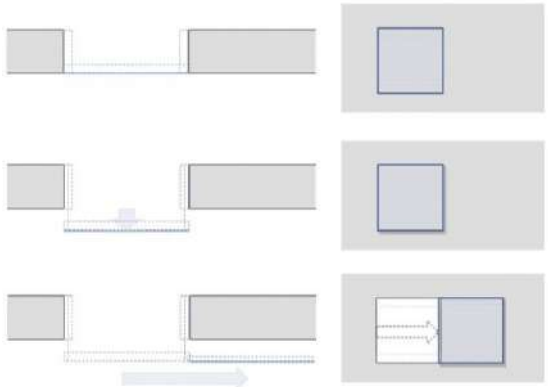

Fig. 3 – Conceptual view and section of prototype D

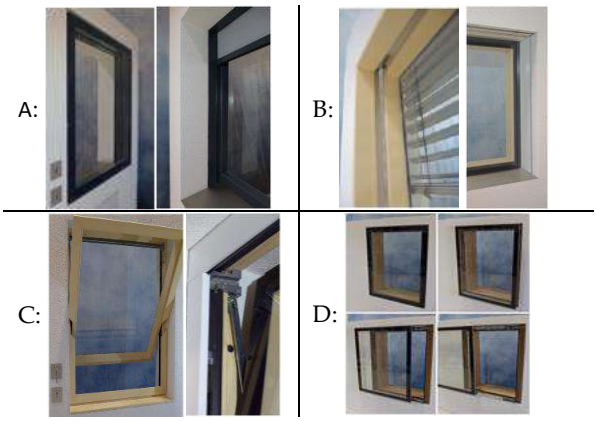

Fig. 4 – Opening/operation schemes of prototype A – D.

Fig. 2 illustrates the opening scheme of all four windows, while Fig. 3 provides some additional insight into prototype D. Fig. 4 shows photos of the finalized prototypes.

3.2 Performance Aspects of Developed Windows

A full documentation of the conducted thermal performance simulation efforts can be found in (Wölzl, 2019) and (Pont et al., 2020a). Exemplarily, Tables 3 to 6 illustrate some Key Performance Indicators (KPIs) of both the windows and the most crucial building construction joint, which is the lower connection between wall and window. The presented KPIs encompass U_{Win}-value, as well as f_{Rsi}-values and minimum surface temperature $\Theta_{min,i}$. Note that the latter KPIs have been simulated assuming steady-state boundary temperatures (external temperature of -10 °C, internal temperature 20 °C). The tables always provide the same structure: KPIs on top, followed by a false color image denoting the temperature distribution within the mentioned construction joint, and section through the same joint highlighting the assumed materials (compare Table 1 and 2).

Table 3 – Thermal Simulation of Window A

Turn window opening to inside (A)
f_{Rsi} 0.74 [-] ǀ $\theta_{min,i}$ 12.23 °C ǀ U_{win} 0.78 W.m^{-2}.K^{-1}

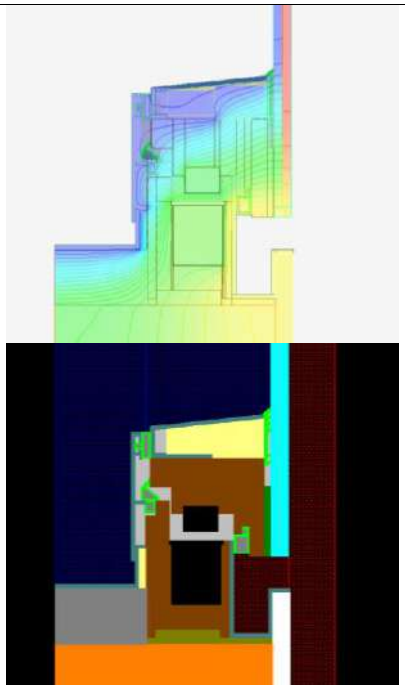

Table 4 – Thermal Simulation of Window B

Turn window opening to outside (B)
f_{Rsi} 0.77 [-] ǀ $\theta_{min,i}$ 13.05 °C ǀ U_{win} 0.72 W.m^{-2}.K^{-1}

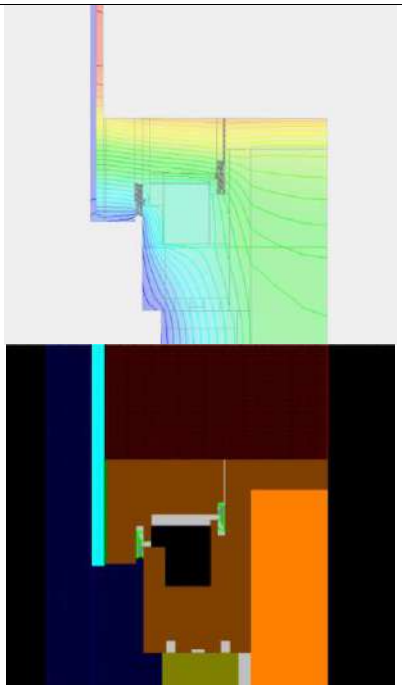

Table 5 – Thermal Simulation of Window C

Swing window (C)
f_{Rsi} 0.75 [-] ǀ $\theta_{min,i}$ 12.55 °C ǀ U_{win} 0.68 W.m^{-2}.K^{-1}

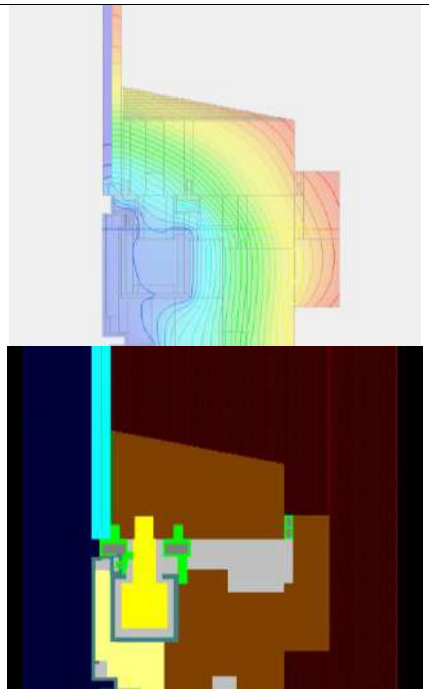

Table 6 – Thermal Simulation of Window D

Sliding window (D)
f_{Rsi} 0.76 [-] ǀ $\theta_{min,i}$ 12.07 °C ǀ U_{win} 0.64 W.m^{-2}.K^{-1}

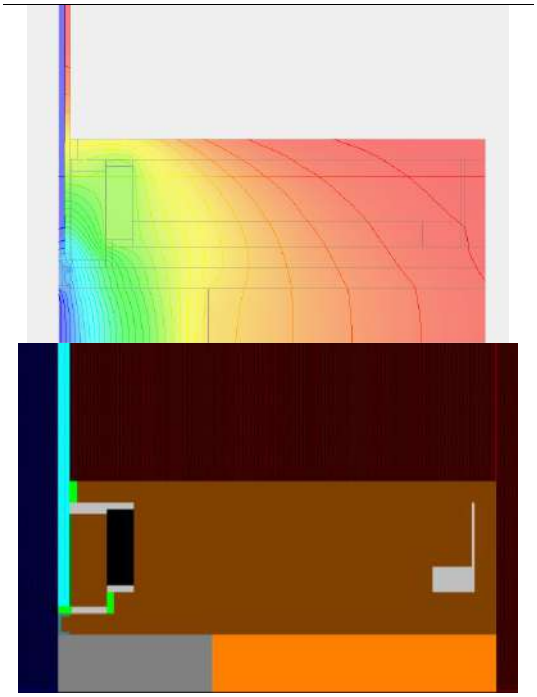

Note that for all of these window prototypes, a vacuum glass pane of 8.15 mm thickness was assumed (U_g-value 0.7 $W.m^{-2}.K^{-1}$). The presented KPIs of all of the window prototypes well surpassed the minimum criteria for condensation risk assessment (which is a threshold f_{Rsi}-value of 0.71 following typical standards for opaque building constructions). Moreover, the U_{Win}-values that were reached are in the range of heavyduty triple glazing windows. Needless to say, the window constructions presented are featherweights in comparison with the triple-glazing windows mentioned.

3.3 Subjective Evaluation of Window Prototypes

The questionnaire-based evaluation of the prototypes was conducted during the FTT2020 (Fenster Türen Treff, 2020) in Salzburg, which is a trade fair and knowledge exchange event of the domain-relevant industry. All four window prototypes were exhibited there, and a talk about the project was held (Pont et al., 2020b). Fig. 5 shows the window prototypes in the exhibition. The grading results of the questionnaire are summarized in Table 7. Pertaining to the question as to which of the windows was preferred by the respondents, results showed that window D was favored, closely followed by A. This can be considered interesting, because these windows are fundamentally different: window D provides a disruptive new design with a very innovative and aesthetically attractive appearance and operation, and is thus far from what we see in most contemporary buildings. Prototype A, in contrast, is the contemporary adaptation of a well-established traditional window operation scheme. The rating by the domain experts thus hints at the fact that both tracks - disruptive change and continuing traditional technologies – need to be followed up.

Fig. 5 – Window prototypes exhibited during FTT2020 (Salzburg)

Table 7 – Domain experts' evaluation of the window prototypes (Austrian school grades: 1… excellent, 2… good, 3…average, 4… sufficient, 5…insufficient)

Criterium	A	B	C	D
Esthetics	1.7	2	2.4	1.2
Contemporaneity	1.8	2,4	2.6	1.6
Degree of innovation	2.1	2	2.2	1.2
Feasibility of the construction	1.8	2.4	2.6	2.1
Aspects of mounting	1.8	2.4	2.2	2.4
Aspects of operation	1.7	2.4	2.5	1.7
Acceptance amongst customers	1.9	2.4	3	1.8
Average	1.8	2.3	2.5	1.7

4. Conclusion and Future Research

The present contribution illustrated the outcome of a collaborative R&D effort which emphasized a set of interesting aspects:

- Shared projects between the building industry and academia can lead to disruptive developments in the AEC-context. Given the Paris climate goals and the rather slow innovation processes in the built environment, we are in urgent need of such fast-forward developments.
- The design of vacuum-glass-equipped windows should be carried out from scratch, even if traditional window operation concepts such as "turn-to-inside" are deployed. It is not feasible to simply take existing frame constructions and replace multi-pane insulation glass with vacuum glass, as such constructions cannot regularly fulfil the specific requirements of vacuum glass, such as a sufficient glass edge-cover length.
- While the window wing should be constructed around the vacuum glass, it seems wise to construct the fixed part of the window frame around the fittings system. As such, motorization of contemporary windows is facilitated, as no electricity needs to be interfaced to the moving part.

- Vacuum glass windows are capable of providing a very good performance in terms of thermal insulation at very slim (and thus lightweight) system thickness.

Needless to say, the prototypes presented are not yet available on the market and should be understood as "showcase" suggestions. Future R&D efforts shall address the development of specific parts (motorization and fittings) given that the elements used in FIVA were individually crafted. To become feasible, the motorization shall employ standard components and products. Moreover, the impact of vacuum glass and vacuum glass windows both on normative guidelines on windows and modeling in other (whole building) simulation tools has yet to be worked upon.

Acknowledgement

The project FIVA was generously funded by the Austrian Research Promotion Agency FFG (project-no. 867352). A set of partners contributed to the project, including domain experts of the window-producing companies Gaulhofer, Internorm, Katzbeck, Svoboda and Wick. Likewise, experts from the components industry contributed to the project, including Maco (fittings), ieb Eisele (sealings) and AGC Interpane (vacuum glass).

References

AnTherm. n.d. http://antherm.at/antherm/Waermebruecken.htm

CEN. 2017. *EN ISO 10077. 2017. EN ISO 10077-1:2017 Thermal performance of windows, doors and shutters — Calculation of thermal transmittance — Part 1: General; EN ISO 10077-2 Thermal performance of windows, doors and shutters — Calculation of thermal transmittance — Part 2: Numerical method for frames; International Standardization Institute*.

Pont, U., and A. Mahdavi. 2017. "A comparison of the performance of two- and three-dimensional thermal bridge assessment for typical construction joints"; in: "Building Simulation Applications Proceedings", bu.press, 3. (2017), ISSN: 2531-6702; Paper ID 75, 8 pages.

Pont, U., E. Heiduk, P. Schober, F. Romierer, F. Dolezal, O. Proskurnina, M. Schuss, C. Sustr, H. Hohenstein, and A. Mahdavi. 2018a. „Sondierung von Fenstersystemen mit innovativen Gläsern, speziell Vakuum-Isoliergläsern, zur Gebäudesanierung", Berichte aus Energie- und Umweltforschung 33/2018. Available via www.nachhaltigwirtschaften.at (last visit: March 2022)

Pont, U., M. Schuss, P. Schober, P., and A. Mahdavi. 2018b. „Conception and Assessment of Technical Solutions for the Application of Vacuum Glazing in Contemporary Window Constructions" in: "Proceedings of BauSim2018", A. Wagner, P. von Both et al. (ed.); (2018), Paper ID 1107, 8 pages.

Pont, U., M. Schuss, A. Mahdavi, P. Schober, K. Hauer, and C. Lux. 2018c. „MOTIVE Modellierung, Optimierung und technische Integration von Vakuumglas-Elementen." Berichte aus Energie- und Umweltforschung 24/2018. Available via www.nachhaltigwirtschaften.at (last visit: March 2022)

Pont, U., M. Wölzl, M. Schuss, A. Mahdavi, P. Schober, J. Haberl, and C. Lux. 2020a. „Fensterprototypen mit integriertem Vakuumglas – FIVA". Berichte aus Energie- und Umweltforschung 47/2020. Available via www.nachhaltigwirtschaften.at (last visit: March 2022)

Pont, U., P. Schober, M. Wölzl, M. Schuss, and J. Haberl. 2020b. „Das Morgenfenster - Entwicklung smarter und energieeffizienter Fensterprototypen" in: "Happy Birthday - Fenster-Türen-Treff 2020 - Tagungsband 5.-6. März 2020 Salzburg", Holzforschung Austria (ed.); (2020), ISBN: 978-3-9504488-8; 30 - 38.

Wölzl, M. 2019. "Fensterkonstruktionen mit Vakuumglas: Simulationsbasierte Weiterentwicklung von innovativen Fensterkonstruktionen.", Master Thesis, TU Wien.

Zoller, A. 1913. „Hohle Glasscheibe". Patent-Nummer: No 387655., see: shorturl.at/lmEHO

Influence of Sound-Absorbing Ceiling on the Reverberation Time. Comparison Between Software and Calculation Method EN 12354-6

Nicola Granzotto – Free University of Bozen-Bolzano, Italy – nicolagranzotto74@gmail.com
Paolo Ruggeri – University IUAV of Venice, Italy – pruggeri@iuav.it
Fabio Peron – University IUAV of Venice, Italy – fperon@iuav.it
Marco Caniato – Free University of Bozen-Bolzano, Italy – marco.caniato@unibz.it
Andrea Gasparella – Free University of Bozen-Bolzano, Italy – andrea.gasparella@unibz.it

Abstract

The correct acoustic design of rooms such as classrooms, conference rooms and offices is of fundamental importance to ensure high speech intelligibility and to contain internal noise levels. The use of sound-absorbing ceilings alone is not always sufficient to guarantee adequate comfort, as the reflections between parallel walls could introduce unwanted phenomena such as flutter echo or the accentuation of modal resonances. One more issue is related to the use of Sabine or Eyring models, which could lead to an underestimation of the reverberation times. This article compares the reverberation time measured and simulated in two small rooms with (i) Sabine and Eyring models, (ii) two commercial simulation software and (iii) the EN 12354-6 standard method valid for rooms, with absorption not homogeneously distributed between the surfaces.

1. Introduction

Correct room acoustic design is of fundamental importance to increase comfort and speech intelligibility.

Many studies have been carried out regarding room acoustics optimization (Farina et al., 1998; Meissner, 2017; Nowoświat et al., 2016 and 2022; Prato et al., 2016; Tronchin et al., 2016, 2021a, 2021b, 2021c and 2022) and regarding acoustic building materials (Fabbri et al., 2021). The tools available to designers are simple equations, such as those of Sabine and Eyring or the EN 12354-6 standard or dedicated calculation software.

The Sabine and Eyring formulations are reliable under the following conditions:

1) diffuse sound field;
2) average absorption coefficient of the room less than 0.2;
3) homogeneous absorption.

Often in rooms such as offices, only the sound-absorbing ceiling is used both for cost and positioning reasons. In this case, the absorption is not homogeneous, since it is concentrated in just one part of the room. Thus, the Sabine and Eyring models may not provide reliable results.

To design rooms with non-homogeneous absorption, the calculation method described in EN 12354-6 Annex D can be used.

A further problem concerns the input data in the calculation software. The measurement of the absorption coefficient in the reverberation room, according to the ISO 354 standard, assumes a perfectly diffused sound field and the use of the Sabine formulation. Unfortunately, this is not possible in real laboratories, since these conditions are only ideal. Another problem of the measurement in a reverberant room is the presence of diffusers, which make the volume of the room lower than that actually used in the Sabine formula, with a consequent overestimation of the results (Scrosati et al., 2019).

On the other hand, methods such as normal incidence measurements according to ISO 10534-2 cannot be directly correlated with measurements carried out in a diffuse field in a reverberation room (Di Bella et al., 2019). The uncertainty of measurement of the absorption coefficient according to ISO 354 standard is also high (Scrosati et al., 2019 and 2020).

This paper presents measurements made on two small, unfurnished offices with sound-absorbing ceilings and simulations carried out with simplified

formulations (Sabine, Eyring), EN 12354-6 calculation method and two dedicated room acoustic software packages.

2. Calculation Models

For the acoustic simulations the following models were compared:

1) equations of Sabine and Eyring;
2) calculation method EN 12354-6;
3) two different room acoustic simulation software.

The Sabine formula is:

$$T_{Sabine} = \frac{55.3}{c_0}\frac{V}{A} \quad (1)$$

The equivalent absorption area A, considering only flat surfaces and not objects, is calculated with Eq. (2):

$$A = \sum_i \alpha_i S_i \quad (2)$$

Eyring equation is:

$$T_{Eyring} = \frac{55.3}{c_0}\frac{V}{-Sln(1-\alpha_m)} \quad (3)$$

The calculation method of EN 12354-6 (Annex D) for rooms with non-homogeneous absorption considers the following reverberation time (without the absorption of objects):

$$T_{est} = \frac{55.3V}{4c_0}\left(\frac{1}{A_x^*}+\frac{1}{A_y^*}+\frac{1}{A_z^*}+\frac{1}{A}\right) \geq T_{Sabine} \qquad f \geq f_t = \frac{8.7c_0}{V^{1/3}} \quad (4)$$

$$T_{est} = \frac{55.3}{c_0}\frac{V}{A_{xyzd}^*} \qquad f < f_t = \frac{8.7c_0}{V^{1/3}} \quad (5)$$

A^*_x, A^*_y, A^*_z, A^*_d are the effective sound absorption area for each sound field, while A^*_{xyzd} is the effective sound absorption area for the total field for low frequency ($f < f_t$).

The commercial software used are based on ray-tracing (A) and pyramid-tracing (B) techniques.

3. Case Studies

Two unfurnished rooms with an access floor with plan surfaces of 16.3 m² (Room 1) and 32.9 m² (Room 2) were examined. The walls are made of gypsum board and plastered concrete, the ceiling is made with square rock wool panels, with dimensions of 600 mm x 600 mm. The windows equal in length to the façade are positioned 108 cm from the floor and have a height of 118 cm. The dimensions of the rooms are shown in Figs. 1, 2, 3 and 4.

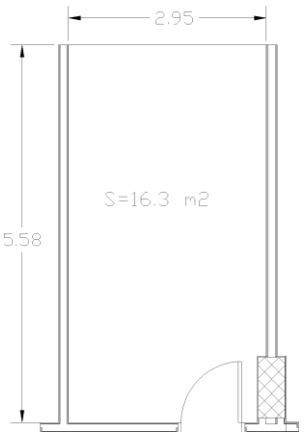

Fig. 1 – Room 1 plan

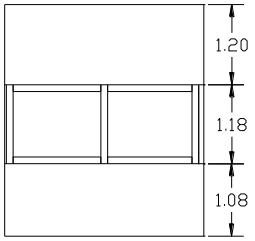

Fig. 2 – Room 1 Façade

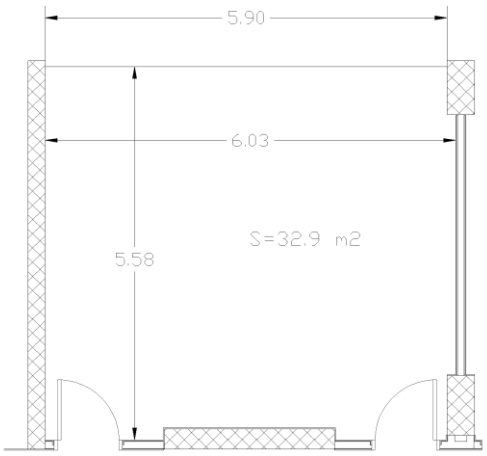

Fig. 3 – Room 2 plan

Fig. 4 – Room 2 Façade

The geometric characteristics of the rooms are shown in Table 1. The mean free path (MFP) calculated as Sabine, or obtained with the software, is also reported. It can be noted that the MFP obtained with the software is very similar to the ones obtained using the Sabine model.

Table 1 – Mean free path

	Room 1	**Room 2**
V	56.2	113.5
S	91.5	147.2
MFP=4V/S	2.460	3.084
MFP-Software A	2.480	3.100
MFP-Software B	2.470	3.090

4. Reverberation Time Measurements

Reverberation time measurements T_{20} on the two offices (Room 1 and Room 2) were carried out to verify the reliability of the different calculation methods. Measurements were made with the interrupted noise method according to ISO 3382-2 standard.
In Room 1, one sound source position and three microphone positions were used, while in Room 2, two source positions and three microphone positions were used. Omnidirectional sound source was placed at 1.7 m height and a microphone was placed at 1.5 m height. Measurements were repeated twice for each source-microphone combination.
The results obtained are shown in Fig. 5.

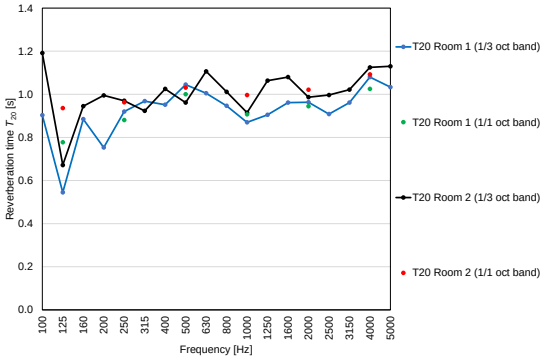

Fig. 5 – Measured reverberation time T_{20} for Room 1 and Room 2 in 1/3 and 1/1 octave bands

It can be noted that the volume of room 1 is about half of the one of room 2, but the reverberation time is only slightly lower.

5. Acoustic Simulations

To verify the reliability of the different calculation methods, simulations of the reverberation time T_{20} were performed. 3D models were realized with two different types of room acoustic software, one based on ray-tracing and the other based on pyramid tracing. Models are reported in Figs. 6 - 9.

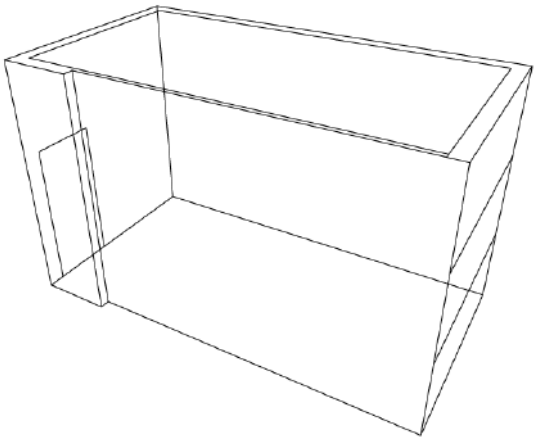

Fig. 6 – Room 1 - 3D simulation model - Software A

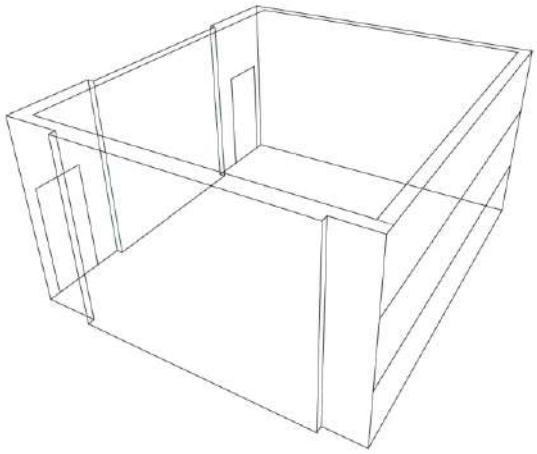

Fig. 7 – Room 2 - 3D simulation model - Software A

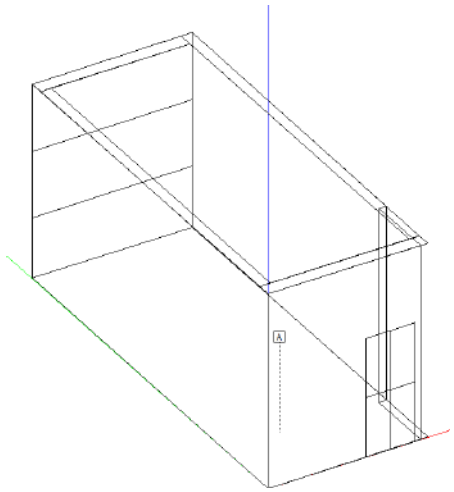

Fig. 8 – Room 1 - 3D simulation model - Software B

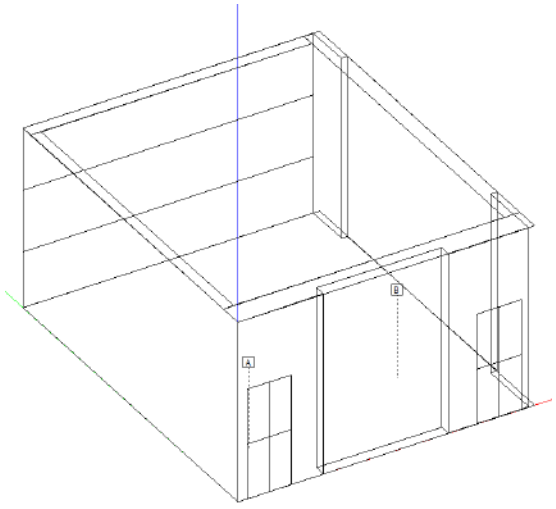

Fig. 9 – Room 2 - 3D simulation model - Software B

The acoustic absorption coefficients used are reported in Table 2.

Table 2 – Acoustic absorption coefficient

	125	250	500	1000	2000	4000
Ceiling	0.45	0.90	1.00	0.85	0.95	0.95
Plastered wall	0.02	0.03	0.03	0.04	0.05	0.07
Access floor	0.20	0.15	0.10	0.10	0.05	0.10
Gypsum board wall	0.15	0.10	0.06	0.04	0.04	0.05
Window	0.18	0.06	0.04	0.03	0.02	0.02
Door	0.14	0.10	0.06	0.08	0.10	0.10

6. Results and Discussion

The reverberation times obtained are shown in Fig. 10 (Room 1) and in Fig. 11 (Room 2). Some noise maps are shown in Fig. 12 (Room 1 - software B) and Fig. 13 (Room 2 - software B).

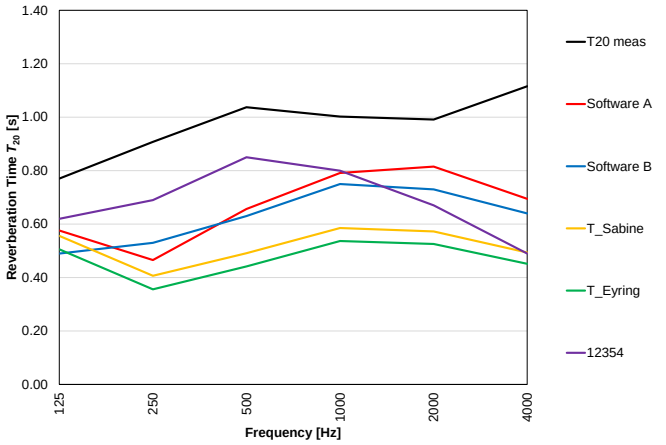

Fig. 10 – Measured and simulated reverberation time T_{20} (Room 1)

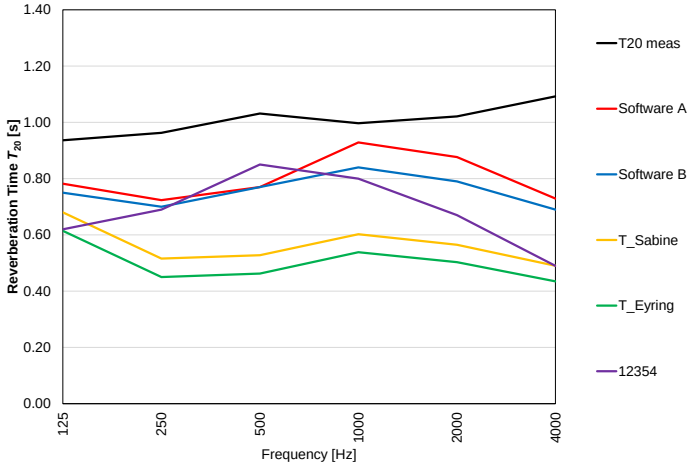

Fig. 11 – Measured and simulated reverberation time T_{20} (Room 2)

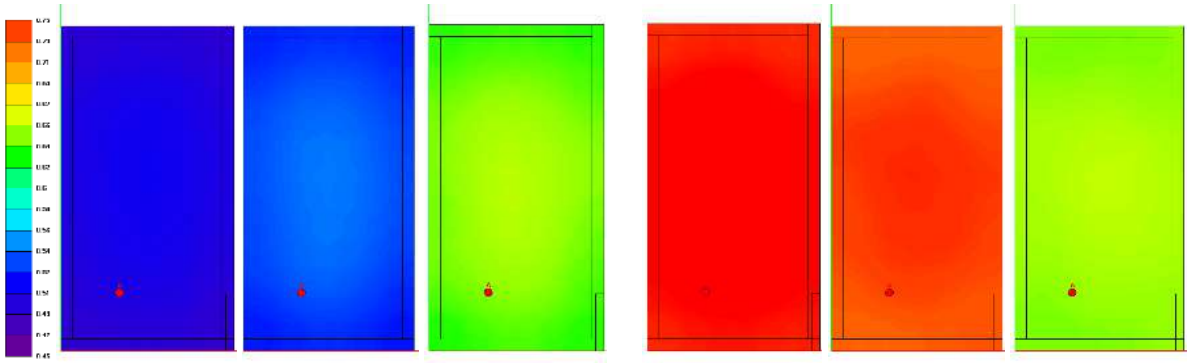

Fig. 12 – Reverberation time T_{20} simulation software B – Room 1 (125 Hz - 4000 Hz)

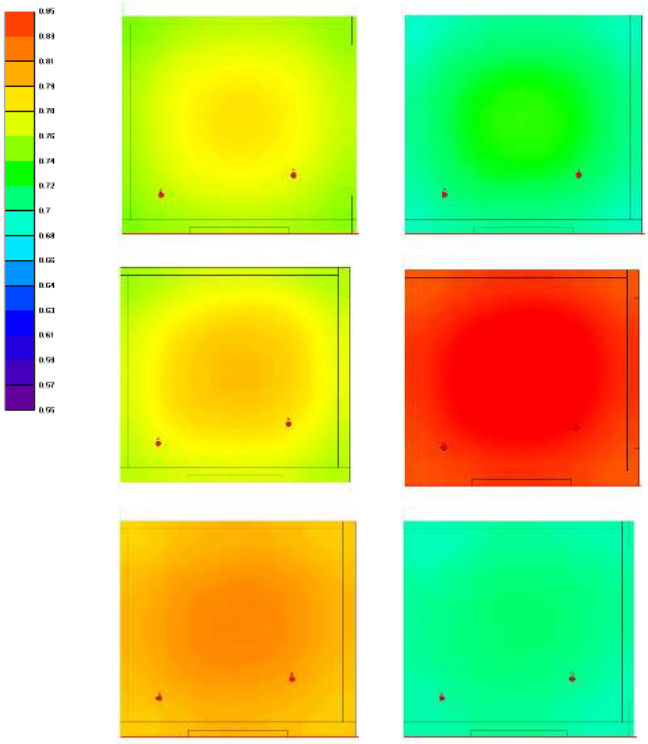

Fig. 13 – Reverberation time T_{20} simulation software B – Room 2 (125 Hz - 4000 Hz)

An underestimation of the simulated reverberation time compared to the measured one can be noted. In particular, the Sabine and Eyring formulas are not usable for rooms of this type. Accordingly, the simulated values obtained are about half of those measured (Farina, 1998). The results obtained with the EN 12354-6 model and with the calculation software are also lower than those measured, in particular, for room 1, the best estimate is represented by EN 12354-6 up to 1000 Hz and by software A over 1000 Hz. For room 2, the best estimate is represented by software A, as reported in Figs. 14 and 15.

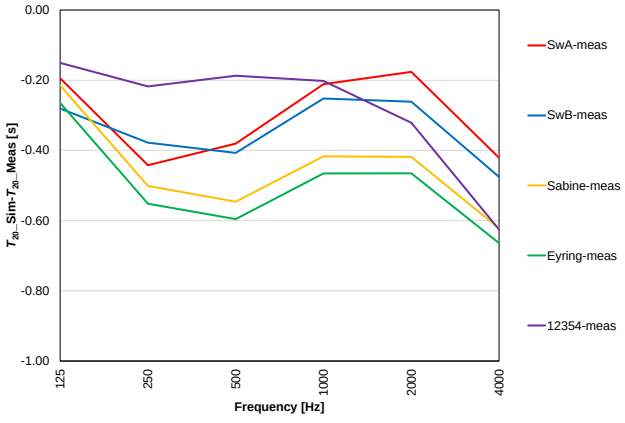

Fig. 14 – Difference between simulated and measured reverberation time T_{20} (Room 1)

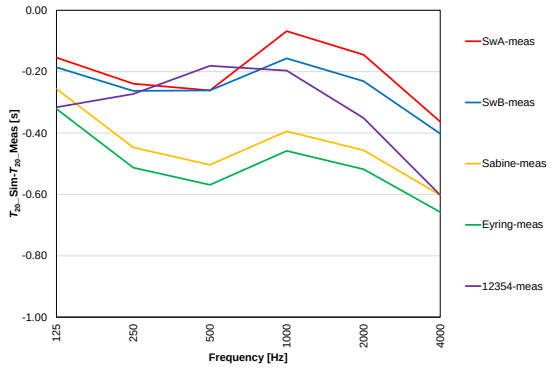

Fig. 15 – Difference between simulated and measured reverberation time T20 (Room 2)

This underestimation is due to an overestimation of the absorption coefficients obtained in the reverberation room according to ISO 354 standard. This is due to the not-perfectly-diffuse sound field and to the modification of the MFP, due to the diffusers hanging to the ceiling of the reverberation room, compared with the one predicted by the Sabine formula contained in the measurement method.

According to Scrosati et al. (2019), the MFP of their empty reverberation room changes from 3.853 m (without diffusers) to 3.377 m (with diffusers), while with specimen MFP varies from 3.750 m (without diffusers) to 3.295 m (with diffusers). The statistical value calculated for this reverberation room was 3.810 m. By modifying the Sabine formula of ISO 354 standard with the correct MFP specific for this reverberation room, the authors found an absorption coefficient about 20-23 % lower than the one measured according to ISO 354.

To better understand the phenomenon, the best fit acoustic absorption coefficients which best approximate the measured reverberation times were calculated both with software A and B. The results are shown in Fig. 16.

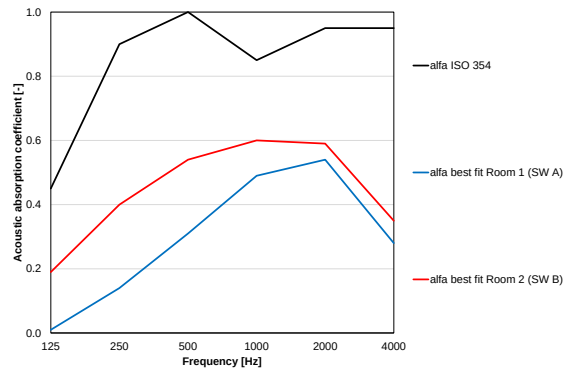

Fig. 16 – Best fit acoustic absorption coefficient

It can be noted that the best fit acoustic absorption coefficient is lower for room 1 than for room 2. This could be due to the different ceiling surface-to-total surface ratio (17.8 % for Room 1 and 22.8 % for Room 2). Furthermore, the celling angle of view concerning the sound source is 78° for Room 1 compared with 101° for Room 2 (Figs. 17 and 18) and differences could actually affect the real sound absorption.

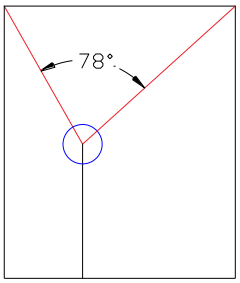

Fig. 17– Celling angle of view (Room 1)

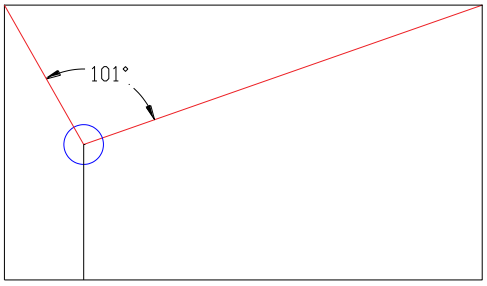

Fig. 18 – Celling angle of view (Room 2)

7. Conclusion

In this work, the acoustic simulation of the reverberation time of two small rooms with volumes of 56.2 m^3 and 113.5 m^3 was considered. These rooms feature sound-absorbing panels only on the ceiling. Therefore, they do not have a homogeneous surfaces absorption.

Simple equations such the Sabine and Eyring formulas, the EN 12354-6 standard model, and two dedicated calculation software were considered.

It was possible to note how all the computational models examined led to an underestimation of the reverberation time. In particular, since reverberation time values obtained with these methods are about half of those measured, the Sabine and Eyring models are not suitable for this type of room.

Better results were obtained using software based

on ray-tracing and pyramid-tracing and on the calculation model based on the EN 12354-6 standard. However, even in this case the reverberation time is underestimated.

A possible explanation of this phenomenon is the overestimation of the absorption coefficients obtained in the reverberation room, according to the ISO 354 standard, due to the not-perfectly-diffuse sound field and to the presence of the diffusers hanging from the ceiling. These do modify the effective volume of the reverberation room and the MFP compared with the one predicted by the Sabine formula.

It is therefore advisable to reduce the values of the acoustic absorption coefficients in the acoustic design.

Nomenclature

Symbols

T_{60}	Reverberation time (s)
V	Volume of the room (m^3)
A	Equivalent absorption area (m^2)
α	Acoustic absorption coefficient (m)
α_m	Mean acoustic absorption coefficient (m)
S	Surface (m^2)

Subscripts/Superscripts

i	i-th surface

References

CEN (European Committee for Standardization). 2006. EN 12354-6:2006 Building acoustics - Estimation of acoustic performance of buildings from the performance of elements - Part 6: Sound absorption in enclosed spaces.

Di Bella, A., N. Granzotto, P. Ruggeri and F. Peron. 2019. "Analysis of the acoustic absorption of fabrics in a diffuse sound field and for normal incidence." *In: Proceedings of the 26th International Congress on Sound and Vibration, ICSV 2019.* Toronto.

Farina, A. A. Langhoff, and L. Tronchin. 1998. "Acoustic characterisation of "virtual" musical instruments: using MLS technique on ancient violins." *Journal Of New Music Research* 27(4):359-379. doi: https://doi.org/10.1080/09298219808570753

Fabbri, K., L. Tronchin, and F. Barbieri. 2021. "Coconut fibre insulators: The hygrothermal behaviour in the case of green roofs." *Construction and Building Materials* 266: 1-9. doi: https://doi.org/10.1016/j.conbuildmat.2020.121026

ISO. 1998. ISO 10534-2, Acoustics – Determination of sound absorption coefficient and impedance in impedance tubes – Part 2: Transfer-function method.

ISO. 2003. ISO 354, Acoustics – Measurement of sound absorption in a reverberation room.

ISO. 2008. ISO 3382-2, Acoustics — Measurement of room acoustic parameters — Part 2: Reverberation time in ordinary rooms.

Meissner, M. 2017. "Acoustics of small rectangular rooms: Analytical and numerical determination of reverberation parameters." *Applied Acoustics* 120: 111-119. doi: https://doi.org/10.1016/j.apacoust.2017.01.020

Nowoświat, A., M. Olechowska, and J. Ślusare. 2016. "Prediction of reverberation time using the residual minimization method." *Applied Acoustics* 106: 42-50. doi: https://doi.org/10.1016/j.apacoust.2015.12.024

Nowoświat, A., and M. Olechowska. 2022. "Experimental Validation of the Model of Reverberation Time Prediction in a Room." *Buildings* 12(3): 347. doi: https://doi.org/10.3390/buildings12030347

Prato, A., F. Casassa, and A. Schiavi. 2016. "Reverberation time measurements in non-diffuse acoustic field by the modal reverberation time." *Applied Acoustics* 110: 160–169. doi: https://doi.org/10.1016/j.apacoust.2016.03.041

Scrosati, C., F. Scamoni, M. Depalma, and N. Granzotto. 2019. "On the diffusion of the sound field in a reverberation room." *Proceedings of the 26th International Congress on Sound and Vibration, ICSV 2019.*.

Scrosati, C., F. Martellotta, F. Pompoli, A. Schiavi, A. Prato, D. D'Orazio, M. Garai, N. Granzotto, A.

Di Bella, F. Scamoni, M. Depalma, C. Marescotti, F. Serpilli, V. Lori, P. Nataletti, D. Annesi, A. Moschetto, R. Baruffa, G. De Napoli, F. D'Angelo, and S. Di Filippo. 2020. "Towards more reliable measurements of sound absorption coefficient in reverberation rooms: An Inter-Laboratory Test." *Applied Acoustics* 165: 107298. doi: https://doi.org/10.1016/j.apacoust.2020.107298

Tronchin, L., and D. J. Knight. 2016. "Revisiting Historic Buildings through the Senses. Visualising Aural and Obscured Aspects of San Vitale, Ravenna." *International Journal of Historical Archeology* 20: 127-145. doi: https://doi.org/10.1007/s10761-015-0325-2

Tronchin, L., and A. Bevilacqua. 2021a. "Acoustic study of different sceneries at the São Carlos national theatre of Lisbon." *Applied Acoustics* 180: 1-11. doi: https://doi.org/10.1016/j.apacoust.2021.108102

Tronchin, L., F. Merli, and M. Dolci. 2021b. "Virtual acoustic reconstruction of the Miners' Theatre in Idrija (Slovenia)." *Applied Acoustics* 172: 1-9. doi: https://doi.org/10.1016/j.apacoust.2020.107595

Tronchin, L. 2021c. "Variability of room acoustic parameters with thermo-hygrometric conditions." *Applied Acoustics* 177: 1-14. doi: https://doi.org/10.1016/j.apacoust.2021.107933

Tronchin, L., and A. Bevilacqua. 2022. "Historically informed digital reconstruction of the Roman theatre of Verona. Unveiling the acoustics of the original shape." *Applied Acoustics* 185: 1-18. doi: https://doi.org/10.1016/j.apacoust.2021.108409

Simulation of Thermal and Acoustic Façade Insulation Starting From the Characteristics of the Individual Elements

Nicola Granzotto – Free University of Bozen-Bolzano, Italy – nicolagranzotto74@gmail.com
Paolo Ruggeri – IUAV, Italy – pruggeri@iuav.it
Fabio Peron – IUAV, Italy – fperon@iuav.it
Marco Caniato – Free University of Bozen-Bolzano, Italy – marco.caniato@unibz.it
Andrea Gasparella – Free University of Bozen-Bolzano, Italy – andrea.gasparella@unibz.it

Abstract

The thermal and acoustic insulation of individual building elements such as walls, windows and systems for roller shutters significantly affects the thermal and acoustic insulation of a building. This paper considers the acoustic and thermal performance of the individual elements evaluated in laboratory with simulation of both the façade sound reduction index and thermal transmittance of a typical room. The scope of this work is to verify if there are any correlations between acoustic and thermal performance; for this reason, 4 types of opaque wall, 3 window systems for roller shutters and 5 windows for a total of 60 façade configurations have been considered and combined.

1. Introduction

The correct acoustic and thermal design of a building is of fundamental importance for increasing indoor comfort.

Many studies have been carried out regarding acoustic and thermal comfort (Fabbri et al., 2014; Granzotto, 2021; Tronchin et al., 2018; Tronchin et al., 2021), façade acoustic insulation (Hua et al., 2021; Jagniatinskis et al., 2021) and thermal insulation (Theodosiou et al., 2019).

Other studies comparing acoustic and thermal characteristics of walls can be found (Di Bella et al., 2014; Di Bella et al., 2015). Sound insulation is one important factor for façade performance optimization. As an example, Ryu et al. (2010) proved that the sound insulation of a building façade influenced indoor annoyance due to transportation noise and the frequency content of intrusive noise.

For façade thermal insulation, Sierra-Peréz et al. (2016) demonstrated how an optimized combination of elements could affect indoor thermal perception.

In this work, the acoustic and thermal insulation of a façade has been considered, varying the performance of single elements. 4 walls, 3 shutter systems and 5 windows.

The acoustic performance was determined in a laboratory while the thermal performance was simulated from the thermal conductivity data, considering, in addition, linear thermal transmittance.

2. Calculation Models

The sound reduction index, R, of a building element is defined as:

$$R = 10\lg\left(\frac{1}{\tau}\right. \quad (1)$$

The transmission coefficient τ is the ratio of the sound power, W_1, which is incident on the test element to the sound power, W_2, radiated by the test element to the other side.

R was measured in laboratory conditions according to the ISO 10140 (2021) series standard:

$$R = L_1 - L_2 + 10\lg\left(\frac{S}{A}\right. \quad (2)$$

The composed sound reduction index, R_{tot}, was calculated as:

$$R_{\mathrm{tot}} = 10\lg\left(\frac{\sum_{\mathrm{i}=1}^{\mathrm{n}} S_{\mathrm{i}}}{\sum_{\mathrm{i}=1}^{\mathrm{n}} 10^{(-R_{\mathrm{i}}/10)} S_{\mathrm{i}}}\right) \quad (3)$$

The weighted sound reduction index, R_{w} and the spectrum adaptation term for pink noise, C, and for traffic noise, C_{tr}, were calculated according to ISO 717-1 (2020). The thermal conductivity, λ, of materials such as rock wool, EPS and XPS is measured according to EN 12667 standard (2021), while the thermal transmittance, U, and the linear thermal transmittance, Ψ, were simulated by means of a FEM software according to ISO 10077-2 (2017) and ISO 10211 (2017) standards.

The composed thermal transmittance, U_{tot}, of the façade was obtained according to ISO 10077-1 (2017) with the following formula:

$$U_{\mathrm{tot}} = \frac{\sum_{\mathrm{i}=1}^{\mathrm{n}} U_{\mathrm{i}} S_{\mathrm{i}} + \sum_{\mathrm{k}=1}^{m} \Psi_{\mathrm{k}} l_{\mathrm{k}}}{\sum_{\mathrm{i}=1}^{\mathrm{n}} S_{\mathrm{i}}} \quad (4)$$

3. Building Elements

The building elements considered are reported in Tables 1, 2 and 3.

Table 1 – Building elements - Walls

ID	Description
A	Aerated concrete blocks (350 kg/m³, 300 mm) lined with rock wool panels (45 mm) and gypsum board (12.5 mm).
B	Hollow brick plastered one side (250 mm) lined with rock wool panels (140 mm) and plaster (5 mm).
C	Hollow brick plastered one side (250 mm) lined with EPS panels (140 mm) and plaster (5 mm).
D	Aerated concrete blocks (300 kg/m³, 400 mm).

Table 2 – Building elements - Windows systems for roller shutters

ID	Description
a	Integrated windows system for roller shutter for window flush with the internal wall. S=0.75 m².
b	Integrated windows system for roller shutter for window in the middle of the wall. S=0.75 m².
c	Box for roller shutter suitable for building renovations. S=0.45 m².

Table 3 – Building elements - Windows

ID	Description
1	One sash window with glass: 6 mm + 0.76 mm acoustic PVB + 6 mm / 16 mm Argon / 4 + 0.50 mm acoustic PVB + 4 mm.
2	One sash window with glass: 3 mm + 0.50 mm acoustic PVB + 3 mm / 15 mm Argon / 4 mm / 15 mm Argon / 3 mm + 0.50 mm acoustic PVB + 3 mm.
3	Two sash windows with glass: 4 mm + 0.76 mm acoustic PVB + 4 mm / 15 mm Argon / 4 mm / 15 mm Argon / 4 mm + 0.76 acoustic PVB + 4 mm.
4	One sash window with glass: 6 mm + 0.76 acoustic PVB + 6 mm / 12 mm Argon / 4 mm / 12 mm Argon / 4 mm + 0.76 acoustic PVB + 4 mm.
5	Two sash windows with glass: 3 + 0.38 PVB + 3 mm / 18 Argon / 4 + 0.50 acoustic PVB + 4 mm.

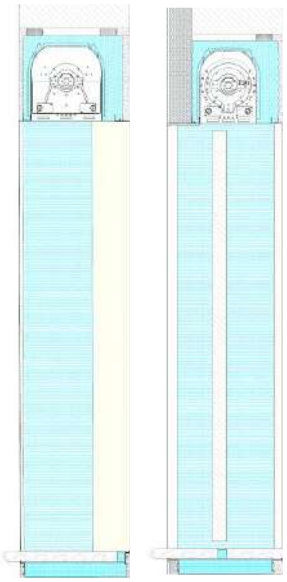

Fig. 1 – Window system for roller shutter “a” and “b”

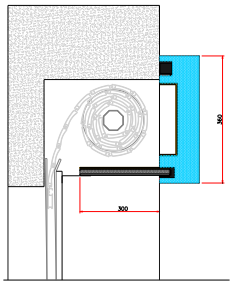

Fig. 2 – Window system for roller shutter “c”

Fig. 1 and 2 show the windows system for roller shutter used in the simulations. Window dimension was 1230 mm x 1480 mm, and wood frame thickness was 80 mm.

4. Acoustic Measurements and Thermal Simulations

The sound reduction index of the building elements was measured in the laboratory according to ISO 10140 (2021) series standard (Figs. 3, 4 and 5). The sound reduction index, *R*, of the building elements in the 1/3 octave frequency band is shown in Fig. 6. The weighted sound reduction and the thermal transmittance are shown in Table 4.

The thermal transmittance of the windows and window systems for roller shutters was simulated with FRAME SIMULATOR software.

From the thermal profiles in Fig. 7, it is possible to consider the “a” box shutter as the one with the best performance followed by “b” and “c”.

Fig. 3 – Window – Laboratory test according to ISO 10140 (2021) series standard

Fig. 4 – Window system for roller shutter “a” – Laboratory test according to ISO 10140 (2021) series standard

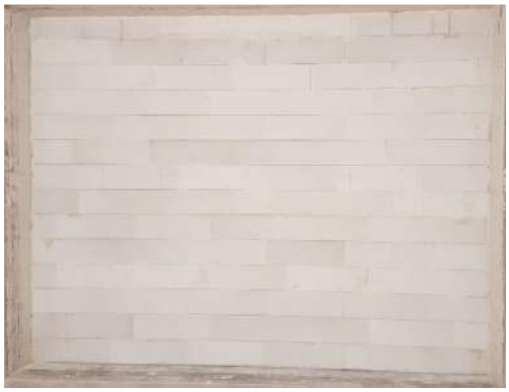

Fig. 5 – Wall – Laboratory test according to ISO 10140 (2021) series standard

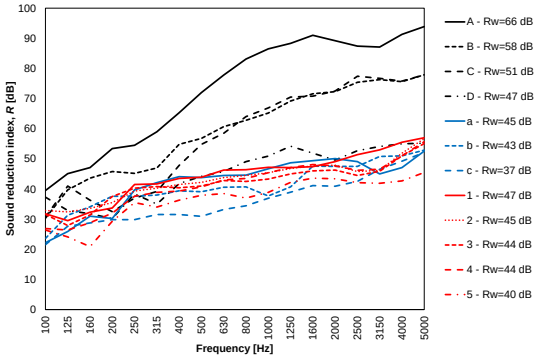

Fig. 6 – Sound reduction index of building elements in 1/3 octave bands

Table 4 – Building elements acoustic and thermal performance

Element	Type	$R_w(C;C_{tr})$	U
A	Wall	66(-2;-9)	0.201
B	Wall	58(-3;-9)	0.219
C	Wall	51(-2;-7)	0.193
D	Wall	47(-2;-6)	0.170
a	Shutter box	45(-2;-8)	0.385
b	Shutter box	44(-2;-5)	0.842
c	Shutter box	37(-1;-3)	1.061
1	Window	47(-2;-5)	1.200
2	Window	45 (-1;-3)	0.890
3	Window	44 (-1;-3)	1.100
4	Window	44(-1;-5)	0.890
5	Window	40(-2;-5)	1.300

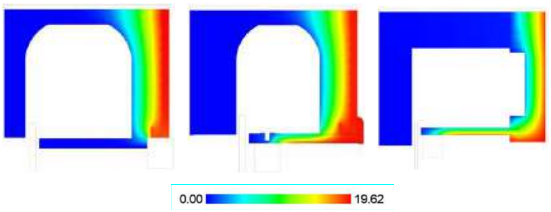

Fig. 7 – Temperature for windows system for roller shutter (left: "a", center: "b", right: "c")

The linear thermal transmittances, Ψ, of the shutter-wall interface, wall-window interface and shutter-window interface were calculated with Finite Element Method software MOLD SIMULATOR, according to ISO 10211 (2017). Ψ_1 is the linear thermal transmittance for wall-shutter box, Ψ_2 is the linear thermal transmittance for wall-shutter-window, Ψ_3 is the linear thermal transmittance for shutter-window (Fig. 8 and Table 5).

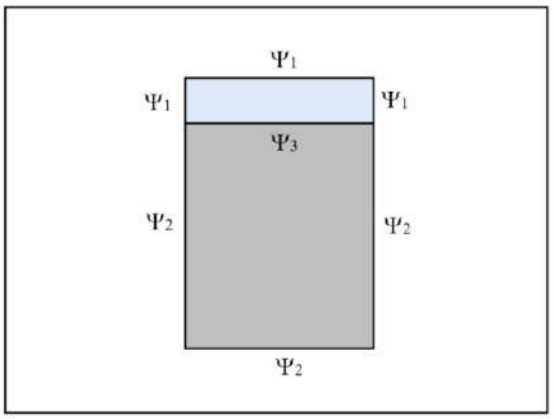

Fig. 8 – Linear thermal transmittance scheme

Table 5 – Building elements – Linear thermal transmittance

Configuration	Ψ_1	Ψ_2	Ψ_3
Aa	0.33	0.08	0.23
Ab	0.33	0.08	0.38
Ac	0.10	0.10	0.55
Ba	0.40	0.11	0.23
Bb	0.40	0.08	0.38
Bc	0.45	0.11	0.55
Ca	0.40	0.12	0.23
Cb	0.40	0.09	0.38
Cc	0.45	0.11	0.55
Da	0.33	0.08	0.23
Db	0.33	0.08	0.38
Dc	0.10	0.09	0.55

Figs. 9, 10 and 11 show some temperature examples of linear thermal transmittance simulations.

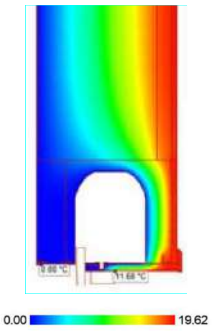

Fig. 9 – Example of Ψ_1 simulation with MOLD software for "b" shutter box and wall "D"

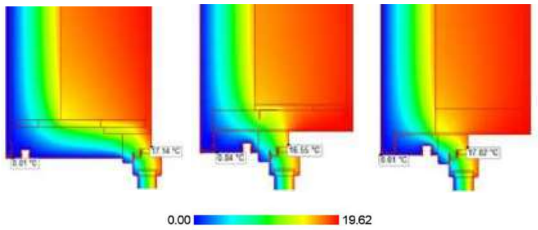

Fig. 10 – Example of Ψ_2 simulation with MOLD software for "a", "b" and "c" shutter box (with Wall "B")

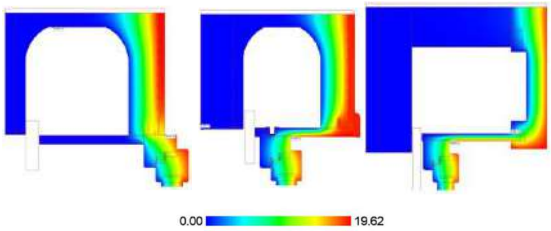

Fig. 11 – Ψ_3 simulation with MOLD software for "a", "b" and "c" shutter box

5. Results

The acoustic and thermal insulation of a 2.7-m-high and 4-m-wide façade has been considered.

The composed weighted sound reduction index, R_w, vs composed thermal transmittance, U, is shown in Fig. 12.

The composed weighted sound reduction index, R_w+C_{tr}, vs composed thermal transmittance, U, is shown in Fig. 13. R_w+C_{tr} considers weighted sound reduction index in dB(A) for traffic noise.

The best configurations are located in the upper left quadrant.

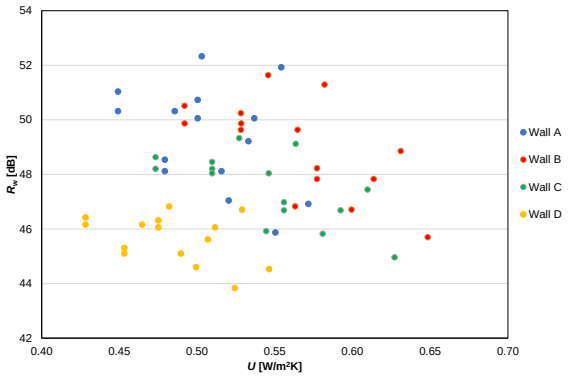

Fig. 12 – R_w vs U

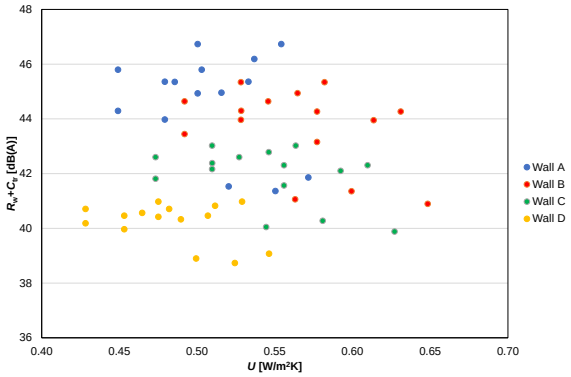

Fig. 13 – R_w+C_{tr} vs U

It can be noted that there are no correlations between acoustic and thermal performance at all. Indeed, poor correlations are obtained even considering single wall results.

For R_w:

- $R^2_{\_wallA}$ is 0.13;
- $R^2_{\_wall\ B}$ is 0.41;
- $R^2_{\_wall\ C}$ is 0.42;
- $R^2_{\_wall\ D}$ is 0.15.

For R_w+C_{tr}:

- $R^2_{\_wall\ A}$ is 0.09;
- $R^2_{\_wall\ B}$ is 0.16;
- $R^2_{\_wall\ C}$ is 0.18;
- $R^2_{\_wall\ D}$ is 0.14.

Fig. 14 shows the configurations examined as the thermal transmittance, U, decreases. In the same graph, the indices R_w and R_w+C_{tr} are indicated (dotted line indicates the calculated transmittance without considering the linear thermal transmittance).

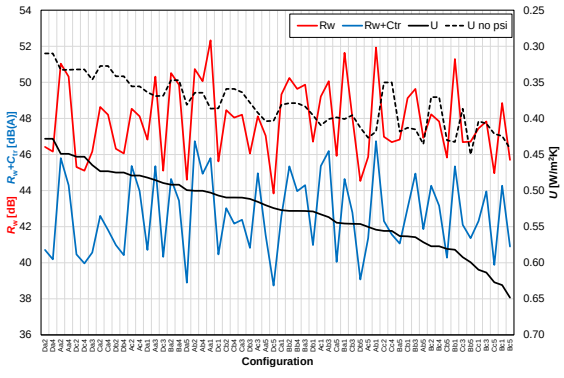

Fig. 14 – U vs R_w and U vs R_w+C_{tr}

Considering the variation in the performance of a single element (wall, window systems for roller shutters and window), it can be noted how the variations in the overall performance of the façade are different from an acoustic and thermal point of view (Fabbri et al., 2021; Tronchin, 2005). Interestingly, it can be noted that, if linear thermal transmittances are not considered, considerable errors are made (ΔU = 0.12-0.21 W/(m²K)).

Furthermore, it can be noted that the configurations with "D" wall are the best in terms of thermal insulation because of low U and reduced thermal bridges, while in terms of sound insulation they are not as effective as the other walls.

The configurations with shutter box type "c" provide good results even if the performances of this element are not optimal. This is due to the small surface of the element, which leads to a small overall influence.

It can be noted that the combination providing better acoustic and thermal performance is represented by the "Aa2" configuration.

In Figs. 15-23, the values of U, R_w, R_w+C_{tr} of the whole façade are reported and parametrically compared with the values of the walls (A, B, C and D), of the shutter boxes (a, b, and c) and of the windows (1, 2, 3, 4 and 5).

Configurations with the lowest value are indicated with a grey dashed line. In Fig. 15, it can be seen how wall A implies a lower value of U for the façade. This is due to the fact that wall A has a lower Ψ_2 value because of its composition (thermal insulating blocks). As regards the acoustic insulation, it can be noted that as the performance of the single element increases, the range of R_w and R_w+C_{tr} increases.

In Figs. 16 and 17, the overall acoustic performance is studied parametrically and compared to the wall ones. Interestingly, an important influence is assessed below 55 dB, while over this threshold no significant difference is found.

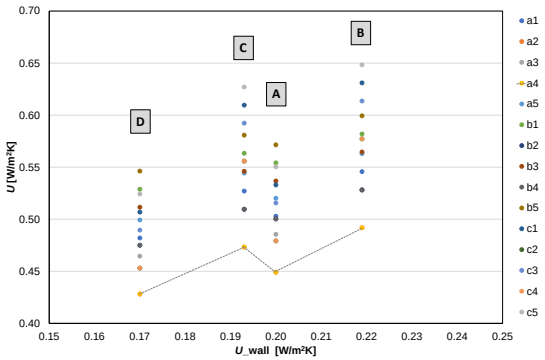

Fig. 15 – Overall U compared to the thermal transmittance of the wall (A, B, C and D), U_wall

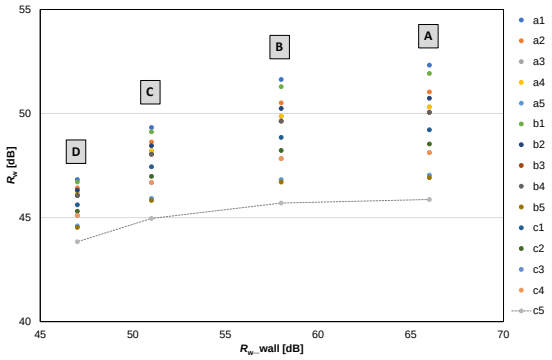

Fig. 16 – Overall R_w compared to the weighted sound reduction index of the wall (A, B, C and D), R_w_wall

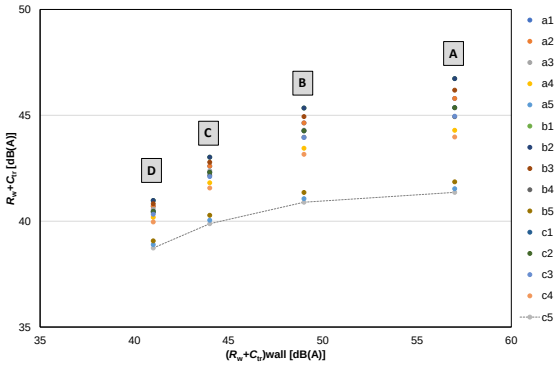

Fig. 17 – Overall R_w+C_{tr} compared to the weighted sound reduction index of the wall (A, B, C and D), (R_w+C_{tr}) wall

The influence of the shutter box transmittance is reported in Fig. 18. It is clear that shutters affect the final performance, but do not drive the overall final result because of their reduced area.

Moving on to the shutter box acoustic performances (Figs. 19-20), it can be seen that their influence affects overall results more when the wall provides high acoustic insulation.

The window parametric influence on overall results is depicted in Fig. 21.

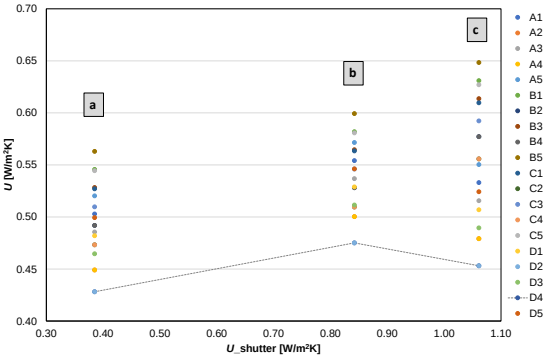

Fig. 18 – Overall U compared to the thermal transmittance of the shutter box, (a, b and c) U_shutter

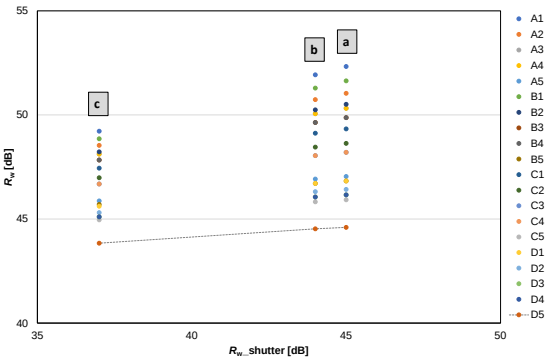

Fig. 19 – Overall R_w compared to the weighted sound reduction index of the shutter box (a, b and c), R_w_shutter

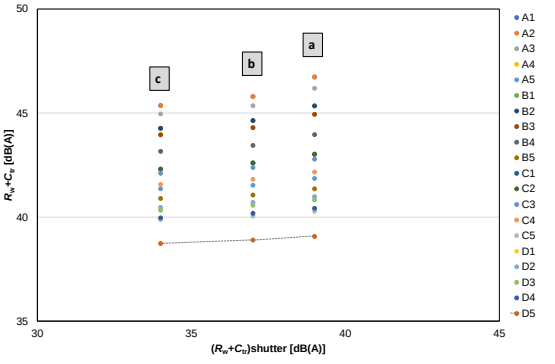

Fig. 20 – Overall R_w+C_{tr} compared to the weighted sound reduction index of the shutter box (a, b and c), (R_w+C_{tr}) shutter

Here, it can be seen how, almost linearly, window thermal transmittances increase the overall final performances as expected because of their significant area.

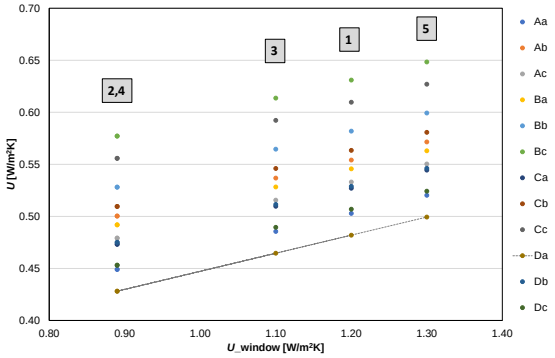

Fig. 21 – Overall U compared to the thermal transmittance of the window, (1, 2, 3, 4 and 5) U_window

When moving on to window acoustic parametric influence (Figs. 22-23), it can be highlighted that, when the sound insulation increases, the overall acoustic performance increases too. Again, this is due to window area, which is significant in the façades considered.

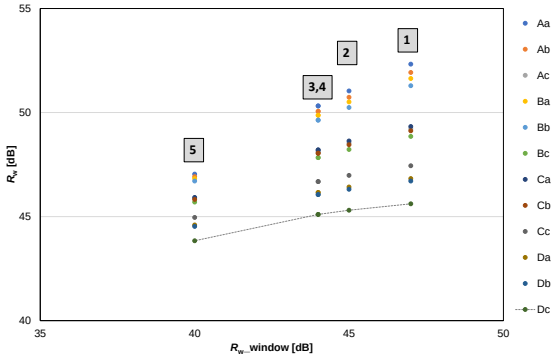

Fig. 22 – Overall R_w compared to the weighted sound reduction index of the window (1, 2, 3, 4 and 5), R_w_window

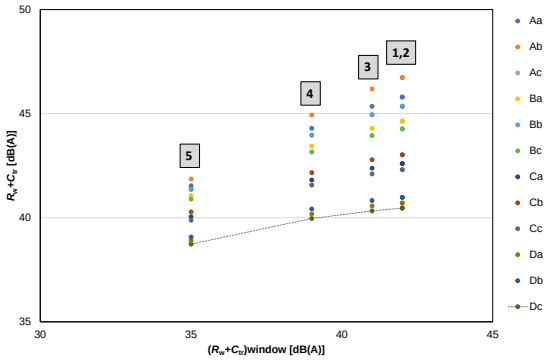

Fig. 23 – Overall R_w+C_{tr} compared to the weighted sound reduction index of the window (1, 2, 3, 4 and 5), (R_w+C_{tr}) window

6. Conclusion

In this work, the acoustic and thermal insulation of 60 different combinations of façade elements was studied. 4 walls, 3 shutter systems and 5 windows were considered. It was possible to verify that there is no correlation between the overall final acoustic and thermal performances.
Some further considerations can be made:
- the best solutions from the thermal point of view are not the best ones from the acoustic point of view;
- the best combined thermal and acoustic performances are obtained using thermally insulating blocks (aerated concrete block) with internal lining and use of integrated window systems for roller shutters
- if linear thermal transmittance is not considered, considerable errors can be made (ΔU=0.12-0.21 W/(m^{2}K)).
- it can finally be pointed out how, from a thermal point of view, all three elements equally contribute to the final performance, while, regarding acoustic insulation, the wall and the windows play a more important role due to their more extended area.

Acknowledgement

This work was financed by the European Interreg BIGWOOD project, IT AT 1081 CUP: I54I18000300006.
Alpac S.r.l. and Punto Infissi S.r.l. are gratefully acknowledged for providing the acoustic and thermal data of their products.

References

CEN (European Committee for Standardization). 2001. *EN 12667:2001 Thermal performance of building materials and products - Determination of thermal resistance by means of guarded hot plate and heat flow meter methods - Products of high and medium thermal resistance.*

Di Bella, A., N. Granzotto and C. Pavarin. 2014. "Comparative analysis of thermal and acoustic performance of building elements." In: *Proceedings of Forum Acusticum 2014*.

Di Bella, A., N. Granzotto, H. H. Elarga, G. Semprini, L. Barbaresi and C. Marinosci. 2015. "Balancing of thermal and acoustic insulation performances in building envelope design." In: *Proceedings of Inter-Noise 2015*. doi: https://dx.doi.org/10.13140/RG.2.1.1435.9122

Fabbri, K., L. Tronchin and V. Tarabusi. 2014. "Energy Retrofit and Economic Evaluation Priorities Applied at an Italian Case Study." *Energy Procedia* 45:379-384. doi: https://doi.org/10.1016/j.egypro.2014.01.041

Fabbri, K., L. Tronchin, and F. Barbieri. 2021. "Coconut fibre insulators: The hygrothermal behaviour in the case of green roofs." *Construction and building materials* 266:1-9. doi: 10.1016/j.conbuildmat.2020.121026

Granzotto, N. 2021. "Optimization of Controlled Mechanical Ventilation Systems for Indoor Acoustic Comfort." *Designs* 5:48. doi: https://doi.org/10.3390/designs5030048

Hua, Z., L. Maxit and L. Cheng. 2021. "Acoustic design and analyses of a double Skin Façade system." *Applied Acoustics* 173. doi: https://doi.org/10.1016/j.apacoust.2020.107727

ISO (International Organization for Standardization). 2021. *ISO 10140-2:2021 Acoustics — Laboratory measurement of sound insulation of building elements — Part 2: Measurement of airborne sound insulation.*

ISO (International Organization for Standardization). 2020. *ISO 717-1:2020 Acoustics — Rating of sound insulation in buildings and of building elements — Part 1: Airborne sound insulation.*

ISO (International Organization for Standardization). 2017. *ISO 10077-1:2017 Thermal performance of windows, doors and shutters — Calculation of thermal transmittance — Part 1: General.*

ISO (International Organization for Standardization). 2017. *ISO 10077-2:2017 Thermal performance of windows, doors and shutters — Calculation of thermal transmittance — Part 2: Numerical method for frames.*

ISO (International Organization for Standardization). 2017. *ISO 10211:2017 Thermal bridges in building construction — Heat flows and surface temperatures — Detailed calculations*

Jagniatinskis, A., B. Fiksa and M. Mickaitis. 2021. "Acoustic classification of building façades using statistical methods." *Applied Acoustics* 172. doi: https://doi.org/10.1016/j.apacoust.2020.107653

Ryu, J. and H. Song. 2019. "Effect of building façade on indoor transportation noise annoyance in terms of frequency spectrum and expectation for sound insulation." *Applied Acoustics* 152: 21–30. doi: https://doi.org/10.1016/j.apacoust.2019.03.020

Theodosiou, T., K. Tsikaloudaki, S. Tsoka, and P. Chastas. 2019. "Thermal bridging problems on advanced cladding systems and smart building facades." *Journal of Cleaner Production* 214: 62-69. doi: https://doi.org/10.1016/j.jclepro.2018.12.286

Tronchin, L. 2005. "Modal analysis and intensity of acoustic radiation of the kettledrum." *The Journal Of The Acoustical Society Of America* 117(2):926-933. doi: https://doi.org/10.1121/1.1828552

Tronchin, L., K. Fabbri and C. Bertolli. 2018. "Controlled Mechanical Ventilation in Buildings: A Comparison between Energy Use and Primary Energy among Twenty Different Devices." *Energies* 11:1-20. doi: https://doi.org/10.3390/en11082123

Tronchin, L. 2021. "Variability of room acoustic parameters with thermo-hygrometric conditions." *Applied Acoustics* 177:1-14. doi: https://doi.org/10.1016/j.apacoust.2021.107933

Climate Change Impact on Historical Buildings: A Case Study Within the Interreg Ita-Slo Secap Project

Marco Manzan – University of Trieste, Italy – manzan@units.it
Amedeo Pezzi – University of Trieste, Italy – amedeopezzi@hotmail.com

Abstract

Climate change effects on human activities have become more and more evident in the last few decades and human society is looking for new solutions to deal with such consequences. One of the measures that can be developed to tackle this problem is the development of the Sustainable Energy and Climate Action Plans (SECAPs), aiming at reducing the mutual impact between human activities and climate at municipal level. To develop such policies, an extensive study of the building stock, of its current and future performances, and its possible improvements is fundamental. Therefore, an energy analysis for a historical building used as a museum and situated in Trieste, a location included in the Interreg ITA-SLO Secap Project, is carried on in this work. The building represents a challenging task due to its historical nature and architectural features. The current climate for Trieste was represented through a Test Reference Year that was then projected into the future using different climate models. The building was numerically modeled, highlighting its main structural and plant features and usage patterns. Future projections for the climate of Trieste showed a general increase in temperatures for all the studied models, leading to a forecasted decrease in heating gas consumption and an increase in electricity-cooling usage of the base building. Regarding the refurbishment interventions applicable in accordance with the preservation regulations, the results show an obtainable reduction of both gas and electricity consumption for every climatic condition considered. However, the interventions proved not to be economically feasible, showing a too-long simple economic return on the investment.

1. Introduction

In recent years climate change has proved to be an extremely influential parameter for consideration in the development of human society. Nowadays the scientific community has recognized the impact of anthropogenic activities on global warming and climate in general (Cook et al., 2016). This is a mutual influence, since climate evolution is also affecting several sectors of human assets. In literature, many authors focused their studies on global warming effects on the building sector, showing that climate change has significant impacts on the energy consumption of buildings (Cui et al., 2017; Radhi, 2009; Wan et al., 2012). In fact, even if sometimes the projections show a reduced/minor impact of climate change in the short term for many aspects, significant variations are forecasted for long-term scenarios and should be considered within the design procedures. Generally, depending on climate type, a decrease in heating energy consumption and an increase in cooling energy consumption is forecast (Crawley, 2008).

Considering that, worldwide, the building sector accounts for a great part of total energy usage and of Greenhouse Gas emissions, it has become crucial for both mitigation and adaptation purposes to study and to reduce as much as possible the mutual interaction between this sector and climate evolution (Jentsch et al., 2008; Robert et al., 2012).

Many measures have been defined to tackle climate change on different scales, from global to local ones. About the former, the most well-known initiative is the Paris Agreement on Climate, aiming to limit global warming compared to the pre-industrial age to under 2 °C and pursuing efforts to limit it to 1.5 °C. It also aims to improve the capacity of countries and local governments to deal with the inevitable effects of climate change and support them in their efforts (Paris Agreement, 2015). Regarding local measures, one of the main ones is the evolution of the Sustainable Energy Action Plans, i.e., SEAPs, into Sustainable Energy and Climate Action Plans, i.e., SECAPs. These policies are draft-

ed at municipal level with the aim of reducing the impact of cities on the climate, and adapting them to the inevitable changes likely to happen in the future.

Because the municipalities are usually lacking the knowledge to develop these plans fully, different projects have been set up to support this process. One of these is the Interreg ITA-SLO Secap Project, aiming to stimulate the sustainable development of human activities within the cross-border territory composed of the metropolitan city of Venice, the Friuli Venezia Giulia region and the western part of Slovenia (Interreg, 2018).

The main aim of the project is to provide reliable bases and experiences that could help cities, both directly and indirectly, to reduce their environmental impact and develop suitable adaptation strategies to climate change. One of the main measures to achieve this objective is to reduce energy use in public and private buildings. In fact, in the European Union the building sector accounts for 26-28 % of the total energy usage (Borozan, 2018; Eurostat, 2020), and 19 % of Greenhouse Gas emissions (Eurostat, 2015). In Italy, this feature is even more relevant because of this sector accounting for about 31% of the total national energy consumption (Directorate-General for Energy, 2021). Regarding this, the municipalities developing their SECAPs normally focus their efforts on the building stock of their own property, accounting for a remarkable 46 % of the total of implemented policies (Palermo et al., 2020). In fact, this is the sector where they can intervene through a more systematic approach, having a full knowledge and control of their own buildings and equipment. Therefore, they can directly implement measures and monitor the results accurately.

Because of this situation, one of the main outputs developed in the Interreg ITA-SLO Secap Project and presented in this paper is the energy analysis of a building, representing a case study that municipalities could exploit when developing their SECAPs. The case study includes a dynamic energy simulation of the building-plant system, of its functioning in present and future climatic situations and the evaluation of the effects of its possible refurbishment improvements.

The building analysed for the case study is the Revoltella Museum of Trieste, a location included in the program area of the Project, and managed by the municipality itself. The choice fell on this building for several reasons. First, it is a historical building preserved by the regulations of the fine arts, a very common situation in Italy, where particular attention is required when dealing with refurbishment interventions (De Santoli, 2015). Because of this, the design solutions are limited and therefore it is of interest to highlight the effects of these restrictions on the analysis output. Moreover, the museum is a place of public utility, a category for which the government is allocating funds to improve energy efficiency. Finally, yet importantly, the municipality of Trieste openly stated a willingness to intervene in this particular building to improve its energy performance, therefore this will not be only a theoretical case study, but it will be effectively carried out.

2. Climate Change Modeling

The source data to represent the current climatic situation were detected between 1995 and 2019 by a meteorological station located less than 1 km away from the building analysed. Raw data were treated to assess their quality, fill the gaps and reject the periods having too-low data quality.

The actual climate for Trieste was represented through a Test Reference Year generated using the Finkelstein-Schfer statistic (Finkelstein et al., 1971).

Climate change was modeled through five different Global-Regional circulation model couplings, assessed to be the most reliable for climate projections in the Friuli Venezia Giulia region, where Trieste is located, by the Regional Agency for Environment Protection, ARPA FVG:

- HadGEM2-ES RACMO22E;
- MPI-ESM-LR REMO2009;
- EC-EARTH CCLM4-8-17;
- EC-EARTH RACMO22E;
- EC-EARTH RCA4.

Before using them, the five models were calibrated through the quantile mapping method (Cannon et al., 2015) to better fit their outputs to the historical data detected for Trieste for a period common to both historical recordings and model outputs. This

allowed more reliable results for the future climate projections to be obtained. The corrected models were then applied to the RCP8.5 scenario, representing a situation where no relevant climate mitigation measures are implemented, therefore similar to the current global situation. The future timeframes considered in the analysis are 2021-2035 and 2036-2050 to represent climate evolution in the near future. Then, the mathematical morphing procedure (Belcher et al., 2005) was used to project the current TRY into the future considering these two periods.

Fig. 1 displays the Heating (a) and Cooling (b) Degree Days for Trieste for current and projected situations. It can be immediately noted that for all the climatic models considered an increase in temperature is forecast as it can be assessed by the decrease of the HDDs and the increase of CDDs. Moreover, it can be noted that climate warming will happen in both the timeframes considered, though with different magnitudes.

Among the projected situations, the one deriving from the HadGEM2-ES RACMO22E model proved to be the warmest one. This being the configuration that most differs from the actual climate, it was used as the future boundary condition for the building-plant analysis.

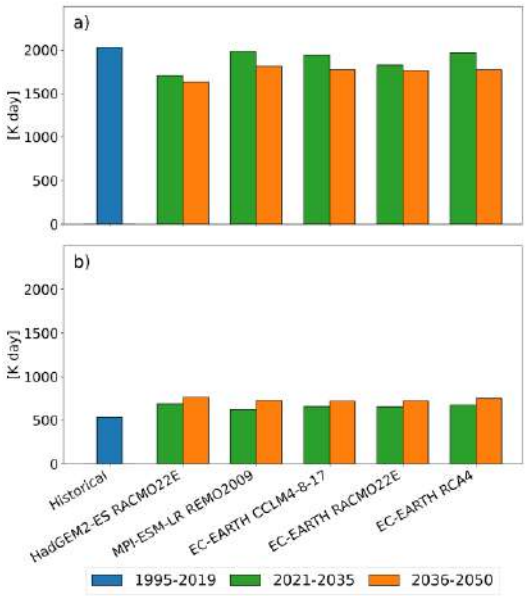

Fig. 1 - Heating (a) and Cooling (b) Degree Days of the historical and projected TRYs for Trieste

3. State-Of-The-Art Modeling

The geometry of the building was modeled using DesignBuilder software, the graphic interface of EnergyPlus calculation engine.

Fig. 2 shows the building within its urban context (a), and its model (b); the presence of the surrounding buildings inserted as elements of solar obstruction for a more accurate analysis can be appreciated in the model.

a)

b)

Fig. 2 – Revoltella Museum view (a) and numerical model (b)

To reduce the computational burden, the model was simplified by removing some internal partitions and unifying spaces sharing the same characteristics. Partitions were still considered as internal masses to correctly model the thermal inertia of the system. Fig. 3 presents as an example the spaces modeling for the second-last floor, with the internal masses added to ensure the correct thermal capacity of the building visible in blue.

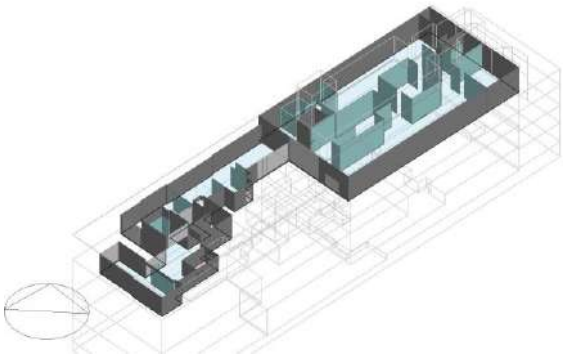

Fig. 3 – Internal spaces modeling for the second-last floor

In total, a building volume of 26,307 m^3 was modeled. Envelope element stratigraphy was obtained through site inspections and data gathered from the municipality of Trieste. Table 1 reports the transmittance values for all opaque elements of the building.

Table 1 – Transmittance values of envelope opaque elements

Element	**U** [W/(m^2 K)]
External walls	0.72
Earth retaining walls	1.20
Ground floor	0.41
Internal floor	1.94
Roof	1.77

Double-glazed windows with air-filled gap and wooden frame having transmittances of 3.21 W/(m^2 K) are present. The building also presents skylights having a transmittance of 5.59 W/(m^2 K).
Regarding the characteristics of the internal spaces and their use patterns, three main zones were identified for the typical floors and are reported in Fig. 4. Zone A is the historical residence museum and is architecturally preserved both internally and externally. Zone B hosts a modern art museum while zone C is intended for office use, and both are subject to preservation rules regarding only the façades.

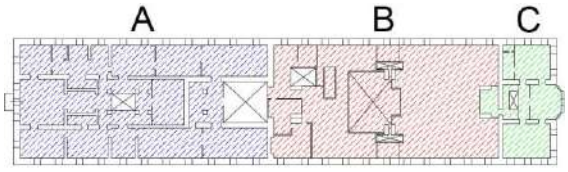

Fig. 4 – Building main zones: A (blue) – historical residence museum, B (red) – modern art museum, C (green) - offices

Because of this situation, internal gains due to illumination, people density and activity, as well as the features of the plant, vary between these three zones. Table 2 reports the principal features for every zone.

Table 2 – Building internal zones features and plant terminals

Parameter \ Zone	**A**	**B**	**C**
People density [people/m^2]	0.143	0.143	0.070
Lighting norm. power dens.[W/(m^2 – 100 lx)]	6	6	4
Illuminance [lx]	200	200	300
Plant terminals [/]	Fan-coils	Fan-coils + CAV units	Radiators + VRF units

People density during the day was modified through a schedule following the typical occupation pattern detected during the opening time of the museum, 9 a.m. – 7 p.m., Tuesday excluded. People density in the office area was instead considered constant during the opening time, as well as lighting for all zones. People metabolic rates were fixed at 140 and 120 W/person for museum and office spaces respectively.
Regarding the plant, various terminals are used in this building, as can be deduced from Table 2; this is due to the different uses and working conditions of the building zones. In particular, only fan-coils are present in Zone A because of the preservation regulations limiting the possibilities in the historical internal spaces. Plant temperature set-points are 20 °C for heating and 25 °C for cooling respectively; humidity control is not present. Heating is available from October 15 to April 15, following the calendar of the Italian Climatic Zone E; cooling is always available. The former is working 14 hours per day, the maximum allowed from 7 a.m. to 9 p.m.; the latter is working during the opening time of the museum. Both are deactivated on Tuesday, the closing day of the museum. As it can also be noted by Table 2, the plant serving the building presents a complex configuration depending on the three main areas. The generators of zones A and B are gas-fired condensing boilers and a water chiller for heating and cooling purposes respectively. These generators serve both the fan-coils and the Air Handling Unit (AHU) for the functioning of the CAV system. Zone C generation is given by a dedicated gas-fired condensing boiler coupled with

VRF units for heating and cooling respectively. Finally, an evaporative cooling tower is present on the roof working with the chiller for summer season cooling.

In the analysis, the existing system was modeled as precisely as possible to determine the energy vectors involved in the most coherent way possible, also by exploiting the technical data sheets available for the boilers and the chiller. In addition to the synthetic data, the chiller performance was properly modeled as a function of the condenser and evaporator water temperatures. Through this, and to take the operation of the system in the different conditions into account, the correction curves for the nominal power and for the Energy Efficiency Ratio (EER) were obtained (UNI, 2018). In the same way, the efficiency and the nominal power of the gas-fired condensing boilers were parameterized according to the load and to the returning water temperature. Regarding the AHU, the cooling tower and the VRF units, their characteristics were hypothesized on the bases of the expected behavior of the whole plant and of historical consumption data. The whole audit process was carried out following what is reported in UNI CEI EN 16247-2 standard (UNI, 2014).

3.1 Model Calibration

To obtain reliable results, the state-of-the-art model has been calibrated through a comparison between its results and the historical recordings of gas and electricity consumption. Historical gas consumption data were available as an average for the years 2010-2012 and on a yearly basis for 2019 and 2020. The latter was characterized by the effects of the COVID-19 pandemic and therefore is not representative of the normal behaviour of the building. Year 2019 instead was not usable for the calibration due to the scarcity of climatic data detected by the meteorological station of Trieste, not allowing the execution of a yearly calibration simulation. Therefore, the mean gas consumption value for years 2010-2012 was used for the calibration. Regarding electricity, monthly consumption values for the years 2017-2020 were available. Year 2018 was chosen to calibrate the model because of the local meteorological station having good data quality for that period. To perform the calibration, a special climatic file containing the 2010-2012 values for the winter season and 2018 values for the summer one was created. The calibration process led to some modifications regarding the envelope elements' transmittance, the internal gains due to people and lighting and the characteristics of the hypothesized elements of the plant. Because of these adjustments, the calibrated model achieved remarkable precision in reproducing the historical consumption recordings, as can be noted through Table 3. The calibrated model was the base to run the energy simulation with the different climatic conditions defined in Section 2 and to assess the effects of the refurbishment interventions described in the next section.

Table 3 – Model calibration results

Energy vectors consumption	**Historical**	**Model**	**Model Error [%]**
Gas [m^3]	56 056	52 458	-6.86
Electricity [kWh]	313 020	319 371	+2.03

4. Refurbishment Interventions

Given the preservation restrictions described in Section 3, the room for improvements to increase the energy performance of the building is very narrow. All the façades, windowed elements included, cannot be modified, and therefore it is not possible to massively intervene on the envelope. Moreover, zone A of the building is also internally protected, limiting the possibilities even further. Regarding the plant, most of its components are still pretty new, therefore solutions concerning this are not considered in this work. Because of this situation, three improvements were hypothesized for the analysed building:

- **A:** Internal insulation of walls pertaining to the modern art museum;
- **B:** Substitution of the existing skylights with new ones featuring solar control window panes;
- **C:** A combination of the previous two.

The internal insulation of the modern art museum

walls was carried out through the insertion of 10 cm of rock wool having a conductivity of 0.038 W/(m K), a density of 35 kg/m^3 and specific heat of 840 J/(kg K), coupled with 2cm of plaster.

The skylights used in the second solution were composed of a PVC frame, of an external coated glass layer, 6 mm thick, having a reduced solar transmission value, 0.3622, a 16mm thick Argon-filled cavity and a standard clear glass layer 4 mm thick. This structure presented a transmittance of 1.554 W/(m^2 K) and the coated external layer aim was to reduce the solar heat gains during the summer season, therefore trying to reduce electricity consumption for cooling.

All three solutions were evaluated regarding their energy and economic aspects. The latter was considered in a simplified way by computing the simple return of the economic investment. Intervention costs were computed using the prices reported in the public regional administration price list "Prezzario Regionale dei Lavori Pubblici" (FVG Region, 2021). By using the reported prices of rock wool per square meter comprehensive of materials and manpower costs, applied to the surface to insulate, a cost of 409,264 € was computed for solution A. The same was done for skylight substitution, in this case considering the price per element and the number of elements to install, and a cost of 67,783 € was computed for solution B. The third solution cost is simply given by summing up the previous two, equal to 477,047 €.

5. Analysis Results

The energy dynamic analysis was first carried out for the state-of-the-art building using the current and the two future TRYs. The results, reported in Table 4, highlight a remarkable reduction of heating gas consumption, and an increase in electricity used for cooling and lighting. The variations compared to the current situation proved to be much more marked in the period 2021-2035 and then to slow down in 2036-2050.

This behavior is in line with the climatic projections, which foresee a slowdown of temperature rise in the second period, as can also be noted by looking at the Degree Days reported in Fig. 1. It is then evident that the cooling component will become more influential in the energy consumption composition of this building.

Table 4 – State-of-the-art simulation results

TRY	Gas use [m^3]	Electr. use [kWh]	Var. Gas [%]	Var. Electr. [%]
1995-2019	52,931	289,193	\	\
2021-2035	43,961	318,398	-16.95	+10.10
2036-2050	42,654	325,025	-19.42	+12.39

Regarding the effects of the refurbishment interventions, reported in Table 5, the analysis highlighted a beneficial effect on both gas and electricity consumption.

Table 5 – Refurbishment effects for every climatic set

ID	Gas use [m^3]	Electr. use [kWh]	Var. Gas [%]	Var. Electr. [%]	Simple Return [years]
1995-2019 TRY					
SOTA	52,931	305,032	\	\	\
A	44,794	304,034	-15.37	-0.33	41
B	50,454	298,267	-4.68	-2.22	17
C	41,699	294,746	-21.22	-3.37	32
2021-2035 TRY					
SOTA	43,961	318,398	\	\	\
A	36,875	317,161	-16.12	-0.39	47
B	41,840	311,235	-4.82	-2.25	19
C	34,395	307,362	-21.76	-3.47	36
2036-2050 TRY					
SOTA	42,654	325,025	\	\	\
A	35,768	323,689	-16.14	-0.41	48
B	40,618	317,525	-4.77	-2.31	19
C	33,345	313,582	-21.82	-3.52	37

As can be seen in Table 5, the obtainable gas consumption reduction varies between 4 and 21 % compared with the state-of-the-art for every climatic set considered. The obtainable electricity consumption reduction is instead much smaller, between 0.3 and 3.5 %, mainly due to the reduced surface treated with the insertion of the new skylights. In general, the best reduction in energy consumption comes from solution C.

However, the economic analysis of these interventions highlighted that they are not economically convenient, showing too-long return times on investment, for every climatic set.

Therefore, coupling these actions with interventions on the plant should be considered. Considering that the generators were replaced a few years ago, and are therefore still functioning well, major interventions could rather focus on the distribution and emission parts of the plant, these being older and less efficient.

6. Conclusions

An energy audit was carried out for the Revoltella museum of Trieste. Great attention was placed on information gathering, this being a historical building featuring particular characteristics.

An evaluation of climate change effects has been carried out for the state-of-the-art building. The present climate was represented through a TRY that was then projected into the future by using different climate models applied to the RCP8.5 scenario. The results showed a steady increase in temperature for the near future, to year 2050, for every climatic model considered. By using the model giving the greatest rise in temperature, climate change effects were evaluated for the museum. Results showed that climate evolution will greatly influence the energy consumption of this building, leading to a decrease in gas consumption, up to 19 %, and an increase in electricity consumption , up to 12 %. Therefore, the municipality of Trieste, owner of the building, should start considering interventions on the building to adapt it to the incoming new working conditions.

In order to provide the municipality with a starting base for this purpose, some refurbishment interventions were modeled for the building for both the current and future climates. By considering the preservation restrictions to which the building is subject, internal insulation of walls and substitution of skylights were considered as feasible interventions. The analysis results showed that a good gas consumption decrease, between 4 and 21 %, would be obtainable for every climatic condition considered. Regarding electricity on the other hand, the beneficial effects would be much less evident, featuring a reduction of between 0.3 and 3.5 % of consumption. This minor effect on electricity is due to the possibility of intervening only on the skylights to reduce solar heat gains during the summer season, the windows on the façades not being replaceable due to the preservation rules. Regarding the economic aspect of the interventions, these did not prove to be economical, showing a too-long return time on investment for every climatic set considered.

Considering all the aspects that emerged from this work, it is strongly recommended for the municipality of Trieste to start designing adaptation measures to address the incoming changes in climate conditions. Results in fact highlighted that in the immediate future the focus of the building performance should be shifted gradually from heating to cooling functioning. That said, internal envelope insulation and skylight substitution proved to be good solutions for heating consumption reduction, but not so much for the cooling solution for every climatic set considered in this work. Therefore, these interventions should be coupled with others mainly pertaining to the plant, mainly focusing on distribution and emission components, given the relative novelty of the generators.

Acknowledgement

The authors wish to thank the municipality of Trieste for providing the valuable information used in this study and for giving access to the building analysed to carry out on-site inspections.

References

Belcher, S., J. Hacker, and D. Powell. 2005. "Constructing design weather data for future climates". *Building Services Engineering Research and Technology* 26: 49-61. doi: https://doi.org/10.1191/0143624405bt112oa

Borozan, D. 2018. "Decomposing the changes in European final energy consumption". *Energy Strategy Reviews* 22: 26-36. doi: https://doi.org/10.1016/j.esr.2018.08.002

Cannon, A. J., S. R. Sobie, T. Q. Murdock. 2015. "Bias Correction of GCM Precipitation by Quantile Mapping: How Well Do Methods Preserve Changes in Quantiles and Extremes?". *Journal of Climate* 28: 6938-6959. doi: https://doi.org/10.1175/JCLI-D-14-00754.1

Cook, J., N. Oreskes, P. T. Doran, W. R. L. Anderegg, B. Verheggen, E. W. Maibach, J. Stuart Carlton, et al. 2016. "Consensus on consensus: A synthesis of consensus estimates on human-caused global warming". *Environmental Research Letters* 11. doi: http://dx.doi.org/10.1088/1748-9326/11/4/048002

Crawley, D. B. 2008. "Estimating the impacts of climate change and urbanization on building performance". *Journal of Building Performance Simulation* 1: 91-115. doi: https://doi.org/10.1080/19401490802182079

Cui, Y., D. Yan, T. Hong, C. Xiao, X. Luo, and Q. Zhang. 2017. "Comparison of typical year and multiyear building simulations using a 55-year actual weather data set from China". *Applied Energy* 195: 890-904. doi: https://doi.org/10.1016/j.apenergy.2017.03.113

De Santoli, L. 2015. "Guidelines on energy efficiency of cultural heritage". *Energy and Buildings* 86: 534-540. doi: https://doi.org/10.1016/j.enbuild.2014.10.050

Directorate-General for Energy. 2021. *EU energy in figures - Statistical pocketbook 2021*. doi: https://doi.org/10.2833/975418

Eurostat. 2020. *Energy data - 2020 edition*. https://doi.org/10.2785/68334

Eurostat. 2015. *Eurostat Manual for air emission accounts - 2015 edition*. doi: https://doi.org/10.2785/527552

Finkelstein, J.M., and R.E. Schafer. 1971. "Improved goodness of fit tests". *Biometrika* 58: 641-645. doi: https://doi.org/10.1093/biomet/58.3.641

Friuli-Venezia Giulia Region. 2021. "Prezzario Regionale dei Lavori Pubblici", 2021. https://www.regione.fvg.it/rafvg/cms/RAFVG/infrastrutture-lavori-pubblici/lavori-pubblici/FOGLIA7/

Interreg ITA-SLO Secap Project 2018. Accessed March 20, 2022. https://www.ita-slo.eu/en/secap

Jentsch, M. F., A. S. Bahaj, and P. A.B. James. 2008. "Climate change future proofing of buildings - Generation and assessment of building simulation weather files". *Energy and Buildings* 40: 2148-2168. doi: https://doi.org/10.1016/j.enbuild.2008.06.005

Palermo, V., P. Bertoldi, M. Apostolou, A. Kona, and S. Rivas. 2020. "Assessment of climate change mitigation policies in 315 cities in the Covenant of Mayors initiative". *Sustainable Cities and Society* 60. doi: https://doi.org/10.1016/j.scs.2020.102258

Paris Agreement 2015. Accessed March 17 2022. https://ec.europa.eu/clima/policies/international/negotiations/paris_en

Radhi, H. 2009. "Evaluating the potential impact of global warming on the UAE residential buildings - A contribution to reduce the CO_2 emissions". *Building and Environment* 44: 2451-2462. doi: https://doi.org/10.1016/j.buildenv.2009.04.006

Robert, A., and M. Kummert. 2012. "Designing net-zero energy buildings for the future climate, not for the past". *Building and Environment* 55: 150-158. doi: https://doi.org/10.1016/j.buildenv.2011.12.014

UNI. 2014. *EN 16247-2: Energy audits – Part 2: Buildings*.

UNI. 2018. *EN 14825: Air conditioners, liquid chilling packages and heat pumps, with electrically driven compressors, for space heating and cooling - Testing and rating at part load conditions and calculation of seasonal performance*.

Wan, K. K.W., D. H.W. Li, W. Pan, and J. C. Lam. 2012. "Impact of climate change on building energy use in different climate zones and mitigation and adaptation implications". *Applied Energy* 97: 274-282. doi: https://doi.org/10.1016/j.apenergy.2011.11.048

Hourly Dynamic Calculation of the Primary Energy With Heat Pump Generation System (EN 15316-4-2): A Case Study in Italy

Giada Remia – Università Politecnica delle Marche, Italy – g.remia@pm.univpm.it
Serena Summa – Università Politecnica delle Marche, Italy – s.summa@univpm.it
Luca Tarabelli – Università Politecnica delle Marche, Italy – l.tarabelli@univpm.it
Costanzo Di Perna – Università Politecnica delle Marche, Italy – c.diperna@univpm.it

Abstract

With the aim of reducing greenhouse gas emissions, more and more heat pump generators are being used in the residential space heating sector to replace traditional condensing gas boilers. This paper discusses the application to an Italian case study of the new draft of EN 15316-4-2, which provides a methodology for the calculation of the energy performance of heat pump systems used for domestic hot water preparation or space heating purpose. The case study involves a two-storey residential building equipped with several modulating air-to-water heat pumps.

Two different daily profiles for heating were considered: continuous heating mode (heating system on 24 hours a day) and intermittent heating mode. Hourly building energy need for heating, calculated according to EN ISO 52016-1:2017, were used as input.

The seasonal coefficient of performance (SCOP) of heat pumps analysed with an intermittent profile are 45.77 % higher on average than those in continuous heating mode, even if, in the intermittent system configuration, there is always an amount of missing energy.

Finally, the results show that oversizing the heat pump leads to low SCOP and high non-renewable primary energy; while undersizing the heat pump leads to high SCOP but non-negligible missing energy values.

1. Introduction

The need to reduce greenhouse gas (GHG) emissions related to building energy production has led Europe to implement policies to reduce energy demand while promoting the use of renewable energy sources to replace fossil fuels.

Residential space heating is one of the sectors most responsible for producing greenhouse gas; one of the most feasible solutions to decarbonise this sector is to electrify consumption by using heat pumps to replace gas boilers. (Famiglietti et al., 2021; Lin et al., 2021).

In the regulatory field, the European Committee for Standardisation (CEN) has approved a set of standards for the implementation of the EPBD (Energy Performance Building Directive) (European Parliament, 2018). These interconnected standards define calculation methodologies for the energy consumption and performance of buildings.

In this package of standards are EN ISO 52016-1:2017 (European Committee for Standardization, 2017) and the new draft of EN 15316-4-2 (European Committee for Standardization, 2018).

Specifically, EN ISO 52016-1 (European Committee for Standardization, 2017) introduces an hourly methodology for calculating the energy need for heating and cooling, while EN 15316-4 deals with the calculation of system energy requirements and system efficiencies according to the different types of generation system.

In the literature, different studies show how the use of the dynamic hourly method defined in UNI EN ISO 52016-1 (European Committee for Standardization, 2017) allows a more accurate assessment of energy needs than a semi-stationary model (Di Giuseppe et al., 2019; van Dijk, 2018) and how the hourly energy needs for heating calculated with the aforementioned standard is comparable with that obtained with TRNSYS (Summa et al., 2022; Zakula et al., 2021).

Regarding the application of the new draft of EN 15316-4-2, there are some studies concerning boilers (Mattarelli & Piva, 2014) and solar thermal

panels (Teodorescu & Vartires, 2016), but not heat pump systems.
To this purpose, this works aims to apply the calculation algorithm provided by the new draft of EN 15316-4-2 (European Committee for Standardization, 2018), concerning heat pump generation systems, on an Italian case study, using as input the hourly energy need for heating, calculated according to EN ISO 52016-1 (European Committee for Standardization, 2017).

2. Methods

2.1 EN ISO 52016-1:2017

The calculation algorithm of EN ISO 52016-1:2017 (European Committee for Standardization, 2017) provides the values of the following hourly parameters: indoor air temperature, mean radiant temperature, operative temperature, surface temperature of building elements and the energy needs for heating and cooling.
These parameters are determined for each thermal zone by providing input of climatic data defined on an hourly basis.
To determine the surface temperatures of the building elements and, consequently, all other parameters, the calculation algorithm provides the procedure for spatial discretization of the capacitive nodes and resistive layers of the opaque and transparent elements based on the thermoelectric analogy.
Transparent elements are discretized by two capacitive nodes and one resistive layer, and opaque elements by five capacitive nodes and four resistive layers.

2.2 EN ISO 15316-4-2

The calculation algorithm of the new draft of EN 15316-4-2 (European Committee for Standardization, 2018) provides as output the following hourly parameters: the total electrical energy, the energy from the cold source, the coefficient of performance (COP) of the heat pump, and the energy not supplied by the heat generator.
The algorithm also provides the amount of energy supplied by back-up systems (electrical resistance) if the heat pump is not able to supply the required energy.
All these parameters are calculated separately for heating and domestic hot water.
The hourly profiles of outdoor temperature, indoor operative temperature, energy needs for heating, and domestic hot water, and the water flow temperature according to the system must be provided as input.
Finally, data concerning the heat pump must be entered, identifying its technology, the source and sink type.
The services the heat pump is used for, the presence of any back-up systems and its power and COP at full load, declared by the manufacturer, must also be specified.

3. Case Study

The case study is a two-storey residential building (Fig.1) with a bathroom, a storage room, a kitchen and a living room on the ground floor and two single rooms, a double room, a bathroom and a hallway on the first floor.
The stairwell and attic are unheated thermal zones. The net floor height is 2.70 m, while the net floor area is 129.64 m^2. The thermo-physical characteristics of the building elements are shown in Table 1.
Aiming at evaluating different climatic contexts, the case study focuses on three Italian locations: Milan, Rome and Palermo. The input hourly climate data were calculated according to UNI 10349 (Ente Nazionale Italiano di Unificazione, 2016). The analysis was carried out for the winter period in order to evaluate the behavior of the heat pump for the heating season only.
Two daily profiles for heating were considered, both with a set-point temperature of 20 °C: (i) the first ON 24h/24h and (ii) the second intermittent with a number of working hours equal to the maximum allowed by Presidential Decree 412/93 (Presidente della Repubblica, 1993) depending on the climatic zone considered (Tab.2).
As an evaluation of the operation of the only heat pump for heating is intended, the production of domestic hot water, the thermal storage and back-up heater have not been considered. Four modulat-

ing air-to-water heat pumps (AWHP) were analysed, with increasing powers of 2.3 kW, 4.6 kW, 5.8 kW and 8.3 kW, values declared according to UNI EN 14511-1:2018.

The hourly profile of water flow temperature for the heat pump was determined through a climatic curve as a function of the air outside temperature and the design temperature of the location considered. Furthermore, distribution, emission and regulation efficiency were not taken into account as assumptions.

4. Results

Using the hourly energy needs for heating calculated according to EN ISO 52016-1 (European Committee for Standardization, 2017) as input values, the electrical energy, the thermal energy from cold external source (air) and the COP of the heat pump per hour were determined using the new draft of EN 15316-4-2 EN 15316-4-2 (European Committee for Standardization, 2018).

Moreover, the primary renewable and non-renewable energy was calculated based on the energy sources used. The comparison between the different heat pumps was made using the SCOP, which is calculated as the ratio between the supplied energy and the respective electricity consumption during the heating season.

Fig. 2 shows how the SCOP are, on average, 45.77 % higher in the case of intermittent use of heating system than constant use.

Considering the four heat pumps used, switching from a constant to an intermittent profile, the average SCOP increase for Milan, Rome and Palermo is 20.10 %, 48.53 % and 68.67 %, respectively.

Considering the same heat pump and varying the daily heating profiles of the buildings analyzed, qualitatively the same pattern is observed for each location: (i) in the case of constant use, the load factor decreases to values of 0.30 or less, with consequent reduction of COP, which happens during the hours when heating energy need is reduced; (ii) in the intermittent mode, on the other hand, having a higher power demand for the heat pump, the load factor is higher, with a consequent higher COP.

For this reason, in the case of Rome and Palermo, where the number of hours the system is switched on is lower than in Milan, the average SCOP variation between intermittent and continuous use is higher.

Therefore, a more intermittent system implies a higher power demand in the first hours of operation and a limited number of hours with reduced load factors.

These two aspects result in higher seasonal COP in the intermittent regime than in the constant daily profile for heating.

In order to assess the different behavior of heat pumps, it is not sufficient to analyze only the SCOP. For this reason, it is also necessary to evaluate the possible presence of missing energy, i.e., not supplied by the heat pump ($Q_{H,gen,add}$).

This analysis was carried out for all the locations considered. Since the results obtained follow the same trend for each location, the decision to specifically analyze the results obtained for the coldest location, i.e., Milan, was made.

Table 3 shows the missing energy for each heat pump used and for the two daily profiles of the heating system considered. Moreover, the percentage of missing energy in relation to the energy required by the heat pump ($Q_{H,gen,out,req}$) and the percentage of hours when the missing energy is present compared to the heating period are listed.

Table 3 shows how, in the intermittent system configuration, there is always an amount of energy not supplied by the heat pump.

The SCOP are higher in the intermittent mode but, on the other hand, the heat pumps always return a higher missing energy than in the constant profile, where there is no missing energy, except for the smallest heat pump.

Table 3 also provides useful information for determining the correct heat pump size for the building analyzed. Results show how the AWHP 4.6 kW does not result in an amount of missing energy in the case of constant mode, while, for the intermittent profile, the energy not provided is equal to 2.76 % of the energy required for heating.

Moreover, AWHP 5.8 kW has a similar operation to the AWHP 4.6 kW for intermittent operation but would be oversized for constant daily profile use.

Oversizing or undersizing a heat pump has conse-

quences in terms of both primary energy and missing energy. An undersized heat pump (AWHP 2.3 kW) is characterized by a high SCOP (Fig. 2), but also by significant missing energy values (Table 3).
An oversized heat pump (e.g., AWHP 8.3 kW) is characterized by a reduced SCOP, which is reflected in a higher primary energy, while not resulting in missing energy. In fact, Fig. 3 shows that the primary energy is higher in the case of the largest generator, i.e., AWHP 8.3 kW. Furthermore, the increase in primary energy leads to an increase of the non-renewable energy.

5. Conclusion

The new draft of EN 15316-4-2 (European Committee for Standardization, 2018), which provides a methodology for calculation of system energy requirements and system efficiencies for heat pump systems, has so far limited application in the literature. For this reason, in this paper the above-mentioned standard was tested by applying it to a residential building located in three different Italian cities and using the hourly energy need, calculated according to EN ISO 52016-1 (European Committee for Standardization, 2017), as input data.
This application shows that

- the use of an intermittent heating profile brings the heat pump to higher COP than a constant continuous heating mode;
- higher intermittency of the system implies a higher power demand in the first hours of operation and a limited number of hours with reduced load factors. These two aspects result in higher SCOP in the intermittent regime than in the constant on regime;
- in contrast, in the intermittent system configuration, an amount of energy not supplied by the heat pump is always present; this leads to an increase in non-renewable primary energy due to the need for an integrated back-up system (e.g., electrical resistance) or a second generator;
- undersizing the heat pump leads to high SCOP but non-negligible missing energy values.
- oversizing the heat pump leads to low SCOP and high non-renewable primary energy.

These results concern the case studies proposed and the methodologies associated with the standards used. The future development of this work will be to extend the calculation by considering an integrated back-up system (electrical resistance) and a storage system in order to assess their possible impact on the results.

Nomenclature

Symbols

COP	Coefficient of performance (-)
SCOP	Seasonal coefficient of performance (-)
M_s	Surface mass (kg/m^2)
U	Thermal transmittance (W/(m^{2}K))
Y_{IE}	Periodic thermal transmittance (W/(m^{2}K))
EP	Primary energy (kWh)
AWHP	Air-to-water heat pump

References

Di Giuseppe, E., G. Ulpiani, S. Summa, L. Tarabelli, C. Di Perna, and M. D'Orazio. 2019. "Hourly dynamic and monthly semi-stationary calculation methods applied to nZEBs: Impacts on energy and comfort." *IOP Conference Series: Materials Science and Engineering* 609: 1–8. doi: https://doi.org/10.1088/1757-899X/609/7/072008

Ente Nazionale Italiano di Unificazione. 2016. *UNI 10349-1:2016 - Riscaldamento e raffrescamento degli edifici - Dati climatici - Parte 1: Medie mensili per la valutazione della prestazione termo-energetica dell'edificio e metodi per ripartire l'irradianza solare nella frazione diretta e diffusa e per calcolare l'irradianza solare su di una superficie inclinata.*

European Committee for Standardization. 2018. *EN 15316-4-2:2018 - Energy performance of buildings - Method for calculation of system energy requirements and system efficiencies - Part 4-2: Space heating generation systems, heat pump systems, Module M3-8-2, M8-8-2.*

European Committee for Standardization. 2017. *EN ISO 52016-1:2017 - Energy performance of buildings — Energy needs for heating and cooling, internal temperatures and sensible and latent head*

loads — Part 1: Calculation procedures Performance.

European Parliament. 2018. "Directive (EU) 2018/844 of the European Parliament and of the Council of 30 May 2018 amending Directive 2010/31/EU on the energy performance of buildings and Directive 2012/27/EU on energy efficiency." *Official Journal of the European Union.*

Famiglietti, J., T. Toppi, L. Pistocchini, R. Scoccia, and M. Motta. 2021. "A comparative environmental life cycle assessment between a condensing boiler and a gas driven absorption heat pump." *Science of the Total Environment* 762: 144392. https://doi.org/10.1016/j.scitotenv.2020.144392

Lin, H., J. Clavreul, C. Jeandaux, J. Crawley, and I. Butnar. 2021. "Environmental life cycle assessment of heating systems in the UK: Comparative assessment of hybrid heat pumps vs. condensing gas boilers." *Energy and Buildings* 240: 110865. https://doi.org/10.1016/j.enbuild.2021.110865

Mattarelli, A., and S. Piva. 2014. "EN 15316 Calculation Methods for the Generation Sub-system: The Influence of Input Data on the Results." *Energy Procedia* 45: 473–481. https://doi.org/10.1016/j.egypro.2014.01.051

Presidente della Repubblica. 1993. *DECRETO DEL PRESIDENTE DELLA REPUBBLICA 26 agosto 1993, n. 412*. Italy.

Summa, S., G. Remia, and C. Di Perna. 2022. "Comparative and Sensitivity Analysis of Numerical Methods for the Discretization of Opaque Structures and Parameters of Glass Components for EN ISO 52016-1." *Energies* 15. https://doi.org/10.3390/en15031030

Teodorescu, D., and A. Vartires. 2016. "A Study of the Influence of Solar Panels Coupled with Thermal Systems for a Residential Building, by Applying Methods of Evaluation as EN 15316-4-3:2014 and TRANSOL." *Energy Procedia* 85: 530–538. https://doi.org/10.1016/j.egypro.2015.12.240

van Dijk, D. 2018. "EPB standards: Why choose hourly calculation procedures?" *REHVA Journal.*

Zakula, T., N. Badun, N. Ferdelji, and I. Ugrina. 2021. "Framework for the ISO 52016 standard accuracy prediction based on the in-depth sensitivity analysis." *Applied Energy* 298: 117089. https://doi.org/10.1016/j.apenergy.2021.117089

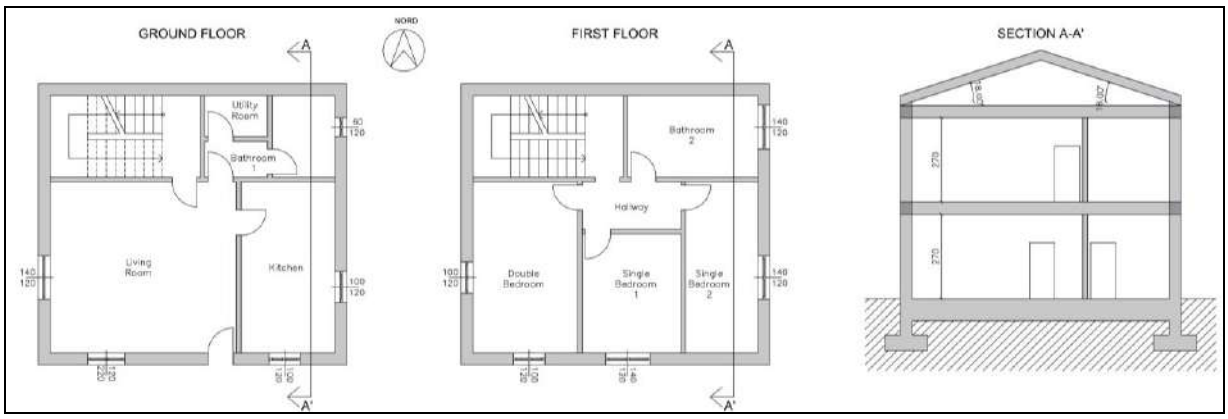

Fig. 1 – Plan view of the ground floor, first floor and section of the case study

Table 1 – Thermo-physical characteristics of the structures

	Thermophysical Parameters	Milan	Rome	Palermo
External Wall	U [W/(m²K)]	0.22	0.24	0.36
	M_s [kg/m²]	227.80	228.86	274.85
	Y_{IE} [W/(m²K)]	0.007	0.007	0.018
Ground Floor	U [W/(m²K)]	0.25	0.27	0.35
	M_s [kg/m²]	1370.60	1370.30	1369.40
	Y_{IE} [W/(m²K)]	0.007	0.007	0.010
Sub-roofing Floor	U [W/(m²K)]	0.24	0.27	0.37
	M_s [kg/m²]	363.60	363.00	362.10
	Y_{IE} [W/(m²K)]	0.038	0.028	0.064
Internal Floor	U [W/(m²K)]	1.13	1.13	1.13
	M_s [kg/m²]	111.60	111.60	111.60
	Y_{IE} [W/(m²K)]	0.673	0.673	0.673
Roof	U [W/(m²K)]	0.70	0.70	0.70
	M_s [kg/m²]	427.20	427.20	427.20
	Y_{IE} [W/(m²K)]	0.120	0.120	0.120
Internal Wall	U [W/(m²K)]	0.35	0.35	0.35
	M_s [kg/m²]	403.80	403.80	403.80
	Y_{IE} [W/(m²K)]	0.039	0.039	0.039

Table 2 – Different daily profiles for heating system, according to the three thermal zone considered.

Climatic Zone	Time Intervals	Heating Period
Milan	6:00-12:00/17:00-23:00	15 October - 15 April
Rome	6:00-11:00/18:00-23:00	1 November - 15 April
Palermo	7:00-10:00/19:00-22:00	1 December - 31 March

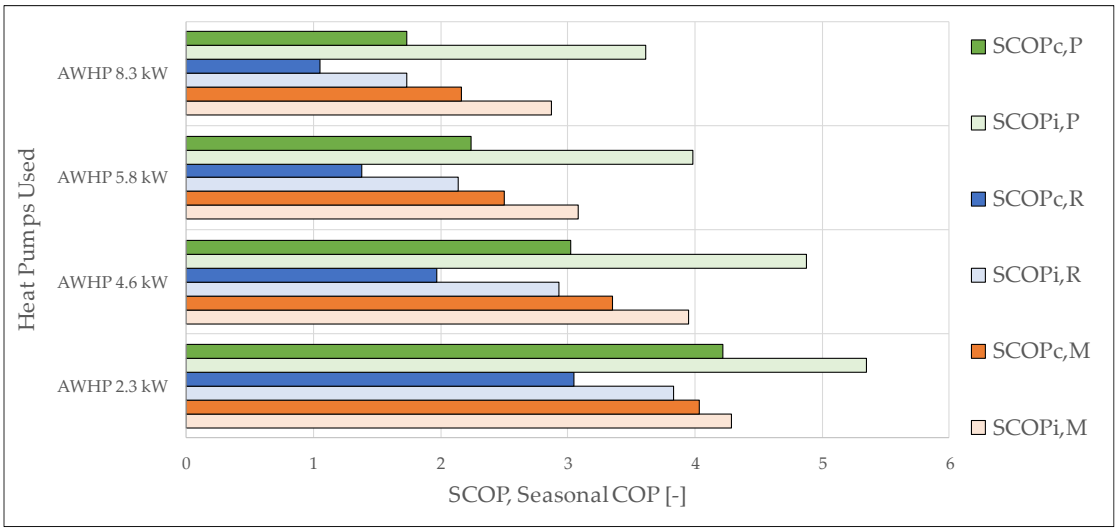

Fig. 2 – Seasonal COP for the three locations, two daily profiles for heating, four heat pumps: c/i:continuos/intermittent heating, P/R/M: Palermo, Rome, Milan

Table 3 – Energy not provided by the heat pump ($Q_{H,gen,add}$); percentage between energy not supplied and energy required for heating ($Q_{H,gen,add}$/ $Q_{H,gen,out,req}$); percentage between the number of hours corresponding to missing energy and the total heating period ($h_{Q,gen,add}$/ $h_{QH,gen,out,req}$)

	Milan					
	Intermittent Heating			Continuous Heating		
Heat Pump	$Q_{H,gen,add}$ [kWh]	$Q_{H,gen,add}$/ $Q_{H,gen,out,req}$ [%]	$h_{Q,gen,add}$/ $h_{QH,gen,out,req}$ [%]	$Q_{H,gen,add}$ [kWh]	$Q_{H,gen,add}$/ $Q_{H,gen,out,req}$ [%]	$h_{Q,gen,add}$/ $h_{QH,gen,out,req}$ [%]
AWHP 2.3 kW	641	18.62 %	30,29 %	18	0.51 %	5.20 %
AWHP 4.6 kW	95	2.76 %	3.72 %	0	0 %	0 %
AWHP 5.8 kW	75	2.17 %	3.19 %	0	0 %	0 %
AWHP 8.3 kW	1	0.04 %	0.33 %	0	0 %	0 %

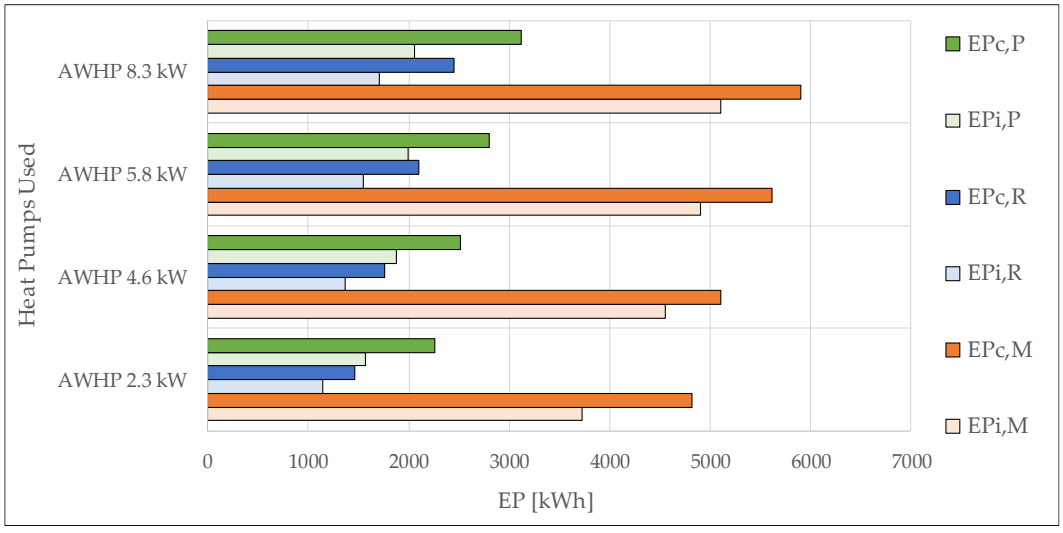

Fig. 3 – Primary energy for the three locations, two daily profiles for heatings, four heat pumps: c/i:continuos/intermittent heating, P/R/M: Palermo, Rome, Milan

A Project Focused on Sound Diffusion: The Acoustics of the Auditorium Yves St Laurent of Marrakech in Combination With its Innovative Architectural Design

Lamberto Tronchin – University of Bologna, Italy – lamberto.tronchin@unibo.it
Antonella Bevilacqua – University of Parma, Italy – antonella.bevilacqua@unipr.it
Ruoran Yan – University of Bologna, Italy – ruoran.yan2@unibo.it

Abstract

Yves St Laurent Auditorium was built at the core of Morocco as part of the museum that honors the French fashion designer. The interior and architectural design of the Auditorium evokes the colors and the materials typical of Marrakech, with bricks and wood being the primary structural resources of construction there. The shoebox envelope was modeled to accommodate ergonomically the select audience attending specific performances oriented towards fashion design. The sound diffusion was realized with the application of quadratic residue diffusers (QRD) installed on all the walls in a vertical configuration. These acoustic panels increase the phenomenon of sound scattering in all directions, making listening very warm and comfortable. This paper deals with the assessment of the main acoustic parameters gathered by the acoustic simulations of a digital model. The simulated values were compared with the optimal values of performing arts spaces of similar room volume.

1. Introduction

Auditoria have often been considered multipurpose places thanks to their suitability for hosting conferences and musical performances (Bettarello et al., 2021). The challenges that architects and acousticians have to face are varied, going from interior design to materials selection based on geometrical characteristics, as well as for energy building and musical instruments simulation, (Fabbri et al., 2014; Manfren et al., 2021a, 2021b, and 2022; Tronchin et al., 2020) and lighting comfort for all the different events. The YSL Auditorium of Marrakech summarises all the aspects that a design project finds as opportunities to extract the best architectural product from certain constraints. This paper deals with the acoustic simulations of the Yves St Laurent Auditorium based on different absorption coefficients assigned to different materials of the 3D models. The results of the simulated values were compared based on the main acoustic parameters.

2. Historical Background

Yves St Laurent Auditorium is located in the Saint Laurent Museum in Marrakesh, which was built in memory of the famous French fashion designer, Yves Saint Laurent (Sabbah, 2021; Vorländer, 2007) (www.museeyslmarrakech.com/en/auditorium/).
The main purpose of the museum is to encourage cultural projects by displaying Yves Saint Laurent's masterpieces, and to preserve and disseminate his works in France and the rest of the world.
Fondation Pierre Bergé launched the Musée Yves Saint Laurent Paris project in 2017. However, this was not enough to show all the designer's artistic heritage, so they found another place to display Yves Saint Laurent's works.

Fig. 1 – Internal view of the Auditorium YSL of Marrakech

The Auditorium, jointly designed by the consulting experts of theatre projects and Ko architectural office studio (Sabbah, 2021), is located at the center of the museum with the aim of hosting conferences, screen shows, concerts, plays, films and other activities.

3. Architectural Characteristics

Seen from the outside, the entire building is composed of cubical shapes dressed in terracotta bricks as a reminder of the fabric of the local place, as shown in Fig. 1.

The auditorium was designed for a total capacity of 113 seats, with a total volume of 650 m^3 and a high degree of flexibility, high acoustic quality and a lighting system capable of fulfilling a variety of activities (Sabbah, 2021). This multi-functionality is visible by the integration of a series of design elements with the technical tools to create a perfect experience for both performers and audience. The streamlined organization inside the auditorium is very logical and highly accessible. The adjustable sound-diffusing panels in the acoustic walls have excellent flexibility (for controlling reverberation time based on several different needs: natural or amplified musical shows, conference hall, or cinema screen (Tronchin, 2005; Tronchin et al., 2021a). Figs. 2 and 3 show the longitudinal section and the internal view of the auditorium, respectively.

Fig. 2 – Longitudinal section of Yves St Laurent Auditorium of Marrakech

Fig. 3 – Internal view of Yves St Laurent Auditorium of Marrakech

The ceiling of the auditorium is equipped with motorized wooden slats to regulate the sense of spaciousness based on the diffusing geometry that they can assume (Tronchin & Bevilacqua, 2022). The lateral walls are characterised by quadratic residue diffusers (QRDs), which contribute to the uniform distribution of the sound across the sitting area (Farina et al., 1998; Tronchin, 2021). The purpose of the diffusing panels is to spread uniformly sound energy in all directions and to reduce energy concentration and/or undesired reflections across the volume (Manfren et al., 2019). In the case of the QRDs, the reflections are spatially dependent and follow a numerical sequence provided by a uniform spatial Fourier transform (Tronchin et al., 2021b). The external envelope is composed of a double skin wall able to provide enough airborne sound insulation to stop intrusive noise (Bettarello et al., 2010).

4. Acoustic Simulation Setup

A digital model was created by using AutoCAD software (Caniato et al., 2020a and 2020b), where the 3D face entities were grouped based on type of material (Tronchin et al., 2020, 2021c; Vorländer, 2007). A view of the digital model is shown in Fig. 4.

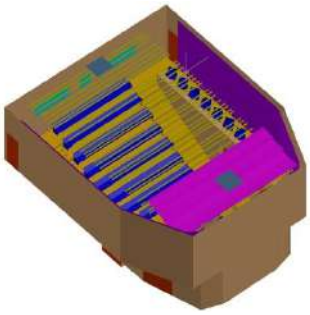

Fig. 4 – Digital model of Yves St Laurent Auditorium of Marrakech

The 3D model was exported in dxf format ready to be employed in the acoustic simulations. An omnidirectional sound source was placed on the stage, while 113 receivers were placed at different heights by homogeneously covering all area of the stalls.
The simulation process was undertaken in two different steps: the first by applying the absorption coefficients as per the literature (Caniato et al., 2019; Farina et al., 1998; Tronchin & Bevilacqua, 2021; Tronchin & Farina, 1997), the second by calibrating the absorption coefficient based on experience of similar auditoria of comparable volume size. The difference between the two simulations is in the adjustment of the spectra related to the fabric, lowered by up to 0.6, and to the ceiling panels, lowered by up to 0.4.

5. Simulated Results

The main acoustic parameters were analysed by considering the bandwidth ranging from between 125 Hz and 8 kHz to be considered the average values of all the receivers.

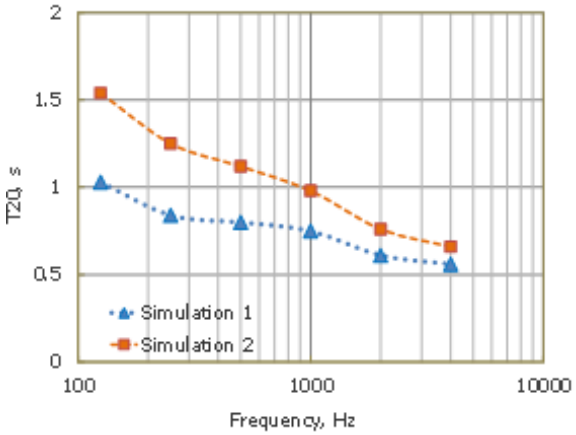

Fig. 5 – Simulated values of T_{20}

Fig. 5 indicates the simulated T_{20} values. The first simulation had absorption coefficients of the fabric close to 0.9, while the second one had absorption coefficients fluctuating around 0.3. Considering that the fabric covers a surface area equal to 58 m^2, it is considered the main determining factor of the T_{20} difference, highlighted especially at low frequencies (Wang et al., 2004).
Due to the multipurpose function assigned to this auditorium, intended to be suitable for both musical and conference events (Mickaitis et al., 2021; Tronchin & Knight, 2016), the overall T_{20} value of the two simulations was compared to the room volume, as indicated in Fig. 6.

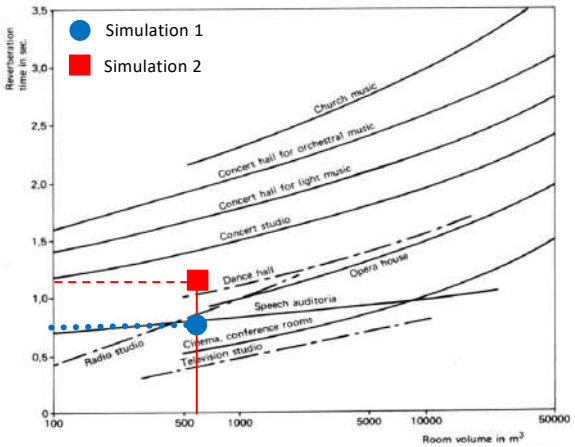

Fig. 6 – Optimal T_{20} values based on room volume

Fig. 6 highlights that the first simulation meet the criteria of a speech auditorium, while the second one turns out to be closer to a musical performance.

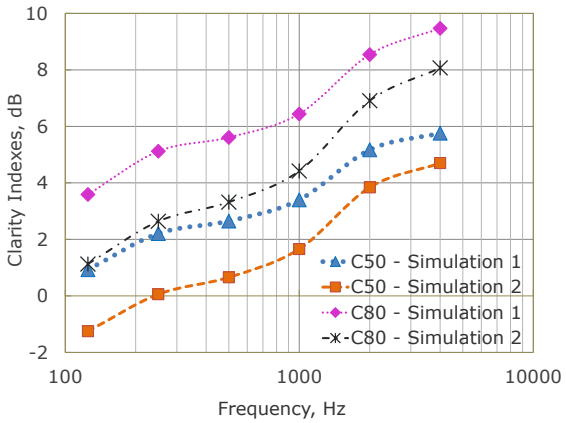

Fig. 7 – Simulated values of Clarity Indexes

Fig. 7 indicates the results of clarity indexes. In relation to speech (C_{50}), the values of the second simulations are within the optimal range (-2 dB < C < +2 dB) (Tronchin et al., 2020) for the octaves ranging from between 125 Hz and 1 kHz, while the higher frequencies are up to 4 dB above the upper range limit. In terms of music, (C_{80}), the results of both simulations were found to be up to 7 dB above the upper range limit across all the spectra.

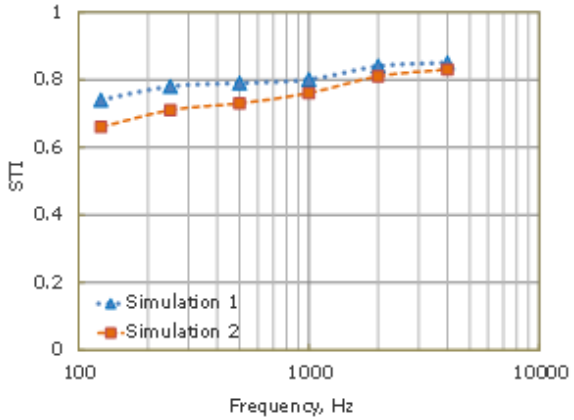

Fig. 8 – Simulated STI values

Fig. 8 shows the results related to speech comprehension. The simulated values of both simulations have been found to be above 0.6 for all octaves. This means that the overall result falls into a "good" category, even "excellent" at mid-high frequencies, as defined by the intelligibility rating according to ISO 9921.

6. Conclusion

This paper deals with two acoustic simulations of the YSL Auditorium of Marrakech. The contained room volume, allocating 113 seats, was designed with motorised wooden slats on the ceiling that can optimize the reverberation time based on the required functionality. The multipurpose hall, intended to be suitable for both speech and musical performances, also involves the design accuracy of the construction elements, like the side walls characterised by the QRD panels.

Two acoustic simulations were carried out by changing mainly the fabrics and the diffuser absorption coefficients. The difference between these is more evident at low frequencies for the T_{20}, while the clarity index for speech and music both proved to be up to 6 dB above the upper range limit, especially at mid-high frequencies. The STI values, found to be more than 0.65 across all the spectra, fall within the excellent category rating.

Further research studies will deepen the investigation by comparing the simulated values with the on-site acoustic measurements (Caniato et al., 2021) in order to define the tuning process.

References

Bettarello, F., P. Fausti, V. Baccan, and M. Caniato. 2010. "Impact Sound Pressure Level Performances of Basic Beam Floor Structures". *Building Acoustics* 17(3): 305-316. doi: https://doi.org/10.1260/1351-010X.17.4.305

Bettarello, F., M. Caniato, G. Scavuzzo, and A. Gasparella. 2021. "Indoor Acoustic Requirements for Autism-Friendly Spaces". *Applied Science* 11: 3942. doi: https://doi.org/10.3390/app11093942

Caniato, M., F. Bettarello, C. Schmid, and P. Fausti. 2019. "The use of numerical models on service equipment noise prediction in heavyweight and lightweight timber buildings". *Building Acoustics* 26(1): 35-55. doi: https://doi.org/10.1177/1351010X18794523

Caniato, M., F. Bettarello, P. Bonfiglio, and A. Gasparella. 2020a. "Extensive Investigation of Multiphysics Approaches in Simulation of

Complex Periodic Structures". *Applied Acoustics* 166: 107356. doi: https://doi.org/10.1016/j.apacoust.2020.107356

Caniato, M., C. Schmid, and A. Gasparella. 2020b. "A comprehensive analysis of time influence on floating floors: Effects on acoustic performance and occupants' comfort". *Applied Acoustics* 166: 107339. doi: https://doi.org/10.1016/j.apacoust.2020.107339

Caniato, M., F. Bettarello, and A. Gasparella. 2021. "Indoor and outdoor noise changes due to the COVID-19 lockdown and their effects on individuals' expectations and preferences". *Scientific Reports* 11: 16533. doi: https://doi.org/10.1038/s41598-021-96098-w

Fabbri, K., L. Tronchin, and V. Tarabusi. 2014. "Energy Retrofit and Economic Evaluation Priorities Applied at an Italian Case Study". *Energy Procedia* 45: 379-384. doi: 10.1016/j.egypro.2014.01.041

Farina, A., A. Langhoff, and L. Tronchin. 1998. "Acoustic characterisation of "virtual" musical instruments: using MLS technique on ancient violins." *Journal Of New Music Research* 27(4): 359-379. doi: https://doi.org/10.1080/09298219808570753

Manfren, M., B. Nastasi, E. A. Piana, and L. Tronchin. 2019. "On the link between energy performance of building and thermal comfort: An example". *AIP Conference Proceedings* 2123: 1-9. doi: https://doi.org/10.1063/1.5116993

Manfren, M., B. Nastasi, L. Tronchin, D. Groppi, and D. A. Garcia. 2021a. "Techno-economic analysis and energy modelling as a key enablers for smart energy services and technologies in buildings". *Renewable and Sustainable Energy Reviews* 150: 1-14. doi: https://doi.org/10.1016/j.rser.2021.111490

Manfren, M., M. Sibilla, and L. Tronchin. 2021b. "Energy Modelling and Analytics in the Built Environment—A Review of Their Role for Energy Transitions in the Construction Sector". *Energies* 14:1-29. doi: https://doi.org/10.3390/en14030679

Manfren, M., P. A. B. James, and L. Tronchin. 2022. "Data-driven building energy modelling – An analysis of the potential for generalisation through interpretable machine learning". *Renewable and Sustainable Energy Reviews* 167: 1-13. doi: https://doi.org/10.1016/j.rser.2022.112686

Mickaitis, M., A. Jagniatinskis, and B. Fiks. 2021. "Case study of acoustic comfort in conference room". *Proc. 27th International Congress of Sound & Vibration*.

Sabbah, C. 2021. *Studio KO. Yves Saint Laurent Museum Marrakech*.

Tronchin, L. 2005. "Modal analysis and intensity of acoustic radiation of the kettledrum." *The Journal Of The Acoustical Society Of America* 117(2): 926-933. doi: https://doi.org/10.1121/1.1828552

Tronchin, L. 2021. "Variability of room acoustic parameters with thermo-hygrometric conditions." *Applied Acoustics* 177: 1-14. doi: https://doi.org/10.1016/j.apacoust.2021.107933

Tronchin, L., and A. Bevilacqua. 2021. "Acoustic study of different sceneries at the São Carlos national theatre of Lisbon." *Applied Acoustics* 180: 1-11. doi: https://doi.org/10.1016/j.apacoust.2021.108102

Tronchin, L., and A. Bevilacqua. 2022. "Historically informed digital reconstruction of the Roman theatre of Verona. Unveiling the acoustics of the original shape." *Applied Acoustics* 185: 1-18. doi: https://doi.org/10.1016/j.apacoust.2021.108409

Tronchin, L., and A. Farina. 1997. "Acoustics of the former Teatro "La Fenice" in Venice." *Journal of the Audio Engineering Society* 45(12): 1051-1062.

Tronchin, L, and D. J. Knight. 2016. "Revisiting Historic Buildings through the Senses. Visualising Aural and Obscured Aspects of San Vitale, Ravenna." *International Journal of Historical Archaeology* 20: 127-145. doi: https://doi.org/10.1007/s10761-015-0325-2

Tronchin, L., F. Merli, M. Manfren, and B. Nastasi. 2020. "The sound diffusion in Italian Opera Houses: some examples." *Building Acoustics* 27(4): 333-355. doi: https://doi.org/10.1177/1351010X20929216

Tronchin, L., F. Merli, and M. Manfren. 2021a. "On the acoustics of the Teatro 1763 in Bologna." *Applied Acoustics* 172: 1-9. doi: https://doi.org/10.1016/j.apacoust.2020.107598

Tronchin, L., A. Farina, A. Bevilacqua, F. Merli,

and P. Fiumana. 2021b. "Comparison failure and successful methodologies for diffusion measurements undertaken inside two different testing rooms." *Applied Sciences* 11: 10523. doi: https://doi.org/10.3390/app112210523

Tronchin, L., F. Merli, and M. Dolci. 2021c. "Virtual acoustic reconstruction of the Miners' Theatre in Idrija (Slovenia)." *Applied Acoustics* 172: 1-9. doi: https://doi.org/10.1016/j.apacoust.2020.107595

Vorländer, M. 2007. "Fundamentals of Acoustics, Modelling, Simulation. Algorithms and Acoustic Virtual Reality".

Wang, L. M., J. Rathsam, and S. R. Ryherd. 2004. "Interactions of model detail level and scattering coefficients in room acoustic computer simulation." *Proc ISRA.*

www.museeyslmarrakech.com/en/auditorium/. Accessed March 10, 2022.

On the Prints of Another Horseshoe-Shaped Historical Building: Acoustic Studies of the Bonci Theatre of Cesena

Antonella Bevilacqua – University of Parma, Italy – antonella.bevilacqua@unipr.it
Ruoran Yan – University of Bologna, Italy – ruoran.yan2@unibo.it

Abstract

The Bonci theatre in Cesena was built in 1846, becoming a stable public construction after a period when theatrical shows used to be privately performed inside aristocratic palaces. The architectural design, to be composed of 5 orders of balconies and the shape of the plan layout follow, in reduced dimensions, the Alla Scala theatre in Milan. Acoustic measurements were taken across the stalls and inside some selected boxes according to BS3382-1. The main acoustic parameters gathered by the measured values were compared with the acoustic simulations of a 3D model, which faithfully reproduces the Bonci theatre. The scope of this paper is the analysis of the acoustic behavior of the Bonci theatre, which can be used to calibrate a digital model before the executions of any acoustic simulations. This practice is fundamental for the accuracy of the results, which shall be carried out by comparing the measured with the calibrated values. A review of the historical background has been introduced to allow an appreciation of the architectural value of this cultural heritage.

1. Introduction

The acoustic discoveries of cultural heritage buildings have always been appreciated by the amateurs that experience these places on a regular basis. Additionally, this enriches the knowledge of experts and scholars focused on existing architectural patrimony of important value (Bettarello et al., 2021; Dordevic, 2016; Vecco, 2010). On this basis, this paper deals with the acoustic characteristics of Bonci theatre of Cesena, measured in line with the standard requirements outlined by ISO 3382 (Iannace & Ianniello, 2008; ISO, 2009; Tronchin et al., 2021a). The shape of the horseshoe plan layout is typical of a 19th century opera theatre characterised with four orders of balconies and a top gallery at the last level (Azzaroni et al., 1997; Battaglia et al., 1992; Iannace & Ianniello, 2008). The results highlight that the acoustic response of the Bonci theatre is suitable for both speech and music, which is what these building types were built for (Farina, 2007; Jordan, 1981; Tronchin et al., 2006). The acoustic parameters meet the criteria of a theatre having similar room volume. This analysis shall be considered as a preparatory study taken into account before any acoustic simulations are carried out upon a digital model.

2. Historical Background

Bonci theater in Cesena was formerly known as Spada theatre in the Aledossi Palace (Azzaroni et al., 1997; Iannace et al., 2019; Puglisi et al., 2021). In 1822, the community of Cesena wanted to purchase the noble theatre from the gonfalonier and build new walls and a solid public theatre (Iannace et al., 2000; Tronchin & Knight, 2016; Tronchin et al., 2020).

In 1842, the construction of Bonci theatre was planned under the supervision of the architect Ghinelli, but, due to financial difficulties, the project started the year after. In 1846, the main frame of the building, decoration, scene construction and furniture of the theater were completed (Battaglia et al., 1992).

Fig. 1 – Internal view of the Bonci theatre in Cesena

Bonci theater represents the paradigm of an Italian theater, with harmonious internal space organization, reflecting the perfect combination of functionality with aesthetics (Tronchin & Bevilacqua, 2022). The internal decorations show the characteristics of the neoclassical style, as indicated in Fig. 1.
Bonci theater is characterized by four orders of balconies and a top gallery (*loggione*). The plan layout of the theater presents a horseshoe shape geometry. In particular, the final design opted for a total number of 23 boxes per balcony, to be 1.7 m wide at the parapet line.

The main hall is richly decorated, and the ceiling, with its allegorical representations, is embedded in a circular panel carved with gold-plated vine patterns. The walls of the main hall are treated with polished plaster, as shown in Fig. 2. The interior design of the boxes is also characterised by polished and stuccoed walls.

Fig. 2 – Decorations of the ceiling

Due to the existence of underground waterways, the foundation of the theater is built on wooden poles, which support a peripheral wall cage containing separated functional units and a large roof supported by huge trusses (Farina & Tronchin, 2000; Tronchin, 2021).
Nowadays, the theater is considered a real "machine" for the artistic shows that run throughout the year.

3. Architectural Organization

Bonci theater has a horseshoe-shaped plan layout, as shown in Fig. 3, having a total capacity of 930 seats, distributed as 364 in the stalls, 130 in the top gallery (*loggione*), and the rest across four orders of balconies composed of 25 boxes.
The surface area of the fly tower is a square of 24 m side having a height of 18 m and an inclination of 5 %. The proscenium arch is 12 m wide with a height of up to 7.8 m.

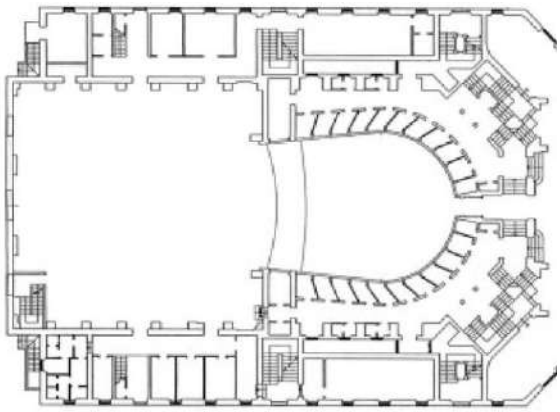

Fig. 3 – Plan layout of Bonci theater of Cesena

4. Acoustic Measurements

Acoustic measurements were carried out inside Bonci theater by using the following equipment:

- Equalised omnidirectional loudspeaker (Look Line);
- Binaural dummy head (Neumann KU-100);
- B-Format (Sennheiser Ambeo);

The sound source and the receivers were located across the stalls and in some selected boxes at different orders, as shown in Fig. 4.

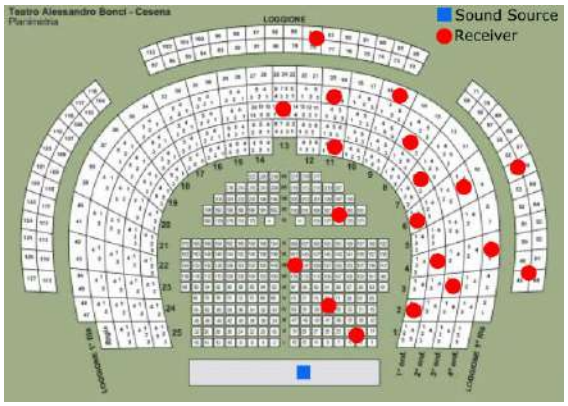

Fig. 4 – Equipment positions during the acoustic survey

The sound source was placed on the stage at a height of 1.4 m and the receivers were moved across the stalls and in the boxes by recording the Impulse Responses (IRs). The excitation signal (Bettarello et al., 2010) was the Exponential Sine Sweep (ESS) (Farina, 2007; Tronchin et al., 2021b), which was 15 s long, by covering a spectrum bandwidth ranging between 40 Hz and 20 kHz. The measurements were taken in unoccupied conditions.

5. Results

The recorded IRs were processed with the Aurora plugin, suitable for Audition 3.0, to gather the main acoustic parameters that are shown in Figs. 5 to 10 for the octave bands going from 125 Hz and 8 kHz.

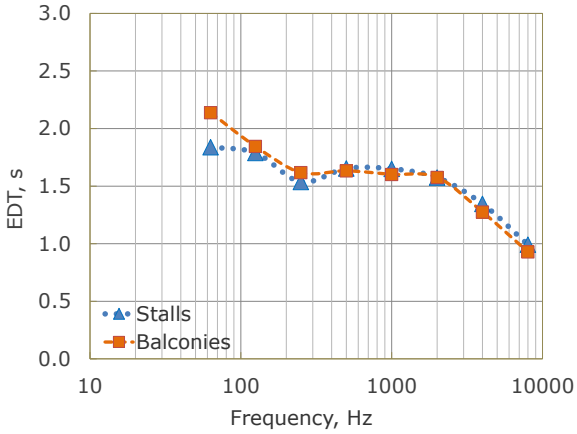

Fig. 5 – Measured values of Early Decay Time (EDT)

Fig. 5 shows the measured values of Early Decay Time (EDT), found to be very similar between stalls and balconies. Between 250 Hz and 2 kHz, the values fluctuate around 1.6 s, while at lower frequencies the results rise to 2.2 s and at higher octaves the values drop to 1.0 s. The overall outcome is within the optimal range set for opera houses (Farina & Tronchin, 2005; Farina et al., 1998; Tronchin & Bevilacqua, 2021).

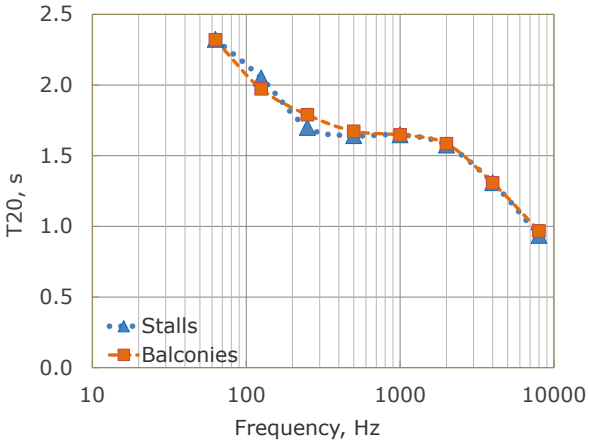

Fig. 6 – Measured values of reverberation time (T_{20})

Fig. 6 indicates that the averaged values of T_{20} are around 1.7 s at mid-frequencies, found to be very similar for stalls and balconies. This result meets the criteria of an opera house of such a volume size, as indicated in Fig. 7.

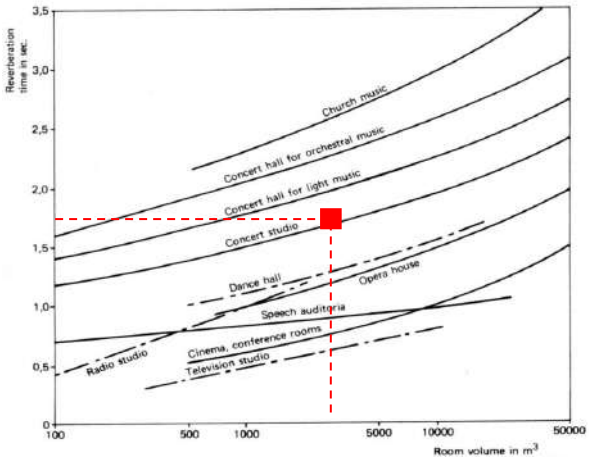

Fig. 7 – Optimal T_{20} values at 500 Hz, based on room volume

Fig. 8 shows the results of speech clarity index (C_{50}), found to be better in the stalls than on the balconies (Tronchin et al., 2006). The values in the stalls meet the optimal range (-2 dB to +2 dB) (ISO, 2003; Puglisi et al., 2021) for the mid-frequencies; the results of 63 Hz and 8 kHz are not included in the target set by the criteria. On the balconies, the

results are slightly below the lower range limit, except at 8 kHz, where the value is within the optimal range.

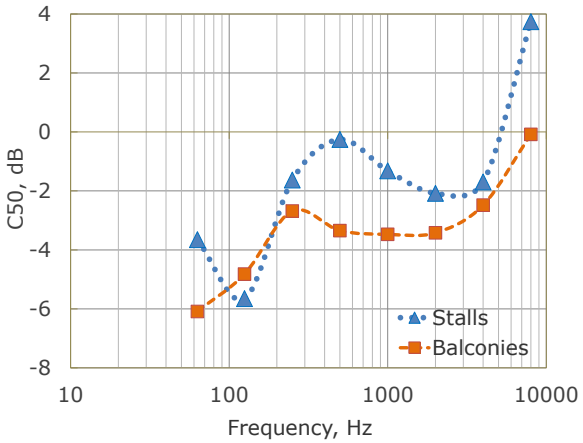

Fig. 8 – Measured values of speech clarity index (C_{50})

In terms of music, Fig. 9 indicates that the clarity index related to music (C_{80}) for both stalls and balconies was found to be within the optimal range for the mid octaves. This outcome highlights the suitability of Bonci theater for both opera and symphonic music (Beranek, 1962; Iannace et al., 2019; Tronchin, 2005).

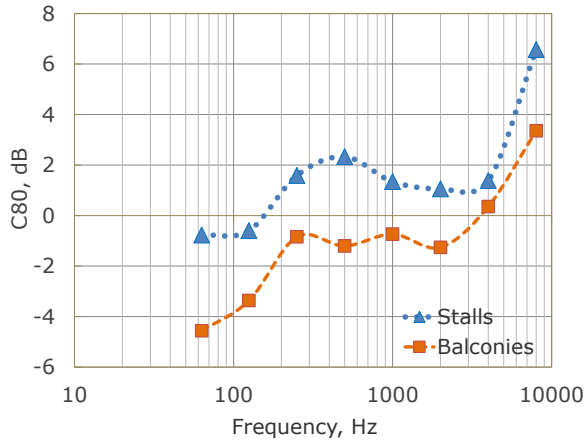

Fig. 9 – Measured values of music clarity index (C_{80})

The results related to definition (D_{50}) turned out to be 0.4 in the stalls and 0.3 on the balconies, as indicated in Fig. 10. This means that the definition is slightly better for music even if the overall outcome confirms what has been assessed for the other acoustic parameters (Iannace et al., 2000; Tronchin et al., 2020; Tronchin et al., 2021b).

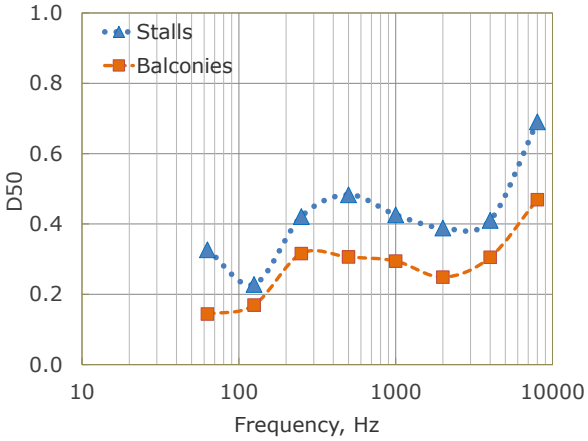

Fig. 10 – Measured values of D_{50}

6. Conclusion

The assessment of the acoustic measurements taken inside Bonci theater in Cesena outlines a good response regarding both speech and music. The best results were found at mid-frequencies, while a shortfall was found at the octaves below 125 Hz, and the results above 4 kHz were found to be slightly above the upper range limit. Based on the acoustic survey, future research studies will be focused on the acoustic simulations (Caniato et al., 2019 and 2020b) of a certain typology of scenery, with and without the audience, in order to highlight the differences of the acoustic parameters in stalls and balconies, as well as for energy building and musical instrument simulation (Fabbri et al., 2014; Manfren et al., 2019, 2021a, 2021b and 2022; Tronchin et al., 2020). On the basis of this, this preparatory analysis would be of fundamental importance during the calibration process of the digital model (Caniato et al., 2020a), where the absorption coefficients would be applied to all the 3D elements.

References

Azzaroni, G., F. Dell'Amore, P. G. Fabbri, R. Pieri, and A. Maraldi. 1997. *Un palcoscenico per Cesena. Storia del Teatro Comunale*. Il Ponte Vecchio, Cesena.

Battaglia, F., M. Gradara, G. Conti, and G. Foschi. 1992. *Il Teatro Comunale Bonci e la Musica a Cesena*.

Beranek, L. 1962. *Music, acoustics and architecture*. Wiley: New York.

Bettarello, F, P. Fausti, V. Baccan, and M. Caniato. 2010. "Impact Sound Pressure Level Performances of Basic Beam Floor Structures". *Building Acoustics* 17(3):305-316,. doi: https://doi.org/10.1260/1351-010X.17.4.305

Bettarello, F., M. Caniato, and A. Gasparella. 2021. "The Influence of Floor Layering on Airborne Sound Insulation and Impact Noise Reduction: A Study on Cross Laminated Timber (CLT) Structures". *Applied Science* 11(13): 5938. doi: https://doi.org/10.3390/app11135938

Caniato, M., F. Bettarello, C. Schmid, and P. Fausti. 2019. "The use of numerical models on service equipment noise prediction in heavyweight and lightweight timber buildings". *Building Acoustics* 26(1): 35-55. doi: https://doi.org/10.1177/1351010X18794523

Caniato, M., F. Bettarello, P. Bonfiglio, and A. Gasparella. 2020a. "Extensive Investigation of Multiphysics Approaches in Simulation of Complex Periodic Structures". *Applied Acoustics* 166: 107356. doi: https://doi.org/10.1016/j.apacoust.2020.107356

Caniato, M., C. Schmid, and A. Gasparella. 2020b. "A comprehensive analysis of time influence on floating floors: Effects on acoustic performance and occupants' comfort". *Applied Acoustics* 166: 107339. doi: https://doi.org/10.1016/j.apacoust.2020.107339

Dordevic, Z. 2016. "Intangible tangibility: Acoustical heritage in architecture." *Structural Integrity and Life* 6: 59–66.

Fabbri, K, L. Tronchin, and V. Tarabusi. 2014. "Energy Retrofit and Economic Evaluation Priorities Applied at an Italian Case Study". *Energy Procedia* 45: 379-384. doi: https://doi.org/10.1016/j.egypro.2014.01.041

Farina, A. 2007. "Advancements in impulse response measurements by sine sweeps." In *Proceedings of the 122nd AES Convention*.

Farina, A., and L. Tronchin. 2000. "On the"virtual" reconstruction of sound quality of trumpets." *Acta Acustica united with Acustica* 86(4): 737-745.

Farina, A., and L. Tronchin. 2005. "Measurements and reproduction of spatial sound characteristics of auditoria." *Acoustical Science and Technology* 26(2): 193-199. doi: https://doi.org/10.1250/ast.26.193

Farina, A., A. Langhoff, and L. Tronchin. 1998. "Acoustic characterisation of "virtual" musical instruments: using MLS technique on ancient violins." *Journal Of New Music Research* 27(4): 359-379. doi: https://dx.doi.org/10.1080/09298219808570753

Iannace, G., and E. Ianniello. 2008. "Sound-focusing effects in the plan of horse-shoe shaped opera theatres." In *Proceedings of European Conference on Noise Control*: 1639–1643.

Iannace, G., C. Ianniello, L. Maffei, and R. Romano. 2000. "Objective measurement of the listening condition in the old Italian opera house Teatro di San Carlo." *Journal of Sound and Vibration* 232: 239-249. doi: https://doi.org/10.1006/jsvi.1999.2696

Iannace, G., G. Ciaburro, A. Trematerra, and C. Foglia. 2019. "Acoustic correction of a renaissance period hall." *Canadian Acoustics* 47(2): 57–66.

ISO. 2003. *ISO 9921:2003. Ergonomics - Assessment of speech communication.* Geneva, Switzerland.

ISO. 2009. *ISO 3382-1:2009. Acoustics - Measurement of Room Acoustic Parameters; Part 1: Performance Spaces*. Geneva, Switzerland.

Jordan, V. L. 1981. "A group of objective acoustical criteria for concert halls." *Applied Acoustics* 14: 253-266. doi: https://doi.org/10.1016/0003-682X(81)90021-9

Manfren, M., B. Nastasi, E. A. Piana, and L. Tronchin. 2019. "On the link between energy performance of building and thermal comfort: An example." *AIP Conference Proceedings* 2123: 1-9. doi: https://doi.org/10.1063/1.5116993

Manfren, M., B. Nastasi, L. Tronchin, D. Groppi, and D. A. Garcia. 2021a. "Techno-economic analysis and energy modelling as a key

enablers for smart energy services and technologies in buildings." *Renewable and Sustainable Energy Reviews* 150: 1-14. doi: https://doi.org/10.1016/j.rser.2021.111490

Manfren, M., M. Sibilla, and L. Tronchin. 2021b. "Energy Modelling and Analytics in the Built Environment—A Review of Their Role for Energy Transitions in the Construction Sector." *Energies* 14: 1-29. doi: https://doi.org/10.3390/en14030679

Manfren, M., P. A. B. James, and L. Tronchin. 2022. "Data-driven building energy modelling – An analysis of the potential for generalisation through interpretable machine learning". *Renewable and Sustainable Energy Reviews* 167: 1-13.
doi: https://doi.org/10.1016/j.rser.2022.112686

Puglisi, G. E., A. Warzybok, A. Astolfi, and B. Kollmeier. 2021. "Effect of competitive acoustic environments on speech intelligibility." *Journal of Physics* 2069(1): 175180. doi: https://doi.org/10.1088/1742-6596/2069/1/012162

Tronchin, L. 2005. "Modal analysis and intensity of acoustic radiation of the kettledrum." *The Journal of the Acoustical Society of America* 117(2): 926-933. doi: https://doi.org/10.1121/1.1828552

Tronchin, L. 2021. "Variability of room acoustic parameters with thermo-hygrometric conditions." *Applied Acoustics* 177: 1-14. doi: https://doi.org/10.1016/j.apacoust.2021.107933

Tronchin, L., and A. Bevilacqua. 2021. "Acoustic study of different sceneries at the São Carlos national theatre of Lisbon." *Applied Acoustics* 180: 1-11. doi: https://doi.org/10.1016/j.apacoust.2021.108102

Tronchin, L., and A. Bevilacqua. 2022. "Historically informed digital reconstruction of the Roman theatre of Verona. Unveiling the acoustics of the original shape." *Applied Acoustics* 185: 1-18. doi:
https://doi.org/10.1016/j.apacoust.2021.108409

Tronchin, L, and D. J. Knight. 2016. "Revisiting Historic Buildings through the Senses. Visualising Aural and Obscured Aspects of San Vitale, Ravenna." *International Journal of Historical Archaeology* 20: 127-145. doi: https://doi.org/10.1007/s10761-015-0325-2

Tronchin, L., R. Shimokura, and V. Tarabusi. 2006. "Spatial sound characteristics in the Theatre Comunale in Bologna, Italy." In *Proceedings of the 9th Western Pacific Acoustics Conference (WESPAC)*, Seoul, Korea, June 26-28.

Tronchin, L., F. Merli, M. Manfren, and B. Nastasi. 2020. "The sound diffusion in Italian Opera Houses: some examples." *Building Acoustics* 27(4): 333-355. doi: https://doi.org/10.1177/1351010X20929216

Tronchin, L., F. Merli, and M. Manfren. 2021a. "On the acoustics of the Teatro 1763 in Bologna." *Applied Acoustics* 172: 107598. doi: https://doi.org/10.1016/j.apacoust.2020.107598

Tronchin, L., F. Merli, and M. Dolci. 2021b. "Virtual acoustic reconstruction of the Miners' Theatre in Idrija (Slovenia)." *Applied Acoustics* 172: 1-9. doi:
https://doi.org/10.1016/j.apacoust.2020.107595

Vecco, M. 2010. "A definition of Cultural Heritage: From the tangible to the intangible." *Journal of Cultural Heritage* 11: 321–324. doi: https://doi.org/10.1016/j.culher.2010.01.006

Acoustic Discoveries of Another Masterpiece by Antonio Galli Bibiena: The Communal Theatre of Bologna

Antonella Bevilacqua – University of Parma, Italy – antonella.bevilacqua@unipr.it
Ruoran Yan – University of Bologna, Italy – ruoran.yan2@unibo.it

Abstract

The Communal Theater of Bologna was built in 1763, after a fire destroyed the previous Renaissance construction. The project was assigned to the architect Antonio Galli Bibiena, who belonged to a family of artists and scenographers. The interior design represents Baroque style, with its four orders of balconies surmounted by a top gallery. Acoustic measurements were carried out inside the theater in line with BS3382-1. The values measured were compared with the acoustic simulations of a digital model reproducing the shape and volume of this cultural heritage. The historical background of the building has been summarised to aid understanding of the construction development overseen by Antonio Galli Bibiena.

1. Introduction

The Communal Theater of Bologna, created by Antonio Galli Bibiena, was criticised at the beginning of the 18th century for being composed of a bell-shaped plan layout marking the main hall. This architectural choice was considered outside the traditional construction rules developed at that time, especially under the influence of Pierre Patte and his studies on the elliptical shapes of spaces for the performing arts. Nonetheless, the architect found a way to combine architectural finesse with a good acoustic response due to the specific materials employed on the finishes as well as to geometry very favourable to sound diffusion (Caniato et al., 2020; Fabbri et al., 2021; Tronchin & Farina, 1997).

The Communal Theater of Bologna was studied in depth during the 20th century, particularly after restoration work on the modification of the orchestra pit and of the initial part of the stage closer to the audience damaged by a fire. Other work was completed on the structural frame of the boxes, on the main trusses of the roof and for the allocation of the electrical system. Fortunately, the interventions did not involve the acoustics, which represent one of the best masterpieces that Antonio Galli Bibiena left to post generations (Tronchin et al., 2021a and 2021b).

2. Historical Notes

The Communal Theater of Bologna was built in the location of the previous Malvezzi Theater, a wooden structure that burned down in 1745. In 1756, the City Council approved the proposal to build a new theater in Baroque style and assigned the project to the architect Antonio Galli Bibiena (Tronchin et al., 2020a, 2020b and 2020c). In 1763, the Communal Theater of Bologna was officially opened to the public.

Fig. 1 – Internal view of the Communal Theater of Bologna

Between 1818 and 1820, the theater underwent some restoration work, including the renovation of the dome, the reconstruction of the auditorium, and the stage. The second restoration campaign

took place between 1853 and 1854, when the architect C. Parmenani was responsible for the transformation work (Tronchin et al., 2020a, 2020b and 2020c). In 1865, the façade was restored along with some safety measures adopted in line with the new building regulations, as shown in Fig. 1.
In 1931, the theater experienced another fire, burning down the stage and the curtain, while many rooms survived. The restoration was completed in 1935 and, after than this event, the theater was closed again due to World War II, but it reopened in 1946 (Tronchin et al., 2006).

3. Architectural Description

The main hall of the Communal Theater of Bologna, completed in 1763, has a total capacity of 1176 seats distributed as 644 seats in the stalls and 532 seats on the elevated boxes. The preferred shape of a bell was designed by Galli Bibiena for the plan layout, having the axes measuring 22.4 m and 15.4 m (L, W), as shown in Fig. 2.

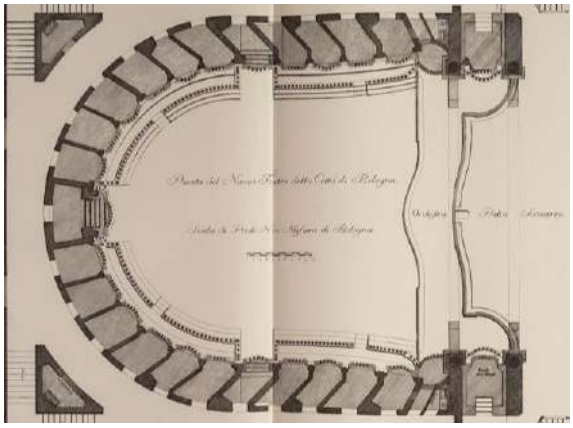

Fig. 2 – Plan layout of the Communal Theater of Bologna. Drawing by A. Galli Bibiena

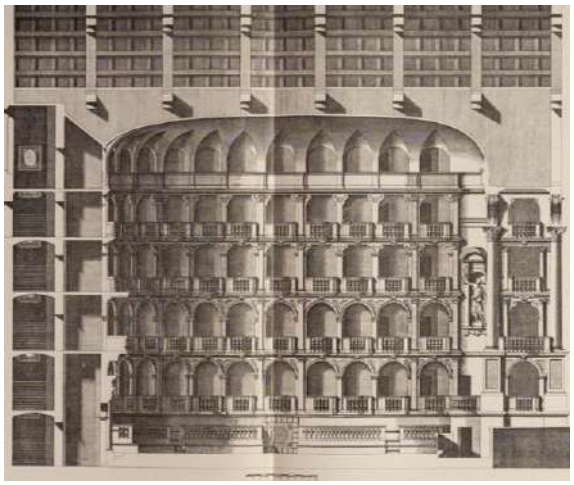

Fig. 3 – Longitudinal section of the Communal Theater of Bologna. Drawing by A. Galli Bibiena

The total height is about 16.9 m, which includes four orders of balconies surmounted by a gallery, as indicated in Fig. 3.
The architect also introduced a series of new constructive solutions, such as the use of load-bearing masonry rather than wooden frames (Amoruso, 2019).
However, these new schemes caused him serious slander, although it was proved that these innovations show excellent acoustic performance.

Fig. 4 – Wooden mechanical system located beneath the finish floor of the stalls

Beneath the floor of the main hall, a wooden mechanical system can regulate the height of the seating area, so to be at the same level as the stage, as shown in Fig. 4.

3.1 Digital Model

From the architectural drawings, a digital model was made, considering all the architectural elements and discarding the details of capitals and tiny decorations (Vorländer, 2011), as shown in Fig. 5. The layers represented in different colours were grouped based on the characteristics of the materials.

Thereafter, the model was exported in dxf format, ready to be used within Ramsete software (Farina, 1995). The attribution of the absorbing and scattering coefficients was carried out based on the acoustic measurements, as indicated in Fig. 6. The sound source and the receivers of the model were located in the same positions used for the survey (Caniato et al., 2021), in order to make the model calibration accurate (Manfren et al., 2020, 2021a and 2021b)

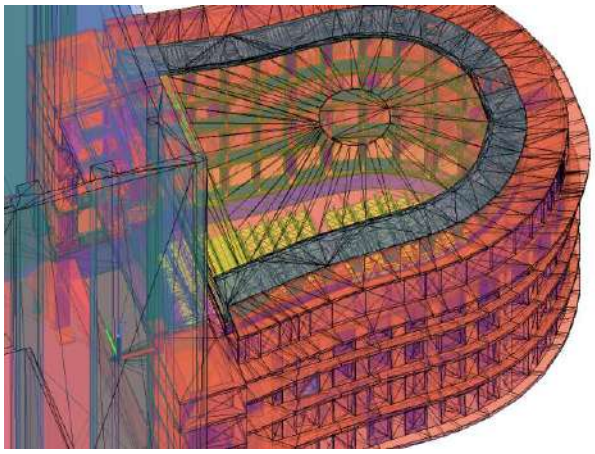

Fig. 5 – View of the 3D model

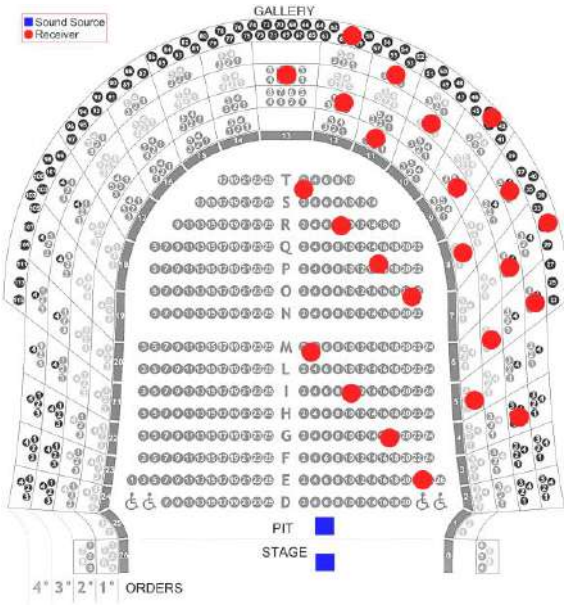

Fig. 6 – Scheme of the equipment positions during the acoustic survey

4. Acoustic Simulation

The acoustic simulations were carried out based on the absorption coefficients that were attributed by considering the materials inside the theater (Shtrepi, 2019). The simulations were calculated without any scenery on the stage, nor any audience; they faithfully represent the conditions found on site.

For the simulations, two omnidirectional sound sources were placed in the locations where they were positioned during the acoustic measurements (Iannace et al., 2000), in particular, on the stage and in the orchestra pit.

Figs. 7 to 11 show the main acoustic parameters for a bandwidth comprising a range of between 125 Hz and 8 kHz. The results shall be considered as the average of measured and simulated values related to stalls and balconies (Tronchin et al., 2021a and 2021b).

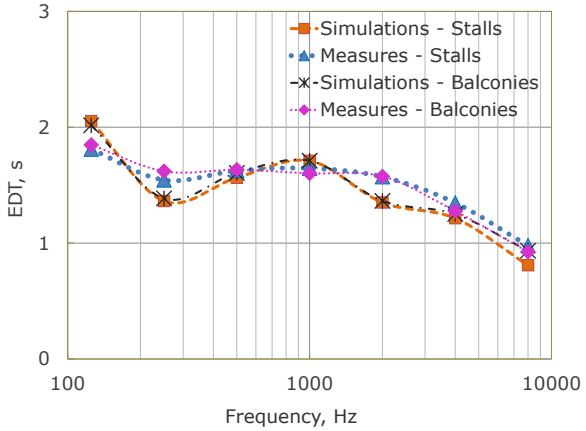

Fig. 7 – Measured and simulated values of EDT

Fig. 7 shows the comparison of the acoustic measurements and simulations of the EDT results. For this acoustic parameter, the difference between stalls and balconies is minimal across all the frequency bands. However, a drift between measurements and simulations does not exceed 5 % for the considered bandwidth (Caniato et al. 2019; Sakai et al., 2002).

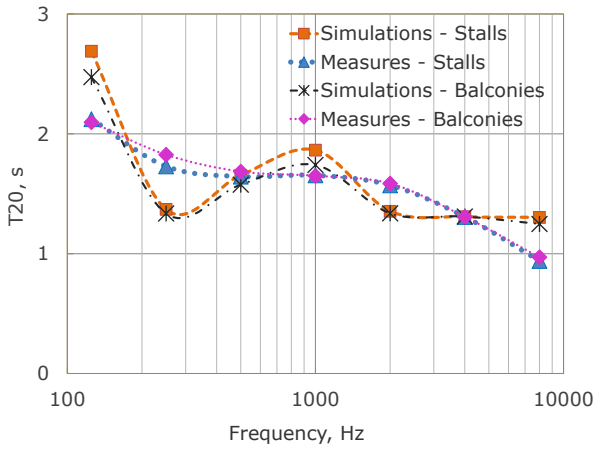

Fig. 8 – Measured and simulated values of T_{20}

Fig. 8 indicates that the T_{20} measured results around 1.8 s at mid-frequencies highlight a good reverberation time for a hall having a volume size equal to approximately 4,200 m^3, and similar to other Italian opera theaters built in the same period (Vodola, 2019). The simulated values at 250 Hz and 2 kHz were calibrated to be up to 0.5 s away from the measured results; this was assessed along with the other acoustic parameters (Bettarello et al., 2021; Guarnaccia et al., 2019).

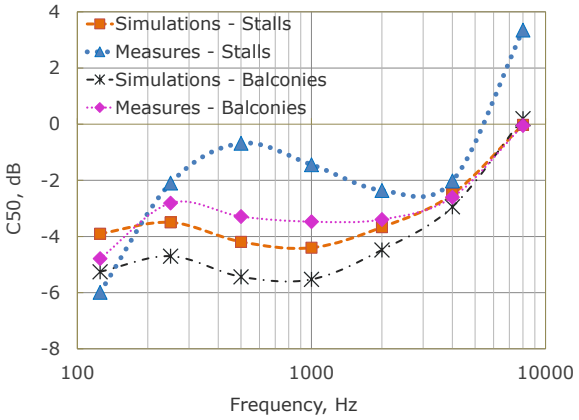

Fig. 9 – Measured and simulated values of C_{50}

Fig. 9 shows the results of the speech clarity index (C_{50}) to be between the optimal range (-2 dB and +2 dB) (Beranek, 1962) from 250 Hz onwards in relation to stalls, while the measured values in the balconies fall slightly below the lowest range limit, with the exception of 8 kHz being equal to 0 dB. The simulated values are shifted below the measurements of up to 2 dB for mid-frequency bands, while at 4 kHz the difference is minimised.

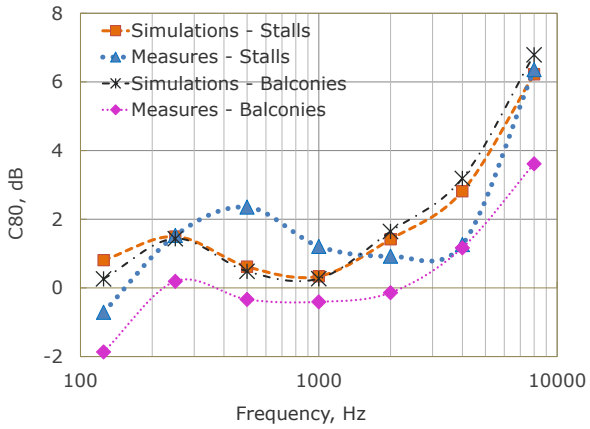

Fig. 10 – Measured and simulated values of C_{80}

In terms of music, the clarity index measured (C_{80}) falls within the optimal range (-2 dB and +2 dB) across all the frequency bands, with the exception of 8 kHz, where the values are up to 4 dB above the upper range limit. A difference of up to 2 dB was found between the measurements in the stalls and in the balconies, to be maximum at 500 Hz and negligible at 4 kHz. The difference in the simulated values between balconies and stalls is less, to approximately 1.5 dB at mid-octave and null at very high frequencies.

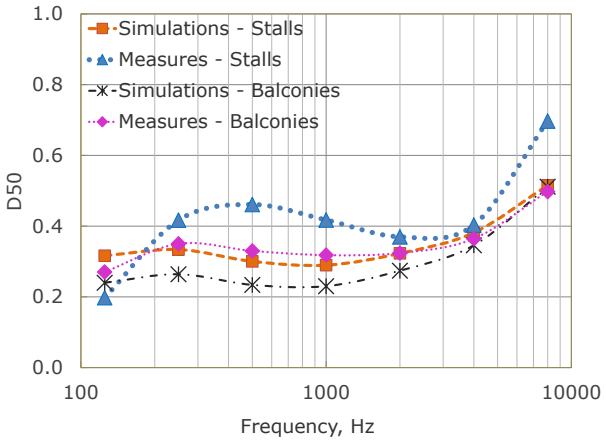

Fig. 11 – Measured and simulated values of D_{50}

Fig. 11 highlights that the measured values of definition (D_{50}) were found to be around 0.38 in the balconies and 0.42 across the stalls. This means that the acoustic response of the Communal Theater of Bologna is more suitable for music, with a shortfall at low frequency related to speech (Bettarello et al., 2010; Puglisi et al., 2021). The simulated values are shifted up to 1.5 below the trend lines related to balconies and stalls, despite the difference at high frequencies being negligible.

5. Conclusion

This paper deals with the acoustics of the Communal Theater of Bologna, one of the best architectural masterpieces designed by Antonio Galli Bibiena. The main acoustic parameters were analysed in comparison with the simulated results obtained by applying the absorbing and scattering coefficients to a digital model that faithfully reproduces the architectural composition of the theater. The results highlight an acoustic response suitable for both music and speech, while the simulated values were assessed to be within 5 % away from the values measured if averaged across all the spectrum bandwidth. The calibration process considered all the acoustic parameters as well as to be fruit of the authors' experience on acoustic simulations taken for similar room shapes.

References

Amoruso, G. 2019. "The teatro of Bologna as a transformable space: drawing, geometry and invention in the study of the wooden model of the theatre by Antonio Galli Bibiena." *Lecture Notes in Civil Engineering* 24:375-394. doi: https://doi.org/10.1007/978-3-030-03676-8_13

Beranek, L. 1962. *Music, Acoustics and Architecture*. John Wiley & Sons, Inc..

Bettarello, F., P. Fausti, V. Baccan, and M. Caniato. 2010. "Impact Sound Pressure Level Performances of Basic Beam Floor Structures". *Building Acoustics* 17(3): 305-316. doi: https://doi.org/10.1260/1351-010X.17.4.305

Bettarello, F., M. Caniato, G. Scavuzzo, and A. Gasparella. 2021. "Indoor Acoustic Requirements for Autism-Friendly Spaces". *Applied Science* 11: 3942. doi: https://doi.org/10.3390/app11093942

Caniato, M., F. Bettarello, C. Schmid, and P. Fausti. 2019. "The use of numerical models on service equipment noise prediction in heavyweight and lightweight timber buildings". *Building Acoustics* 26(1): 35-55. doi: https://doi.org/10.1177/1351010X18794523

Caniato, M., F. Bettarello, P. Bonfiglio, and A. Gasparella. 2020a. "Extensive Investigation of Multiphysics Approaches in Simulation of Complex Periodic Structures". *Applied Acoustics* 166: 107356. doi: https://doi.org/10.1016/j.apacoust.2020.107356

Caniato, M., C. Schmid, and A. Gasparella. 2020b. "A comprehensive analysis of time influence on floating floors: Effects on acoustic performance and occupants' comfort". *Applied Acoustics* 166: 107339. doi: https://doi.org/10.1016/j.apacoust.2020.107339

Caniato, M., F. Bettarello, and A. Gasparella. 2021. "Indoor and outdoor noise changes due to the COVID-19 lockdown and their effects on individuals' expectations and preferences". *Scientific Reports* 11: 16533. doi: https://doi.org/10.1038/s41598-021-96098-w

Fabbri, K., L. Tronchin, and F. Barbieri. 2021. "Coconut fibre insulators: The hygrothermal behavior in the case of green roofs". *Construction and building materials* 266: 1-9. doi:

https://doi.org/10.1016/j.conbuildmat.2020.121026

Farina, A. 1995. "RAMSETE – a new pyramid tracer for medium and large-scale acoustic problems". In *Proceedings of Euro-Noise Conference*, Lyon, France.

Guarnaccia, C., L. Tronchin, and M. Viscardi. 2019. "Special issue on modelling, simulation and data analysis in acoustical problems." *Applied Sciences* 9: 5261. doi: https://doi.org/10.3390/app9235261

Iannace, G., C. Ianniello, L. Maffei, and R. Romano. 2000. "Objective measurement of the listening condition in the old Italian opera house Teatro di San Carlo." *Journal of Sound and Vibration*, 232(1): 239-249. doi: https://doi.org/10.1006/jsvi.1999.2696

Manfren, M., B. Nastasi, E. A. Piana, and L. Tronchin. 2019. "On the link between energy performance of building and thermal comfort: An example". In *AIP Conference Proceedings* 2123: 1-9. doi: https://doi.org/10.1063/1.5116993

Manfren, M., B. Nastasi, L. Tronchin, D. Groppi, and D. A. Garcia. 2021a. "Techno-economic analysis and energy modelling as a key enabler for smart energy services and technologies in buildings". *Renewable and sustainable energy reviews* 150: 1-14. doi: https://doi.org/10.1016/j.rser.2021.111490

Manfren, M., M. Sibilla, and L. Tronchin. 2021b. "Energy Modelling and Analytics in the Built Environment—A Review of Their Role for Energy Transitions in the Construction Sector". *Energies* 14: 1-29. doi: https://doi.org/10.3390/en14030679

Puglisi, G. E., A. Warzybok, A. Astolfi, and B. Kollmeier. 2021. "Effect of competitive acoustic environments on speech intelligibility." *Journal of Physics* 2069(1): 175180. doi: https://doi.org/10.1088/1742-6596/2069/1/012162

Sakai, H., Y. Ando, N. Prodi, and R. Pompoli. 2002. "Temporal and spatial acoustical factors for listeners in the boxes of historical opera theatres." *Journal of Sound and Vibration*, 258(3): 527-547. doi: https://doi.org/10.1006/jsvi.2002.5274

Shtrepi, L. 2019. "Investigation on the diffusive surface modeling detail in geometrical acoustics-based simulations." *Journal of Acoustic Society of America* 145(3): EL215–21. doi: https://doi.org/10.1121/1.5092821

Tronchin, L., and A. Farina. 1997. "Acoustics of the former Teatro "La Fenice" in Venice." *Journal of the Audio Engineering Society* 45(12):1051-1062.

Tronchin, L., R. Shimokura, and V. Tarabusi. 2006. "Spatial sound characteristics in the Theatre Comunale in Bologna, Italy". Proceedings of the 9th Western Pacific Acoustics Conference (WESPAC), Seoul, Korea, June 26-28.

Tronchin, L., M. Manfren, and V. Vodola. 2020a. "Sound characterization through intensity of acoustic radiation measurement: A study of persian musical instruments". *Applied Sciences* 10(2): 633. doi: https://doi.org/10.3390/app10020633

Tronchin L., M. Manfren, and V. Vodola. 2020b. "The carabattola - vibroacoustical analysis and intensity of acoustic radiation (IAR)". *Applied Sciences* 10(2): 641. doi: https://doi.org/10.3390/app10020641

Tronchin, L., F. Merli, M. Manfren, and B. Nastasi. 2020c. "The sound diffusion in Italian Opera Houses: some examples." *Building Acoustics*, 27(4): 333-355. doi: https://doi.org/10.1177/1351010X20929216

Tronchin, L., F. Merli, and M. Dolci. 2021a. "Virtual acoustic reconstruction of the Miners' Theatre in Idrija (Slovenia)". *Applied Acoustics* 172: 1-9. doi: https://doi.org/10.1016/j.apacoust.2020.107595

Tronchin, L., F. Merli, and M. Manfren. 2021b. "On the acoustics of the Teatro 1763 in Bologna." *Applied Acoustics* 172: 107598. doi: https://doi.org/10.1016/j.apacoust.2020.107598

Vodola, V. 2019. "The renovation of the Teatro Nuovo in Spoleto: analysis of the acoustic quality of an Italian Opera House." *Journal of Physics Conference Series* 1351: 012013. doi: https://doi.org/10.1088/1742-6596/1351/1/012013

Vorländer, M. 2011. "Models and algorithms for computer simulations in room acoustics." In *Proceedings of the International Seminar on Virtual Acoustics (ISVA)*, Valencia, Spain, November 24-25.

In Situ Measurement of Wall Thermal Properties: Parametric Investigation of the Heat Flow Methods Through Virtual Experiments Data

Andrea Alongi – Politecnico di Milano, Italy – andrea.alongi@polimi.it
Luca Sala – Politecnico di Milano, Italy – luca11.sala@mail.polimi.it
Adriana Angelotti – Politecnico di Milano, Italy – adriana.angelotti@polimi.it
Livio Mazzarella – Politecnico di Milano, Italy – livio.mazzarella@polimi.it

Abstract

Energy retrofit of existing buildings is based on the assessment of the starting performance of the envelope. The procedure to evaluate thermal conductance through in situ measurements is described in the technical standard ISO 9869-1:2014, which provides two alternative techniques to process collected data: the Average Method (AM) and the Dynamic Method (DM).

This work studies their effectiveness using virtual data from numerical simulations of three kinds of walls, performed using a Finite Difference model.

The AM always provides acceptable estimates in winter, with better outcomes when indoor heat flux is considered in every case except the highly insulated wall. Summer conditions do not lead to acceptable measurements, despite the fulfillment of the check required by the standard. The DM results show acceptable estimations of the thermal conductance in both climates, for most of the virtual samples considered, although critically depending on some parameters of the DM that are left to the user's discretion, without strict indications by the standard. This work highlights a possible approach for overcoming this issue, which requires deeper future investigation.

1. Introduction

To reduce the energy needs related to the existing building stock, great effort is oriented towards envelope renovation. As a first step in this direction, the thermal properties (thermal transmittance and conductance) of the existing building components are usually assessed through in situ measurements. To this purpose, the international technical standard ISO 9869-1:2014 describes the so-called Heat Flow Meter method and two data processing techniques: the Average and the Dynamic Method.

Within the dedicated literature there is a wide variety of results (Atsonios et al., 2017; Gaspar et al., 2018; Lucchi et al., 2017). This is possibly due to the diversity of wall typologies investigated and boundary conditions occurring. Moreover, even when different walls are studied in the same work (Atsonios et al., 2017), experimental measurements are not performed at the same time.

To overcome the limitations inherent with experimental approaches, this work analyzes the efficacy of the Average and the Dynamic Method in finding the wall conductance by using virtual wall samples with different known properties, simulated through a Finite Difference model with controlled and repeatable boundary conditions. Moreover, these analyses are also aimed at looking for supplementary criteria concerning some key parameters of each methodology.

2. Methods and Materials

In this paper the Average and the Dynamic methods of analysis suggested by ISO 9869-1:2014 are applied to virtual data obtained through virtual Heat Flow Meter experiments i.e., heat transfer numerical simulations on wall components. The purpose of the data analysis is to derive the "experimental" thermal conductance, that in this case can be compared with the exactly known true value. In this section the experimental and data processing approaches by the standard are briefly illustrated. Secondly, the

numerical model for heat transfer across the wall is described and the three virtual walls and boundary conditions provided.

2.1 The HFM Method According to the Standard

The in situ estimation of the thermal conductance is based on the monitoring of the indoor and outdoor surface temperatures (T_{si} and T_{se} respectively) of a given wall, along with the heat flux density (φ) at one of these surfaces. More precisely, the ISO 9869-1:2014 suggests sampling this quantity at the indoor surface, due to a generally greater stability.

Data processing is then performed according to two possible techniques, the Average Method (AM) and the Dynamic Method (DM).

The sampling period is suggested as being at least 72 h, but it can be longer if required. This parameter is subject of discussion later in this work. As far as sampling frequency is concerned, it can be around 0.5÷1 h for the AM, while for the DM no explicit indication is provided. However, in this work the sampling frequency is significantly increased, reducing the sampling interval to 5 minutes to allow more accurate estimations.

2.1.1 The Average Method

According to the AM approach, the overall thermal conductance Λ of the building envelope component is progressively evaluated while the measurement itself is ongoing, through the following equation:

$$\Lambda = \frac{\sum_{i=1}^{n} \varphi_i}{\sum_{i=1}^{n} \left(T_{si,i} - T_{se,i}\right)} \qquad (1)$$

where φ_i, $T_{si,i}$, and $T_{se,i}$ are heat flux density [Wm^{-2}], indoor and outdoor surface temperature [°C] respectively at the *i-th* sampling moment (with $i = 1 \div N$). Both summations in Eq. 1 progress with time and their ratio should reach a stable value that approximates the real thermal conductance of the investigated component. This approach is based on the steady state assumption. For this reason, the standard suggests performing the sampling in winter periods, when outdoor conditions are more stable and larger heat flow densities usually occur. For elements with an expected thermal capacity lower than 20 kJ m^{-2}K^{-1}), only data acquired during the nights should be used. The standard also provides three conditions for good estimation, i.e.:

- the test should last more than 72 h;
- the deviation between the result at the end of the test and the value reached 24 h before should be within ±5 %;
- the deviation between the results obtained considering the first 2/3 and the last 2/3 of the test duration should be within ±5 %.

In this work the constraint on the overall test duration is not strictly considered in order to investigate how much the sampling period can be reduced while maintaining an acceptable outcome of the procedure. At the same time, the other two conditions are always checked. Moreover, the standard suggests either the use of a thermal mass factor correction or the implementation of the DM whenever the change in internal energy of the wall is more than 5 % of the heat passing through the wall during the test. Since it is not clearly explained how this condition should be assessed and this work deals with the DM anyway, no thermal mass factor correction is considered.

2.1.2 The Dynamic Method

This second processing technique is suggested as a way of estimating the steady-state properties of a building element starting from highly variable temperatures and heat fluxes and is applied at the end of their acquisition. It is based on the solution of the Fourier equation through the Laplace transformation method (Ahvenainen et al., 1980):

$$\begin{aligned}\varphi_i &= \Lambda\left(T_{si,i} - T_{se,i}\right) + \\ &+ K_1 T'_{si,i} - K_2 T'_{se,i} + \\ &+ \sum_n P_n \sum_{j=i-p}^{i-1} T_{si,j}(1-\beta_n)\beta_n(i-j) + \\ &+ \sum_n Q_n \sum_{j=i-p}^{i-1} T_{se,j}(1-\beta_n)\beta_n(i-j)\end{aligned} \qquad (2)$$

where $T'_{si,i}$ and $T'_{se,i}$ are the surface temperature time derivatives [K s^{-1}] at the *i-th* sampling moment (approximated using the incremental ratio referred to the sampling interval Δt), K_1, K_2, P_n and Q_n are unknown dynamic characteristics of the wall that depend on the *n-th* time constant τ_n (also unknown). Even though the number of time constants should be theoretically infinite, a limited number m (generally from 1 to 3) is adequate to correctly describe the system behaviour. Finally, β_n is defined as:

$$\beta_n = e^{-\Delta t/\tau_n} \quad (3)$$

Once the m time constants are initialized, the $(2m+3)$ unknowns are iteratively calculated optimizing the τ_n, through the minimisation of the square deviation between the measured and the estimated (φ^*_i) heat flux densities:

$$S^2 = \sum(\varphi_i - \varphi_i^*)^2 \quad (4)$$

The sums over the index j in Eq. 2 are the approximation of the integration process and are performed over a supplementary subset of p data, with $p = M-N$ and M the number of data triplets (φ_i, $T_{si,i}$, and $T_{se,i}$) that are actually used in the estimation of φ^*_i, as shown in Fig. 1.

Therefore, the user is expected to choose the number of time constants m (and their starting value for the iteration process) and M. While the standard provides some indications about the former, the latter is left to the user's experience (the only constraint is $M > 2m+3$). No univocal criterion is provided to assess the quality of the estimation and, ultimately, of the thermal conductance Λ achieved: the technical standard reports only an equation to calculate the confidence interval I for the estimated Λ (see ISO 9869-1:2014), stating that whenever I is lower than 5 % of the estimated conductance, the latter is generally close to the real value.

As far as the DM is concerned, this work aims at:

- assessing its effectiveness for different wall kinds, both in winter and summer conditions;
- evaluating the sensitivity of the outcomes on the number and the initial values of the time constants considered;
- evaluating the sensitivity of the method to the parameter M, possibly finding useful indications for the user.

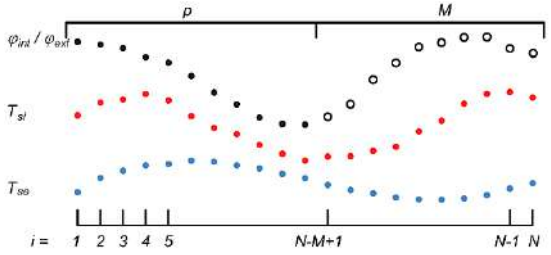

Fig. 1 – data utilization representation for the DM, with indication of p and M

2.2 The Numerical Model

In this work virtual experiments are performed using a one-dimensional Finite Difference model based on the one presented and validated in (Alongi et al., 2021). For a given k-th layer of the wall ($k = 1 \div K$), the discretized version of the Fourier equation is:

$$\frac{T_i^{j+1} - T_i^j}{\Delta t} = \alpha_k \frac{T_{i+1}^{j+1} - 2T_i^{j+1} + T_{i-1}^{j+1}}{\Delta x^2} \quad (5)$$

where α_k is the thermal diffusivity, T_i is the temperature at the i-th node ($i = 1 \div N_{FD}$) and at the j-th timestamp ($j = 1 \div M_{FD}$), Δx and Δt are the space and time discretization respectively. The numerical model uses a central difference scheme for the spatial derivative and a fully implicit representation of the time variation.

Third type boundary conditions are imposed at both edges of the domain, along with an imposed heat flux at the outdoor surface to take into account solar radiation, while temperature and heat flux continuity is imposed at the interface between adjacent layers. In all simulations performed, a structured grid is considered, with a constant step $\Delta x = 0.001$ m (which in (Alongi et al., 2021) is suggested as a good compromise between accuracy and computational cost), and the timestep Δt is set equal to 300 s.

The main outcomes of the simulations used by both the AM and the DM are the surface temperature trends, along with the corresponding heat flux densities. For the latter, the three-points formulation is chosen as in (Alongi et al., 2021):

$$\varphi_{ext}^j = -\lambda_1 \frac{3T_3^j - 4T_2^j + T_1^j}{2\Delta x} \quad (6)$$

$$\varphi_{int}^j = -\lambda_K \frac{3T_{N_{DF}}^j - 4T_{N_{DF}-1}^j + T_{N_{DF}-2}^j}{2\Delta x} \quad (7)$$

where φ_{ext} and φ_{int} are the heat flux densities at the outer and the inner edges of the domain, respectively, both positive when directed inward.

2.3 The Virtual Samples

The effectiveness of the two methods is evaluated on three walls with different thermophysical properties, used as virtual samples: a light and well insulated dry wall (W1); a heavy wall (W2); an externally insulated wall (W3). Layer sequences and material thermal properties are reported in Table 1 (density ρ, thermal conductivity λ, specific heat c and thickness s), along with the following reference quantities, calculated as follows:

- thermal conductance

$$\Lambda_{ref} = \left(\sum R_{cd,i} + \sum R_{cav,j}\right)^{-1} \quad (8)$$

- Specific heat capacity per unit area

$$C_{ref} = \sum (\rho_i \cdot c_i \cdot s_i) \quad (9)$$

- time constant

$$\tau_{ref} = \sum \left(R_{cd,i} \cdot C_i\right) \quad (10)$$

where C_i [J·m^{-2} K^{-2}] and $R_{cd,i}$ [m^2 K·W^{-1}] are the heat capacity per unit surface and the conductive resistance, respectively, of the *i-th* solid layer, $R_{cav,j}$ is the convective-radiative resistance of the *j-th* gap. It can be noticed that for all the walls C_{ref} is larger than 20 kJ m^{-2} K^{-1}.

Table 1 – names and main properties of the virtual samples

	ρ [kgm^{-3}]	λ [Wm^{-1}K^{-1}]	c [Jkg^{-1}K^{-1}]	s [m]
W1 - light and insulated wall				
sandwich	230	0.532	1500	0.04
rock wool	70	0.033	1030	0.2
air gap	-	-	-	0.055
rock wool	40	0.035	1030	0.04
Λ_{ref} = 0.134 Wm^{-2}K^{-1}	C_{ref} = 30 kJm^{-2}K^{-1}		τ_{ref} = 0.54 d	
W2 - heavy wall				
plaster	1800	0.9	1000	0.03
brick wall	1800	0.787	1000	0.425
plaster	1400	0.7	1000	0.02
Λ_{ref} = 1.661 Wm^{-2}K^{-1}	C_{ref} = 847 kJm^{-2}K^{-1}		τ_{ref} = 5.00 d	
W3 - externally insulated wall				
plaster	1300	0.3	840	0.03
rock wool	120	0.035	1030	0.06
hollow bricks	1000	0.163	1000	0.3
plaster	1400	0.7	1000	0.02
Λ_{ref} = 0.271 Wm^{-2}K^{-1}	C_{ref} = 368 kJm^{-2}K^{-1}		τ_{ref} = 6.50 d	

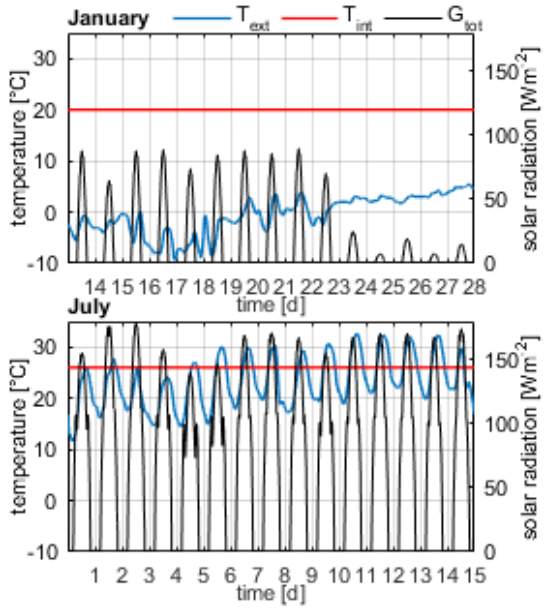

Fig. 2 – Indoor and outdoor boundary conditions for the two 14-day periods considered

As boundary conditions, two alternative indoor constant values for operative temperatures are considered: 20 °C in winter (from October 15th to April 15th) and 26 °C in summer (the rest of the year). Daily variations are neglected, limiting fluctuations to those caused by the outdoor conditions, which are based on the Typical Meteorological Year for Milan-Linate (Italy). More in detail, both external operative temperature and total solar radiation on a vertical surface facing North are used. Finally, even though the whole year is simulated, only the two most relevant 14-day periods are considered: from the 14th to the 28th of January for winter and from the 1st to the 15th of July for summer (Fig. 2).

3. Results And Discussion

The simulations provide the trends of the surface temperatures and the heat fluxes for each wall. For the sake of brevity, Fig. 3 shows only the results for W1 as an example, while Table 2 reports the main performance of each virtual sample (average, minimum and maximum for every quantity).

During the winter period, the three walls show stable thermal conditions, with indoor-outdoor temperature differences constant in sign. Heat flux densities, however, feature higher oscillations on the outer boundaries, with several sign inversions for all walls except W1. A more stable behavior can be observed on the indoor side (no sign inversions), with heat flux density always below 1 W m^{-2} for W1. Greater instability can be observed during the summer period, with multiple sign changes for both temperature difference and heat fluxes. These virtual measurements are then used to estimate Λ.

3.1 The Average Method Results

This method has been applied for each wall to the two complete 14-day periods, starting the average process at the beginning of each time window and considering the indoor and outdoor heat flux densities alternatively. Fig. 4 shows the conductance curves obtained in both periods for each wall investigated. The time needed to achieve a reliable estimation is actually the minimum time period

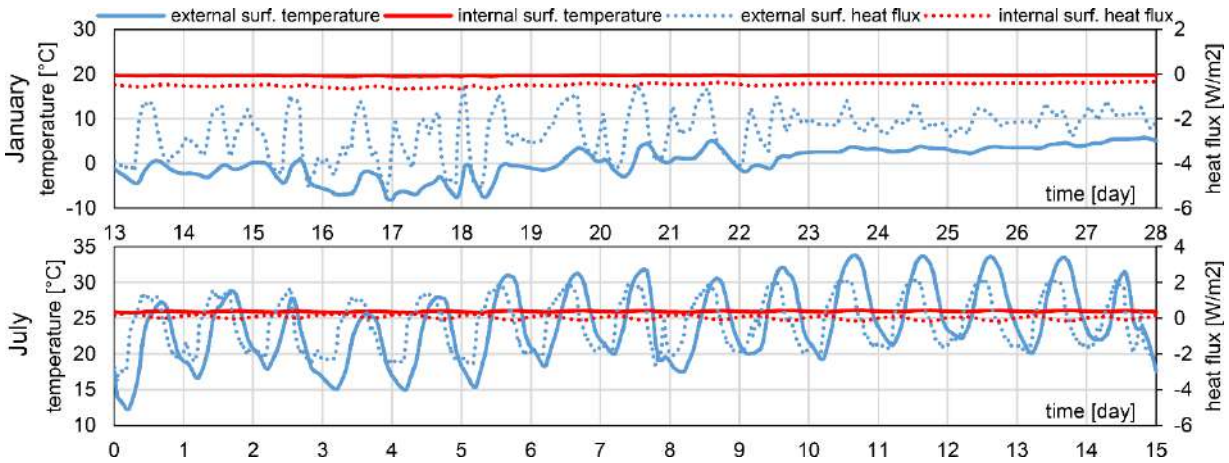

Fig. 3 – Simulation results (indoor and outdoor temperature and heat flux density fluctuations) for the W1 virtual sample

Table 2 – Average, minimum and maximum indoor and outdoor surface temperatures and heat flux densities for each virtual sample

		W1				*W2*				*W3*			
		T_{se} [°C]	T_{si} [°C]	φ_{ext} [Wm^{-2}]	φ_{int} [Wm^{-2}]	T_{se} [°C]	T_{si} [°C]	φ_{ext} [Wm^{-2}]	φ_{int} [Wm^{-2}]	T_{se} [°C]	T_{si} [°C]	φ_{ext} [Wm^{-2}]	φ_{int} [Wm^{-2}]
Jan.	*av.*	0.23	19.67	-2.55	-0.48	0.58	16.48	-25.15	-27.14	-0.23	19.29	-5.04	-5.49
	min	-8.15	19.54	-5.40	-0.66	-6.63	15.69	-79.90	-33.22	-8.79	19.16	-26.31	-6.45
	max	5.78	19.76	-0.45	-0.35	5.92	17.26	28.72	-21.10	5.48	19.42	24.54	-4.44
July	*av*	24.12	25.97	-0.30	0.04	24.13	25.64	-2.29	2.77	24.06	25.92	-0.47	0.60
	min	12.23	25.78	-3.54	-0.18	14.31	25.01	-94.45	-2.26	12.05	25.83	-38.56	-0.24
	max	33.84	26.12	2.18	0.32	32.26	26.29	63.20	7.66	33.90	26.03	27.15	1.32

required to fulfil the constraints provided by the ISO 9869-1:2014. The main results for each wall are reported in Table 3, where *n.a.* means that for a given condition it was not possible to satisfy the standard constraints within the 14-day period. It is possible to observe that acceptable outcomes (i.e., up to 5 % accuracy) can be achieved for every wall in the winter conditions minimum period required by the standard, provided that the proper heat flow density is chosen. In general, while both W2 and W3 feature acceptable outcomes with both heat flux densities, with an improvement when the indoor one is considered, for W1 only φ_{ext} provides accurate results, while φ_{int} leads to an unacceptable value of Λ. This is possibly due to the small values of the indoor heat flux density, as a consequence of the high insulation level. Table 3 also shows that increasing the evaluation period up to 14 days does not lead to a significant improvement, as the corresponding estimated conductance Λ_{14} shows.

As far as the summer conditions are concerned, the constraints of the standard are never met for W2 and W3, while 5 days are needed for W1. However, despite satisfying the constraints given by the ISO 9869-1:2014 for W1, estimations based on the indoor heat flux density lead to an unacceptable value of the thermal conductance (-82 %), while with φ_{ext}, Λ never stabilizes around an asymptotic value (Fig. 3). This oscillatory trend is also present in W2 and W3, wherever the heat flux is measured. These analyses show that the indications provided by the standard are only partially effective: first of all, a stable heat flux is not enough to achieve a reliable estimate of the thermal conductance, but it needs to be above a threshold (even the -6 to -4 W m^{-2} observed for W3 seem to suffice); more reliable outcomes are achieved with highly insulated walls when φ_{ext} is used. Moreover, the constraints in the standard only deal with the apparent stability of the thermal conductance estimate and can be misleading in some cases, like what happens for W1 either considering φ_{in} in the winter period or both heat flux densities in the summer period. Thus, the calculations required by the standard must be supported by a critical evaluation of the outcome and a visual inspection of the thermal conductance trend during the whole period.

3.2 The Dynamic Method Results

The DM has been tested on each wall considering several time windows within the two simulated periods to evaluate the shorter time needed to achieve a reliable estimation. A first sensitivity analysis demonstrated that the number of time constant has little effect on the outcomes. Thus, only one time constant is considered ($m = 1$), to reduce computational costs. Fig. 5 shows the thermal conductance and the square deviation achieved with the shorter data set, among the several investigated, used for each wall and each climate, both as function of M. Moreover, conductance trends feature the confidence interval (coloured areas), calculated as indicated by the ISO 9869-1:2014.

Outcomes for W1 are similar to those achieved with the AM: despite the better stability, φ_{int} does not provide acceptable results, while better agreement between estimated and reference Λ is obtained using φ_{ext}. Moreover, winter conditions lead to more stable results, while summer ones show a great dependence on M. In both seasons two days are enough to achieve acceptable results (Table 3).

As far as W2 is concerned, better outcomes are achieved using the heat flux density at the indoor surface both in January and in July, with a greater stability observable in the winter period (Table 3), when two days of data are enough. Indeed, the summer period needs a three-day data set and leads to a trend with a great dependence on the M parameter and, therefore, is more difficult to interpret. Finally, W3 seems to be more difficult to investigate:

Table 3 – Main outcomes of the AM and the DM for the three virtual samples and the two periods investigated

				W1				W2				W3			
				January		July		January		July		January		July	
				int	ext	int	ext	int	ext	int	ext	int	ext	int	ext
AM		t	[d]	3	3	5	5	3	5	n.a.	n.a.	3	5	n.a.	n.a.
		Λ	[W/(m²K)]	0.024	0.139	0.024	0.145	1.609	1.826	n.a.	n.a.	0.258	0.305	n.a.	n.a.
		err.		-81.9%	3.7%	-82.0%	8.4%	-3.1%	10.0%	n.a.	n.a.	-4.5%	13.1%	n.a.	n.a.
		Λ_{14}	[W/(m²K)]	0.025	0.131	0.023	0.163	1.707	1.582	1.833	1.520	0.282	0.258	0.321	0.250
		err.	[%]	-81.7%	-2.0%	-82.5%	21.8%	2.8%	-4.7%	10.4%	-8.4%	4.3%	-4.4%	18.9%	-7.4%
DM	best case	t	[d]	2	2	2	2	2	2	3	3	3	3	6	6
		N	[-]	575	575	575	575	575	575	863	863	863	863	1727	1727
		Λ	[W/(m²K)]	0.029	0.134	0.027	0.133	1.663	1.656	1.518	2.057	0.259	0.271	0.227	0.350
		err.	[%]	-78.2%	0.0%	-79.8%	-0.5%	0.2%	-0.3%	-8.6%	23.9%	-4.2%	0.5%	-15.9%	29.6%
		τ_1	[d]	0.85	0.12	0.63	0.13	0.48	0.01	0.07	0.08	0.24	0.01	0.17	0.16
		M	[-]	86	466	76	446	296	326	786	796	726	736	1606	1636
	S^2 loc.	Λ	[W/(m²K)]	0.025	0.136	0.025	0.133	1.620	1.746	1.499	2.234	0.254	0.285	0.227	0.455
		err.	[%]	-81.7%	1.3%	-81.6%	-0.5%	-2.4%	5.2%	-9.7%	34.6%	-5.8%	5.5%	-15.9%	68.6%
		M	[-]	416	536	436	446	506	526	796	816	806	846	1606	1456

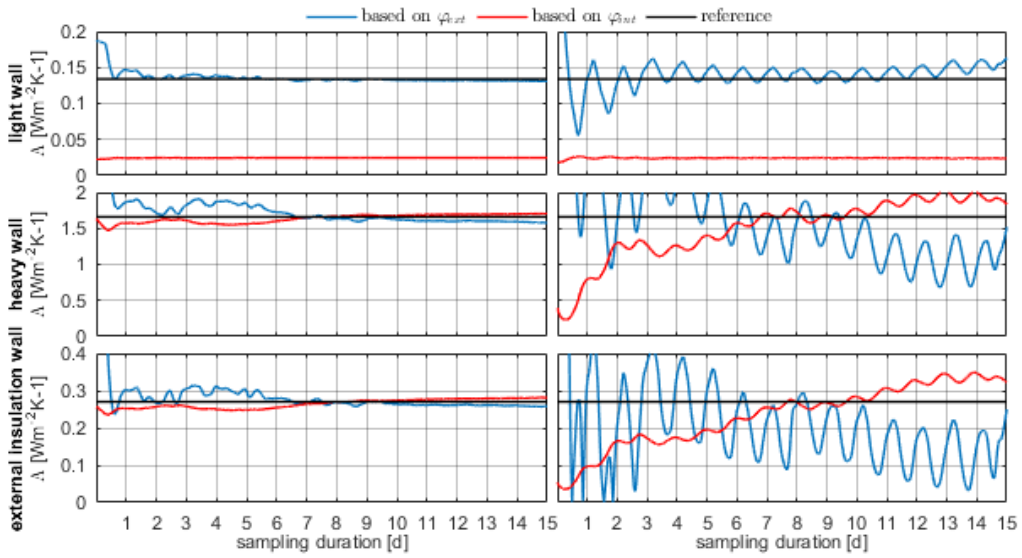

Fig. 4 – Outcomes of the AM: progressive estimate of Λ for the three walls in January and July, considering φ_{ext} and φ_{int}

three days of data are needed in winter to achieve an acceptable result, for both indoor and outdoor heat flux densities, while in summer several time frames have been considered (1 to 14 days) without success (the six-day one is shown in Fig. 5).

In general, the interpretation of the outcomes of each analysis is not straightforward: the sensitivity to M is great in several cases and the lack of clear indications by the ISO 9869-1:2014 may be an issue in a real implementation of this method, since the reference thermal conductance to validate the estimations is usually unknown. Moreover, the indication on the value of the confidence interval mentioned previously does not provide any guidance: the fulfilment of this criterion, shown in Fig. 5 as horizontal coloured bars in the S^2 graphs, occurs for many values of M, even when the discrepancy between reference and estimated thermal conductance is unacceptable. Also, the post-fitting value of the time constant does not provide any indication about the reliability of the results: τ_1 in the best conductance estimates shown in Table 3 (grouped under *best case*) differs significantly from the respective lumped capacity reference τ_{ref} (Eq. 10), suggesting that it is not possible to assign this physical meaning to τ_1.

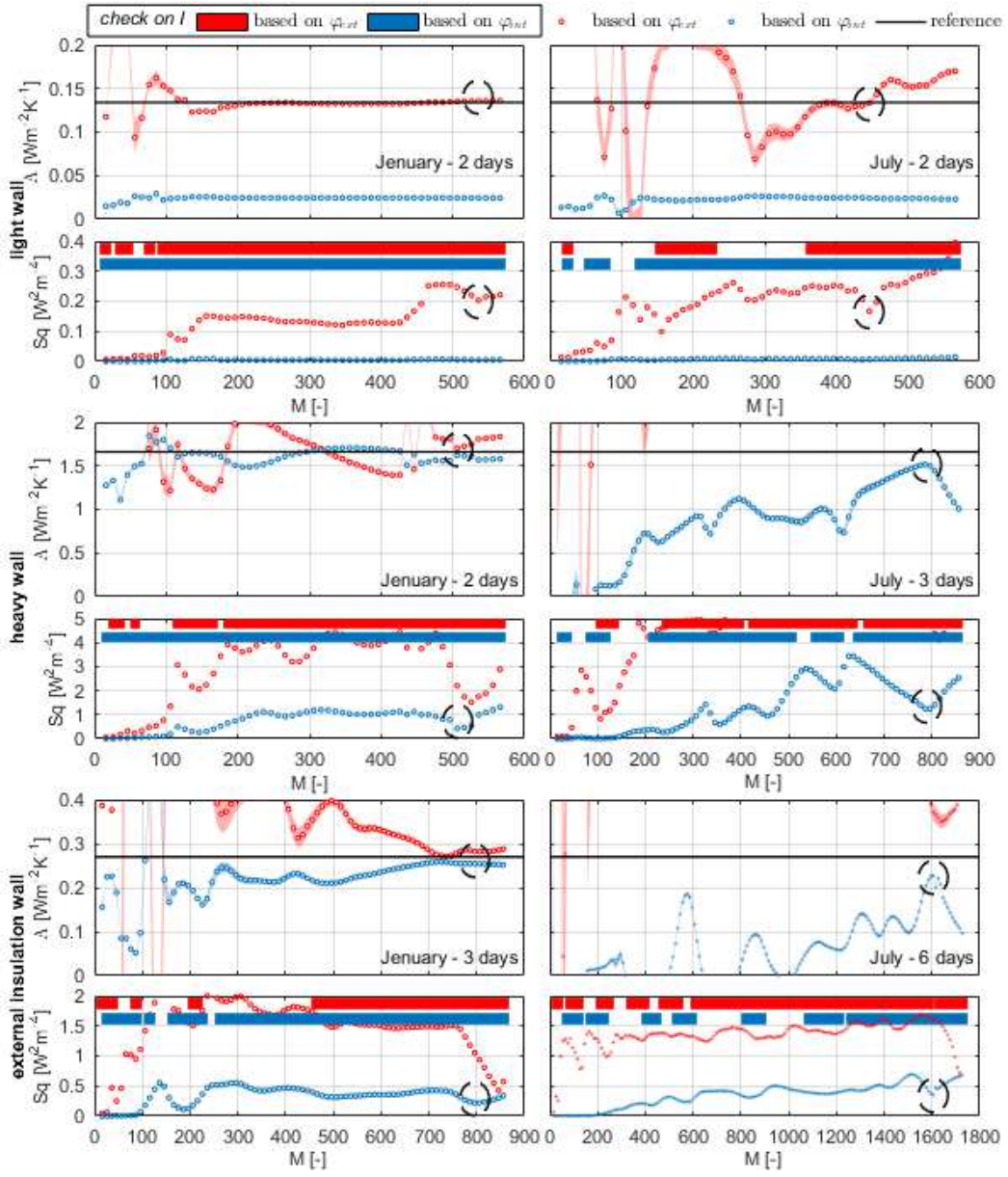

Fig. 5 – Outcomes of the DM: estimate of Λ and S^2 as function of M for the three walls in January and July, considering φ_{ext} and φ_{int}

To identify the most accurate estimate of Λ, a possible indication might come from the S^2 trend as function of M: good outcomes are indeed achieved for values of M greater than $N/2$ and corresponding to the last local minimum of S^2 (highlighted by dashed circles in Fig. 5 and grouped in Table 3 as S^2 *loc min*). This behaviour has been observed in several other cases, when different time frames have been considered. Therefore, it suggests that a technician should perform a sensitivity analysis on M and evaluate the outcomes using the S^2 trend as described above. Yet, this observation only suggests a possible line of investigation: this approach will need further analyses to provide a mathematical explanation and verify its repeatability.

4. Conclusions

This work investigates the accuracy of the post processing techniques provided by the ISO 9869-1:2014 by means of numerical simulations on three virtual wall samples, and focuses on two 14-day periods in January and July.

The analyses on the AM show that the best period to implement this technique is winter, in agreement with the standard. However, even though the latter suggests considering the heat flux density at the surface where it is more stable, it has been proven that a proper amplitude of the signal is more important than stability when dealing with highly insulated walls. Moreover, the criteria included in the standard can be misleading at times, as observed for W1, either in summer or, if φ_{int} is considered, in winter. Thus, a careful analysis of the conductance trend with time is needed to verify convergence to a stable and reasonable value.

As far as the DM is concerned, it generally leads to acceptable outcomes with acquisition periods shorter than the AM in winter, and summer measurements can be used too. W1 shows the same behavior described above, providing acceptable Λ only when the outdoor heat flux is considered in both periods. Results for both W2 and W3 are less sensitive to the choice between φ_{int} and φ_{ext} in winter, while in summer only the indoor one is useful for W2 and no reasonable outcome is obtained for W3 for every timespan considered. Dealing now with the parameters of the method, while the number and the initial values of the time constants do not affect the final outcomes, great sensitivity on M is observed, which makes the results difficult to interpret when the method is applied, as expected, to a wall with unknown properties.

However, there is a correspondence between an acceptable thermal conductance value and the local minimum of the S^2 for M near to N. This finding will need further investigations in order for it to be confirmed and formally systematized.

References

Ahvenainen, S., E. Kokko, and A. Aittomaki. 1980. "Thermal conductance of wall-structures" Report 54. Espoo: Technical Research Centre of Finland, Laboratory of Heating and Ventilating.

Alongi, A., A. Angelotti, and L. Mazzarella. 2021. "A numerical model to simulate the dynamic performance of Breathing Walls". *Journal of Building Performance Simulation* 14 (2): 155-180. doi: https://doi.org/10.1080/19401493.2020.1868578

Atsonios, I. A., I. D. Mandilaras, D. A. Kontogeorgos, and M. A. Founti. 2017. "A comparative assessment of the standardized methods for the in-situ measurement of the thermal resistance of building walls." *Energy and Buildings* 154: 198-206. doi: https://doi.org/10.1016/j.enbuild.2017.08.064

Gaspar, K., M. Casals, and M. Gangolells. 2018. "In situ measurement of façades with a low U-value: avoiding deviations." *Energy and Buildings* 170: 61–73. doi: https://doi.org/10.1016/j.enbuild.2018.04.012

International Standard. 2014. ISO 9869-1:2014 - Thermal insulation — Building elements — In-situ measurement of thermal resistance and thermal transmittance — Part 1: Heat flow meter method.

Lucchi, E. 2017. "Thermal transmittance of historical stone masonries: a comparison among standard, calculated and measured data." *Energy and Buildings* 151: 393–405. doi: https://doi.org/10.1016/j.enbuild.2017.07.002

Investigating the Performance of Different Window Opening Styles for Single-Sided Wind-Driven Natural Ventilation Using CFD Simulations

Akshit Gupta – Eurac Research, Italy – akshit.gupta@eurac.edu
Annamaria Belleri – Eurac Research, Italy – annamaria.belleri@eurac.edu
Francesco Babich – Eurac Research, Italy – francesco.babich@eurac.edu

Abstract

Natural ventilation can be an effective means of providing healthy and comfortable indoor environments while minimizing energy consumption. However, the use of diverse types of windows and control strategies usually leads to different indoor local thermal conditions. Previous studies have focused on indicators of ventilation effectiveness, but too little is known about the spatial variations of thermal comfort generated by different window opening styles. CFD is a powerful numerical modeling technique to compare the air distribution within a room, and therefore to evaluate the performances of different type of window in terms of delivered thermal comfort and indoor air quality (including local effects). Thus, the aim of this research is to investigate the effectiveness of diverse type of window, such as bottom-hung, horizontal pivot and top-hung fanlight for single-sided wind-driven natural ventilation. In this study, two wind speeds and two wind-window angles were investigated, for two weather conditions typical for the region of South Tyrol, Italy. In this study, thermal comfort was evaluated based on standards EN ISO 7730 and ASHRAE Standard 55. Using transient RANS CFD simulations, the performance of different window configurations for the different boundary conditions were numerically evaluated. The boundary conditions, geometrical simplifications, grid-independence tests, discretization, and basic principles for a transient simulation were chosen based on previous studies and then tested to ensure the correct modelling of a wind-driven natural ventilation flow. The results show 25 %-200 % higher incoming airflow when the wind enters at an acute angle as compared with perpendicular wind. Furthermore, the horizontal-pivot window reports a 39 % higher incoming airflow when compared with bottom-hung window style, while the draught risk in winter conditions was similar for both.

1. Introduction

Across the world, buildings are a big consumer of energy. In the EU alone, buildings account for 40 % of our energy consumption and 36 % of greenhouse gas emissions (European Commission 2020). The energy in buildings is largely used for heating, ventilation, and air conditioning (HVAC) in order to achieve the necessary air changes and provide a good quality of indoor environment (Zhong et al., 2022). To reduce dependence on fossil fuels, Natural Ventilation (NV) is being widely recognised as an effective means of delivering fresh air and comfort cooling in buildings, but the performance depends greatly on design (Nomura & Hiyama, 2017; Zhong et al., 2022). A well-designed NV system can ensure removal of indoor contaminants, provide thermal comfort and occupant control at a much lower cost compared with a mechanical ventilation system (Belleri et al., 2014; Gupta et al., 2021; Zhong et al., 2022). Designing a NV strategy depends on several factors, such as opening styles, arrangement of the opening, indoor-outdoor condition, wind condition, among others (Wang et al., 2017; Zhong et al., 2022). A building's architectural arrangement is a crucial factor in incorporating a suitable NV strategy in a room. In many cases, such as residential buildings, hostels, and dormitories, openings are possible only on one side of the room, thus falling under the single-sided ventilation category (Gupta et al., 2021).

Many studies in the past have focused on the performance of ventilation for single-side natural ventilation for different window configurations, but not so much on the thermal comfort aspects.

This study focuses on providing a deeper understanding of efficiently using a CFD simulation tool to replicate wind-driven single-sided NV flow and

choosing different window opening styles based on parameters of ventilation effectiveness and thermal comfort, as per EN-ISO 7730, for draught risk calculations and parameters of thermal discomfort in winter conditions; and the American Society of Heating, Refrigerating and Air-Conditioning Engineers (ASHRAE) Standard 55, for thermal comfort parameters in summer conditions.

In the subsequent sections, the three different window opening types are discussed for wind-driven single-sided natural ventilation flow to evaluate parameters of ventilation effectiveness and thermal comfort for different boundary conditions and geometrical simplifications for high quality CFD simulations.

2. Methodology

A CFD study was conducted for different window configurations to evaluate the flow rates based on different internal-external pressure differences. In this section, the model configuration and geometrical assumptions considered for the CFD analysis are presented, followed by the parameters considered for comparing the performance of different window types.

2.1 Geometric Model and Discretization

In natural ventilation flows, the airflow through an opening is affected by several factors, such as the opening configuration, indoor-outdoor temperature difference, heat sources, room geometry, wind speed, direction, among others.

The geometry of one of the two test chambers of Eurac Research's Façade System Interaction Lab is used for the internal domain (8 m x 4 m x 3 m). To replicate outdoor conditions, an external domain of the size 48 m x 36 m x 12 m is used. It should be noted that the computational domains (Fig. 1) for carrying out the CFD simulations were modeled based on the conclusions of Wang et al. (2018) and Gupta et al. (2021), to accurately replicate the physics of a single-sided wind driven flow, while keeping the computational time within a reasonable range. The resulting blockage ratio of this domain size is 2.8 %, which is below the recommended limits of 3 % (Blocken, 2015). This ensures a large enough domain for correct development of the airflow (Liu & Niu, 2016).

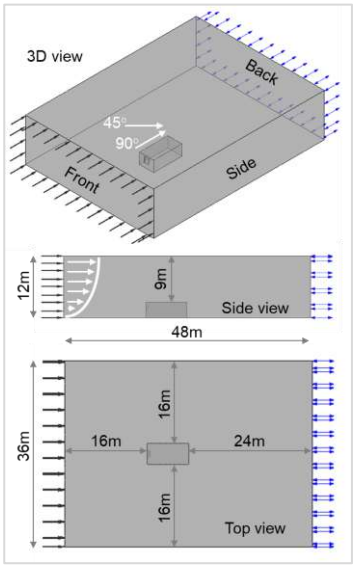

Fig. 1 – CFD model of the domains

For better flexibility, domain discretization is carried out using an unstructured meshing technique, and the mesh is finest at critical points, such as the opening, less coarse for the internal chamber and coarse for the external domain. The meshing technique, as well as the conclusions of the grid independence study inside the chamber, follow the methodology of Gupta et al. (2021). The three different window con-figurations considered in this study were chosen after a preliminary market analysis (Gupta et al., 2021). Fig. 2 shows the 3 window types and their opening areas. Type_1 (6° open) and Type_2 (20° open) cases have an overall area of 1190 x 1450 mm, and Type_3 (20° open) top-hung fanlight has a top area of 1190 x 450 mm, with a fixed bottom glazed area.

2.2 Basic CFD Principles

The CFD software used a parallel, implicitly coupled multigrid solver. The simulation period was 120 seconds, in transient condition, using steady-state solution for initialisation. An adaptive time-step was used, varying between 10 and 0.5 seconds, as a function of root-mean-square (RMS) courant number of 5, to keep under the residual target within 20 coefficient loops (Babich et al., 2017;

Gupta et al., 2021). A thermal energy transfer is considered, and, since the fluid is air, a Newtonian fluid, Boussinesq approximation was used to consider the buoyancy effects caused due to variations in air density, and was applied by setting up the reference buoyancy temperature equal to the glass temperature (ANSYS Inc., 2013; Babich et al., 2017; Gupta et al., 2021; Wang et al., 2018). The convergence criteria for the RMS residuals was 1e-05 and a conservation target was 0.01 (Babich et al., 2017; Gupta et al., 2021). The Reynolds-averaged Navier–Stokes (RANS) model and SST (Shear Stress Transport) k-omega turbulence model were selected to effectively solve the airflow characteristics (ANSYS Inc. 2013; Gupta et al., 2021; Babich et al., 2017; Zhong et al., 2022). All the simulations were performed with Ansys CFX 2021, and meshing with Ansys ICEM, on a work-station of 16 GB RAM and a 6-core Intel Xenon Gold 6154 CPU.

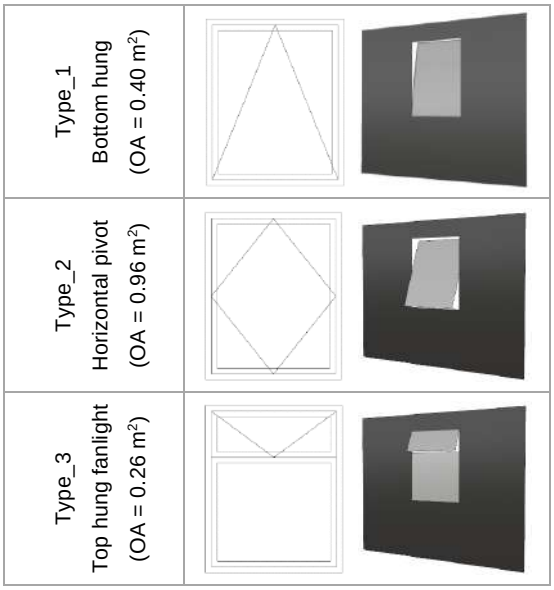

Fig. 2 – Window configurations (OA = opening area)

2.3 Boundary Conditions

Two weather conditions representing typical winter and summer conditions, with internal–external temperature of 20 °C – 10 °C and 30 °C – 25 °C, were considered. Table 1 shows the boundary conditions and temperatures for each domain.

The glass temperature was set to an approximate average of the two domains and is also used as the reference buoyancy temperature as well. The wind force is applied at the front face of the external domain as an inlet condition, and the wind speed is defined based on the power law, as per Eq. 1:

$$u = u_{ref} \cdot \alpha \cdot (y/y_{ref})^{\gamma} \quad (1)$$

where u is the wind speed at y height on the surface, and u_{ref} is the reference velocity of 1 m/s, at a reference height of y_{ref} (equal to the Lab height 5 m), as shown in Fig. 1 (side view), and parameters α=1, γ=0.143 refer to a terrain with few trees or small buildings (Wang et al., 2018; Yi et al., 2019).

Table 1 – Boundary conditions and temperatures (air/surface)

Location	Boundary Condition	Temperature	
		Winter	Summer
(a) Chamber Air		**20 °C**	**30 °C**
Wall surfaces	No-slip	20 °C	30 °C
Ceiling surface	No-slip	20 °C	30 °C
Floor surface	No-slip	23 °C	30 °C
Window Glass	No-slip	14 °C	28 °C
(b) External Domain Air		**10 °C**	**25 °C**
Top surface	Free slip	10 °C	25 °C
Front surface	Inlet	10 °C	25 °C
Ground surface	No-slip	10 °C	25 °C
Side surfaces	Free slip	10 °C	25 °C
Back surface	0Pa opening	10 °C	25 °C
Window Glass	No-slip	14 °C	28 °C

Two wind speeds (1 m/s and 2 m/s), and two wind angles (90°-wind coming perpendicular to the window from the front, and 45°) were chosen for this study, as representative conditions of the region of South Tyrol, Italy. For the wind angle of 45°, the inner domain was rotated for the CFD simulations, as represented in Fig. 1 (3D view), while the external domain remains the same.

2.4 Performance Parameters

The main parameters of ventilation effectiveness and thermal comfort, to compare the performance of different windows, are based on a previous study on buoyancy-driven single sided NV flow (Gupta et al., 2021):

1. Temperature profile – the temperature contour at the vertical plane in the middle of the room.
2. Velocity field – the velocity fields at the same vertical plane in the middle of the room.
3. Incoming airflow rate (Q) – the airflow rate entering the room through the window.

4. Mean Age of Air (MAA) – average time the air entering a building through an opening takes to reach a specific point in the zone (Zhong et al., 2022). It is calculated locally at every point in space, as a scalar quantity in the CFD solver (Gupta et al., 2021).
5. Air changes per hour (ACH) – the total number of times the air inside a space is completely replaced in one hour, as per the Eq. 2:
   $ACH = (Q / V) * 3600$ (2)
   where Q is the incoming airflow rate (m^3/s), and V is the total volume (m^3).
6. Effective penetration depth – the longitudinal distance traveled by the air entering from the inlet inside the room. This indicator represents the effective ventilating ability of NV and is an important parameter for single-side ventilated spaces (Zhou et al., 2021). For the context of this study, a maximum length of 8 m is considered.
7. Discharge coefficient (C_d) – this is a function of volume flow rate and pressure difference for a fluid flowing through an opening. It is calculated by rearranging the orifice equation (Yi et al., 2019).
   $C_d = Q / A \cdot \sqrt{(\varrho/2\Delta p)}$ (3)
   where Q is the airflow rate entering the opening (m^3/s), A is the opening area (m^2), ϱ is the air density in the room (kg/m^3) and Δp is the difference between the pressure at the opening area and in the room (Pa).
8. Temperature stratification – the difference in temperature along different planes based on EN ISO 7730 and ASHRAE Standard 55, in order to estimate the local thermal discomfort: (a) vertical air temperature difference between the head level (1.8 m from the floor for standing, and 1.1 m from the floor for sitting position) and ankles (0.1 m from floor), and (b) temperature difference at distances 0.5 m, 1 m, 1.5 m and 2 m from the window.
9. Draught risk (DR) – the discomfort caused in winter due to draught is calculated using Eq. 4 (Section 6.2 EN ISO 7730-2005):
   $DR=(34-t_a)\cdot(v_a-0.05)^{0.62}(0.37\cdot v_a\cdot T_u+3.14)$ (4)
   where t_a is the local air temperature (°C), v_a is the local mean air velocity (m/s), and T_u is the local turbulence intensity (%).
10. Mean air velocity at different heights – the average air velocity at 1.8 m, 1.1 m, and 0.1 m distance above the floor. Based on EN ISO 7730, the effects on the perceived air temperature due to variations in air velocity is evaluated.
11. Mean air velocity near surfaces – this helps to compare the convective heat transfer which is enhanced due to the fluid motion near the surface. Predicting the air velocity near surfaces can be very complicated, but using CFD it can be computed. The air velocity is averaged at a plane 5 cm away from each surface.

3. Results And Discussion

Based on the performance parameters listed in Section 2.4, the results are discussed in this section.

1. Temperature distribution – in Fig. 3 the thermal profiles are presented at the vertical plane in the middle of the room for the wind at a 90° angle. The focus is laid on the inner chamber, without showing the entire external domain. The air enters inside differently according to the different window opening styles and modifies the indoor environment differently. A greater drive of buoyancy is seen at 1 m/s speed, where the colder outdoor wind enters from the lower parts of the window, such as the winter case for Type_1 and Type_2. On the contrary, for 2 m/s wind, the colder wind from outside is dominant and enters through the upper portions. Type_2 shows higher inflow and lower indoor temperatures. In winter conditions, the reduction in the mean indoor temperature for Type_1 at 2 m/s is only 0.6 % higher than the reduction achieved at 1 m/s, whereas for Type_2 this difference is 6.3 %. While in summer, the reduction for Type_1 is only 1.1 %, and for Type_2 is 12.2 %. Type_3 shows a much lower incoming airflow, higher indoor temperature, and a more homogeneous distribution due to low opening area. Up until the part to which the wind penetrates, the profiles are similar to the thermal profiles at the central plane of Wang et al. (2018).

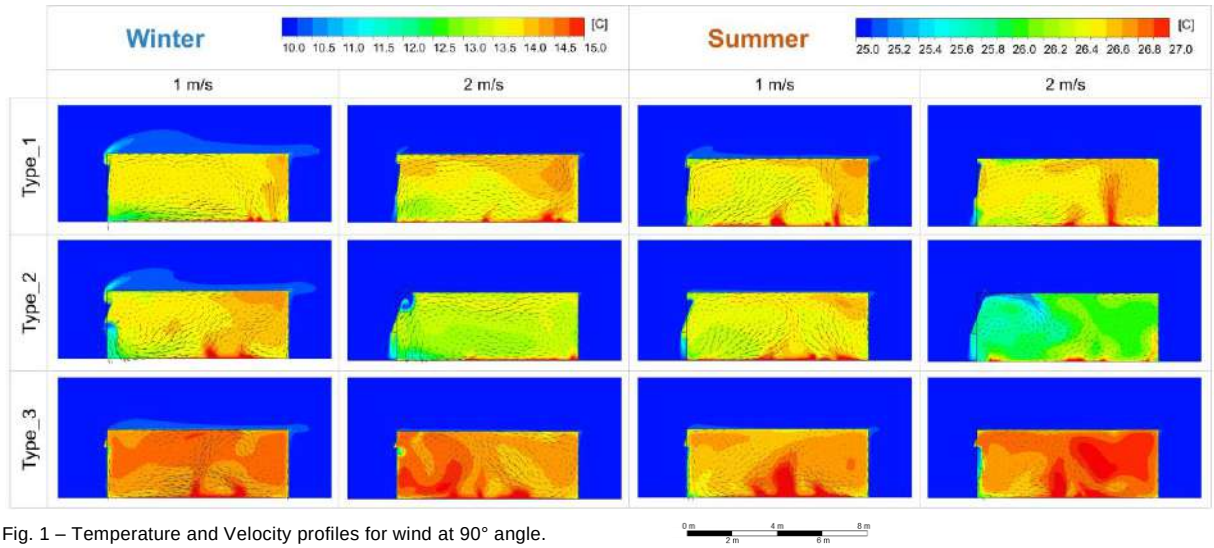

Fig. 1 – Temperature and Velocity profiles for wind at 90° angle.

2. Velocity fields – the velocity profile in the inner chamber, for wind at a 90° angle, are shown in Fig. 3. In the winter case, at lower speed, the buoyant forces are dominant, due to high temperature differences. For Type_3, the buoyancy forces are always dominant due to the geometrical configuration of the window, which does not allow the wind to directly enter inside, and the cold air can be seen entering the lower part and immediately falling. Similar fields for these types of windows can be noticed in the results obtained by Wang et al. (2018), but a direct comparison is not possible due to different opening sizes.
3. Incoming airflow rate (Q) – as shown in Fig. 4 (a), Q varies largely by the opening types, wind angle and wind speed, and not due to the indoor-outdoor temperature conditions tested. Q for summer and winter conditions do not vary more than 20 %, except for Type_2 for 1 m/s wind at a 90° angle when Q in summer conditions is 33 % less than in winter conditions. Based on wind speed, Q for 2 m/s wind is always higher than Q for 1 m/s wind, with the minimum difference of 44 % for Type_1 for wind at 45° in winter, up to a maximum of 342 % higher rate for Type_2 for wind at 90° in summer. Based on the angle of wind, Q is always higher for wind at a 45° angle, with a difference of 25 % for Type_1 for 2 m/s wind in summer, up to 210 % for Type_3 for 2 m/s wind in winter and both speeds in summer. This is due to the geometrical advantage of wind coming at an angle and entering indirectly.
4. Mean Age of Air (MAA) – as shown in Fig. 4 (b), for the same wind speed and angle, MAA in summer is higher than in winter conditions, because the air changes are slower for lower temperature differences in the summer case, except for Type_2 for 2 m/s wind at a 90° angle where MAA in summer is 17 % lower than in

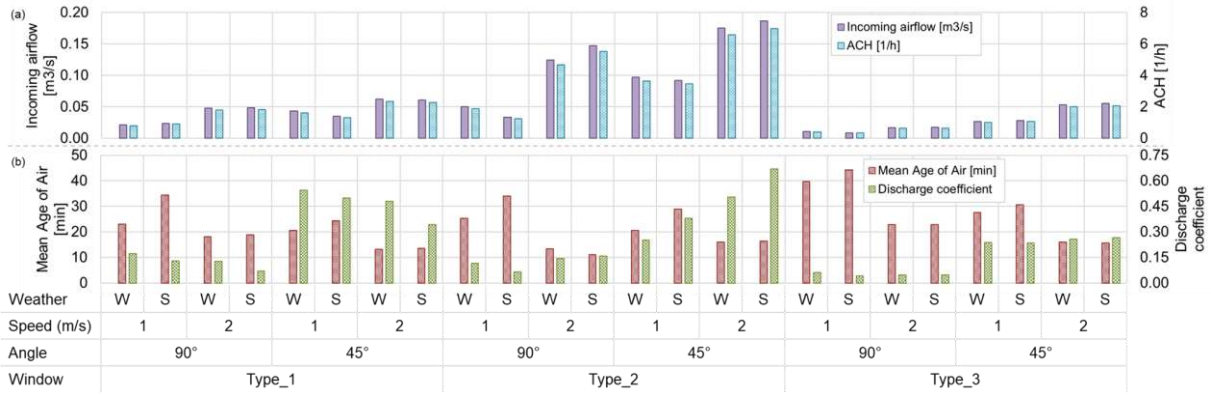

Fig. 2 – Results for (a) incoming airflow and air changes per hour (ACH); (b) mean age of air and discharge coefficient. [W=winter, S=summer]

winter conditions. Based on the wind speed, MAA for 2 m/s is always lower than for 1 m/s wind, from 22 % lower for Type_1 for wind at 90° in winter, as well as for Type_2 for wind at 45° in winter, up to 67 % lower for Type_2 for wind at a 90° angle in summer, due to the corresponding lower Q. For the same wind speed and temperature, MAA for wind at 45° is lower than wind at a 90° angle, except for Type_2 for 2 m/s wind in both weathers.

5. Air changes per hour (ACH) – trends for ACH are observed similar to Q. On comparison with previous studies, ACH for Type_2 shows consistent behavior on increasing wind speed, as well as the range of ACH being consistent for the two wind speeds (Wang et al., 2018).
6. Effective penetration depth – as visible in the velocity profile at the vertical plane in the middle of the room, shown in Fig. 3, it can be observed that the effective penetration depth in all cases varies for each window type, as the influence of the incoming air is different.
7. Discharge coefficient (C_d) – shown in Fig. 4 (b), the C_d of the same type of window varies largely with temperature, wind speed and wind angle, as concluded by previous studies (Heiselberg et al., 2001; Karava et al., 2004; Yi et al., 2019). Based on the wind speed, Type_1 always shows a low C_d for 2 m/s speed, whereas the other Type_2 shows a high C_d at 2 m/s wind. This is due to the geometrical structure of the window opening. Based on the wind angle, C_d is always higher for wind at a 45° angle, with a minimum difference of 118 % for Type_2 for 1 m/s wind in winter, up to 500 % higher for Type_2 for 2 m/s wind in summer. The variation of C_d with wind angle is consistent with the conclusions of Yi et al. (2019), and is due to decreased resistance, as also noticed with the incoming airflow rate.
8. Temperature stratification – the temperature differences at different heights and distances from the window are represented in Fig. 6 (a). More stratification is noticed in winter, due to higher indoor-outdoor temperature difference. The maximum differences at the horizontal and vertical planes are seen for Type_2 in winter for 2 m/s wind at a 90° angle, whereas in the summer cases, the overall differences are quite low. This shows a good level of air mixing inside the chamber. The temperature differences between head level (1.1 m) and ankles (0.1 m) are in accordance with Category A of ISO 7730, since it is always lower than 2 °C in all cases (Section A.3 EN ISO 7730-2005), and in accordance with ASHRAE 55 (Section 5.3 ASHRAE Standard 55-2017).
9. Draught risk (DR) – Fig. 5 shows the DR and mean indoor temperatures in winter. The maximum DR of 15.8 % is observed for Type_2 at 2 m/s wind at a 45° angle. For the same wind angle, DR is always observed as higher for wind speed 2 m/s, up to 29 % higher for Type_2 for wind at a 90° angle, due to higher mean air velocity indoors. Based on wind angle, DR is always higher for wind at a 45° angle. The thermal environment lies in Category B of the ISO 7730, since DR lies between 10-20 % (Section A.1 EN ISO 7730-2005).
10. Mean air velocity at different heights – as represented in Fig. 6 (b), higher velocity of air is observed at the lowest level of 0.1 m, because of colder air entering and flowing downwards. Based on the ISO 7730, for occupancy similar to office spaces, the maximum mean air velocity lies in Category B for both winter and summer cases (Section A.4 EN ISO 7730-2005).
11. Mean air velocity near surfaces – as per Fig. 6 (b), air velocity is higher near the floor surface and lowest near the ceiling. A maximum of 0.21 m/s is observed near the sidewall for Type_1 for 2 m/s wind at a 45° angle. Due to higher velocity at the floor, a heat source near the floor could be a good option for promoting convective heat transfer, as it is enhanced due to the fluid motion near the surface.

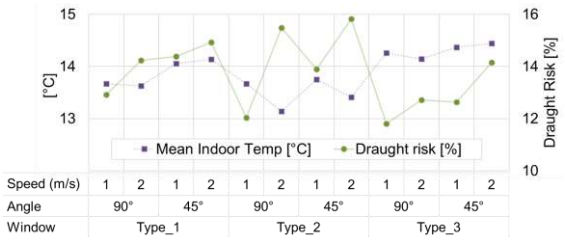

Fig. 5 – Draught risk and mean indoor temperatures in winter for the different window types in different weather conditions

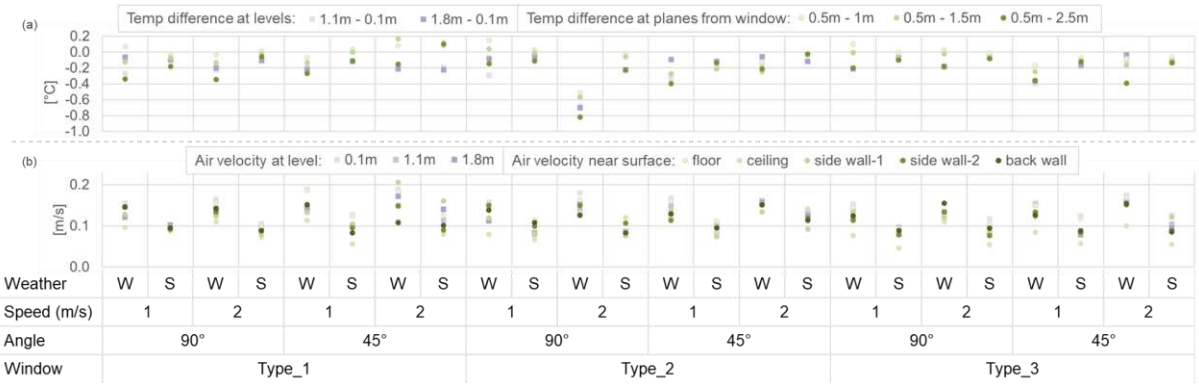

Fig. 6 – Results showing (a) temperature differences at various levels, and (b) air velocity. [W=winter, S=summer]

4. Conclusion

The aim of this study was to investigate the effectiveness of different types of windows for single-sided wind-driven natural ventilation using CFD simulations. A methodology of geometrical modeling of a one-room zone, which is a common condition for student dormitories and many residential apartments with openings only on one side, was studied. The model considered was tested for three different window configurations, two weather conditions, two wind speeds and two different wind angles. The performance of the windows was tested for its ventilation performance, as well as thermal comfort.

It was observed that the ventilation performance is sensitive to the ambient conditions, but for the different opening configuations this senstivity varies. At low wind speed (1 m/s), the buoyant forces dominate, whereas at higher wind speed (2 m/s), the wind pressure becomes dominant and air enters from the upper portions of the windows. Based on wind speed, for 2 m/s wind, the incoming airflow and air changes per hour are always higher, whereas the mean age of air is always lower when compared with 1 m/s wind. Based on wind angle, for the wind at a 45° angle, the airflow and the air changes per hour are always higher, whereas the mean age of air is generally lower when compared with wind at 90° to the window. The mean age of air in summer is generally higher than in winter, because the air changes are slower for lower temperature differences in the summer case.

The discharge coefficient is dependent on various factors, and the traditional concept of a unique constant discharge coefficient is not suitable, as the value obtained in the cases modeled was generally below the recommended value of 0.6, which can overestimate the natural ventilation performance. Type_2 (horizontal pivot) shows an increase in discharge coefficient for increasing wind speed, whereas Type_1 (bottom-hung) shows inverse behavior. Based on the wind angle, the discharge coefficient is always higher for wind at a 45° angle. For Type_2 (horizontal pivot) window, higher differences of temperature at different vertical and horizontal places were observed. Based on wind speed, the draught risk is higher for 2 m/s wind, and, based on wind angle, it is higher for wind at a 45° angle. The air velocities are generally high at lower heights, which can promote convective heat transfer.

Therefore, for different window configurations, the aspects of local weather conditions, such as wind speed, angle, indoor-outdoor temperature, should be carefully considered by the designers to better determine ventilation performance and the natural ventilation strategy for each context.

Acknowledgement

The research presented in this paper is supported by funding from the European Regional Development Fund POR FESR 2014-2020 of the Province of Bolzano, under Project number 1116, NEW-AIR: Nuovo approccio per una qualità degli ambienti interni energeticamente efficiente: ricerca e aziende fanno sistema in Alto Adige (English: New approach for an energy efficient IEQ: research and firms systemizing cooperation in South Tyrol).

References

ANSYS Inc. 2013. "ANSYS CFX Solver Modeling Guide 15.0."

Babich, F., M. Cook, D. Loveday, R. Rawal, and Y. Shukla. 2017. "Transient Three-Dimensional CFD Modelling of Ceiling Fans." *Building and Environment* 123: 37–49. doi: https://doi.org/10.1016/J.BUILDENV.2017.06.039

Belleri, A., R. Lollini, and S. M. Dutton. 2014. "Natural Ventilation Design: An Analysis of Predicted and Measured Performance." *Building and Environment* 81: 123–38. doi: https://doi.org/10.1016/J.BUILDENV.2014.06.009

Blocken, B. 2015. "Computational Fluid Dynamics for Urban Physics: Importance, Scales, Possibilities, Limitations and Ten Tips and Tricks towards Accurate and Reliable Simulations." *Building and Environment* 91: 219–45. doi: https://doi.org/10.1016/J.BUILDENV.2015.02.015

European Commission. 2020. "Energy Efficiency in Buildings." February 17. https://ec.europa.eu/info/news/focus-energy-efficiency-buildings-2020-lut-17_en

Gupta, A., A. Belleri, and F. Babich. 2021. "Evaluating the Performance of Different Window Opening Styles for Single-Sided Buoyancy-Driven Natural Ventilation Using CFD Simulations." In *Proceedings of Building Simulation 2021 Conference*. Bruges, Belgium.

Heiselberg, P., K. Svidt, and P. V. Nielsen. 2001. "Characteristics of Airflow from Open Windows." *Building and Environment* 36(7): 859–69. doi: https://doi.org/10.1016/S0360-1323(01)00012-9

Karava, P., T. Stathopoulos, and A. K. Athienitis. 2004. "Wind Driven Flow through Openings-A Review of Discharge Coefficients." *International Journal of Ventilation* 3(3). doi: https://doi.org/10.1080/14733315.2004.11683920

Liu, J., and J. Niu. 2016. "CFD Simulation of the Wind Environment around an Isolated High-Rise Building: An Evaluation of SRANS, LES and DES Models." *Building and Environment* 96: 91–106. https://doi.org/10.1016/J.BUILDENV.2015.11.007

Nomura, M., and K. Hiyama. 2017. "A Review: Natural Ventilation Performance of Office Buildings in Japan." *Renewable and Sustainable Energy Reviews* 74: 746–54. doi: https://doi.org/10.1016/J.RSER.2017.02.083

Wang, J., S. Wang, T. Zhang, and F. Battaglia. 2017. "Assessment of Single-Sided Natural Ventilation Driven by Buoyancy Forces through Variable Window Configurations." *Energy and Buildings* 139: 762–79. doi: https://doi.org/10.1016/J.ENBUILD.2017.01.070

Wang, J., T. Zhang, S. Wang, and F. Battaglia. 2018. "Numerical Investigation of Single-Sided Natural Ventilation Driven by Buoyancy and Wind through Variable Window Configurations." *Energy and Buildings* 168: 147–64. doi: https://doi.org/10.1016/J.ENBUILD.2018.03.015

Yi, Q., X. Wang, G. Zhang, H. Li, D. Janke, and T. Amon. 2019. "Assessing Effects of Wind Speed and Wind Direction on Discharge Coefficient of Sidewall Opening in a Dairy Building Model – A Numerical Study." *Computers and Electronics in Agriculture* 162: 235–45. doi: https://doi.org/10.1016/J.COMPAG.2019.04.016

Zhong, H.Y., Y. Sun, J. Shang, F.P. Qian, F.Y. Zhao, H. Kikumoto, C. Jimenez-Bescos, and X. Liu. 2022. "Single-Sided Natural Ventilation in Buildings: A Critical Literature Review." *Building and Environment* 212: 108797. doi: https://doi.org/10.1016/J.BUILDENV.2022.108797

Zhou, J., Y. Hua, Y. Xiao, C. Ye, and W. Yang. 2021. "Analysis of Ventilation Efficiency and Effective Ventilation Flow Rate for Wind-Driven Single-Sided Ventilation Buildings." *Aerosol and Air Quality Research* 21(5): 200383. doi: https://doi.org/10.4209/AAQR.200383

The Management of the Energy Performance Simulation of a Complex Building Portfolio. The Case of the School Building Asset of an Italian Municipality

Claudia Bo – Politecnico di Milano, Italy – claudia.bo@polimi.it
Enrico De Angelis – Politecnico di Milano, Italy – enrico.deangelis@polimi.it
Andrea Augello – Politecnico di Milano, Italy – andrea.augello@polimi.it

Abstract

This paper aims at presenting a methodology for the management of multiple energy simulations of complex building assets. The educational buildings of the Milan municipality have been chosen as case studies: several retrofit strategies are tested on hundreds of buildings, evaluating their feasibility and calculating the potential energy savings. The results, obtained with dynamic simulations using SketchUp and the "Intelligent Community Design (iCD)" plugin, are then compared with a static calculation implemented on a regional scale in Lombardy. Besides, a methodology for the collection of the input parameters is proposed, based on the combination of data coming from several sources.

1. Introduction

Due to the increasing risks derived from global warming, proved to be caused by human activities, a dramatic reduction of the greenhouse gas emissions in the atmosphere will be crucial in the near future (Pörtner et al., 2022). The built environment plays a dominant role, since it is one of the largest sources of direct and indirect greenhouse gas emissions (36 %, in Europe) and the share (40 %, ibid.) of energy consumption. In this framework, urban areas play a fundamental role and are deeply involved in meeting the main decarbonization objectives. Educational buildings account for a small percentage of built stock (about 4 % of the European one, in terms of net floor area, and even less, about 3 %, in terms of energy consumption, due to their short time use, (Re Cecconi, 2020), but they represent a critical asset, in particular in Italy (we can refer to the periodic reports edited by Legambiente and the most recent one in particular, Legambiente 2021), because of their age, their maintenance needs and, in general, their social role. Unfortunately, a precise understanding of the energy and carbon footprint of the built asset is rare and often unreliable (this is particularly true for the Italian educational building asset; the Legambiente 2021 report, for example, mentions that the energy-rated buildings are less than ¼ of the total). Data – when easily available – report consumptions only as averages and even their physical description is often unreliable (but improving, see the MIUR OpenData). As a consequence, energy retrofit strategies are usually referred to as one or more "typical" buildings or "archetypes", representatives of the average energy need of the asset and the average retrofit potentials, without defining the real priorities of the asset. This approach is investigated by Mohammadiziazi et al. (2021), who estimated the energy performances of the commercial building stock in Pittsburgh by analyzing twenty building archetypes with a dynamic tool, i.e., EnergyPlus. The same methodology was applied by Caputo et al. (2013), who proposed the estimation of the energy consumption of residential and commercial buildings in Milan, analyzing 56 archetypes different in geometry, construction period, and function. Also, in this case, they use a dynamic tool, i.e., EnergyPlus, whose results were later validated and compared with the energy consumptions reported in the SIRENA (Sistema Informativo Regionale Energia Ambiente) database. Another dynamic tool, i.e., DOE-2.2, was adopted by Krarti et al. (2020) to analyze 54 building archetypes and assess the energy and non-energy benefits in investing in retrofitting existing residential building stock in

Saudi Arabia. Other authors prefer to assess the energy performances of building archetypes using steady-state methods, using Microsoft Excel (Tuominen et al., 2014) or national energy certification software (Dascalaki et al., 2016). Other methods used for the energy analysis of building archetypes are based on the EN ISO 13790 (Yang et al., 2020; Yang et al., 2022) or multiple regression analysis (Wong et al., 2019). Bottom-up approaches without building archetypes were studied by Costanzo et al. (2019) and Wang et al. (2018). Costanzo et al. (2019) developed a bottom-up engineering approach applied to the Yuzhong District of Chongqing municipality in China, based on EnergyPlus with the Urban Modelling Interface. Similarly, Wang et al. (2018) analyzed the energy demand and the retrofitting potential for three Swiss residential districts of Zurich and Zernez, adopting a bottom-up approach without building archetypes based on EnergyPlus. Other bottom-up approaches investigated are based on statistical methods, e.g., multiple linear regression techniques, as proposed by Mastrucci et al. (2014), Torabi Moghadam et al. (2018), and de Rubeis et al. (2021). These methods can predict the energy consumption on a large scale with reduced computational time and without the need for complex input data as with the physics-based models. The advantages of physical models and data-driven methods are combined and investigated by Li & Yao (2021) and Zygmunt & Gawin (2021), who proposed hybrid approaches based on building archetypes with machine learning and artificial neural network models, respectively. Other analysis methods are based on the energy performance certificates available, as demonstrated by Hjortling et al. (2017) and Gangolells et al. (2016), who respectively mapped the energy performances of existing Swedish and Spanish buildings.

This paper presents a methodology for the assessment of energy retrofit scenarios applied to Italian educational buildings. The energy performances of the school buildings belonging to the Milan municipality were assessed with both dynamic and steady-state tools, testing the effect of three retrofit strategies. The research allowed us to evaluate the energy consumption innovatively; it eliminates the concept of the archetype: the whole urban area of Milan was modeled, assessing the energy performances of each school building. Furthermore, it gave us a clear idea about the available database open sources, cross-checking of the input data, mainly about the buildings' geometry and envelope/plant properties, thus increasing the model reliability and finding a compromise when data were missing.

2. Methodology

2.1 Data Sources and Reliability

This paragraph describes the primary data sources of the modelled school buildings and their related uncertainties. The geometrical models are based on geographic information system (GIS) data, which were later compared with AutoCAD drawings; the buildings' characteristics are obtained from several data sources, such as European projects, national open data, energy performances certificates, etc.

GIS data: OpenStreetMap and Lombardy geographical data

OpenStreetMap (OSM), a crowd-sourcing editable world map, is currently the biggest freely available geodata platform; it provides different kinds of open data, such as building footprints, function, name, height, etc. These maps are based on polylines created with GPS tracks, satellite photos, and various data provided by local governments or volunteers. However, OSM contains two main levels of errors: a systematic one due to the uncertainty of the GIS data, and a casual error, i.e., an unpredictable error due to the inaccuracy of users themselves; besides, for many buildings, we observed an additional lack of information, for example, related to the height of the buildings, which was not consistent with the real values. To overcome these uncertainties, the GIS database of the Lombardy region and the city of Milan was analyzed, visualizing their metadata (shapefile, JSON or CSV format, raster data) on the software QGIS.

AutoCAD drawings

The plans, sections, and elevations for about 20 school buildings, provided as AutoCAD files by the Municipality of Milan, have been analyzed to validate the geometrical information reported in the other data sources.

IEE TABULA project database

The Intelligent Energy Europe Tabula project, published in May 2012 and updated in July 2014, assesses the energy performances of the existing Italian residential buildings, predicting the impact of retrofit measures on both building envelope and plants. This project is chosen as a reference since it contains useful information about the building envelope components: according to the period of construction, it provides a general description of its typical construction elements with their related thermal performances.

Ministero dell'istruzione, dell'università e della ricerca (MIUR) open data

The Italian ministry of education, university, and research provide open data about the whole Italian school asset. For each Italian school, represented by a unique building code, data about location, total areas, and volumes, number of floors, typology of installed plants, year of construction, etc. is provided.

Energy Performance Certificates

The Energy Performance Certificates (EPCs) of the Lombardy region provide more detailed information about the school building asset: heated surfaces and volumes, typology of installed plants, electricity and gas consumptions, envelope thermal transmittances, primary energy consumptions, etc. However, these data are not available for all school buildings, since they refer only to the Italian schools having certified energy performances. Besides, another limitation of these data is related to the certified building unit: in many cases, the energy certificate is provided only for a part of the entire school building, and therefore, in these cases, the data are not representative of the whole building.

EnergyPlus Weather data

The chosen weather data come from the World Meteorological Organization Region and Country and is referred to as a Typical Meteorological Year based on the Milano Malpensa climate. Due to the distance between the airport weather station and the city center, a source of uncertainty arises, since the weather file does not consider the urban heat island effect, which could determine an increased air temperature for several parts of the city.

2.2 Calculation Methods

Two calculation methodologies were chosen: a dynamic one, based on the simulation tool "Intelligent Community Design (iCD)" and applied to 277 educational buildings in Milan, and a steady-state one, based on the UNI/TS 11300-1 and applied to 1036 educational buildings of Lombardy. The first one is a plug-in to SketchUp, a 3D master planning modeling tool able to perform energy analysis scalable from individual buildings up to entire cities. It could be used for both new interventions and retrofit projects, assessing: the heating and cooling energy consumption, the effects of retrofit strategies on the overall performances (i.e., addition of insulation to the building envelope, replacement of the HVAC systems, etc.), energy produced with renewable sources, accessibility to transport and amenities, total building water consumption, etc. The building geometries can be drawn manually on SketchUp or imported from the OpenStreetMap database; all the other characteristics of the buildings can be later assigned by choosing from lists of predefined values. The applied steady-state method is a simplification of the procedure described in the UNI/TS11300-1 standard, and it aims at calculating the final and primary energies according to the following equations:

$$Q_U = (Q_L - \eta Q_G)/\varepsilon_P \quad (1)$$

$$EP_H = Q_U \cdot fp_{nren} \quad (2)$$

For the steady-state calculations, the following hypothesis was assumed: an average air change per hour of 0.4 was considered for each school building, without any heat recovery; the transmission losses were calculated starting from the average envelope thermal transmittances, calculated as weighted values. Concerning the total gains, intended as the sum of internal and solar gains, reference was made to the UNI 10349 for the climatic data and the UNI/TS 11300-1 for the applied average internal gains, equal to 4 W/m^2; besides, a boiler efficiency of 0.83 was assumed to consider the possible losses of the building's systems. In the end, a primary energy conversion of 1.05 was used to estimate the primary energy, choosing natural gas as the primary energy source.

2.3 The Building Geometrical Model

Starting from the OpenStreetMap database, the volumes of all the buildings in Milan were modeled. However, the chosen database contains uncertainties and inaccuracies, mainly linked to the footprint area and height of the buildings: for this reason, the geometry of about 20 educational buildings was later checked and compared with detailed AutoCAD drawings; the rest of the school buildings were instead checked with the data, even if approximate, provided by Google Earth, since no architectural drawings were available for those buildings. The geometric GIS data of different layers are metadata containing technical information and are identified by alphanumeric codes. The school's name or its unique identification code is the link between the geometric and the envelope information. Three actions were performed to achieve the input data needed for the steady-state calculations, based on "Scuole Lombardia", "A020101" and "corpo edificato massima estensione" layers:

1) Filtration in Mapshaper Console: the volumetric unit who have "servizio pubblico - istruzione - sede scuola" were considered.
2) Data Process in Qgis: NN Join Plugin, based on the shorter distance, linked the school's name with the geometry.
3) Data transformation: the surface to volume ratio (S/V) was calculated for all the Lombardy schools based on the procedure proposed by Vicentini and Mutani (2012).

Moreover, the calculated volumes of the buildings were used as reference to check the ones provided by MIUR open data.

2.4 The Building Technological Model

The Lombardy Region Database and MIUR provide very useful but generic information, giving a general description of the building envelope (e.g., "double glazing" or "single glazing" as information for the windows). On the contrary, the Certificazione Energetica degli Edifici (CENED) data provide more specific information that could be, however, as stated in the previous paragraph, related to a small portion of the school buildings modeled. For this reason, the envelope properties were estimated starting from the IEE TABULA project database, assigning the material properties according to the buildings' year of construction. The chosen thermal properties are shown in Table 1.

Table 1 – Envelope thermal transmittance [W/m^{2}K] according to the construction year of the buildings (dynamic and steady-state models)

	?-1975	1976-1990	1991-2005	After 2006
Roof	2.02	1.05	0.68	0.3
Ext. wall	1.74	0.79	0.6	0.34
Int. floor	2.28	0.93	0.65	0.36
Windows	5.23	3.17		2.3
Ground floor	0.79	0.79	0.79	0.79
Int. wall	1.06	0.76 - 0.59		

However, not all the building characteristics were defined using the previously cited sources of data, due to their limitations in terms of information provided. For example, the window to wall ratios (WWR), i.e., the ratio between glazed and opaque envelopes was estimated using Google Earth, calculating these quantities for 49 school buildings. Consequently, the calculated average WWR of 23 % was applied to all 277 school buildings.

2.5 The Building Plant Model

A "central heating radiators" system was applied to all the school buildings as HVAC system; no cooling system is considered. The technical data of the modeled building plants of the dynamic analysis, taken from the iCD database, are summarized in Table 2.

Table 2 – Building system characteristics (dynamic model)

SCOP [kW/kW]	0.83
Heating setpoint [°C]	20
SEER [kW/kW]	-
Cooling setpoint [°C]	-
Auxiliary energy [W/m^2]	0.95
Ventilation heat recovery [%]	-
Air supply [l/(s·m$^{2)}$]	0.27
Infiltration rate [ach]	0.167
Domestic Hot Water efficiency [%]	0.5
Average Cold Water temperature [°C]	10
Average Hot Water temperature [°C]	60

2.6 The Building Usage Model

iCD contains several predefined usage profiles, specific for each building typology and human activity. The internal gains are thus assigned to the model, selecting, among the available ones, the usage

profiles defined as "School or University", which are summarized in Table 3 and plotted in Fig. 1 along with the building system schedules.

Table 3 – Applied internal gains (dynamic model)

Daily average internal gains [W/m²]			Average people density [m²/pers]
People	Lighting	Appliances	
4	3.4	4	6.8

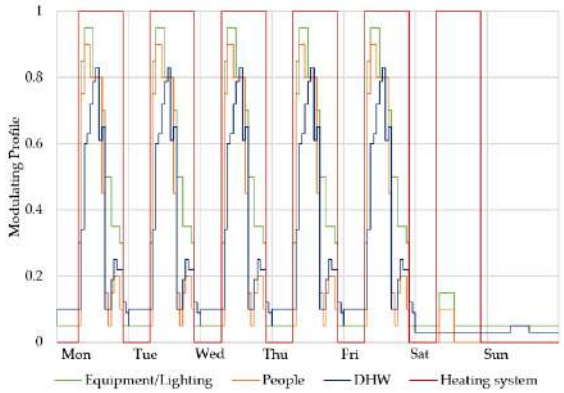

Fig. 1 – Weekly schedules of internal gains and plants (dynamic model)

3. Results and Discussion

3.1 Energy Consumption

The dynamic simulation for all 277 buildings was performed on iCD, analyzing the energy consumption concerning the following: domestic hot water production, auxiliary energy, heating system, equipment, and lighting. These results are plotted in Fig. 2, which summarizes the energy consumption of the school asset as average values. The results show that the highest consumptions, i.e., 69 % of the total, are due to the heating system, probably due to the high heat losses through the envelope and the low efficiency of the installed systems. Therefore, the average total energy of 179.9 kWh/m² is obtained, of which 123.4 kWh/m² are due to heating consumption. This value is consistent with the Italian average heating consumption, estimated equal to 115 kWh/m² (Dias Pereira et al., 2014). Starting from the baseline results, three retrofit scenarios are tested:

1) S1: Replacement of the external windows with double glazing with a thermal transmittance equal to 1.4 W/(m² K)
2) S2: Installation of 10 cm of thermal insulation on the external side of external walls and roof. Fiberglass with a thermal conductivity of 0.034 W/(m K) is chosen for the external walls, while a glass wool panel with thermal conductivity of 0.037 W/(m K) is proposed for the roof.
3) S3: Replacement of the existing boiler with a heat pump with a COP equal to 3.5

The averages and frequencies of the total energy consumption are reported and compared in Fig. 2 and Fig. 3. The replacement of the windows (S1) determines a reduction of the heat losses by transmission, thanks to the reduced thermal transmittance values; in this way, it is possible to reduce the average heating energy consumption, going from 123.4 kWh/m² to 105.7 kWh/m². This solution is optimal for buildings with several floors and a restricted footprint area because the most significant slice of dispersion area will be due to the external area of the wall also influenced by the WWR. The results of the S2 scenario demonstrate the importance of having a well-insulated envelope: we registered a further decrease in the average heating consumption, which arrives at 74.7 kWh/m². Certainly, this solution is more effective than the S1 scenario, due to the larger area of the opaque envelopes. The best results are obtained with the S3 scenario: the replacement of the heat generator determines a reduction of 87 % of the average heating consumption compared with the baseline configuration, decreasing the heating need to 16.5 kWh/m².

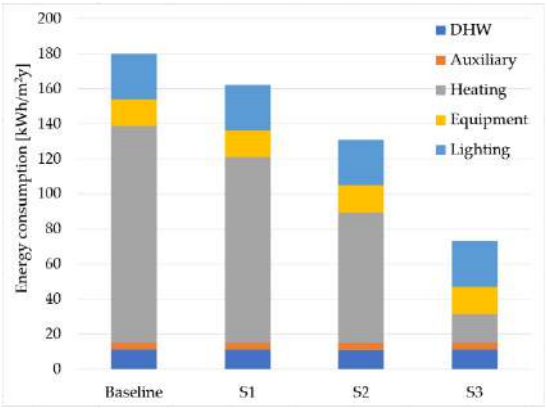

Fig. 2 – Comparison of the average energy consumption

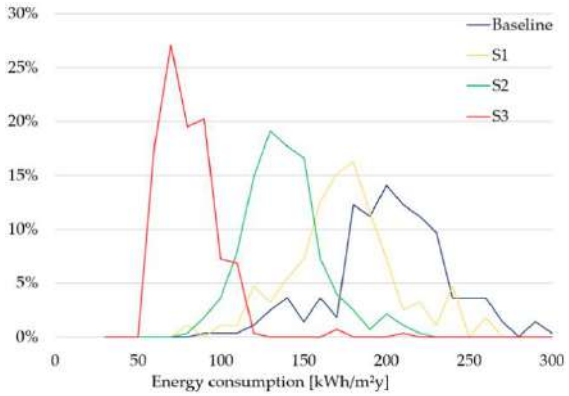

Fig. 3 – Frequency distribution of the total energy consumption

Furthermore, the heating consumption of the school buildings in Lombardy was calculated with a steady-state method: however, to compare these results with those coming from the dynamic model, the initial sample of 1036 schools was reduced to 144 buildings, i.e., the number of buildings common for both steady-state and dynamic models. Comparing the frequencies of several ranges of heating consumption (Fig. 4), we notice that the results of the dynamic calculation do not exceed 240 kWh/m², while for the steady-state model we register energy consumption even higher than 340 kWh/m². Besides, using the dynamic tool, more than half of the school buildings in Milan are characterized by a heating consumption lower than 140 kWh/m²; on the contrary, with the steady-state tools, they reach 240 kWh/m². Therefore, significant differences between the results compared are presented, which seems higher for the steady-state method. This difference could be related to the methodology itself, highlighting the advantages of dynamic simulation tools, or to the input data and assumptions.

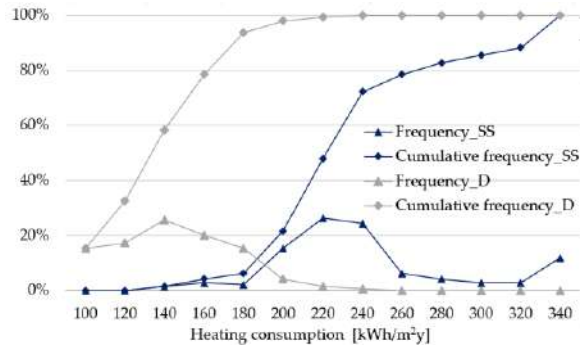

Fig. 4 – Frequency distribution for the steady-state (SS) and dynamic (D) heating consumption

3.2 Limitations and Open Questions

The main limitation of the present methodology concerns the input data needed: several sources have been used to define the buildings' geometries, envelope performances, usage profiles, etc., which might not be consistent with the actual buildings' characteristics. Therefore, the results reported should be compared with measured energy consumption, thus improving and validating the proposed methodology.

4. Conclusion

This paper proposes a methodology for the assessment of the energy performances of urban areas. The educational building asset of Milan was chosen as a case study, calculating its energy consumption with a dynamic tool and obtaining results close to the ones proposed by other authors (e.g., Dias Pereira et al., 2014). Three retrofit strategies were proposed and their effect was assessed: the best results were obtained by replacing the existing heat generators with heat pumps, decreasing the average heating consumption by about 87 % compared to the baseline one. Furthermore, the results obtained with the dynamic tool were compared with steady-state calculations analysing a sample of 144 educational buildings: we registered higher energy consumption with the steady-state method, which could be related to the methodology itself or the different input and sources of data. Hence, future investigations will improve and validate the proposed methodology by comparing the obtained results with actual measured energy consumption.

Acknowledgments

We wish to thank the ICL consultancy team and, in particular, Mario Favalli Ragusini, Fergus Ross, and Valeria Ferrando for their support with the Intelligent Communities Lifecycle ICL software.

Nomenclature

Symbols

ε	Efficiency (-)
η	Utilization factor (-)
EP	Primary energy (kWh)
fp	Primary energy conversion factor (-)
Q	Energy (kWh)

Subscripts/Superscripts

G	Gains
H	Heating
L	Losses
nren	Non-renewable
P	Plants
U	Useful

References

Caputo, P., G. Costa, and S. Ferrari. 2013. "A supporting method for defining energy strategies in the building sector at urban scale". *Energy Policy* 55: 261-270. doi: http://dx.doi.org/10.1016/j.enpol.2012.12.006

Certificazione ENergetica degli EDifici (CENED). Accessed on April 15. https://www.cened.it/

Costanzo, V., R. Yao, X. Li, M. Liu, and B. Li. 2019. "Urban building energy model: Database development, validation, and application for commercial building stock." *Cities* 95. doi: https://doi.org/10.1016/j.cities.2019.102467

Dascalaki, E. G., C. A. Balaras, S. Kontoyiannidis, and K. G Droutsa. 2016. "Modeling energy refurbishment scenarios for the Hellenic residential building stock towards the 2020 & 2030 targets". *Energy and Buildings* 132: 74-90. doi: http://dx.doi.org/10.1016/j.enbuild.2016.06.003

de Rubeis, T., L. Giacchetti, D. Paoletti, and D. Ambrosini. 2021. "Building energy performance analysis at urban scale: A supporting tool for energy strategies and urban building energy rating identification". *Sustainable Cities and Society 7*: 74. doi: https://doi.org/10.1016/j.scs.2021.103220

Dias Pereira, L., D. Raimondo, S. P. Corgnati, and M. G. da Silva. 2014. "Energy consumption in schools – A review paper." *Renewable and Sustainable Energy Reviews* 40: 911–922. doi: http://dx.doi.org/10.1016/j.rser.2014.08.010

EnergyPlus. Accessed on May 16. https://energyplus.net/

Gangolells, M., M. Casals, N. Forcada, M. Macarulla, and E. Cuerva. 2016. "Energy mapping of existing building stock in Spain". *Journal of Cleaner Production* 112: 3895-3904. doi: http://dx.doi.org/10.1016/j.jclepro.2015.05.105

Geoportale della Regione Lombardia. Accessed on August 5. https://www.geoportale.regione.lombardia.it/

Hjortling, C., F. Bjork, M. Berg, and T. af Klintberg. 2017. "Energy mapping of existing building stock in Sweden – Analysis of data from Energy Performance Certificates". *Energy and Buildings* 153: 341-355. doi: http://dx.doi.org/10.1016/j.enbuild.2017.06.073

Intelligent Energy Europe Project TABULA. Accessed on July 18. https://episcope.eu/welcome/

Krarti, M., M. Aldubyan, and E. Williams. 2020. "Residential building stock model for evaluating energy retrofit programs in Saudi Arabia". *Energy* 195. doi: https://doi.org/10.1016/j.energy.2020.116980

Li, X., and R. Yao. 2021. "Modelling heating and cooling energy demand for building stock using a hybrid approach". *Energy and Buildings* 235. doi: https://doi.org/10.1016/j.enbuild.2021.110740

Mastrucci, A., O. Baume, F. Stazi, and U. Leopold. 2014. "Estimating energy savings for the residential building stock of an entire city: A GIS-based statistical downscaling approach applied to Rotterdam". *Energy and Buildings* 75: 358-367.doi: http://dx.doi.org/10.1016/j.enbuild.2014.02.032

Ministero dell'istruzione, dell'università e della ricerca. Accessed on April 7. https://dati.istruzione.it/opendata/opendata/

Mohammadiziazi, R., S. Copeland, and M. M. Bilec. 2021. "Urban building energy model: Database development, validation, and application for commercial building stock." *Energy and Buildings* 248. doi: https://doi.org/10.1016/j.enbuild.2021.111175

Pörtner, H.-O., et al. 2022. *Climate Change 2022: Impacts, Adaptation and Vulnerability. Contribution of Working Group II to the Sixth Assessment Report of the Intergovernmental Panel on Climate Change*. doi: https://doi.org/10.1017/9781009325844.002

OpenStreetMap. Accessed on March 15. https://www.openstreetmap.org/

Re Cecconi, F., L. C. Tagliabue, N. Moretti, E. De Angelis, A. G. Mainini, and S. Maltese. 2019. "Energy retrofit potential evaluation: The Regione Lombardia school building asset", in: Della Torre, S., M. Bocciarelli, L. Daglio, R. Neri (2019), *Buildings for Education, A Multidisciplinary Overview of The Design of School Buildings*. doi: https://doi.org/10.1007/978-3-030-33687-5_27

Torabi Moghadam, S., J. Toniolo, G. Mutani, and P. Lombardi. 2018. "A GIS-statistical approach for assessing built environment energy use at urban scale". *Sustainable Cities and Society* 37: 70-84. doi: https://doi.org/10.1016/j.scs.2017.10.002

Tuominem, P., R. Holopainen, L. Eskola, J. Jokisalo, and M. Airaksinen. 2014. "Calculation method and tool for assessing energy consumption in the building stock." *Building and Environment* 75: 153–160. doi: http://dx.doi.org/10.1016/j.buildenv.2014.02.001

Vicentini, G., and G. Mutani. 2012. "L'analisi del fabbisogno di energia elettrica e termica del parco edilizio esistente attraverso un sistema informativo geografico open source". *GFOSS-DAY 2012 - Fifth Italian conference on geographic free software and open geodata*.

Wang, D., J. Landolt, G. Mavromatidis, K. Orehounig, and J. Carmeliet. 2018. "CESAR: A bottom-up building stock modelling tool for Switzerland to address sustainable energy transformation strategies". *Energy and Buildings* 169: 9-26. doi: https://doi.org/10.1016/j.enbuild.2018.03.020

Wong, I. L., E. Kruger, A. C. M. Loper, and F. K. Mori. 2019. "Classification and energy analysis of bank building stock: A case study in Curitiba, Brazil". *Journal of Building Engineering* 23: 259-269. doi: https://doi.org/10.1016/j.jobe.2019.02.003

Yang, X., M. Hu, A. Tukker, C. Zhang, T. Huo, and B. Steubing. 2022. "A bottom-up dynamic building stock model for residential energy transition: A case study for the Netherlands". *Applied Energy* 306: 118060. doi: https://doi.org/10.1016/j.apenergy.2021.118060

Yang, X., M. Hu, N. Heeren, C. Zhang, T. Verhagen, A. Tukker, and B. Steubing. 2020. "A combined GIS-archetype approach to model residential space heating energy: A case study for the Netherlands including validation". *Applied Energy* 280. doi: https://doi.org/10.1016/j.apenergy.2020.115953

Zygmunt, M., and D. Gawin. 2021. "Application of Artificial Neural Networks in the Urban Building Energy Modelling of Polish Residential Building Stock". *Energies* 14(24): 8285. doi: https://doi.org/10.3390/en14248285

Hourly-Simplified Calculation to Identify Cost-Optimal Energy Performance Requirements for the Italian Building Stock

Matteo Piro – Politecnico di Torino, Italy – matteo.piro@polito.it
Franz Bianco Mauthe Degerfeld – Politecnico di Torino, Italy – franz.bianco@polito.it
Giovanna De Luca – Politecnico di Torino, Italy – giovanna.deluca@polito.it
Ilaria Ballarini – Politecnico di Torino, Italy – ilaria.ballarini@polito.it
Vincenzo Corrado – Politecnico di Torino, Italy – vincenzo.corrado@polito.it

Abstract

The 2010/31/EU Directive established a comparative methodology framework to determine minimum energy performance requirements based on a cost-optimal approach. This research investigates the cost-optimal outcomes resulting from the application of the monthly quasi-steady state method (UNI/TS 11300-1) and the simplified hourly dynamic model (EN ISO 52016-1), both aimed at determining the thermal energy needs for space heating and cooling. The technical building systems have been modelled by means of a monthly steady-state method, in agreement with the UNI/TS 11300 series. The global cost has been calculated from a financial perspective according to EN 15459-1. The proposed methodology has been applied to two buildings that differ in their climatic zone, construction period, and intended use. For this purpose, a single-family house located in Palermo and an office building sited in Milan have been assessed. To investigate the deviations between the two energy models, the results in terms of packages of energy efficiency measures and global cost have been compared.

1. Introduction

1.1 The Comparative Methodology Framework and the *EP* Assessment

The Commission Delegated Regulation No. 244/2012 (European Commission, 2012a), which supplements European Directive 2010/31/EU (European Commission, 2010a), specifies a comparative methodology framework and prescribes Member States to define minimum energy performance requirements for buildings to achieve "cost-optimal levels", i.e., the lowest global cost (*GC*) during the building lifecycle. Moreover, the European Directive requires the Member States to update the applied methodology regularly. The Guidelines accompanying Commission Delegated Regulation No. 244/2012 (European Commission, 2012b) established three different applicable calculation methods to determine the building energy needs: monthly quasi-steady state, simple hourly, or fully dynamic approach. In Italy, the deployed comparative methodology, described by Corrado et al. (2018), provides for performing the calculations through a monthly quasi-steady state method, according to the UNI/TS 11300 series (UNI, 2010-2019).

Recently, the mandate of the European Commission M480 (European Commission, 2010b), aimed at developing a new harmonized package of EPB directives, has conceived the EN ISO 52016-1 standard (CEN, 2017b). Italy is finalizing its National Annex (NA) of EN ISO 52016-1 (CTI, 2021), providing some main improvements that are related to: a) a new discretization approach of opaque building components (Mazzarella et al., 2020); b) a more accurate method to determine the solar heat gains and the longwave radiation heat exchange with the sky vault; c) the introduction of a weighting factor for the *g*-value calculation that accounts for incident angle dependency on direct and diffuse solar irradiance.

1.2 Aim of the Research

This work is part of a study carried out in collaboration with the Italian National Agency for New Technologies, Energy and Sustainable Economic

Development (ENEA; Corrado et al., 2021); it investigates the employment of the simplified dynamic hourly model, introduced by EN ISO 52016-1, for determining the minimum energy performance requirements to achieve the cost-optimal level. For this work, two representative case studies (a single-family house located in Palermo and an office building sited in Milan) have been selected between twenty-six buildings and have been simulated to upload the comparative methodology. These results have been compared, in terms of the optimal set of energy efficiency measures (EEMs) and global cost, with those derived from the application of the monthly quasi-steady state method, carried out in accordance with the UNI/TS 11300-1 (UNI, 2014) calculation procedures.

2. Methodology

The EPBD recast establishes the comparative methodology framework to set out the minimum energy performance requirements for new buildings and existing buildings undergoing a major renovation. This approach requires Member States to:

a) identify an adequate number of real and/or 'virtual' residential and non-residential reference buildings, representative of the national building stock,
b) define energy efficiency measures for the refurbishment of the building envelope and the technical building systems for each reference building, also detecting technologies that exploit renewable energy sources,
c) calculate the primary energy demand deriving from the application of different packages of energy efficiency measures for each identified reference building,
d) calculate the global cost associated with the different building energy renovation scenarios,
e) derive the cost-optimal level for each reference building that minimises the global cost value.

2.1 Thermal Energy Needs Calculation Models

The calculation tool used in Corrado et al. (2018) has been updated for the sake of the present study to determine the thermal energy needs for space heating and cooling according to the EN ISO 52016-1 simplified hourly method (Corrado et al., 2021). For consistency with the quasi-steady state UNI/TS 11300-1 calculation method, some of the improved calculation options introduced by the Italian NA have been implemented, namely the hourly variations of the sky temperature and of the total solar energy transmittance of the glazed components. In the NA, the sky temperature is determined by means of the formulation presented in UNI/TS 11300-1, and it depends on the external vapor pressure. Moreover, the solar gains through windows are determined with a weighting factor for the g-value. The correction factor is formulated as a function of the solar angle, exposure, and glazing type. While in the quasi-steady method, the values are determined for each month through a tabular approach, in the Italian NA the properties are defined on an hourly basis.

2.2 The Cost-Optimal Approach

The cost-optimization procedure employed in this work is a single-objective optimization approach that applies discrete energy efficiency options (EEOs) one at a time to obtain a new partial optimized building for each step of the calculation. The full procedure is described in Corrado et al. (2014) and is based on the methodology proposed by Christensen et al. (2006). In particular, the identification of the cost-optimal level has been performed by applying at the same time more EEMs in an iterative procedure, to exploit the synergy effects of different measures. For each step of the calculation, the algorithm identifies a new renovation scenario, associated with a combination of EEMs, and calculates both the primary energy demand and the global cost. If the subsequent package of energy efficiency measures results in a lower *GC*, then the procedure sets a new partial optimum. The optimization proceeds until the package of EEMs that determines the lowest global cost is found.

Starting from a reference set of EEMs, the optimiza-

tion procedure will test the different EEOs until the energy efficiency package of measures that guarantees the minimum global cost is found.

The energy efficiencies of the technical building subsystems have been evaluated considering the UNI/TS 11300 series monthly steady-state method. The investment costs of EEMs have been derived from DEI (2017). Then, the global cost has been calculated according to EN 15459-1 (CEN, 2017a), considering a lifespan of 30 years and the financial perspective, i.e., analysing the mere evaluation of the private investment. In the assessment, a real interest rate of 4% has been assumed. Moreover, the cost-optimality approach, being a comparative methodology for the determination of the *GC*, neglects the same cost categories repeated for several measures (safety costs, ancillary charges, etc.), and the cost items on building materials whose installation does not have an impact on the energy performance of the building.

3. Application

3.1 Case Studies

In the present work, the reference buildings have been assumed to be located in two different Italian climatic zones (Palermo and Milan), and two construction periods have been considered (an existing building, built in the period 1977-90, and a new building). Two different intended uses have been assumed: residential and non-residential.

The single-family house sited in Palermo was selected from the IEE-TABULA project (*Typology Approach for Building Stock Energy Assessment*; Loga et al., 2012), while the office located in Milan was derived from the survey of Margiotta & Puglisi (2009). Both buildings present a reinforced concrete structure, with reinforced concrete and hollow brick slabs. Brick masonry cavity walls for the single-family house and hollow brick masonry walls for the office have been assumed, respectively. The upper slabs face the external environment, while the bottom floor is adjacent to an unconditioned zone (cellar). Table 1 reports the main geometrical characteristics.

In its current state, the single-family house, located in Palermo, presents single-glazed windows without external solar shading devices installed. The residential house is equipped with a heat generator for space heating and domestic hot water, and a multi-split system for space cooling (see Table 2).

Table 1 – Geometrical characteristics of the case studies

	Residential/Existing bldg/Palermo	**Office/New bldg/Milan**
V_g [m^3]	725	6100
A_f [m^2]	199	1519
A_{env} / V_g [m^{-1}]	0,72	0,35
A_w [m^2]	25	434
no. storeys	2	4

3.2 Energy Efficiency Measures

Sixteen categories of EEMs have been defined, considering up to five different energy efficiency options for each EEM, characterised by increasing levels of performance. The EEMs are classified into three different groups according to their application field: a) the thermal insulation of the building fabric (i.e., opaque and transparent building envelope components) and installation of solar shading devices; b) the replacement of technical building systems components (i.e., heating, cooling, and domestic hot water generators, ventilation, and lighting systems); c) the installation of renewable energy plants. The considered number of EEOs is variable depending on both the reference building and the specific EEM. In Table 2, the thermophysical parameters and costs associated with each EEO are reported per each EEM.

3.3 Consistency Options

As introduced, the cost-optimal packages of energy efficiency measures determined by means of the monthly and the simplified hourly dynamic methods respectively are compared in the present work. To make the results of the two calculation methods comparable, some consistency options have been considered:

a) Typical Meteorological Years (TMY) elaborated by the Italian Thermo-technical Committee (CTI, 2015) have been adopted in both calculation methodologies,
b) diversity factors for energy calculation on an hourly basis have been introduced to eval-

Table 2 – EEOs per EEMs for residential and non-residential buildings

EEMs		Residential/Existing bldg/Palermo					Office/New bldg/Milan				
		EEOs					EEOs				
		1 (*)	**2**	**3**	**4**	**5**	**1**	**2**	**3**	**4**	**5**
External wall thermal insulation	U_{wl} [W m^{-2}K^{-1}]	-	0,54	0,45	0,40	0,26	1,50	0,36	0,30	0,26	0,17
	c_{eli} [€ m^{-2}]	-	79	83	85	96	-	58	62	66	80
or Cavity wall thermal insulation	U_{wl} [W m^{-2}K^{-1}]	1,10	0,37	-	-	-					
	c_{eli} [€ m^{-2}]	-	21	-	-	-					
Roof thermal insulation	$U_{fl,up}$ [W m^{-2}K^{-1}]	2,16	0,41	0,34	0,32	0,26	1,50	0,30	0,25	0,22	0,18
	c_{eli} [€ m^{-2}]	-	45	50	52	59	-	40	45	48	55
Floor thermal insulation	$U_{fl,lw}$ [W m^{-2}K^{-1}]	0,78	0,58	0,48	0,42	0,28	1,50	0,36	0,30	0,26	0,17
	c_{eli} [€ m^{-2}]	-	9	9	9	12	-	12	14	16	26
Windows	U_w [W m^{-2}K^{-1}]	4,90	3,80	3,20	3,00	1,60	5,00	2,20	1,80	1,40	1,10
	c_{eli} [€ m^{-2}]	-	300	306	346	624	200	365	379	388	391
Solar shading devices	F *or* M (**) / τ_{sh} [-]	-	F / 0,20	M / 0,20	-	-	F / 0,20	M / 0,20	-	-	-
	c_{eli} [€ m^{-2}]	-	170	26	-	-	170	26	-	-	-
Chiller	*EER* [-]	2,35	3,30	-	-	-	3,30	-	-	-	-
	C [k€]	-	3,77	-	-	-	71,90	-	-	-	-
plus Heat generator for space heating	*COP* [-]	-	3,70	4,10	-	-					
	c [€ kW^{-1}]	-	451	493	-	-					
plus Heat generator for domestic hot water	$\eta_{W,gn}$ [-]	-	0,93	1,00	-	-					
	c [€ kW^{-1}]	-	210	629	-	-					
or Combined heat generator for space heating and domestic hot water	$\eta_{H+W,gn}$ [-]	0,73	0,93	1,00	-	-	0,93	1,05	-	-	-
	c [€ kW^{-1}]	-	264	209	-	-	179	124	-	-	-
or Heat pump for space heating, domestic hot water, and space cooling	*COP* [-] *and* *EER* [-]	-	4,10 3,50	-	-	-	3,00 2,80	3,50 3,20	-	-	-
	c [€ kW^{-1}]	-	967	-	-	-	329	372	-	-	-
Thermal solar system	A_{coll} [m^2]	-	1	2	3	-	2	4	6	8	10
	c_{coll} [k€ m^{-2}]	-	1,40	1,40	1,40	-	1,40	1,40	1,20	1,00	0,80
Photovoltaic system	W_P [kW]	-	1,36	1,70	2,04	-	8,80	11,00	13,20	-	-
	c [k€ kW^{-1}]	-	1,50	1,50	1,50	-	1,25	1,25	1,25	-	-
Heat recovery ventilation system	η_{ru} [-]						0,60	0,70	0,90	-	-
	C [k€]						3,79	9,76	17,67	-	-
Space heating control sub-system	$\eta_{H,rg}$ [-]	0,78÷ 0,89	0,94	0,98	0,99	-	0,94	0,98	0,99	-	-
	C [€]	-	52	288	90	-	358	1.075	394	-	-
Lighting system	P_n [W m^{-2}]						6,00	6,00			
	F_O [-]						1,00	0,80	-	-	-
	F_C (F_D) [-]						1,00	0,90			
	c_f [€ m^{-2}]						24	30	-	-	-

(*) For the existing building the first column represents the current state

(**) F = fixed louvres, M = mobile louvres

uate the temporal distribution of the internal heat gains, in accordance with EN 16798-1 (CEN, 2019),

c) in the simplified hourly model, the mass of the internal horizontal partitions has been associated with the internal node of the conduction model. Moreover, the specific heat capacity of air and furniture has been neglected.

4. Results

The results of the optimization procedure are presented in terms of the overall non-renewable energy performance ($EP_{gl,nren}$) vs. the global cost in Fig. 2 and Fig. 1 for the single-family house and the office building respectively. Both partial optimum and the cost-optimal points, calculated on a monthly and hourly basis, are shown. Moreover, Table 3 specifies the cost optimal EEMs packages for each reference building and for the two calculation methods (monthly and hourly).

The comparative analysis shows slight differences between the global costs and the cost-optimal package of energy efficiency measures. In light of the comparison between the two case studies and the two calculation methodologies, *GC* and $EP_{gl,nren}$ of the cost-optimal levels present negligible deviations. The $EP_{gl,nren}$ deviation of the hourly cost-optimal level with respect to the monthly one is equal to 11% and -3% for the single-family house and the office respectively. For both buildings, from the global cost view, the relative variation of the global cost is close to 1%. The cost-optimal combination of EEMs varies between the two calculation models, as highlighted in Table 3 (coloured cells). For both buildings, a different level of thermal insulation of the bottom floor in the cost-optimal EEMs is displayed when applying a different calculation model. More evident variations occur for the single-family house, in which different levels of the EEOs for the solar shading devices and the photovoltaic system are reported.

Primarily, deviations in the results can be ascribed to major differences in the calculation methods, such as the deployment of a different model for the heat conduction assessment in every building component and the approach to determine the heat transfer through unconditioned zones. From the optimal package of EEMs view, although the determination of the thermal energy needs for space heating and cooling is strictly related to the building fabric energy performance, this does not necessarily imply that the EEOs of the technical building system cannot vary between the two calculation methods. In fact, the energy cost, which is a term of the global cost calculation, is directly influenced by the building energy needs. Moreover, most of the sensitivity in the EEO variation is related to the measures with the minimal difference cost as a consequence of the energy efficiency increase. A significant example that describes this phenomenon is represented by the floor thermal insulation (see Table 3).

5. Conclusion

The comparative methodology applied in 2018 to identify the cost-optimal minimum energy performance requirements for the Italian building stock has been updated with the new simplified hourly model specified by EN ISO 52016-1 and by its National Annex. In the present work, the outcomes of the comparative analysis for a single-family house located in Palermo and for an office building situated in Milan have been presented. For each building, the cost-optimal energy efficiency measures resulting from the calculation of the thermal energy needs for space heating and cooling both on a monthly basis (UNI/TS 11300-1) and on an hourly basis (EN ISO 52016-1) have been assessed and compared. The outcomes, which are presented in terms of the cost-optimal package of EEMs and global cost, do not lead to significant differences under application of a different calculation method.

Future works will provide an update of the cost-optimal methodology to assess the technical building system performance on an hourly basis.

Table 3 – Optimal EEM packages resulting from different calculation methods, for residential and non-residential buildings

EEM		Optimal EEO Residential/Existing bldg/Palermo		Optimal EEO Office/New bldg/Milan	
		Monthly method	*Hourly method*	*Monthly method*	*Hourly method*
External wall thermal insulation *or* cavity wall thermal insulation	U_{wl} [W m^{-2}K^{-1}]	-	-	0,36	0,36
		1,10	1,10		
Roof thermal insulation	$U_{fl,up}$ [W m^{-2}K^{-1}]	0,41	0,41	0,30	0,30
Floor thermal insulation	$U_{fl,lw}$ [W m^{-2}K^{-1}]	0,28	0,78	0,30	0,36
Windows	U_w [W m^{-2}K^{-1}]	4,90	4,90	1,10	1,10
Solar shading devices	F *or* M (*) / τ_{sh} [-]	F / 0,20	M / 0,20	M / 0,20	M / 0,20
Chiller	*EER* [-]	2,35	2,35	-	-
plus Heat generator for space heating	*COP* [-]	-	-		
plus Heat generator for domestic hot water	$\eta_{W,gn}$ [-]	-	-		
or Combined heat generator for space heating and domestic hot water	$\eta_{H+W,gn}$ [-]	1,00	1,00	-	-
or Heat pump for space heating, domestic hot water, and space cooling	*COP* [-]	-	-	3,50	3,50
	EER [-]	-	-	3,20	3,20
Thermal solar system	A_{coll} [m^2]	absent	absent	2,00	2,00
Photovoltaic system	W_p [kW]	1,36	2,04	13,20	13,20
Heat recovery ventilation system	η_{ru} [-]			0,60	0,60
Space heating control sub-system	$\eta_{H,rg}$ [-]	0,99	0,99	0,99	0,99
Lighting system	P_n [W m^{-2}]			6,00	6,00
	F_O [-]			0,80	0,80
	F_C (F_D) [-]			0,90	0,90

(*) F = fixed louvres, M = mobile louvres

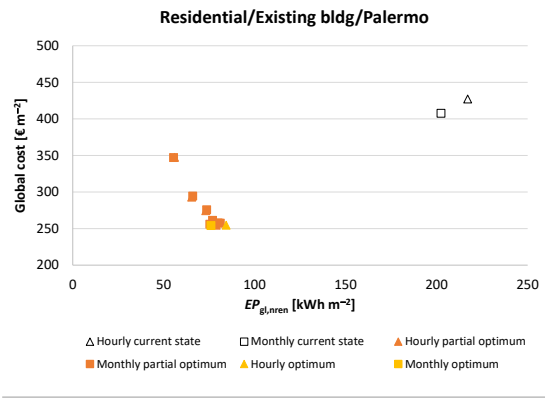

Fig. 1 – Cost-optimal level for the single-family house

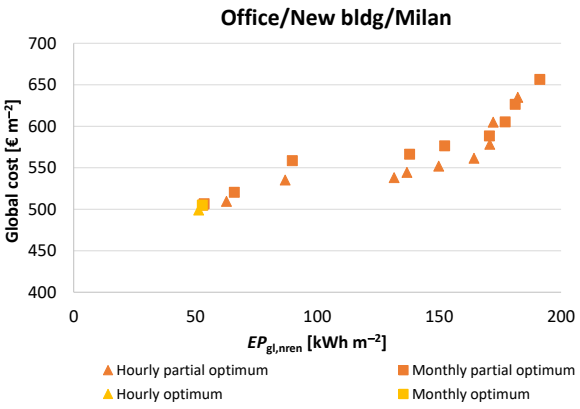

Fig. 2 – Cost-optimal level for the office building

Acknowledgement

This work is part of research supported by the Italian National Agency for New Technologies, Energy and Sustainable Economic Development (ENEA), regarding the application of the simplified hourly calculation model (UNI EN ISO 52016-1) and the update of methodology for calculating cost-optimal levels of energy performance.
For the research, a tool developed by the EPB Center and made available within a cooperation agreement with the Department of Energy "Galileo Ferraris" of the Politecnico di Torino was implemented.

Nomenclature

Symbols

A	area (m^2)
C	cost (€)
c	specific cost (€ m^{-2}) *or* (€ kW^{-1})
COP	coefficient of performance (-)
EER	energy efficiency ratio (-)
EP	energy performance indicator (kWh m^{-2})
F	factor (-)
P	lighting power density (W m^{-2})
U	thermal transmittance (W $m^{-2}K^{-1}$)
V	volume (m^3)
W	peak power (kW)
η	efficiency (-)
τ	coefficient of transmission (-)

Subscripts/Superscripts

C	constant illuminance
coll	solar collector
D	daylight dependency
eli	building element
env	building envelope
f	net floor
fl,lw	lower floor
fl,up	upper floor
g	gross
gl	overall
gn	generation sub-system
H	space heating
n	number of luminaires in the zone
nren	non-renewable
O	occupancy dependency
p	peak
rg	control sub-system
ru	heat recovery unit
sh	shading
W	domestic hot water
w	window
wl	wall

References

Christensen, C., R. Anderson., S. Horowitz, A. Courtney, and J. Spencer, 2006. *BEoptTM Software for Building Energy Optimization: Features and Capabilities*. Golden, Colorado (USA): U.S. Dep. of Energy, National Renewable Energy Laboratory. https://www.nrel.gov/docs/fy06osti/39929.pdf

Corrado, V., I. Ballarini, F. Bianco Mauthe Degerfeld, and M. Piro, 2021. "Aggiornamento della metodologia di calcolo dei livelli ottimali di prestazione energetica in funzione dei costi". Rome: Agenzia Nazionale per le Nuove Tecnologie, l'Energia e lo Sviluppo Economico Sostenibile (ENEA). ENEA. In print.

Corrado, V., I. Ballarini, G. De Luca, and E. Primo, 2018. "Aggiornamento della metodologia comparativa per la determinazione dei livelli ottimali di prestazione energetica negli edifici". Report RdS/2017/141. Rome: Agenzia Nazionale per le Nuove Tecnologie, l'Energia e lo Sviluppo Economico Sostenibile (ENEA). ENEA. https://www.enea.it/it/Ricerca_sviluppo/documenti/ricerca-di-sistema-elettrico/adp-mise-enea-2015-2017/edifici-nzeb/report-2017/rds-par2017-141.pdf

Corrado, V., I. Ballarini, and S. Paduos, 2014. "Assessment of cost-optimal energy performance requirements for the Italian residential building stock". *Energy Procedia* **45**: 443–452. doi: https://doi.org/10.1016/j.egypro.2014.01.048

EPB Center. 2019. "Demo (EN) ISO 52016-1 (energy needs heating and cooling, internal

temperatures and loads)". Accessed June 1, 2021. https://epb.center/support/documents/demo-en-iso-52016-1

European Commission. 2010a. "Directive 2010/31/EU of 19 May 2010 on the energy performance of buildings (recast)". *Official Journal of the European Union*, 19 May 2010.

European Commission. 2010b. "M/480 EN: Mandate to CEN, CENELEC and ETSI for the elaboration and adoption of standards for a methodology calculating the integrated energy performance of buildings and promoting the energy efficiency of buildings, in accordance with the terms set in the recast of the directive on the energy performance of buildings (2010/31/EU)". 14 December 2010.

European Commission. 2012a. "Commission delegated regulation (EU) No 244/2012 of 16 January 2012 supplementing Directive 2010/31/EU of the European Parliament and of the Council on the energy performance of buildings by establishing a comparative methodology framework for calculating cost-optimal levels of minimum energy performance requirements for buildings and buildings elements". *Official Journal of the European Union*, 16 January 2012.

European Commission. 2012b. "Guidelines accompanying Commission Delegated Regulation (EU) No 244/2012 of 16 January 2012 supplementing Directive 2010/31/EU of the European Parliament and of the Council on the energy performance of buildings by establishing a comparative methodology framework for calculating cost-optimal levels of minimum energy performance requirements for buildings and building elements". *Official Journal of the European Union*, 19 April 2012.

European Committee for Standardization (CEN). 2017a. *EN 15459-1: Energy performance of buildings - Economic evaluation procedure for energy systems in buildings - Part 1: Calculation procedures, Module M1-14*. CEN: Brussels, Belgium.

European Committee for Standardisation (CEN). 2017b. *EN ISO 52016-1: Energy Performance of Buildings – Energy Needs for Heating and Cooling, Internal Temperature and Sensible and Latent Heat Loads. Part 1: Calculation procedures (ISO 52016-1:2017)*. CEN: Brussels, Belgium.

European Committee for Standardization (CEN). 2019. *EN 16798-1: Energy performance of buildings. Ventilation for buildings. Indoor environmental input parameters for design and assessment of energy performance of energy performance of buildings addressing indoor air quality, thermal environment, lighting and acoustics. Module M1-6*. CEN: Brussels, Belgium.

Italian Organisation for Stardardisation (UNI). 2010-2019. *UNI/TS 11300 (series): Energy performance of buildings*. UNI: Milan, Italy.

Italian Organisation for Stardardisation (UNI). 2014. *UNI/TS 11300-1: Energy performance of buildings - Part 1: Evaluation of energy need for space heating and cooling*. UNI: Milan, Italy.

Italian Thermo-technical Committee (CTI). 2015. "Typical Metereological Year (2015)". Accessed June 1, 2021. https://try.cti2000.it.

Italian Thermo-technical Committee (CTI). 2021. *Documento n. 020200134, Bozza di Appendice Nazionale UNI EN ISO 52016-1*. CTI: Milan, Italy.

Loga, T., N. Diefenbach, B. Stein, 2012. "Typology Approach for Building Stock Energy Assessment. Main Results of the TABULA Project". Institut Wohnen und Umwelt GmbH: Darmstadt, Germany. https://doi.org/10.1016/j.enbuild.2016.06.094

Margiotta, M., and G. Puglisi, 2009. "Caratterizzazione del parco edilizio nazionale. Determinazione dell'edificio tipo per uso ufficio". Report RdS/2009/164. Rome: Agenzia Nazionale per le Nuove Tecnologie, l'Energia e lo Sviluppo Economico Sostenibile (ENEA). ENEA.https://www.enea.it/it/Ricerca_sviluppo/documenti/ricerca-di-sistema-elettrico/condizionamento/rse164.pdf

Mazzarella, L., R. Scoccia, P. Colombo, and M. Motta, 2020. "Improvement to EN ISO 52016-1:2017 hourly heat transfer through a wall assessment: the Italian National Annex". *Energy and Buildings* **210**: 109758. Doi: https://doi.org/10.1016/j.enbuild.2020.109758

Tipografia del Genio Civile (DEI). 2017. "Prezzi informativi dell'edilizia". DEI: Rome, Italy.

A Novel Methodology for Risk Assessment of Airborne Transmission due to Covid-19 in University Classrooms

Giulia Lamberti – University of Pisa, Italy – giulia.lamberti@phd.unipi.it
Roberto Rugani – University of Pisa, Italy – roberto.rugani@phd.unipi.it
Fabio Fantozzi – University of Pisa, Italy – fabio.fantozzi@unipi.it

Abstract

The Covid-19 pandemic revolutionized the way of designing buildings, which should be created to improve health conditions and limit the spread of contagion. Among these, schools certainly need special attention. To improve indoor conditions, the first step of this study was conducted by simulating three classrooms having different ventilation strategies, using a CFD analysis. Then the infection probability was calculated using the Gammaitoni-Nucci model to analyse the risk in the classrooms according to different ventilation and building characteristics. The study showed the need for providing adequate ventilation to ensure healthy conditions for the students. Furthermore, the infection probability was calculated considering non-uniform environments, which can result from various air distributions in the classroom due to local non-uniformities. The configuration obtained from the CFD analysis was then compared to the standard condition. which considers the classrooms as uniform environments. This allows an understanding of the effective conditions to which students are exposed and to comprehend whether the classical models do not risk underestimating the infection probability. This study provides a new methodology for airborne transmission risk assessment in non-homogeneous environments and supports designers with a new tool to evaluate HVAC systems layout and classroom operation.

1. Introduction

The importance of providing Indoor Environmental Quality (IEQ) in buildings has been always a necessity for enhancing people's health and well-being (Lamberti, 2020), especially in educational buildings, where students can improve their learning abilities (Bluyssen, 2016; Lamberti et al., 2021). This issue became even more evident after the Covid-19 outbreak, when improving IEQ to guarantee occupants' health became a priority, both during normal and critical operations (Awada et al., 2021). This new awareness led building practitioners to focus on the aspect of Indoor Air Quality (IAQ) (Awada et al., 2022). Overall, there was a tendency to rethink building design strategies (Megahed & Ghoneim, 2021) to prepare buildings for post-pandemic architecture.

Since airborne transmission was recognized as a possible route of infection (Morawska et al., 2020), researchers focused on the relationship between ventilation rate and infection risk. Indeed, ventilation can be an important preventive measure to reduce infection probability, even if most existing ventilation standards are comfort-based and not sufficient to control the risk (Ding et al., 2022). For this reason, studies that relate the ventilation rate and infection probability have been carried out considering diverse building types (Dai & Zhao, 2020). The most used models for assessing these relationships are the well-established Wells-Riley (Riley & Nardell, 1989) and the Gammaitoni-Nucci (Gammaitoni & Nucci, 1997) models. In this scenario, educational buildings present particularly critical situations, as students spend a consistent amount of time indoors (Lamberti et al., 2020) and are in close contact with other occupants. Thus, the infection risk was often analyzed in these types of buildings (Pavilonis et al., 2021; Fantozzi et al., 2022) to ensure healthy conditions for students.

However, these models assume that the air in the indoor environment is uniformly distributed, which is not necessarily true. Indeed, there is the possibility of underestimating infection risk if, in some locations of the room, the ventilation rate is below the assumed uniform value. This fact may

have negative consequences on students' health, especially if the infection probability is underestimated in the positions occupied by their desks. Building simulation and CFD analysis, which have often been used to evaluate various aspects of IEQ (Rugani et al., 2021) and validated on the real conditions encountered in classrooms (Fantozzi et al., 2021), are valid tools for analyzing the distribution patterns of the air in the rooms. In fact, CFD simulations were recently used to minimize Covid-19 spread (Ascione et al., 2021).

The aim of this paper is, then, to analyze the air patterns through a CFD analysis using university classrooms with different room characteristics, occupancy, and operation mode as a case study. This analysis will provide important information regarding the estimation of infection risk considering the classrooms as non-uniform spaces and validation of the models predicting infection risk. Furthermore, an innovative methodology for enhancing classroom management and improving the health conditions of the students is proposed.

2. Methodology

2.1 The Case Study

In this study, the classroom environments were studied as a non-homogeneous space, investigating the infection probability from an individual-oriented perspective. Three different classrooms at the School of Engineering of the University of Pisa were simulated, which present three different HVAC configurations. The three classrooms are located in different buildings: the first is under construction and will be equipped with a VRF system with a mechanical air exchange ventilation system (Class A), the second was built in 2006 and is air-conditioned by an air-to-air heat pump with ceiling fan coil distribution (Class B); the latter was built in 1930 and has a traditional hydronic radiator system (Class C).

Table 1 shows the characteristics of the three classrooms studied. Ideal manikins were placed in the stalls to study the infection risk that the users are actually exposed to.

Several points mainly corresponding to students' positions were identified.

Table 1 – Characteristics of the classrooms

Class	Surface [m²]	Volume [m³]	Occupancy	Ventilation rate [m³/h]
Class A	130	390	129	3250
Class B	131	468	130	1000
Class C	70	182	49	370

2.2 Simulation of the Classrooms and Infection Probability

The three classrooms were analyzed by means of a 3D CFD analysis, using Autocad CFD. CFD decomposes the environment of a zone into a large number of control volumes and can provide a detailed description of the airflow by solving the Navier-Stroke's equations. CFD was used with the Finite Volume Method (FMV) approach, as it can perform detailed computation on heat transfer and air-flow simulation. The standard k-ε turbulence model was used for air turbulence due to its accuracy in predicting indoor airflows (Hughes et al., 2012).

Classes A, B, and C were modeled and simulated in two different scenarios: one lesson on a summer day and on a winter day. The boundary conditions were set as the output of a Building Energy Simulation (BES) campaign carried out using the well-known EnergyPlus software with a Typical Mean Year weather file. The room investigated and all adjacent classrooms were modeled as different thermal zones. An airflow network was used to simulate internal air movements, aimed at assessing the effective boundary conditions, i.e., mainly wall surface temperatures, for CFD analysis. The aim was to obtain the local value of the Local Mean Age (LMA) and the air velocity at the previously identified points of the environment.

The infection probability in the classroom was calculated using the well-established Gammaitoni-Nucci model (Gammaitoni & Nucci, 1997), which relates the ventilation rate to the infection probability. First, P was calculated considering the air distribution in the classroom uniform using the values from Table 1, then the infection probability was evaluated for the different zones that were established in the different classrooms, obtaining the Air

Changes per Hour for each zone from the simulated local mean age. The ACH for each zone corresponded to the position occupied by the students to assess their actual condition. The number of infectors was considered equal to 2 % of the total number of occupants.

3. Results

3.1 Local Mean Age

From the LMA, obtained from the CFD simulation, it was possible to derive the ventilation rate, so the Air Changes per Hour (ACH) were assumed for each zone, considering summer (yellow) and the winter (light blue) conditions (Fig. 1). The dashed line represents the ACH assumed for the simulations, which was considered uniform in the entire classroom ($ACH_{uniform}$), and is calculated from the ventilation rate given in Table 1.

Fig. 1 shows that the most favorable conditions can be encountered in Class A, which presents the highest ACH, both considering the $ACH_{uniform}$ and the single zones. On the other hand, the most critical conditions are in Class C, which is the naturally ventilated classroom, and whose ventilation was poorer both during summer and winter conditions. From the simulation of summer and winter conditions, it can be noticed that, for Class A, the winter scenario was generally less critical than the summer one, while, for Class B, the trend was the opposite. In general, mechanically ventilated classrooms present better indoor conditions, with higher values of ACH. It can be immediately noticed that the $ACH_{uniform}$ remains lower in each case than the ACH obtained in the different zones, which is a good indicator that assuming this parameter for the calculation of the infection probability does not lead to underestimation of the risk. The ventilation rate in the different zones of the classroom tends to be higher than the one assumed if the air distribution of the room is considered uniform. This tendency is particularly evident in the mechanically ventilated classrooms (Class A and B), while it is less clear for the naturally ventilated ones (Class C). This fact shows that, in the naturally ventilated classroom, the air distribution tended to be more uniform and closer to the value assumed for $ACH_{uniform}$, probably also due to the reduced volumetric dimensions of Class C.

3.2 Calculation of the Infection Probability for the Different Classrooms

The infection probability for five hours of exposure was then calculated using the Gammaitoni-Nucci model for Classes A, B, and C (Fig. 2). Five hours of exposure were considered, as they are the most critical representative period in which students may remain in a classroom. Two typical activities that can be performed in classrooms were reported: the infector breathing and the infector speaking while the occupants are resting. The winter scenario was chosen for the analysis and Fig. 2 reports the infection probability calculated in the case that the air distribution in the classroom is considered uniform (continuous line), for the zone with the lowest ACH ("worst condition", dashed line) and the zone with the highest ACH ("best condition", dotted line). This allows a comparison of the results of the different conditions in classrooms, as all the other zones will be included between the best and the worst conditions for each class.

It can be noticed that, for all the classrooms, the in-

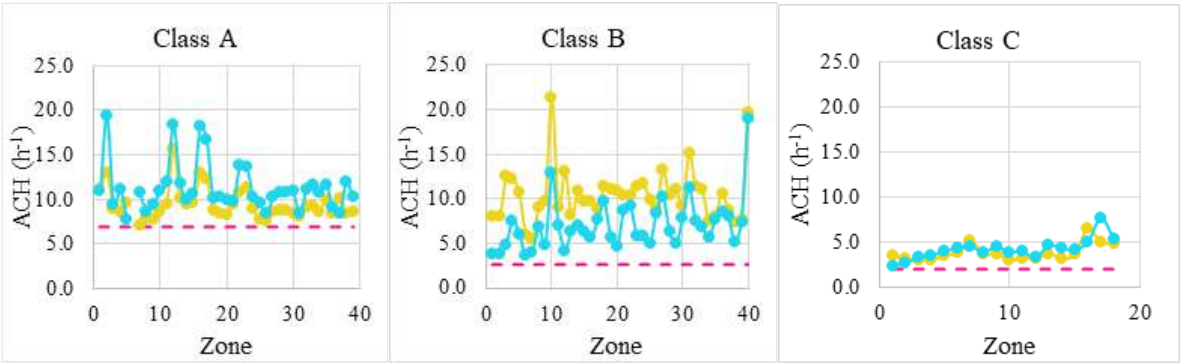

Fig. 1 – ACH obtained for each zone in the three classrooms for summer (yellow) and winter (light blue) conditions. The dashed line represents the ACH assumed for the entire classroom.

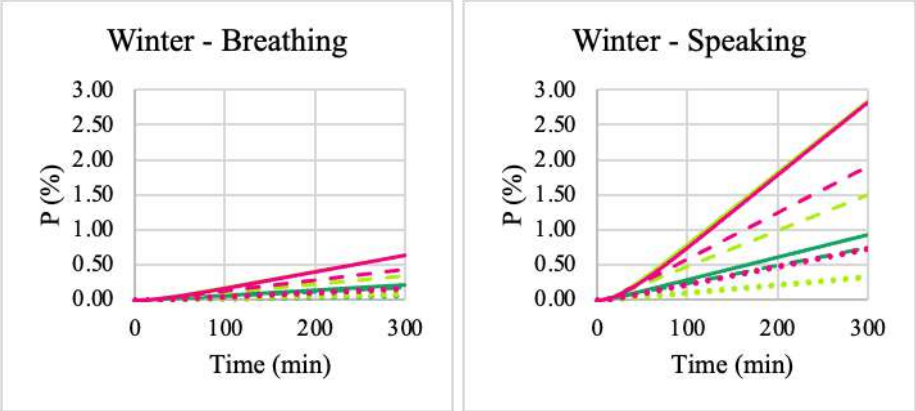

Fig. 2 – Infection probability for 5 hours of exposure in the three classrooms considered. Classes A, B, C are represented by the green, yellow, and red colors, respectively. The continuous line shows the uniform case, the dashed line the worst, and the dotted line the best condition

fection probability for the worst and the best conditions remained below the one calculated considering the $ACH_{uniform}$. This means that using the typical conditions assumed in infection risk models, namely the hypothesis of well-mixed air distribution, there is no risk of underestimating infection probability. On the contrary, the ventilation required to reduce infection probability can lead to an increased demand for ventilation, which may affect energy costs.

Fig. 2 shows that the most critical cases are represented by Classes B and C, due to the reduced ventilation. Furthermore, results show a high influence of the infector's activity on the infection probability. Indeed, the infection probability remains below 1 % for all the classrooms if the infector is only breathing, considering the five hours of exposure. On the contrary, if the infector is speaking, P exceeds 1 % after about 140 minutes in Class C and 200 minutes in Class B, considering the most critical zone (dashed line). On the contrary, Class A reports the most favorable conditions, where the critical infection probability of 1 % is never exceeded for all the scenarios and in five hours of exposure, showing the importance of providing adequate ventilation in educational buildings. Indeed, correct ventilation design can have a consistent influence on the maintenance of healthy indoor conditions. The infection probability calculated for the best condition (dotted line) shows that some positions are particularly favorable for maintaining the health of the occupants, which suggests that the students should favor certain locations in the class over more risky ones.

Since the real challenge is to design buildings that are healthy and comfortable for everyone, in the design phase it is necessary to consider the most critical scenario, which is represented by the activity of speaking. In this case, for Classes B and C, the threshold infection probability is soon exceeded, and preventive measures, such as increasing the ventilation rate, reducing the number of occupants, or including breaks during the duration of the lecture, are needed.

3.2.1 Relation between the ACH and infection probability in different classrooms

The relation between ventilation rate, expressed by the ACH, and infection probability was analyzed for different classrooms for the activity of speaking, as shown in Fig. 3. The exposures of one and five hours were considered, as they represent the minimum and the maximum time that students usually spend in university classrooms. The activity of speaking was chosen, as it represents the most critical scenario that can be probably encountered in university classrooms.

Regarding ventilation, Class A presents the most uniform conditions, as can be noticed by the range in which the ACH was varying. Classes B and C are less uniform, as they present Air Changes per Hour varying between about 5 h^{-1} and 25 h^{-1}. Non-uniformity in classroom ventilation can lead to different exposures to the infection risk, which means that some locations are less favorable than others. There is then the need for avoiding students being exposed to unhealthy conditions and, therefore, for providing indications on the correct management of university classrooms.

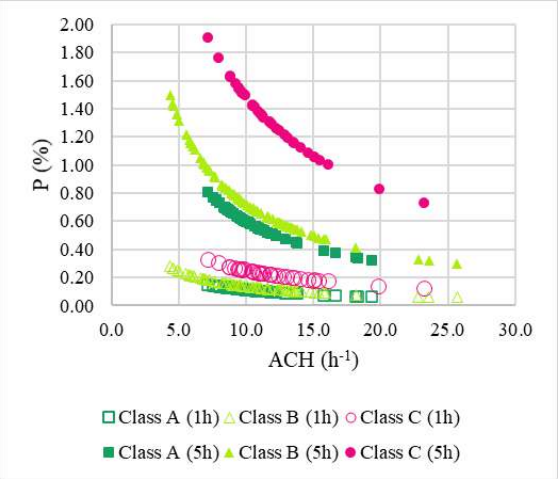

Fig. 3 – Relation between the infection probability for 1 and 5 hours of exposure and the ACH in the three classrooms considered with an infector speaking.

Concerning exposure time, for one hour of exposure, infection probability remains below the threshold value of 1 % for all the classrooms, while, for five hours, only Class A remains below this limit. This implies that, for long exposures, not all the locations should be occupied, but only the ones with acceptable risk values, or that breaks should be guaranteed to reduce infection probability.

Also noteworthy is the fact that there are some differences in the relationship between the ACH and infection probability considering the characteristics of different classrooms. Indeed, despite Class A and B presenting a higher occupation and therefore a higher number of possible infectors, the reduced room volume of Class C largely influences infection probability, as the curve of this class is much higher. The difference between the classrooms is particularly evident for long exposures, as can be noticed in Fig. 3.

4. Discussion

To assess the relationship between ventilation rate and infection probability, the models that are commonly used adopt the hypothesis that ventilation is uniformly distributed in all the locations in the room. However, from the previous results obtained from CFD simulations, it can be noticed that the local mean age of the air, and therefore the ventilation rate, may vary greatly between different positions. In this paper, mechanically and naturally ventilated university classrooms were analyzed to understand how different ventilation strategies, building characteristics, and occupancy can influence indoor infection probability. The crucial point is that the risk must not be underestimated by considering the air in the space to be uniformly distributed.

For this reason, the deviation between infection probability in the different zones (P_{zone}) and infection probability calculated considering ventilation uniform in all the classrooms ($P_{uniform}$) was calculated. Table 2 reports the minimum and maximum deviation for the three classes for the activity of speaking. The choice of infection probability for speaking is related to the fact that it is the most critical and common condition that can be encountered in university classrooms.

The deviation was calculated as the maximum difference between the effective infection probability in the zone and the one calculated considering the ventilation uniformly distributed in the environment. The negative sign in the deviation is associated with the fact that the $P_{uniform}$ was higher than the P_{zone} for all the zones of the classrooms, even in the case of the ventilation rate being the lowest, thus their difference is negative. This means that there is no risk of underestimating the infection probability by using uniform air distribution in the classroom, which is a fundamental issue if the health and the safety of the students are to be guaranteed.

Table 2 – Minimum and maximum deviation for the three classes for the activity of speaking

Class	Season	Minimum deviation	Maximum deviation
Class A	Summer	-0.11	-0.53
	Winter	-0.17	-0.58
Class B	Summer	-1.79	-2.55
	Winter	-1.35	-2.51
Class C	Summer	-1.20	-2.00
	Winter	-0.92	-2.10

This result shows that, in certain cases, the effective infection probability P_{zone} was much lower than the $P_{uniform}$, especially for Classes B and C. Therefore, even if some differences occur, these results demonstrate that assuming the air to be

uniformly distributed in the classroom is an acceptable hypothesis, which benefits student safety. However, from the previous results, it can be noticed that, in several cases, infection probability exceeded the threshold value of 1 % for five hours of exposure. This implies more responsible management of the classrooms to ensure healthy conditions for the students. For this reason, the classrooms used as a case study were divided into homogeneous-risk zones, as can be noticed from Fig. 4. As expected, the lowest infection probability can be found in Class A, while the worst conditions for Class C also present the most homogenous ventilation pattern. This subdivision provides homogeneous risk zones, which permit the identification of the conditions of higher risk for students. In this case, an exposure time of five hours was considered the most critical condition, but similar trends

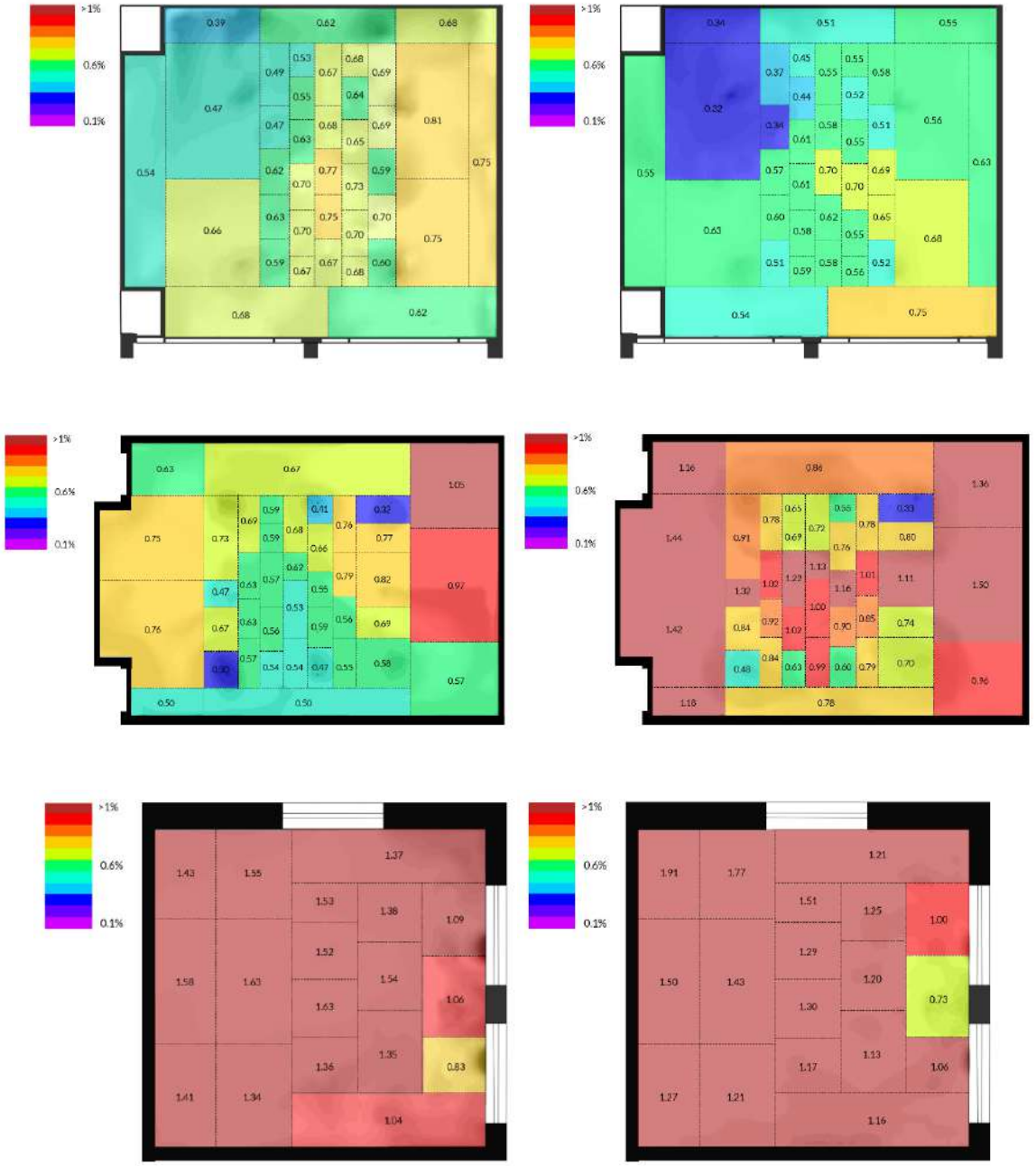

Fig. 4 – Infection probability calculated for the different zones in Class A (above), B (central) and C (below) during summer (left) and winter (right) conditions. The gray area below the graph identifies the flux of fresh air provided by the ventilation system or the window

are found for lower exposures. This division enables more efficient management of classrooms favoring student health. For example, it is possible to recommend certain positions in the classroom depending on the probability of infection, especially if room capacity is not at the maximum.

The extreme cases are Class A, which remains totally below the critical probability of 1 %, and Class C, with a probability above 1 % in practically every position. In the latter case, it is necessary to find solutions that do not involve the positioning of students, since there are no areas of lower risk.

The case of Class B is interesting, since it presents a great variety of situations within it. The best area is in the middle, near the ventilation system, and at the back where there are windows (albeit closed). The side at the back of the classroom furthest from the windows is more critical, although this is not a problem, since this area is a corridor that is not usually occupied by students.

In conclusion, this methodology allows for the efficient management of university spaces, favoring the health of the occupants.

5. Conclusion

The importance of guaranteeing safe and healthy conditions in classrooms has become increasingly relevant, especially after the Covid-19 pandemic. However, the impact of adequate ventilation on students' health and productivity has always been a crucial point for researchers and building designers. Indeed, there is a necessity to provide sufficient air changes to enhance indoor air quality.

In this scenario, to assess the conditions of health indoors, infection probability has been often associated with ventilation rate, using predictive models that assume that air distribution in the room is uniform. However, it can be noticed that, in several cases, classrooms do not present uniform conditions due to the positioning of the ventilation systems or the window or door openings. It is necessary to verify that these non-uniformities do not lead to an underestimation of the infection risk, compromising students' health. With a CFD model, it was possible to simulate different scenarios using university classrooms that presented diverse building characteristics and operation modes as a case study. Results indicate that the less critical situation can be found in mechanically ventilated classrooms, which provide adequate ventilation for the duration of exposure. Furthermore, results show that these models can be applied, despite the different conditions that can be encountered in classrooms, as the assumption of uniform distribution of the air tends to be pro-safety with no risk of underestimating infection probability.

Furthermore, division into equal-risk zones allows for intelligent management of the classroom, which permits students' positioning according to the most favorable conditions indoors, improving their health. Moreover, the new methodology has an important practical application, since it is possible to optimize the HVAC system position in the design phase.

References

Ascione, F., R.F. De Masi, M. Mastellone, and G.P. Vanoli. 2021. "The Design of Safe Classrooms of Educational Buildings for Facing Contagions and Transmission of Diseases: A Novel Approach Combining Audits, Calibrated Energy Models, Building Performance (BPS) and Computational Fluid Dynamic (CFD) Simulations." *Energy and Buildings* 230: 110533. https://doi.org/10.1016/j.enbuild.2020.110533

Awada, M., B. Becerik-Gerber, S. H. Zheng O'Neill, et al. 2021. "Ten Questions Concerning Occupant Health in Buildings during Normal Operations and Extreme Events Including the COVID-19 Pandemic." *Building and Environment* 188: 107480. doi: https://doi.org/10.1016/j.buildenv.2020.107480

Awada, M., B. Becerik-Gerber, E. White, et al. 2022. 'Occupant Health in Buildings: Impact of the COVID-19 Pandemic on the Opinions of Building Professionals and Implications on Research." *Building and Environment* 207: 108440. doi: https://doi.org/10.1016/j.buildenv.2021.108440

Bluyssen, P. M. 2016. "Health, Comfort and Performance of Children in Classrooms – New Directions for Research." *Indoor and Built*

Environment 26(8): 1040–50. doi: https://doi.org/10.1177/1420326X16661866

Dai, H., and B. Zhao. 2020. "Association of the Infection Probability of COVID-19 with Ventilation Rates in Confined Spaces." *Building Simulation* 13(6): 1321–27. doi: https://doi.org/10.1007/s12273-020-0703-5

Ding, E., D. Zhang, and P. M. Bluyssen. 2022. "Ventilation Regimes of School Classrooms against Airborne Transmission of Infectious Respiratory Droplets: A Review." *Building and Environment* 207: 108484. doi: https://doi.org/10.1016/j.buildenv.2021.108484

Fantozzi, F., G. Lamberti, F. Leccese, and G. Salvadori. 2022. "Monitoring CO2 Concentration to Control the Infection Probability Due to Airborne Transmission in Naturally Ventilated University Classrooms." *Architectural Science Review*: 11-13. doi: https://doi.org/10.1080/00038628.2022.2080637

Fantozzi, F., G. Lamberti, and R. Rugani. 2021. "Thermal Comfort in University Classrooms: Analysis of Simulated and Real Conditions. " In *2021 IEEE International Conference (EEEIC/ I&CPS Europe)*. Bari, Italy. doi: https://doi.org/10.1109/EEEIC/ICPSEurope51590.2021.9584490

Gammaitoni, L., and M. C. Nucci. 1997. "Using a Mathematical Model to Evaluate the Efficacy of TB Control Measures." *Emerging Infectious Diseases* 3: 335–42. doi: https://doi.org/10.3201/eid0303.970310

Hughes, B. R., J. K. Calautit, and S. A. Ghani. 2012. "The Development of Commercial Wind Towers for Natural Ventilation: A Review." *Applied Energy* 92: 606–27. doi: https://doi.org/10.1016/j.apenergy.2011.11.066

Lamberti, G. 2020. "Thermal Comfort in the Built Environment: Current Solutions and Future Expectations." In *2020 IEEE International Conference (EEEIC / I&CPS Europe)*, 1–6. doi: https://doi.org/10.1109/EEEIC/ICPSEurope49358.2020.9160558

Lamberti, G., F. Fantozzi, and G. Salvadori. 2020. 'Thermal Comfort in Educational Buildings: Future Directions Regarding the Impact of Environmental Conditions on Students' Health and Performance'. In 2020 IEEE International Conference (EEEIC/I&CPS Europe). doi: https://doi.org/10.1109/EEEIC/ICPSEurope49358.2020.9160680

Lamberti, G., G. Salvadori, F. Leccese, F. Fantozzi, and P. M. Bluyssen. 2021. "Advancement on Thermal Comfort in Educational Buildings: Current Issues and Way Forward." *Sustainability* 13(18). doi: https://doi.org/10.3390/su131810315

Megahed, N. A., and E. M. Ghoneim. 2021. "Indoor Air Quality: Rethinking Rules of Building Design Strategies in Post-Pandemic Architecture." *Environmental Research* 193: 110471. doi: https://doi.org/10.1016/j.envres.2020.110471

Morawska, L., J. W. Tang, W. Bahnfleth, et al. 2020. "How Can Airborne Transmission of COVID-19 Indoors Be Minimised?." *Environment International* 142: 105832. doi: https://doi.org/10.1016/j.envint.2020.105832

Pavilonis, B., A. M. Ierardi, L. Levine, F. Mirer, and E. A. Kelvin. 2021. "Estimating Aerosol Transmission Risk of SARS-CoV-2 in New York City Public Schools during Reopening." *Environmental Research* 195: 110805. doi: https://doi.org/10.1016/j.envres.2021.110805

Riley, R. L., and E. A. Nardell. 1989. "Clearing the Air: The Theory and Application of Ultraviolet Air Disinfection." *The American review of respiratory disease* 139(5): 1286–1294. https://doi.org/10.1164/ajrccm/139.5.1286

Rugani, R., M. Picco, M. Marengo, and F. Fantozzi. 2021. "Can PCS Help Us Save Energy? Initial Assessment Using Dynamic Energy and CFD Analyses." In *2021 IEEE International Conference (EEEIC/I&CPS Europe)*. doi: https://doi.org/10.1109/EEEIC/ICPSEurope51590.2021.9584694

Integrated Approach to Assess the Energy and Environmental Payback Time of Buildings Refurbishment: A Case Study

Marta Roncone – Roma Tre University, Roma, Italy – marta.roncone@uniroma3.it
Francesco Asdrubali – Roma Tre University, Roma, Italy – francesco.asdrubali@uniroma3.it
Gianluca Grazieschi – EURAC, Bolzano, Roma, Italy – gianluca.grazieschi@eurac.edu
Chiara Tonelli – Roma Tre University, Roma, Italy – chiara.tonelli@uniroma3.it

Abstract

The design of nZEB buildings, as well as the implementation of retrofit interventions in existing structures, are essential tools for reducing energy consumption in buildings and increasing decarbonization of the building sector. To describe the effectiveness of a retrofit intervention, in addition to the analysis of the benefits in terms of costs and energy savings, an environmental analysis should also be performed, introducing various indicators, such as energy and environmental payback times. In this article, we considered a residential building located in Montemarcello (Liguria, North-west of Italy) that had been subjected to a refurbishment and an expansion, with the aim of evaluating the energy and carbon savings achievable due to the interventions carried out. The life cycle analysis approach was applied to calculate the environmental payback times. The main purpose of this work is the application of an integrated approach to assess the economic, energetic and environmental convenience of retrofit interventions during the entire life cycle of the building, underlining the importance of considering LCA and environmental aspects to achieve decarbonisation of the construction sector. The results show that energy and environmental payback times are lower than the useful life of the building and of its components, and that LCA proves to be a strategic methodology for studying the problems deriving from global warming and energy supply in the building sector.

1. Introduction

It is well known that the construction sector is nowadays one of the most energy-intensive, and that, in Europe, it is responsible for about 40 % of final energy consumption and 36 % of greenhouse gas emissions, representing about one third of EU energy-related emissions (European Commission, 2020). These emissions arise partly from the direct use of energy from fossil fuels in buildings and partly from the indirect emissions due to the generation of electricity used in buildings.

Although the EU's total greenhouse gas emissions from buildings decreased significantly by 29 % over the period 2005-2019 (EEA, 2021), Member States' emissions should continue declining in the future in order to achieve the EU climate change policy goals. Indeed, to achieve the overall EU target of a 55 % reduction in emissions by 2030, the construction sector would need to reduce its emissions by 60 % (EEA, 2021). For this to happen, the current energy renewal rate of building stock must greatly increase. In this context, to reduce energy consumption and to increase the decarbonisation of the construction sector, the design of nearly Zero Energy Buildings - nZEB (European Parliament and Council, 2010), as well as the implementation of retrofit interventions on existing structures or the selection of materials and building elements with low environmental impact are essential actions to be undertaken. Concerning the embodied burdens, different literature works have already shown that certification with Environmental Product Declarations – EPD (CEN, 2019) – can help in the determination of the environmental performance of building materials, such as insulation (Grazieschi et al., 2021) and windows (Asdrubali et al., 2021).

The implementation of retrofit interventions on existing structures is of additional importance.

However, in order to identify the most efficient and sustainable retrofit intervention, in addition to an assessment in terms of economic benefits, environmental and energy analyses must also be

considered, using appropriate indicators, such as environmental and energy payback times (Asdrubali et al., 2019; Asdrubali & Grazieschi, 2020).

Most of the scientific literature reviewed (Ardente et al., 2011; Webb, 2017) focuses on the evaluation of retrofit interventions of existing buildings or on the energy and environmental performances of new constructions. This work presents, on the other hand, a combined intervention that is characterized by the retrofitting of an existing house that involves a new add-on part. These typologies of retrofit interventions, sometimes referred as parasite architecture (Rinaldi et al., 2021), nowadays represent one of the possible architectural solutions for increasing living spaces, indoor comfort conditions and, if necessary, reducing energy consumption (Assimakopoulos et al., 2020).

In particular, a residential building located in Montemarcello (Liguria, North-west of Italy) subjected to a renovation and construction of an extension was considered, evaluating the energy and carbon savings due to the interventions and applying the life cycle analysis (LCA) to calculate the environmental payback times.

Therefore, this work presents the application of an integrated approach for estimating the environmental convenience of some structural and energy redevelopment interventions during the entire life cycle of the building.

The paper is organized as follows: Section 2 describes the materials and methodologies used in this work for the life cycle, energy and economic analysis of the pre- and post-energy requalification study building; in Section 3, the case study is presented; in Sections 4 and 5, the results of the study are reported and discussed, respectively, while in Section 6, conclusions are provided.

2. Materials and Methods

2.1 LCA and Dynamic Energy Simulation

Life Cycle Analysis (LCA) is a methodology that aims at determining the overall environmental impacts of a product or a service during the entirety of its life stages. This analysis addresses a comprehensive evaluation so that it is able to detect burden shifting or a trade-off between life cycle phases or between different categories of environmental impact.

The methodology is standardized at international level by ISO 14040 (ISO, 2006) and 14044 (ISO, 2006). These two standards give a general overview of the phases that every LCA study should follow, defining a framework that is not characterized by a rigid temporal order, but which permits a shift from one phase to another also in reverse order when there is the need for updating or revising the assumptions previously made. The LCA phases individuated by the ISO standards are: goal and scope definition, life cycle inventory (LCI), life cycle impact assessment (LCIA), results reporting and sensitivity analysis.

The LCA application is very useful for identifying the most effective scenario in building retrofit interventions, also starting from the early design stage when there is the need to choose the solution that minimizes the cumulative environmental impacts during the whole life cycle of the construction.

In this work, the aim of the study was to compare the environmental impacts of a building, chosen as a case study, which was subjected to an energy retrofit intervention that also includes an extension of its useful volume, thus a new part. The life cycle environmental burdens of the ex-ante scenario and of the retrofitted solution were compared to confirm the environmental benefit deriving from the intervention proposed.

The functional unit that was chosen for the comparison was equal to the gross internal area of the building. The boundaries of the analysis included the raw material supply (A1), the transportation to the fabrication site (A2), the manufacturing process (A3), the transportation to the construction site (A4), the replacement of materials and components after their useful service lives (B4), the operational energy uses (B6) and, finally, the end-of-life stages (C1-C4).

The "cradle-to-grave" approach is so adopted for the analysis, excluding some stages that are considered negligible for the scopes of the evaluation (see Fig. 1 for more details).

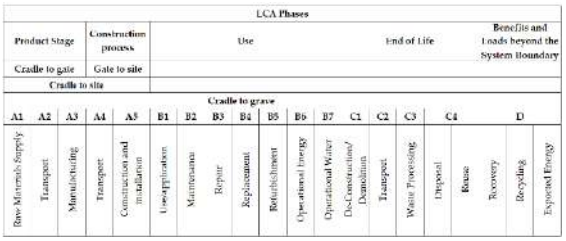

Fig. 1 – Building life cycle stages and related system boundaries - modified from PCR (Wiklund, 2019)

The environmental impacts determined employing the SimaPro software (PRé Sustainability, 2022) were the primary energy non-renewable requirement (PENR), calculated from the Cumulative Energy Demand (Frischknecht et al., 2015) single issue indicator, and the IPCC Global Warming Potential – GWP 100y (IPCC, 2007). Ecoinvent database (ecoinvent, 2021) was used as the background source of data.

The operational energy requirements were evaluated through a dynamic simulation of the building using the EnergyPlus code implemented in DesignBuilder environment (DesignBuilder Software Ltd., 2022).

The assumptions that were made for the development of the LCA are detailed in the following bullet points:

- The useful life of the building (after the intervention) was considered equal to 50 and 100 years, as recommended by the Product Category Rules (Wiklund, 2019) for the compilation of buildings Environmental Product Declarations and other LCA studies (Asdrubali et al., 2019; Asdrubali and Grazieschi, 2020; Blengini and Carlo, 2010). A 100-year lifespan is quite a long time-frame but it permits consideration of the long service life that interventions undertaken with good construction quality generally have.
- The analysis was performed for a rough building, thus external spaces, technical rooms, internal furniture, potable water grids, sewage grids, electrical plants, and any swimming pools were not considered in the evaluation, which was limited to the external envelope, to the internal walls and to energy systems. The consumption of water, DHW, electricity for lighting and household appliances was also excluded.
- Only heating and cooling energy requirements were accounted for in the analysis.
- A complete substitution of the components after their service life was foreseen without fractioning their environmental impacts in case of maintenance of the functionality after the end-of-life of the building.
- Load-bearing structures were supposed to have a service life of 100 years; secondary constructions and insulating materials were supposed to have a duration of 50 years, while for windows it was 35 years; energy systems and plants were modeled with a 20-year life span.
- The transportations means were supposed to be 16-ton trucks (diesel-fueled), while the transportation distance was always considered equal to 60 km.
- Construction and demolition waste material was considered but excavated soils (about 600 m^3) were not accounted for in the evaluation.

2.1 Energy and Carbon Payback Times

The energy and carbon payback time are the two indicators that were considered to describe the effectiveness of the interventions proposed from an energetic and environmental point of view. These two indicators were calculated only for the retrofit intervention of the existing building and for the combined solution. which also includes the realization of the new extension: in fact, the evaluation for the new part was not possible because no ex-ante baseline scenario could be individuated.

The Energy Payback Time (EPBT) is the ratio between the difference of Embodied Energy (EE), after and before the retrofit, and the annual saved energy due to the retrofitting (see Eq. 1).

$$EPBT = \frac{EE_{A1-A4}+EE_{B1-B4}+EE_{C1-C4}}{E_{sav}} \quad (1)$$

The Carbon Payback Time (CPBT) is the ratio between the difference in Embodied Carbon, after and before the retrofit, and the annual carbon reduction due to the retrofitting (see Eq. 2).

$$CPBT = \frac{GWP_{A1-A4}+GWP_{B1-B4}+GWP_{C1-C4}}{GWP_{sav}} \quad (2)$$

The numerators of equations (1) and (2) represent the energy consumptions and the CO_2 emissions due to the construction of the system (stages A1-A4,

B1-B4 and C1-C4) and E_{sav} and GWP_{sav} are the annual reductions of PENR consumption and CO_2 emission due to the system operation, respectively.

3. Case Study

The residential complex under study is located in Montemarcello, in the Liguria region (Italy). The building is in a countryside area (226 m a.s.l.) and was built around the year 1930.
According to Italian legislation, the climatic zone of the property is C (on a scale from A to F, where A corresponds to the hottest places and F to the coldest), with a value in degree days between 1400 and 2100 (President of Italian Republic, 1993).
The building was subject to redevelopment and expansion interventions with the aim of ensuring an adequate level of internal environmental well-being and the containment of the consumption of energy and environmental resources. Fig. 2 shows the structural demolition and reconstruction interventions carried out on the property.

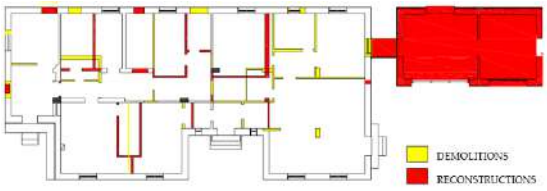

Fig. 2 - Demolitions and reconstructions conducted on the study building for the refurbishment and expansion of the building

The ante operam building, with an area of 211 m², consisted mainly of a brick-cement structure with single-glazed wooden windows. The heated space was separated from the roof by an accessible, unventilated and uninsulated attic, while the roof, also not insulated, was made of a brick-cement structure with tile cladding. The floor slab was raised above the ground level on a dry and damp air space. Instead, the infill walls are of the empty box type with a 10 cm thick air gap. Regarding the heating system, this consisted of 2 natural gas boilers with a nominal power of 24.4 kW and heat input between 12.5 and 27.1 kW. The emission system consisted of a radiant floor with copper pipes embedded in a cement screed directly laid on the brick-cement floor, for an overall average thickness determined by means of a span, including the tiles, of 11 cm. Finally, the regulation system included the room thermostat.
The interventions carried out on the building consisted of a major energy renovation, since the intervention involved more than 50 % of the dispersant envelope (Italian Ministry of Economic Development, 2015) and consisted of: the insulation of the floors, the insulation of the walls, the replacement of fixtures, the reduction of thermal bridges, the replacement of the thermal system, the integration of the summer cooling system, the dehumidification of the air during the winter and summer with heat recovery, and finally the remote management of the heating system.
Fig. 3 illustrates some elevations of the building ante operam, inter operam and post operam.

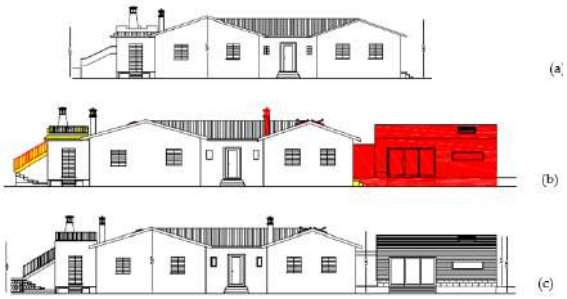

Fig. 3 - Prospects of the studio building ante operam (a), inter operam (b) and post operam (c)

The redeveloped building has a total area of 255 m², including an extension structure of 44 m². In the energy efficiency project, much importance was given to the insulation of the building envelope. In particular, windows with a transmittance between 1.1 and 1.5 W/(m²K) (< 2.0 W/(m²K) of limit value (Italian Ministry of Economic Development, 2015)) and glazed components with a transmittance between 1.332 and 1.687 W/(m²K) were installed. Finally, opaque elements with overall values lower than 0.42 W/(m²K) were obtained, as prescribed by the legislation in force in Italy on the minimum requirements about energy efficiency in buildings (Italian Ministry of Economic Development, 2015).
While the toilets are to be heated with towel-warmer radiators, the heating system of the redeveloped building is of the low-temperature type with radiant floor panels. This system is also capable of cooling in the summer.

The older system was based on a traditional boiler fed by natural gas, with radiators as terminal units and split air-to-air heat pumps for summer cooling. Before the retrofit, the control system was characterized by an on-off termostat installed in the living room, while after the retrofit each room was also equipped with its own thermostat in order to manage and differentiate the temperature independently.

The central heating and cooling system involves the use of a 500-liter boiler (technical water) and an integrated solar thermal circuit, designed to be combined with a single phase heat pump of 10.6 kW.

4. Results

The results showed that the application of energy efficiency measures can bring significant savings in terms of operational non-renewable primary energy consumption and GHG emissions. In particular, the retrofitting of the existing building permitted a reduction of the non-renewable primary energy demand for heating and cooling of 62 % to be obtained, increasing the coverage of renewable energy (see Fig. 4). The overall intervention, on the other hand, produced a reduction of the non-renewable energy demand equal to 60 % if compared with the ante operam situation.

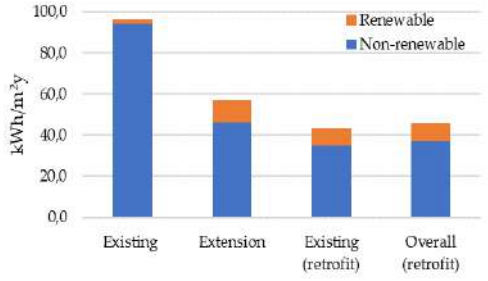

Fig. 4 – Overall annual energy consumptions per square meter for the different scenarios considered (operational energy)

The effort in reducing the operational non-renewable energy demand, however, caused an increase in the embodied impacts due to the introduction of new materials and energy systems. Tables 1, 2 and 3 show the PENR and GWP that characterize the extension, the retrofitted building and the overall combined intervention (composed of the requalification of the existing part and the addition of the new volume).

Table 1 – PENR and GWP of the new extension

LCA stage	PENR (kWh/m²y)	GWP (kg CO_2eq/m²y)
A1-A3	21.3	5.78
A4	1.3	0.28
B1-B4	17.0	3.90
B6	41.7	7.90
C1-C4	1.9	1.70

Table 2 – PENR and GWP of the existing part after the retrofit

LCA stage	PENR (kWh/m²y)	GWP (kg CO_2eq/m²y)
A1-A3	12.0	2.73
A4	0.3	0.07
B1-B4	12.0	2.51
B6	35.0	6.70
C1-C4	0.4	0.42

Table 3 – PENR and GWP of the overal intervention: retrofit of the existing building and new extension

LCA stage	PENR (kWh/m²y)	GWP (kg CO_2eq/m²y)
A1-A3	13.6	3.26
A4	0.5	0.11
B1-B4	12.9	2.75
B6 (post)	36.9	7.04
C1-C4	0.7	0.64

The increase in embedded impacts was relevant and cannot be discarded. Considering the existing construction, for example, the retrofit produces an increment of about 25 kWh/(m²y) in the embedded PENR that corresponds to 26 % of the initial operational non-renewable energy requirement. Looking at the results for the new extension (Table 1), the embodied components (stages A1-A4 and B1-B4) account for 47 % of the total PENR and 57 % of the life cycle GWP of the building. Moreover, if we consider a building lifespan equal to 50 years, the percentage incidence of the embodied components reaches 57 % and 68 % of the life cycle PENR and GWP, respectively, becoming the most important sources of environmental impact.

Fig. 5 displays the overall non-renewable life cycle energy of the scenarios analysed versus its operational component. As can be noted, the increment of the embodied impacts is beneficial, since it is followed by a reduction of the overall life cycle non-renewable primary energy of the building.

The calculation of the energy and environmental payback times (see Table 4) confirmed the environmental advantages of the intervention, showing values that are much lower than the useful life of the building (50 or 100 years are both considered) and of its components.

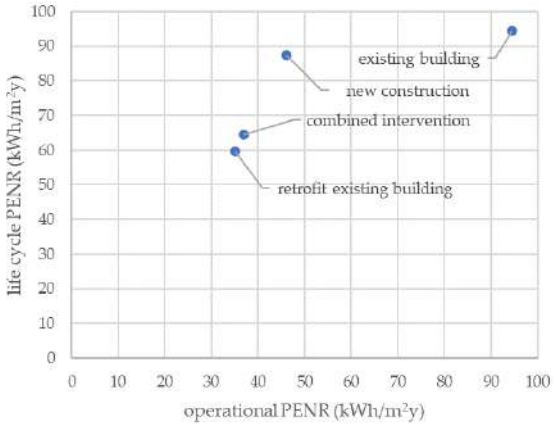

Fig. 5 – Life Cicle-PENR versus operational PENR for the existing building and for the intervetions supposed

Table 4 – Payback times of the overall intervetion

	Payback (months) 100-year life span	Payback (months) 50-year life span
	retrofit existing part	
PENR	5	6
GWP	3	4
	combined intervention	
PENR	6	8
GWP	4	6

5. Discussion

The analysis showed that the most sustainable intervention resulted in the energy requalification of the existing part. The addition of the extension results, on the other hand, is a much less competitive solution in the whole life cycle if compared with the retrofit of the old part: the interventions related to the extension, in fact, have a higher PENR in the entire life cycle. This result depends on different aspects:

1. The operational energy requirements of the old construction after the retrofit are lower than the ones of the new built volume. This is linked with the higher S/V ratio and with the higher window-to-wall ratio of the extension.
2. The retrofit definitely involves a lower embodied energy and carbon because only the roof is completely re-built, while external walls and foundations are conserved.
3. The retrofit implies a higher production of construction and demolition waste, but the management of this waste has relatively low environmental impact. In particular, the demolition waste generated was composed of 46.8 tons of mineral materials, 226 kg of metal waste (ferrous material), 361 kg of glass waste and 720 kg of wood waste.

The overall combined intervention is mainly affected by the retrofit of the existing part, albeit still slightly higher than the one concerning only the redevelopment of the existing building. However, it is characterized by life cycle environmental performances that are still very interesting, even if slightly higher than the ones of the most sustainable solution (namely retrofitting only the existing building): the calcuation of the payback times for the overall intervention shows that they are much lower than the service lives of the installed construction materials and components and it confirms the environmental benefit and the compatibility of the solution.

6. Conclusions

The energy and structural refurbishment of existing buildings implies the selection of a series of strategies and solutions.

In order to identify the most sustainable ones from an environmental point of view, it is necessary to take into consideration an integrated approach that also considers the environmental impacts in terms of the energy and carbon that are incorporated in the building materials and components.

In this study, a residential building subject to an energy retrofit, a structural intervention and an

extension was analyzed. The energy consumptions of the building were simulated in an EnergyPlus environment, while the overall LCA was performed employing an ecoinvent life cycle database.

Therefore, using the PENR, GWP, EPBT and CPBT indicators, the results for the new construction, for the existing building after and before the retrofit and for the combined intervention were compared.

The results are in accordance with other literature studies regarding single buildings with a residential function. In particular, as already shown by other works (Asdrubali & Grazieschi, 2020; Blengini & Carlo, 2010), the operational PENR can be significantly reduced (from 94 to 35 kWh/(m^{2}y) in our case study) if an adequate combination of passive and active solutions is designed and implemented. Consequently, in such low energy solutions, the embodied impacts can represent a very significant part of the total impact, even more than 50 %.

The adoption of a life cycle approach therefore proved to be very useful for the evaluation of the overall environmental burdens. It permitted detection of the burden shifting between the operational and production stages that characterizes the energy retrofit interventions or the construction of new energy-efficient buildings. Moreover, the study made it possible to understand the heaviest interventions and the most impacting phases from an energetic and environmental point of view, while underlining that the energy and environmental payback times are much lower than the useful life of the building and its components. Also in this case, the outcomes obtained agree with the results of other literature works (Ardente et al., 2011; Asdrubali et al., 2019). The trade-off turns out to be only temporary, while environmental benefits are obtainable in the long term.

The new add-on volume, which represents the most peculiar aspect of the retrofit intervention, increased the energy requirement and the environmental burdens of the building, also delaying the payback times of the intervention. That is mainly linked to the fact that the two parts were not integrated, but conceived of as separate units. A higher integration between the two could have been more interesting from the environmental perspective, particularly if the add-on volume had contributed to the reduction of the energy requirement of the existing part.

References

Ardente, F., M. Beccali, M. Cellura, and M. Mistretta. 2011. "Energy and environmental benefits in public buildings as a result of retrofit actions." *Renewable and Sustainable Energy Reviews* 15: 460–470. https://doi.org/10.1016/j.rser.2010.09.022

Asdrubali, F., I. Ballarini, V. Corrado, L. Evangelisti, G. Grazieschi, and C. Guattari. 2019. "Energy and environmental payback times for an NZEB retrofit". *Building and Environment* 147: 461-472. doi: https://doi.org/10.1016/j.buildenv.2018.10.047

Asdrubali, F., and G. Grazieschi. 2020. "Life cycle assessment of energy efficient buildings." *Energy Reports* 6 (8): 270-285. doi: https://doi.org/10.1016/j.egyr.2020.11.144

Asdrubali, F., M. Roncone, and G. Grazieschi. 2021. "Embodied energy and embodied GWP of windows: A critical review." *Energies* 14 (13). doi: https://doi.org/10.3390/en14133788

Assimakopoulos, M. N., R. F. de Masi, A. Fotopoulou, D. Papadaki, S. Ruggiero, G. Semprini, and G. P. Vanoli. 2020. "Holistic approach for energy retrofit with volumetric add-ons toward nZEB target: Case study of a dormitory in Athens." *Energy and Buildings* 207. doi: https://doi.org/10.1016/j.enbuild.2019.109630

Blengini, G.A, and T. Di Carlo. 2010. "The changing role of life cycle phases, subsystems and materials in the LCA of low energy buildings". *Energy and Buildings* 42 (6): 869-880. doi: https://doi.org/10.1016/j.enbuild.2009.12.009

CEN. 2019. EN 15804-2019 - Sustainability of Construction Works. Environmental Product Declarations, Core Rules for the Product Category of Construction Products. Bruxelles, Belgium.

DesignBuilder Software Ltd. 2022. "DesignBuilder." Accessed on January 16. https://designbuilder.co.uk/

Ecoinvent. 2021. "ecoinvent Database." Accessed on February 8. https://ecoinvent.org/

EEA. 2021. "Greenhouse gas emissions from energy use in buildings in Europe." Accessed May 20. https://www.eea.europa.eu/data-and-

maps/indicators/greenhouse-gas-emissions-from-energy/assessment

European Commission – Department of Energy. 2020. "Energy efficiency in buildings." Accessed on 29 October 2021. https://ec.europa.eu/info/news/focus-energy-efficiency-buildings-2020-lut-17_en

European Parliament and Council of the European Union. 2010. "Directive 2010/31/EU of the European Parliament and of the Council of 19 May 2010 on the energy performance of buildings." Accessed on 29 October 2021. https://eur-lex.europa.eu/legal-content/EN/TXT/?uri=celex%3A32010L0031

Frischknecht, R., F. Wyss, S.B. Knöpfel, T. Lützkendorf and M. Balouktsi. 2015. "Cumulative energy demand in LCA: the energy harvested approach." *The International Journal of Life Cycle Assessment* 20: 957–969. doi: https://doi.org/10.1007/s11367-015-0897-4

Grazieschi, G., F. Asdrubali, and G. Thomas. 2021. "Embodied energy and carbon of building insulating materials: A critical review." *Cleaner Environmental Systems* 2. doi: https://doi.org/10.1016/j.cesys.2021.100032

Intergovernmental Panel on Climate Change (IPCC). 2007. "Fourth Assessment Report." Accessed on January 11. https://www.ipcc.ch/assessment-report/ar4/

International Organization for Standardization. 2006. ISO 14040:2006 Environmental management — Life cycle assessment — Principles and framework. Geneva, Switzerland.

International Organization for Standardization. 2006. ISO 14044:2006 Environmental management — life cycle assessment — Requirements and guidelines. Geneva, Switzerland.

Italian Ministry of Economic Development. 2015. Ministry Decree of 26 June 2015 "Applicazione delle metodologie di calcolo delle prestazioni energetiche e definizione delle prescrizioni e dei requisiti minimi degli edifici". Accessed on 29 October 2021. https://www.gazzettaufficiale.it/eli/id/2015/07/15/15A05198/sg

PRé Sustainability. 2022. LCA software for informed change-makers. Accessed on January 11. https://simapro.com/

President of the Italian Republic. 1993. Decree of 26 August 1993 n. 412 "Regolamento recante norme per la progettazione, l'installazione, l'esercizio e la manutenzione degli impianti termici degli edifici ai fini del contenimento dei consumi di energia". Accessed on 4 December 2021. https://www.gazzettaufficiale.it/eli/id/1993/10/14/093G0451/sg

Rinaldi, S., G. Frunzio, M. Guadagnuolo, L. Di Gennaro, and L. Massaro. 2021. "A sustainable material for sustainable architecture: wood in parasite architecture." In *Congresso Internacional Sobre Patologia e Reabilitação Das Construções, Universidade Federal do Ceará*, 481–488. doi: https://doi.org/10.4322/CINPAR.2021.061

Webb, A. L.. 2017. "Energy retrofits in historic and traditional buildings: A review of problems and methods." *Renewable and Sustainable Energy Reviews* 77: 748–759. doi: https://doi.org/10.1016/j.rser.2017.01.145

Wiklund, U. 2019. Product Category Rules for Buildings - version 2.01. Accessed on January 11. https://portal.environdec.com/

Comparison Between Measured and Calculated Values in Relation to Noise From Wind Turbines

Antonella Bevilacqua –University of Parma, Italy - antonella.bevilacqua@unipr.it
Gino Iannace - University of Campania "Luigi Vanvitelli", Italy - gino.iannace@unicampania.it
Ilaria Lombardi - University of Campania "Luigi Vanvitelli", Italy - ilaria.lombardi@unicampania.it
Amelia Trematerra - University of Campania "Luigi Vanvitelli", Italy - amelia.trematerra@unicampania.it

Abstract

The noise from wind turbines is generally assessed according to ISO 9613 in order to preserve the internal noise levels of the nearest sensitive receptors. Following the standard requirements, the wind turbines are considered point sources with an attenuation decay equal to 6 dB by doubling the distance. These indications should be taking into account also the air absorption at different octave bands and the gradient effects due to outdoor environmental conditions. This paper deals with the comparison of some acoustic measurements carried out in Campania (Italy) with the theoretic outcomes obtained in line with the standard ISO 9613. Different types of wind turbines have been assessed, based on a variety of power supply, distance between source and receiver and gradient of wind speed and direction. The surveys have been undertaken inside the nearest sensitive receptors with the conditions of open windows. The results highlight a drift between results, where the calculated are found to be lower than the measured-on site, underestimating the real environmental conditions.

1. Introduction

Wind energy contributes significantly to reducing the use of fossil fuels in the production of electricity, having the benefit of little surface area of occupation. The first wind towers built for the transformation of wind energy into electricity occurred in the United States during 1950s and thereafter it spread rapidly during the 1970s, following the fossil energy crises. Nowadays, wind energy is the most competitive renewable energy source to produce electricity, contributing to both limiting the use of fossil fuels and reducing the effects of atmospheric pollution. Therefore, it is considered a growing business market. The uprising growth at global scale can be translated in numbers as summarised in Table 1.

Table 1 – Global growth of wind power in the last decades

Time	Wind Tower Production (MW)
1996	6100
2001	24000
2017	540000

The areas with the most significant increase are Asia (China and India), Europe (especially France, Spain and Germany) and the United States. In Italy the first wind towers were built in 1990. Based on the geographical morphology, Italy has a significant number of sites suitable for the productivity of wind power, especially in the south and on the islands, where strong winds are dominant. Many wind farms have been built nearby existing residential properties, rising nuisance concerns for the occupants living in the surrounding areas (Sardaro et al., 2019; Shaheen et al., 2016). Noise emission by the operation of wind turbines is potentially causing sleep disturbance and other disease, depending on time of exposure and level of noise. According to the World Health Organization (WHO), limits from nuisance have been established in relation to night-time period (Guillemette & Larsen, 2012). In particular, thresholds of 40 dB(A) for outdoor areas and 30 dB(A) within bedrooms are considered the recommended limits to avoid sleep disturbance which may be potentially causing distress and having negative impact on health (Raman et al., 2016).

Specifically, the noise coming from wind turbines is due to both the effects of air interaction during the blades rotation and the systems inside the nacelle (Wagner et al., 2012). As such, the components of the generated noise are the following (Zajamsek et al., 2014):

- Airborne emission due to the blades' rotation, characterised by a broadband spectrum; and
- Structural-borne emission produced by the electro-mechanical pieces, like the generator, turning over-gear, cooling systems and other components).

Based on a comparison between the two, the levels of the second type of noise are lower than the first one (Bowdler et al., 2011; Burton et al., 2001). By calculating predictions according to ISO 9613 (ISO) the wind turbines are considered as point sources, and the major contribution of the total sound energy is considered to be issued by the gearbox. Generally, the higher the electric power production, the higher the sound pressure levels emitted by a wind tower. By detailing the noise at the gear box, a variation of sound levels is generated whereas the blade crosses the pole during the rotation. This variation can be defined as an amplitude modulation and is one of the most important factors of annoyance since the human hearing is more sensitive to impulsive than steady (or tonal) noise (Doolan et al., 2012; Rogers et al., 2006; Van den Berg, 2004). When compared to other noise sources (e.g. aircraft, railways, etc.) the degree of annoyance of noise from wind turbines is consistent (Pedersen et al., 2004; Waye & Öhrström, 2002).

This paper deals with the acoustic measurements of noise generated by wind turbines of different power supply undertaken inside sensitive residential properties; the measured results have been compared with the outcomes of the numerical predictions calculated in accordance with ISO 9613 (ISO, 2006). The two main scenarios (with the noise source on and off) have been compared with each other and with the predictions carried out by model simulations (Krijgsveld et al., 2009; Ladenburg, 2009; Lee et al., 2011; Shepherd et al., 2011; Voicescu et al., 2016).

2. Sound Propagation Based On Simulated Predictions

The assessment of the acoustic impact generated by the operation of wind turbines is one of the concerns considered since the design phase. The predictions herein calculated have been assessed according to ISO 9613-2 (ISO, 2006; Wszołek et al., 2019), which considers the sound emission as a point source: a numerical model that can match the reality if the receiver is located at a large distance from the source. For the determination of environmental noise levels, the standard ISO 9613-2 provides a theoretical method to evaluate the sound attenuation based on free field conditions.

The calculation of the equivalent continuous sound pressure level (L_{Aeq}) is summarized in equation (1).

$$Lp = Lw + D_{i\vartheta} - A_{div} - A_{atm} - A_{gr} - A_{bar} - A_{misc} \quad (1)$$

where:

- L_p: sound pressure level, dB(A),
- L_W: sound power level, dB(A),
- $D_{i\theta}$: directivity factor,
- A_{div}: attenuation due geometric divergence,
- A_{atm}: attenuation due to atmospheric absorption,
- A_{gr}: attenuation due to the ground effect,
- A_{bar}: attenuation due to any barrier,
- A_{misc}: attenuation due to foliage, industrial sites, housing.

By simplifying equation (1) and considering the geometric divergence only, the sound pressure level becomes as indicated in equation (2).

$$L_p = L_w - A_{div} \quad (2)$$

where A_{div} is calculated according to UNI ISO 9613-2, which is given in equation (3).

$$A_{div} = 20 \log(d) + 11 \quad (3)$$

where d is the distance between the sound source and the receiver. In line with the ISO 9613 (ISO, 2006), the sound pressure level at the nearest sensitive locations shall include the attenuation effect of the open window, or the difference between the sound levels measured outdoor and inside the building.

3. Acoustic Measurements

The acoustic measurements were carried out with a First-Class sound level meter LXT1 Larson Davis. The equipment was calibrated before and after the survey and no drift in calibration was noted. Sets of 5-minute were made at the 3-hour long term attended measurement locations, identified inside the nearest sensitive receptors. The measurements recorded overall A-weighted L_{eq} and L_{95} sound pressure levels, with the time averaging constant set to 'Fast' (Ciaburro et al., 2021). The sound level meter was installed on a tripod at a height of 1.4 m from the finish floor and a minimum of 2 m from any vertical surface. The acoustic measurements were carried out under the condition of having open window. The noise levels have been recorded for wind turbines in operation and out of any activity, in order to assess, under the same wind speed condition, the noise contribution from the wind farms in operation against the background noise levels without any activity running (Iannace, 2016; Iannace et al., 2019a; Trematerra & Iannace, 2017).

3.1 First Case Study

The first measurement campaign has been conducted in autumn, with a relative humidity equal to 50 %, a temperature around 10 °C, and a wind speed averaging between 8 m/s and 10 m/s, from South-West direction (Iannace et al., 2019a; Iannace et al., 2019b). With wind towers provided with 3.0 MW power supply. The rotation speed is about 12 rpm. The microphone was installed in a room having dimensions of 2 × 3 × 3 m (W, L, H). Given the different orientation, the wind turbines were operating singularly during the survey, such that each contribution has been calculated singularly (Iannace et al., 2020). The measured equivalent sound pressure levels at the receiving positions have been summarized in Table 2.

Table 2 – Measured results related to the first case study

Activity of Wind Towers	L_{eq} (dBA)	L_{95} (dBA)	Average wind speed (m/s)
On	45	39	8 - 9
Off	35	31	9 - 10
On	52	48	10 - 11
On	43	36	9 - 10

Table 2 indicates that the noisiest condition occurs when the wind speed fluctuates around 10-11 m/s; in this case the equivalent sound pressure level is equal to L_{eq} = 52 dB(A). With similar wind speed conditions (9-10 m/s), when the wind turbines are off, the background noise level drops to L_{eq} = 35 dB(A), up to 17 dB below. By comparing the sound pressure levels measured at the nearest sensitive receptor and the predictions as outlined by the standard requirements, it is possible to calculate the sound pressure level for each distance of the three towers from the receiver. Considering the distance of each wind tower equal to 450 m, 650 m, and 950 m, that a nominal power of each wind turbine is 3.0 MW (equivalent to L_W =104 dB(A)), the predicted sound pressure levels emitted by a wind turbine according to ISO 9613 are summarised in Table 3. A total predicted equivalent sound pressure level at the receiver location would be equivalent to L_p = 42 dB(A). Additionally, the effect of the open window shall be counted to be around 4-5 dB. Therefore, the sound level inside the sensitive receptor is equal to L_p = 37-38 dB(A), meaning that the regulation underestimates the overall value if compared with the measured results.

Table 3 – Predicted noise levels according to ISO 9613. First case study

Distance of the Towers from Receiver	A_{div} values (dBA)	L_P values (dBA)
450	64	40
650	67	37
950	71	33

3.2 Second Case Study

This second acoustic survey deals with wind towers provided with 60 kW power supply. The tower is located about 250 m from the nearest sensitive receptor, and it is composed of a 40 m high pole and three blades. The rotation speed is about 30 rpm. The rotation is discontinuous because it depends on instantaneous wind speed, that therefore generates an intermittent noise. The measured equivalent sound pressure levels at the receiving positions have been summarized in Table 4.

Table 4 – Measured results related to the second case study

Activity of Wind Towers	L_{eq} (dBA)	L_{95} (dBA)	Average wind speed (m/s)
On	45	40	8 - 9
Off	32	33	8 - 9
On	48	46	11 - 12
On	50	47	12 - 15
On	41	38	7 - 8

When the wind turbine is not in operation, the background noise level measured inside the sensitive receptor is equal to L_{eq} = 32 dB(A), while results of the wind farm in operation is between L_{eq} = 41 dB(A) and L_{eq} =50 dB(A). Considering the theoretical methodology based on ISO 9613 standard, with a distance equal to 250 m, the sound attenuation indicated in equation (4) is the following.

$$A_{div} = 20\ \log(250) + 11 = 59\ dB(A) \quad (4)$$

The nominal power of the wind turbine is 60 kW (equivalent to L_W = 100 dB(A)); as such, the predicted sound pressure levels emitted by a wind turbine considered a point source in accordance with ISO 9613 is given in equation (5).

$$L_p = 100 - 59 = 41\ dB(A) \quad (5)$$

By applying a further attenuation for the open window equal to 4 dB, the predicted noise levels is L_p =37 dB(A). For this second case study, the methodology outlined by the standard underestimates effective noise level and highlights a difference of up to 13 dB between the maximum measured results and the calculated value.

3.3 Third Case Study

The third acoustic survey has been performed inside a sensitive receptor that is 250 m distant from the wind towers. With wind towers provided with 1.0 MW power supply. A South-West wind direction has been recorded to have a speed of approximately 8-9 m/s. The rotation speed of these blades is equal to 15 rpm. The measured equivalent sound pressure levels at the receiving positions have been summarized in Table 5.

Table 5 – Measured results related to the third case study

Activity of Wind Towers	L_{eq} (dBA)	L_{95} (dBA)	Average wind speed (m/s)
On	45	31	8 - 9
Off	33	31	8 - 9

Table 5 indicates that when the wind turbine is in operation the equivalent sound pressure levels measured inside the sensitive receptor is equal to L_{Aeq} = 45 dB(A), with a difference of 12 dB by considering the quiet condition (i.e., background noise level). Considering the theoretical methodology based on ISO 9613 standard, with a distance equal to 250 m, the sound attenuation is similar to what calculated in equation (4) to be equal to A_{div} = 59 dB(A). The nominal power of this wind turbine is 1.0 MW, which is equivalent to L_W = 104 dB(A). Based on these values, the predicted sound pressure level emitted by a wind turbine considered a point source in accordance with ISO 9613 is given in equation (6).

$$L_p = 104 - 59 = 45\ dB(A) \quad (6)$$

By applying a further attenuation for the open window equal to 4 dB, the predicted noise levels is L_p = 41 dB(A). Similarly, this third case study highlights an underestimation of the predicted calcula-

tions of 4 dB compared to the measured value.

3.4 Fourth Case Study

The fourth acoustic survey has been performed inside the nearest sensitive receptor located 200 m from the wind farm. With wind towers provided with 1.0 MW power supply. The North wind direction has been recorded to have a speed equal to 15 m/s. The rotation speed for this wind turbines is equal to 15 rpm. The acoustic measurements were performed by placing the microphone in a room facing the wind turbines, with the window open. The measured equivalent sound pressure levels at the receiving positions have been summarized in Table 6 (Berardi et al., 2020).

Table 6 – Measured results related to the fourth case study

Activity of Wind Towers	L_{eq} (dBA)	L_{95} (dBA)	Average wind speed (m/s)
On	52	49	15
Off	44	40	15

Table 6 indicates that when the wind turbine is in operation the equivalent sound pressure levels measured inside the sensitive receptor is equal to L_{Aeq} = 52 dB(A), with a difference of 8 dB by considering the quiet condition (i.e., background noise level). Considering the theoretical methodology based on ISO 9613 standard, with a distance equal to 200 m, the sound attenuation expressed in equation (7) is given as follows.

$$A_{div} = 20\ \log(200) + 11 = 57\ dB(A) \quad (7)$$

Having a nominal power of 1.0 MW, which is equivalent to L_W = 104 dB(A) the predicted noise levels based on theoretical concepts is given in equation (8).

$$L_p = 104 - 57 = 47\ dB(A) \quad (8)$$

With the open window attenuation, the final predicted noise level emitted by the wind turbine is equal to L_p = 43 dB(A). On this basis, it has been demonstrated that a difference of 9 dB has been found between measured and estimated values.

3.5 Fifth Case Study

The fifth acoustic survey has been performed inside the nearest sensitive receptor located 450 m from the wind farm. With wind towers provided with 1.0 MW power supply. The North wind direction has been recorded to have a speed around 6-8 m/s. The rotation speed of the blades is equal to 11 rpm. The acoustic measurements were performed by placing the microphone in a room facing the wind turbines, with the window open. The measured equivalent sound pressure levels at the receiving positions have been summarized in Table 7.

Table 7 – Measured results related to the fourth case study

Activity of Wind Towers	L_{eq} (dBA)	L_{95} (dBA)	Average wind speed (m/s)
On	40	37	6 - 8
Off	35	31	6 - 8

Table 7 indicates that when the wind turbine is in operation the equivalent sound pressure levels measured inside the sensitive receptor is equal to L_{Aeq} = 40 dB(A), with a difference of 5 dB by considering the background noise level. Considering the theoretical methodology based on ISO 9613 standard, with a distance equal to 450 m, the sound attenuation expressed in equation (9) is given as follows.

$$A_{div} = 20\ \log(450) + 11 = 64\ dB(A) \quad (9)$$

Given the nominal power produced by the sound source equal to L_W = 104 dB(A) the theoretical sound pressure level emitted by a wind turbine according to ISO 9613 is summarised in equation (10).

$$L_p = 104 - 64 = 40\ dB(A) \quad (10)$$

With the additional open window attenuation, the

final predicted noise level emitted by the wind turbine is equal to L_P = 36 dB(A). On this basis, it has been demonstrated that a difference of 4 dB has been found between measured and estimated values.

4. Discussion

Different campaigns of measurements have been carried out inside sensitive receptors near to the wind farms. The nominal power of the wind turbine varied from 60 kW, 1.0 MW to 3.0 MW. The surveys were carried out in rooms having similar volume size and with the window open, with the microphone directly facing the sound sources. This paper has demonstrated that the difference between measured results and predicted values calculated in accordance with ISO 9613 is consistent, to be up to 13 dB. From the five case studies it has been shown how the predicted values are lower than the measured results therefore underestimating the effective impact that the wind farms have on the sensitive receptors. The effects of the disturbance due to the noise perceived inside the houses is a function of the difference in the noise level measured when the wind turbine is off or in operation. If from the analysis of the acoustic measurements between the sound source switched off or in operation, a difference is detected then we are in the presence of a disturbing noise, that is generates annoyance. It may happen that for wind speeds above 15 m/s the wind noise covers the noise emitted by the wind turbines, in this condition the noise emitted by the wind turbines is not perceived by the people living inside the houses, but this is a condition limit that happens a few times.

5. Conclusions

The theoretical assessment of the noise propagation from wind turbines in operation has been performed in accordance with the ISO 9613 standard requirements. The predictions are based on the simulation of a wind turbine as a point source and on the open window attenuation. The variety of case studies, characterised by different distance between source and receiver, has demonstrated that the predictions underestimate the effective noise levels of the wind farms as they have been measured on site. One of the main factors that the regulation shall take into account is the wear of the rotating elements that is cause of an increase of noise levels compared to the initial assessment carried out in laboratory conditions, before the wind farms are installed. This outcome highlights the limits of the existing regulation (ISO 9613) that shall be implemented with further considerations in order to produce results to be close to the acoustic measurements.

References

Berardi, U., G. Iannace, G. Ciaburro, D. D'Orazio, and A. Trematerra. 2020. "Mini-Wind Turbine Noise Measured Inside Near-by Houses". *Canadian Acoustics* 48(3): 18-20.

Bowdler, D., and L. Leventhall. 2011. *Wind turbine noise,* Multi-science Publishing Co. Ltd.

Burton, T., D. Sharpe, N. Jenkins, and E. Bossanyi. 2001. *Wind energy handbook* (Vol. 2). New York: Wiley.

Ciaburro, G., G. Iannace, V. Puyana-Romero, and A. Trematerra. 2021. "Machine learning-based tools for wind turbine acoustic monitoring". *Applied Sciences* 11(142) doi: https://doi.org/10.3390/app11146488

Doolan, C. J., D. J. Moreau, and L. A. Brooks. 2012. "Wind turbine noise mechanisms and some concepts for its control". *Acoustics Australia* 40(1): 7–13.

Guillemette, M., and J. K. Larsen. 2002. "Post development experiments to detect anthropogenic disturbances: the case of sea ducks and wind parks". *Ecological Applications* 12: 868–877.

Iannace, G. 2016. "Effects of noise from wind turbines inside home". *Wind Engineering* 40(1): 25-30. doi: https://doi.org/10.1177/0309524X15624339

Iannace, G., U. Berardi, G. Ciaburro, and A. Trematerra. 2019. "Wind turbines noise measurements inside homes". In *Proc. of INTER-NOISE and NOISE-CON* 259(7): 2845-2854.

Iannace, G., G. Ciaburro, and A. Trematerra. 2019. "Wind turbine noise prediction using random forest regression". *Machines* 7(4): 69. doi: https://doi.org/10.3390/machines7040069

Iannace, G., Berardi, U., Ciaburro, G., Trematerra, A., 2019. Wind turbines noise measurements inside homes. *In proc. of Internoise Conference*, Madrid.

Iannace, G., G. Ciaburro, and A. Trematerra. 2020. "Using neural networks to detect wind turbine functioning conditions". *International Journal of Automation and Smart Technology* 10(1): 145-152. doi: https://doi.org/10.5875/ausmt.v10i1.2225

ISO. 1996. *ISO 9613-2: 1996, Acoustics - Attenuation of sound during propagation outdoors*.

Krijgsveld, K. L., K. Akershoek, F. Schenk, F. Dijk, and S. Dirksen. 2009. "Collision risk of birds with modern large wind turbines". *Ardea* 97(3), 357-366.

Ladenburg, J. 2009. "Visual impact assessment of offshore wind farms and prior experience". *Applied Energy* 86(3): 380-387.

Lee, S, K. Kim, W. Choi, and S. Lee. 2011. "Annoyance caused by amplitude modulation of wind turbine noise". *Noise Control Engineering Journal* 59(1): 38-46

Pedersen, E., and K. P. Waye. 2004. "Perception and annoyance due to wind turbine noise - a dose – response relationship". *Journal of Acoustical Society of America* 116(6): 3460 – 3470.

Raman, G., R. C. Ramachandran, and M. R. Aldeman. 2016. "A review of wind turbine noise measurements and regulations". *Wind engineering* 40(4): 319-342.

Rogers, A. L., J. F. Manwell, and S. Wright. 2006. *Wind turbine acoustic noise*. Renewable Energy Research Laboratory, Amherst: University of Massachusetts.

Sardaro, R., N. Faccilongo, and L. Roselli. 2019. "Wind farms, farmland occupation and compensation: Evidences from landowners' preferences through a stated choice survey in Italy". *Energy Policy* 133: 110885.

Shaheen, M., and M. Z. Khan. 2016. "A method of data mining for selection of site for wind turbines". *Renewable and Sustainable Energy Reviews* 55: 1225-1233.

Shepherd, D., D. McBride, D. Welch, K. N. Dirks, and E. M. Hill. 2011. "Evaluating the impact of wind turbine noise on health-related quality of life". *Noise and Health* 13(54): 333.

Trematerra, A., and G. Iannace. 2017. "Wind turbines acoustic measurements". *In AIP Conference Proceedings* 1859(1): 020001.

Van den Berg, G. P. 2004. "Effects of the wind profile at night on wind turbine sound". *Journal of sound and vibration* 277(4-5): 955-970.

Voicescu, S. A., D. S. Michaud, K. Feder, L. Marro, J. Than, M. Guay, A. Denning, T. Bower, F. van den Berg, N. Broner, and E. Lavigne. 2016. "Estimating annoyance to calculated wind turbine shadow flicker is improved when variables associated with wind turbine noise exposure are considered". *The Journal of the Acoustical Society of America* 139(3): 1480-1492.

Wagner, S., R. Bareiss, and G. Guidati. 2012. *Wind turbine noise*. Springer Science & Business Media.

Waye, K. P., and E. Öhrström. 2002. "Psycho-acoustic characters of relevance for annoyance of wind turbine noise". *Journal of sound and vibration* 250(1): 65-73.

Wszołek, T., B. Stępień, and D. Mleczko. 2019. "Comparison of ISO 9613-2 and CNOSSOS-EU methods in noise modelling of a large industrial plant". *In Proc. of INTER-NOISE*.

Zajamsek, B., D. J. Moreau, and C. J. Doolan. 2014. "Characterizing noise and annoyance in homes near a wind farm". *Acoustics Australia* 42(1): 14-19.

Thermo-Hygrometric Comfort Analysis in a Real Public Conference Room to Support a Digital-Twin Targeted to Parametric Investigations

Roberto Bruno – University of Calabria, Italy – roberto.bruno@unical.it
Piero Bevilacqua – University of Calabria, Italy – piero.bevilacqua@unical.it
Daniela Cirone – University of Calabria, Italy – daniela.cirone@unical.it
Natale Arcuri – University of Calabria, Italy – natale.arcuri@unical.it

Abstract

In this paper, the efficient use of a building-plant system in terms of thermal comfort conditions for a real conference room was verified in the summer by its digital twin. A DesignBuilder model was calibrated by experimental data concerning the indoor air temperature, average radiant temperature, relative humidity and CO_2 concentration. Different situations for people's well-being were studied by varying emitter typology, control strategies, subjective parameters and internal loads. The EMS tool was used to simulate high-level control strategies. It was found that radiant ceilings in continuous operation could promote situations of undercooling, whereas a predicted plant operation is appropriate with intermittent functioning. People's metabolism affects comfort conditions more than internal loads, determining an increase of about 3 degrees in indoor air and mean radiant temperature. Inlet temperature variations in fan coils modify comfort conditions marginally. However, these emitters interact worse with internal loads than radiant ceilings. Aside from the Fanger PMV, discomfort indices following EN 15251 were also evaluated. However, in prevision of the implementation of predictive control strategies, the degree hour approach is not recommended because it does not consider clothing resistance properly.

1. Introduction

Recent studies confirm how the implications of thermal comfort in human activities are increasingly relevant, from energy management to ensuring energy efficiency, up to contexts linked to environmental impact and economy (Abdelrahman et al., 2022). People, indeed, spend up to 90 % of their lives in buildings, therefore proper management of indoor spaces is required, also to have a positive impact on people's productivity (Asadi et al., 2017). Recently, targeted investigations have shown that, beyond the subjective parameters involved in ISO 7730, a sort of dependence on gender, age, lighting, CO2 concentration and noise occurs (Crosby & Rysanek, 2021). How-ever, also the more updated thermal comfort models produce accuracy in results of less than 33 % when compared with measured data (Li et al., 2018). In the light of this, the procedures based on the development of a tuned digital twin of the building plant systems could improve the reliability of the result. Moreover, predictive control strategies can be developed to attain simultaneously well-being and energy savings when significant parameters change dynamically. Despite the elevated potential, also to favor the intuitive visualizations of the monitored data in appropriate dashboards, digital twins have rarely been studied for thermal comfort evaluation. A vector-based spatial model, called Build2Vec, for predicting spatial-temporal occupants' indoor environmental preferences was studied in (Abdelrahman et al., 2022), showing a 14 %–28 % accuracy improvement. In (Zhang et al., 2022) a web-based digital twin platform combined with IoT allowed real-time control of the relative humidity level of underground heritage sites to promote preservation to be achieved. A system architecture for the live PMV/PPD calculation based on ASHRAE 55 and enrichment of BIM-based representations of building spaces in virtual reality environments, with live IoT-enabled monitoring data, was proposed in (Shahinmoghadam et al., 2021). In this paper, referring to a real conference room lo-

cated at the University of Calabria, experimental data of indoor air temperature, relative humidity, CO_2 concentration and mean radiant temperature were used to calibrate the digital twin developed in the DesignBuilder environment (DesignBuilder Software Ltd, 2018), a user interface based on an EnergyPlus engine (Berkeley et al., 2019). In this study, the model was employed to determine the influence of different parameters on thermal comfort indices. This work is targeted for the successive implementation of predictive control strategies that assure appropriate thermal comfort conditions in transient regimes. So, the real-time monitoring associated with IoT will be able to intervene by apposite actuators in order to maintain comfort indices within a suitable range.

2. Materials and Methods

Indoor microclimatic measurements were carried out from 11 on 19 July 2019 to 11 on 22 July 2019 using the BABUC control unit (*LSI - Babuc System*, 2022). The aim was to obtain experimental data necessary for validating a dynamic model in DesignBuilder and then proceed to further parametric analyses. In Figure 1, the conference room monitored is shown in blue. The variables strictly related to people, such as metabolism and clothing thermal resistance, were changed related to the different seasons following UNI EN ISO 9920 (Italian Unification Institution, 2009). Environmental parameters refer to the UNI EN ISO 7726 (Italian Unification Institution, 2001).

2.1 The Building-Plant System

The experimental site is located at the University of Calabria (Southern Italy, 39°19'58"80N - 16°11'6"72 E) with typical Mediterranean climatic conditions, defined as subtype CSa following the Köppen climate classification (Peel et al., 2007).

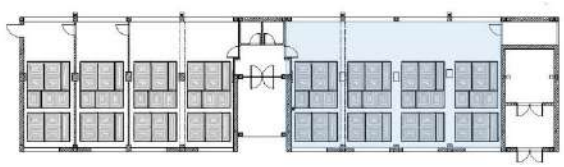

Fig. 1 – Ground floor plane and highlighted monitored area

Table 1 – Layers of the vertical walls

Layer	T [m]	TC [W m^{-1} K^{-1}]	SH [J kg^{-1} K^{-1}]	D [kg m^{-3}]
Plaster	0.02	0.900	800	1400
Hollow brick	0.30	0.157	1000	1250
Plaster	0.02	0.900	800	1400

Table 2 – Layers of the ground floor

Layer	T [m]	TC [W m^{-1} K^{-1}]	SH [J kg^{-1} K^{-1}]	D [kg m^{-3}]
Tiles	0.005	1	1000	2000
Light concr.	0.050	2	800	900
EPS	0.090	0.035	800	55
Stru. element	0.140	2. 2	1000	2600

Table 3 – Layers of the ceiling deck

Layer	T [m]	TC [W m^{-1} K^{-1}]	SH [J kg^{-1} K^{-1}]	D [kg m^{-3}]
Tiles	0.005	1	1000	2000
Light concr.	0.050	2	800	900
EPS	0.090	0.035	800	55
Stru. element	0.140	2. 2	1000	2600
Plaster	0.020	0.9	800	1400

The structure is made of reinforced concrete with transparent surfaces located in the South and North. Stratigraphies of vertical and horizontal opaque walls are listed from Tab. 1 to Tab. 3 with thickness (T), Thermal conductivity (TC), Specific heat (SH) and density (D), all derived from material datasheets.

Highly efficient technological solutions were implemented inside the building, with a control system capable of optimizing renewable energy resources. Two air-water heat pumps in master/slave functioning with a rated thermal power of 5 kW and cooling capacity of 3.8 kW each, connected with a 4 kW_P PV generator, provided heating and cooling by an 800-litre storage tank, configured as a sui-generis electrical storage system to manage PV surpluses. A cogenerative biomass boiler with a Stirling engine (14 kW of thermal power, 1 kW of electric load) was used as an integration system. Emitters consisted of radiant ceilings in mineral fibre, thermally decoupled from the structure, installed in a false ceiling, with an active radiant surface of 124.8 m² distributed in eight independent sectors (see Fig. 1). The main novelty lay in the

management of the experimental set-up: while integrating different systems and devices, the system carries out checks on a single decision-making level to rationalize and manage resources in the best possible way by creating an electrical island grid-independent.

2.2 Measurement System

The BABUC instrument line consists of an assembly of instruments, sensors, accessories and software programs for acquisition, display, storage and processing purposes. Different sensors adopting different physical principles can be connected simultaneously to BABUC, and those employed are listed in Tab. 4. All the probes were positioned in the centre of the conference room.

2.3 Simulation Model

DesignBuilder is based on an EnergyPlus calculation engine and allows for managing the degree of detail with which it intends to set envelope and technological aspects, internal loads, occupancy scenarios, clothing and others.
Climatic data were provided by an *.epw file on an hourly basis using the real values acquired by the weather stations located at the University of Calabria (external air temperature, relative humidity, atmospheric pressure, global horizontal irradiation, beam and diffuse components). Schedules were set for light activity with a metabolism of 1.2 met and a summer clothing factor of 0.5 clo. Air infiltration was set following EN 12831 and it was evaluated as a discriminating element for the calibration of the model. On the other hand, natural ventilation was neglected.

Table 4 – Probes employed for room monitoring

Code	Probe	Measured parameter
BSU102	Psychrometer	Dry bulb temperature (°C) Wet Bulb Temperature (°C) Relative Humidity (%) Dew point temperature (°C) Enthalpy (J)
BST131	Globe Thermometer	Globe temperature (°C) Mean radiant temperature (°C)
BSO103.1	CO_2 sensor	CO_2 concentration (ppm)
BSR001	Lux meter	Illuminance (lux)

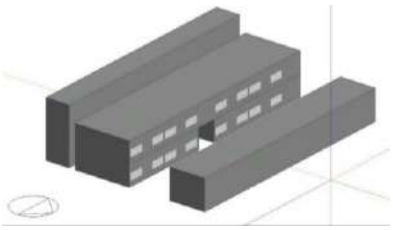

Fig. 2 – Reference building model in DesignBuilder

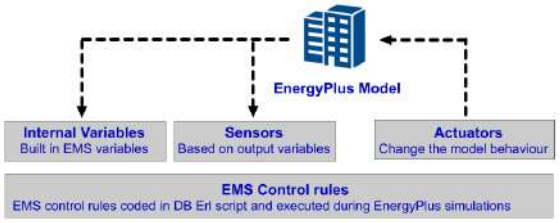

Fig. 3 – Scheme of operation of an EMS control

The HVAC system assumed an ideal setting with unlimited power to attain a setpoint of 22 °C. An EMS (Energy Management System) was employed to carry out an advanced control of the CO_2 concentration. This tool is one of the high-level control methods available in EnergyPlus. An EMS script can access a wide variety of "sensor" data to direct various types of control actions. The EMS uses the concept of sensors to obtain information from elsewhere to use in control calculations. Actuators determine changes in the model and these commands will be used in future studies for the evolution of the model and for the control of air flows to control CO_2 levels by adding control logic following the scheme of Fig. 3

3. Results

3.1 Experimental Data and Validation

The microclimatic surveys for the validation of the model were carried out considering the presence of nine people on 19 July from 14:00 to 18:30 and on 20 July from 9:00 to 14:00, following the real occupation profile. Calibration was carried out by considering closed windows and non-activated shading devices. In order to tune the results, in the model the specific heat and the density of the layers (from Tab. 1 to Tab. 3), the infiltration flow rate and the optical properties of the transparent surfaces were varied. After a fair number of attempts, the temperature profiles of the indoor air matched,

with a slight temporal shift between the experimental and modeled trends (imperfect tuning of the building thermal mass), as depicted in Fig. 4. This aspect is more evident with the indoor mean radiant temperature (Fig. 6). Instruments do not record variations of the relative humidity in the presence of occupants, while the simulation returns a sudden increase (Fig. 5). It can be assumed that real ventilation produces a considerable lowering of humidity ratio in the indoor environment, without affecting the indoor relative humidity. A good match can be observed also for the CO_2 concentration (Fig. 7). Validation was analytically confirmed by statistical indices: mean square error (RMSE), mean bias error (MBE) and correlation factor "r", listed in Tab. 5. It can be appreciated, as temperature and CO_2 concentration are met quite well; relative humidity is slightly underestimated, as indicated by the negative MBE value.

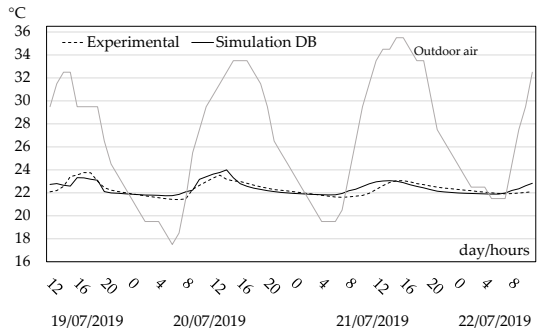

Fig. 4 – Experimental and modeled indoor air temperature

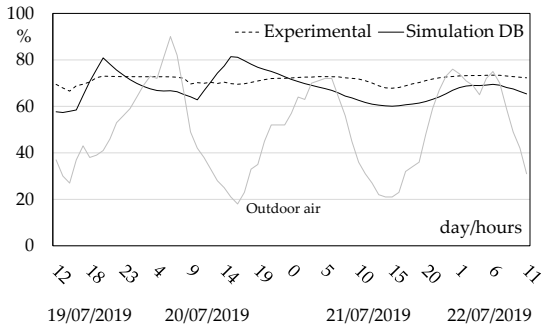

Fig. 5 – Experimental and modeled indoor relative humidity

Table 5 – Some statistical indices for the validation procedure

	RMSE	r	MBE
Indoor air temperature	0.37	0.8	0.00004
Relative humidity	6.61	0.41	-0.00068
Mean radiant temperature	0.48	0.66	0.00014
CO_2	272.17	0.92	-0.00170

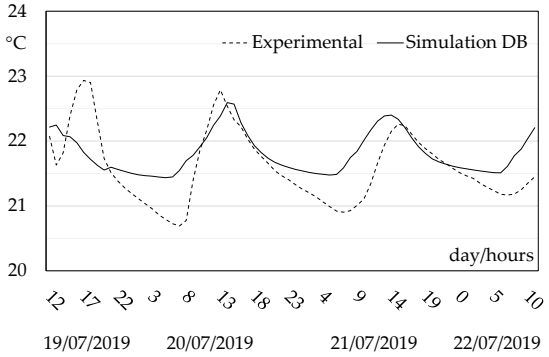

Fig. 6 – Experimental and modeled mean radiant temperature

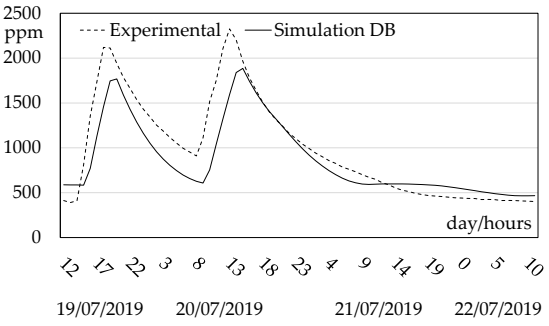

Fig. 7 – Experimental and modeled indoor CO_2 concentration

3.2 Thermal Comfort Evaluation

After validation, the model results were used to proceed with parametric studies for thermal comfort evaluation inside the conference room. Initially, the use of fan-coils and radiant ceilings (both installed in the conference room, with fan-coils provided mainly for dehumidification purposes) and the variation of the inlet temperature was considered by referring to the whole month of July and 9 to 18 users from Monday to Friday (with an hour and a half of lunch break from 13:00 to 14:30). Lightings (dimming LED system with 5 W of electric power each) were scheduled with the same profile relating to user presence. The cases listed in Tab. 6 were considered.

Table 6 – Cases considered for the thermal comfort evaluation

	Emitter	Cooling time	Clothing/ Metabolism
Case 1	Radiant ceiling 15 °C	7-18 Mo- Fr	0.5 clo/1.2 me
Case 2	Radiant ceiling 15 °C	24h Mo- Fr	0.5 clo/1.2 me
Case 3	Fan coil 15 °C	7-18 Mo- Fr	0.5 clo/1.2 me
Case 4	Fan coil 7 °C	7-18 Mo- Fr	0.5 clo/1.2 me

Regarding the plant operation, two modes were envisaged: the first follows the occupation profile starting one hour earlier. The second mode provides continuous functioning for weekdays to overcome the issues related to the inertia of the radiant ceilings. The Fanger PMV, the Pierce PMV SET, the PMV ET and the operative temperature, as described in the EN 15251 standard, were determined. For the latter, assuming a category II, an operative temperature range is recommended in summer at 23 ÷ 26 °C. The Degree Hours criterion, which defines the time during which the operative temperature exceeds the comfort range by the weight factor w_f, was also calculated. It can be noticed that a continuous functioning regime of radiant ceilings allows for the best result (-5.03 °C/month), followed by the intermittent functioning (+119.4 °C/month), whereas fan-coils always involve a worsening of the operative temperature due to the prevalent convective exchange inside the indoor environment (422.11 and 324.08 °C/month, respectively, for Cases 3 and 4). The daily average comfort indexes obtained by DesignBuilder confirmed Case 2 as the situation that allows for achieving values falling within the comfort range with the greatest frequency, while fan coils produce marked overheating conditions.

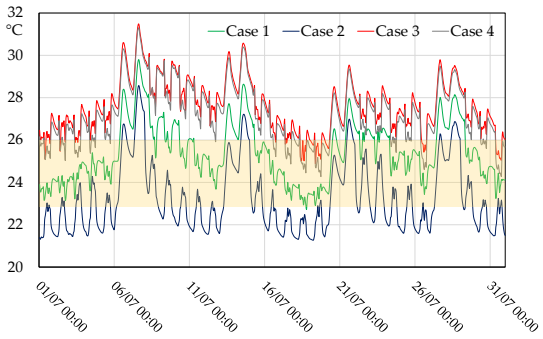

Fig. 8 – Operative temperature in July for the cases considered

Case 2 often guarantees thermal neutrality, but sometimes also a slight undercooling, confirmed both by the w_f index and by the Fanger PMV, whereas the other indices denote a position closer to a slightly warm condition. In Case 1, a slight overheating is detected, meaning that a proper activation in advance is needed to attain adequate comfort. Fan coils supplied at 7 °C guarantee better comfort conditions than Case 4. However, similar comfort indices were obtained, meaning that the inlet temperature is not suitable for regulating thermal comfort when these emitters are employed.

3.3 Parametric Studies

For cases 1, 2 and 4, the role of some parameters on the thermal comfort conditions was evaluated. Case 3 was not considered because it produced the worst scenario. The situation VAR1 involves an increase of internal loads by adding 10 computers supplying 100 Watts each of sensible load. VAR2, instead, considers an increase in 10 people suppling 2 met, whereas in VAR3, a change in clothing insulation to 0.72 clo was implemented. Table 7 highlights how the three situations affect the operative temperature values in Case 1. An evident similarity was detected between the base case and VAR 3, because the indoor air and the mean radiant temperature are the same by changing the clothing thermal resistance. Conversely, a considerable increase was observed in VAR 1 and VAR 2. In particular, 10 people suppling 2 met led to an indoor air temperature growth of 3.6 °C, and the average radiant temperature increased up to 3.4 °C. The weight factor w_f increases in VAR 1 and VAR 2, with the latter affecting results more than the addition of 10 computers (2 met per person for a body area of 1.8 m² corresponds approximately to 200 W following Dubois). It can be appreciated that the mean and maximum temperatures slightly vary, the minimum temperature is almost constant, whereas the degree hour criterion shows considerable worsening with people's metabolism increase.

Table 7 – Operative temperatures with variations in Case1

Base Case	VAR 1	VAR 2	VAR 3
Mean = 25.4 °C	Mean = 26 °C	Mean = 26.9 °C	Mean = 25.5 °C
Max = 29.8 °C	Max = 30 °C	Max = 30.7 °C	Max = 29.8 °C
Min = 22.8 °C	Min = 23.4 °C	Min = 23.6 °C	Min = 22.7 °C
w_f = 119.4 °C/month	w_f = 179.43 °C/month	w_f = 347.57 °C/month	w_f = 119 °C/month

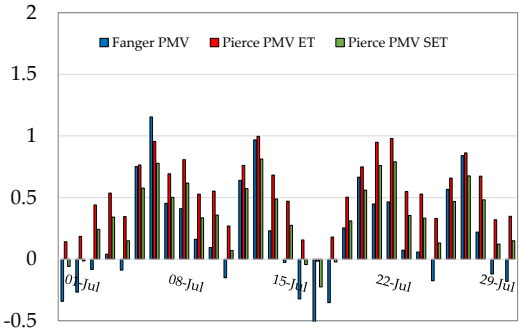

Fig. 9 – Some comfort indices for July 2012, Case 1-base case

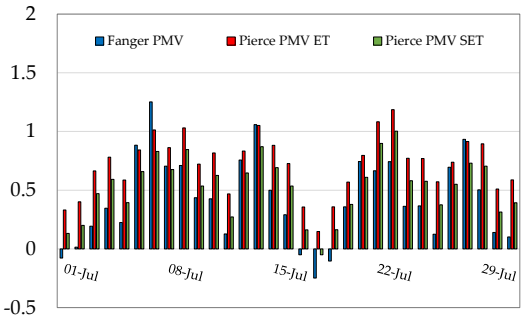

Fig. 10 – Some comfort indices for July 2012, Case 1-VAR1

It can be appreciated that, in the base case, the mean daily Fanger PMV allows for remaining frequently in the desirable range -0.5/+0.5, whereas both Pierce PMV ET and PMV SET produce a situation with slight overheating. In particular, the latter are majorly affected by people's metabolism increase, therefore the use of these indices has to be evaluated carefully because it is more sensitive than Fanger PMV. In accordance with the w_f index, the PMV also records the greatest discomfort in VAR 2. For VAR 3, on the other hand, the PMV indices highlight an exceeding of the comfort threshold, nevertheless offering more consistency than the w_f index.

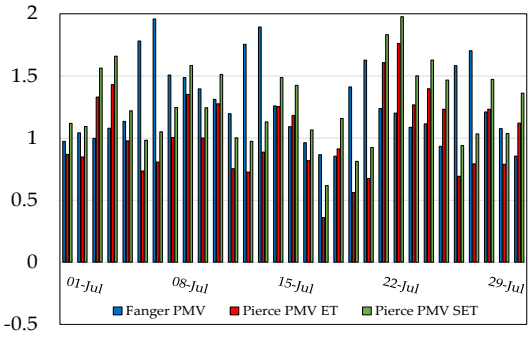

Fig. 11 – Some comfort indices for July 2012, Case 1-VAR2

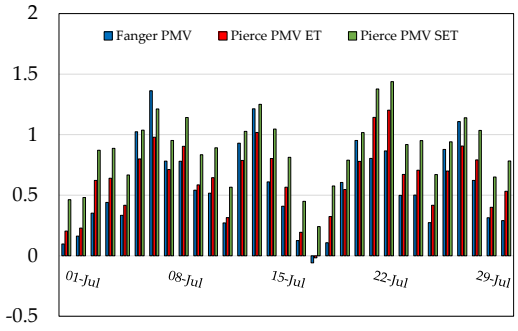

Fig. 12 – Some comfort indices for July 2012, Case 1-VAR3

Case 2 produces similar results to those obtained for case 1. The addition of internal loads and clothing resistance growth determined a Fanger PMV less than 1 with VAR 1 and VAR 3. VAR 2 produced a slightly warm thermal zone with PMV up to 1.5. This result shows that a continuous operation of the radiant ceiling system can guarantee proper thermal comfort conditions when people's activity level is high, so control systems must intervene to limit cooling loads by acting, for instance, on the shading device of the transparent surfaces. Furthermore, even in this case, in the situation of VAR 3, the w_f value fails to return the discomfort increase. On the other hand, all the indices confirm VAR 2 as the situation that causes the greatest discomfort. Nevertheless, the functioning of the radiant ceilings 24 hours per workday allows for more easily meeting the comfort range than an intermittent functioning, but with obvious energy repercussions.

Table 8 – w_f index determined with Case 2 in different situations

Base Case	VAR 1	VAR 2	VAR 3
w_f = -5.03	w_f = 45.87	w_f = 61.94	w_f = -5.03

Passing to fan-coils (case 4), again operative temperatures remain almost the same with VAR 3. Unlike the other two previous cases, VAR 2 produced a slight increase. Conversely, VAR 1 determined a significant increase (Figure 13 and Table 9). Indeed, PCs were set mainly as a radiative load (which in the previous cases is instantaneously removed from radiant ceilings), whereas metabolism is prevalently a convective load. This means that fan-coils interact in a worse manner to contrast the endogenous loads. Similarly, regarding the w_f index, the operative temperature increases more with the presence of PCs and not with people's metabolism, and, again, the increase in clothing resistance does not affect its value.

Table 9 – Operative temperatures with variations in Case 4

Base Case	VAR 1	VAR 2	VAR 3
Mean = 27.2 °C	Mean = 28.8 °C	Mean =27.5 °C	Mean = 27.2 °C
Max = 31.3 °C	Max = 31.8 °C	Max =31.5 °C	Max =31.3 °C
Min = 24.3 °C	Min = 24.7 °C	Min = 24.4 °C	Min =24.3 °C
w_f = 324.08 °C/month	w_f = 418.45 °C/month	w_f = 331.05 °C/month	w_f = 324.08 °C/month

As for Case 1, in Figure 14 and Figure 15, the average daily values concerning the comfort indices are displayed for the base case and VAR 1. It can be noticed that the variant records significant discomfort compared with the base case. In accordance with the w_f index, the PMV indices record the greatest discomfort in VAR 2, even if the PMV is more sensitive to the increase in met than the other indices. These results are in line with radiant ceilings. However, it is highlighted that thermal comfort conditions are more difficult to control in presence of fan coils.

4. Conclusions

Thermal comfort conditions were analyzed by a digital twin for a conference room located in South Italy. This allows, in successive steps, for the implementation of predictive control strategies to apply by IoT for preserving thermal comfort conditions, without exceeding energy consumption, by acting on envelope and cooling plant.

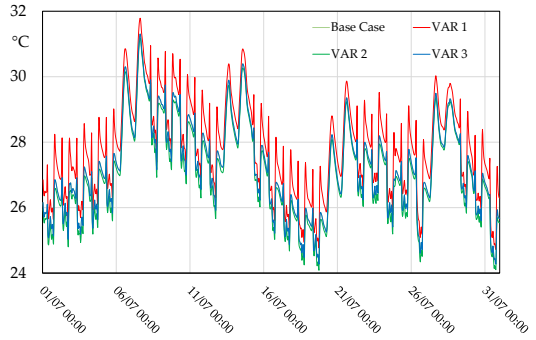

Fig. 13 – Operative temperatures in Case 4 with variants

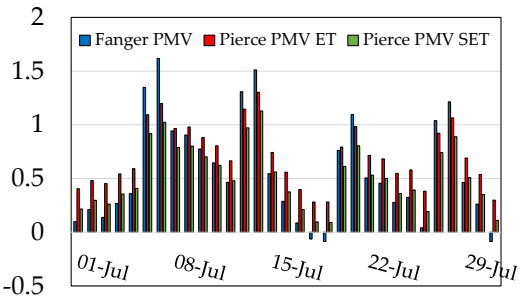

Fig. 14 – Some comfort indices for July 2012, Case 4-base case

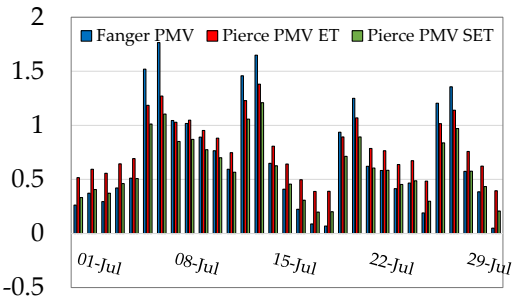

Fig. 15 – Some comfort indices for July 2012, Case 4- VAR 1

A DesignBuilder model was validated by statistical indices calculated starting from experimental data of the indoor microclimatic parameters. Analyses referred to the degree hours criterion (EN 15251) and the Fanger and Pierce comfort indices.

The latter agree with the results of the degree hours criterion. However, when clothing resistance has to be considered is not indicated. Radiant ceilings in a continuous regime offer more days in which the average comfort remains within the range of -0.5 and +0.5. Nevertheless, the risk of zone undercooling occurs. Intermittent functioning produces appreciable comfort conditions only when plant activation is planned in advance. In a parametric study, the Fanger PMV denoted negligible variations, while, conversely, wider deviances were observed for Pierce PMV ET and PMV SET,

which are more sensitive. In particular, with the modification of clothing resistance, the degree hours criterion fails and only Fanger and Pierce comfort indices provide accuracy. In these situations, the Fanger PMV varies from -0.5 to -0.05 with intermittent functioning, and from -0.79 to -0.29 in continuous operation. The same index varies from -0.09 to 0.31, assuming fan coils supplied at 15 °C. The variation of the inlet temperature in fan coils does not modify the comfort indices noticeably. The variation of internal loads and people's metabolism shows a considerable increase both in the w_f coefficient and in the other comfort indices. The slight undercooling detected by the Fanger PMV in the continuous operation of radiant ceilings can be easily overcome by increasing internal gains. The increase in people's metabolism produces overheating both with the Fanger PMV and the Pierce PMV. Therefore, the activation of solar shadings is recommended. Fan coils are more difficult to manage because they are ineffective against removing radiative loads instantaneously, so a predictive control is highly recommended for these emitters.

References

Abdelrahman, M. M., A. Chong, and C. Miller. 2022. "Personal thermal comfort models using digital twins: Preference prediction with BIM-extracted spatial–temporal proximity data from Build2Vec." *Building and Environment* 207. doi: https://doi.org/10.1016/j.buildenv.2021.108532

Asadi, I., M. Mahyuddin, and P. Shafigh. 2017. "A review on indoor environmental quality (IEQ) and energy consumption in building based on occupant behavior." *Facilities* 35: 684–695. doi: https://doi.org/10.1108/F-06-2016-0062

Berkeley, L. et al. EnergyPlus Essentials. 2019. Available online: https://energyplus.net/documentation

Crosby, S., and A. Rysanek. 2021. "Correlations between thermal satisfaction and non-thermal conditions of indoor environmental quality: Bayesian inference of a field study of o_ces." *Journal of Building Engineering* 35. doi: https://doi.org/10.1016/j.jobe.2020.102051

DesignBuilder Software Ltd. 2018. *User manual of the software Design Builder 6*.

Italian Unification Institution. 2001. *UNI 7726. Ergonomia Degli Ambienti Termici - Strumenti per La Misurazione Delle Grandezze Fisiche*.

Italian Unification Institution. 2009. *UNI 9920. Ergonomia Dell Ambiente Termico - Valutazione Dell Isolamento Termico e Della Resistenza Evaporativa Dell Abbigliamento.*

Li, H., S. Wang, and H. Cheung. 2018. "Sensitivity analysis of design parameters and optimal design for zero/low energy buildings in subtropical regions." *Applied Energy* 228: 1280–1291. doi: https://doi.org/10.1016/j.apenergy.2018.07.023

LSI – Babuc. 2022. https://www.lsi-lastem.com

Peel, M. C., B. L. Finlayson, and T. A. McMahon. 2007. "Updated world map of the Köppen-Geiger climate classification." *Hydrology.* doi: https://doi.org/10.5194/hess-11-1633-2007

Shahinmoghadam, M., W. Natephra, and A. Motamedi. 2021. "BIM- and IoT-based virtual reality tool for real-time thermal comfort assessment in building enclosures." *Building and Environment* 199. doi: https://doi.org/10.1016/j.buildenv.2021.107905

Zhang, H. H., L. Kwok, H. Luo, J. C. Tong, J. C. Cheng. 2022. "Automatic relative humidity optimization in underground heritage sites through ventilation system based on digital twins." *Building and Environment* 216. doi: https://doi.org/10.1016/j.buildenv.2022.108999

Validation of Energy Simulations of a Sustainable Wooden House in a Mediterranean Climate

Piero Bevilacqua – University of Calabria, Italy – piero.bevilacqua@unical.it
Roberto Bruno – University of Calabria, Italy – roberto.bruno@unical.it
Daniela Cirone – University of Calabria, Italy – daniela.cirone@unical.it
Stefania Perrella – University of Calabria, Italy – stefania.perrella@unical.it
Natalia Shushunova – Moscow State University of Civil Engineering, Russia – nshushun@gmail.com
Natale Arcuri – University of Calabria, Italy – natale.arcuri@unical.it

Abstract

Wood has become an appealing solution in the building sector compared with traditional materials such as stone, steel, concrete, and brick for several reasons: it is more sustainable, it provides good thermal properties, and allows for fast construction processes in dry-assembled applications. However, wooden buildings in the Mediterranean area are still not very widespread , mainly due to social prejudices about their resistance to seismic events and doubts concerning durability and fire resistance. The paper focuses on the validation of an energy model of a sustainable wooden building that is the prototype of a research project aiming at producing advancement in the development of residential settlement models with solutions to implement in new single or multi-story buildings. The single-family building is located in the province of Cosenza (South Italy). The building was equipped with a monitoring system for the acquisition of quantities of interest for thermal analysis and was subject to an experimental campaign conducted in the summer of 2021. The building was then modeled in the TRNSYS environment accounting for the detailed modeling of solar radiation. Simulations were performed in free-floating conditions, allowing the thermal model to be validated. Then, further energy simulation allowed an evaluation of the thermal performances of building in different Italian localities, allowing the viability of wooded solution in a Mediterranean climate to be demonstrated.

1. Introduction

Sustainability has become a major concern nowadays where worldwide policies aim at achieving the sustainable development of society, with minimal depletion of material and energy (Shushunova et al., 2020). The building sector is an important field where lots of efforts have been made to reduce the energy consumption associated with annual operation and enhance the sustainability of construction (Korol et al., 2018). Wood has been used in the past as the main construction element, especially in cold climates (Arumägi & Kalamees, 2014), but then disregarded in favor of materials such as steel, concrete, and brick rendered more available by the strong industrialization of manufacturing.

Recently, wood has been rediscovered thanks to its appealing characteristics (Slávik et al., 2019) since it is recyclable, reusable, and naturally renewable. Moreover, it has excellent strength-to-weight ratios, thermal insulating and acoustical properties (Caniato et al., 2022) that make it appropriate for different kinds of applications in buildings (Asdrubali et al., 2017). A comparison of the sustainability impacts of both wood- and concrete-based building materials (Žemaitis et al., 2021) shows that that glue-laminated timber and sawn timber value chains have more positive sustainability impacts, especially when referred to environmental indicators. The study also highlighted the socio-economic advantage of wood, which could increase the competitiveness of the regions and contributes to their sustainable development.

Despite the growth and numerous advantages of timber construction, the global scale of multi-story timber construction is still relatively low (Leskovar & Premrov, 2021) compared to reinforced concrete

and steel construction. One of the reasons lies in the complexity of their design, whereby the architectural design, the selection of a suitable structural system, and the energy efficiency concept heavily depend on the specific features of the location, particularly climate conditions, wind exposure, and seismic hazard. An interesting construction solution combining a timber frame with a precise layout of cross-laminated timber panels for a multistory building has been proposed (Bruno et al., 2019). Such a building was capable of attaining both seismic safety and nZEB requirements.

An experimental research study on a wooden frame house was conducted in France to better understand hygrothermal phenomena, and to allow the validation of numerical models for heat, air, and moisture transfers in wooden frame buildings (Piot et al., 2011). Another study in France focused on the desorption and adsorption behavior of exotic wood, then modeled heat and mass transfer through a wooden wall (Simo-Tagne et al., 2021).

This paper focuses on the energy performance of a single-story wooden building in the Mediterranean area. The prototype was built as part of a research project aiming at producing advancement in the development of residential settlement models. A monitoring campaign was conducted in the summer and the thermal model developed in TRNSYS environment was validated thanks to the experimental data. Finally, a series of simulations showed the thermal behavior and winter and summer energy consumption of the proposed building in different Italian localities.

2. Methodology

2.1 The Building Prototype

The demonstrator is a single-family building, classified as a single-story /insulated house, located in Zumpano, a town in the province of Cosenza (South Italy), in the climatic zone D with 1647 degree-days. The building is the output of a regional research project and has a gross surface area of 96 m^2 including the patios on the main front and back, and an inter-floor height of 2.70 m. The building presents a platform frame constructive system.

The project aims at proposing innovative modular solutions for buildings that can be easily assembled and disassembled providing flexibility in the creation of new spaces, and with the use of sustainable materials for their construction.

Fig. 1 – Prototype building of the project Sweethome

The massive employment of wood confers characteristics of celerity of construction and ultimately pushes toward the development of a local production chain of wooden elements, given the abundance of woods in the Calabria. The thermal properties of the layers of the vertical opaque elements are reported in Table 1.

Table 1 – Thermal properties and layers of the opaque vertical envelope

Material	S [cm]	λ [W m^{-1} K^{-1}]	ρ [kg m^{-3}]	c_P [kJ kg^{-1} K^{-1}]
Rock Wool	5	0.035	78	1.03
OSB panel	1.5	0.130	650	1.7
Wood beams +Mineral wool	12	0.192*	105	1.3
OSB panel	1.5	0.130	650	1.7
Air	5	0.28	1.23	1
OSB panel	1.5	0.130	650	1.7
Plasterboard panel	1.2	0.210	816	1

* equivalent thermal conductivity

The resultant thermal transmittance is 0.23 W/(m^2 K), due to the high presence of thermal insulation. The wall facing North presents an additional layer of fir wood, mainly for aesthetic appearance. The ground floor has 6 cm of EPS insulation, reaching an overall U-value of 0.24 W m^{-2} K^{-1}. The roof cover has the same value.

Different types of windows were employed in the prototype. In the main room, the East façade has a double-glazed window with lamellar chestnut frames and a U-value of 1.73 W m^{-2} K^{-1}, whereas the North and South façades have a glazed window with PVC frame with a U-value of 1.47 W m^{-2} K^{-1} and 1.68 W m^{-2} K^{-1}, respectively.

2.2 The Experimental Campaign

In order to assess the thermal performance of the proposed solution, a monitoring campaign was performed in the summer of the year 2021. Several thermo-hygrometric quantities have been monitored with the help of a conspicuous number of sensors and probes. In particular, only the central room of the building was monitored, since it has the largest area, and is the most representative space of the house.

Data logger M-log from LSI LASTEM was placed in the middle of the room to measure:

- Air temperature
- Relative humidity
- Air velocity
- Wet-bulb temperature
- Mean radiant temperature

The psychrometer measures the dry bulb temperature with a Pt100 class 1/3 and an accuracy of 0.10 °C at 0 °C. The relative humidity is measured with an accuracy of 2 %.

Furthermore, a series of Resistance Thermal Detectors were placed in correspondence with each opaque and glazed surface to measure the internal surface temperature of each wall and window. In particular, 4-wire Pt100 sensors class 1/3 with an accuracy of 0.10 °C at 0 °C were employed. Such data were acquired by a datalogger Hioki LR8400-20.

Fig. 2 – Sensors and instruments installed in the central room of the building prototype

A further thermohygrometer DELTAOHM HD2101.2 was placed outdoors behind the main entrance, covered by the external patio to avoid direct exposition to solar radiation, to measure external temperature and relative humidity. The probe used is the HP474AC R with an accuracy of ±1.5 % (0…90 % RH) for relative humidity and ± 0.3 °C for temperature. The datalogger has an internal memory allowing the storage of data that can be successively downloaded to a pc.

2.3 The Simulation Model

The simulation model of the building prototype was developed in a TRNSYS 18 environment. This well-known software allows for dynamic energy simulation of buildings and energy systems in general. The 3D model of the building was realized in Sketchup with the TRNSYS 3D plug-in allowing for a detailed geometry representation. To increase the accuracy of the model and account for the effect of shadings and overhangs, the detailed model for beam radiation and diffuse radiation was set for calculation in TRNBUILD. Likewise, a detailed approach was chosen for the longwave radiation exchange. Internal and external heat transfer coefficients were set to 11 kJ h^{-1} m^{-2} K^{-1} and 64 kJ h^{-1} m^{-2} K^{-1} respectively. The solar absorption coefficient was set to 0.14 for external white surfaces and 0.75 for the north one with a wooden finish. For windows, the g value was assumed to be 0.62 for the window on the north façade and 0.66 for all other windows.

Since during the monitoring campaign there were

no internal loads in the building, the thermal gains were set to 0.

Furthermore, because of the careful construction of the building with a high degree of air tightness, it was possible to exclude infiltration through the envelope.

Type 9 was used to provide hourly data on solar radiation, dry bulb temperature, and relative humidity. Type 16g was then used to evaluate irradiation on different tilted surfaces; Type 69b and 33e were used to evaluate the sky temperature and finally Type 77 provided the ground temperature at different depths.

3. Results and Discussion

The validation of the model was performed with data acquired from 01/06/2021 to 16/06/2021 when the building was operating in a free-floating regime. The main quantity considered for validation was the internal air temperature of the zone. The values of simulated and measured temperature are reported in Fig. 3.

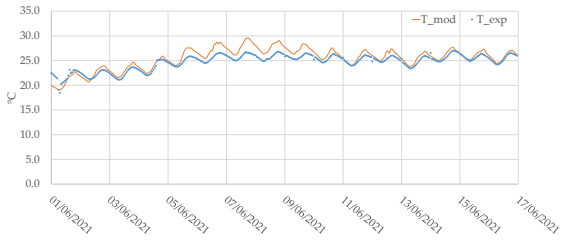

Fig. 3 – Trends of simulated and experimental internal air temperature in the free-floating regime for the period 01/06/2021 – 16/06/2021

The model showed an excellent capability for predicting the internal air temperature variations. Some differences can be observed in the central days of Fig. 3, which are mainly attributed to uncertainty in the values of solar radiation employed for simulation and because of some deviances in the prediction of the temperature of some internal surfaces. Overall, the performance was fairly satisfactory, with an average difference between predicted and measured temperatures of -0.74 °C. The results are further confirmed by Fig. 4, which reports the simulated versus the measured temperature. As can be observed, the data are well aligned along the bisector and a global correlation coefficient R^2 of 0.9683 can be obtained.

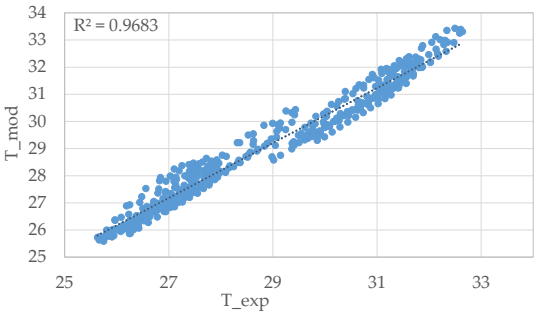

Fig. 4 – Simulated versus experimental internal air temperature in the period 01/06/2021 – 16/06/2021

3.1 Thermal Performance of the Prototype Building

In order to obtain more detailed information on the energy performance of the prototype building in different climatic conditions, a series of subsequent simulations have been performed. To describe more realistically the operation of the building, internal gain according to the Italian reference UNI EN TS 11300 was defined and set in the building model. In particular, for the main room of the building, a daily profile as in Fig. 5 was defined, with a maximum load of 20 W m^{-2}.

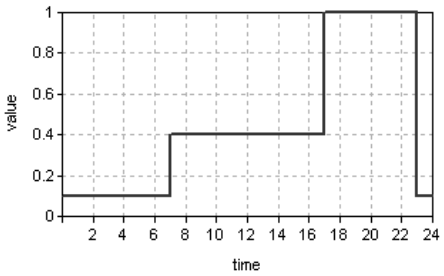

Fig. 5 – Internal gain profile for the main room of the building

Simulations were then performed in different Italian cities, each one representative of a different climatic zone. The heating setpoint temperature was set to 20 °C, whereas the cooling one was set to 26 °C.

In the warm locality of Palermo, with an average yearly temperature of 18.60 °C and global solar horizontal radiation of 1662 kWh m^{-2}, the results are reported in Fig. 6.

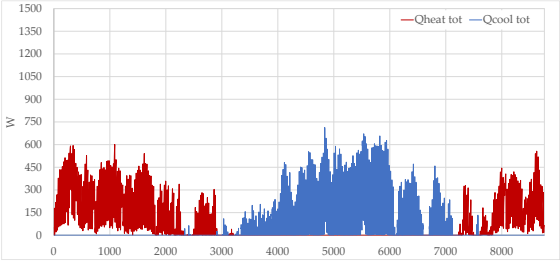

Fig. 6 – Heating and cooling load for the locality of Palermo

The annual energy consumption amounts to 668 kWh for heating and 514 kWh for cooling.

In the milder location of Rome with an average yearly temperature of 15.5 °C and a global solar horizontal radiation of 1559 kWh m^{-2}, the results are reported in Fig. 7.

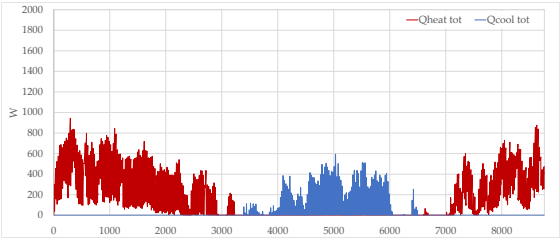

Fig. 7 – Heating and cooling load for the locality of Rome

The annual energy consumption amounts to 1430 kWh for heating and 270 kWh for cooling.

In the colder locality of Bolzano with an average yearly temperature of 12.1 °C and a global solar horizontal radiation of 1250 kWh m^{-2}, the results are reported in Fig. 8.

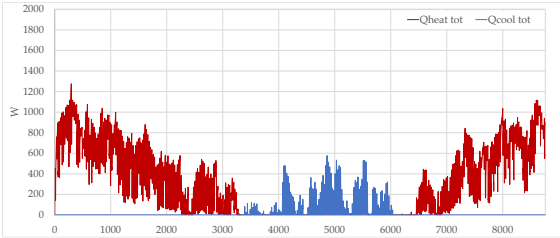

Fig. 8 – Heating and cooling load for the locality of Bolzano

The annual energy consumption amounts to 2563 kWh for heating and 178 kWh for cooling.

4. Conclusion

Recently, the use of wood in building construction has increased noticeably since it is recognized that wood is an environmentally friendly material and can contribute to the achievement of sustainable development goals. However, the rate of these construction solutions is still low compared to reinforced concrete and steel constructions, mainly because the selection of a suitable structural system and the energy efficiency strongly depend on the specific location and in particular climate conditions and seismic hazards. The paper presents the validation of the energy model of a single-storey wooden building in the Mediterranean area. The building was equipped with a complete monitoring and data acquisition system, and an experimental campaign was conducted in the summer of 2021. The energy model of the building was developed in TRNSYS environment and was validated thanks to the experimental data acquired. With reference to the internal air temperature of the main room of the building, a correlation index R^2 of 0.9683 was obtained for a simulation period of 17 consecutive days.

Then the model was employed to evaluate the energy consumption of the building in winter and summer conditions in different climatic localities in Italy.

The results showed the limited energy needs of the building. Heating requirements ranged from 668 kWh in Palermo to 2563 kWh in Bolzano. In the same two cities, the cooling requirements amounted to 514 kWh and 178 kWh

Acknowledgment

The paper was partly supported by Regione Calabria POR CALABRIA FERS FSE 2014-2020 ASSE I – promozione della ricerca e dell'innovazione through the grant of project SWEET HOME - Sustainable Wooden and Energy Efficient HOuse in the Mediterranean. CUP J18C17000600006

References

Arumägi, E., and T. Kalamees. 2014. "Analysis of energy economic renovation for historic wooden apartment buildings in cold climates." *Applied Energy* 115: 540-548. doi: https://doi.org/10.1016/j.apenergy.2013.10.041

Asdrubali, F., B. Ferracuti, L. Lombardi, C. Guattari, L. Evangelisti, and G. Grazieschi. 2017. "A review of structural, thermo-physical, acoustical, and environmental properties of wooden materials for building applications." *Building and Environment* 114: 307–332. doi: https://doi.org/10.1016/J.BUILDENV.2016.12.033

Bruno, R., P. Bevilacqua, T. Cuconati, and N. Arcuri. 2019. "Energy evaluations of an innovative multi-storey wooden near Zero Energy Building designed for Mediterranean areas." *Applied Energy* 238: 929-941. doi: https://doi.org/10.1016/j.apenergy.2018.12.035

Caniato, M., A. Gasparella, F. Bettarello, A. Santoni, P. Fausti, N. Granzotto, F. X. Bécot, F. Chevillotte, L. Jaouen, G. Borello, O. Robin, and N. Atalla. 2022. "A reliability study concerning the acoustic simulations of timber elements for buildings." *Construction and Building Materials* 315: 125765. doi: https://doi.org/10.1016/J.CONBUILDMAT.2021.125765

Korol, S., N. Shushunova, and T. Shushunova. 2018. "Indicators of the resource efficiency development in Russia", in: MATEC Web of Conferences. doi: https://doi.org/10.1051/matecconf/201819305075

Leskovar, V. Ž., and M. Premrov. 2021. "A Review of Architectural and Structural Design Typologies of Multi-Storey Timber Buildings in Europe." *Forests* 12(6): 757. doi: https://doi.org/10.3390/F12060757

Piot, A., M. Woloszyn, J. Brau, and C. Abele. 2011. "Experimental wooden frame house for the validation of whole building heat and moisture transfer numerical models." *Energy and Buildings* 43: 1322–1328. doi: https://doi.org/10.1016/J.ENBUILD.2011.01.008

Shushunova, T., N. Shushunova, E. Pervova, R. Dernov, and K. Nazarova. 2020. "Tendencies of the green construction in Russia." *IOP Conference Series: Materials Science and Engineering* 960. doi: https://doi.org/10.1088/1757-899X/960/4/042022

Simo-Tagne, M., R. Remond, R. Kharchi, L. Bennamoun, M. C. Ndukwu, and Y. Rogaume. 2021. "Modeling, numerical simulation and validation of the hygrothermal transfer through a wooden building wall in Nancy, France.£ *Thermal Science and Engineering Progress* 22: 100808. doi: https://doi.org/10.1016/J.TSEP.2020.100808

Slávik, R., M. Čekon, and J. Štefaňák. 2019. "A Nondestructive Indirect Approach to Long-Term Wood Moisture Monitoring Based on Electrical Methods." *Materials* 12(15): 2373. doi: https://doi.org/10.3390/MA12152373

Žemaitis, P., E. Linkevičius, M. Aleinikovas, and D. Tuomasjukka. 2021. "Sustainability impact assessment of glue laminated timber and concrete-based building materials production chains – A Lithuanian case study." *Journal of Cleaner Production* 321: 129005. doi: https://doi.org/10.1016/J.JCLEPRO.2021.129005

Thermal and Acoustic Simulation of a Technical Enclosure for High Voltage Control Equipment

Edoardo A. Piana – University of Brescia, Italy – edoardo.piana@unibs.it
Somayan Basu – University of Brescia, Italy – s.basu@unibs.it
Francesco Palone – TERNA Rete Italia SpA, Italy – francesco.palone@terna.it
Simone Sacco – TERNA Rete Italia SpA, Italy – simone.sacco@terna.it
Roberto Spezie – TERNA Rete Italia SpA, Italy – roberto.spezie@terna.it

Abstract

The development of the electric power grid addresses the needs deriving from the growing use of renewable sources and from the dispatching flexibility required by mobility electrification. New infrastructures to control the grid parameters and configuration are also being installed in the urban environment, and the relative equipment must generally be enclosed in technical rooms to prevent unauthorised access. Such enclosures must fulfil two conflicting requirements: on the one hand, they must be closed enough to reduce the potentially disturbing noise emitted by the inner equipment, and, on the other hand, they must feature openings for natural ventilation, as high-voltage elements may get damaged due to overheating. Therefore, cooling and sound insulation aspects must be properly integrated during the design phase, keeping an eye on other potential issues, such as condensation. This paper presents a possible strategy of dual acoustic and thermal simulation applied to the design of a new high-voltage control system that allows the expensive technical equipment to be safeguarded while reducing the risk of noise annoyance.

1. Introduction

As detailed in the Electricity Ten Year Statement (Leslie, 2021), with the growing requirement of having smart electric distribution grids capable of adapting to the different needs of the users, transmission system operators (TSO) are developing new solutions with the aim of achieving a remotely operated fast re-configuration of the power grid (Chen et al., 2016). The expansion of green power and the refurbishment of old plants able to withstand the shortage of natural gas have shown the importance of voltage regulation and reactive power compensation (Leborgne & Stypulkowski, 2017). This situation overlaps with the increasing demand for electricity due to the development of electric vehicles and the ever-growing expansion of air conditioning systems. The need for having a flexible distribution network is even more important in the light of the recent developments related to the international situation.

In many cases, the devices used to re-configure or control the power grid are better integrated into the distribution system if they are placed close to the users, and then in the proximity of residential areas (Cohen et al., 2014). Since these devices are based on mechanisms that, under certain circumstances, can produce noise (Piana et al., 2018), it is important to control the sound emitted by the installations. For TSO it is not possible to decrease the noise emissions through a better design of the source itself. The next step is to work on the structures through the implementation of sound insulating shelters containing the noise sources and the related control systems. One drawback of this type of solution is that, in order to avoid damage due to overheating, the thermal power generated by the current flowing through the conductors must be properly dissipated. A sensible solution to avoid adding further noise sources is the use of natural ventilation (Izadyar et al., 2020). If the shelter is properly designed, the ventilation openings will be responsible for the main noise contributions in the surroundings.

These must be large enough to allow a certain air mass flow and, at the same time, small enough to

prevent noise spreading in the neighborhood. For this reason, an accurate thermal and acoustic design of the shelter is necessary. The goal of the present article is to give the reader an idea of the procedure that can be adopted to design the openings necessary to guarantee a sufficient degree of cooling to the high-voltage-control equipment contained in the enclosure, assuring, at the same time, that the noise produced by the devices is compatible with the limits applied to very quiet areas. The amount of heat dissipated by the openings can be improved by using conductive materials (Neri & Pilotelli, 2019; Neri et al., 2020).

The study will be carried out through two different types of simulation software: the first one to predict the indoor thermal conditions and the second one to assess the acoustic impact of the installation.

The structure of the article is as follows. Section 2 briefly gives the geometric, thermal, and acoustic parameters needed for the simulations. Section 3 describes the thermal model implemented in EnergyPlus. In Section, 4 the outcomes of the thermal simulations in terms of opening dimensions will be used to assess the sound pressure level distribution around the shelter using Ramsete. Finally, Section 5 will draw the conclusions.

2. Materials and Methods

The shelter considered in the present study consists of a single volume having dimensions 7 x 7 x 6 m^3. The size has been specifically chosen by the TSO research and development team so that it can contain all the devices needed to implement the remotely controlled system and all the related auxiliary components, maintaining at the same time a suitable occupation of public land. Due to safety reasons, the main volume must be kept apart from undesired accesses of people and animals. For this reason, the walls and the roof must be made of solid materials. Moreover, the structures must be strong enough to withstand natural events (wind, rain, and snow). For aesthetic reasons, the main volume will be enclosed in a buffer of panels acting as a second skin with camouflage purposes. If properly selected, such panels can also behave as a sound barrier. The distance of the second skin from the main volume is about 500 mm. After a discussion with the technical team responsible for the structural design, it was decided that the panels selected for the main structure can be standard sound-insulating sandwich panels made of two external 1 mm thick steel laminates and a 300 mm gap filled with 70 kg/m^3 stone wool. The aesthetic panels can be selected from a wide range of solutions. For the purposes of the present study, their mass per unit area is of importance since they must behave as sound barriers. For this reason, it was decided that the mass per unit area of such panels must be higher than 30 kg/m^2.

The sound source placed inside the shelter is represented by a set of mechanical switches generating impulsive noise (Fig. 1).

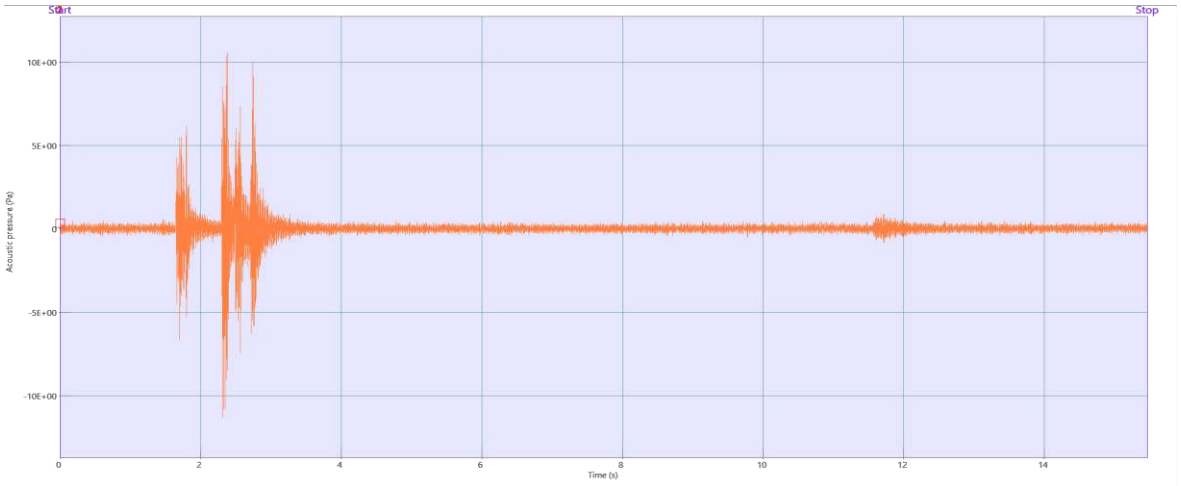

Fig. 1 – Recording of the pressure signal measured at 2 m distance from the switch

The average sound pressure level measured at 2 m distance from one of these switches is reported in Fig. 2. The overall sound energy level due to the single event, according to the international standard ISO 3744 (ISO, 2010), is equal to 114 dB(A) *re* 1pW. It is interesting to note that most of the sound pressure level encompasses between 250 Hz and 20 kHz. This means that, since the sound insulation in the low frequency range is usually dominated by the mass-per-unit area, the required value of this parameter for the panels surrounding the noise sources does not need to be extremely high.

Concerning the thermal simulations, the main parameter to be considered is the thermal power, which needs to be dissipated inside the volume. The current generates heat due to the joule effect. This contribution can be computed once the electric current running through the switching apparatus, the length of the conductors and their resistance known. From a first evaluation of the current (900 A) and of the resistance and length of the conductors, a total thermal power of 4 kW caused by the joule effect can be estimated. In addition, the control and anti-dew systems placed inside the shelter add a further 2 kW to the thermal load, bringing the total amount of thermal power to be dissipated at 6 kW. To prevent damage to the electrical systems, the average temperature inside the volume must be kept below 40 °C.

Fig. 2 – Average sound pressure level measured at 2 m distance from the switch

Since the decision was made to use a natural ventilation system, the amount of heat dissipated depends on the dimensions of the openings and on the external air temperature.

It is known that a fluid possesses a density which decreases with its temperature. If a fluid is less dense than the surrounding one, it tends to shift upwards, generating a convective motion. The two openings of the shelter must be located in such a way that the cold air flowing through the inlet is heated when passing through the volume. The density reduction due to heating generates a convective motion towards the higher part of the shelter, where the air can exit the volume through the outlet. Hence, it is necessary to place the outlet in a position which simplifies the discharge of the warm air. In the simulations, the inlet and the outlet does not have initial mean flow assigned and the pressure is assumed to be atmospheric. Concerning the walls, they are assumed to be rigid but not adiabatic. From this point of view, it is important to find suitable materials possessing both thermal and acoustic properties, as stated by (D'Amore et al., 2020) and (Caniato et al., 2017). The region where the shelter is located is very important. For the purposes of the present study, the thermal simulations were made considering the shelter located in Brescia, northern Italy. The meteorological data of this location, such as the wind speed, the wind direction and the solar gain were given as an input to EnergyPlus.

3. Thermal Simulations

The thermal simulations were carried out using EnergyPlus. A first drawing of the shelter was made in Sketchup. After the work of Correia et al. (2020), and a section of the openings equal to 3 x 1 m^2 to guarantee at least 20 air volume changes each hour was chosen. To exploit the chimney effect due to the different density of the air inside the shelter volume, the two openings (inlet and outlet) have a height difference of 4 m. For the purpose of properly considering the thermal transmittance of the walls, these were virtually assembled in EnergyPlus according to the description given in Section 2 and using the characteristics of the materials shown in Table 1.

The total transmittance for the entire envelope of the main volume is 0.377 W/(m^2 K).

Table 1 – Materials used for the walls of the shelter

Material	Thickness [mm]	Density [kg/m³]	Thermal conductivity [W/(m K)]
Steel plate	1	8000	52
Mineral wool	98	70	0.04
Steel plate	1	7800	52

The thermal load acting on the shelter can be divided into two contributions: the internal thermal load (6 kW distributed on the floor of the main volume) and the solar gain. A reasonably accurate way of simulating the heat source within the volume is to let the heat enter the volume through its floor. This can be considered a reasonable assumption because the components which dissipate heat are located close to the bottom of the shelter. The heat source can be assumed to be a uniformly distributed 122.5 W/m² heat flux, for a total amount to 6 kW.

The solar gain is automatically taken into account by EnergyPlus once the location of the construction is selected as an input.

In the case at hand, the shelter is considered as being situated in Brescia. In this way, EnergyPlus can also consider the average external air temperature, the solar gain and wind speed/direction. These parameters represent the boundary conditions of the simulation. The dataset used encompasses a one-year span, so that the outputs can cover both winter and summer times.

EnergyPlus can give a large number of parameters as outputs. For the present work, the most interesting ones are the average temperature inside the volume, the temperature of the walls and the mass flow rate of the air through the openings. Fig. 3 shows a plot of the mean radiant temperature (black line), the mean air temperature inside the volume (blue line) and the outdoor air temperature (cyan line). In Fig. 4, the mass flow rate of the air running through the openings is given. Fig. 3 and Fig. 4 are yearly-based plots. They can give a reasonable projection of what happens during one "average" year as a function of the meteorological conditions and of the solar gain. It is interesting to note that such simulations give temperatures that are always between -8 °C and 40 °C. This last value represents the limit fixed for the overheating protection of the devices. The natural ventilation of the volume is then able to assure that the temperature is kept below the limit with a certain safety margin, which can be assumed as 4 °C.

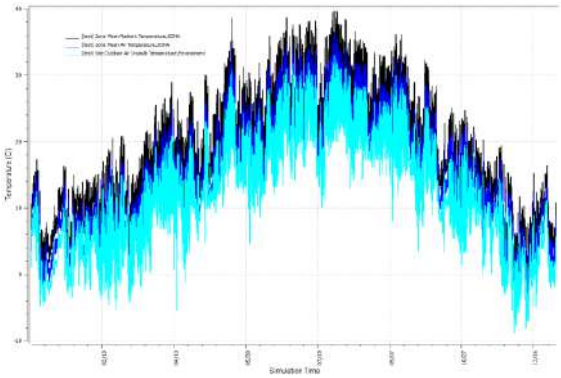

Fig. 3 – Average temperature of the air inside the technical volume of the shelter

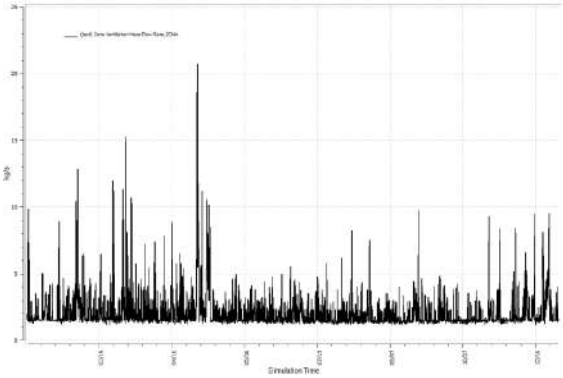

Fig. 4 – Mass flow rate of the air through the openings

Of course, the simulation run assuming a certain location, thus the results cannot be extended to any other possible construction site. The situation can be very different in other contexts like, for example, southern Italy. In this case, a new thermal simulation can be easily made using the specific meteorological dataset of the location chosen as final installation site. In case the proposed dimension of the opening is not sufficient, it can be easily increased, or, in extreme cases, a ventilation system can be added to ensure proper cooling. In the latter case, the noise contribution of the fan must be considered as an additional contribution to the acoustic simulations.

4. Acoustic Simulations

Once the thermal simulation gives feasible results, suggesting a reasonable dimension for the openings, it is possible to run the acoustic simulation to check the sound pressure level distribution around the shelter. The use of acoustic simulation on thin structures was already proved to be effective (Caniato et al., 2020). The simulations were carried out using Ramsete, a software specifically developed for the simulation of the acoustic quality of rooms (Tronchin, 2013), which is also capable of performing the calculation of the noise spreading outdoors (Farina, 2000). One of the characteristics of this software is that it can take sound absorption, sound insulation and the diffraction of the structures into account. This means that the second skin represented by the lightweight panels can be properly represented both in terms of its sound reduction index and diffraction effect. In this sense, the position of the openings is extremely important since the effectiveness of a sound barrier depends on the additional path of the sound wave compared to the direct path. The inlet is placed close to the ground and has an area of 3 x 1 m². The outlet placed on the opposite vertical face of the shelter has the same area, and its lower side is at 4 m from the ground. The walls of the shelter have the sound absorption coefficient and the sound reduction index reported in Fig. 5.

	31 Hz	63 Hz	125 Hz	250 Hz	500 Hz	1 kHz	2 kHz	4 kHz	8 kHz	16 kHz
α	0.092	0.137	0.277	0.608	0.855	0.840	0.794	0.741	0.679	0.639
R	11.0	17.0	23.4	25.6	30.4	26.6	38.2	44.0	50.0	56.0

Fig. 5 – Sound absorption coefficient α and sound reduction index R – shelter walls

The choice of the material for the aesthetic lightweight panels surrounding the shelter was made by architects. The material chosen for these panels is Perspex. The sound-absorption coefficient and the sound-reduction index of the Perspex panels is shown in Fig. 6.

	31 Hz	63 Hz	125 Hz	250 Hz	500 Hz	1 kHz	2 kHz	4 kHz	8 kHz	16 kHz
α	0.040	0.070	0.050	0.030	0.020	0.020	0.030	0.020	0.010	0.010
R	16.0	14.0	18.0	24.0	30.0	36.0	42.0	40.0	48.0	56.0

Fig. 6 – Sound absorption coefficient α and sound reduction index R – aesthetic walls (Perspex glass)

Fig. 7 shows a 3D sketch of the acoustic model imported in Ramsete. The model can give the sound pressure level distribution of the sound emitted by the installation as an output. This means that the sound pressure level computed by Ramsete represents only the contribution of the source placed in the shelter, without the contribution of the background noise. According to Italian legislation (Italian Parliament, 1995), the allowed "Emission Level" in built-up areas depends on the destination of the area itself and on the time of day. Considering the daytime (6-22) and the nighttime (22-6), the emission level limits are summarized in Table 2.
Looking at Table 2 and given the intention of installing the shelter in residential areas, it is sensible to design the shelter so that the limits for Class II during the nighttime (40 dB(A)) are fulfilled. Since the final installation site is not known in advance, satisfying the limits for Class I (35 dB(A)) is still a goal that, if possible, represents an optimal achievement for the project.

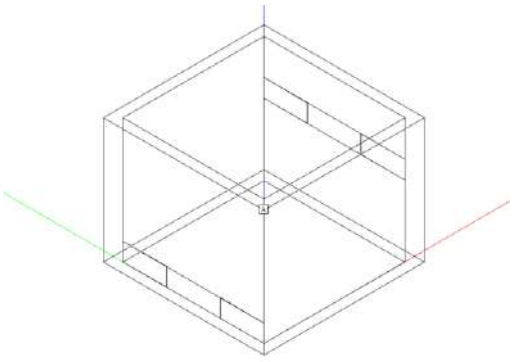

Fig. 7 – Sketch of the acoustic model

Fig. 8 and Fig. 9 show the sound pressure level computed by Ramsete on a horizontal grid of receivers placed at 2 m one from the other, at a height of 1.5 m from the ground and on the vertical mid-section of the shelter, up to a height of 16 m. The sound pressure level inside the shelter is very high and reaches values close to 97 dB(A).

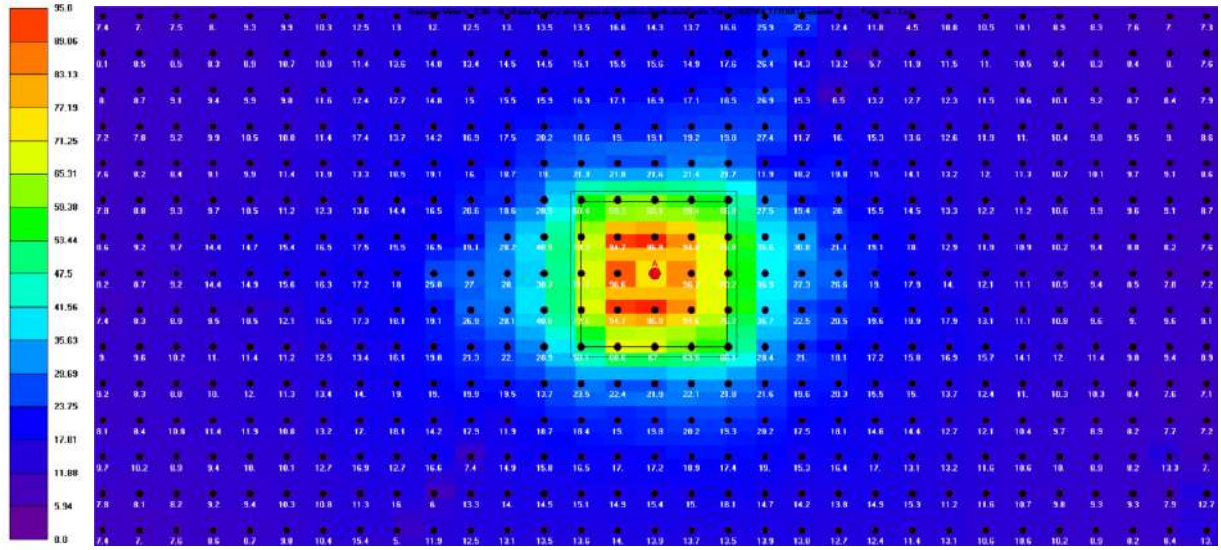

Fig. 8 – Sound pressure level distribution around the shelter – site map

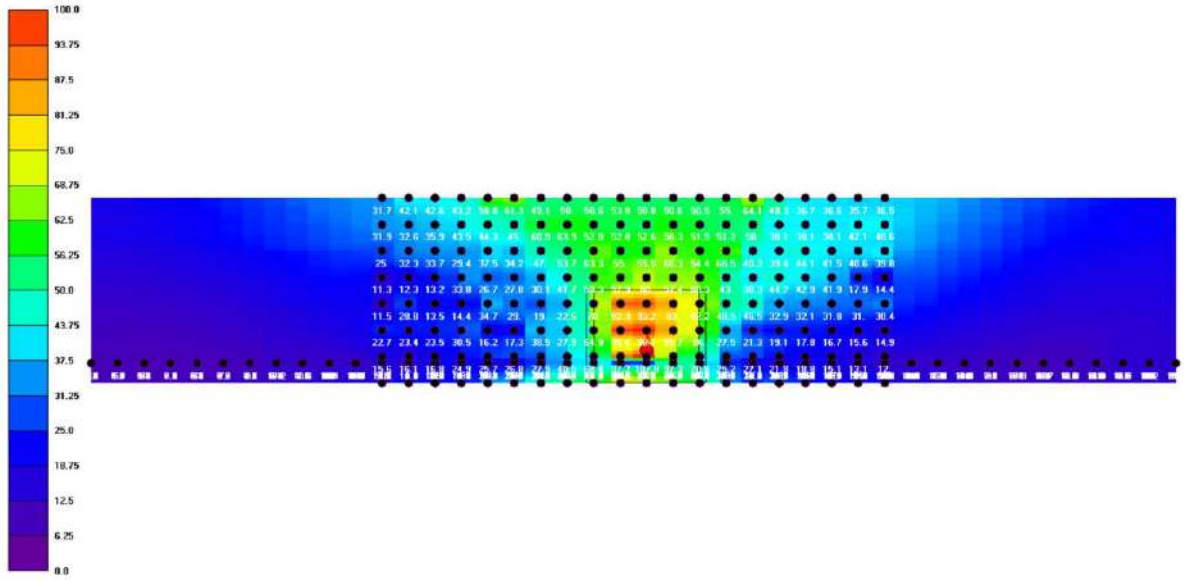

Fig. 9 – Sound pressure level distribution around the shelter – vertical section

Table 2 – Emission level limits

Area destination	Daytime [dB(A)]	Nighttime [dB(A)]
I - Sensitive	45	35
II - Residential	50	40
III - Mixed	55	45
IV - Intense activity	60	50
V - Industrial	65	55
VI – Excl. industrial	65	65

It is important to note that, for keeping sound pressure level as low as possible, the inner side of the shelter walls must feature a certain sound absorption. From Fig. 9 it can be noted also that the sound pressure level in the gap between the shelter and the aesthetic panels depends on the position considered. If a point in front of the opening placed closer to the ground is selected, then the sound pressure level is near 76 dB(A), while on the side where the opening is at 4 m from the ground the sound pressure level is around 72 dB(A). The other two sides of the shelter are characterized by sound pressure levels around 60 dB(A). The result is that,

beyond the aesthetic panel, the sound pressure level is more than acceptable.

Looking at the zones characterized by the higher sound pressure levels, the values at different distances are reported in Table 3.

The sound pressure level values reported in Table 3 show that the sound emission of the shelter is compatible with the limits of Class I starting from 10 m from the wall featuring the air outlet, which is the one giving the highest sound pressure level values. Since it can be expected that no buildings can be erected at a distance lower than 30 m from the shelter, the result achieved allows full compatibility of the installation with the built environment also in the case of the class featuring the lowest emission limits.

Table 3 – Sound pressure levels at different distances from the walls [dB(A)]

Distance [m]	Inlet side	Outlet side
5	30	37
10	19	26
20	10	15

5. Conclusions

A flexible distribution grid, capable of being configured in real time depending on the needs of the customers, is becoming an important point for transmission system operators. This capability has strong advantages when discontinuous green power technologies or loads are integrated in the transmission line. TERNA Rete Italia is working to develop a set of remotely operated systems allowing a fast reconfiguration of the distribution grid.

Since the devices used for the reconfiguration can emit noise and the system is more effective if placed in close vicinity of the users, the acoustic compatibility of this solution with the residential areas is crucial. Nonetheless, assuring acoustic compatibility requires the noisy devices to be enclosed in a shelter having sufficient sound insulation and, at the same time, the capability of allowing a certain cooling of the high voltage systems contained in it.

The present paper presented the thermal and acoustic simulations used to verify the compatibility of the system with the noise limits proposed by Italian legislation for a residential area. The study started with the dimensioning of the openings required for cooling the shelter volume. To avoid additional sound sources, reliance on only natural ventilation was chosen. The simulations were carried out using EnergyPlus and considering the solar gain as well as the temperature distribution outdoors across the entire year. As a result, the dimensions and the position of the openings required for a proper cooling were set. The next step was to check the noise emission of the entire installation. The sound power level of the devices to be placed in the shelter was derived from experimental measurements. Using Ramsete software and properly selecting the materials for the walls and the roof of the shelter, it was possible to run the simulations necessary to predict the noise emissions. A big advantage derived from the choice of the architects to improve the visual impact of the installation by placing four “aesthetic walls” around the shelter. Such structures, from an acoustic point of view, act as noise barriers, shielding the sound spreading from the ventilation openings.

Merging the results of the thermal simulations with the results of the acoustic simulations, it was possible to predict the full compatibility of the installation with the limits of Italian legislation for residential areas. Moreover, the sound emissions are so low that compatibility is assured also for sensitive areas featuring the lowest emission limits allowed by Italian legislation.

References

Caniato, M., F. Bettarello, P. Bonfiglio, and A. Gasparella. 2020. “Extensive Investigation of Multiphysics Approaches in Simulation of Complex Periodic Structures”. *Applied Acoustics* 166. doi: https://doi.org/10.1016/j.apacoust.2020.107356

Caniato, M., F. Bettarello, A. Ferluga, L. Marsich, C. Schmid, and P. Fausti. 2017. “Thermal and acoustic performance expectations on timber buildings.” *Building Acoustics* 24(4): 219–37. doi: https://doi.org/10.1177/1351010X17740477

Chen, L., H. Y. Li, S. Cox, and K. Bailey. 2016. "Ancillary Service for Transmission Systems by Tap Stagger Operation in Distribution Networks." *IEEE Transactions on Power Delivery* 31(4): 1701–9. doi: https://doi.org/10.1109/TPWRD.2015.2504599

Cohen, J. J., J. Reichl, and M. Schmidthaler. 2014. "Refocussing research efforts on the public acceptance of energy infrastructure: A critical review." *Energy* 76: 4–9. doi: https://doi.org/10.1016/j.energy.2013.12.056

Correia, A., L. Ferreira, P. Coimbra, and A. de Almeida. 2020. "Impacts of Automated Natural Ventilation in the Temperature and Humidity of a Distribution Transformer Room." In *Proceedings of 2020 IEEE 14th International Conference on Compatibility, Power Electronics and Power Engineering (CPE-POWERENG)*, Setubal, Portugal. doi: https://doi.org/10.1109/CPE-POWERENG48600.2020.9161687

D'Amore, G. K. O., F. Mauro, A. Marinò, M. Caniato, and J. Kašpar. 2020. "Towards the Use of Novel Materials in Shipbuilding: Assessing Thermal Performances of Fire-Doors by Self-Consistent Numerical Modelling." *Applied Sciences* 10(17). doi: https://doi.org/10.3390/APP10175736

Farina, A. 2000. "Validation of the pyramid tracing algorithm for sound propagation outdoors: Comparison with experimental measurements and with the ISO-DIS 9613 standards." *Advances in engineering software* 31(4): 241–50. doi: https://doi.org/10.1016/S0965-9978(99)00053-8

Farina, A. "Ramsete Home Page". Last accessed in December 2019. http://www.ramsete.com/

ISO. 2010. *ISO 3744:2010 -- Acoustics -- Determination of Sound Power Levels and Sound Energy Levels of Noise Sources Using Sound Pressure -- Engineering Methods for an Essentially Free Field over a Reflecting Plane.*

Italian Parliament. 1995. *Legge 26/10/1995, n. 447 -- Legge quadro sull'inquinamento acustico (Law 26/10/1997, n. 447 -- Framework law on environmental noise, in Italian).*

Izadyar, N., W. Miller, B. Rismanchi, and V. Garcia-Hansen. 2020. "Impacts of Façade Openings' Geometry on Natural Ventilation and Occupants' Perception: A Review." *Building and Environment* 170: 106613. doi: https://doi.org/10.1016/j.buildenv.2019.106613

Neri, M., and M. Pilotelli. 2019. "Device for limiting the temperature at chimney-roof penetration in very critical chimney operating conditions." *Fire Technology*, 55(6): 1937-1965. doi: 10.1007/s10694-019-00837-5

Neri, M., P. Leppanen, M. Alanen, D. Luscietti, S. Bani, and M. Pilotelli. 2020. "Effects of the coupling of insulating and conductive materials to limit the temperature at chimney-roof penetration." *Fire Technology*, 56(4): 1655-1680. doi: 10.1007/s10694-020-00947-5

Leborgne, R. C., and Y. S. Stypulkowski. 2017. "Optimal Reactive Power Compensation in Weak Grids with Insertion of Wind and Solar Sources." In *Proceedings of 2017 Brazilian Power Electronics Conference (COBEP)*, Juiz de Fora, Brazil. doi: https://doi.org/10.1109/COBEP.2017.8257362

Leslie, J. 2021. «ETYS 2021».

Piana, E. A., F. Bignucolo, A. Donini, and R. Spezie. 2018. "Maintenance of a high-voltage overhead transmission line: Sustainability and noise impact assessment." *Sustainability* 10(2). doi: https://doi.org/10.3390/su10020491

Tronchin, L. 2013. "Francesco Milizia (1725-1798) and the Acoustics of His Teatro Ideale (1773)." *Acta Acustica United with Acustica* 99(1): 91–97. doi: https://doi.org/10.3813/AAA.918592

Investigating the Role of Humidity on Indoor Wellness in Vernacular and Conventional Building Typologies

Suchi Priyadarshani – Indian Institute of Science, Bangalore, India – suchip@iisc.ac.in
Roshan R Rao – Indian Institute of Science, Bangalore, India – roshanrao@iisc.ac.in
Monto Mani – Indian Institute of Science, Bangalore, India – monto@iisc.ac.in
Daniel Maskell – University of Bath, United Kingdom – D.Maskell@bath.ac.uk

Abstract

Moisture in air is essential for human life. It drives all physiological processes and determines occupant wellness. As a crucial parameter of Indoor Environmental Quality (IEQ), it is regulated by building typology and its constituent materials. Besides affecting heating and cooling energy requirements, indoor moisture also determines occupants' comfort and health.

Occupant comfort, commonly referred to as thermal comfort, is paramount for building and indoor environment design. Currently available building simulation tools majorly incorporate temperature-related comfort models like PMV, PPD, and adaptive thermal models. In conjunction with temperature, indoor moisture levels impact occupants' skin-related and respiratory comfort, resulting in health issues such as skin irritation, allergies, respiratory infections, asthma, etc. Humidity has not been adequately dealt with in comfort studies. This study proposes a novel computational approach derived from an existing model to explain and assess humidity-related comfort in buildings. The study also involves real-time monitoring of indoor-outdoor temperature and humidity and occupant comfort-votes.

The hygroscopic properties of building materials impact the regulation of indoor moisture, thereby impacting occupant comfort and health. This article examines humidity-related comfort aspects between conventional and vernacular building typologies. Results from the simulation have been used to explain the comfort votes obtained from an on-field survey of occupants. Skin temperature and wettedness derived through energy balance between the human skin and the indoor air parameters can be used as an indicator to assess skin-related comfort in indoor environments.

Comfort is an essential indicator of wellness in an indoor environment. Clarity on approaches to evaluate different aspects of comfort attributed to building materials is crucial for built environment design for occupant wellness. Incorporating humidity-associated comfort parameters in building simulation tools could be beneficial in selecting materials for building design to cater to varying functionalities and health co-morbidities.

1. Introduction

Moisture is omnipresent and fundamental to life. The human body comprises 70 % water. Water balance between the surrounding air and the human body is essential for life. Human beings spend 90 % of their time indoors. Indoor surfaces (building envelope) determine the Indoor Air Quality (IAQ), impacting occupant comfort and health (al Horr et al., 2016; Petty, 2017). Indoor air is the connecting link between the building typology (and materials used) and the occupant. Moisture in the air is a critical determinant of IAQ. Indoor air moisture (as affected by building typology due to heat and moisture transport mechanisms) determines the occupant's thermo-physiological balance, thereby determining comfort. Unregulated (high/low) moisture is generally considered detrimental to health.

Majorly, simulation-based indoor comfort analysis accounts for thermal comfort using indices like PDD (Predicted Percentage of Dissatisfied) and PMV (Predicted Mean Vote). Thermal comfort is determined majorly by environmental (air temperature, relative humidity, wind velocity, and radiation) and personal (metabolism and clothing) factors. Heat-Stress indices like WBGT (Wet-Bulb Globe Temperature) Index, Oxford index, and Effective Temperature are used for varied applications other than indoor comfort like sports, clothing design etc.

Numerous empirical studies have also indicated the impact of (de Dear et al., 1991; de Dear et al., 2015; Jokl, 2002; Kong et al., 2019; Parsons, 2003; van Hoof et al., 2010) indoor humidity on thermal comfort.

While humidity is also accepted as a significant determinant of skin-related and respiratory comfort (Wolkoff & Kjærgaard, 2007); it has not been dealt with explicitly. Tools for evaluating skin-related or respiratory comfort due to changing indoor air parameters are not incorporated in commonly used building simulation softwares.

Vernacular (earth-based materials) and conventional (standardized bricks and RCC) buildings in Jamgoria village, Jharkhand (India), situated in composite climate zone, were monitored (Priyadashani et al., 2021a) for indoor air parameters. This study revealed a significant moderation of indoor RH exhibited by vernacular building typology. The variations in humidity seen in different building typologies provided clear grounds for understanding the humidity-related comfort parameters of occupants with varying indoor environments. Thus, further extension of this study (Priyadarshani et al., 2021b) was carried out to record the response of occupants to skin and respiratory comfort throughout the year in both the building typologies.

Skin acts as the interface with the ***indoor air moisture*** and can be witnessed as wettedness/dryness. The aims of this work are:

1. To compute diurnal/seasonal variations of skin temperature (T_{sk}) and wettedness (w) in vernacular and conventional dwellings using an energy balance-based simulation approach.
2. To explain the changing skin-related comfort votes (oily/very-dry skin) of occupants in vernacular and conventional dwellings using computed Tsk and w.

2. Applied Approach and Methods

2.1 Energy Balance of the Human Body (Core-Skin-Indoor Air)

Simulation-based analysis was done to derive the skin wettedness and temperature corresponding to diurnally/seasonally varying indoor temperature and RH in conventional and vernacular building typologies. The Gagge 2-node model, validated for occupants in indoor environments (Atmaca & Yigit, 2006), was used to represent the energy balance between the human body and indoor air. Factors concerning ethnicity and regional stereotypes were not examined. The model considers 16 cylindrical segments (see Fig. 1) representing different human body parts, each comprising two nodes (core and skin).

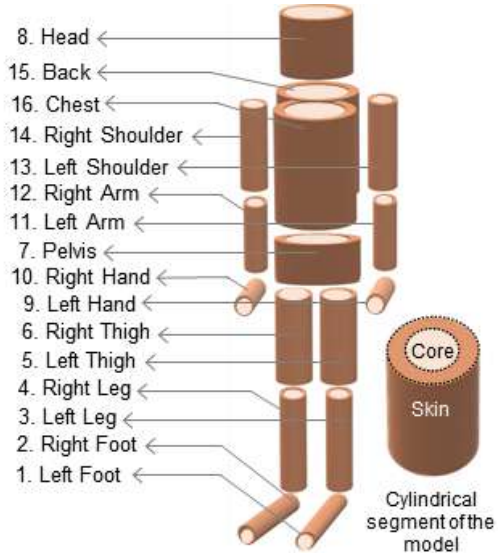

Fig. 1 – Description of segments of the human body in Gagge-2 Core, 16 segment model

Indoor temperature and RH data obtained from real-time monitoring of vernacular and conventional building typologies were used as input parameters for the model. The energy balance between the core and the skin for each segment was expressed as:

$$S_{cr}(i) = M - W[C_{res}(i) + E_{res}(i)] - Q_{cr,sk}(i) \quad (1)$$

$$S_{sk}(i) = Q_{cr,sk}(i) - [C(i) + R(i) + E_{sk}(i)] \quad (2)$$

Here, $C_{res}(i) + E_{res}(i)$ correspond to the respiration at the core of the chest segment.

The rate of change of internal energy in the core and the skin layers is given by:

$$S_{Cr}(i) = \frac{[1 - \alpha(i)]m(i)c_{p,b}\left[\frac{dt_{cr}(i)}{d\theta}\right]}{A(i)} \quad (3)$$

$$S_{sk}(i) = \frac{\alpha(i)m(i)c_{p,b}\left[\frac{dt_{sk}(i)}{d\theta}\right]}{A(i)} \quad (4)$$

Heat losses from each segment, and exchange from the core to the skin (and vice versa) within the segment are given by:

$$C(i) + R(i) = \frac{[t_{sk}(i) - t_o]}{R_t(i)} \quad (5)$$

$$C_{res}(i) + R_{res}(i) = [(0.0014)M(34 - t_o)] + \left[(0.0173)M\left(5.87 - p_{wv,a}\right)\right] \quad (6)$$

$$E_{sk}(i) = w(i)\frac{\left[p_{sk,s}(i) - p_{wv,a}\right]}{R_{e,t}(i)} \quad (7)$$

$$Q_{cr,sk}(i) = \left[K + c_{p,bl}m_{bl}(i)\right][t_{cr}(i) - t_{sk}(i)] \quad (8)$$

For the analysis, air temperature [t_o] was assumed to be the same as operative temperature. RH recorded on-field was used to calculate the partial pressure of ambient air [$p_{wv,a}$]. The total thermal resistance [R_t] and evaporative resistance [$R_{e,t}$] were computed for single-layer, 1.2 mm-thick cotton weave cloth for each body segment using Equations 9 and 10, respectively. Head, left foot, right foot, left hand, and right-hand segments were considered unclothed.

$$R_t(i) = R_a(i) + \left[R_f(i) + R_{al}(i)\right] \quad (9)$$

$$R_{e,t}(i) = R_{e,a}(i) + \left[R_{e,f}(i) + R_{e,al}(i)\right] \quad (10)$$

Segment-wise convective heat transfer coefficients were obtained from (de Dear et al., 1997). Metabolic heat loss [M] and heat loss due to external work [W] was taken as 60 and 30 W/m2, respectively.

2.2 Aggregated Comfort Survey

A questionnaire-based field survey was conducted using an aggregated comfort survey approach (Shastry et al., 2016). 62 occupants living in conventional (Total=32, M=18 and F=14) and vernacular (Total=30, M=13 and F=17) building typologies, aged between 20-56 years, were interviewed. The survey was conducted when the subjects were indoors and not involved in any exhaustive physical activity. Their comfort votes (thermal, respiratory, and skin-related) and health symptoms were recorded for each month of the year. Indoor Air Quality (IAQ) is determined by the constituents of the indoor air (water vapor, carbon dioxide, volatile organic compounds etc.); however, in this study, only indoor air humidity-related skin stickiness/dryness was examined. Also, their clothing, activity (standing, walking, sleeping, lying down), environmental temperature, and RH during the interview were recorded.

3. Results and Discussions

The comfort votes of the occupants (Thermal, Skin-related, and Respiratory) for all the months are shown in Fig. 2. There is a close relation between thermal comfort and the skin-related (IAQ) comfort votes of occupants, suggesting that the occupants felt that their skin was stickier/oilier during warmer months. During the colder months, occupants experienced dry skin. However, the response varied within the building typologies. The response of occupants in vernacular dwellings is more consistent than that of the occupants of conventional buildings. Comfort votes of occupants represents their expectations from the built environment, reflecting adaptive strategies. Skin-related comfort/discomfort is often manifested as a change in thermal comfort vote, making it challenging to discern.

Occupants report neutral respiratory comfort mostly, other than the cold winter months when the Humidity Ratio (HR) of the air goes low. Low HR values can cause serious difficulty in respiration due to inefficient nasal mucociliary clearance, especially in the elderly. As regulated by the building material and anthropogenic factors, the humidity of the indoor air is responsible for maintaining the homeostasis of the human airways (Hugentobler, 2021). Even though the average daily humidity ratio was higher than that suggested by ASHRAE for comfort, i.e., 0.012 kg-wv/kg-da in both the building typologies, a deficit was observed from the saturated (trachea) airway HR of 0.041kg-wv/kg-da (at saturated core temperature 36.7 °C), more so in the winter months. The humidity ratio in the conventional building remains lower than in the vernacular building throughout the year. Also, as illustrated in Fig. 3 and Fig. 4, the diurnal variation of the moisture deficit remains very high in the conventional room, especially when the HR of outdoor air is low in the winters (see Fig. 4).

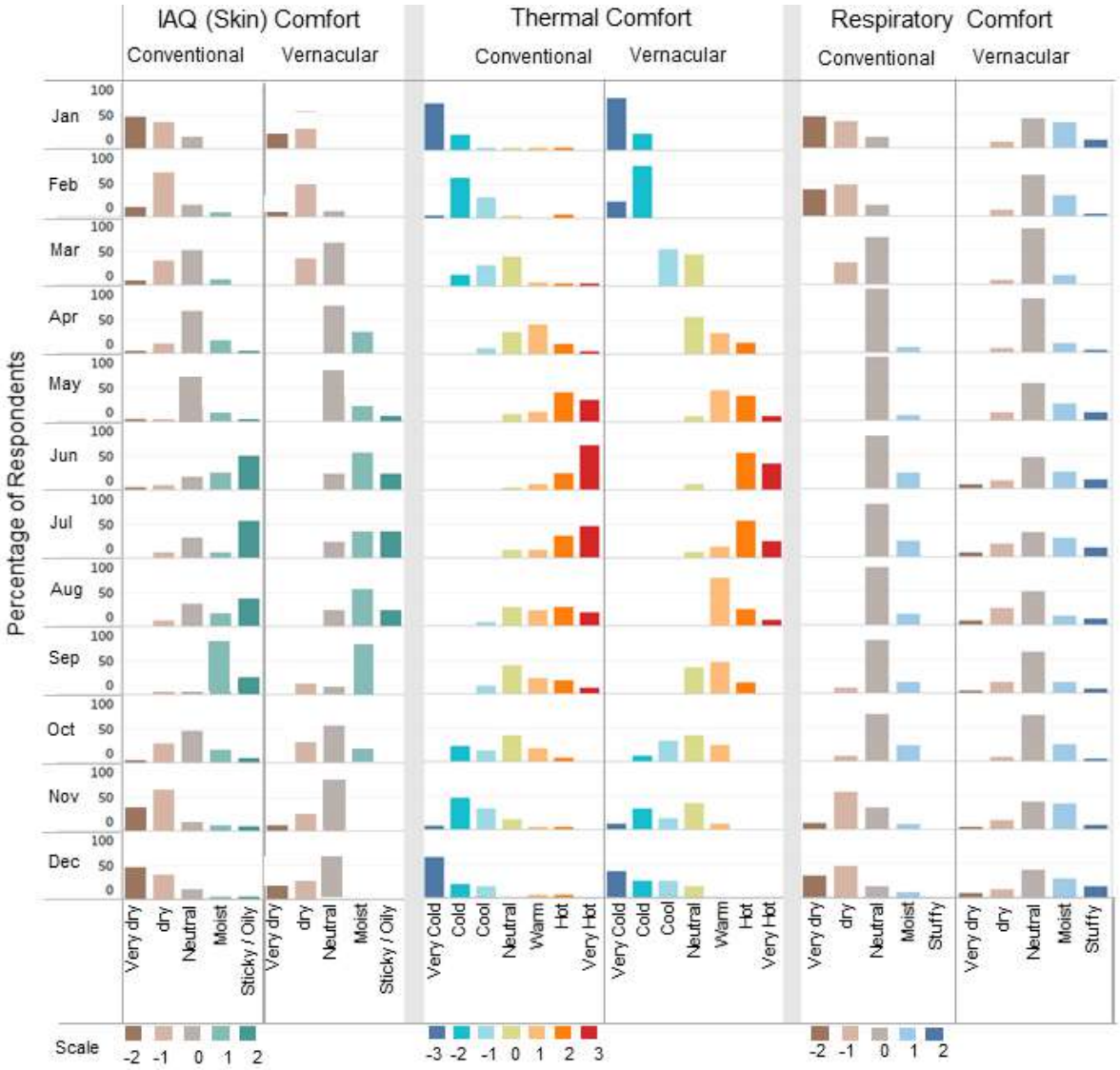

Fig. 2 – Aggregated Comfort Votes of occupants

The equilibrium (heat and mass) between the skin and the indoor air is associated with heat loss or gain by the human body, leading to thermal comfort perception. The local changes in the skin's temperature due to the heat loss/gain to attain equilibrium leads to skin-related discomfort.

In this article, skin temperature and wettedness, computed using the Gagge-2 core model, were used to understand the interaction of skin with indoor air. The system of differential equations for energy balance was solved using an iterative approach until the difference between two consecutive skin temperature values was less than 10^{-8} °Celsius. Convergence of the model was ensured in the entire range of temperature and humidity conditions recorded during the field study.

The trends of Mean Skin Temperature (MTsk), Evaporative heat loss (Esk), and skin wettedness (w) of occupants in different buildings (and outdoors) for four typical seasons, Spring (March), Summer (May), Monsoon (September), and Winter (November) are shown in Figs. 5, 6 and 7, respectively. During September, the average MTsk variation is close to the neutral MTsk; occupants report feeling hot and humid. The corresponding Esk is lower, with higher values of w. This implies that the evaporative losses are restricted in the humid months from the skin causing sweat accumulation on the skin surface, resulting in the occupants feeling sticky.

In November, when the occupants feel cold and dry, the variation in average MT_{sk} is the highest, implying more deviation from the neutral MT_{sk}. However,

even though the MT_{sk} is lower than the neutral, and the human body needs to gain heat, E_{sk} is higher, and the skin is still losing energy. This negative response of the skin is due to active perspiration from the skin (high HR) into the outdoor air (low HR) to attain mass equilibrium, further cooling the skin. This loss of moisture leads to skin dryness.

In May, even though the MT_{sk}, E_{sk}, and w remain the highest, the skin-related (IAQ) comfort vote remains close to neutral. High E_{sk} and moderate w have a cooling effect on the skin, promoting the lowering of skin temperature to the neutral MT_{sk}.

The building clusters in the survey locality are designed to accommodate open, closed, and semi-open spaces (courtyard/verandah). Transitions from outdoor/semi-outdoor to indoors are inevitable for daily activities. Thermoregulation on the skin's surface is perturbed in this transition.

Human skin tries to maintain a balance through active perspiration, leading to a spontaneous skin temperature change. These variations in the skin temperature and wettedness due to environmental air parameters can cause dryness.

In Fig. 8 and Fig. 9, the computed skin temperatures of each body segment in the courtyard (outdoors), vernacular room, and conventional room at different times of the day are illustrated. The indoor environmental parameters in the vernacular buildings are very close to the outdoor environment on the low humidity cold days, implying lowered discomfort. It may be noted that some segments reach MT_{sk} as high as 40° C, which may not occur in reality. The calculated MT_{sk} indicates an equilibrium temperature between the skin and the indoor air. However, the skin responds instantaneously with indoor air temperature/RH perturbation, not necessarily after the equilibrium is reached.

Nonetheless, the temperatures illustrated are valid for understanding the stress that human skin may undergo. Also, the thermal stress on the skin in the courtyard, conventional and vernacular rooms is contrasted.

The change in temperature and RH outdoors diurnally also changes skin parameters. Vernacular indoor environments are regulated, moderating the thermal exchanges between the human body and the indoor air throughout the day.

Other reported health outcomes like colds, coughs, headaches, etc., need further scrutiny for their association with Indoor Environmental Quality (IEQ). Also, the present humidity-related comfort standards need to be validated for their applicability given the varying building typologies, acclimatization, personal habits, and occupants' preferences.

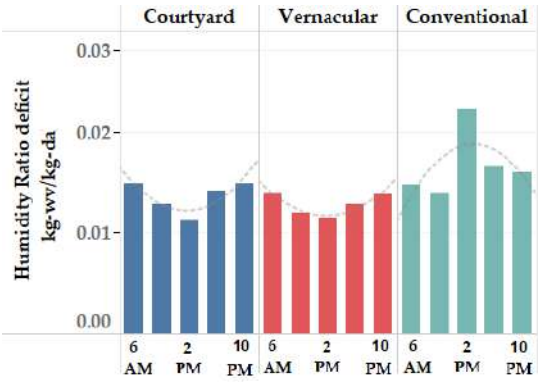

Fig. 3 – HR deficit on highest outdoor humidity day (23 Sept 2020)

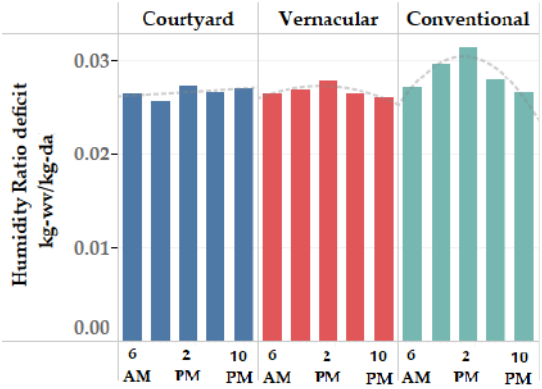

Fig. 4 – HR deficit on lowest outdoor humidity day (4 Nov 2020)

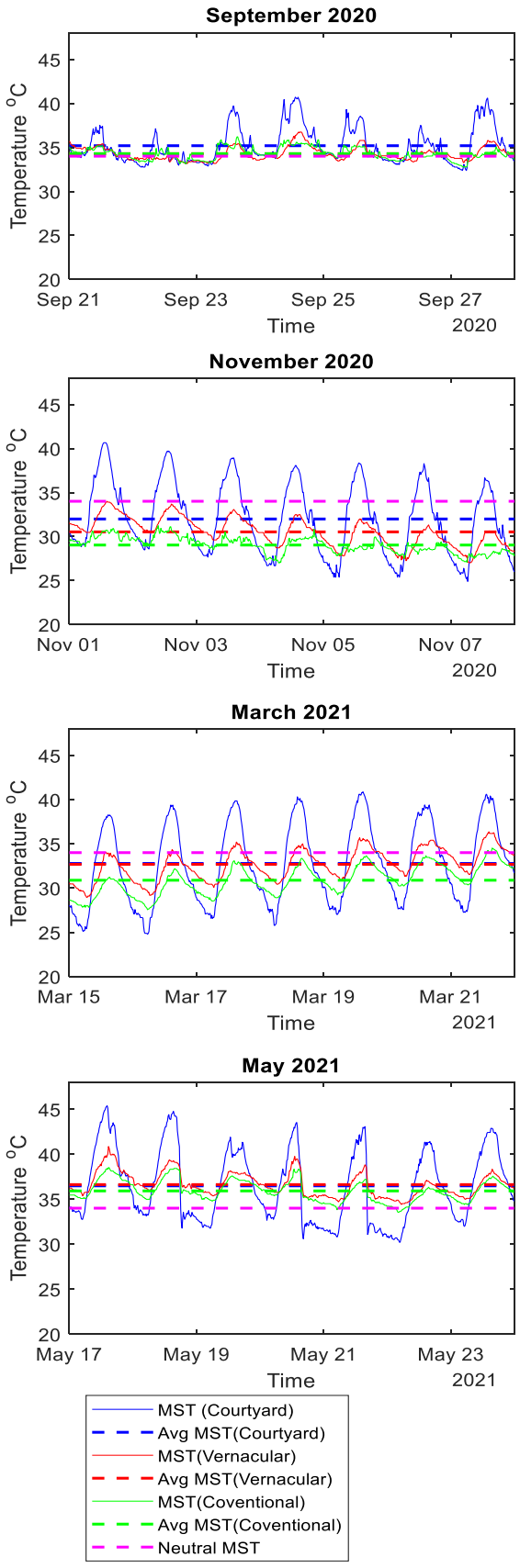

Fig. 5 – Seasonal variations of Mean Skin Temperature in Courtyard, Vernacular and Conventional Rooms

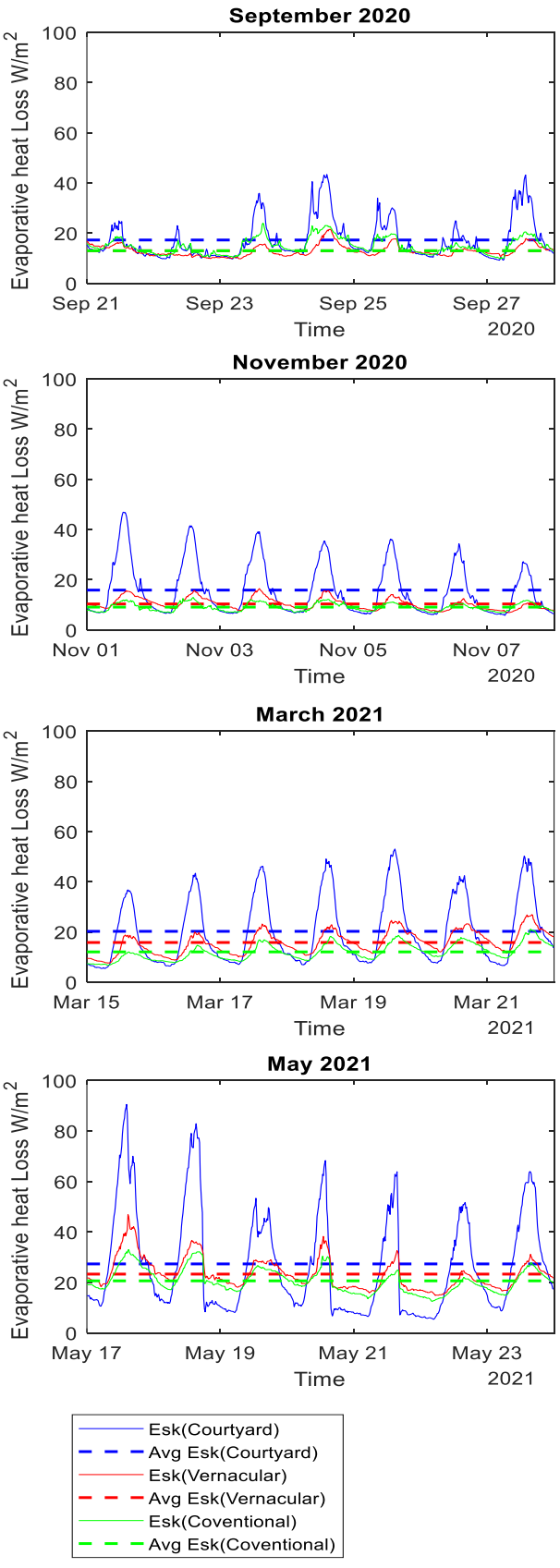

Fig. 6 – Seasonal variations of Evaporative heat loss in Courtyard, Vernacular and Conventional Rooms

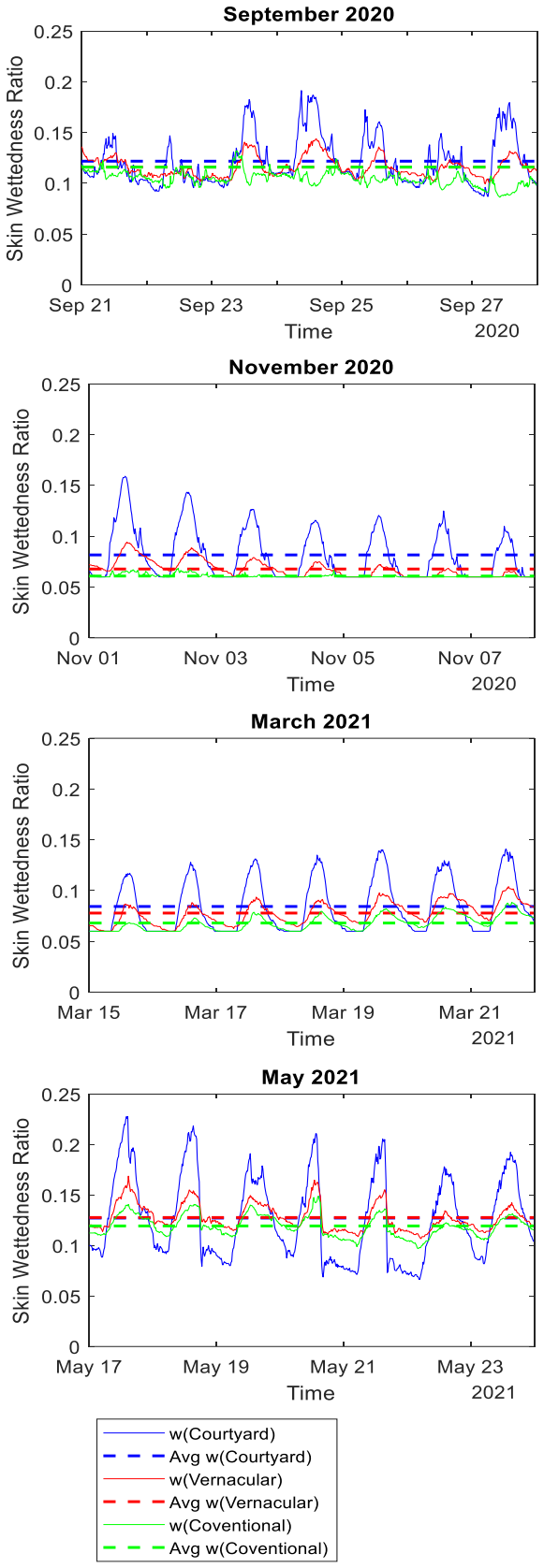

Fig. 7 – Seasonal variations of skin wettedness in courtyard, vernacular and conventional rooms

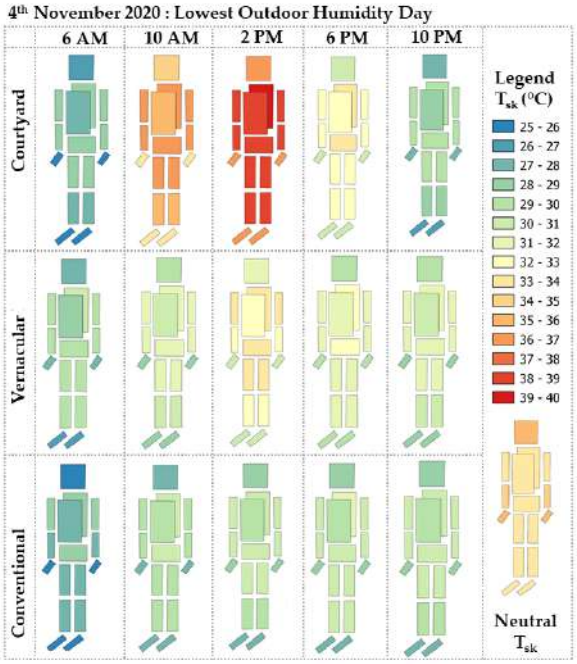

Fig. 8 – Variation of skin temperatures diurnally in the courtyard, vernacular dwelling, and conventional dwelling on lowest outdoor humidity day (4 Nov 2020)

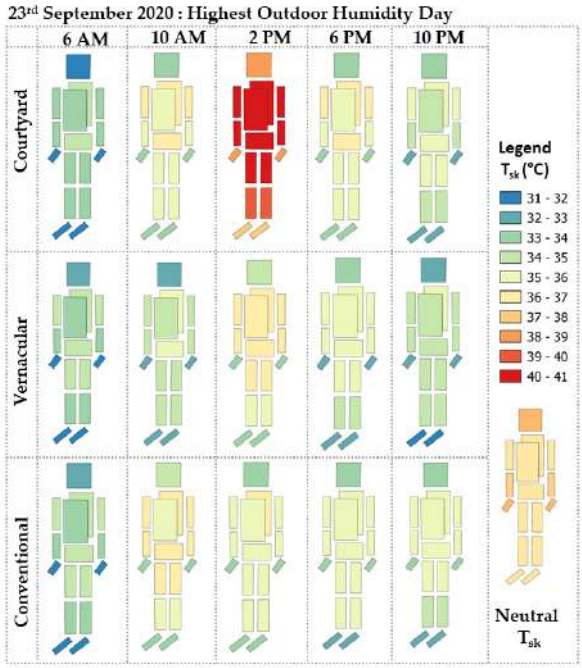

Fig. 9 – Variation of skin temperatures diurnally in the courtyard, vernacular dwelling, and conventional dwelling on highest outdoor humidity day (23 Sept 2020)

4. Conclusion

This study attempts to explain the impact of varying indoor RH in vernacular and conventional building typologies on humidity-related comfort and health outcomes. It involves real-time monitoring and a computational approach. Skin temperature and wettedness were computed corresponding to real-time indoor conditions in vernacular and conventional buildings based on the energy balance between the skin and indoor air. Humidity is an essential determinant of thermal, respiratory, and skin-related comfort, determining everyday habits like clothing, use of cosmetics etc., water intake etc. thereby impacting health. Although the current building simulation tools incorporate examination of thermal comfort associated with humidity, skin and respiratory comfort are not explicitly examined. Integration of this approach in building simulation tools could improve understanding into occupants' skin and respiratory comfort. The results show that building typology (materials) is vital in enhancing humidity-related IEQ parameters. Vernacular dwelling was more conducive to occupants' comfort and health in this study. Vernacular dwellings are earth-based and carry a lower carbon/ecological footprint. There is immense scope for occupant wellness in their adoption in modern buildings.

Acknowledgment

This study was supported by Prime Minister's Research Fellowship at the Indian Institute of Science and the British Academy's Wellbeing achieved from Earthen Residence (WAFER) project (UWB190086).

Nomenclature

Symbols

A	Surface Area (m^2)
$c_{p,b}$	Constant pressure specific heat of tissue (kJ/(kg K))
$c_{p,bl}$	Constant pressure specific heat of blood (kJ/(kg K))
C	Convective heat transfer (W/m^2)
C_{res}	Sensible heat loss due to respiration (W/m^2)
E_{res}	Evaporative heat loss due to respiration (W/m^2)
E_{sk}	Evaporative heat loss from the skin (W/m^2)
HR	Humidity Ratio (kg-wv/kg-da)
i	Body segment (dimensionless)
K	Effective conductance between core and skin ($W/(m^2K)$)
m	Mass (kg)
m_{bl}	Blood flow (core-skin) ($kg/(m^2s)$)
M	Metabolic heat production (W/m^2)
$p_{sk,s}$	Partial pressure of saturated water vapor at skin temperature (kPa)
$p_{wv,a}$	Partial pressure of water vapor in the air (kPa)
$Q_{cr,sk}$	Heat flow from core to skin (W/m^2)
R	Radiative heat transfer (W/m^2)
R_a	Thermal resistance of outer air layer ($m^2°C/W$)
R_{al}	Thermal resistance of intermediate air layer ($m^2°C/W$)
$R_{e,a}$	Evaporative resistance of outer air layer (m^2kPa/W)
$R_{e,al}$	Evaporative resistance of intermediate air layer (m^2kPa/W)
$R_{e,f}$	Evaporative resistance of fabric layer (m^2kPa/W)
$R_{e,t}$	Total evaporative resistance (m^2kPa/W)
R_t	Total thermal resistance ($m^2°C/W$)
S_{cr}	Heat storage in the core (W/m^2)
S_{sk}	Heat storage in the skin (W/m^2)
t_o	Air temperature (°C)
t_{cr}	Core temperature (°C)
$t_{cr,n}$	Neutral core temperature (°C)
t_{sk}	Skin temperature (°C)
$t_{sk,n}$	Neutral skin temperature (°C)
w	Skin wettedness ratio (dimensionless)
W	Heat due to external work (W/m^2)
α	Body mass fraction at the skin (dimensionless)
θ	Time (s)

References

al Horr, Y., M. Arif, A. Kaushik, A. Mazroei, M. Katafygiotou, and E. Elsarrag. 2016. "Occupant Productivity and Office Indoor Environment Quality: A Review of the Literature". *Building and Environment* 105: 369–89. doi: https://doi.org/10.1016/j.buildenv.2016.06.001

Atmaca, I., and A. Yigit. 2006. "Predicting the Effect of Relative Humidity on Skin Temperature and Skin Wettedness". *Journal of Thermal Biology* 31(5): 442–52. doi: https://doi.org/10.1016/j.jtherbio.2006.03.003

de Dear, R. J., K. G. Leow, and S. C. Foo. 1991. "Thermal Comfort in the Humid Tropics: Field Experiments in Air Conditioned and Naturally Ventilated Buildings in Singapore". *International Journal of Biometeorology* 34(4): 259–65. doi: https://doi.org/10.1007/BF01041840

de Dear, R. J., E. Arens, Z. Hui, and M. Oguro. 1997. "Convective and Radiative Heat Transfer Coefficients for Individual Human Body Segments". *International Journal of Biometeorology* 40(3): 141–56. doi: https://doi.org/10.1007/s004840050035

de Dear, R. J., J. Kim, C. Candido, and M. Deuble. 2015. "Adaptive Thermal Comfort in Australian School Classrooms". *Building Research and Information* 43(3): 383–98. doi: https://doi.org/10.1080/09613218.2015.991627

Hugentobler, W. 2021. "Mucociliary Clearance Is Humidity Dependent-Contrary to Common Belief". *Proceedings of the 17th International Healthy Buildings Conference*: 66–69.

Jokl, M. V. 2002. "Thermal Comfort and Optimum Humidity". *Acta Polytechnica* 42(1): 12–24.

Kong, D., H. Liu, Y. Wu, B. Li, S. Wei, and M. Yuan. 2019. „Effects of Indoor Humidity on Building Occupants' Thermal Comfort and Evidence in Terms of Climate Adaptation". *Building and Environment* 155: 298–307. doi: https://doi.org/10.1016/j.buildenv.2019.02.039

Parsons, K. C. 2003. "Human Thermal Environments: The Effect of Hot, Moderate and Cold Environments on Human Health". *Comfort and Performance*: 262–294.

Petty, S. E. 2017. *Indoor Environmental Quality, Forensic Engineering: Damage Assessments for Residential and Commercial Structures*. doi: https://doi.org/10.1201/b14052

Priyadarshani, S., M. Mani, and D. Maskell. 2021a. "Discerning Relative Humidity Trends in Vernacular and Conventional Building Typologies for Occupant Health". *Proceedings of the 17th International Healthy Buildings Conference*: 587–98.

Priyadarshani, S., M. Mani, and D. Maskell. 2021b. "Influence of Building Typology on Indoor Humidity Regulation". *REHVA Journal* 6: 48–52.

Shastry, V., M. Mani, and R. Tenorio. 2016. "Evaluating Thermal Comfort and Building Climatic Response in Warm-Humid Climates for Vernacular Dwellings in Suggenhalli (India)." *Architectural Science Review* 59(1): 12–26. doi: https://doi.org/10.1080/00038628.2014.971701

van Hoof, J., M. Mazej, and J. L. M. Hensen. 2010. "Thermal Comfort: Research and Practice". *Frontiers in Bioscience* 15(2): 765–88. doi: https://doi.org/10.2741/3645

Wolkoff, P., and S. K. Kjærgaard. 2007. "The Dichotomy of Relative Humidity on Indoor Air Quality". *Environment International* 33(6): 850–57. doi: https://doi.org/10.1016/j.envint.2007.04.004

An Investigation Into Thermal Performance of Buildings Built Using Upcycled End-Of-Life Photovoltaic Panels

Roshan R Rao – Indian Institute of Science, India – roshanrao@iisc.ac.in
Suchi Priyadarshani – Indian Institute of Science, India – suchip@iisc.ac.in
Monto Mani – Indian Institute of Science, India – monto@iisc.ac.in

Abstract

End-of-Life, or discarded, Solar Photovoltaic panels are rising in huge numbers every year throughout the world. This is of grave concern as the environmentally safe handling of EoL-PV is not yet established fully. We propose a novel approach to upcycle End-of-Life (EoL)-PV as a building material that can extend the life of PV by another 2~3 decades. PV panels are a multi-layered laminate of different materials. In the course of environmental exposure and use, degradation induces variation in the optical properties of EoL-PV. Variations in thermal properties have not been explicitly examined, which has a bearing on the thermal performance of a building when integrated as a building material. This work studies the influence of the thermal conductivity and solar transmittance of PV panels on the surface temperatures using a steady-state energy balance model. Also, through the whole building simulation, the implications on the mean radiant temperature and the heating/cooling load of the building by using EoL PV compared to a new PV are understood. Other factors, like the area of PV to wall ratio, seasonal changes, and climate zone are found to play a role in the relative changes in the MRT and Heating/Cooling Load attributed to EoL-PV integration in buildings.

1. Introduction

Solar Photovoltaic (PV) installations are growing exponentially worldwide, leaving behind a massive pile of PV waste after its decommissioning. By 2050, cumulative PV waste would be 60~78 million tons (IEA-PVPS and IRENA, 2016). Currently, most PV panels end up in shredders and/or landfills, contaminating and disrupting our ecosystem. We propose a novel approach to upcycle End-of-Life (EoL)-PV as a building material that can extend the life of PV by another 2~3 decades. On another note, the number of people living in slums or informal settlements is over 1 billion, with 80 % in Eastern and South-Eastern Asia, sub-Saharan Africa and Central and Southern Asia. About 3 billion people will require adequate and affordable housing by 2030 (United Nations, 2021).

EoL-PV panels are a low-cost alternate durable option as a building material, and this approach promotes planetary wellness by offsetting the use of conventional materials and preventing toxic elements in PV entering the ecosystem. On using PV panels as a building façade, the occupants are exposed to the backsheet of the PV panel. Backsheet chalking (presence of white coloured powder on the backsheet) is commonly observed in field degraded PV. In a few cases, it has been investigated and discovered to be TiO_2 (Gebhardt et al., 2018), and usage of such PV panels in buildings exposes the occupants to such powders. Also, the release of fluorine from the backsheet has been examined at high temperatures (> 300 °C) (Danz et al., 2019). The release of fluorine at room temperature or the nature of the impact of chalking on occupants has not been understood. Studies involving any emissions from PV backsheet (due to cracking, chalking, burns, etc.) and its negative impact on occupants is essential.

PV panels are laminate of different materials. A typical PV panel configuration is Glass / EVA / Cell / EVA / Backsheet and layers of anti-reflective coating subject to the manufacturer. A commonly observed degradation mode in PV is EVA (ethylene vinyl acetate) discoloration, which occurs due to acetic acid formation (Pern & Czanderna, 1992). Also, the adhesion strength of the EVA (primarily used as an adhesive layer in panels) is compromised in aged PV (Desai et al., 2022), which could lead to delamination of PV panels. A change in vinyl acetate (VA)

content has been reported in the aged PV panel (Desai et al., 2022). VA content change can imply a change in the thermal conductivity of the EVA (Jia and Zhang, 2022) layer in the PV panel. Also, due to discoloration of the EVA layer, optical transmittance is reported to have dropped (Desai et al., 2020; Jeong et al., 2013). Due to the inherent nature of PV panels being composed of multiple layers of different materials, unlike a homogenous panel, physical and chemical changes in any layer impact the optical and thermal properties of the bulk material. Our preliminary investigations include understanding the influence of physical degradation on optical and thermal transmittance of EoL-PV (aged) and its influence on the building's thermal performance and indoor thermal comfort. A steady-state energy balance model is used to understand the effect of changes in optical and thermal properties on PV surface temperatures. When PV panels are integrated as a building elements, multiple other factors influence the thermal performance of the building. Hence, a whole building simulation is performed using Design Builder software with EoL-PV integrated with the building.

2. Methodology

2.1 Energy Balance Model

An optical model considering the interaction of light through multiple layers of PV is used to calculate the spectral transmittance, reflectance and absorptance of the PV panel at each layer (Lu & Yao, 2007). The heat transfer modes among the layers considered are shown in Fig. 1. The transmittance, reflectance, and absorptivity of n (number of layers) layers of the PV panel are calculated using the multi-layered optical model developed (Lu & Yao, 2007).

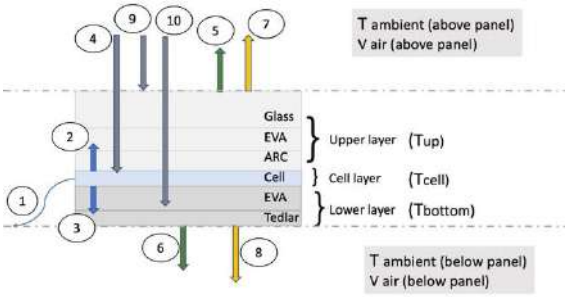

1. Electricity generation
2. Conduction from cell to upper layer
3. Conduction from cell to lower layer
4. Energy from sun, absorbed by cell layer
5. Convective heat from upper layer to air
6. Convective heat from lower layer to air
7. Radiative heat from upper layer (towards sky+ ground)
8. Radiative heat from lower layer (towards sky+ ground)
9. Energy by sun, absorbed by upper layers
10. Energy by sun, absorbed by bottom layers

Fig. 1 - Heat transfer modes at different layers of a typical PV module

A steady-state energy balance model for PV panel is used, which considers the heat transfer through multiple layers of PV panel (Glass, EVA, ARC, Si-cell, EVA, Tedlar). The angle between the sun and the normal to PV panel is calculated using the following equations

$$a = (sin\,\emptyset\,.\,sin\,\delta\,.\,cos\,\beta) - (cos\,\emptyset\,.\,sin\,\delta\,.\,cos\,\gamma_m\,.\,sin\,\beta) \quad (1)$$

$$b = (\sin\emptyset\,.\,cos\,\delta\,.\,cos\,\gamma_m\,.\,sin\,\beta) + (cos\,\emptyset\,.\,cos\,\delta\,.\,cos\,\beta) \quad (2)$$

$$c = (cos\,\delta\,.\,sin\,\gamma_m\,.\,sin\,\beta) \quad (3)$$

$$\theta = cos(a + b\,cos\,\omega + c\,sin\,\omega) \quad (4)$$

Electricity generated depends on the net radiation transmitted through the first three layers and the efficiency of the solar cell (Zarei & Abdolzadeh, 2016). The rate of energy absorption by a Solar cell depends on the absorptivity of the cell layer.

$$\boldsymbol{q_4} = \int_0^\infty A_{cell}(\lambda).\,g(\lambda)\,d\lambda \quad (5)$$

$$\boldsymbol{q_1} = \eta_{electricity} \int_0^\infty \tau_u(\lambda).\,g(\lambda)\,d\lambda \quad (6)$$

Bi-directional (towards the upper and lower layers) conduction from the cell depends on the temperature differences and the thermal conductivity of the corresponding layers (Zarei & Abdolzadeh, 2016).

$$\boldsymbol{q_{2,3}} = \frac{T_{cell} - T_{u,b}}{R_{u,b}} \quad (7)$$

Convective heat transfer occurs at the top layers-air interface, and the bottom layers-air interface is a function of the temperature difference and heat transfer co-efficient. The heat transfer coefficient approximations are adapted from (Zarei & Abdolzadeh, 2016).

$$\boldsymbol{q_{5,6}} = h_{u,b}.\left(T_{u,b} - T_{air-film\,u,b}\right) \quad (8)$$

Radiative heat transfer between the top layers-sky, top layers-ground and bottom layers-sky, bottom layers- ground is a function of view factor and temperature difference (Zarei & Abdolzadeh, 2016).

$$\boldsymbol{q_7} = \varepsilon_u \sigma F_{u,sky,ground} \left({T_u}^4 - {T_{sky,ground}}^4\right) \quad (9)$$

$$\boldsymbol{q_8} = \varepsilon_b \sigma F_{b,sky,ground} \left({T_b}^4 - {T_{sky,ground}}^4\right) \quad (10)$$

$$\boldsymbol{q_{9,10}} = \int_0^\infty A_{u,b}(\lambda,\theta).\, g(\lambda)\, d\lambda \quad (11)$$

The above system of equations was solved for top, bottom, and cell temperatures through an iterative approach. The thickness of Glass, EVA, Cell and Backsheet is in the range of 3~4 mm, 0.4~0.5 mm, 0.2~0.4 mm, and 0.1~0.35 mm, respectively.

The thermal conductivity of Glass, EVA, Cell and Backsheet are in the range of 0.98 – 1.8 W/(m K), 0.23~0.35 W/(m K), 148~150 W/(m K), and 0.2~0.36 W/(m K), respectively (Chamkha & Selimefendigil, 2018; Hammami et al., 2017; Lee et al., 2008; Popovici et al., 2016; Sahli et al., 2018; Syafiqah et al., 2019). The thickness and thermal conductivity used as a base case in the steady-state model: glass (3 mm, 0.98 W/(m K)), EVA (0.5 mm, 0.35 W/(m K)), cell (0.4 mm, 148 W/(m K)), back sheet (0.1 mm, 0.2 W/(m K)).

To understand the influence of the thermal conductivity of each layer on the surface temperatures, thermal conductivity values were varied from -100 % ~ +200 % of the base-case values.

2.2 Design Builder Model

A whole building simulation has been performed for the modified BESTEST case 600FF (DesignBuilder v6.1 with EnergyPlus v 8.9, 2021) model (a block of 6 m X 8 m and height of 2.7 m) (Fig. 2). PV panels have been integrated in the buildings as Glazing integrated Photovoltaics. PV panels are applied to substitute for the walls and roof and not over the existing wall or roof. The properties of the PV (250 Wp typical crystalline Silicon PV panel): (a) front and back emissivity is 0.8, infrared transmittance is 0.2, inside and outside reflectance (solar and visible) is 0.1, and the thermal conductivity, solar transmittance is varied in the range tabulate in Table 1. The PV panels are not connected to any power sources in the simulation and are only considered a building material. Simulations are performed for varying PV area in the wall (varied as window-to-wall ratio in the Design Builder) for two cases, 25 % and 75 %. Multiple scenarios of PV integration in all four walls and roof are considered. The wall (without PV) is the 'BESTEST Lightweight Wall', which has a concrete cast (dense) with a thickness of 0.1m (see Fig. 2). The floor construction is 'BESTEST Ground Floor', which has a thickness of 0.225 m and a U value of 0.039 W/(m² K). The roof (without PV) is 'BESTEST Roof' with a U value of 0.319 W/(m² K) and thickness of 0.1 m. The simulation is performed with an occupancy density of 0.04 people/m² and no furniture/furnishings in the building. The BESTEST building being simulated is a block with a heating and cooling setpoint temperatures of 20 °C and 26 °C, respectively. India has varied climate zones, and simulations are performed for five representative cities corresponding to five climate zones (Table 2).

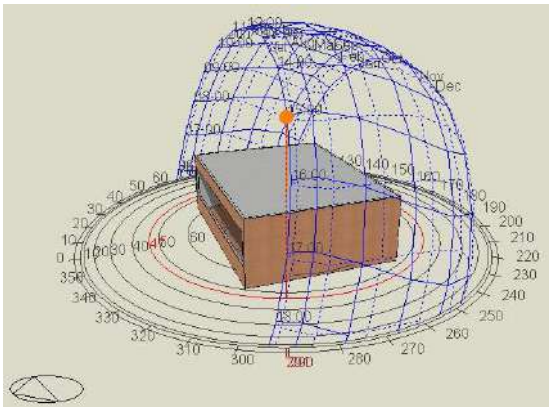

Fig. 2 – Design Builder model (600FF) modified by integrating PV in all the walls and roof

The thermal conductivity of the EVA layer varies due to the variation in the % VA content. An empirical relation has been proposed (Jia et al., 2022) to describe the relationship between thermal conductivity and % VA content.

With ageing, a maximum change in VA content in EVA was seen, with an increase from 18.1 % to 21.9 % (Desai et al., 2022). This is estimated to cause a drop in thermal conductivity of EVA and the bulk of PV panels. But this does not explain any changes in the bulk thermal conductivity. There are possibilities of reduction in the thickness (Hu et al., 2016; Jahn, 2018) of the back sheet due to weathering, and

this can cause the bulk thermal conductivity to rise. Hence, there is a possibility that the bulk thermal conductivity may get altered depending on the combination and severity of multiple degradation modes. To accurately quantify the change in thickness, thermal conductivity of the individual layers and bulk properties associated with aged PV panels (EoL-PV) requires sophisticated measurements. To broadly understand the impact of such a change at the building level, we have varied the bulk thermal conductivity (equivalent thermal conductivity of a PV panel including all the layers) and solar transmittance of the PV panels in 5 steps each. A total of 25 scenario combinations of PV panel have been considered for whole building simulations (Table 1).

Table 1 – Range of Thermal conductivity and Solar Transmittance values. Corresponding SHGC and U-value of all the possible combinations

Parameter	Range	Steps
Thermal Conductivity	0.1 ~ 2.8 W/(m K)	0.7 W/(m K)
Solar Transmittance	0.1 % ~ 16 %	4 %
SHGC (calculated)	0.271 ~ 0.408	-
U- Value (calculated)	4.763 ~ 5.782 W/(m^2 K)	-

Table 2 – The representative cities selected for each climate zone in India

Climate Zone	City	Lat/Long (^{o}North / ^{o}East)	Mean Daily Temp ($^\circ$C) (min ~ max)
Temperate	Bangalore	12.97 / 77.58	15.0 ~ 33.9
Composite	Lucknow	26.75 / 80.88	7.3 ~ 40.3
Warm-Humid	Kolkata	22.65 / 88.45	13.7 ~ 35.7
Hot-Dry	Ahmedabad	23.07 / 72.63	13.1 ~ 41.4
Cold	Shillong	25.58 / 91.89	4.4 ~ 24.0

To allow for a comparative assessment between an EoL PV panel and a new panel, the new panel has been considered to have a thermal conductivity of 0.7 W/(m K) and 8 % solar transmission. Mean Radiant Temperature (used as a heat index to indicate thermal comfort) and Heating/Cooling loads resulting from 25 combinations of PV panels have been analyzed. Simulations are performed to understand the influence of PV covered area to wall area ratio, the direction of the envelope on which the PV panels are integrated and Climate zone.

3. Results and Discussion

When the thermal conductivity of the glass layer is varied from -100 % to 200 % of its reference value (0.9 W/(m K)), the top layer's thermal resistance increases exponentially with the decrease in the thermal conductivity of glass. The increase in the thermal resistance in the top layer causes a drop in the rate of conduction heat transfer between cell and top layer. This causes a reduction in the top layer energy, as the radiation absorption by the top layer is unaffected by the change in the thermal conductivity of the glass. The decrease in the top layer energy is associated with the reduction in the top layer temperature. As the energy balance between energy into the cell and out of the cell has to be maintained at the steady-state, the conduction heat transfer between cell-bottom layer increases. This causes the bottom layer energy to increase and results in the rise in temperature of the bottom layer (Fig. 3). Each layer's thermal conductivity variation impacts the PV panel's bulk thermal conductivity (equivalent thermal conductivity). The PV panel's bulk thermal conductivity (equivalent thermal conductivity) was varied to understand the bottom surface temperature variation, as this is the surface that will interact with the indoor air when integrated in the building. A surface temperature calculation is made for the scenario where the PV panel is horizontal, and solar radiation of 900 W/m^2 is incident on the PV panel (Fig. 4). Further, in the whole building simulation, the degradation of PV was parameterized as a variation in solar transmittance (tau) and thermal conductivity (k) (equivalent thermal conductivity) of PV. The different scenarios of PV are compared with the base case of PV, and only relative changes in MRT and Heating Cooling load with respect to the base case is reported throughout.

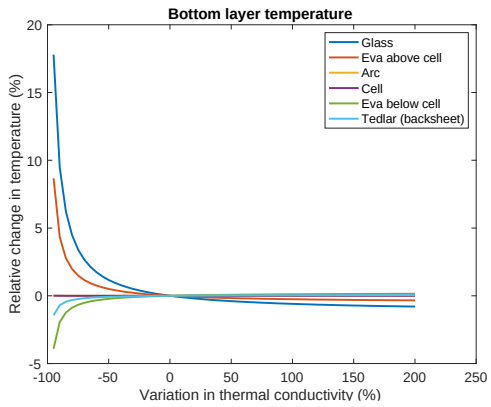

Fig. 3 – Bottom surface temperature variation with variation in the thermal conductivity of each layer of PV module

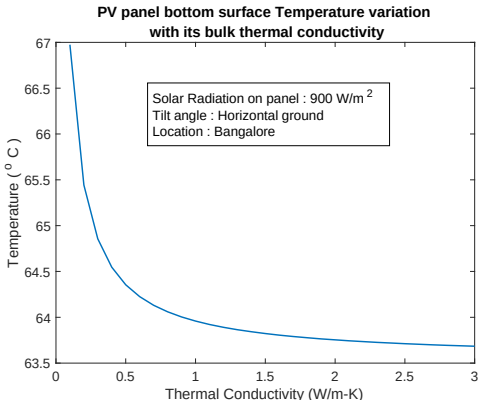

Fig. 4 – PV bottom surface temperature variation with the bulk thermal conductivity of PV panel (equivalent thermal conductivity of PV panel)

PV was integrated in the roof, and a typical summer week simulation revealed that, as the solar transmittance drops, there is about 2 % and 15 % drop in the relative change in Mean Radiant Temperature (MRT) and Heating Cooling load, respectively (Fig. 5). We understand from the literature that there are higher chances of solar transmittance drop due to EVA degradation, glass degradation, etc. The maximum and minimum relative changes in MRT and Heating Cooling load occur at maximum and minimum solar transmittance conditions. A typical summer week and winter week are compared for the maximum and minimum relative changes. Fig. 6 shows that the ranges of relative changes are broadened during winter, indicating that the external temperature has a role in indoor and MRT changes.

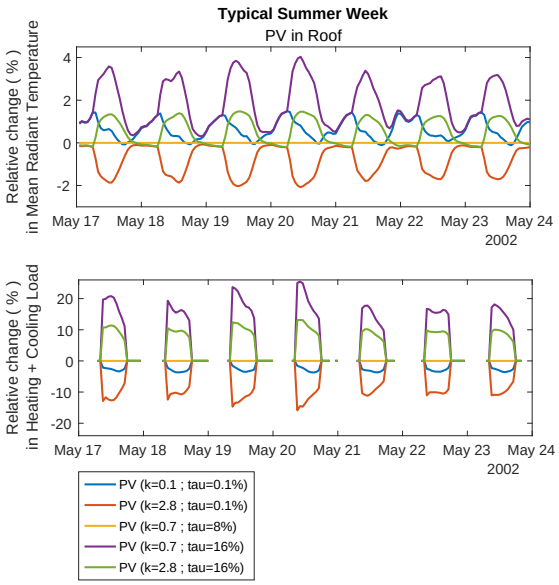

Fig. 5 – Relative change (%) in the Mean Radiant Temperature and Heating+Cooling Load for a typical summer week in Bangalore

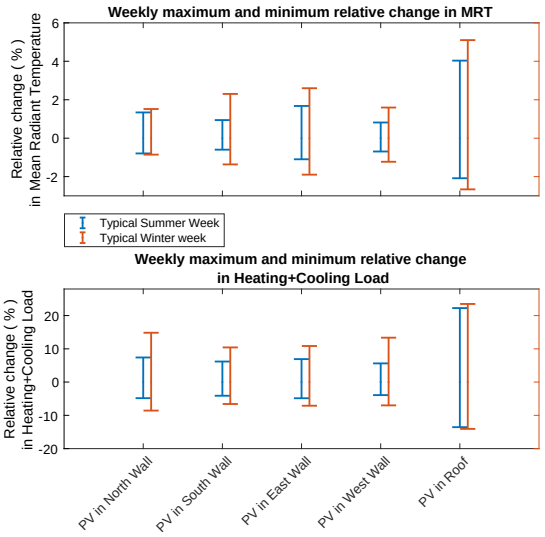

Fig. 6 – Weekly maximum and minimum relative change in MRT and Heating+Cooling Load when PV is integrated in North wall, South wall, East wall, West wall and Roof

The relative changes in MRT and Heating Cooling load variation with thermal conductivity of PV are investigated with a simulation of PV in the roof for a summer month (Fig. 7). The trend is similar to the trend observed using the steady-state energy balance model at the PV panel level (Fig. 4). The area ratio of PV to the wall also magnifies the range of minimum and maximum relative changes in the MRT and Heating Cooling load (Fig. 8).

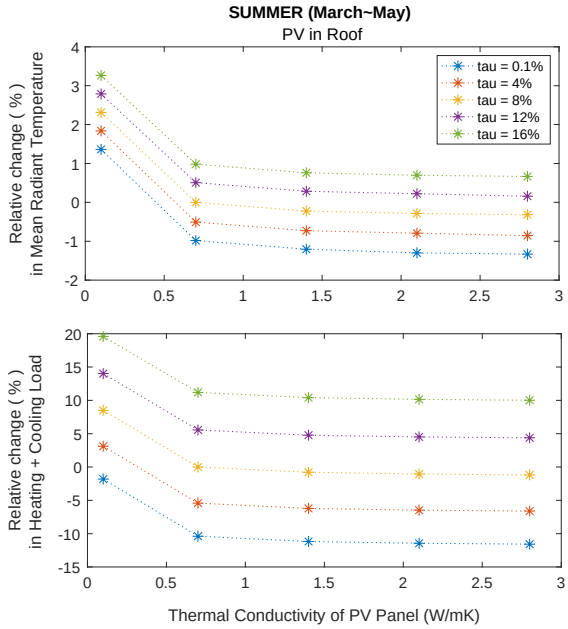

Fig. 7 – Influence of Solar Transmittance and Thermal Conductivity on the Relative change in MRT and Heating+Cooling Load

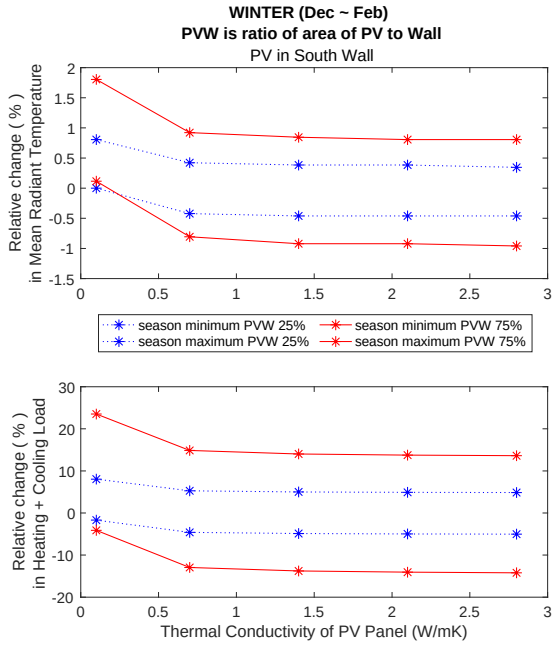

Fig. 8 – Influence of ratio of PV area-to-wall area on minimum and maximum relative changes in annual mean MRT and heating/cooling load

Annual mean MRT and Heating Cooling loads are calculated based on simulations run for all the days of the year. Such a simulation was performed to compare the relative changes in different climate zones and the location of application of PV in a building.

Annual Minimum relative change (%) in MRT

	North	South	East	West	Roof
Bangalore	-0.3824	-0.5977	-0.5568	-0.5241	-1.453
Ahmedabad	-0.2911	-0.5626	-0.5306	-0.4654	-1.388
Lucknow	-0.346	-0.6282	-0.522	-0.5281	-1.44
Kolkata	-0.2579	-0.5005	-0.3276	-0.4323	-1.112
Shillong	-0.823	-0.3065	-0.8039	-1.087	-1.963

Annual Maximum relative change (%) in MRT

	North	South	East	West	Roof
Bangalore	0.9178	1.121	0.928	0.9734	3.702
Ahmedabad	0.5459	0.8439	0.7075	0.6445	3.311
Lucknow	0.7305	1.109	0.8949	0.8299	3.567
Kolkata	0.5158	0.7508	0.5461	0.6844	2.813
Shillong	1.875	0.6567	1.697	1.914	5.207

PV location

Fig. 9 – Minimum and Maximum relative changes in annual mean MRT for different cities and PV application location in building

Fig. 9 and Fig. 10 tabulate the relative changes in the annual mean MRT and Heating Cooling load for different cities and the location in the building where PV is applied. The application of EoL PV on the roof seems to be more beneficiary in terms of reduction in MRT and Heating Cooling load. This could be possible due to the larger area exposed to the sun for longer hours than the walls.

4. Conclusion

This work has discussed a novel approach to upcycle EoL PV panels into building applications. The bottom surface temperature of PV rises when the thermal conductivity of the PV panel reduces. Specifically, glass layer's thermal conductivity variation has a dominant impact on temperature variation due to its thickness. Furthermore, whole building simulations also confirm the exponential temperature variation of mean radiant temperature with thermal conductivity. Our simulation indicates a drop of about 2 % in MRT and close to 13 % in Heating Cooling load due to the loss in solar transmittance and thermal conductivity of PV. The reduction of solar transmittance due to EVA degradation is widely reported in the literature, making it favorable for EoL PV in building applications. The application of EoL PV on the roof seems to be more beneficiary in terms of reduction in MRT and Heating Cooling load.

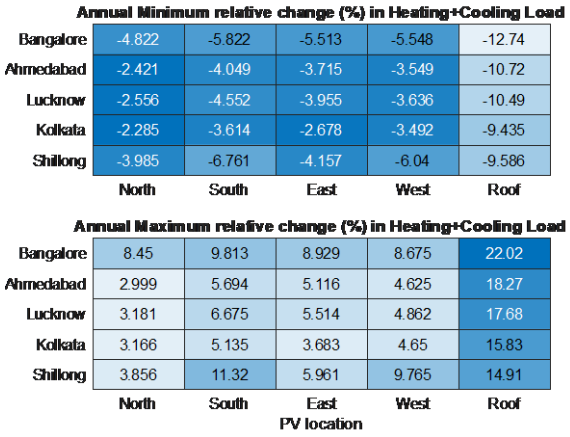

Fig. 10 – Minimum and Maximum relative changes in annual mean Heating Cooling load for different cities and PV application location in building

The benefit is achieved in the case of lower solar transmittance conditions, which also implies lesser daylight entry into the building. The implication of this on the marginal rise in electricity consumption for artificial lighting is the scope of further study. There is no significant difference in the magnitude of relative changes in MRT or Heating Cooling loads at different climate zones. At this point, it can be argued that application of EoL PV has the potential to be used as a building material in general and provide better thermal performance at the same time. A more detailed understanding of the variations of optical and thermal properties due to different degradation modes permits us to speculate on the possible implication of EoL-PV applications in buildings more accurately.

Nomenclature

Symbols

$A_{cell,u,b}$	Absorptivity (cell, upper or bottom layers)
$F_{b,sky,ground}$	View Factor (bottom layer - sky or bottom layer - ground)
$F_{u,sky,ground}$	View Factor (upper layer - sky or upper layer - ground)
$h_{u,b}$	Convectional heat transfer coefficient (W/m²K) (upper or bottom layers)
$R_{u,b}$	Resistance in conduction (K/W) (upper or bottom layer)
$T_{air-film\ u,b}$	Temperature (°C) (air film upper or bottom layers)
$T_{cell,u,b}$	Temperature (°C) (cell, upper or bottom layer)
$T_{sky,ground}$	Temperature (°C) (sky or ground)
$\eta_{electricity}$	PV conversion efficiency
$\tau_{u,b}$	Transmittivity (upper or bottom layers)
$\emptyset$	Latitude
g	Solar radiation (W/m²) incident on PV panel
tau	Solar Transmittance
β	Tilt angle (degrees from horizontal)
δ	Declination angle (degrees)
θ	Inclination angle (degrees) between sun and normal to PV panel
ω	Hour angle (degrees)

References

Chamkha, A. J. and F. Selimefendigil. 2018. "Numerical Analysis for Thermal Performance of a Photovoltaic Thermal Solar Collector with SiO2-Water Nanofluid". *Applied Sciences* 8(11). doi: https://doi.org/10.3390/app8112223

Danz, P., V. Aryan, E. Möhle, and N. Nowara. 2019. "Experimental Study on Fluorine Release from Photovoltaic Backsheet Materials Containing PVF and PVDF during Pyrolysis and Incineration in a Technical Lab-Scale Reactor at Various Temperatures". *Toxics* 7(47).

Desai, U., B. K. Sharma, A. Singh, and A. Singh. 2020. "Enhancement of Resistance against Damp Heat Aging through Compositional Change in PV Encapsulant Poly (Ethylene-Co-Vinyl Acetate)". *Solar Energy* 211: 674–82. doi: https://doi.org/10.1016/j.solener.2020.09.083

Desai, U., B. Kumar Sharma, A. Singh, and A. Singh. 2022. "A Comparison of Evolution of Adhesion Mechanisms and Strength Post Damp-Heat Aging for a Range of VA Content in EVA Encapsulant with Photovoltaic Backsheet". *Solar Energy* 231: 908–20. doi: https://doi.org/10.1016/j.solener.2021.12.031

DesignBuilder v6.1 with EnergyPlus v 8.9, ANSI/ASHRAE Standard 140-2017 Building

Thermal Envelope and Fabric Load Tests - Validation Report, 2021.

Gebhardt, P., L. P. Bauermann, and D. Philipp. 2018. "Backsheet Chalking - Theoretical Background and Relation to Backsheet Cracking and Insulation Failures". In *35th European PV Solar Energy Conference and Exhibition*.

Hammami, M., S. Torretti, F. Grimaccia, and G. Grandi. 2017. "Thermal and Performance Analysis of a Photovoltaic Module with an Integrated Energy Storage System". *Applied Sciences* 7(11). doi: https://doi.org/10.3390/app7111107

Hu, H., W. M. Wang, O. Fu, A. Bradley, T. Felder, W. Gambogi, and T. J. Trout. 2016. "Typical Photovoltaic Backsheet Failure Mode Analysis under Different Climates in China". *SNEC International Photovoltaic Power Generation Conference*.

IEA-PVPS and IRENA. 2016. *End-of-Life Management: Solar Photovoltaic Panels*.

Jahn, U. 2018. *Methoden Zur Fehlererkennung Bei PV-Modulen Und Anlagen-Qualitaetssicherung Im Feld*, pp. 1–22.

Jeong, J. S., and N. Park. 2013. "Field Discoloration Analysis and UV/Temperature Accelerated Degradation Test of EVA for PV". *2013 IEEE 39th Photovoltaic Specialists Conference (PVSC)*.

Jia, Y. and J. Zhang. 2020. "Thermal Conductivity of Ethylene-Vinyl Acetate Copolymers with Different Vinyl Acetate Contents Dependent on Temperature and Crystallinity". *Thermochimica Acta* 708:179141. doi: https://doi.org/10.1016/j.tca.2021.179141

Lee, B., J. Z. Liu, B. Sun, C. Y. Shen, and G. C. Dai. 2008. "Thermally Conductive and Electrically Insulating EVA Composite Encapsulant for Solar Photovoltaic (PV) Cell". *Express Polymer Letters* 2(5): 357–63. doi: https://doi.org/10.3144/expresspolymlett.2008.42

Lu, Z. H., and Q. Yao. 2007. "Energy Analysis of Silicon Solar Cell Modules Based on an Optical Model for Arbitrary Layers". *Solar Energy* 81: 636–47, 2007. doi: https://doi.org/10.1016/j.solener.2006.08.014

Pern, F. J., and A. W. Czanderna. 1992. "Characterization of Ethylene Vinyl Acetate (EVA) Encapsulant: Effects of Thermal Processing and Weathering Degradation on Its Discoloration". *Solar Energy Materials and Solar Cells* 25(1–2): 3–23, 1992. doi: https://doi.org/10.1016/0927-0248(92)90013-F

Popovici, C. G., S. V. Hudişteanu, T. D. Mateescu, and N. C. Cherecheş. 2016. "Efficiency Improvement of Photovoltaic Panels by Using Air Cooled Heat Sinks". *Energy Procedia* 85: 425–32. doi: https://doi.org/10.1016/j.egypro.2015.12.223

Sahli, M., J. P. de Magalhaes Correia, S. Ahzi, and S. Touchal. 2018. "Thermomechanical Investigation of PV Panels Behaviour under NOCT Conditions". *Proceedings of 2017 International Renewable and Sustainable Energy Conference, IRSEC 2017*. doi: https://doi.org/10.1109/IRSEC.2017.8477292

Syafiqah, Z., N. Amin, M. Irwanto, W. Z. Leow, and A. R. Amelia. 2019. "Thermal and Electrical Study for PV Panel with Cooling System". *Indonesian Journal of Electrical Engineering and Computer Science* 17(2): 941–49, 2019. doi: http://doi.org/10.11591/ijeecs.v7.i2.pp492-499

United Nations. 2021. *Make Cities and Human Settlements Inclusive, Safe, Resilient and Sustainable*.

Zarei, T., and M. Abdolzadeh. 2016. "Optical and Thermal Simulations of Photovoltaic Modules with and Without Sun Tracking System". *Journal of Solar Energy Engineering* 138(1): 1–12. doi: https://doi.org/10.1115/1.4031684

Determining the Energy Benefits from Passive Solar Design Integration through the Sensitivity Analysis of Different Case Studies

Giacomo Cillari – University of Pisa, Italy – giacomo.cillari@phd.unipi.it
Alessandro Franco – University of Pisa, Italy – alessandro.franco@unipi.it
Fabio Fantozzi – University of Pisa, Italy – fabio.fantozzi@unipi.it

Abstract

The increasing energy demand of our buildings is putting stress on the building systems and energy grids in terms of need for efficiency improvements. The maximization of the overall performance requires a multidisciplinary approach towards seeking innovative solutions to help reduce the building loads. In terms of efficient energy planning, the building design phase has often been often disregarded or looked at from a single point of view. In this case, research places its attention either on the performance of the opaque or transparent envelope to define optimization criteria. A comprehensive analysis of the impact of different passive solutions on the energy demand of buildings with different uses is the core of the present paper. The main goal is to define design guidelines for the integration of simple to complex passive configurations into the building design to help reduce the heating demand by better exploiting solar radiation. The paper gathers data from 384 simulations, on different test buildings, with the permutation of various design parameters, including window-to-wall ratio, wall heat transfer coefficient and heat capacity. Simulations were run in two different locations, typical of southern and northern Italian climate conditions, for both residential and office use. After the best solutions according to the heating or total energy performance over a nominal year were highlighted, the guidelines were applied to a case study. The aim is to determine a methodology to properly integrate passive solutions on the basis of energy performance. This performance, indeed, constitutes a trade-off of the potential of passive systems to understand when it can be profitable to integrate these. The building analyzed, a cohousing project still in the design phase, showed that 10 to 16 % of the total energy demand can be saved. The energy saving is reached by simply integrating and declining the passive configuration suggested with marginal modifications to the initial design.

1. Introduction

The impact of the residential sector share on global energy consumption is known to be relevant. Therefore, practice has increasingly paid attention to energy conservation and efficiency strategies, use of efficient building plants and, recently, integration of renewable energy systems (RES). Among the latter, photovoltaic and solar thermal technologies have spread all over the market as the most user-friendly RES to integrate into buildings (O'Shaughnessy et al., 2018), but proper sizing and management of these systems is crucial to avoid wasting the energy produced (Cillari et al., 2021a and 2021b). From the perspective of nearly-zero-energy buildings (Albayyaa et al., 2019), the rational use of available sources must be further increased. Solar energy being one of the most suitable for exploitation in the building sector, the design of the building envelope must take into account the impact of an integrated passive solar system (Bajcinovci & Jerliu, 2016). to maximize the potential benefits,. Even if passively exploiting green and renewable energy, such as solar radiation, can be regarded to as a relevant advantage in the application of these solutions, their integration, especially in modern buildings, has been limited to a few, broad projects, due to the prediction of the final performance being hard to estimate. The prediction of passive solar potential on a suburban scale may help the performance of neighborhood design and find the optimal starting configuration (Nault et al., 2017). The energy behavior of the passive solar design, however, is influenced by many different factors, either intrinsic or extrinsic to the design, from latitude and orientation to specific solution details, such as cavity depth (Cillari et al.,

2021a and 2021b). Various optimization techniques and objective functions can be used to improve the behavior of solar passive design due to its multi-disciplinary nature, as it can positively affect heating, cooling, lighting and ventilation demand (Stevanović, 2013).

Based on the operational characteristic of each solution, such as adaptability, overheating sensitivity and estimated cost, a schematic view of different suggested solutions has been already proposed (Cillari et al., 2020). The present work deals with the modeling of the integration of different passive solar solutions and evaluation of the related energy results achievable. The purpose is to define a methodological approach for the integration of such solutions based on the trade-off regarding their energy performance. To deal with different affecting parameters, a permutation of the most impactful factors was implemented, as described in Methodology, Section 2. Section 3 presents the results and discussion of both general investigation and case study. Finally, conclusions are drawn in Section 4.

2. Methodology

Passive strategies are usually divided, according to the relative position of the solar collector, the thermal mass and the indoor environment, into direct gain systems, indirect systems, and isolated gain systems (Givoni, 1991). In the first category, we have wide windows systems, shading systems and solar paintings, while indirect gain systems include the most complex configurations, such as roof pond, massive and Trombe walls. The last class consists of sunspaces and Barra-Costantini systems. In order to develop a comprehensive analysis of passive solar design, four different solutions were analysed, namely *direct gain systems*, *Trombe walls*, *direct sunspaces* and *nanopainting*, which can affect cooling savings. The present investigation is based on a sensitivity analysis of these passive configurations through an extensive dynamic energy simulation with the software EnergyPlus™. Simulations are based on two different climate conditions and building destinations: residential and office buildings in location 1, Palermo, and location 2, Bolzano. The two climatic contexts are defined by an average annual solar irradiation of 1673 kWh/m² and 1218 kWh/m² respectively, with an average air temperature of 18.8 °C and 13.7 °C. Maximum, minimum and average monthly temperature and average monthly global horizontal solar radiation are shown for the two locations in Fig. 1. The three orientations were investigated. Lightweight and heavyweight structures were considered for the simulation, with average heat capacity per unit area values using 30-cm-thick concrete and wooden structures as a reference.

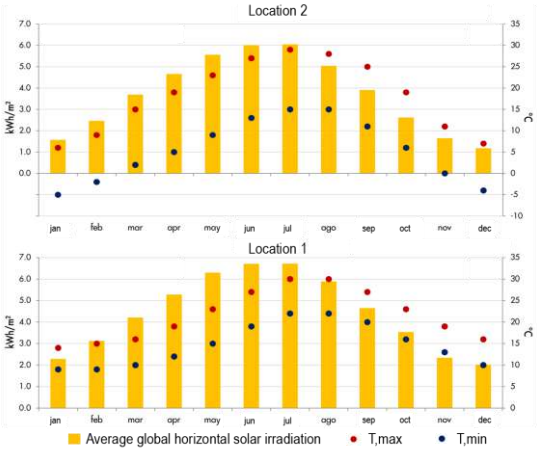

Fig. 1 – Temperature and radiation for location 1 and 2

The direct gain systems simulation consists of the increase of the reference window-to-wall ratio (WWR), according to Table 1, as with glass U-values. The Trombe wall was simulated as a detached thermal zone, with different constructions for the heat capacity and the WWR of the outer glass collector values of Table 1. Within the air cavity of the zone, for the modeling of the Trombe Wall, the ISO 15099 correlation, as validated by (Ellis, 2003), was adopted. For the summer period, the following equation was used to model the thermal chimney behavior of the opened air cavity:

$$Q = C_d A_o \sqrt{[2*(T_{fo}-T_r)/(T_r)*gL]/(1+A_{rt})^2} \quad (1)$$

$$A_{rt} = A_o/A_i \quad (2)$$

where C_d is the discharge coefficient, A_o and A_i are the cross-sectional areas of air channel outlet and inlet, respectively, T_{fo} is the outlet air temperature,

T_r is the room air temperature and L is the total length of the thermal chimney. The sunspace was simulated as a detached sunspace, thus in a different thermal zone, with a local airflow network. Walls and roof are completely glazed; the floor construction is the same of the main building. Finally, nanopainting characteristics were included in the outer plaster layer of the wall, according to reflexivity and emissivity parameters of Table 1. For each passive solution analysed, the simulation included all the permutation of the two values of each parameter. To manage the results, an alphanumeric code was adopted based on the acronyms in brackets showed in Table 1. The simulated building, with average heat transmittance coefficients given in Table 2, has a surface-to-volume ratio of 0.715 over 77.44 m^2.

The sensitivity analysis of the parameters listed with relative ranges of variation in Table 1 provides results based on the mutual effects of common design factors already investigated in previous research separately, such as orientation (Morrissey et al., 2011), glass U-value (Nielsen et al., 2001) and thermal mass (Albayyaa et al., 2019).

As the objective is to gain potential energy savings during the heating season, the simulation is set accordingly. The blinds activate in winter to reduce night losses, and in the summer period, when the solar radiation on the windows rises over 250 W/m^2. Natural ventilation was added in summer, reproducing full opening of the windows in daytime during building occupation. The aim and novelty of the analysis is to provide not an optimization method, but a preliminary optimized set of parameters for specific solutions. Through the application to a case study, the scope is to determine an energy-related trade-off for the possible application of such passive solutions providing designers with a starting set of design parameters to investigate the benefits of integrating passive solutions in their projects. A multi-objective approach, including comfort indexes to modify system set points according to an adaptive approach, will be explored in future work.

Table 1 – Acronyms of the alphanumeric code

Category	**Acronyms**	**Characteristics/Value**
Building reference	B1	
Building destination	R	Residential
	O	Office
Location	L1	Palermo
	L2	Bolzano
Passive solution	DG	Direct gains
	TW	Trombe wall
	SS	Sunspace
	NP	Nanopainting
Orientation	E	East
	W	West
	S	South
Window to Wall Ratio (WWR)	*first parameter*	0.2 – 0.6
Glass U-value [W/m^2K]	*second parameter*	0.8 - 2.3/1.0*
Heat capacity per unit area [kJ/m^2K]	*third parameter (TS1-TS2)*	160-800
Reflectivity	*fourth parameter*	0.1 – 0.9
Emissivity	*fifth parameter*	0.1 – 0.9

**limit in North Italy*

Table 2 – Heat transfer coefficients of building constructions

Construction	**U-value [W/(m^2K)]**
Roof	2.2
Floor	2
Wall	1.26

3. Discussion of the Results

3.1 Passive Solar Design Guidelines

On the basis of Table 1, four reference cases can be detected, based on location and building use: Table 3 shows the related energy demand.

Table 3 – Energy demand of the reference cases

CODE ID	Heating demand [kWh]	Cooling demand [kWh]	Total demand [kWh]
B1_R_L1	961	1671	2632
B1_O_L1	977	1896	2873
B1_R_L2	4494	391	4885
B1_O_L2	2854	436	3290

It can be noticed that a slight difference occurs in terms of destination for L1, larger in L2. In this section, the best results of each specific simulated solution from the sensitivity analysis in terms of heating and global energy saving are introduced. **Direct gain** systems show the highest performance in residential applications and close to the highest in offices. From Fig. 2 it is clear how south can be seen as the best orientation option, with more thermal mass needed in the northern areas. **Trombe wall** systems perform slightly better than direct gains in offices, with a still-high share of energy saving in residential buildings. Fig. 3 highlights how south-bound systems are still the best choice, with heavyweight structures generally preferred, to limit nighttime losses and prevent excessive heat transfer from the air cavity. **Sunspace** best configurations still include south, with one west-bound configuration, as in the previous cases. In this scenario, the heavyweight system is preferred due to the high amount of solar radiation to dispose of. As described by Fig. 4, they perform better in residential applications, thanks to the delay guaranteed by the thermal mass. **Nanopainting**, in Fig. 5 shows very low shares for heating performance, while they mainly impact on the cooling load.

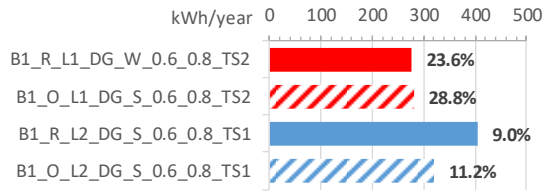

Fig. 2 – Best direct gain configurations

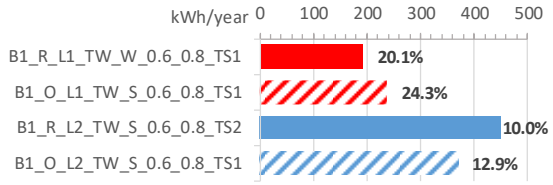

Fig. 3 – Best Trombe wall configurations

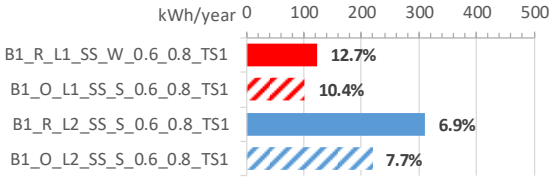

Fig. 4 – Best sunspaces configurations

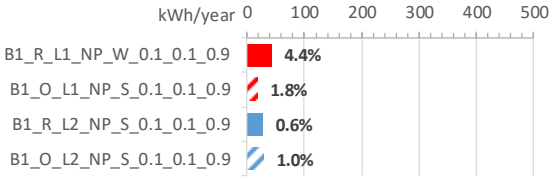

Fig. 5 – Best nanopainting configurations

South orientation proved to be the best solution, as described in Fig. 6, with west in second place, performing better than east in order to get heat late in the afternoon when people are back home. Almost all the configurations prefer 0.6 and 0.8 as WWR and glass U-value. It is worth noting that direct gain systems are the suggested solution for Palermo, while Trombe walls should be preferred in Bolzano.

Finally, Table 4 shows the best configuration for the four base case scenarios in terms of heating performance, while Table 5 shows the code of the passive solar design configurations that perform better in terms of total energy saving.

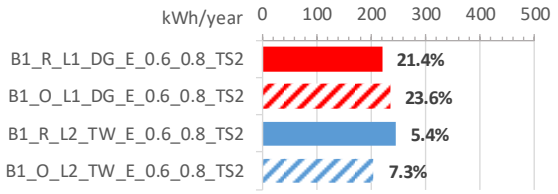

(a)

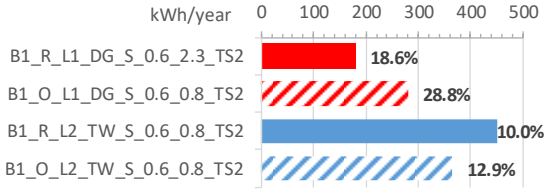

(b)

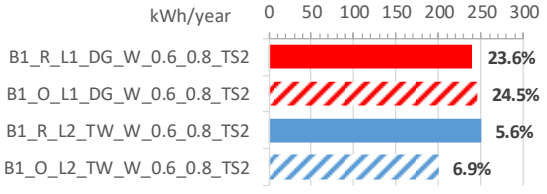

(c)

Fig. 6 – Best east (a), south (b) and west (c) bound configurations

Table 4 – Best configuration for heating energy savings

CODE ID	Heating [%]	Cooling [%]	Total [%]
B1_R_L1_DG_W_0.6_0.8_TS2	-23.6	+120.3	+67.8
B1_O_L1_DG_S_0.6_0.8_TS2	-28.8	+64.3	+32.6
B1_R_L2_TW_S_0.6_0.8_TS2	-10	+33.2	-6.6
B1_O_L2_TW_S_0.6_0.8_TS2	-12.9	+20.6	-8.5

Table 5 – Best configuration for total energy savings

CODE ID	Heating [%]	Cooling [%]	Total [%]
B1_R_L1_NP_W_0.1_0.9_0.9	+1.8	-2.5	-0.9
B1_O_L1_TW_S_0.2_0.8_TS2	-11.3	+3.3	-1.7
B1_R_L2_TW_S_0.6_0.8_TS2	-10	+33.2	-6.6
B1_O_L2_TW_S_0.6_0.8_TS2	-12.9	+20.6	-8.5

In Palermo, L1, the high solar irradiation leads to an increase of the cooling loads, which, as a result, generates an increment in the total energy loads. In Table 5, total energy savings are achieved as long as they are low. This is mainly due to the simulation set, as it focuses on the heating performance, with no optimized shading system for the summer period. However, for Bolzano (L2), the best heating configurations correspond to the best in total energy savings, between 6-8 %. The solution is Trombe Wall, with a high WWR and a low heat transfer coefficient. Direct gain configurations are the best passive heating systems for Palermo (L1), but can even double the cooling demand. In terms of total performance, nanopainting and Trombe walls slightly reduce the total demand even in a hot climate with a short heating season. As in previous cases, south-bound solutions are the most useful ones, with west limited to the residential case in location 1.

3.2 Optimization of the Case Study

The analysis of the case study allows a generalization of the approach to the previous solutions. The test case demonstrates the benchmark of the potential savings achievable through passive systems. The trade-off between passive and active solutions depends on the energy benefit the building can obtain, which is related to the climatic conditions, the kind and use of buildings, and the behavior of the occupants. The case analyzed is a co-housing project located in central Italy. Fig. 7 provides a schematic view. The building is a part of a masterplan for the development of 16 blocks. Developed on 4 floors, 180 m² each, the building hosts a co-working space and standardized flats for families. Each flat consists of a wide living space, a private terrace, one bathroom and two bedrooms, for a total of 78 m². The approach to the case study started from the application of the configuration suggested by the analysis previously described. Starting from the simulation of the base case, reference loads were identified, with an overall demand of 30.11 MWh per year. Fig. 8 shows the results of the cumulative application of suggested solutions in terms of energy savings. The case study took place in the center of Italy, Pisa, defined by L3: the cli-

matic conditions, 14.8 °C average air temperature and 1500 kWh/m² of annual solar irradiation, fall between the two locations previously analyzed. The solution applied, taken from L1 results, will then be linearized according to both series of results. Firstly, direct gains on the west façade were integrated: the increase of the WWR led to 7.8 % heating energy saving. However, the cooling load increased to 16.5 %, causing the total demand to rise around 6 %. Looking at the orientation solutions in Fig. 8, east appears to be the second-most efficient for residential application. Direct gain systems are thus simulated on the east façade, with a close heating performance and a slightly lower cooling increase compared to west orientation. In the third step, the increase in the WWR was split between the two façades to better exploit solar radiation early in the morning and late in the afternoon - basically when passive heating is needed by the house occupants. To reduce the cost of the intervention, the increase in the WWR is compensated for by moving out the windows from the north-facing façade.

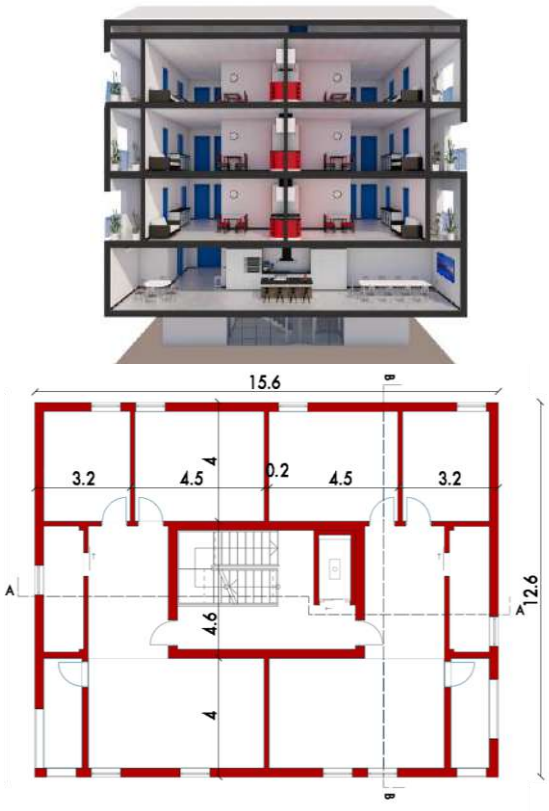

Fig. 7 – Schematic section of the building

This results in a higher heating performance, with an increase of the total demand, due to the cooling demand, being almost imperceptible. To reduce the cooling load, the best configurations in terms of total energy, in Table 5, were applied in step 4, starting with nanopainting. The cooling load is drastically reduced, 8 % compared to the base case, and finally energy saving is achieved in a total basis, even if the improvement in the heating performance is halved. Step 5 includes the optimization of summer shading, to further reduce the cooling load, -23.6 %. Finally, in step 6, sunspaces were implemented. This configuration was included due to the specific design of the building, whose terraces can be easily closed. Sunspace management system is optimized to get passive heating in winter, and assure natural ventilation through opening in summer. Shading system is implemented too. The result is a 14.3 % reduction in heating energy demand, 18.4 % in cooling and a total energy saving of 16.7 %.

Fig. 9 shows the changes in the building design. By moving additional windows from the north façade, the cost of the intervention is low, while the modular rhythm of the façades is preserved.

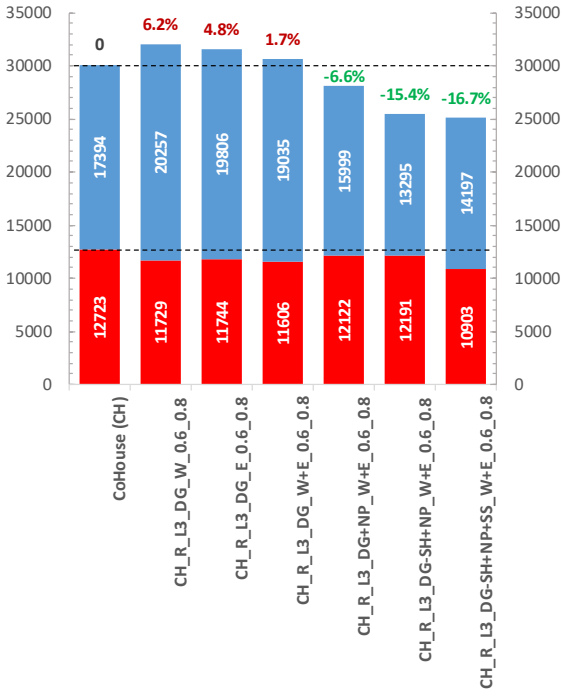

Fig. 8 – Heating, cooling and total energy saving of the case study design steps

Fig. 9 – Starting (left) and final (right) project design

While nanopainting has no influence on the overall architectural design, the integration of sunspaces in the terrace does have a minimal impact, limited to the winter time. The test case confirms the limits of complex passive configurations in terms of energy benefits and management, to balance passive heating with cooling request. The integration of wide direct systems or sunspaces led to relative savings in the heating demand, but their counter effect on the cooling load unbalanced their effect on the overall consumption. More simple solutions, such as shading systems and nanopainting, on the other hand, proved to perform equally. The use of nanopainting, with its impact on the cooling demand, and the integration of a properly set shading system brings a reduction of the overall demand, allowing for a higher degree management of the passive heating load. Being easier to integrate, in technical and economic terms, their trade-off makes them more appealing for building application.

4. Conclusion

Passive solar design strategies are a tool for reducing building energy demand by exploiting solar energy. High heating energy savings can be passively achieved by simply optimizing the building design through the integration of passive solar solutions. The focus on the energy performance of the different passive configurations analyzed allowed the most proficient solutions in terms of both passive heating and energy saving for office and residential buildings in two different climates to be determined. The sensitivity analysis was based on both extrinsic and intrinsic factors, such as building use, location, WWR and glass U-value. The present work aims to address the lack of guidelines or suggested solutions and a methodology for a rational application of such configurations in different kinds of buildings. The purpose is to define an analysis to determine the possible energy-related trade-off for simple to complex passive configurations. A general methodology for the application and integration of the configuration during the design step of a new building was proposed through the analysis of a case study. The analysis moves from the solutions suggested by the general investigation to the integration of elements due to the specific building design:

- marginal savings can be achieved by simply applying the suggested solution for passive heating (direct gains, -7 % of the heating demand)
- the integration of the suggested solution in terms of total energy saving reduces the cooling load (nanopainting, -7 % of the demand)
- the optimization of the shading system helps to prevent the overheating risk in summer (optimized shading system, -15 % of the demand)
- finally, building specific solutions boost the performance (sunspaces, -14 % of the heating demand, -16 % of the total demand).

The results are achieved by minimizing two relevant factors for the promotion of passive solar design integration: impact on the building design, and thus architectural interferences, and the cost of interventions. A relevant element for a widespread application of passive solar design, which this paper attempts to address, is the development of design guidelines. The results of the present analysis can be generally applied as preliminary suggested parameters for the integration of passive systems in the Italian climate, by properly scaling values according to local climate conditions. To generalize the application of these guidelines, the trade-off of the application of passive solutions must be addressed. As seen by the test case, simple kinds of passive measures, such as nanopainting and shading, have a comparable performance on the demand of the building: with easier integration and lower cost, their trade-off suggests a wider application when compared with complex solutions. Fur-

ther analysis must be carried out to take into account the effect of climate-related parameters, such as solar radiation, and local economy factors on the trade-off of these systems. Cost analysis and comfort models should be integrated into the sensitivity analysis.

Acknowledgement

The authors acknowledge Alessio Bardelli for his work within the framework of his Master's Thesis.

Nomenclature

Symbols

A	cross-sectional area (m^2)
Ar	aspect ratio of the cavity
C	discharge coefficient
g	gravity acceleration (m/s^2)
L	length of the chimney (m)
Q	air flow rate (m^3/s)
T	temperature (K)

Subscripts/Superscripts

d	discharge
fo	outlet air
i	inlet
o	outlet
r	room air
rt	ratio

References

Albayyaa, H., D. Hagare, and S. Saha. 2019. "Energy conservation in residential buildings by incorporating Passive Solar and Energy Efficiency Design Strategies and higher thermal mass." *Energy and Buildings* 182: 205–213. doi: https://doi.org/10.1016/j.enbuild.2018.09.036

Bajcinovci, B., and F. Jerliu. 2016. "Achieving Energy Efficiency in Accordance with Bioclimatic Architecture Principles." *Environmental and Climate Technologies* 18(1): 54–63. doi: https://doi.org/10.1515/rtuect-2016-0013

Cillari, G., F. Fantozzi, and A. Franco. 2020. "Passive solar systems for buildings: performance indicators analysis and guidelines for the design." E3S Web of Conferences 197: 02008. doi: https://doi.org/10.1051/e3sconf/202019702008

Cillari, G., F. Fantozzi, and A. Franco. 2021a. "Passive Solar Solutions for Buildings: Criteria and Guidelines for a Synergistic Design." *Applied Sciences* 11(1): 376. doi: https://doi.org/10.3390/app11010376

Cillari, G., A. Franco, and F. Fantozzi. 2021b. "Sizing strategies of photovoltaic systems in nZEB schemes to maximize the self-consumption share." *Energy Reports* 7. doi: https://doi.org/10.1016/j.egyr.2021.09.117

Ellis, P. G. 2003. "Development and validation of the unvented Trombe wall model in EnergyPlus." Master Degree Thesis, University of Illinois.

Givoni, B. 1991. "Characteristics, design implications, and applicability of passive solar heating systems for buildings." *Solar Energy* 47(6): 425–435. doi: https://doi.org/10.1016/0038-092X(91)90110-I

Morrissey, J., T. Moore, and R. E. Horne. 2011. "Affordable passive solar design in a temperate climate: An experiment in residential building orientation." *Renewable Energy* 36(2): 568–577. doi: https://doi.org/10.1016/j.renene.2010.08.013

Nault, E., P. Moonen, E. Rey, et al. 2017. "Predictive models for assessing the passive solar and daylight potential of neighborhood designs: A comparative proof-of-concept study." *Building and Environment* 116: 1–16. doi: https://doi.org/10.1016/j.buildenv.2017.01.018

Nielsen, T. R., K. Duer, and S. Svendsen. 2001. "Energy performance of glazings and windows." *Solar Energy* 69: 137–143. doi: https://doi.org/10.1016/S0038-092X(01)00062-7

O'Shaughnessy, E., D. Cutler, K. Ardani, et al. 2018. "Solar plus: Optimization of distributed solar PV through battery storage and dispatchable load in residential buildings." *Applied Energy* 213: 11–21. doi: https://doi.org/10.1016/j.apenergy.2017.12.118

Stevanović, S. 2013. "Optimization of passive solar design strategies: A review." *Renewable and Sustainable Energy Reviews* 25: 177–196. doi: https://doi.org/10.1016/j.rser.2013.04.028

A Novel Personal Comfort System: A Radiant Desk With a Loop Heat Pipe

Roberto Rugani – University of Pisa, Italy – roberto.rugani@phd.unipi.it
Marco Bernagozzi – University of Brighton, United Kindom – M.Bernagozzi3@brighton.ac.uk
Marco Picco – University of Brighton, United Kindom – M.Picco@brighton.ac.uk
Giacomo Salvadori – University of Pisa, Italy – giacomo.salvadori@unipi.it
Fabio Fantozzi – University of Pisa, Italy – fabio.fantozzi@unipi.it

Abstract

This study is the second step toward the development and prototyping of a Personal Comfort System for tertiary sector working environments. The entire industrial sector, and, in particular, offices, have seen changes in working habits, with a large increase in smart working also due to prevention of COVID infection. The chance to partialize the HVAC system and maintain rooms in an under-conditioned state is the obligatory way towards reducing energy waste, providing each workstation with an independent system that guarantees the operator's comfort conditions. The goal of the second step presented in this work was to size and optimize the radiating desk, with the aim of testing an experimental demonstrator. A LHP was chosen to bring heat from the source to the desk, decoupling the heat generation and heat distribution system, without the need for additional parasitic power consumption or moving parts, adding to the innovation of the proposed design. The ergonomic optimization of the surface and its power reduction did not affect its ability to improve localized comfort, since the operators' conditions move from a slightly cold to a neutral situation. Moreover, no discomfort due to vertical temperature differences or radiant asymmetries were found. Therefore, the next research step will lead to prototype creation and its analyses, conducted in a climatic room to test if the distribution system can satisfy comfort thermal requirements with probes as well as real users.

1. Introduction

Reducing energy consumption is a current issue, made increasingly stringent with the progress of the 21st century (Allouhi et al., 2015; Almasri & Alshitawi, 2022). The total energy consumption associated with HVAC services (heating, ventilation, and air conditioning) in buildings accounts for 40 % of total energy consumption in Europe and 36 % of greenhouse gas emissions (EU. Buildings, 2020).

New methods of building design and HVAC systems are becoming increasingly popular, yet people still often complain of thermal discomfort (Fantozzi et al., 2020; Ortiz et al., 2017), and inadequate attention is paid to reducing energy waste (Carmenate et al., 2016; Li et al., 2019). Moreover, buildings do not meet the regulations' modest goal of having no more than 20 % unsatisfied occupants, primarily due to building over-conditioning and occupants' inability to adjust the environment individually to meet their personal needs (Brager et al., 2015).

The importance of providing Indoor Environmental Quality (IEQ) is widely recognised (Lamberti, 2020), especially in the work-place, where not only personal well-being increases productivity (Greenberger et al., 1989; Rocca et al., 2020), but it also makes up the greatest component towards dissatisfaction (Frontczak et al., 2012; Huizenga et al., 2006). The IEQ is defined by many interacting factors (Bluyssen, 2020), among which thermal comfort is the most significant on the perception of environmental quality and the energy consumption associated with IEQ achievement (Lamberti, 2020). As the individual differences based on age, gender, or body fat content show, thermal comfort is not only a simple function of the thermal environment, but it is also influenced by a whole set of individual factors. Thermal neutrality is considered to provide the best comfort, but this does not respect individual preferences (Fantozzi et al., 2021; van Hoof, 2008).

Personal ability to thermoregulate oneself plays a key role in this process (de Dear et al., 2013). Therefore, the local microenvironment needs to become personalized to fit the preferences of everyone.
Individually oriented new approaches are under development in this emerging research area, to evaluate the average zone thermal comfort metrics. For instance, a personal comfort model predicts individuals' thermal comfort responses, instead of the average response of a large population with an improved comfort predictive power compared to conventional models (PMV, Adaptive) (Kim et al., 2018).
A noteworthy model is the Berkeley Comfort Model, which predicts the sensation for each local body part with input data related to skin temperature (Huizenga et al., 2001); a physical measurement campaign or a thermophysiological computer program that treats the body as multiple segments would be needed to simulate this data (Zhang et al., 2010a; Zhang et al., 2010b). Thermal sensation and comfort for local body parts vary greatly and affect thermal sensation and comfort perceived for the whole body (Arens et al., 2006a). In a cool environment, hands and feet feel colder than other body parts, and feet are the major sources of discomfort (Arens et al., 2006b; Zhang et al., 2010c). In the tests performed by Arens et al, people perceived neutral conditions as "comfortable", but the "very comfortable" rating was achieved only in the asymmetric or transient environment conditions, which can be achieved through local Personal Comfort Systems (PCS), defined as systems that heat and cool individuals without affecting the environments of surrounding occupants (Arens et al., 2006a).
PCSs play an important role in this landscape with the target of conditioning only the "personal" microclimate rather than the volume of the entire building, in contrast to traditional HVAC systems (Kalaimani et al., 2020).
PCSs provide a series of benefits to indoor environments, like ensuring comfort conditions (Tsuzuki et al., 1999; Warthmann et al., 2018; Zhang et al., 2010) and reducing energy waste (Godithi et al., 2019; Shahzad et al., 2018; Zhang et al., 2015). They can provide comfort conditions with an environment temperature as low as 15 °C (Veselý & Zeiler, 2014). Zhang et al. found that there are several benefits to providing personal control over an environmental feature capable of providing a local pleasurable sensation (Zhang et al., 2010c).
The present study is the second step of a research study aimed at prototyping a radiant-conductive system to guarantee microclimatic comfort conditions in open-space offices, transferring heat directly to the person (Rugani et al., 2021). Furthermore, reducing air movement will bring about the additional benefit of reducing the movement of pollutants and micro-particulates.
The global COVID-19 pandemic has increased cases of smart-working, often causing office staff presence to be significantly lowered. The direct consequence was seen in the wasted energy needed to air-condition entire offices where most desks remained empty (Jiang et al., 2021). PCSs can provide microclimatic comfort for operators, and the possibility of reducing the setpoint temperatures of the primary HVAC system would lead to a drastic reduction in energy losses (Rugani et al., 2021). The trend is generally to rethink design strategies as a result of the pandemic (Megahed & Ghoneim, 2021), rethinking buildings both from a spatial point of view, but also in terms of HVAC systems.
Therefore, the prototypisation of a bespoke radiant surface embedded in a desk and the study of the comfort conditions that this can provide is the objective of the research. In this second research step, the preparatory analyses were carried out considering a Loop Heat Pipe (LHP) as the thermal vector from the heat source and the radiant plate. LHPs are a passive devices, whose heat transfer and fluid motions are ensured by cycles of evaporation and condensation of a working fluid. Hence the lack of need for pumps or additional energy sources for their operation makes up their great scientific interest.

2. Method

2.1 Overview

The aim of the study is to prototype and optimise a Personal Comfort System (PCS). In the previous phase, the PCS was conceived and studied as a complete radiant desk, analysing the comfort provided to the user according to the potential energy savings in offices (Rugani et al., 2021).

Two possibilities were identified for transferring heat to the desk - via a hydronic system and via an electric infrared surface. The objective of the current research is the sizing of the hydronic one, with the application of a Loop Heat Pipe. It allows the parasitic energy consumption of the pump for a standard hydronic system to be saved and a plug-in desk, versatile and easily interfaced with the energy sources, with no moving parts and no risk of failure to be created.

The analysis consisted of a first phase of the LHP condenser sizing, i.e., the radiant plate to be placed in the desk, simulating it in the operating conditions. Several condensers designed were studied to find the most efficient one. Meanwhile, CFD analysis with a similar methodology to the previous study by the Authors was conducted, simulated in two different heating system configurations: heating with standard setpoint and underconditioned state with local PCS.

2.2 LHP Design

LHPs have been widely implemented in space applications and thermal management, for which they were first created in the early 70s. They are a two-phase passive heat exchanger, able to transfer heat over several meters without the need for moving parts or any additional energy for its functioning. This would reduce power consumption and the noise in using a hydraulic active system, the complexity, and the risk of failure, hence increasing the overall system efficiency. LHPs work thanks to the cyclic evaporation/condensation processes of a working fluid, whose motion is ensured by a positive pressure gradient arising in a porous structure, due to capillarity (Maydanik, 2005). LHPs have been extensively studied in recent years in several applications, like aircraft (Pagnoni et al., 2021) and electric vehicle thermal management (Bernagozzi et al., 2021), solar water heating (Wang & Yang, 2014), and electronics cooling (Domiciano et al., 2022).

The LHP has the function of transferring heat from the source (evaporator) to the radiating desk (condenser). Its sizing was performed thanks to a validated Lumped Parameter Model (LPM) code validated by Bernagozzi et al. (2018). The power of the system was chosen according to the previous analysis performed. Compared with the first study, the power range was reduced because the radiating surface was optimized, according to an ergonomic study about the user's position. Values aligned with those previously identified by Mao et al. (2017), who provided the desk with a palm warmer with a power consumption of 26 W at steady state (typical surface temperature of 35 °C).

Fig. 1 shows the condenser, which represents the heating plate, located in the desk. Fig. 2 shows the desk section with the embedded condenser of the LHP. This will be a small diameter meandering pipe where condensation of the working fluid takes place, ensuring a constant temperature profile along the radiating surface, ultimately increasing the individual's feeling of comfort.

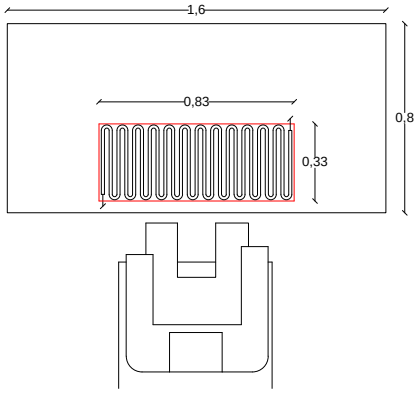

Fig. 1 – Example of a desk configuration, with the heating plate facing the user

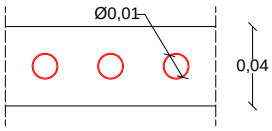

Fig. 2 – Desk section

2.3 CFD Modeling

A CFD analysis was conducted using Autocad CFD software. The purpose was to obtain the local environmental conditions on an ideal manikin placed on a chair in front of the desk. Solving the Navier-Stokes equations allowed an assessment of the local comfort conditions and the convective and radiant energy contributions of the PCS, which are impossible to evaluate with a Building Energy Simulation (BES).

CFD models have been widely adopted as effective tool for natural ventilation simulations, while BES is more stable with the heat transfer between solid and

fluid (Zhang et al., 2013). Moreover, the effect of air mixing considerably affects the zone temperatures. Thus, CFD analysis is the most suitable option for assessing the temperature variation (Jones et al., 2020; Salimi & Hammad, 2020).

Following the previous methodology, two configurations were studied: heating with standard set-point (21 °C), and PCS in an under-conditioned environment (17 °C).

The CFD simulations aimed at evaluating the size and shape of the condenser in ensuring user comfort. Thus, this phase was conducted in parallel with the calculation of the LHP system.

2.4 Comfort Assessments

To determine thermal comfort, several models were developed. Most of the research conducted on the assessment of comfort conditions were based on Fanger's thermal model and the calculation of the two indices: the Predicted Mean Vote (PMV) and the Predicted Percentage of Dissatisfied (PPD) (ISO 7730:2005 2005).

Individual-oriented models, such as the Berkeley Comfort Model, while more effective at predicting local response, require experimental data on a physical person. Although Fanger's indexes were created for the evaluation of general comfort, several studies demonstrated its ability to compare thermal comfort from different setups (Orosa Jose, 2010; Shahzad et al., 2018; Zhang et al., 2015).

To compare the case study results to the previous analysis (Rugani et al., 2021) and to the research conducted by Shahzad et al. (2018), the applied conditions are those shown in Table 1.

Table 1 – Comfort evaluation parameters for Fanger's model

Humidity (RH)	30%
Metabolic rate (MET)	1
Clothing insulation (CLO)	0.7

Furthermore, two local models based on environmental data were applied (ASHRAE, 2021): discomfort due to vertical temperature difference (1), and discomfort due to radiant asymmetry (2-3). Also, specific standards on heating radiant systems such as EN ISO 11855 (ISO, 2021) indicate following the previous models for local discomfort evaluation.

$$PD = 100/1 + \exp(5.76 - 0.856 \cdot \Delta t_{a,v}) \quad (1)$$

$$PD = 100/1 + \exp(6.61 - 0.345 \cdot \Delta t_{pr}) \quad (2)$$

$$PD = 100/1 + \exp(9.93 - 0.50 \cdot \Delta t_{pr}) \quad (3)$$

Where PD is the Percentage Dissatisfied and Δt are the temperature differences in each case.

The limits prescribed by the regulations are applied, with particular attention to temperature differences. The vertical temperature gradient between head and feet is prescribed as 3 °C/m by ASHRAE 55 (ASHRAE 2020) and ISO 7730 (ISO 7730:2005 2005). Nevertheless, Liu et al. (2020) found that vertical temperature gradient changes with thermal sensation votes and could be increased to 5 °C/m when the subject is thermally neutral.

3. Results

Different heating inputs were provided to the LHP evaporator to achieve the optimum desk surface temperature of 36 °C, namely 15 W, 20 W, 25 W, and 30 W. Moreover, several working fluids were investigated for the LHP: water, acetone, ethanol, R1233, and Novec649. Finally, tubes of various sizes were tested, with internal radius of 4, 5, and 6 mm.

Figs. 3, 4, and 5 show the superficial temperature variation of the desk as a function of the working fluid, the heating power, and the pipes dimension.

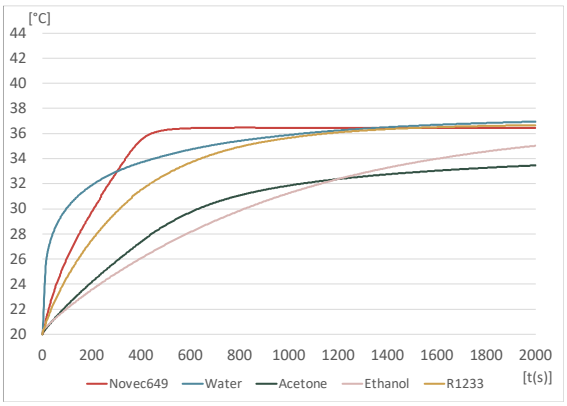

Fig. 3 – Radiant surface temperature of the desk as a function of the liquid in the LHP loop, with a power of 20W and an internal radius of 6 mm

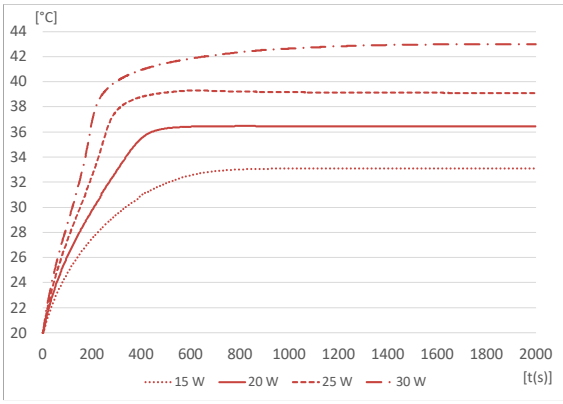

Fig. 4 – Radiant surface temperature of the desk as a function of the power applied to the evaporator, Novec649 in the loop and an internal radius of 6 mm

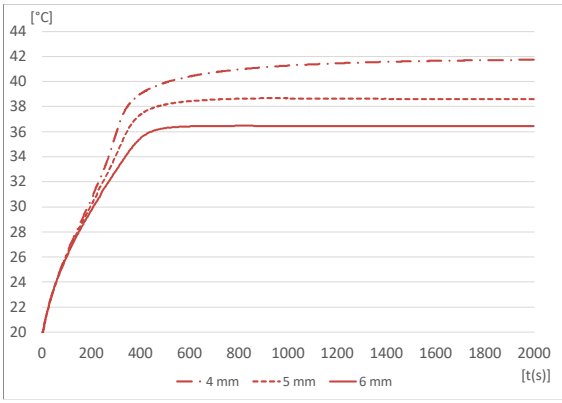

Fig. 5 – Radiant surface temperature of the desk as a function of the pipes dimension, Novec649 in the loop and a power of 20W

The CFD results allowed the overall comfort situation (Fig. 6) and the temperature distributions around the workers to be studied (Fig. 7).

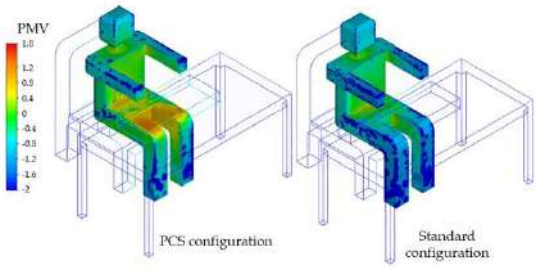

Fig. 6 – PMV distribution at each point of the environment

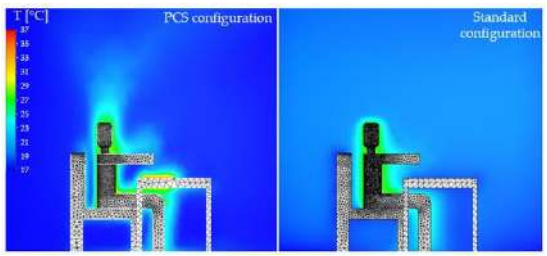

Fig. 7 – Temperature distribution at each point of the environment

4. Discussion

The coupling of CFD and LHP sizing calculations allowed optimization of the heating plate, i.e., the LHP condenser, with the aim of creating a real prototype.

Sizing results showed that the most efficient working fluid was the heat transfer fluid Novec™ 649, produced by 3M™, as it condensed earlier than other liquids and allowed the system to be operative in the shortest time. Interestingly, in the design configuration, 20 W was the power that allows the desired desk surface temperature to be reached, associated with pipes whose inner radius was 6 mm. This low value of power opens up different avenues on heat recovery, for instance, suggesting the use of the waste heat from the electronic components present on the desk, e.g., laptop.

The CFD results show an alignment with those of the first step of the research (Rugani et al., 2021). Although the heating surface area was reduced to 0.27 m², as well as the power delivered, the general comfort situation was not affected. The ergonomic study prior to prototyping thus succeeded in optimizing the panel while maintaining its ability to ensure local comfort (Table 2).

Table 2 – Localized results of CFD analyses

	PCS		**Standard**	
	PMV	*PPD*	*PMV*	*PPD*
Face	-0.06	5	-0.27	7
Torso	0.11	5	-0.42	9
Knee	0.23	6	-0.47	10

A further step conducted in this analysis phase was to verify the compliance of local discomfort models for vertical air temperature difference and radiant asymmetry. There are no major temperature differences between the ankles and the head, as the surface heats in both directions. The PD value is below 1. Likewise, vertical radiant asymmetry discomfort from cold ceilings hardly exceeds PD value 1. On the other hand, if the radiating desk were located near a cold wall, the discomfort from radiant asymmetry could lead to a PD value of 2 with a temperature difference of 8 °C, which in any case is lower than the 10 °C indicated as the standard limit.

5. Conclusion

Today's society demands quality and comfort, especially in the workplace. This study aims to increase comfort and satisfaction with the thermal microclimate in large offices.

The global pandemic has accentuated smart working. Thus, the possibility of being able to partialize thermal systems and to locally heat and cool only occupied workstations is a winning strategy for reducing energy waste.

A first step of this research was conducted to analyze the thermal comfort provided by a radiant desk combined with the associated energy savings. The goal of the second step presented in this work was to size and optimize the radiating desk, with the aim of testing an experimental demonstrator.

A LHP was chosen to bring heat from the source to the serpentine on the horizontal table. Its sizing was performed thanks to a validated Lumped Parameter Model (LPM). 20 W was the power that allows reaching the desired desk surface temperature, associated with pipes whose inner radius was 6 mm.

The CFD results confirmed the ability of the PCS to ensure comfortable conditions even at sub-comfort room temperatures, moving to a neutral situation with PMV value near to 0 (face -0.06, torso 0.11, knee 0.23), thus reducing energy losses from heating entire rooms, such as open space offices, recently left almost empty due to the increase in smart working. The ergonomic optimisation of the surface and its power reduction did not affect its ability to improve localised comfort. Moreover, no discomfort due to vertical temperature differences or radiant asymmetries was found, with PD below 1 and temperature gradients not exceeding regulatory limits.

Summarizing, the contribution of this work is twofold: firstly, the improvement of the individual's comfort by the adoption of microclimatic comfort; secondly, the system allows an increase in the efficiency of the building's HVAC system, reducing energy consumption and moving a few steps in the net-zero direction.

Future research developments include the comparison of this hydronic desk with a similar electrically powered desk. The reason for this analysis is to conduct an exergetic comparison by contrasting the quality of energy with the versatility and efficiency of systems to ensure local comfort and reduce energy consumption.

Moreover, analyses will be conducted in a climatic room to test that the distribution system can satisfy comfort thermal requirements with probes, as well as real users. Additionally, The CFD model will be rebuilt and validated with ANSYS Fluent software.

References

Allouhi, A., Y. el Fouih, T. Kousksou, A. Jamil, Y. Zeraouli, and Y. Mourad. 2015. "Energy Consumption and Efficiency in Buildings: Current Status and Future Trends." *Journal of Cleaner Production* 109: 118–130. https://doi.org/10.1016/j.jclepro.2015.05.139

Almasri, R. A., and M. S. Alshitawi. 2022. "Electricity Consumption Indicators and Energy Efficiency in Residential Buildings in GCC Countries: Extensive Review." *Energy and Buildings* 255: 111664. https://doi.org/10.1016/j.enbuild.2021.111664

Arens, E., H. Zhang, and C. Huizenga. 2006a. "Partial- and Whole-Body Thermal Sensation and Comfort - Part II: Non-Uniform Environmental Conditions." *Journal of Thermal Biology* 31:60–66. doi: https://doi.org/10.1016/j.jtherbio.2005.11.027

Arens, E., H. Zhang, and C. Huizenga. 2006b. "Partial- and Whole-Body Thermal Sensation and Comfort - Part I: Uniform Environmental Conditions." *Journal of Thermal Biology* 31:53–59. doi: https://doi.org/10.1016/j.jtherbio.2005.11.028

ASHRAE. 2020. *ANSI/ASHRAE Standard 55: 'Thermal Environmental Conditions for Human Occupancy*.'

ASHRAE. 2021. *Handbook of Fundamentals*.

Bernagozzi, M., S. Charmer, A. Georgoulas, I. Malavasi, N. Michè, and M. Marengo. 2018. "Lumped Parameter Network Simulation of a Loop Heat Pipe for Energy Management Systems in Full Electric Vehicles." *Applied Thermal Engineering* 141: 617–629. doi: https://doi.org/10.1016/j.applthermaleng.2018.06.013

Bernagozzi, M., A. Georgoulas, N. Miché, C. Rouaud, and M. Marengo. 2021. "Novel Battery

Thermal Management System for Electric Vehicles with a Loop Heat Pipe and Graphite Sheet Inserts." *Applied Thermal Engineering* 194: 117061. doi: https://doi.org/10.1016/j.applthermaleng.2021.117061

Bluyssen, P. M. 2020. "Towards an Integrated Analysis of the Indoor Environmental Factors and Its Effects on Occupants." *Intelligent Buildings International* 12(3): 199–207. doi: https://doi.org/10.1080/17508975.2019.1599318

Brager, G., H. Zhang, and E. Arens. 2015. "Evolving Opportunities for Providing Thermal Comfort." *Building Research & Information* 43(3): 274–287. doi: https://doi.org/10.1080/09613218.2015.993536

Carmenate, T., P. Inyim, N. Pachekar, G. Chauhan, L. Bobadilla, M. Batouli, and A. Mostafavi. 2016. "Modeling Occupant-Building-Appliance Interaction for Energy Waste Analysis." *Procedia Engineering* 145: 42–49. doi: https://doi.org/10.1016/j.proeng.2016.04.012

de Dear, R. J., T. Akimoto, E. A. Arens, G. Brager, C. Candido, K. W. D. Cheong, B. Li, et al. 2013. "Progress in Thermal Comfort Research over the Last Twenty Years." *Indoor Air* 23(6): 442–461. doi: https://doi.org/10.1111/ina.12046

Domiciano, K. G., L. Krambeck, J. P. M. Flórez, and M. B. H. Mantelli. 2022. "Thin Diffusion Bonded Flat Loop Heat Pipes for Electronics: Fabrication, Modelling and Testing." *Energy Conversion and Management* 255: 115329. doi: https://doi.org/10.1016/j.enconman.2022.115329

EU. Buildings. 2020. "Energy Performance of Buildings Directive." https://ec.europa.eu/energy/topics/energy-efficiency/energy-efficient-buildings/energy-performance-buildings-directive_en

Fantozzi, F., G. Lamberti, F. Leccese, and G. Salvadori. 2020. "The Indoor Thermal Environment in Fencing Halls: Assessment of the Environmental Conditions Through an Objective and Subjective Approach." *Advances in Physical, Social & Occupational Ergonomics*, edited by W. Karwowski, R. S. Goonetilleke, S. Xiong, R. H. M. Goossens, and A. Murata, 223–229. Cham: Springer International Publishing.

Fantozzi, F., G. Lamberti, and R. Rugani. 2021. "Thermal Comfort in University Classrooms: Analysis of Simulated and Real Conditions." 2021 IEEE (EEEIC / I&CPS Europe). Bari. doi: https://doi.org/10.1109/EEEIC/ICPSEurope51590.2021.9584490

Frontczak, M., S. Schiavon, J. Goins, E. Arens, H. Zhang, and P. Wargocki. 2012. "Quantitative Relationships between Occupant Satisfaction and Satisfaction Aspects of Indoor Environmental Quality and Building Design." *Indoor Air* 22(2): 119–131. doi: https://doi.org/10.1111/j.1600-0668.2011.00745.x

Godithi, S. B., E. Sachdeva, V. Garg, R. Brown, C. Kohler, and R. Rawal. 2019. "A Review of Advances for Thermal and Visual Comfort Controls in Personal Environmental Control (PEC) Systems." *Intelligent Buildings International* 11 (2): 75–104. https://doi.org/10.1080/17508975.2018.1543179

Greenberger, D. B., S. Strasser, L. L. Cummings, and R. B. Dunham. 1989. "The Impact of Personal Control on Performance and Satisfaction." *Organizational Behavior and Human Decision Processes* 43(1): 29–51. https://doi.org/10.1016/0749-5978(89)90056-3

Huizenga, C., S. Abbaszadeh, L. Zagreus, and E. Arens. 2006. "Air Quality and Thermal Comfort in Office Buildings: Results of a Large Indoor Environmental Quality Survey." Proceedings of Healthy Buildings 2006, Lisbon, Vol. III, 393-397.

Huizenga, C., H. Zhang, and E. Arens. 2001. "A Model of Human Physiology and Comfort for Assessing Complex Thermal Environments". *Building and Environment* 36. doi: https://doi.org/10.1016/S0360-1323(00)00061-5

ISO. 2021. *ISO 11855-1:2021, 'Building Environment Design — Embedded Radiant Heating and Cooling Systems. Part 1: Definitions, Symbols, and Comfort Criteria.'*

ISO. 2005. *ISO 7730:2005. 2005. Ergonomics of the Thermal Environment -- Analytical Determination and Interpretation of Thermal Comfort Using Calculation of the PMV and PPD Indices and Local Thermal Comfort Criteria*.

Jiang, P., Y. van Fan, and J. J. Klemeš. 2021. "Impacts of COVID-19 on Energy Demand and Consumption: Challenges, Lessons and Emerging Opportunities." *Applied Energy* 285.

doi: https://doi.org/10.1016/j.apenergy.2021.116441

Jones, N. L., I. Chaires, and A. Goehring. 2020. "Detailed Thermal Comfort Analysis from Preliminary to Final Design." Proceedings of Building Simulation 2019: 16th Conference of IBPSA 16: 2675–2682. doi: https://doi.org/10.26868/25222708.2019.210875

Kalaimani, R., M. Jain, S. Keshav, and C. Rosenberg. 2020. "On the Interaction between Personal Comfort Systems and Centralized HVAC Systems in Office Buildings." *Advances in Building Energy Research* 14(1): 129–157. doi: https://doi.org/10.1080/17512549.2018.1505654

Kim, J., S. Schiavon, and G. Brager. 2018. "Personal Comfort Models – A New Paradigm in Thermal Comfort for Occupant-Centric Environmental Control." *Building and Environment* 132: 114–124. doi: https://doi.org/10.1016/j.buildenv.2018.01.023

Lamberti, G. 2020. "Thermal Comfort in the Built Environment: Current Solutions and Future Expectations." Proceedings - 2020 IEEE, EEEIC / I and CPS Europe 2020. doi: https://doi.org/10.1109/EEEIC/ICPSEurope49358.2020.9160558

Li, J., K. Panchabikesan, Z. Yu, F. Haghighat, M. el Mankibi, and D. Corgier. 2019. "Systematic Data Mining-Based Framework to Discover Potential Energy Waste Patterns in Residential Buildings." *Energy and Buildings* 199: 562–578. doi: https://doi.org/10.1016/j.enbuild.2019.07.032

Liu, S., Z. Wang, S. Schiavon, Y. He, M. Luo, H. Zhang, and E. Arens. 2020. "Predicted Percentage Dissatisfied with Vertical Temperature Gradient." *Energy and Buildings* 220. doi: https://doi.org/10.1016/j.enbuild.2020.110085

Mao, N., D. Pan, Z. Li, Y. Xu, M. Song, and Sh. Deng. 2017. "A Numerical Study on Influences of Building Envelope Heat Gain on Operating Performances of a Bed-Based Task/Ambient Air Conditioning (TAC) System in Energy Saving and Thermal Comfort." *Applied Energy* 192: 213–221. doi: https://doi.org/10.1016/j.apenergy.2017.02.027

Maydanik, Y. F. 2005. "Loop Heat Pipes." *Applied Thermal Engineering* 25(5): 635–657. doi: https://doi.org/10.1016/j.applthermaleng.2004.07.010

Megahed, N. A, and E. M. Ghoneim. 2021. "Indoor Air Quality: Rethinking Rules of Building Design Strategies in Post-Pandemic Architecture." *Environmental Research* 193: 110471. doi: https://doi.org/10.1016/j.envres.2020.110471

Orosa Jose, J. A. 2010. "A Review of General and Local Thermal Comfort Models for Controlling Indoor Ambiences." *Air Quality* 1966. doi: https://doi.org/10.5772/9763

Ortiz, M. A., S. R. Kurvers, and P. M. Bluyssen. 2017. "A Review of Comfort, Health, and Energy Use: Understanding Daily Energy Use and Wellbeing for the Development of a New Approach to Study Comfort." *Energy and Buildings* 152: 323–335. doi: https://doi.org/10.1016/j.enbuild.2017.07.060

Pagnoni, F., V. Ayel, Y. Bertin, J. Coulloux, and M. Zebian. 2021. "Loop Heat Pipe for Thermal Management of Aircraft Engine Equipment." *Journal of Thermophysics and Heat Transfer* 35(2): 323–334. doi: https://doi.org/10.2514/1.T6049

Rocca, M., F. Leccese, and G. Salvadori. 2020. "Health and Well-Being in Indoor Work Environments: Features of an Expert Assessment Campaign in an Italian University Hospital." Proceedings - 2020 IEEE, EEEIC / I and CPS Europe 2020, 0–5. doi: https://doi.org/10.1109/EEEIC/ICPSEurope49358.2020.9160493

Rugani, R., M. Picco, G. Salvadori, M. Marengo, and F. Fantozzi. 2021. "Can PCS Help Us Save Energy? Initial Assessment Using Dynamic Energy and CFD Analyses." 2021 IEEE (EEEIC / I&CPS Europe), Bari, Italy.

Salimi, S., and A. Hammad. 2020. "Optimizing Energy Consumption and Occupants Comfort in Open-Plan Offices Using Local Control Based on Occupancy Dynamic Data." *Building and Environment* 176: 106818. doi: https://doi.org/10.1016/j.buildenv.2020.106818

Shahzad, S., J. Kaiser Calautit, K. Calautit, B. Hughes, and A. I. Aquino. 2018. "Advanced Personal Comfort System (APCS) for the Workplace: A Review and Case Study." *Energy*

and Buildings 173: 689–709. https://doi.org/10.1016/j.enbuild.2018.02.008

Tsuzuki, K., E. Arens, F. Bauman, and D. Wyon. 1999. "Individual Thermal Comfort Control with Desk-Mounted and Floor-Mounted Task/Ambient Conditioning (TAC) Systems." Indoor Air 99, August 8-13, Edinburgh, UK.

van Hoof, J. 2008. "Forty Years of Fanger's Model of Thermal Comfort: Comfort for All?" *Indoor Air* 18(3): 182–201. https://doi.org/10.1111/j.1600-0668.2007.00516.x

Veselý, M., and W. Zeiler. 2014. "Personalized Conditioning and Its Impact on Thermal Comfort and Energy Performance - A Review." *Renewable and Sustainable Energy Reviews* 34: 401–408. https://doi.org/10.1016/j.rser.2014.03.024

Wang, Z., and W. Yang. 2014. "A Review on Loop Heat Pipe for Use in Solar Water Heating." *Energy and Buildings* 79: 143–154. https://doi.org/10.1016/j.enbuild.2014.04.051

Warthmann, A., D. Wölki, H. Metzmacher, and C. van Treeck. 2018. "Personal Climatization Systems-a Review on Existing and Upcoming Concepts." *Applied Sciences* 9(1). https://doi.org/10.3390/app9010035

Zhang, H., E. Arens, C. Huizenga, and T. Han. 2010a. "Thermal Sensation and Comfort Models for Non-Uniform and Transient Environments: Part I: Local Sensation of Individual Body Parts." *Building and Environment* 45(2): 380–388. https://doi.org/10.1016/j.buildenv.2009.06.018

Zhang, H., E. Arens, C. Huizenga, and T. Han. 2010b. "Thermal Sensation and Comfort Models for Non-Uniform and Transient Environments, Part II: Local Comfort of Individual Body Parts." *Building and Environment* 45(2): 389–398. https://doi.org/10.1016/j.buildenv.2009.06.015

Zhang, H., E. Arens, C. Huizenga, and T. Han. 2010c. "Thermal Sensation and Comfort Models for Non-Uniform and Transient Environments, Part III: Whole-Body Sensation and Comfort." *Building and Environment* 45(2): 399–410. https://doi.org/10.1016/j.buildenv.2009.06.020

Zhang, H., E. Arens, D. E. Kim, E. Buchberger, F. Bauman, and C. Huizenga. 2010. "Comfort, Perceived Air Quality, and Work Performance in a Low-Power Task-Ambient Conditioning System." *Building and Environment* 45(1): 29–39. https://doi.org/10.1016/j.buildenv.2009.02.016

Zhang, H., E. Arens, and Y. Zhai. 2015. "A Review of the Corrective Power of Personal Comfort Systems in Non-Neutral Ambient Environments." *Building and Environment* 91: 15–41. https://doi.org/10.1016/j.buildenv.2015.03.013

Zhang, R., K. P. Lam, S. Yao, and Y. Zhang. 2013. "Coupled EnergyPlus and Computational Fluid Dynamics Simulation for Natural Ventilation." *Building and Environment* 68: 100–113. https://doi.org/10.1016/j.buildenv.2013.04.002

Energy Signature Modeling Towards Digital Twins – Lessons Learned From a Case Study With TRV and GAHP Technologies

Massimiliano Manfren – ENEA, Italy – M.Manfren@soton.ac.uk
Maria Cristina Tommasino – ENEA, Italy – cristina.tommasino@enea.it
Lamberto Tronchin – University of Bologna, Italy – lamberto.tronchin@unibo.it

Abstract

In building refurbishment projects, efficient technologies such as heat pumps are increasingly being used as a substitute for conventional technologies such as condensing boilers, with the aim of reducing carbon emissions and determining operational energy and cost savings. Measured building performance, however, often reveals a significant gap between the predicted energy use (design stage) and actual energy use (operation stage). For this reason, a scalable energy signature modeling approach is presented in this paper to verify building energy performance from measured data. Regression models are built with data at multiple temporal resolutions (monthly and daily) and are used to verify the performance improvement due to smart heating controllers (TRV) and Gas Absorption Heat Pumps (GAHP). The capabilities of energy signature analysis are enhanced by including additional variables in the modeling process and by running the models as "digital twins" with a rolling horizon of 15 days of data. Finally, a regression model for GAHP technology is developed to validate the results measured in the monitoring process in a comparative way. The case study chosen is Hale Court sheltered housing, located in the city of Portsmouth (UK). The results obtained are used to illustrate possible extensions of the use of energy signature modeling, highlighting implications for energy management and innovative building technologies development.

1. Introduction

The necessity of achieving high energy efficiency targets while maintaining an adequate level of services in the building stock is one of the topics driving the built environment today. Innovative heating technologies are part of this research and Gas Absorption Heat Pump (GAHP) can be used as an alternative to conventional and condensing boilers. Additionally, smart heating controllers, such as Smart TRVs (Thermostatic Radiator Valves) are often reported as a promising technology, even if this depends on multiple factors and, in particular, operational patterns and user behavior (Manfren et al., 2021a, 2021b and 2022; Tronchin et al., 2018).
The case study of Hale Court, considering intervention in the North Block allows testing of the new methodology in question. In particular, the area was monitored before and after the retrofit intervention – namely, first with the installation of Smart TRVs (Thermostatic Radiator Valves) and then with the installation of Gas Absorption Heat Pumps (GAHPs). The monitored data are split into three periods: explicitly before retrofit, after the installation of TRVs and after the installation of GAHPs and plant room upgrade. The performance before retrofit represents for us the baseline for evaluation. Data are summarized and aggregated at different time scales (monthly and daily), energy signatures are calculated from energy metering data and piecewise linear regression models are fitted for the different monitoring periods to enable performance comparison. Finally, the savings monitored are compared to the ones calculated by a regression model of GAHP performance

2. Methods

First of all, the methods used in this research are aimed at giving primarily a reliable assessment of the actual impact of different technologies in terms of efficiency. For this reason, the regression-based approaches proposed by state-of-the-art Measurement and Verification (M&V) protocols such as ASHRAE 14 (ASHRAE, 2014), Efficiency Value

Organization (EVO, 2003), Federal Energy Management Program (FEMP, 2008), frequently indicated with the term M&V 2.0 (Gallagher et al., 2018), are included. This is crucial because of the necessity of performing an initial screening analysis before proceeding with more in-depth evaluations. Technical state-of-the-art standardization was used as a basis and some innovative elements were introduced. The starting point is a regression-based analysis of energy signatures (i.e., average power in a certain interval of analysis).

Sample models for the whole-building approach (ASHRAE 14:2014 Measurement of Energy, Demand, and Water Savings) are used:

- mean, or one-parameter model, (electricity);
- two-parameter model;
- three-parameter heating model (similar to a variable-base degree-day VBDD model for heating);
- three-parameter cooling model (VBDD for cooling);
- four-parameter heating model;
- four-parameter cooling model;
- five-parameter model.

Energy signature regression is proposed in standardization as a way of "normalizing " energy performance with respect to the main influencing factors - outdoor air temperature in this case. Models can then be used to track performance in time (Manfren et al., 2019 and 2021b).

3. Case Study

Hale Court is a sheltered housing development run by Portsmouth City Council, built in 1984. Hale Court consists of 80 flats with a mix of studio flats, 1 bedroom-, 2 bedroom- and 3-bedroom-flats.

As part of the EU Horizon 2020 project THERMOSS), Smart Thermostatic Radiator Valves were installed and the heating system plant room was refurbished with the installation of Gas Absorption Heat Pumps (GAHP). A monitoring system was set-up to enable detailed building energy performance analysis.

The proposed refurbishment of the heating system for the North Block plant room involves: (1) keeping the existing gas boilers (2) removal of the water heaters (3) addition of a 3-GAHP cascade (4) incorporation of thermal storage and (5) reconfiguration of the piping layout.

Table 1 – Characteristics of the thermal systems

HEAT GENERATORS	
Gas Boilers x2	**REMEHA GAS 110 Eco**
Capacity	115 kW (per boiler)
Boiler design Temperature	80 °C
Typology	Condensing
Gas Absorption Heat Pump	**GHP AWO 38 Three appliance cascade**
Thermal power output A7W50	114.9 kW
Gas Utilization Efficiency A7W50	1.52
Natural gas power input A7W50	75.6 kW
Max. heating water flow temperature	65 °C
Permissible Ambient Temperature	-20 to +40 °C

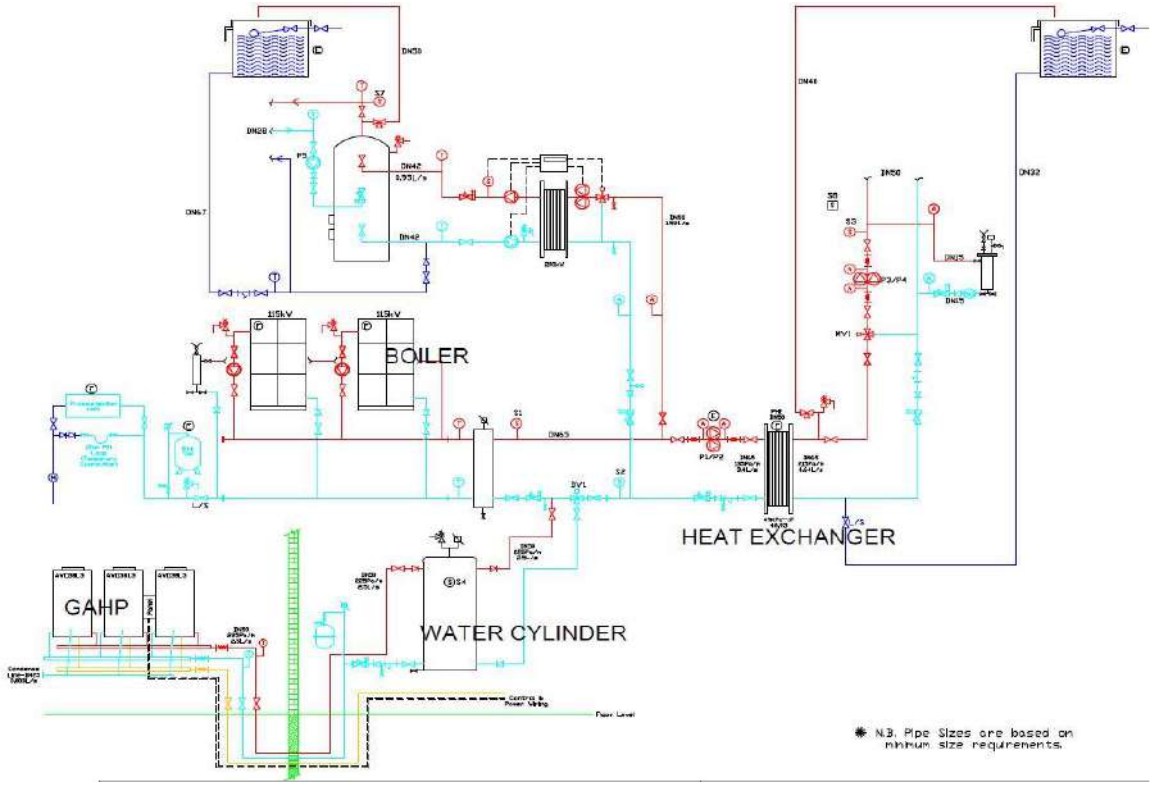

Fig. 1 – Technological scheme of the case study – Hale Court

4. Results and Discussion

Energy signature analysis of natural gas and electricity requires using piecewise linear regression for Hale Court, North Block.

The two models for natural gas demand signature (three-parameter heating model) and electricity signature are in the boundaries fixed by the ASHRAE 14:2014 guidelines.

Table 2 – Results of analysis for natural gas demand signature

Period	Energy indicator			Statistical indicator			
	Energy Measured (M)	Energy Predicted (P)	Relative differences	R^2	MAPE	NMBE	Cv(RMSE)
1	293464	299273	-1.98	93.0	14.3	1.98	11.9
2	93466	93544	-0.08	91.1	15.9	0.08	12.2
3	242586	243004	-0.17	88.3	13.9	0.17	13.3

The energy demand reduction regression model of GAHP performance shows a reduction of 20 %.

Table 3 shows the energy demand reduction using a prediction model, with standard weather and normalized occupant behavior.

Table 3 – Reductions

Period	Description	Overall reduction	Relative reduction
1	Before retrofit	0 (baseline)	-
2	TRVs installation	7.2 %	0 (baseline)
3	GAHPs and plant room upgrade	25.8 %	20.0 %

In order to characterize GAHP performance, we need to consider the *GUE* (Gas Utilization Efficiency), which is the parameter describing its thermal conversion efficiency. *GUE* is defined as the ratio between the delivered thermal energy and the fuel energy (and substantially similar to the COP for an electric heat pump).

Prediction of thermal power output P_{th} and *GUE* in full load conditions as a function of outdoor air temperature and supply water temperature used multivariate regression.

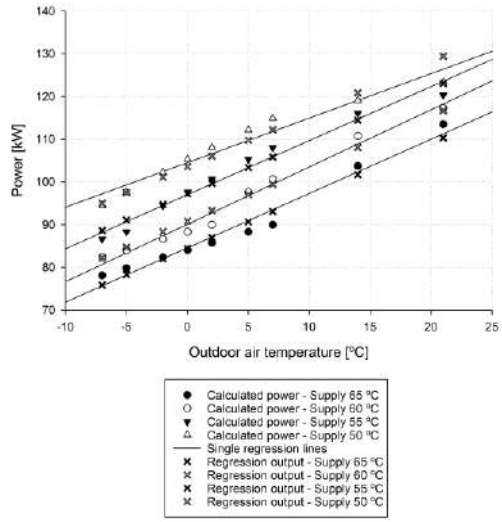

Fig. 2 – Thermal power output as a function of outdoor air temperature

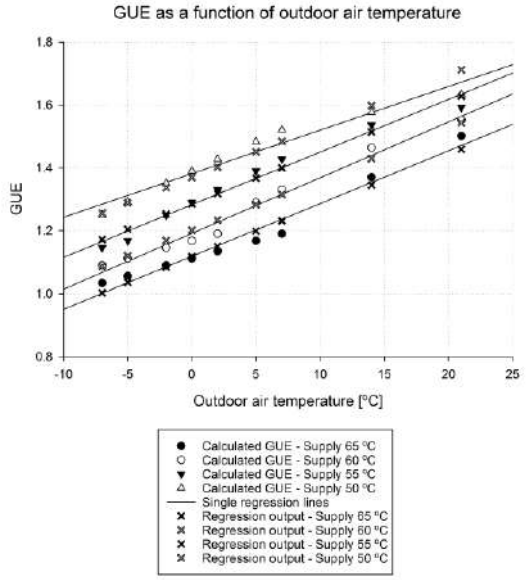

Fig. 3 – GUE as a function of outdoor air temperature

5. Conclusions

Energy signature modeling is a powerful tool for a first screening using monthly data. GAHP performance linearization enables the estimation of performance variability (P_{th}, *GUE)* as a function of outdoor air and supply temperatures and the calculation of part-load performance. Feedback from data analysis can help to improve management and control of GAHP.

Further research concerns application to daily and hourly data, to derived daily and hourly energy signature analysis and performance tracking:

1. Calculation of part-load performance ratio for GAHP using the regression model as reference.
2. Analysis of average thermo-physical properties of building to support detailed energy model calibration.

References

ASHRAE. 2014. *ASHRAE Guideline 14-2014: Measurement of Energy, Demand, and Water Savings*. American Society of Heating, Refrigerating and Air-Conditioning Engineers: Atlanta, GA, USA.

EVO. 2003. *IPMVP New Construction Subcommittee. International Performance Measurement & Verification Protocol: Concepts and Option for Determining Energy Savings*. In New Construction, Volume III; Efficiency Valuation Organization (EVO): Washington, DC, USA.

FEMP. 2008. *Federal Energy Management Program, M&V Guidelines: Measurement and Verification for Federal Energy Projects Version 3.0*. U.S. Department of Energy Federal Energy Management Program.

Gallagher C. V., K. Leahy, P. O'Donovan, K. Bruton, and D. T. J. O'Sullivan. 2018. "Development and application of a machine learning supported methodology for measurement and verification (M&V) 2.0." *Energy and Building* 167: 8–22. doi: https://doi.org/10.1016/j.enbuild.2018.02.023

Manfren, M., B. Nastasi, E. A. Piana, and L. Tronchin. 2019. "On the link between energy performance of building and thermal comfort: An example." *AIP Conference Proceedings* 2123: 1-9. doi: https://doi.org/10.1063/1.5116993

Manfren, M., B. Nastasi, L. Tronchin, D. Groppi, and D. A. Garcia. 2021a. "Techno-economic analysis and energy modelling as a key enablers for smart energy services and technologies in buildings". *Renewable and Sustainable Energy Reviews* 150: 1-14. doi: https://doi.org/10.1016/j.rser.2021.111490

Manfren, M., M. Sibilla, and L. Tronchin. 2021b. "Energy Modelling and Analytics in the Built Environment—A Review of Their Role for Energy Transitions in the Construction Sector."

Energies 14: 1-29- doi: https://doi.org/10.3390/en14030679

Manfren, M., P. A. B. James, and L. Tronchin. 2022. "Data-driven building energy modelling – An analysis of the potential for generalisation through interpretable machine learning". *Renewable and Sustainable Energy Reviews* 167: 1-13. https://doi.org/10.1016/j.rser.2022.112686

Tronchin, L., K. Fabbri, and C. Bertolli. 2018. "Controlled Mechanical Ventilation in Buildings: A Comparison between Energy Use and Primary Energy among Twenty Different Devices." *Energies* 11: 1-20, doi: https://doi.org/10.3390/en11082123

The Amintore Galli Theatre in Rimini: A Dataset of Building Simulation Tools for its Acoustic Design

Antonella Bevilacqua – University of Parma, Italy – antonella.bevilacqua@unipr.it
Massimiliano Manfren – University of Southampton, UK – M.Manfren@soton.ac.uk
Maria Cristina Tommasino – ENEA, Italy – cristina.tommasino@enea.it
Ruoran Yan – University of Bologna, Italy – ruoran.yan2@unibo.it
Lamberto Tronchin – University of Bologna, Italy – lamberto.tronchin@unibo.it

Abstract

The Amintore Galli theater in Rimini re-opened in 2018, after more than 60 years of inactivity. Its acoustics have been studied in depth, starting in 2009 until the re-opening of the theater. This paper analyses the following different steps of the acoustic design of the Opera House: the analysis of the acoustics of similar other theaters, the design of the acoustics of the new main hall, the analysis of the acoustic characteristics of the diffusing panels in the theater, and the acoustic design of other rooms, including the rehearsal room. Moreover, this paper reports some of the most relevant results of the acoustic surveys conducted after the re-opening, comparing the values of some acoustic parameters obtained after the simulation processes, and the values of the same parameters during the final validation of the theater.

1. Introduction

The acoustic studies of Italian opera theater houses have been improved in their accuracy by the development of new generation technology (Farina et al., 1998; Tronchin, 2005 and 2021; Tronchin & Bevilacqua, 2021 and 2022; Tronchin & Knight, 2016; Tronchin et al., 2020a, 2020b, 2021a and 2021b). An acoustic survey was undertaken inside Galli theater of Rimini in order to show the acoustic parameters as required by the regulations (ISO 3382-1). Furthermore, a multichannel spherical array microphone was employed to add value to this acoustic investigation by illustrating the impulse response (IR) through an overlay video. The outcomes of this additional provision were recorded with some snaps related to different moments of the IR decay. The authors of this paper also outline a brief history of Galli theater of Rimini, including a description of the architectural features that characterize this important opera house.

2. Historical Background

The theater was originally named "Teatro Nuovo" (The New Theater), and the project began in 1841, overseen by architect Luigi Poletti. The theater distinguished itself from other theaters in the same period, showing the innovative style of memorial architecture of classical architecture (Toyota, 2020).
The theater was built between 1843 and 1856, and the project was delivered to Pietro Bellini, the Rimini contractor. The cost of the theater was mostly covered by the aristocracy. The theater officially opened in 1857. It was renamed Teatro Vittorio Emanuele II in 1859 (Toyota, 2020).
In 1916-1923, the ceiling of the theater was damaged and cracked in an earthquake. In addition to the necessary repair of the historical structure, it was also equipped with an electrical system (Toyota, 2020). Subsequently, the architect Gaspare Rastelli completed the Ridotto and upper Gallery of the theater with neoclassical elements different from Poletti (Toyota, 2020).
In 1943, the theater was almost completely destroyed by bombing during World War II. At the same time, the theater was looted after becoming a military camp, and the best furniture in the theater was robbed. In 1947, it was officially renamed with its current name in memory of the great composer, Amintore Galli.

Since 1948, any decision on the restoration of the theater was repeatedly postponed because Rimini, a town of Roman origin, contained a lot of Roman relics. Part of the reconstruction of Amintore Galli theater began in 1997, and, in 2010, under the auspices of the municipal authorities, adhering to the concept of being as faithful to the original design as possible while respecting the safety rules, the theater began to be fully rebuilt. After a long period of restoration work, Amintore Galli theater reopened in 2018.

Fig. 1 − Internal view of the Galli theater of Rimini

The main hall of Galli theater could host more than 700 people. All these seats are distributed as 268 seats in the stalls, and 324 seats on the three orders of boxes and 108 seats in the gallery. The dimensions of the main axes of the horseshoe shape plan are 22 m and 16 m [L, W,], which are crowned by three orders of balconies, surmounted by a gallery having a capacity of 108 seats. The total height of the main hall is 20 m. The floor of the stalls is composed of oak planks, slightly inclined (2 %) towards the stage.

The restoration works in Galli theater had previously also included the restoration of the main foyer of the theater, and also other rooms, including the "ballet room", located just beyond the roof, on top of the foyer.

3. Architectural Organization

The main hall of Amintore Galli theater, completed in 1856, is a traditional horseshoe plan, with a total capacity of 700 seats, of which 268 seats are distributed in the stalls, 324 seats are distributed in the elevated box, and 108 seats in the gallery. The main hall is 22 m, 16 m and 20 m [L, W, H], crowned by a three-order balcony, with a gallery at the top that can accommodate 108 seats. The floor of the stalls is slightly inclined towards the stage, composed of oak planks, as shown in Fig. 2.

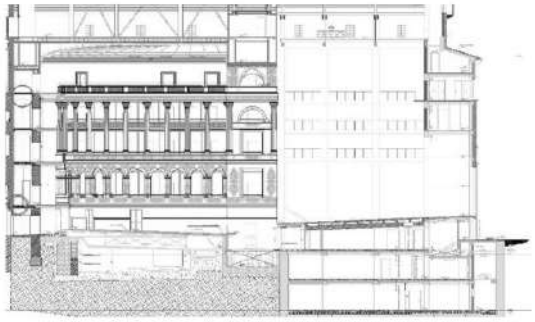

Fig. 2 − Longitudinal section of Amintore Galli Theater

After a period of long repair, the main hall still retains the original historical appearance dominated by ivory and gold. The floor and ceiling have been reinforced, and the decorations and painting have been restored (Toyota, 2020), as shown in Fig. 3. Further, pomegranate red has been used on seats and for the upholstery of the boxes.

Fig. 3 − Reliefs have been restored

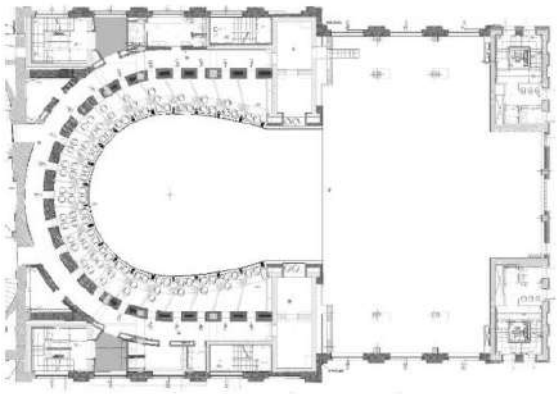

Fig. 4 − Plan layout of the main hall

The total area of the stage is 358 m² and the proscenium arch is 13 m large and 17 m high, the stage inclined by 2 %. The orchestra pit is 5.5 m deep and 12 m wide. Fig. 4 shows the horseshoe-shaped layout of the main hall.
Table 1 summarizes the architectural features of Amintore Galli theater.

Table 1 - Architectural characteristics of Amintore Galli theater

Description	Features
Type of plan layout	Horseshoe box
Total volume (m^3)	14420
Total capacity (no. of seats)	700
Stage dimension (m) [L × W]	30 × 16
Inclination of stage floor (%)	2 %
Inclination of stalls area (%)	2 %
Volume of the flytower (m^3)	8640
Volume of the main hall (m^3)	5780

Fig. 5 − View of the main hall of Teatro Galli of Rimini

Elaborate decoration is installed all around the main hall, with floor finishings , seats, upholstery and the walls of the boxes. having a pomegranate red color. Other dominant colors are ivory and gold, used on the wooden decorations.
The acoustics of Teatro Galli have been studied since 2010, when a specific 3D model was created in order to determine the future sound distribution in the main hall. Fig. 6 reports the numeric model of the theater.

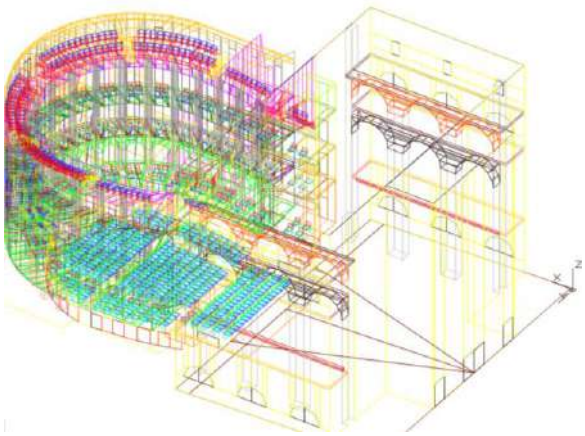

Fig. 6 − 3D numeric model of Teatro Galli

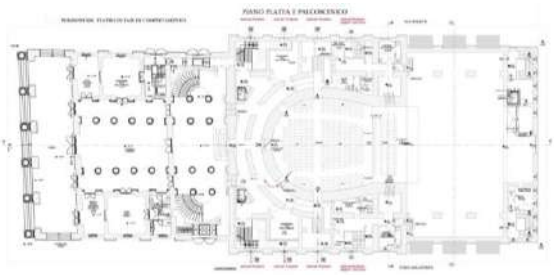

Fig. 7 − Plan layout of Teatro Galli of Rimini

4. Acoustic Surveys

Inside Galli theater, several acoustic measurements were taken during different steps of the reconstruction of the theater, and compared with the simulation conducted during the acoustic design. At the same time, thermo-hygrometric parameters were also taken into consideration, since the variation of the acoustic parameters with thermo-hygrometric conditions are relevant. The acoustic survey was carried out with the following equipment:

1. Equalised omnidirectional loudspeaker (Look Line);
2. Binaural dummy head (Neumann KU-100);
3. B-Format (Sennheiser Ambeo);
4. Omnidirectional microphone (Bruel&Kjaer);
5. 32-channel spherical array (Mh Acoustic em32 Eigenmike®);
6. Ricoh Theta V 360 camera
7. Personal Computer connected to the loudspeaker and all the receivers.

Fig. 8 reports a screenshot of two impulse responses, measured in the stalls and in the box.

Fig. 8 − Impulse responses measured in the stalls (n 2) and box (2nd order (n 12))

Fig. 9 reposts the comparison for reverberation time T30 obtained after reconstruction with the same parameter simulated in 2010.

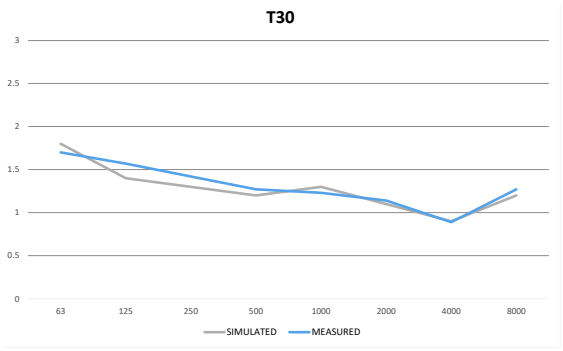

Fig. 9 − Reverberation time measured after reconstruction compared with the values obtained during the acoustic design in 2010

The sound source was located 1.4 m from the stage floor, while the receivers were positioned at a height of 1.2 m on stalls and boxes. The excitation signal emitted by the sound source was the Exponential Sine Sweep (ESS), having a duration of 15 s at a uniform sound pressure level for the between 40 Hz and 20 kHz range. The measurements were undertaken in unoccupied conditions and without any scenery or acoustic chamber mounted. Fig. 10 and Fig. 11 show the measurement positions of sound source and receivers placed across the sitting areas.

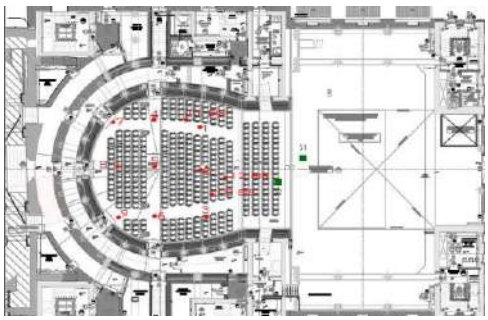

Fig. 10 − Scheme of the equipment location during the acoustic measurements in the stalls of Teatro Galli of Rimini

Fig. 11 − One of the surveys conducted in Teatro Galli in Rimini

5. Results

5.1 Traditional Parameters

The recorded ESS signals were processed by using the Aurora plugin suitable for Audition 3.0. Different acoustic parameters defined by the international standards ISO 3382-1 were analyzed and commented on.To be included are reverberation time (T_{20}), early decay time (EDT), clarity indexes (C_{80} and C_{50}), definition (D_{50}) and strength (G). The main acoustic parameters are reported in the octave bands between 125 Hz and 4 kHz, considered as the average results of all the measurement positions.

Fig. 12 and Fig. 14 show the graphs of the measurements of the main acoustic parameters. Fig. 13 shows the frequency response of the EDT and T_{20} parameters. If optimal values of EDT for concert halls are considered to range between 1.8 and 2.6 s, as defined by the literature, this target was not achieved by the measured values related to the selected bandwidth. However, if compared with several other opera houses, the results for Teatro Galli are much better than the others.

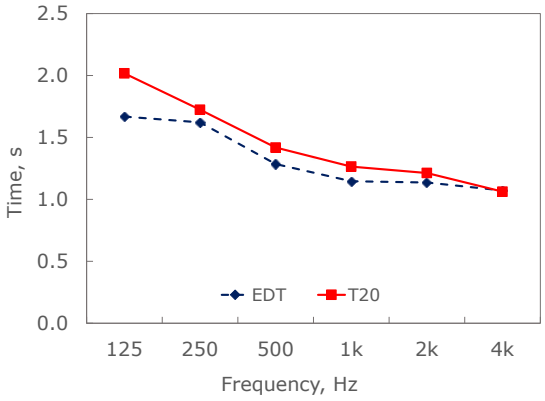

Fig. 12 − Measured results of clarity indexes (C50 and C80)

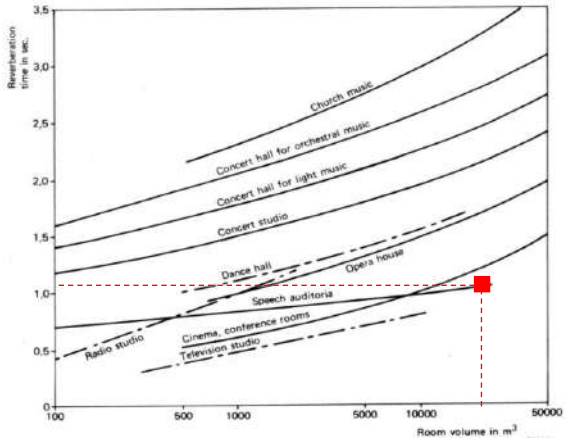

Fig. 13 − Optimum reverberation time values in function of room volume

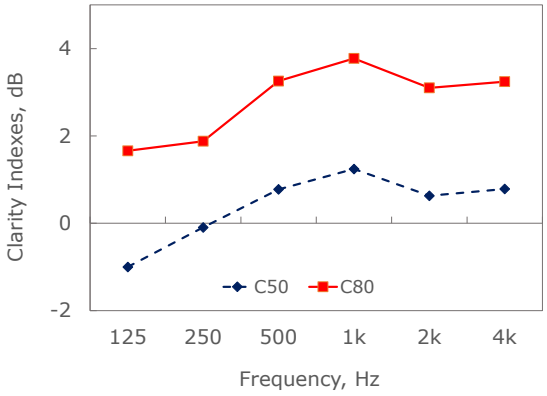

Fig. 14 − Measured results of clarity indexes (C50 and C80)

Following the research studies by Reichardt, the optimum values for the speech clarity index (C_{50}) would be ≥ 0 dB. In Teatro Galli, this parameter floats between +1 and +4 dB, at low and high frequency bands, respectively. Based on the results of Fig. 14, the good response of C_{50} was achieved at frequencies higher than 500 Hz. However, the shortfall at low frequencies found to be slightly below the lowest range limit is not to be interpreted as a negative result.

5.2 Acoustic Analysis of 3D Sound Maps

The employment of the spherical array microphone (i.e., em32 Eigenmike®) allowed the authors to elaborate sound maps obtained for each source-receiver combination. These maps were created by a video-overlay that reproduces the recorded IR.

This different data analysis is obtained by a combination of the omnidirectional sound source, the multichannel microphone (i.e., em32 Eigenmike®) and the panoramic camera (i.e., Rico Teta V, capturing a 360° image herein represented in an equirectangular view). The 32 microphone signals were processed by extracting 122 high-directivity virtual microphones (with 8th order cardioid setup) with the addition of the Spatial PCM Sampling (SPS). By using this methodology, it was possible to encode the direction of arrival of all the sound rays, including the direct sound and the reflections occurring after hitting any surface.

The colors shown in the map overlay range between red tinge (indicating the high level of sound energy) and blue-violet shades (representing a poor energy sound wave). Fig. 15 shows an illustration of the outcomes.

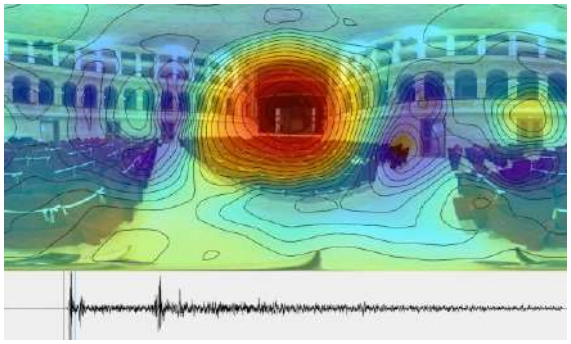

Fig. 15 − Acoustic map showing direct sound arriving to the receiver placed in the stalls

Fig. 15 shows the late reflections hitting the ceiling surface area. As per the above discussion, the overlay videoclip allows the surface areas that contribute toward creating the early and late reflections to be visualized. The bar at the bottom of the image indicates the flow time of the IR.

6. Conclusions

This paper deals with the representation of the acoustic results obtained by the survey undertaken in the Teatro Galli in Rimini Measurements were conducted by using an omnidirectional sound source and four types of microphones.

Overall, the results obtained from the measurement campaign showed that the theater has a good response for speech performance, with some difficulties at low frequencies in terms of strength, which requires the singers to put more effort into the bass tones. In terms of music, the theater turns out to be slightly dry compared to opera houses of similar volume size.

This acoustic study was extended to analyze the specific trajectory of the sound waves during the IR. The capabilities of the multi-channel spherical microphone (i.e., em32 Eigenmike®) allowed the authors to render 3D sound maps, obtained for each source-receiver combination. Such maps indicate the direction of arrival of the sound rays and their intensity, contributing to understanding the specific role of the specific construction elements interacting with the sound waves.

References

Farina, A., A. Langhoff, and L. Tronchin. 1998. "Acoustic characterisation of "virtual" musical instruments: using MLS technique on ancient violins." *Journal Of New Music Research* 27(4): 359-379. doi: https://doi.org/10.1080/09298219808570753

Toyota, Y. 2020. *Concert Halls by Nagata Acoustics: Thirty Years of Acoustical Design for Music Venues and Vineyard-Style Auditoria*.

Tronchin, L. 2005. "Modal analysis and intensity of acoustic radiation of the kettledrum." *The Journal Of The Acoustical Society Of America* 117(2): 926-933. doi: https://doi.org/10.1121/1.1828552

Tronchin, L. 2021. "Variability of room acoustic parameters with thermo-hygrometric conditions." *Applied Acoustics* 177: 1-14. doi: https://10.1016/j.apacoust.2021.107933

Tronchin, L., & A. Bevilacqua. 2021. "Acoustic study of different sceneries at the São Carlos national theatre of Lisbon." *Applied Acoustics* 180: 1-11. doi: https://doi.org/10.1016/j.apacoust.2021.108102

Tronchin, L., and A. Bevilacqua. 2022. "Historically informed digital reconstruction of the Roman theatre of Verona. Unveiling the acoustics of the original shape." *Applied Acoustics* 185: 1-18. doi: https://doi.org/10.1016/j.apacoust.2021.108409

Tronchin, L, and D. J. Knight. 2016. "Revisiting Historic Buildings through the Senses. Visualising Aural and Obscured Aspects of San Vitale, Ravenna." *International Journal of Historical Archaeology* 20: 127-145. doi: https://doi.org/10.1007/s10761-015-0325-2

Tronchin, L., M. Manfren, and V. Vodola. 2020a. "The carabattola - vibroacoustical analysis and intensity of acoustic radiation (IAR)". *Applied Sciences* 10(2): 641. doi: https://doi.org/10.3390/app10020641

Tronchin, L., M. Manfren, and V. Vodola. 2020b. "Sound characterization through intensity of acoustic radiation measurement: A study of persian musical instruments". *Applied Sciences* 10(2), 633. doi: https://doi.org/10.3390/app10020633

Tronchin, L., F. Merli, and M. Dolci. 2021a. "Virtual acoustic reconstruction of the Miners' Theatre in Idrija (Slovenia)." *Applied Acoustics* 172: 1-9. doi: https://doi.org/10.1016/j.apacoust.2020.107595

Tronchin, L., F. Merli, and M. Manfren. 2021b. "On the acoustics of the Teatro 1763 in Bologna." *Applied Acoustics* 172: 1-9. doi: https://doi.org/10.1016/j.apacoust.2020.107598

Data-Driven Building Energy Modelling – Generalisation Potential of Energy Signatures Through Interpretable Machine Learning

Massimiliano Manfren – University of Southampton, UK – M.Manfren@soton.ac.uk
Maria Cristina Tommasino – ENEA, Italy – cristina.tommasino@enea.it
Lamberto Tronchin – University of Bologna, Italy – lamberto.tronchin@unibo.it

Abstract

Building energy modeling based on data-driven techniques has been demonstrated to be effective in a variety of situations. However, the question about its limits in terms of generalization is still open. The ability of a machine-learning model to adapt to previously unseen data and function satisfactorily is known as generalization. Apart from that, while machine-learning techniques are incredibly effective, interpretability is required for a "human-in-the-loop" approach to be successful. This study develops and tests a flexible regression-based approach applied to monitored energy data on a Passive House building. The formulation employs dummy (binary) variables as a piecewise linearization method, with the procedures for producing them explicitly stated to ensure interpretability. The results are described using statistical indicators and a graphic technique that allows for comparison across levels in the building systems. Finally, suggestions are provided for further steps toward generalization in data-driven techniques for energy in buildings.

1. Introduction

Data-driven building energy modeling methods that use machine-learning techniques have been shown to be useful in a variety of applications (Hong et al., 2020), from design (Westermann & Evins, 2019) to operation (Manfren et al., 2020). As a result, they have the potential to become a key tool for accelerating the ongoing process of building stock decarbonisation (Norton et al., 2021; Tronchin, & Knight, 2016) as well as an integral part of innovative services and technologies (Farina et al., 1998; Manfren et al., 2021a). However, the question of whether data-driven approaches can be generalized is still being debated.

The ability of a machine-learning model to adapt to previously unknown data and perform reasonably well, given specified performance criteria, is referred to as generalization. A simple example of generalization is a model trained on building energy consumption data over a period of time and then used to estimate energy consumption during a successive period of time. This is the counterfactual approach used in Measurement and Verification (M&V) protocols, which uses statistical indicators as model acceptability criteria during the calibration phase. A more ambitious form of generalization would be that of using data-driven methods on energy modeling problems involving sets of building with homogeneous characteristics. Using data-driven methods on energy modeling problems involving different sets of buildings with relatively similar characteristics would be a more ambitious type of generalisation.

In this research, we use regression models trained and tested on building energy signatures as a tool for addressing the generalization problem. In fact, methods based on energy signature (ISO, 2013) (i.e., energy divided by the number of operating hours in the time interval of the analysis, corresponding to an average power) are scalable (temporally and spatially) (Manfren et al., 2021b; Tronchin, 2021; Tronchin et al., 2018), can work with unstructured data (using clustering) (Pistore et al., 2019; Westermann et al., 2020) and provide results that are weather normalized (Fazeli et al., 2016). Additionally, energy signatures can be scaled according to the building's size (Pistore et al., 2019; Tronchin et al., 2016), to produce a performance comparison that is independent of the size. Further, regression-based approaches are considered interpretable machine learning techniques (ISO, 2020) because it is possible

to predict how the model output will change in response to a change in input data or algorithmic parameters (i.e., the rationale behind model output and the algorithmic logic can be easily understood in human terms) (Fabbri et al., 2014 and 2021). In this study, we employ this technique to analyze monitored data from a Passive House building in the Province of Forlì-Cesena in northern Italy, with the goal of improving formulations at the state of the art while also considering generalization and interpretability issues (Tronchin, 2005 and 2021).

2. Methods

The regression model proposed in this research is a reformulation of the variable-based degree-days regression, originally proposed by Kissock et al. (2003) in their Inverse Modeling Toolkit (IMT), which has been included in ASHRAE 14:2014 (ASHRAE, 2014) and has been evolving steadily with different algorithmic formulations. Essentially, interpretable regression-based methods can be based on general piecewise linearization methods (Lin et al., 2013) and use dummy (binary variables) to handle non-linearities. Model formulation and calibration criteria are reported hereafter (Tronchin et al., 2021a and 2021b).

2.1 Model Formulation

Separate sub-models (heating, base load and cooling), indicated in Table 1, are combined into a single model (which is the sum of the individual sub-models) by introducing additional variables (dummy, 0-1 binary variables) to the original datasets using rules, indicated in Table 2. The binary variables multiply the original variables and act as interaction terms. Two types of models are tested, type 1 and type 2. In the first case, the independent variable is outdoor air temperature, while, in the second case, the independent variables are outdoor air temperature and total solar radiation on horizontal surface. The dependent variables are the energy signatures calculated from the monitored data described in Section 3.

The rules provided hereafter in Table 2 can be applied both manually and in an automated way to the dataset, for example, using ranges of balance-point temperature (change-points) for heating and cooling (Manfren et al., 2019).

Table 1 – Regression model formulation

Mode	Demand	Sub-models	
Type 1	Heating	$q_h = a_0(X_h) + a_1(X_h\theta_e) + \varepsilon_h$	(1)
	Base load	$q_b = b_0(X_b) + b_1(X_b\theta_e) + \varepsilon_b$	(2)
	Cooling	$q_h = c_0(X_c) + c_1(X_c\theta_e) + \varepsilon_c$	(3)
Type 2	Heating	$q_h = a_0(X_h) + a_1(X_h\theta_e) + a_2(X_h I_{sol}) + \varepsilon_h$	(4)
	Base load	$q_b = b_0(X_b) + b_1(X_b\theta_e) + b_2(X_b I_{sol}) + \varepsilon_b$	(5)
	Cooling	$q_h = c_0(X_c) + c_1(X_c\theta_e) + c_2(X_c I_{sol}) + \varepsilon_c$	(6)

Table 2 – Rules for dummy variable creation

Rule	Description	Variables
1	If the energy demand is greater than 0 for the corresponding sub-model (e.g., heating, cooling or base load), then the dummy variable is equal to 1.	X_h, X_b, X_c
2	If the outdoor air temperature is lower than balance point temperature for heating (i.e., heating base temperature), the dummy variable for heating is equal to 1.	X_h
3	If the outdoor air temperature is greater than balance point temperature for cooling (i.e., cooling base temperature), the dummy variable for cooling is equal to 1.	X_c
4	All the dummy variables (that partition heating, cooling and base load demands) should be coherent with the schedules of operation for building services (i.e., months of heating and cooling system operation).	X_h, X_b, X_c
5	The dummy variables for base load are assumed to be 1 in all the months (i.e., electricity and hot water demand are always present).	X_b

2.2 Model Calibration Criteria

Following the indications proposed by state-of-the-art Measurement and Verification (M&V) protocols, such as ASHRAE 14:2014 (ASHRAE, 2014), Efficiency Value Organization (EVO) IPMVP (EVO,

2003), and Federal Energy Management Program (FEMP) (FEMP, 2008), the thresholds of acceptability for regression models as calibrated with monthly data are reported in Table 3.

Table 3 – Model calibration criteria

Data interval	Metric	ASHRAE Guidelines 14	IPMVP	FEMP
Monthly	*NMBE*	±5	±20	±5
	Cv(RMSE)	15	-	15

3. Case Study

The case study is Passive House building, located in the northern Italian province of Forlì-Cesena; the essential building data are reported in Table 4.

The building was monitored for three years and electric and thermal demand data were split by end use, as indicated in Table 5.

The modeling workflow pursued to test the models reported in Table 1 incrementally is set out in the following steps:

1. Initial training, year 1, 2.
2. Testing, year 3 (model created in step 1).
3. Retraining, year 1, 2 and 3.

The results obtained are reported hereafter in Section 4.

Table 4 – Building design data

Group	Type	Unit	Design
Geometry	Gross volume	m^3	1557
	Net volume	m^3	1231
	Heat loss surface area	m^2	847
	Net floor area	m^2	444
	Glazed area/total wall area ratio percentage	%	22.5
	Surface/volume ratio	1/m	0.54
Envelope	U value external walls	$W/(m^2 K)$	0.18
	U value roof	$W/(m^2 K)$	0.17
	U value transparent components	$W/(m^2 K)$	0.83
HVAC and DHW	Ground-source heat pump (GSHP) - Brine/Water Heat Pump (B0/W35)*	kW	8.4
	Borehole heat exchanger (2 double U boreholes)	m	100
On-site energy production	Building Integrated Photo-Voltaic (BIPV) - Polycrystalline silicon	kW_P	9.2
	Solar thermal - Glazed flat plate collector	m^2	4.32
	Domestic hot water storage	m^3	0.74

* EN 14511 test condition in heating mode, brine at 0 ºC and water 35 ºC with supply-return temperature difference Δt = 10 ºC.

Table 5 – Dataset used for modeling

Data	Enduse	Interval	Monitoring period
Electric	Total	Monthly	3 years
	HVAC, DHW	Monthly	3 years
	Appliances and lighting	Monthly	3 years
Thermal energy	Heating	Monthly	3 years
	Cooling	Monthly	3 years

4. Results and Discussion

In this section, the results of the model training and testing process are reported, indicating both numerical results represented by statistical indicators (Table 3) and visualization of energy signatures for the different models fitted.

4.1 Numerical Results of Regression Models

The results obtained are split with respect to the two types of models considered, namely type 1 and type 2.

4.1.1 Model Type 1

It can be clearly seen that model type 1, after 2 years, obtains values for the indicators *NMBE* and *Cv(RMSE)* that make them acceptable as calibrated (Table 3), with the exception of electricity demand for HVAC and DHW and thermal demand for cooling. In these cases, the values are higher than 15 % for *Cv(RMSE)* but lower than 20 %.

Table 6 – Model type 1 – Initial training (year 1 and 2)

Data	End-use	*EN(M)*	*EN(P)*	R^2	*NMBE*	*Cv(RMSE)*
		kWh	kWh	%	%	%
Electric	Total	23812	23510	84.77	-1.27	12.59
	HVAC, DHW	8611	8499	91.05	-1.30	17.99
	Appliances	15201	15202	70.27	0.01	10.12
Thermal	Heating	17761	17757	98.05	-0.03	8.87
	Cooling	5054	5004	93.50	-0.99	16.45

The model trained for the period indicated in Table 6 (first 2 years) is then tested for the third year of monitoring. In this case, we can see how, for model type 1, the statistical indicators in the testing phase are larger (i.e., the model performance is lower in terms of goodness of fit.

Table 7 – Model type 1 – Testing (year 3)

Data	End-use	*EN(M)*	*EN(P)*	R^2	*NMBE*	*Cv(RMSE)*
		kWh	kWh	%	%	%
Electric	Total	11318	10167	65.37	-10.17	20.15
	HVAC, DHW	3659	3181	90.78	-13.07	20.76
	Appliances	7659	7013	26.83	-8.44	22.13
Thermal	Heating	6029	5460	85.28	-9.53	21.17
	Cooling	1784	1841	63.23	3.19	20.21

Finally, models are retrained with the entire 3-year dataset, obtaining results that are slightly better compared to the ones presented in Table 6, but not largely different.

Table 8 – Model type 1 – Retraining (year 1, 2 and 3)

Data	End-use	*EN(M)*	*EN(P)*	R^2	*NMBE*	*Cv(RMSE)*
		kWh	kWh	%	%	%
Electric	Total	35130	34819	84.41	-0.88	12.12
	HVAC, DHW	12270	12139	91.23	-1.07	17.35
	Appliances	22860	22868	67.34	0.04	10.56
Thermal	Heating	23790	23795	95.91	0.02	12.42
	Cooling	6838	6735	90.91	-1.51	17.77

4.1.2 Model Type 2

The same workflow presented for model type 1 in Section 4.1.1 is repeated here for model type 2. The results are reported in Tables 9, 10 and 11, respectively. In this case, we can see a moderate improvement for the model training (Table 9) and retraining (Table 11), but a much better performance of the models in the testing phase (Table 10). In general, model type 2 performs better than type 1.

Table 9 – Model type 2 – Initial training (year 1 and 2)

Data	End-use	*EN(M)*	*EN(P)*	R^2	*NMBE*	*Cv(RMSE)*
		kWh	kWh	%	%	%
Electric	Total	23812	23518	88.36	-1.23	11.05
	HVAC, DHW	8611	8534	91.74	-0.90	17.16
	Appliances	15201	15204	82.19	0.02	7.84
Thermal	Heating	17761	17759	98.95	-0.01	6.50
	Cooling	5054	5229	93.54	3.46	18.34

Table 10 – Model type 2 – Testing (year 3)

Data	End-use	*EN(M)*	*EN(P)*	R^2	*NMBE*	*Cv(RMSE)*
		kWh	kWh	%	%	%
Electric	Total	11318	10551	85.96	-6.78	12.53
	HVAC, DHW	3659	3248	91.75	-11.24	18.80
	Appliances	7659	7329	66.66	-4.30	12.04
Thermal	Heating	6029	5828	94.13	-3.59	13.52
	Cooling	1784	1964	85.58	10.10	16.66

Table 11 – Model type 2 – Retraining (year 1, 2 and 3)

Data	End-use	*EN(M)*	*EN(P)*	R^2	*NMBE*	*Cv(RMSE)*
		kWh	kWh	%	%	%
Electric	Total	35130	34847	89.75	-0.81	10.16
	HVAC, DHW	12270	12200	92.41	-0.57	16.56
	Appliances	22860	22870	84.05	0.05	7.60
Thermal	Heating	23790	23798	98.32	0.03	7.96
	Cooling	6838	7002	91.61	2.39	17.04

4.2 Energy Signature Visualization

In this section, energy signatures are visualized for both electric and thermal data and divided by end use. Section 4.2.1 focuses on electricity data, while Section 4.2.2 focuses on thermal data.

4.2.1 Energy Signatures – Electricity

The energy signature shapes shown in Fig. 1 for total electricity, Fig. 2 for electricity for HVAC and DHW, Fig. 3 for appliances and lighting, are substantially similar to a 5p or nearly 4p model according to the classification proposed by ASHRAE14:2014. The charts are used to compare models type 1 and 2 at multiple levels in the building

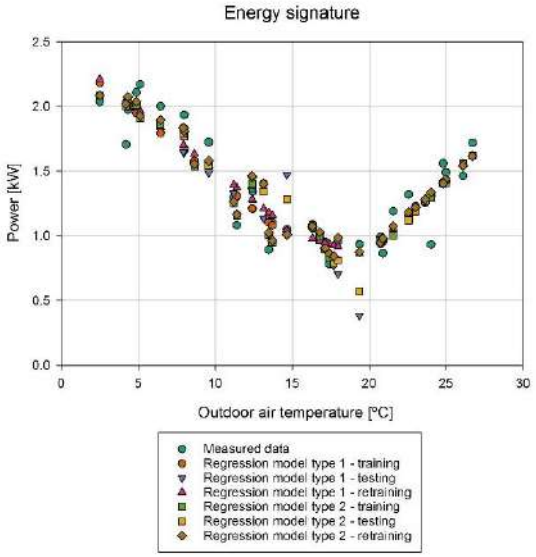

Fig. 1 – Energy signatures, measured data and regression models types 1 and 2 – Total electricity

The spread of data around the trend line is quite limited in Fig. 1 (total electricity) and Fig. 2 (electricity for HVAC and DHW), while it is more pronounced for Fig. 3 (appliances and lighting). In the latter, there is a lower temperature dependence (steepness of the trend line), compared to the other cases. However, the dependence is actually on daylight hours, which are correlated to temperature (lower temperatures correspond to winter condition where daylight hours are less and electric consumption for lighting is higher) and on the actual operation pattern, whose variability also determines the larger spread of values.

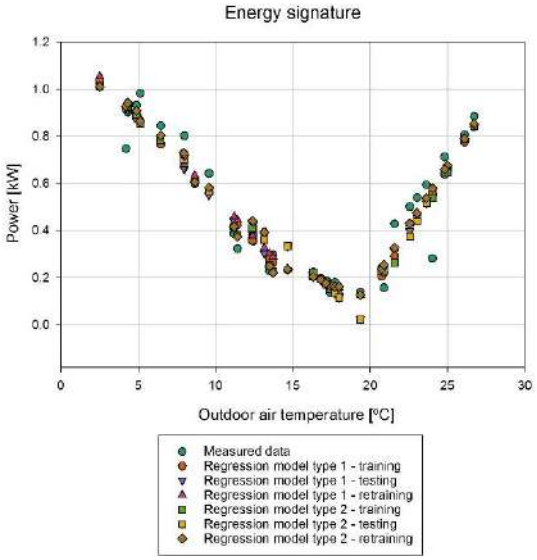

Fig. 2 – Energy signatures, measured data and regression models types 1 and 2 – Electricity for HVAC and DHW

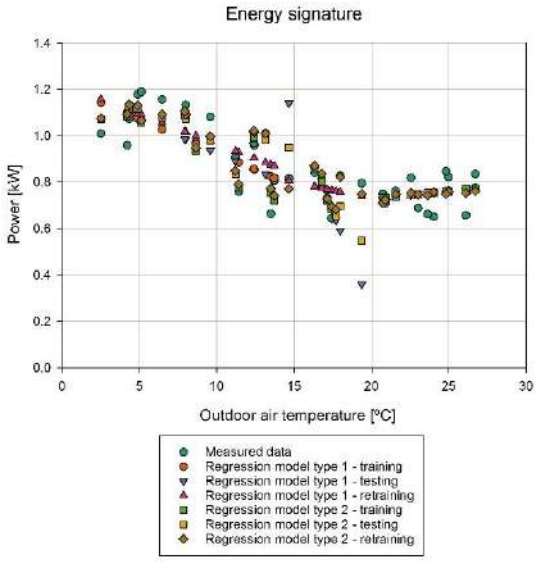

Fig. 3 – Energy signatures, measured data and regression models types 1 and 2 – Electricity for appliances and lighting

4.2.2 Energy Signatures – Thermal Energy

The energy signature shapes shown in Fig. 4 for thermal demand for heating and in Fig. 5 for thermal demand for cooling are essentially similar to a 3p model according to the classification proposed by ASHRAE14:2014. There are clearly some months when the technical systems do not produce either heating or cooling. Finally, it is possible to identify graphically, in an approximated way, the balance-point temperature for heating and cooling, around 14 °C and 19 °C, respectively.

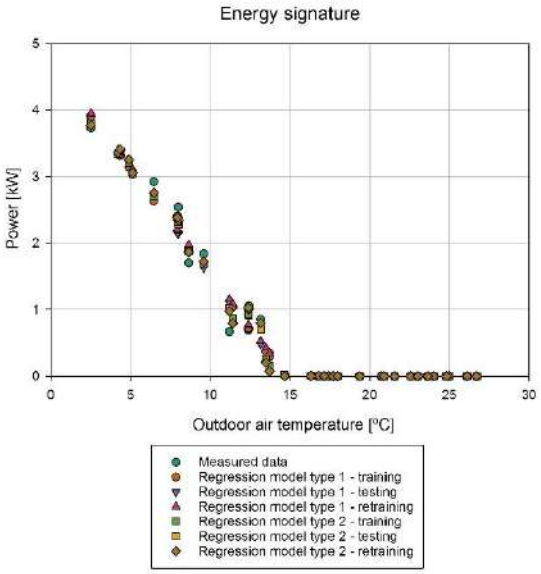

Fig. 4 – Energy signatures, measured data and regression models types 1 and 2 – Thermal energy for heating

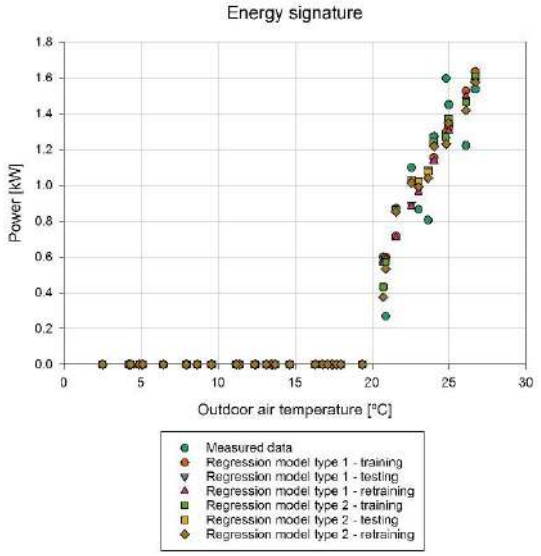

Fig. 5 – Energy signatures, measured data and regression models types 1 and 2 – Thermal energy for cooling

5. Conclusion

Machine learning-based building energy modeling techniques have proved to be effective in a range of applications. However, problems such as generalization and interpretability must be considered in order to enable the widespread adoption of these techniques. A piecewise linear regression model (interpretable) was proposed to analyze monitored data from a Passive House building, located in the northern Italian province of Forlì-Cesena. The

building was monitored for three years, and this technique requires at least two years of monthly interval data to be used effectively. Nonetheless, the formulation provided is quite simple and flexible; the visualization of energy signatures can also help understanding the actual spread of data around the trend line, which represent outdoor air temperature dependence.

Further efforts involving the categorization of building data according to archetypes could be considered to address the generalization issue effectively. Finally, interpretability is extremely relevant because of the necessity to promote a "human-in-the loop" approach when using machine learning tools and the transparent link between regression model formulation and other analytical techniques at the state-of-the-art could represent an interesting research area from the perspective of future studies (Tronchin et al., 2020a and 2020b).

Nomenclature

Symbol	Quantity	Unit
a_0,b_0,c_0	regression coefficients, intercept	kW
a_1,b_1,c_1	regression coefficients, temperature dependence term	kW/K
a_2,b_2,c_2	regression coefficients, solar radiation dependence term	m²
$Cv(RMSE)$	coefficient of variation of RMSE	-
$EN(M)$	measured energy	kWh
$EN(P)$	predicted energy	kWh
I_{sol}	total solar radiation on horizontal surface (direct and diffuse) average hourly value on monthly base	kW/m²
$NMBE$	normalized mean bias error (expressed in percentage)	-
q_h	energy signature heating	kW
q_b	energy signature base load	kW
q_c	energy signature cooling	kW
R^2	determination coefficient (expressed in percentage)	-
X_h	dummy variable (binary 0-1) heating	-
X_b	dummy variable (binary 0-1) base load	-
X_c	dummy variable (binary 0-1) cooling	-
θ_e	outdoor air temperature	ºC
ε_h	error term heating	kW
ε_b	error term base load	kW
ε_c	error term cooling	kW

References

ASHRAE. 2014. *ASHRAE Guideline 14-2014: Measurement of Energy, Demand, and Water Savings.* American Society of Heating, Refrigerating and Air-Conditioning Engineers: Atlanta, GA, US.

EVO. 2003. *IPMVP New Construction Subcommittee. International Performance Measurement & Verification Protocol: Concepts and Option for Determining Energy Savings in New Construction, Volume III.* Efficiency Valuation Organization (EVO): Washington, DC, US.

Fabbri, K., L. Tronchin, and V. Tarabusi. 2014. "Energy Retrofit and Economic Evaluation Priorities Applied at an Italian Case Study". *Energy Procedia* 45: 379-384. doi: 10.1016/j.egypro.2014.01.041.

Fabbri, K., L. Tronchin, and F. Barbieri. 2021. "Coconut fibre insulators: The hygrothermal behaviour in the case of green roofs". *Construction and Building Materials* 266: 1-9. doi: 10.1016/j.conbuildmat.2020.121026.

Farina, A., L. Langhoff, and L. Tronchin. 1998. "Acoustic characterisation of "virtual" musical instruments: using MLS technique on ancient violins". *Journal of new music research* 27(4): 359-379.

Fazeli, R., M. Ruth, and B. Davidsdottir. 2016. "Temperature Response Functions for Residential Energy Demand – A Review of Models." *Urban Climate* 15: 45–59. doi: https://doi.org/https://doi.org/10.1016/j.uclim.2016.01.001

FEMP. 2008. *FEMP. Federal Energy Management Program, M&V Guidelines: Measurement and Verification for Federal Energy Projects Version 3.0*. U.S. Department of Energy Federal Energy Management Program: Washington, DC, US.

Hong, T., Z. Wang, X. Luo, & W. Zhang. 2020. "State-of-the-Art on Research and Applications of Machine Learning in the Building Life Cycle." *Energy and Buildings* 212: 109831. doi: https://doi.org/https://doi.org/10.1016/j.enbuild.2020.109831

ISO. 2013. *ISO 16346:2013, Energy Performance of Buildings — Assessment of Overall Energy Performance*.

ISO. 2020. *ISO/IEC TR 29119-11:2020(En) Software and Systems Engineering — Software Testing — Part 11: Guidelines on the Testing of AI-Based Systems*.

Kissock, J. K., J. S. Haberl, and D. E. Claridge. 2003. "Inverse Modeling Toolkit: Numerical Algorithms." *ASHRAE Transactions* 109: 425.

Lin, M.-H., J. Gunnar Carlsson, D. Ge, J. Shi, and J.-F. Tsai. 2013. "A Review of Piecewise Linearization Methods." *Mathematical Problems in Engineering* 2013: 101376. https://doi.org/10.1155/2013/101376

Manfren, M., B. Nastasi, E. A. Piana, and L. Tronchin. 2019. "On the link between energy performance of building and thermal comfort: An example". In *AIP Conference Proceedings* 2123: 1-9. doi: https://doi.org/10.1063/1.5116993

Manfren, M., B. Nastasi, and L. Tronchin. 2020. "Linking Design and Operation Phase Energy Performance Analysis Through Regression-Based Approaches." *Frontiers in Energy Research* 8: 288. doi: https://doi.org/10.3389/fenrg.2020.557649

Manfren, M., B. Nastasi, L. Tronchin, D. Groppi, and D. Astiaso Garcia. 2021a. "Techno-Economic Analysis and Energy Modelling as a Key Enablers for Smart Energy Services and Technologies in Buildings." *Renewable and Sustainable Energy Reviews* 150: 111490. doi: https://doi.org/https://doi.org/10.1016/j.rser.2021.111490

Manfren, M., M. Sibilla, and L. Tronchin. 2021b. "Energy Modelling and Analytics in the Built Environment—A Review of Their Role for Energy Transitions in the Construction Sector." *Energies* 14(3): 679. doi: https://doi.org/10.3390/en14030679

Norton, B., W. B. Gillett, and F. Koninx. 2021. "Decarbonising Buildings in Europe: A Briefing Paper." Proceedings of the Institution of Civil Engineers - Energy 174(4): 147-155. doi: https://doi.org/10.1680/jener.21.00088

Pistore, L., G. Pernigotto, F. Cappelletti, A. Gasparella, and P. Romagnoni. 2019. "A Stepwise Approach Integrating Feature Selection, Regression Techniques and Cluster Analysis to Identify Primary Retrofit Interventions on Large Stocks of Buildings." *Sustainable Cities and Society* 47: 101438. doi: https://doi.org/https://doi.org/10.1016/j.scs.2019.101438

Tronchin, L., M. Manfren, and L. C. Tagliabue. 2016. "Optimization of Building Energy Performance by Means of Multi-Scale Analysis – Lessons Learned from Case Studies." *Sustainable Cities and Society* 27: 296–306. doi: https://doi.org/https://doi.org/10.1016/j.scs.2015.11.003

Tronchin, L. 2005. "Modal analysis and intensity of acoustic radiation of the kettledrum". *The Journal of the Acoustical Society of America* 117(2): 926-933. doi: https://doi.org/10.1121/1.1828552.

Tronchin, L. 2021. "Variability of room acoustic parameters with thermo-hygrometric conditions". *Applied Acoustics* 177: 1-14. doi: https://doi.org/10.1016/j.apacoust.2021.107933

Tronchin, L., K. Fabbri, and C. Bertolli. 2018. "Controlled Mechanical Ventilation in Buildings: A Comparison between Energy Use and Primary Energy among Twenty Different Devices". *Energies* 11: 1-20. doi: https://doi.org/10.3390/en11082123

Tronchin, L., and D. J. Knight. 2016. "Revisiting Historic Buildings through the Senses. Visualising Aural and Obscured Aspects of San Vitale, Ravenna". *International Journal of*

Historical Archaeology 20: 127-145. doi: https://doi.org/10.1007/s10761-015-0325-2

Tronchin, L., M. Manfren, and V. Vodola. 2020a. "The carabattola - vibroacoustical analysis and intensity of acoustic radiation (IAR)". *Applied Sciences* 10(2): 641 doi: https://doi.org/10.3390/app10020641

Tronchin, L., M. Manfren, and V. Vodola. 2020b. "Sound characterization through intensity of acoustic radiation measurement: A study of persian musical instruments". *Applied Sciences* 10(2): 633. doi: https://doi.org/10.3390/app10020633

Tronchin, L., F. Merli, and M. Manfren. 2021a. "On the acoustics of the Teatro 1763 in Bologna". *Applied Acoustics* 172: 1-9. doi: https://doi.org/10.1016/j.apacoust.2020.107598

Tronchin, L., F. Merli, and M. Dolci. 2021b. "Virtual acoustic reconstruction of the Miners' Theatre in Idrija (Slovenia)". *Applied Acoustics* 172: 1-9. doi: https://doi.org/10.1016/j.apacoust.2020.107595

Westermann, P., C. Deb, A. Schlueter, and R. Evins. 2020. "Unsupervised Learning of Energy Signatures to Identify the Heating System and Building Type Using Smart Meter Data." *Applied Energy* 264: 114715. doi: https://doi.org/https://doi.org/10.1016/j.apenergy.2020.114715

Westermann, P., and R. Evins. 2019. "Surrogate Modelling for Sustainable Building Design – A Review." *Energy and Buildings* 198: 170–86. doi: https://doi.org/https://doi.org/10.1016/j.enbuild.2019.05.057